

**ANALYTICAL MODELING OF A FRACTURE-INJECTION/FALLOFF
SEQUENCE AND THE DEVELOPMENT OF A REFRACTURE-
CANDIDATE DIAGNOSTIC TEST**

A Dissertation

by

DAVID PAUL CRAIG

Submitted to the Office of Graduate Studies of
Texas A&M University
in partial fulfillment of the requirements for the degree of

DOCTOR OF PHILOSOPHY

May 2006

Major Subject: Petroleum Engineering

© 2006

DAVID PAUL CRAIG

ALL RIGHTS RESERVED

**ANALYTICAL MODELING OF A FRACTURE-INJECTION/FALLOFF
SEQUENCE AND THE DEVELOPMENT OF A REFRACTURE-
CANDIDATE DIAGNOSTIC TEST**

A Dissertation

by

DAVID PAUL CRAIG

Submitted to the Office of Graduate Studies of
Texas A&M University
in partial fulfillment of the requirements for the degree of

DOCTOR OF PHILOSOPHY

Approved by:

Chair of Committee,
Committee Members,

Thomas A. Blasingame
W. John Lee
Peter P. Valkó
G. Donald Allen
Stephen A. Holditch

Head of Department,

May 2006

Major Subject: Petroleum Engineering

ABSTRACT

Analytical Modeling of a Fracture-Injection/Falloff Sequence and the Development of a Refracture-Candidate Diagnostic Test. (May 2006)

David Paul Craig, B.S., Texas Tech University;

M.S., Texas A&M University

Chair of Advisory Committee: Dr. Thomas A. Blasingame

Fracture-injection/falloff sequences are routinely used as pre-frac well tests to estimate reservoir pressure and transmissibility, but the current interpretation methods are limited to analyzing specific and very small portions of the pressure falloff data. To remove the current limitations, new analytical fracture-injection/falloff models are developed that account for fracture propagation, fracture closure, and after fracture closure diffusion. A fracture-injection/falloff differs from a conventional injection/falloff sequence in that pressure during the injection is sufficient to initiate and propagate a hydraulic fracture. By considering fracture propagation as time-dependent storage, three new models are presented for a fracture-injection/falloff sequence in a well in an infinite slab reservoir with a single vertical fracture created during the injection and with variable fracture and wellbore storage as follows:

- Equivalent propagating-fracture and before-fracture-closure storage with constant after-fracture-closure storage.
- Time-dependent propagating-fracture storage, constant before-closure storage, and constant after-closure storage.
- Time-dependent propagating-fracture storage, constant before-closure storage with linear flow from the fracture, and constant wellbore storage and skin with after-closure radial flow.

When a fracture-injection can be considered as occurring instantaneously, limiting-case solutions of the new fracture-injection/falloff models suggest the observed pressure difference can be integrated to generate an equivalent pressure difference if the rate were constant. Consequently, a fracture-injection/falloff sequence can be analyzed with constant-rate, variable-storage type curves.

The new fracture-injection/falloff theory is also extended to allow for a fracture-injection in a reservoir containing an existing conductive hydraulic fracture. The new multiple-fracture fracture-injection/falloff model forms the basis of a new refracture-candidate diagnostic test that uses characteristic variable-storage behavior to qualitatively diagnose a pre-existing fracture retaining residual width and to determine if a pre-existing fracture is damaged. A quantitative analysis methodology is also proposed that uses a new pressure-transient solution for a well in an infinite-slab reservoir producing through multiple arbitrarily-oriented finite- or infinite-conductivity fractures.

DEDICATION

This work is dedicated:

*To my wife, Tesha Ann, for her love, encouragement, and patience
and to our twin boys, Justin Patrick and Jarrod Preston.*

ACKNOWLEDGEMENTS

I want to express my gratitude and appreciation to:

Dr. Tom Blasingame, chair of my advisory committee, for his guidance and friendship. In particular, I want to acknowledge two suggestions. First, when the development of the fracture-injection/falloff model stalled, Dr. Blasingame suggested that I review the work of Correa and Ramey, which proved to be the key to developing the new analytical solution. Second, after completing the pressure-transient solution for production through multiple infinite-conductivity fractures, Dr. Blasingame encouraged me to also complete a finite-conductivity solution. After adamantly refusing, I began working on the solution while flying back to Denver, and completed the solution in about six weeks time. Thanks Dr. Blasingame.

Drs. W. John Lee, Peter P. Valkó, and G. Donald Allen for serving as members of my advisory committee.

TABLE OF CONTENTS

	Page
ABSTRACT	iii
DEDICATION	iv
ACKNOWLEDGEMENTS.....	v
TABLE OF CONTENTS	vi
LIST OF FIGURES.....	ix
LIST OF TABLES	xiii
CHAPTER	
I INTRODUCTION – REFRACTURE-CANDIDATE DIAGNOSTIC.....	1
1.1 Introduction	1
1.2 Refracturing.....	2
1.2.1 Fracture Reorientation, Fracture Remediation, and Fracture Bypassed Layers.....	2
1.2.2 Refracture-Candidate Selection.....	6
1.2.3 Tight Gas Restimulation Study.....	8
1.3 Refracture-Candidate Diagnostic Tests	15
1.4 Research Objectives.....	17
1.5 Dissertation Summary	18
II SLUG-TEST AND FRACTURE-INJECTION/FALLOFF TEST ANALYSIS.....	21
2.1 Introduction	21
2.2 Slug-Test Solution	21
2.3 Injection/Falloff Testing at Pressures Greater Than Fracture Initiation Pressure.....	32
2.3.1 G-Function Derivative Analysis.....	32
2.3.2 Before-Closure Pressure Transient Analysis.....	38
2.3.3 Before-Closure Pressure Transient Analysis in Dual-Porosity Reservoirs.....	41
2.4 After-Closure Analysis	43
2.5 Discussion of Existing Injection/Falloff and Fracture-Injection/Falloff Test Analysis Methods	45
III MODELING A FRACTURE-INJECTION/FALLOFF TEST IN A RESERVOIR WITHOUT A PRE-EXISTING FRACTURE	47
3.1 Introduction	47
3.2 Constant-Rate Drawdown Solutions With Variable Fracture Storage.....	48
3.2.1 Constant-Rate Drawdown With Constant Before- and Constant After-Closure Storage.....	48
3.2.2 Constant-Rate Drawdown With Constant Before- and Constant After-Closure Storage With Fracture-Face and Choked-Fracture Skin.....	50

CHAPTER	Page
3.2.3 Constant-Rate Drawdown With Constant Before-Closure Storage, Constant After-Closure Wellbore Storage, and After-Closure Radial Flow With Skin.....	52
3.3 Constant-Rate Drawdown Numerical Solutions With Variable Fracture Storage.....	53
3.3.1 Constant-Rate Drawdown With Constant Before- and Constant After-Closure Storage.....	53
3.3.2 Constant-Rate Drawdown With Constant Before- and Constant After-Closure Storage With Fracture-Face and Choked-Fracture Skin.....	55
3.3.3 Constant-Rate Drawdown With Constant Before-Closure Storage, Constant After-Closure Wellbore Storage, and After-Closure Radial Flow With Skin.....	59
3.4 Fracture-Injection/Falloff Solutions.....	63
3.4.1 Solution Accounting for a Dilating Fracture, Before-Closure Storage, and After-Closure Storage.....	65
3.4.2 Solution Accounting for a Propagating Fracture, Constant Before-Closure Storage, and Constant After-Closure Storage.....	67
3.4.3 Solution Accounting for a Propagating Fracture, Before-Closure Storage, Constant After-Closure Storage, and After-Closure Radial Flow.....	70
3.5 Fracture-Injection/Falloff Limiting Solutions.....	72
3.5.1 Limiting-Case Solutions With a Dilating Fracture, Before-Closure Storage, and After-Closure Storage.....	72
3.5.2 Limiting-Case Solutions With a Propagating Fracture, Before-Closure Storage, and After-Closure Storage.....	73
3.5.3 Limiting-Case Solutions With a Propagating Fracture, Before-Closure Storage, Constant After-Closure Storage, and After-Closure Radial Flow.....	76
3.5.4 Limiting-Case Solutions With a Large Dimensionless Time of Injection.....	78
3.6 Numerical Evaluation of a Fracture-Injection/Falloff Analytical Solution.....	79
 IV MODELING A FRACTURE-INJECTION/FALLOFF TEST IN A RESERVOIR WITH A PRE-EXISTING FRACTURE.....	 86
4.1 Introduction.....	86
4.2 Multiple Arbitrarily-Oriented Vertical Fracture Pressure Transient Solution.....	87
4.2.1 Uniform Flux.....	87
4.2.2 Infinite Conductivity.....	90
4.2.3 Finite Conductivity.....	95
4.3 Multiple Vertical Fracture Constant-Rate Drawdown Pressure Transient Solution With Variable Fracture Storage.....	98
4.3.1 Numerical Evaluation of a Multiple Vertical Fracture Constant-Rate Drawdown Pressure Transient Solution With Variable Fracture Storage.....	100
4.4 Fracture-Injection/Falloff Solution With a Pre-Existing Fracture.....	102

CHAPTER	Page
4.4.1 Limiting-Case Fracture-Injection/Falloff Solutions With a Dilating Pre-Existing Fracture, a Propagating Induced Fracture, Multiple Closures, and Constant After-Closure Storage	107
V A REFRACTURE-CANDIDATE DIAGNOSTIC AND EXAMPLE FIELD APPLICATIONS	111
5.1 Introduction	111
5.2 Refracture-Candidate Diagnostic Test	112
5.2.1 Qualitative Analysis	114
5.2.2 Quantitative Analysis – Before-Closure Pressure-Transient Analysis	118
5.2.3 Quantitative Analysis – After-Closure Analysis	122
5.2.4 Quantitative Analysis – Type-Curve Analysis	130
5.3 Field Examples	142
5.3.1 Pseudoradial Flow Observed After Closure	142
5.3.2 Pseudolinear Flow Observed After Closure	156
5.3.3 Pre-Existing Conductive Hydraulic Fracture With Choked-Fracture Skin Damage	170
VI SUMMARY, CONCLUSIONS, AND RECOMMENDATIONS	172
6.1 Summary and Conclusions	172
6.2 Recommendations for Future Research	174
NOMENCLATURE	176
REFERENCES	183
APPENDIX A — BEFORE-CLOSURE PRESSURE-TRANSIENT ANALYSIS WITH PRESSURE-DEPENDENT RESERVOIR FLUID PROPERTIES	193
APPENDIX B — CONSTANT-RATE DRAWDOWN SOLUTIONS ACCOUNTING FOR BEFORE- AND AFTER-CLOSURE FRACTURE STORAGE	203
APPENDIX C — FRACTURE-INJECTION/FALLOFF SOLUTIONS IN A RESERVOIR WITHOUT A PRE-EXISTING FRACTURE	213
APPENDIX D — ANALYTICAL PRESSURE-TRANSIENT SOLUTION FOR A WELL CONTAINING MULTIPLE INFINITE-CONDUCTIVITY VERTICAL FRACTURES IN AN INFINITE SLAB RESERVOIR	228
APPENDIX E — ANALYTICAL PRESSURE-TRANSIENT SOLUTION FOR A WELL CONTAINING MULTIPLE FINITE-CONDUCTIVITY VERTICAL FRACTURES IN AN INFINITE SLAB RESERVOIR	245
APPENDIX F — FRACTURE-INJECTION/FALLOFF SOLUTIONS IN A RESERVOIR CONTAINING A COMPRESSIBLE FLUID	267
VITA	281

LIST OF FIGURES

FIGURE	Page
1.1 Multilayer Tracerscan log suggesting perforations at 4112-, 4420-, and 4468 ft were ineffectively stimulated or completely bypassed during the completion.	4
1.2 Multilayer Tracerscan log suggesting perforations at 4984-, 5014-, and 5212 ft were ineffectively stimulated or completely bypassed during the completion.	5
1.3 Composite microseismic image of two limited-entry hydraulic fracturing treatments with the sands targeted for hydraulic fracturing shaded, a gamma ray log overlay, and microseismic events (solid circles) recorded along the fracture plane.	7
1.4 Cotton Valley well CGU 3-8T production decline before and after the refracture treatment. Solid curve is the extrapolated production decline without a refracture treatment.....	10
1.5 Cotton Valley well CGU 10-7T production decline before and after the refracture treatment. Solid curve is the extrapolated production decline without a refracture treatment.	10
1.6 Cotton Valley well CGU 15-8T production decline before and after the refracture treatment. Solid curve is the extrapolated production decline without a refracture treatment.....	11
1.7 Frontier well GRBU 45-12 production decline before and after the refracture treatment. Solid curve is the extrapolated production decline without a refracture treatment.	12
1.8 Frontier well WSC 20-09D production decline before and after the refracture treatment. Solid curve is the extrapolated production decline without a refracture treatment.	12
1.9 Frontier well GRBU 27-14 production decline before and after the refracture treatment. Solid curve is the extrapolated production decline without a refracture treatment.	13
1.10 Mesaverde well RMV 55-20 production decline before and after the refracture treatment. Solid curve is the extrapolated production decline without a refracture treatment.	13
1.11 Mesaverde well Langstaff #1 production decline before and after the refracture treatment. Solid curve is the extrapolated production decline without a refracture treatment.	14
2.1 Slug-test type curve for an infinite-slab reservoir with skin.....	26
2.2 Constant-rate drawdown type curves for a radial infinite-slab reservoir with wellbore storage and skin generated from the slug-test type curves shown in Fig. 2.1.	27
2.3 <i>G</i> -Function derivative analysis common leakoff types.	37
3.1 Constant-rate drawdown in a reservoir with an open fracture with constant before-closure storage, decreasing constant after-closure storage, and variable dimensionless closure time.	54
3.2 Constant-rate drawdown in a reservoir with an open fracture with constant before-closure storage, increasing constant after-closure storage, and variable dimensionless closure time.	54
3.3 Comparison of constant-rate drawdown numerical solutions formulated with and without fracture-face and choked-fracture skin.	56

FIGURE	Page
3.4 Constant-rate drawdown in an infinite-slab reservoir with constant before- and decreasing constant after-closure storage with variable fracture-face and no choked-fracture skin.	57
3.5 Constant-rate drawdown in an infinite-slab reservoir with constant before- and decreasing constant after-closure storage with no fracture-face and variable choked-fracture skin.	58
3.6 Constant-rate drawdown in an infinite-slab reservoir with constant before- and decreasing constant after-closure storage with fracture-face and choked-fracture skin.	58
3.7 Constant-rate drawdown in an infinite-slab reservoir with fracture flow before closure, constant before-closure storage, and radial flow after closure with wellbore storage and skin—variable dimensionless wellbore radius.	61
3.8 Constant-rate drawdown in an infinite-slab reservoir with fracture flow before closure, constant before-closure storage, and radial flow after closure with wellbore storage and skin—variable skin.	62
3.9 Constant-rate drawdown in an infinite-slab reservoir with fracture flow before closure, constant before-closure storage, and radial flow after closure with wellbore storage and skin—variable dimensionless wellbore radius and approximation with $r_{wD} = 1$	62
3.10 A typical fracture-injection/falloff sequence in a moderate-permeability gas reservoir.	64
3.11 Pressure extrapolated to beginning of pseudoradial flow.	64
3.12 Comparison of a slug-test solution for $C_{LFD} = 0.001$ with the dimensionless wellbore pressure from an injection/falloff sequence with $q_{wD} = 100$ and $(t_e)_{LFD} = \{10^{-4}, 10^{-5}, 10^{-6}\}$	81
3.13 Comparison of a slug-test solution for $C_{LFD} = 0.01$ with the dimensionless wellbore pressure from an injection/falloff sequence with $q_{wD} = 100$ and $(t_e)_{LFD} = \{10^{-4}, 10^{-5}, 10^{-6}\}$	82
3.14 Comparison of a slug-test solution for $C_{LFD} = 0.10$ with the dimensionless wellbore pressure from an injection/falloff sequence with $q_{wD} = 100$ and $(t_e)_{LFD} = \{10^{-4}, 10^{-5}, 10^{-6}\}$	82
3.15 Comparison of a slug-test solution for $C_{LFD} = 0.001$ with the dimensionless wellbore pressure from an injection/falloff sequence with $q_{wD} = 10$ and $(t_e)_{LFD} = \{10^{-4}, 10^{-5}, 10^{-6}\}$	83
3.16 Comparison of a slug-test solution for $C_{LFD} = 0.01$ with the dimensionless wellbore pressure from an injection/falloff sequence with $q_{wD} = 10$ and $(t_e)_{LFD} = \{10^{-4}, 10^{-5}, 10^{-6}\}$	83
3.17 Comparison of a slug-test solution for $C_{LFD} = 0.10$ with the dimensionless wellbore pressure from an injection/falloff sequence with $q_{wD} = 10$ and $(t_e)_{LFD} = \{10^{-4}, 10^{-5}, 10^{-6}\}$	84
3.18 Comparison of a dilating fracture slug-test solution for $C_{bcD} = 0.01$, $C_{acD} = 0.005$, and $(t_c)_{LFD} = \{2(10)^{-5}, 2(10)^{-4}\}$ with the dimensionless wellbore pressure from a fracture-injection/falloff sequence with $q_{wD} = 10$, $(t_e)_{LFD} = 10^{-5}$, and $(t_c)_{LFD} = \{2(10)^{-5}, 2(10)^{-4}\}$	85
4.1 Cruciform uniform-flux vertical fracture pressure transient solution for $\delta_L = 0.001, 0.01, 0.1$, and 1	89
4.2 A comparison of a pressure-averaging infinite-conductivity solution, the uniform-flux solution, and the semianalytical infinite-conductivity solution for a cruciform fracture with $\delta_L = 1$	94

FIGURE	Page
4.3 Product of $(1 + \delta_L)$ and dimensionless pressure versus dimensionless time for a cruciform infinite-conductivity fracture with $\delta_L = 0, 1/4, 1/2, 3/4,$ and 1	94
4.4 Cruciform fracture log-log type curve with variable conductivity, $\delta_L = 1$ and $\delta_C = 1$	97
4.5 Log-log type curves for oblique fractures with $\delta_L = 1$, and $\delta_C = 1$, $C_{LFD} = 100\pi$ and $\theta_{j2} = \pi/2, \pi/4,$ and $\pi/8$	98
4.6 Cruciform fracture log-log type curve with infinite-conductivity fractures and constant storage, $C_{Lfbcd} = C_{Lfacd} = \{0.005, 0.010\}$	101
4.7 Cruciform fracture log-log constant storage type curve with infinite-conductivity fractures and variable storage, $C_{Lfbcd} = 0.005$ and $C_{Lfacd} = 0.010$	101
5.1 Variable storage drawdown type curve with closure at $(t_c)_{LFD} = 0.0001$, $C_{bcd} = 0.10$, and $C_{acd} = 0$	115
5.2 Variable storage drawdown type curve with closure at $(t_c)_{LFD} = 0.0001$, $C_{bcd} = 0.10$, and $C_{acd} = 0.05$	115
5.3 Variable storage drawdown type curve with closure at $(t_c)_{LFD} = 0.0001$, $C_{bcd} = 0.095$, $C_{acd} = 0.045$, $C_D = 0.005$, and choked-fracture skin, $(S_{fs})_{ch} = 0.05$	116
5.4 Variable storage drawdown type curve with closure at $(t_c)_{LFD} = 0.00001$, $C_{bcd} = 0.01$, and $C_{acd} = 0.009$	117
5.5 Fracture-injection/falloff sequence.	143
5.6 Fracture-injection/falloff sequence G -function derivative analysis.	147
5.7 Fracture-injection/falloff sequence before-closure pressure versus the dimensionless loss-volume function.	147
5.8 Fracture-injection/falloff sequence before-closure pressure-transient analysis.	150
5.9 Fracture-injection/falloff sequence after-closure analysis diagnostic graph.	151
5.10 Fracture-injection/falloff sequence Cartesian after-closure analysis graph.	152
5.11 Fracture-injection/falloff sequence variable-storage type-curve match.	153
5.12 GM 543-33 Mesaverde formation fracture-injection/falloff sequence.	159
5.13 GM 543-33 Mesaverde formation fracture-injection/falloff sequence G -function derivative analysis.	160
5.14 GM 543-33 Mesaverde formation fracture-injection/falloff sequence before-closure pressure versus the dimensionless loss-volume function.	160
5.15 GM 543-33 Mesaverde formation fracture-injection/falloff sequence before-closure pressure-transient analysis.....	162
5.16 GM 543-33 Mesaverde formation fracture-injection/falloff sequence after-closure analysis diagnostic graph.	164
5.17 GM 543-33 Mesaverde formation fracture-injection/falloff sequence after-closure pseudolinear flow graph.	164
5.18 GM 543-33 Mesaverde formation fracture-injection/falloff sequence infinite-conductivity fracture type-curve match.	166

FIGURE	Page
5.19 GM 543-33 Mesaverde formation fracture-injection/falloff sequence infinite-conductivity fracture type-curve match.	168
5.20 Mesaverde formation refracture-candidate diagnostic test pressure and injection rate recorded versus time.	171
5.21 Mesaverde formation refracture-candidate diagnostic equivalent constant-rate adjusted pseudopressure difference and derivative versus adjusted pseudotime.	171

LIST OF TABLES

TABLE	Page
3.1 Fracture stiffness for common two-dimensional fracture models.	65
5.1 Fracture stiffness for 2D fracture models.	119
5.2 Fracture-injection time, pressure, and rate data.	144
5.3 Variables required for before- and after-closure analysis.	146
5.4 Variables required for before-closure pressure transient analysis.	149
5.5 Variables required for type-curve match.	154
5.6 GM 543-33 fracture-injection time, bottomhole pressure, and injection rate.	157
5.7 GM 543-33 time and bottomhole pressure recorded during the pressure falloff.	158
5.8 GM 543-33 time and bottomhole pressure recorded during the pressure buildup.	169
5.9 GM 543-33 summary of results from the interpretation of the fracture-injection/falloff and drawdown/buildup sequences in the Mesaverde formation between 4,948- and 4,962- feet.	170

CHAPTER I

INTRODUCTION – REFRACTURE-CANDIDATE DIAGNOSTIC

1.1 Introduction

Oil and gas wells often contain potentially productive layers bypassed either intentionally or inadvertently during an original completion. Subsequent refracturing programs designed to identify underperforming wells and recomplete bypassed layers have sometimes been unsuccessful in part because the programs tend to focus on commingled *well* performance and *well* restimulation potential without thoroughly investigating individual *layer* properties and the refracturing potential of individual layers. Perhaps the most significant impediment for investigating layer properties is a lack of representative and cost-effective diagnostics that can be used to determine layer permeability, reservoir pressure, and to quantify the effectiveness of previous stimulation treatments.

Fracture-injection/falloff tests, which differ from conventional injection/falloff tests in that a fracture is propagated during the injection, are asserted to be a valid refracture-candidate diagnostic. The assertion is proved using new mathematical models and analytical solutions for a fracture-injection/falloff sequence in an infinite slab reservoir with and without a pre-existing hydraulic fracture.

A special case of interest is a fracture-injection/falloff test with an injection time short relative to the reservoir response. When the finite time of a fracture injection can be considered instantaneous, slug-test analysis methods can be applied to the falloff data. The preferred slug-test analysis method "converts" variable-rate pressure falloff data to equivalent constant-rate pressure data by integration of the recorded pressure difference with respect to time. After conversion, model-based (type curve) analysis is possible with new constant-rate variable-storage drawdown type curves that account for fracture closure and after-closure diffusion.

With a new solution for multiple arbitrarily-oriented uniform-flux, infinite-conductivity, or finite-conductivity hydraulic fractures, the fracture-injection/falloff test theory is extended to the case with a pre-existing hydraulic fracture. Consequently, a fracture-injection/falloff sequence with the injection time short relative to the reservoir response can be used as a refracture-candidate diagnostic to qualitatively determine the existence of a pre-existing fracture that retains residual width and to determine if a pre-existing fracture is damaged. Provided sufficient pressure falloff data are recorded, the new refracture-candidate diagnostic test can also provide estimates of fracture conductivity, fracture half length, reservoir permeability, and average reservoir pressure.

This dissertation follows the style and format of *SPE Journal*.

1.2 Refracturing

Howard and Fast¹ note that between 1947, when hydraulic fracturing was introduced to the industry, and 1970, there were about 500,000 recorded fracturing treatments. Of the half million treatments, an estimated 35% were refracture treatments to further enhance well production. Between 1970 and 1996, a modest number of case histories appear in the literature describing refracturing programs in both oil,²⁻⁷ gas,⁸⁻¹¹ and gas-storage reservoirs,¹² but the number of wells with refracture treatments in each case is on the order of 100 or less.

Reeves¹³ in a 1996 study to identify the technology barriers and potential benefit of restimulation concluded that only 450 to 550 refracture treatments are pumped per year in the United States. Examples of gas reservoirs with refracturing programs originating since 1996 include the Barnett shale of North Texas,¹⁴ the Codell formation in the Denver-Julesburg basin,¹⁵⁻¹⁶ and the Vicksburg in South Texas.¹⁷

1.2.1 Fracture Reorientation, Fracture Remediation, and Fracturing Bypassed Layers. Restimulation following a primary fracturing treatment takes several forms. For example, a premature screenout can result in a very short effective fracture half-length, a damaged fracture face, and a plugged proppant pack. If the cause of a screenout is known or inferred from the treatment records, a refracture treatment is sometimes performed immediately after correcting the problem to obtain the desired fracture half-length and conductivity.¹⁸ Alternatively, a damaging fluid system, for example, a system that does not degrade following a treatment, might allow a fracturing treatment to be pumped as designed, but it can also either plug the proppant pack or significantly reduce fracture conductivity. With a damaging fluid system, the impact can be immediate, that is, a well may not flow back, or the production profile might show the effects of slow fracture clean up over time.¹⁹ Alternatively, formation fines migration or proppant crushing can damage fracture conductivity over time. With proppant-pack damage, a remedial chemical stimulation treatment is sometimes effective, or with severe fracture conductivity damage, a refracture treatment can be required.¹⁸ The current Vicksburg refracturing program in South Texas is an example of a fracture remediation project that attempts to identify refracture-candidates based on unsuccessful primary fracture treatments or suspected proppant-pack damage.¹⁷

Refracturing programs in the Barnett¹⁴ shale and Codell¹⁵⁻¹⁶ are believed to be successful because of secondary fracture azimuth reorientation. Ebel and Mack²⁰ theorized that the directions of maximum and minimum stress change with production. Consequently, a refracture treatment pumped after significant production can initiate and propagate in a different plane than the primary fracture treatment. A definitive study of fracture reorientation was presented by Wright *et al.*²¹ Wright *et al.* used tiltmeter interpretations to demonstrate that the fractures propagated during a 1993 refracturing program in the Lost Hills Diatomite reoriented to a plane different than the original 1990 tiltmeter-mapped primary hydraulic fractures.²¹ In a subsequent study, Wright *et al.*²² and Wright and Conant²³ demonstrated using tiltmeter

interpretations that the fractures from refracture treatments in the Van Austin Chalk oil field in Texas reoriented by as much as 56° from the original fracture azimuth. A field experiment in the Barnett shale using tiltmeters during the original fracture treatment and subsequent refracture treatment, also clearly demonstrated hydraulic fracture reorientation.²⁴

Multilayer completions with hydraulic fractures can contain layers bypassed intentionally to pursue higher grade pay and layers bypassed inadvertently because of ineffective fracture treatment diversion. For example, an average of 26 sands are targeted for fracturing in a typical Piceance basin Mesaverde low permeability gas well using three to five fracturing treatments with perforation-friction controlled diversion (limited entry). Esphahanian and Storhaug²⁵ in a study of 13 Piceance basin production logs, found that after fracturing, 28% of the targeted sands produced less than 10 Mcf/D. A similar production log study in the Jonah field in Wyoming, where each well can contain 30 to 40 low permeability gas sands targeted for fracturing, found that after completion 35% to 40% of the sands were not significantly contributing to production.²⁶ In some cases the noncontributing sands may have been successfully fracture stimulated, but either the reservoir quality is extremely poor or the fracture was damaged by subsequent uphole completion operations.²⁶ In other cases, the fracturing diversion technique failed, and the sands were inadvertently bypassed.

Identifying bypassed layers is sometimes possible with near-wellbore radioactive tracing, far-field tiltmeter fracture imaging, or microseismic fracture imaging.²⁷ Radioactive tracing adds radioactive isotopes to the fracturing fluid during a treatment, and after the treatment uses spectral gamma ray logging to determine the location of the radioactive material. Radioactive tracing is a near-wellbore diagnostic that can help determine if a sand targeted for fracturing was inadvertently bypassed. **Figs. 1.1 and 1.2** contain a post-frac spectral gamma ray log presentation (Tracerscan) from a Mesaverde well with 20 sands targeted for fracturing during three fracturing treatments using limited-entry diversion. Fig. 1.1 shows little or no radioactive material adjacent to perforations at 4,112 ft, 4,420 ft, and 4,468 ft. Similarly, Fig. 1.2 shows no radioactivity measured adjacent to the perforations at 4,984 ft, 5,014 ft, and 5,212 ft. In summary, the near-wellbore image shown in Figs 1.1 and 1.2 suggest that six of the 20 sands, or 30%, were not effectively stimulated or were bypassed entirely. In a study of fracturing treatments in the Almond, Cotton Valley, Delaware, and Red Fork using radioactive tracers and spectral gamma ray logging, Fisher *et al.*²⁸ concluded that between 10% and 33% of layers targeted for fracturing were unstimulated after completion.

Far-field fracturing imaging methods,²⁷ including tiltmeters and microseismic monitoring, can also help determine if targeted sands were bypassed, but the resolution of far-field imaging is not sufficient to definitively identify bypassed layers without other corroborative evidence like production logs or pressure transient tests of individual layers. Tiltmeters can be either surface or downhole deployed, and measure the

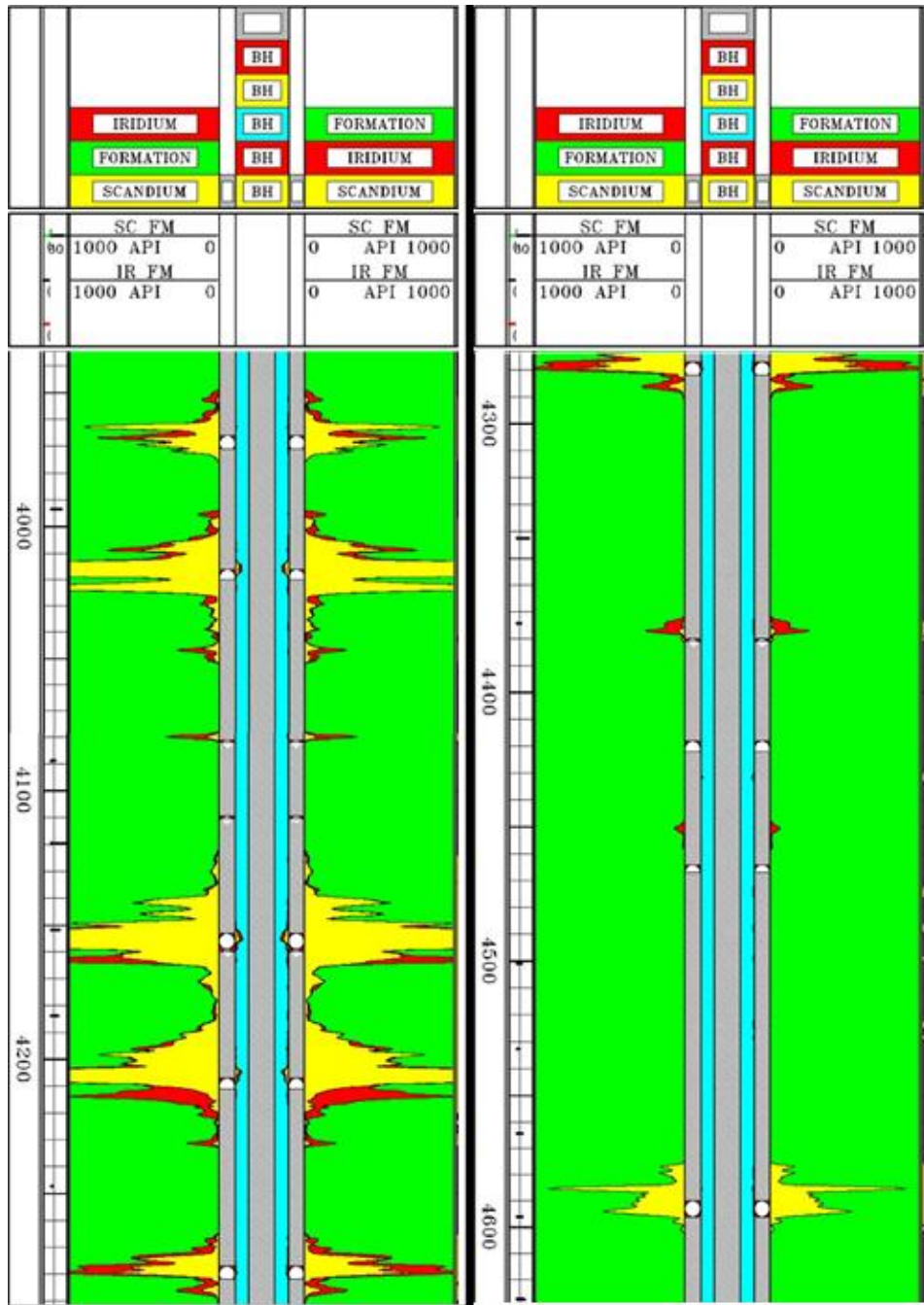


Fig. 1.1—Multilayer Tracerscan log suggesting perforations at 4112-, 4420-, and 4468 ft were ineffectively stimulated or completely bypassed during the completion.

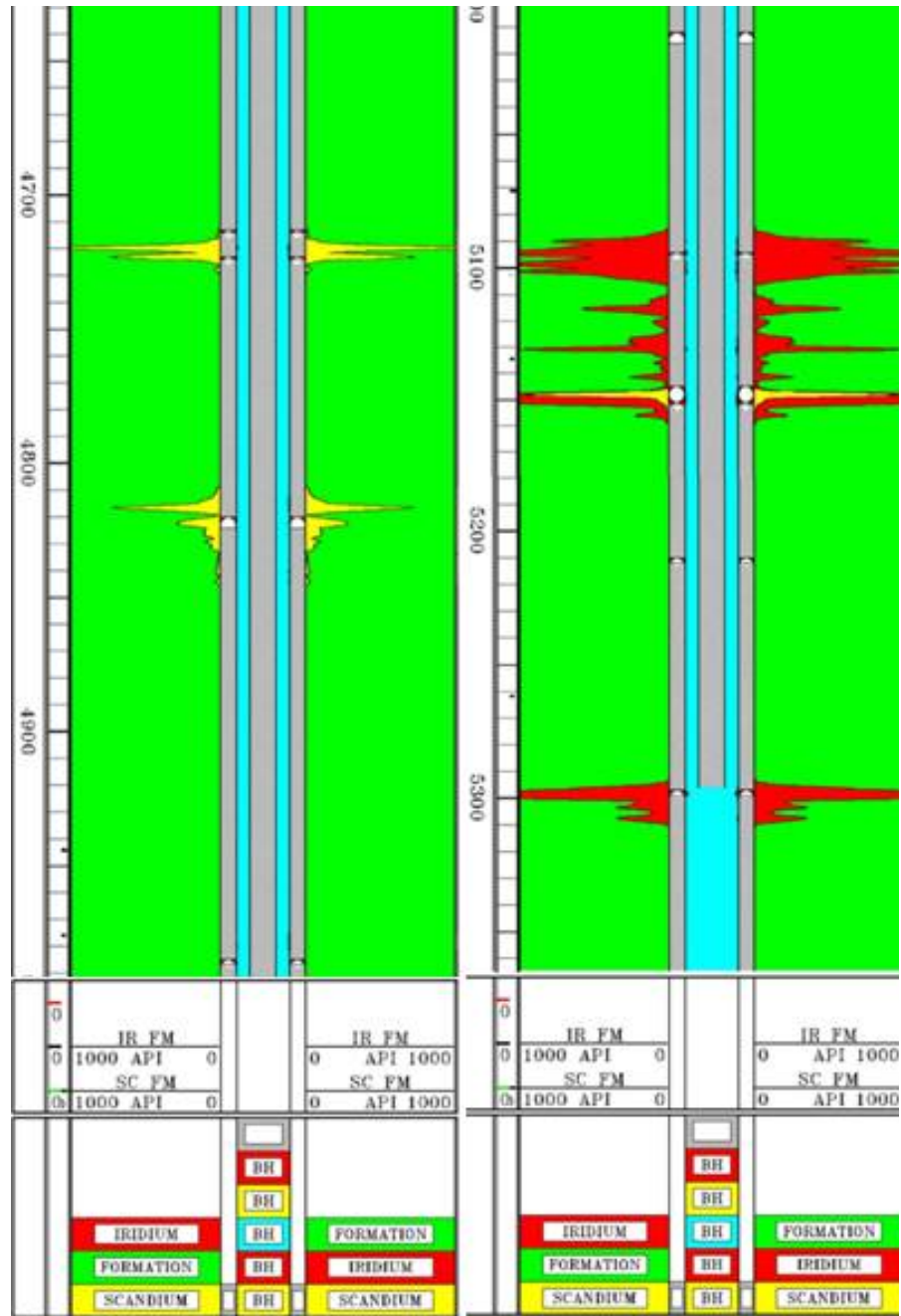


Fig. 1.2—Multilayer Tracerscan log suggesting perforations at 4984-, 5014-, and 5212 ft were ineffectively stimulated or completely bypassed during the completion.

minute distortion of the earth during a fracturing treatment.²⁷ An array of tiltmeters in or adjacent to the treatment well can be used to infer the far field fracture geometry—azimuth, length, and height—based on relatively simple models of fracture growth.²⁷

Microseismic fracturing imaging uses an array of geophones or accelerometers in the treatment well or an offset well to measure the acoustic energy transmitted from the slippage of microfractures and fissures adjacent to a propagating fracture. The slippage creates seismic events that form an "envelope" around the propagating fracture, and by mapping the location of each seismic event, the fracture azimuth, length and height can be inferred.²⁷ **Fig. 1.3** is a composite microseismic image of two limited-entry fracturing stages from a multilayer completion with a total of 10 layers targeted for fracturing. The targeted layers are denoted by the crosshatched shading, and the microseismic events recorded (solid circles) are shown in the fracture plane. Fracture geometry is inferred by distribution of the seismic events in the fracture plane. It's noteworthy that virtually all of the seismic events were confined to five layers, and that the other five layers contained few if any of the recorded seismic events. A lack of seismic events in the five layers strongly suggests the layers were bypassed or ineffectively stimulated by the limited-entry fracture treatments.

Radioactive tracing and far-field fracture imaging are extremely beneficial when developing a refracture program to identify and stimulate bypassed layers; however, the vast majority of wells drilled and completed have no tracing or imaging.

1.2.2 Refracture-Candidate Selection. Howard and Fast¹ proposed refracture-candidate selection criteria for oil wells in 1970 that focused on either identifying wells that responded favorably to an initial treatment but experienced rapid production decline or wells with intentionally bypassed pay that could be targeted during refracturing. They concluded wells that responded favorably during an initial fracture treatment would respond favorably to refracturing, or as phrased by Reese *et al.*,²⁹ "good wells make good refracture candidates." In 1978, however, Crowell and Jennings,³⁰ reported only limited success had been observed following refracturing treatments in low permeability gas wells. More than twenty years later, Kuuskraa *et al.*³¹ noted that identifying refracture-candidate wells is "challenging," and suggested that refracture-candidate selection should include production data analysis to identify suspected underperforming wells, well test analysis to validate the production data analysis, fracture modeling, and a thorough well records review to find potential problems during the original completion.

Other refracture-candidate selection methods have been suggested over the years. Hower and Decker³² identified recompletion candidates in multilayer gas reservoirs by interpreting linear trends in a graph of p/z versus cumulative production. Fetkovich, *et al.*³³ demonstrated that a graph of p/z versus cumulative production will be non-linear in layered, no crossflow reservoirs. Thus, Hower and Decker³²

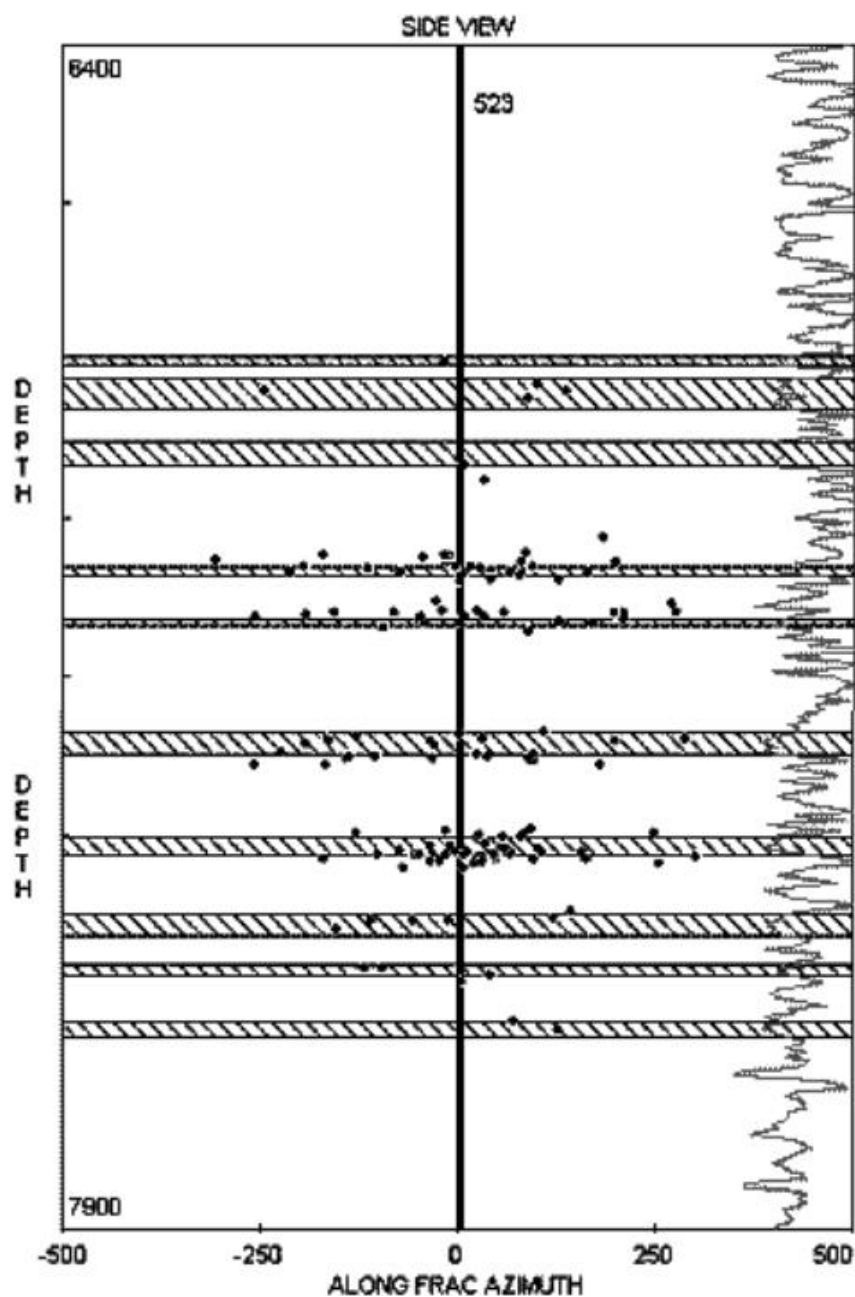


Fig. 1.3—Composite microseismic image of two limited-entry hydraulic fracturing treatments with the sands targeted for hydraulic fracturing shaded, a gamma ray log overlay, and microseismic events (solid circles) recorded along the fracture plane.

concluded a linear trend in a multilayer completion implied an ineffective completion with bypassed layers.

A similar refracture candidate selection method was proposed by Fetkovich³⁴ using production data analysis with Fetkovich type curves to identify layered no-crossflow behavior. Fetkovich³⁴ recognized that selectively stimulating the lower permeability layers would add well productivity and reserves, and he reported that the low permeability layers were targeted for refracturing in wells with strong layered no-crossflow behavior, which is indicated by a decline curve exponent approaching unity. McCoy, Reese, and Johnson,³⁵ extended the work of Fetkovich and developed refracture-candidate selection guidelines for multilayer completions. The guidelines included a thorough review of well records—which the author's conclude is the most important step—production data analysis to identify layered no-crossflow behavior, production logs to identify nonproductive layers, and layer pressure transient testing to determine layer reservoir properties.

In the 1990s a relatively new tool was introduced to help select refracture-candidates. An artificial neural network³⁶⁻³⁸ can be developed for refracture programs by "training" a neural-network with a set of input and output parameters. Training implies the neural-network develops a relationship between a given set of input and output parameters. After training, the neural-network is used as a predictive tool to identify refracture candidates. Shelley³⁷ notes a neural-network trained with public completion and production information is especially beneficial since it can rapidly screen refracture candidates before more detailed analysis—like thoroughly reviewing the well file, production data analysis, and well testing—is required.

In summary, refracture-candidate selection methods in the late 1990s generally consisted of the following.

- A thorough well record review to identify obvious problems or inadequacies of the initial fracturing treatment and to identify target layers intentionally bypassed during the original completion.
- Production data analysis to identify well underperformance. Production data analysis can simply compare offset well production or can entail type-curve analysis and reservoir simulation.
- Refracture-candidate diagnostics including well testing and production logs.

1.2.3 Tight Gas Restimulation Study. Beginning in 1998, the Gas Research Institute (GRI), since renamed the Gas Technology Institute (GTI), embarked on a research and development project to evaluate methods for selecting refracture candidates, to identify the mechanisms for well "underperformance," and to test restimulation techniques.³⁹⁻⁴¹ Three methods were used to evaluate well performance and fracture treatment effectiveness—production statistics, virtual intelligence using a neural network, and production type-curve analysis.

Production statistics, or moving domain analysis as implemented on a computer,⁴²⁻⁴³ compares production indicators of each well with its offsets to identify well underperformance. By comparing a well's

production with only the immediate offset well production, the variability of reservoir quality is minimized in the comparison. Virtual intelligence was utilized by training an artificial neural network with production, completion, and fracturing variables that included fracturing fluid type, breaker type, and breaker concentration. After training, the artificial neural network was used to identify restimulation-candidate wells with relatively poor fracture treatment design or execution by comparing predicted and actual well performance. The production type-curve analysis used in the restimulation study required history-matching well production using analytical type-curves developed specifically for *single layer* hydraulically fractured low permeability gas wells.⁴⁴ Restimulation candidates were identified by a short effective fracture half-length, and the production increase potential of extending the effective fracture half-length with a restimulation treatment.³⁹

An important guiding principle of the study was the "85/15" rule, which presumed that 85% of the incremental recovery from restimulation of all wells could be produced by only 15% of the wells.³⁹ Using the 85/15 rule, the evaluation methods were required to identify only the top 15% of the refracture candidates. Each evaluation method was anticipated to develop a list of candidates, and the overlap between lists would be the preferred restimulation candidates. Unfortunately, little overlap was observed,⁴⁵ and a detailed study of the top candidates from each list was required to develop a prioritized list of restimulation candidates.

After a thorough evaluation process, nine multilayer tight-gas wells were restimulated in the Frontier formation in Wyoming, the Mesaverde in Colorado, and the Cotton Valley in Texas. Eight of the nine restimulation treatments were refracture treatments with three refracture treatments in the Frontier, two in the Mesaverde, and three in the Cotton Valley. In the final report to GRI, Reeves⁴⁵ reported that seven of the eight refracture treatments were economically successful—based on a refracture cost of less than \$0.75/Mcf of incremental gas produced⁴⁶—with 2.9 Bcf of incremental reserves attributed to the restimulation project at a cost of \$0.26/Mcf.

A new review of the well performance after four years of production following the refracture treatments reveals the program as a whole was successful, but the measure of success varied considerably by area and by formation. **Figs. 1.4 through 1.6** contain graphs of gas production versus time for the Cotton Valley restimulation wells, which are the CGU 3-8T, CGU 10-7T, and CGU 15-8T, respectively. Each graph contains estimated incremental gas recovery since the refracture treatment along with a cost in dollars per Mcf of the incremental gas. Clearly the CGU 3-8T and CGU 10-7T can be considered economic successes with 0.67 Bcf of incremental gas produced at a cost of \$0.30/Mcf, but the CGU 15-8T appears to be a failure with only 0.080 Bcf of incremental gas produced at a cost of \$1.23/Mcf. Recognizing that an economic success depends on several factors, including gas price volatility and risk, the incremental gas

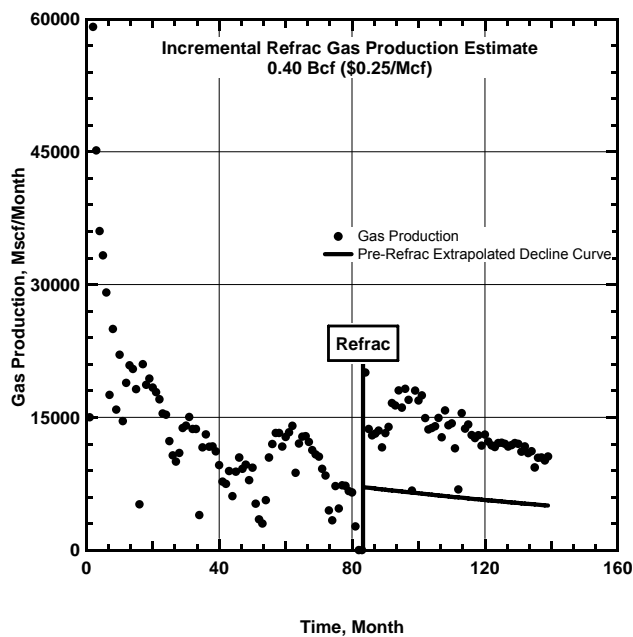


Fig. 1.4—Cotton Valley well CGU 3-8T production decline before and after the refracture treatment. Solid curve is the extrapolated production decline without a refracture treatment.

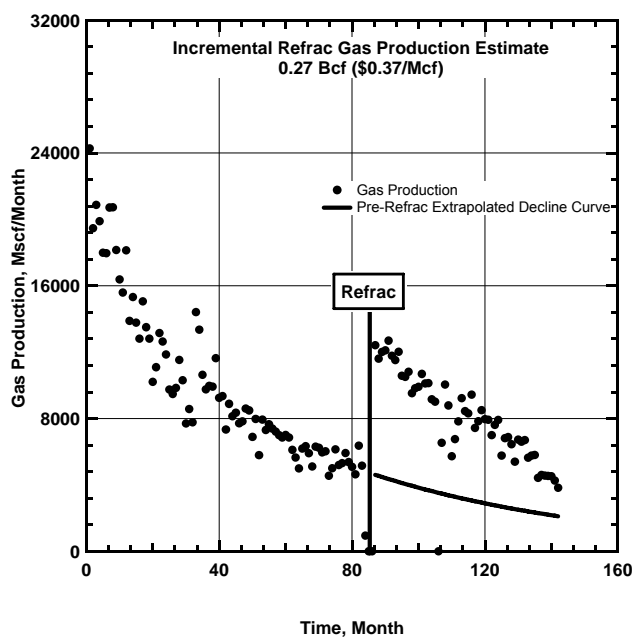


Fig. 1.5—Cotton Valley well CGU 10-7T production decline before and after the refracture treatment. Solid curve is the extrapolated production decline without a refracture treatment.

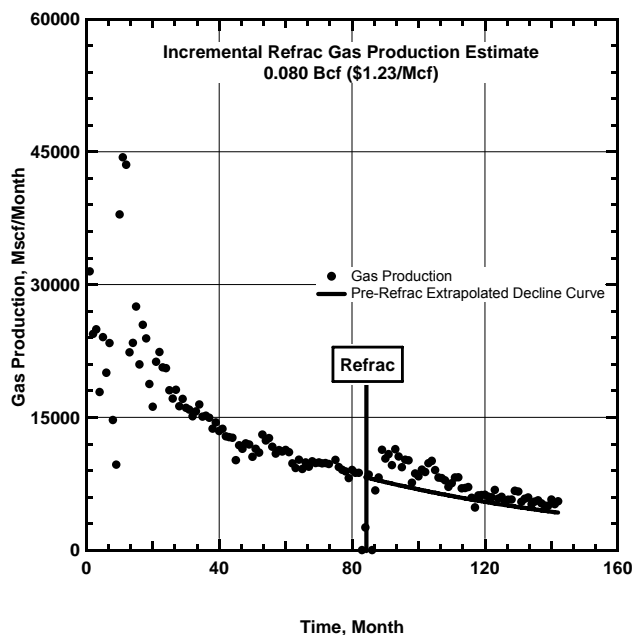


Fig. 1.6—Cotton Valley well CGU 15-8T production decline before and after the refracture treatment. Solid curve is the extrapolated production decline without a refracture treatment.

may be a better measure of success, and as such, the CGU 15-8T refracture treatment was unsuccessful with only 5% of the cumulative gas production attributed to the refracture treatment.

Figs. 1.7 through 1.9 contain graphs of gas production versus time for the Frontier wells with refracture treatments, which are the GRBU 45-12, WSC 20-09D, and the GRBU 27-14, respectively. As observed with the Cotton Valley refracturing results, two of the three refracturing treatments were successful. The refracturing treatment in the GBU 45-12 added 0.30 Bcf of incremental production, and the refracturing treatment in the WSC 20-09D added 0.17 Bcf of incremental production, which corresponds to a cost of \$0.45/Mcf for both wells. Conversely, the refracture treatment in the GRBU 27-14 shown in Fig. 1.9 was detrimental to well performance, and the treatment resulted in a loss of 0.10 Bcf.

Figs. 1.10 and 1.11 contain graphs of gas production versus time for the RMV 55-20 and Langstaff #1 Mesaverde wells. The refracture treatments resulted in incremental gas production of 0.09 Bcf and 0.055 Bcf, respectively. However, the refracture treatment incremental gas production cost \$0.85/Mcf, and the refracture treatments are considered by the operator to be failures.

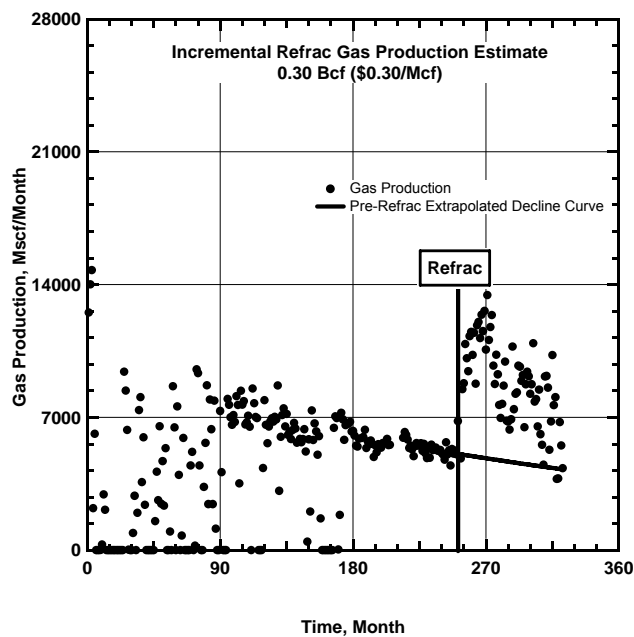


Fig. 1.7—Frontier well GRBU 45-12 production decline before and after the refracture treatment. Solid curve is the extrapolated production decline without a refracture treatment.

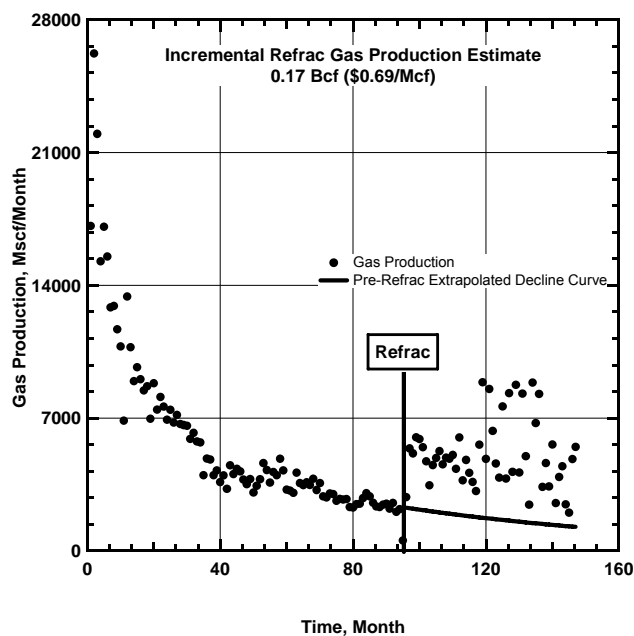


Fig. 1.8—Frontier well WSC 20-09D production decline before and after the refracture treatment. Solid curve is the extrapolated production decline without a refracture treatment.

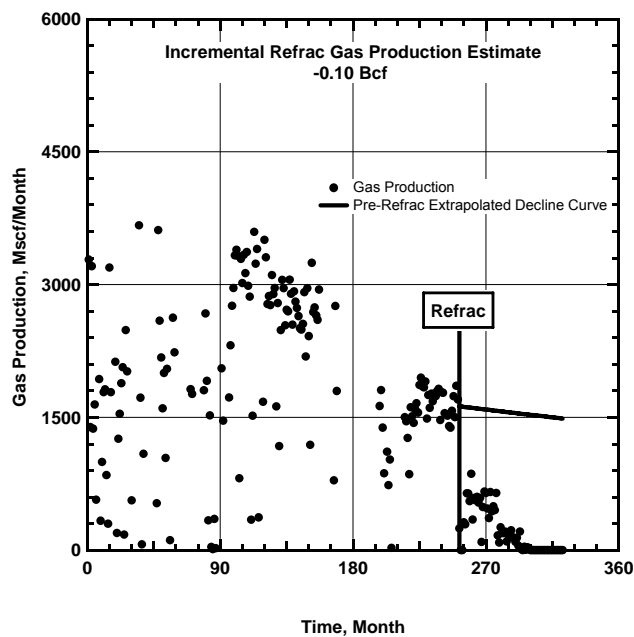


Fig. 1.9—Frontier well GRBU 27-14 production decline before and after the refracture treatment. Solid curve is the extrapolated production decline without a refracture treatment.

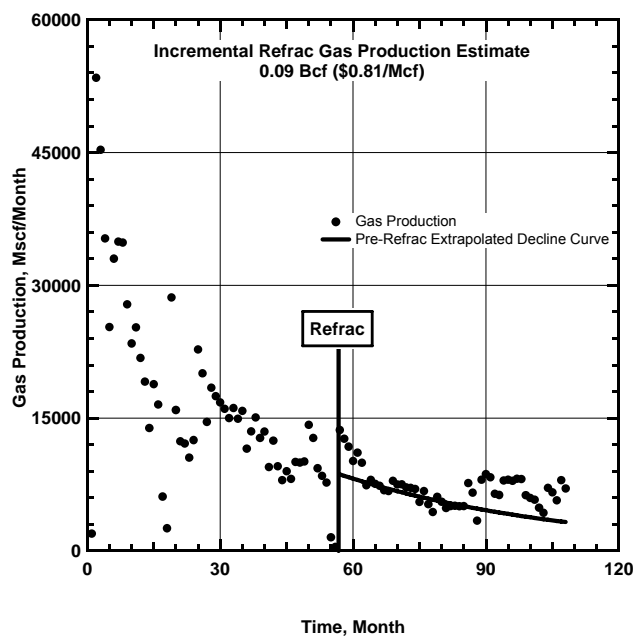


Fig. 1.10—Mesaverde well RMV 55-20 production decline before and after the refracture treatment. Solid curve is the extrapolated production decline without a refracture treatment.

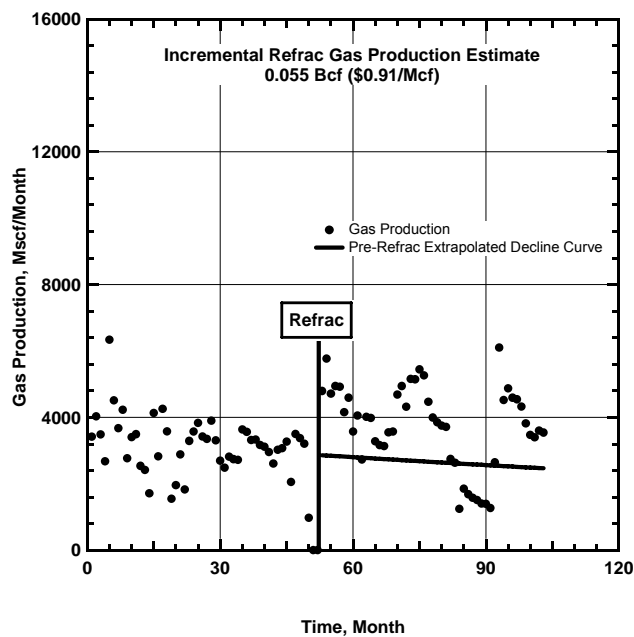


Fig. 1.11—Mesaverde well Langstaff #1 production decline before and after the refracture treatment. Solid curve is the extrapolated production decline without a refracture treatment.

After 4 years of production, it appears that four of eight refracture treatments can be considered successful based on the refracture cost and incremental gas production. Of the other four wells with a refracture treatment, one is a failure that resulted in a loss of 0.10 Bcf of reserves, and the other three are economic failures based on the original Reeves and Wolhart⁴⁶ \$0.75/Mcf refracture treatment cost per incremental gas production economic threshold. It's also noteworthy that the incremental gas production attributed to the successful refracture treatments was on the order of 20% of the well cumulative production, while the incremental gas production from the unsuccessful refracture treatments was less than 5% of the well's cumulative gas production.

Two common characteristics of every well in the refracture program is that each produced from multiple layers, and the original fracturing program consisted of some limited-entry fracture treatments.³⁹⁻⁴⁰ If, as previously suggested, limited-entry fracture treatments ineffectively stimulate or inadvertently bypass on the order of 30% of the targeted layers, then why wasn't the restimulation program more successful?

One possible explanation is that the approach adopted during the restimulation study was to evaluate the restimulation potential of each *well*. All three restimulation candidate evaluation methods—production statistics, virtual intelligence using artificial neural networks, and production type-curve analysis—were

developed to evaluate *well* performance as opposed to identifying bypassed layers that could be at or near virgin reservoir pressure. While recognizing the importance of evaluating layer properties and targeting specific layers or groups of layers for restimulation, a lack of cost-effective diagnostic tests for use in wells producing from multiple layers hindered any attempt to identify specific underperforming layers in the multilayer completions.³⁹⁻⁴¹ Additionally, once the refracture wells were identified, the refracture treatments were designed to restimulate the *well* as opposed to identifying and stimulating isolated individual layers. Mechanical isolation and refracturing in stages were preferred in some cases, but isolation was not allowed either because of operator concerns or project economic constraints.⁴⁷ As a last resort, ball sealers were used periodically throughout several treatments to ensure some fluid diversion, and refracture treatments with radioactive tracing confirmed some diversion was obtained.⁴⁷

1.3 Refracture-Candidate Diagnostic Tests

A refracture-candidate diagnostic test should be used prior to a refracture treatment to complete the following objectives.

- Determine if a pre-existing fracture retaining residual width exists.
- Determine if a pre-existing fracture is damaged.
- Determine pre-existing fracture effective half-length and conductivity
- Determine reservoir permeability and average reservoir pressure.

When the diagnostic test objectives are achieved, the benefits of refracturing can be easily evaluated, and the incremental production from a refracture treatment can be predicted.

Quantitative conventional pressure-transient testing, which includes drawdown, drawdown/buildup, or injection/falloff tests at a pressure less than the fracture propagation pressure, can be used to achieve the objectives of a refracture-candidate diagnostic test. However, conventional pressure-transient tests are best suited for evaluating a single layer. For wells producing from multiple low permeability layers, multilayer pressure-transient tests have been published,⁴⁸ but in practice, determining layer flow rates for test interpretation from multiple layers is problematic—especially with upwards of 20 layers producing.⁴⁹ In general, a cost-effective quantitative diagnostic test does not exist for low permeability wells producing from multiple layers.

Diagnostic testing in low permeability multilayer wells has been attempted, and Hopkins *et al.*⁵⁰ describe several diagnostic techniques used in a Devonian shale well to diagnose the existence of a pre-existing fracture(s) in multiple targeted layers over a 727 ft interval. The diagnostic tests included isolation flow tests, wellbore communication tests, nitrogen injection/falloff tests, and conventional drawdown/buildup tests.

As described by Hopkins *et al.*,⁵⁰ the refracture-candidate well was originally completed in four layers—the Cleveland, Upper Huron, Middle Huron, and Lower Huron—distributed across a 727 ft gross interval with a single limited-entry fracture treatment. Isolation flow tests were used to quantify the post-frac production of each isolated layer, and the tests determined insignificant flow from the Cleveland and Middle Huron layers. Wellbore communication tests were used to determine if a hydraulic fracture connected layers outside of the wellbore. The communication tests established that only the Middle and Lower Huron were communicating beyond the wellbore, which for well testing purposes, effectively reduced the four layer completion to a three layer case.

Three nitrogen injection/falloff tests were completed in the Cleveland, Upper Huron, and Middle/Lower Huron layers. During the test, nitrogen was injected at a pressure less than the fracture propagation pressure, and the pressure falloff during the shut-in period was recorded for one hour. Nitrogen injection/falloff tests suggested a propped hydraulic fracture existed in the Middle/Lower Huron but not in the the Cleveland or Upper Huron. Consequently, the limited-entry fracture treatment effectively stimulated only 50% of the targeted layers. Three pressure buildup tests were completed in Cleveland, Upper Huron, and Middle/Lower Huron, and a finite-difference simulator was used to history-match the nitrogen injection-falloff and pressure buildup tests. Well testing interpretations revealed an infinite-conductivity fracture with a fracture half length of 80 feet had been placed in the poorest quality reservoir rock in the wellbore. Additionally, reservoir simulation suggested gas recovery could be increased by 29% by placing infinite-conductivity fractures in the Cleveland and Upper Huron layers, which are the best quality reservoir rock.⁵⁰

The post-frac diagnostic program described by Hopkins *et al.*⁵⁰ was very thorough and addressed the objectives of a refracture-candidate diagnostic. However, the diagnostic program was also expensive and time consuming for a relatively simple four layer case. Many refracture candidates in low permeability gas wells contain stacked lenticular sands with between 20 to 40 layers which need to be evaluated in a timely and cost effective manner.

Other more cost effective but qualitative refracture-candidate diagnostic tests have been reported. Hopkins, *et al.*⁵¹ also suggested an annulus injection test to qualitatively identify a pre-existing fracture in the Antrim shale. The annulus injection test requires slowly injecting water into a targeted layer until the observed pressure approaches the fracture initiation or propagation pressure of the formation. The injected volume is the "fillup" volume, and a large fillup volume suggests a high conductivity fracture exists. When the objective of a refracture treatment(s) is to stimulate bypassed layers, a qualitative determination of a pre-existing fracture may be the only diagnostic test required, that is, if a fracture exists, a refracture treatment may be deemed unnecessary.

As part of the recent GRI restimulation project,⁴⁵ Huang *et al.*⁵² suggested a quasi-quantitative pressure transient test interpretation method as a refracture-candidate diagnostic. The "short shut-in test interpretation method" is designed to provide only an indication of pre-existing fracture effectiveness. The method uses log-log type curve reference points—the end of wellbore storage, the beginning of pseudolinear flow, the end of pseudolinear flow, and the beginning of pseudoradial flow—and the known relationships between pressure and system properties at those points to provide upper and lower limits of permeability and effective fracture half length. Huang *et al.*⁵² provide a simulated example that unfortunately requires 25 hours of shut-in data to bracket fracture half length to within 10% of the known value and to bracket permeability to within a two order-of-magnitude range.

While not used specifically as a refracture-candidate diagnostic test, nitrogen slug tests have been used effectively as a prefracture diagnostic test in low permeability reservoirs.^{49,53} Jochen *et al.*⁴⁹ describe the nitrogen injection test as a short, small volume injection of nitrogen *at a pressure less than the fracture initiation and propagation pressure* followed by an extended pressure falloff period. A nitrogen slug test is unlike the nitrogen injection/falloff test used by Hopkins *et al.*⁵⁰ in that the injection period is short and can be considered instantaneous. A nitrogen slug test is analyzed using slug-test type curves and by history matching the injection and falloff pressure with a finite-difference simulator.⁴⁹

Since 1998, fracture-injection/falloff tests have been routinely utilized as a prefracture diagnostic to estimate formation permeability and average reservoir pressure.⁵⁴ Fracture-injection/falloff tests differ from nitrogen slug tests in that the pressure during the injection *is greater than the fracture initiation and propagation pressure*. A fracture-injection/falloff test typically requires a low rate, small volume injection of treated water followed by an extended shut-in period, and the permeability to the mobile reservoir fluid and the average reservoir pressure are interpreted from the pressure decline.

The test methods or test programs described are not cost-effective and capable of achieving the objectives of a refracture-candidate diagnostic in a well completed in multiple layers. The annulus injection test is qualitative. The short shut-in time buildup test interpretation method is quasi-quantitative, but the tests require too much time for multilayer testing. Nitrogen slug tests and fracture-injection/falloff tests have only been used as prefracture diagnostics. Only Hopkins' *et al.*⁵⁰ refracture-candidate diagnostic program has proven successful in achieving the refracture-candidate diagnostic objectives in a well completed in multiple layers, but the program is time consuming and may be impractical for low permeability stacked, lenticular gas reservoirs.

1.4 Research Objectives

A fracture-injection/falloff test with the time of injection short relative to the reservoir response is asserted to be a viable refracture-candidate diagnostic test. The research objectives documented in this dissertation include the following.

- Extend fracture-injection/falloff interpretation methodology to account for pressure-dependent reservoir fluid properties by formulating before-closure pressure transient analysis in terms of adjusted pseudopressure and adjusted pseudotime.
- Demonstrate that the pressure difference observed during the falloff of a fracture-injection/falloff sequence in a layer with or without an existing conductive hydraulic fracture and with the reservoir response short relative to the time of injection can be converted to an equivalent pressure difference if the sandface rate were constant.
- Demonstrate that in a layer without a pre-existing conductive hydraulic fracture, a quantitative determination of reservoir transmissibility is possible by matching equivalent constant-rate pressure from the falloff of a fracture-injection/falloff sequence with a variable-storage constant-rate drawdown log-log type curve.
- Demonstrate that a pre-existing hydraulic fracture retaining residual width can be diagnosed from the variable storage behavior exhibited by the equivalent constant-rate pressure difference observed during the falloff of a fracture-injection/falloff sequence.
- Demonstrate that a quantitative determination of primary and secondary fracture half-length, primary and secondary fracture conductivity, and reservoir transmissibility are possible by matching equivalent constant-rate pressure recorded during the falloff of a fracture-injection/falloff sequence with a variable-storage constant-rate drawdown log-log type curve developed a well producing from multiple arbitrarily-oriented uniform-flux, infinite-conductivity, or finite-conductivity fractures in an infinite-slab reservoir.
- Develop a complete refracture-candidate fracture-injection/falloff test methodology to diagnose the following.
 - The existence of a conductive hydraulic fracture.
 - The choked-fracture skin damage of an existing conductive hydraulic fracture.
 - The effective primary fracture half-length and primary fracture conductivity of an existing conductive hydraulic fracture.
 - The average reservoir pressure and reservoir transmissibility.

1.5 Dissertation Summary

Chapter II reviews existing slug-test and fracture-injection/falloff test solutions and interpretation methods that were derived assuming a slightly compressible fluid. A new formulation and interpretation method are presented for before-closure pressure transient analysis of a fracture-injection/falloff sequence when the reservoir fluid is compressible. As shown in **Appendix A**, the formulation is derived in terms of adjusted pseudovariables to account for reservoir fluid compressibility.

Chapter III presents new analytical variable-storage pressure-transient solutions for a constant-rate drawdown in a well producing from an infinite slab reservoir containing a single dilated vertical fracture with the initial reservoir pressure above the minimum insitu or closure stress and with fracture storage and wellbore storage as follows:

- Constant before fracture closure and constant after fracture closure storage.
- Constant before- and constant after-closure storage with fracture-face and choked-fracture skin.
- Fracture flow during closure with constant before-closure storage and radial flow after closure with constant wellbore storage and skin.

Additionally, a new fracture-injection/falloff model accounting for fracture creation, fracture closure, and diffusion after closure is also presented. Limiting-case solutions of the new model are used to demonstrate when a finite injection time can be considered as occurring instantaneously – which allows the pressure difference recorded during the falloff to be transformed to an equivalent pressure difference if the rate were constant. By considering fracture propagation as time-dependent storage, three new models are presented for a fracture-injection/falloff sequence for a well in an infinite slab reservoir with a single vertical fracture created during an injection with fracture and wellbore storage as follows:

- Equivalent propagating-fracture storage and before-closure storage with constant after-closure storage.
- Time-dependent propagating-fracture storage, constant before-closure storage, and constant after-closure storage.
- Time-dependent propagating-fracture storage and before-closure storage with linear flow from the fracture before closure and after-closure radial flow with constant wellbore storage and skin.

Limiting-case solutions of the fracture-injection/falloff models are also presented to demonstrate when a fracture-injection can be considered as occurring instantaneously and the equivalent constant-rate pressure difference can be calculated from the observed pressure during the falloff of a fracture-injection/falloff sequence for quantitative type-curve analysis.

In Chapter IV the new fracture-injection/falloff model developed in Chapter III is extended to a case with a pre-existing hydraulic fracture. Ideally, a refracture-candidate diagnostic should identify a pre-existing hydraulic fracture and allow for estimation of existing fracture half-length, fracture conductivity, average reservoir pressure, and permeability.

An ancillary development required for the fracture-injection/falloff model with a pre-existing fracture is the derivation of a new semianalytical pressure-transient solution for a constant-rate drawdown in a well producing from an infinite slab reservoir through multiple arbitrarily-oriented uniform-flux, infinite-conductivity, or finite-conductivity fractures. The new pressure-transient solution is illustrated by preparing a log-log type curve for a constant-rate drawdown in a well producing from an infinite-slab

reservoir through a cruciform fracture with constant storage. Additionally, a variable-storage case is presented for a constant-rate drawdown through a cruciform fracture in an infinite slab reservoir where the initial reservoir pressure is in excess of the closure stress of the secondary fracture, and during the drawdown, the secondary fracture closes – which creates a case of decreasing storage during the drawdown.

A new refracture-candidate fracture-injection/falloff solution is also presented with time-dependent propagating secondary fracture storage, constant before-closure primary and secondary fracture storage, and constant after-closure storage. Limiting-case solutions of the refracture-candidate fracture-injection/falloff model are also presented to demonstrate when a fracture-injection can be considered as occurring instantaneously and the equivalent constant-rate pressure difference can be calculated from the pressure observed during the falloff and used for quantitative type-curve analysis.

The new single- and multiple-fracture pressure-transient solutions combined with the new fracture-injection/falloff models provide the theoretical basis of a new refracture-candidate diagnostic test method. Chapter V presents the new refracture-candidate diagnostic test and analysis methodology that can be used to rapidly identify a pre-existing hydraulic fracture. Field examples are provided to illustrate the interpretation of a fracture-injection/falloff sequence for the following cases.

- No pre-existing hydraulic fracture with pseudoradial flow observed.
- No pre-existing hydraulic fracture with pseudolinear flow observed.
- A pre-existing conductive hydraulic fracture with choked-fracture skin damage.

Chapter VI itemizes the new pressure-transient solutions and fracture-injection/falloff models developed within the dissertation. Additionally, areas for additional research are recommended for numerically validating the new pressure-transient solutions and fracture-injection/falloff models; for examining complex fracture patterns and different multiple fracture configurations beyond the cruciform and oblique fracture scenarios presented; and for developing a pressure-transient solution for a well producing from multiple fractures in a bounded reservoir.

CHAPTER II

SLUG-TEST AND FRACTURE-INJECTION/FALLOFF TEST ANALYSIS

2.1 Introduction

An injection/falloff sequence requires injecting a fluid (liquid or gas) at a pressure *less than* the pressure required to initiate and propagate a hydraulic fracture followed by an extended shut-in (falloff) period. When the injection period is relatively short, an injection/falloff test is referred to as an impulse test,⁵⁵ but when the finite injection period is very short relative to the reservoir response, the injection can be considered as occurring instantaneously, and the test is referred to as a slug test.⁵⁶

A fracture-injection/falloff test sequence requires injecting a fluid (liquid or gas) at a pressure *greater than* the pressure required to initiate and propagate a hydraulic fracture. Consequently, a fracture is created during the injection, and as the pressure declines during the shut-in period, the created fracture closes, and the pressure continues to decline after closure. The before fracture closure (before-closure) pressure falloff can be analyzed with before-closure pressure transient analysis,⁵⁷⁻⁵⁹ and the after fracture closure (after-closure) falloff can be analyzed using an impulse-fracture technique presented by Gu, *et al.*,⁶⁰ and Aboalsleiman, *et al.*⁶¹

Chapter II reviews existing slug test and fracture-injection/falloff analysis methods, and contains a discussion of the limitation of existing interpretation methods. Pressure and time and adjusted pseudopressure and adjusted pseudotime formulations are reviewed for slug tests, and pressure and time formulations are presented for before-closure pressure transient analysis and after-closure analysis for fracture-injection/falloff tests. A new formulation in terms of adjusted pseudovariabiles is also presented for before-closure pressure transient analysis of a fracture-injection/falloff sequence when the reservoir fluid is compressible. All equations are derived and shown in Darcy units.

2.2 Slug-Test Solution

In the present context, injection/falloff sequences are restricted to relatively small volume, short duration injections followed by a lengthy falloff period. A general injection/falloff solution can be derived using a technique described by Correa and Ramey⁶²⁻⁶⁴ that requires writing a material balance equation valid at all times during the injection/falloff test using the Heaviside unit-step function. The Correa and Ramey⁶²⁻⁶⁴ derivation technique is used repeatedly throughout the dissertation.

Assume a slightly compressible fluid fills the wellbore and is injected at a constant surface rate. A mass balance during an injection is written as

$$\underbrace{m_{in}}_{qB\rho} - \underbrace{m_{out}}_{q_r B_r \rho_r} = \overbrace{V_w \frac{d\rho_w}{dt}}^{\text{Storage}}, \dots\dots\dots (2.1)$$

where q is the surface injection rate, B is the formation volume factor at surface injection conditions, ρ is the fluid density at surface injection conditions, q_r is the flow rate into the reservoir, B_r is the formation volume factor at reservoir conditions, ρ_r is the density of the reservoir fluid, ρ_w is the injected fluid density at average wellbore conditions, and V_w is the wellbore volume.

The derivative with respect to time of the wellbore fluid density is written using the chain rule as

$$\frac{d\rho_w}{dt} = \rho_w \frac{1}{\rho_w} \frac{d\rho_w}{dp_w} \frac{dp_w}{dt} = \rho_w c_w \frac{dp_w}{dt}, \quad (2.2)$$

where c_w is the isothermal wellbore fluid compressibility. The material balance equation can now be written as

$$qB\rho - q_r B_r \rho_r = \rho_w c_w V_w \frac{dp_w}{dt}, \quad (2.3)$$

or assuming a constant density, $\rho = \rho_w = \rho_r$, and a constant formation volume factor, $B = B_r$, the material balance equation during the injection is written as

$$q_r = q - \frac{1}{B} (c_w V_w) \frac{dp_w}{dt}. \quad (2.4)$$

The dimensionless wellbore pressure for the injection/falloff sequence is written as

$$p_{wsD}(t_D) = \frac{p_w(t_D) - p_i}{p_0 - p_i}, \quad (2.5)$$

where p_i is the initial reservoir pressure and p_0 is an arbitrary reference pressure. For an injection slug test the wellbore pressure is increased to a pressure, p_{w0} , at time zero, and the dimensionless wellbore pressure at time zero is written as

$$p_{wsD}(0) = \frac{p_{w0} - p_i}{p_0 - p_i}. \quad (2.6)$$

Generally for a slug test, the pressure at time zero, p_{w0} , is set equal to p_0 , and the dimensionless wellbore pressure at time zero is unity, $p_{wsD}(0) = 1$. For an injection test without an instantaneous change in wellbore pressure, p_0 is arbitrary provided $p_0 \neq p_i$.

Define dimensionless time as

$$t_D = \frac{kt}{\phi \mu_r c_t r_w^2}, \quad (2.7)$$

where k is the permeability, ϕ is the porosity (fraction), μ_r is the reservoir fluid viscosity, c_t is the total compressibility, and r_w is the wellbore radius. The dimensionless reservoir flow rate is defined as

$$q_{sD} = \frac{q_r B_r \mu_r}{2\pi kh(p_0 - p_i)}, \quad (2.8)$$

and the dimensionless well flow rate is defined as

$$q_{wsD} = \frac{qB\mu}{2\pi kh(p_0 - p_i)} \dots\dots\dots(2.9)$$

With the dimensionless variables, the material balance equation during an injection is written as

$$q_{sD} = q_{wsD} - \frac{C}{2\pi\phi c_t h r_w^2} \frac{dp_{wsD}}{dt_D}, \dots\dots\dots(2.10)$$

where the wellbore storage coefficient is written as

$$C = c_w V_w \dots\dots\dots(2.11)$$

Define a dimensionless wellbore storage coefficient as

$$C_D = \frac{C}{2\pi\phi c_t h r_w^2}, \dots\dots\dots(2.12)$$

and the dimensionless material balance equation during an injection is written as

$$q_{sD} = q_{wsD} - C_D \frac{dp_{wsD}}{dt_D} \dots\dots\dots(2.13)$$

During the falloff portion of the test, $q_{wsD} = 0$, and the pressure falloff dimensionless material balance equation is written as

$$q_{sD} = -C_D \frac{dp_{wsD}}{dt_D} \dots\dots\dots(2.14)$$

The Heaviside unit-step function,⁶² is defined as

$$U_a = \begin{cases} 0 & , t < a \\ 1 & , t > a \end{cases} \dots\dots\dots(2.15)$$

and following the technique of Correa and Ramey,⁶²⁻⁶⁴ a material balance equation valid at all times for an injection/falloff sequence with constant wellbore storage is written as

$$q_{sD} = \left(1 - U(t_e)_D\right) \left(q_{wsD} - C_D \frac{dp_{wsD}}{dt_D} \right) - U(t_e)_D C_D \frac{dp_{wsD}}{dt_D} \dots\dots\dots(2.16)$$

where $(t_e)_D$ is the dimensionless time at the end of the injection. The material balance equation can be expanded, simplified, and written as

$$q_{sD} = q_{wsD} - U(t_e)_D q_{wsD} - C_D \frac{dp_{wsD}}{dt_D} \dots\dots\dots(2.17)$$

The Laplace transform of the material balance equation⁶² is written as

$$\bar{q}_{sD} = \frac{q_{wsD}}{s} - \frac{q_{wsD}}{s} e^{-s(t_e)_D} - C_D [s\bar{p}_{wsD} - p_{wsD}(0)], \dots\dots\dots(2.18)$$

where s is the Laplace transform variable. A solution is developed by applying the superposition principle,⁶⁵ which is written as

$$p_{wsD} = \int_0^{t_D} q_{sD}(\tau_D) \frac{dp_D(t_D - \tau_D)}{dt_D} d\tau_D, \dots\dots\dots(2.19)$$

where p_D is the dimensionless reservoir pressure solution for a constant-rate injection with dimensionless pressure defined as

$$p_D = \frac{2\pi kh(p_w(t) - p_i)}{q_r B_r \mu_r} \dots\dots\dots(2.20)$$

The initial condition requires a constant initial pressure, $p_D(t_D) = 0$, and with the initial condition, the Laplace transform of the superposition integral is written as

$$\bar{p}_{wsD} = \bar{q}_{sD} s \bar{p}_D \Leftrightarrow \bar{q}_{sD} = \frac{\bar{p}_{wsD}}{s \bar{p}_D} \dots\dots\dots(2.21)$$

Combining the transformed material balance equation and superposition integral results in

$$\bar{p}_{wsD} (1 + s^2 C_D \bar{p}_D) = q_{wsD} \bar{p}_D - q_{wsD} \bar{p}_D e^{-s(t_e)_D} + p_{wsD}(0) C_D s \bar{p}_D \dots\dots\dots(2.22)$$

The Laplace domain dimensionless pressure solution for a well produced at a constant rate with wellbore storage is written as

$$\bar{p}_{wD} = \frac{\bar{p}_D}{1 + s^2 C_D \bar{p}_D}, \dots\dots\dots(2.23)$$

and the Laplace domain injection/falloff solution is written as

$$\bar{p}_{wsD} = q_{wsD} \bar{p}_{wD} - q_{wsD} \bar{p}_{wD} e^{-s(t_e)_D} + p_{wsD}(0) C_D s \bar{p}_{wD} \dots\dots\dots(2.24)$$

Inverting the Laplace domain solution results in the time domain injection/falloff solution written as

$$p_{wsD}(t_D) = q_{wsD} [p_{wD}(t_D) - p_{wD}(t_D - (t_e)_D)] + p_{wsD}(0) C_D \frac{dp_{wD}(t_D)}{dt_D} \dots\dots\dots(2.25)$$

The injection/falloff solution is applicable to both an impulse test and a slug test, that is, in the limit as the dimensionless injection time approaches zero, $(t_e)_D \rightarrow 0$, the injection/falloff solution reduces to the slug test solution defined by Ramey and Agarwal⁶⁶ and written as

$$p_{wsD}(t_D) = p_{wsD}(0) C_D \frac{dp_{wD}(t_D)}{dt_D} \dots\dots\dots(2.26)$$

The slug test solution is written in a general form in that the dimensionless reservoir pressure solution can be any radial flow solution—infinite-acting, infinite-acting with skin, dual-porosity infinite-acting, etc. The solution is also analogous to the slug-test solution in a reservoir containing a hydraulic fracture, which is written as

$$p_{wsD}(t_{LfD}) = p_{wsD}(0) C_{LfD} \frac{dp_{wD}(t_{LfD})}{dt_{LfD}}, \dots\dots\dots(2.27)$$

where the dimensionless time for a well with a hydraulic fracture is defined as

$$t_{LjD} = \frac{kt}{\phi\mu_r c_t L_f^2}, \dots\dots\dots (2.28)$$

and L_f is the fracture half-length. The dimensionless wellbore storage coefficient for a well containing a hydraulic fracture is defined as⁶⁷

$$C_{LjD} = \frac{C}{2\pi\phi c_t h L_f^2}. \dots\dots\dots (2.29)$$

With a hydraulic fracture, the dimensionless reservoir pressure solution is written in the Laplace domain as

$$\bar{p}_{wD} = \frac{\bar{p}_{jD}}{1 + s^2 C_{LjD} \bar{p}_{jD}}, \dots\dots\dots (2.30)$$

where p_{jD} is any fractured-well solution—infinite-acting reservoir with an infinite-conductivity fracture, infinite-acting reservoir with a finite-conductivity fracture, dual-porosity infinite-acting reservoir with a finite-conductivity fracture, etc.⁶⁷

Ramey *et al.*⁵⁶ recommend analyzing a slug test with a special type curve, which is a semi-log graph of the dimensionless wellbore pressure versus t_D/C_D . **Fig. 2.1** contains slug-test type curves for a radial infinite-acting reservoir with skin. The cylindrical-source reservoir solution with skin, S , is written in the Laplace domain as⁶⁵

$$\bar{p}_{sD} = \frac{1}{s} \frac{K_0(r_{wD}\sqrt{s})}{\sqrt{s} K_1(\sqrt{s})} + \frac{S}{s}, \dots\dots\dots (2.31)$$

where K_0 and K_1 are the modified Bessel functions of order zero and one, respectively. The cylindrical-source solution is used with the slug-test solution to generate the type curves in Fig. 2.1. The slug-test solution is evaluated in the Laplace domain and numerically inverted to the time domain with the Stehfest algorithm.⁶⁸

Slug-test analysis with the Ramey *et al.*⁵⁶ method to determine transmissibility requires calculating a dimensionless pressure plotting function for an injection defined as

$$p_{wsD} = \frac{p_w(t) - p_i}{p_0 - p_i}, \dots\dots\dots (2.32)$$

or for a production slug test, defined as

$$p_{wsD} = \frac{p_i - p_w(t)}{p_i - p_0}, \dots\dots\dots (2.33)$$

where p_i is the initial reservoir pressure, $p_w(t)$ is the observed wellbore pressure, and p_0 is the wellbore pressure at the instant a pressure difference is applied (time zero). The slug-test plotting function is calculated for all observed points during the shut-in period and graphed versus shut-in time, Δt , on semi-log slug-test type curves. Transmissibility is calculated from a time match point, which is written as

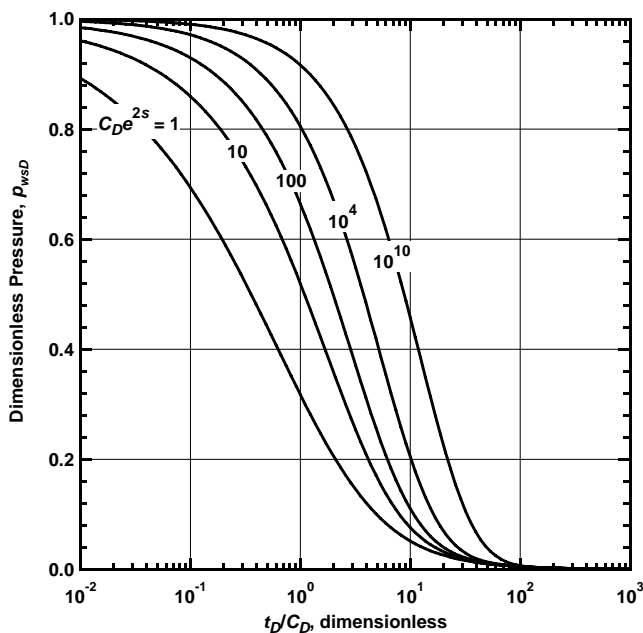


Fig. 2.1—Slug-test type curve for an infinite-slab reservoir with skin.⁵⁶

$$\frac{kh}{\mu} = \frac{C}{2\pi} \left[\frac{t_D/C_D}{\Delta t} \right]_{MP}, \dots\dots\dots(2.34)$$

and the skin is calculated using the definition of the dimensionless storage coefficient and the type-curve match written as

$$S = \frac{1}{2} \ln \left[\left[C_D e^{2S} \right]_{MP} \left[\frac{2\pi\phi c_t h r_w^2}{C} \right] \right] \dots\dots\dots(2.35)$$

Peres *et al.*⁶⁹ published an alternative slug-test interpretation method by recognizing that the slug-test solution written as

$$p_{wsD}(t_D) = p_{wsD}(0) C_D \frac{dp_{wD}(t_D)}{dt_D}, \dots\dots\dots(2.36)$$

can be integrated and written as

$$p_{wD}(t_D) = \frac{1}{p_{wsD}(0) C_D} \int_0^{t_D} p_{wsD}(\tau_D) d\tau_D, \dots\dots\dots(2.37)$$

where τ_D , is a variable of integration. Peres *et al.*⁶⁹ also noted that the well testing pressure derivative could be written as

$$\frac{dp_{wD}}{d(\ln t_D)} = t_D \frac{dp_{wD}}{dt_D} = \frac{t_D}{C_D} p_{wsD}, \dots\dots\dots(2.38)$$

Consequently, the dimensionless pressure observed during a variable-rate slug-test can be converted to an equivalent dimensionless pressure if the rate were constant and plotted on conventional constant-rate drawdown log-log type curves. **Fig. 2.2** is a log-log graph of dimensionless wellbore pressure and pressure derivative versus t_D/C_D . The dimensionless pressure was generated by integrating the slug-test type curves in Fig. 2.1 and dividing by the dimensionless wellbore storage coefficient, and the dimensionless pressure derivative was calculated by multiplying the slug-test type curve dimensionless pressure by t_D/C_D . Both the pressure and pressure derivative curves in Fig. 2.2 reproduce type curves for a constant-rate drawdown in a radial infinite-acting reservoir with wellbore storage and skin exactly; thus, conventional log-log constant-rate drawdown type curves can be used to analyze slug-test data.

With the definition of dimensionless time, dimensionless wellbore-storage coefficient, and the dimensionless slug-test plotting function, the integral equation for equivalent constant-rate dimensionless pressure can be written as

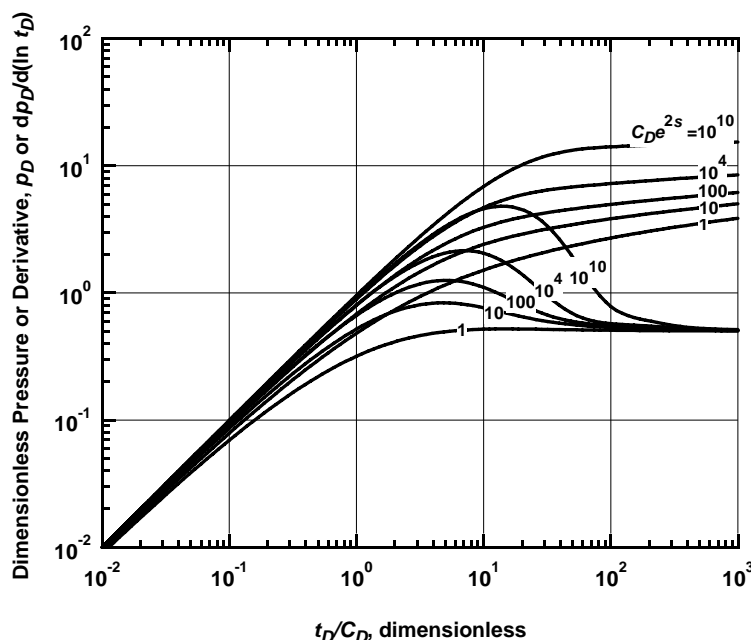


Fig. 2.2—Constant-rate drawdown type curves for a radial infinite-slab reservoir with wellbore storage and skin generated from the slug-test type curves shown in Fig. 2.1.

$$p_{wD}(t_D) = \left(\frac{2\pi}{p_{wsD}(0)C[p_0 - p_i]} \frac{kh}{\mu} \right) \int_0^t [p_w(\tau) - p_i] d\tau, \dots\dots\dots (2.39)$$

which suggests that a log-log graph of the integral of the pressure difference, $p_w(t) - p_i$, versus time during a slug test will overlay a constant-rate drawdown pressure log-log type curve. The pressure derivative can also be written as

$$\frac{dp_{wD}}{d(\ln t_D)} = \left(\frac{2\pi}{p_{wsD}(0)C[p_0 - p_i]} \frac{kh}{\mu} \right) t [p_w(t) - p_i], \dots\dots\dots (2.40)$$

and a graph of the product of time and the pressure difference will overlay a constant-rate drawdown log-log derivative type curve.

Transmissibility is calculated from a pressure type curve match point as

$$\frac{kh}{\mu} = \left(\frac{p_{wsD}(0)C[p_0 - p_i]}{2\pi} \right) \left[\frac{p_{wD}(t_D / C_D)}{\int_0^t [p_w(\tau) - p_i] d\tau} \right]_{MP}, \dots\dots\dots (2.41)$$

and the skin can be calculated from the matching type curve as

$$S = \frac{1}{2} \ln \left(\left[C_D e^{2S} \right]_{MP} \left(\frac{2\pi\phi c_t h r_w^2}{C} \right) \right). \dots\dots\dots (2.42)$$

The slug-test analysis method of Peres *et al.*⁶⁹ is general and can be applied for other reservoir systems—dual porosity, infinite-conductivity hydraulic fracture, finite-conductivity fracture, etc. For example, a slug test in a reservoir with an infinite conductivity fracture is analyzed as before by preparing a log-log graph of the integrated pressure difference and the product of shut-in time and the pressure difference versus the shut-in time. The slug-test data can be matched to a Barker-Ramey⁷⁰ type curve where the transmissibility is calculated from Eq. 2.41 assuming fracture storage is negligibly small relative to wellbore storage and if the reservoir is infinite acting.

When fracture storage is significant, fracture half-length must be known to calculate the storage coefficient and transmissibility, but fracture half-length cannot be determined from the slug-test analysis method. However, if transmissibility is known from a previous well test, the fracture half-length can be calculated from a slug-test using the pressure-curve match, $(C_{LFD})_{MP}$, and the definition of the dimensionless storage coefficient as

$$L_f = \sqrt{\frac{C}{2\pi\phi c_t h [C_{LFD}]_{MP}}}. \dots\dots\dots (2.43)$$

When the reservoir fluid is compressible, Xiao and Reynolds⁷¹ suggested that log-log constant-rate drawdown type curves developed for a slightly compressible fluid can be used for slug-test analysis if the

slug-test pressure and time are transformed to pseudopressure and pseudotime, or for convenience, adjusted pseudopressure and adjusted pseudotime.

Lee and Holditch⁷² previously demonstrated that the governing differential equation for a reservoir containing a compressible fluid can be effectively linearized by the writing in terms of pseudopressure and pseudotime, and Meunier *et al.*⁷³ extended the concept by normalizing the transforms, which results in adjusted pseudopressure and adjusted pseudotime. With adjusted pseudovariables, flow solutions developed for a reservoir with slightly compressible fluid can be used directly in a reservoir containing a compressible fluid.

Recall that a material balance during an injection/falloff is written as

$$qB\rho - q_r B_r \rho_r = \rho_w c_w V_w \frac{dp_w}{dt} \quad (2.44)$$

Following the definitions of Xiao and Reynolds⁷¹ and assuming the wellbore and reservoir fluid are compressible, the wellbore storage, $c_w V_w$, can alternatively be written as

$$c_w V_w = c_{gw0} \frac{\mu_0}{\mu_i} \frac{\mu_i c_{gw}(p_w)}{\mu_0 c_{gw0}} V_w \quad (2.45)$$

where c_{gw0} is the bottomhole fluid compressibility at time zero, μ_0 is the bottomhole fluid viscosity at time zero, μ_i is the bottomhole fluid viscosity at initial reservoir pressure, and $c_{gw}(p_w)$ is the bottomhole fluid compressibility as a function of pressure. An adjusted storage coefficient can be defined as

$$C_a = c_{gw0} V_w \frac{\mu_0}{\mu_i} \quad (2.46)$$

and the material balance equation can be written as

$$qB\rho - q_r B_r \rho_r = \rho_w \frac{\mu_i c_{gw}(p_w)}{\mu_0 c_{gw0}} C_a \frac{dp_w}{dt} \quad (2.47)$$

Adjusted pseudopressure is defined as

$$p_a = \left(\frac{\mu z}{p} \right)_{re} \int_0^p \frac{p dp}{\mu z} \quad (2.48)$$

where the subscript 're' denotes a reference pressure, which Xiao and Reynolds define as the initial reservoir pressure, and adjusted pseudotime is defined as

$$t_a = (\mu c_t)_{re} \int_0^t \frac{dt}{\mu_w c_t} \quad (2.49)$$

where the reference pressure defined by Xiao and Reynolds is the pressure at the instant a differential is applied, p_0 . With the adjusted pseudovariables, and assuming $c_t \approx c_{gw}$, the material balance equation can be written as

$$qB\rho - q_r B_r \rho_r = \rho_w \left(\frac{p}{z} \right)_i \left(\frac{z}{p} \right)_w C_a \frac{dp_{aw}}{dt_a} \quad (2.50)$$

The dimensionless adjusted pseudopressure is defined as

$$p_{awsD}(0) = \frac{p_{aw0} - p_{ai}}{p_{a0} - p_{ai}} \quad (2.51)$$

and dimensionless adjusted pseudotime is defined as

$$t_{aD} = \frac{kt_a}{\phi \mu_i c_{ti} r_w^2} \quad (2.52)$$

With dimensionless adjusted pseudovariabes, the material balance equation can be written as

$$qB\rho - q_r B_r \rho_r = \rho_w \left(\frac{p}{z} \right)_i \left(\frac{z}{p} \right)_w \frac{2\pi kh(p_{a0} - p_{ai})}{\mu_i} \frac{C_a}{2\pi \phi c_{ti} h r_w^2} \frac{dp_{awD}}{dt_{aD}} \quad (2.53)$$

Gas formation volume factor is defined as

$$B = \frac{V}{V_{sc}} = \frac{zT}{p} \frac{p_{sc}}{z_{sc} T_{sc}} \quad (2.54)$$

where the subscript 'sc' denotes standard conditions, and gas density can be written as

$$\rho = \frac{m}{V} = \frac{Mp}{zRT} \quad (2.55)$$

where m is the mass and M is the molecular weight of the gas. With the definition of gas formation volume factor, the ratio of gas formation volume factor at bottomhole and initial conditions can be written as

$$\frac{B_w}{B_i} = \frac{p_i}{z_i} \frac{z_w}{p_w} \frac{T_w}{T_i} \quad (2.56)$$

and with the definition of gas density, the ratio of gas density at reservoir and surface conditions is written as

$$\frac{\rho_r}{\rho} = \frac{B}{B_r} \quad (2.57)$$

or at wellbore and surface conditions written as

$$\frac{\rho_w}{\rho} = \frac{B}{B_w} \quad (2.58)$$

With the definitions of gas formation volume factor and gas density, the material balance equation can be written as

$$q - q_r = \frac{2\pi kh(p_{a0} - p_{ai})}{B_i \mu_i} \frac{C_a}{2\pi \phi c_{ti} h r_w^2} \frac{T_i}{T_w} \frac{dp_{awD}}{dt_{aD}} \quad (2.59)$$

Defining the dimensionless adjusted wellbore injection rate as

$$q_{awsD} = \frac{qB_i\mu_i}{2\pi kh(p_{a0} - p_{ai})}, \dots\dots\dots(2.60)$$

the dimensionless adjusted reservoir injection rate as

$$q_{asD} = \frac{q_r B_i \mu_i}{2\pi kh(p_{a0} - p_{ai})}, \dots\dots\dots(2.61)$$

and defining the dimensionless adjusted storage coefficient as

$$C_{aD} = \frac{C_a}{2\pi\phi c_{ti} h r_w^2} \frac{T_i}{T_w}, \dots\dots\dots(2.62)$$

the dimensionless material balance equation is written in terms of adjusted pseudovariables as

$$q_{asD} = q_{awsD} - C_{aD} \frac{dp_{awsD}}{dt_{aD}}, \dots\dots\dots(2.63)$$

Since the material balance equation in terms of adjusted pseudovariables is identical to the material balance equation for a slightly compressible fluid, the slug-test solution is of the same form and written as

$$p_{awsD}(t_D) = p_{awsD}(0)C_{aD} \frac{dp_{awD}(t_{aD})}{dt_{aD}}, \dots\dots\dots(2.64)$$

where the Laplace domain reservoir solution is written as

$$\bar{p}_{awD} = \frac{\bar{p}_{aD}}{1 + s^2 C_{aD} \bar{p}_{aD}}, \dots\dots\dots(2.65)$$

The radial diffusivity equation for a compressible fluid is written as

$$\frac{1}{r} \frac{\partial}{\partial r} \left(\frac{p}{\mu z} r \frac{\partial p}{\partial r} \right) = \frac{\phi c_g}{k} \frac{p}{z} \frac{\partial p}{\partial t}, \dots\dots\dots(2.66)$$

which is written in terms of dimensionless adjusted pseudovariables as⁷¹⁻⁷³

$$\frac{1}{r_D} \frac{\partial}{\partial r_D} \left(r_D \frac{\partial p_{aD}}{\partial r_D} \right) = \alpha_D \frac{\partial p_{aD}}{\partial t_{aD}}, \dots\dots\dots(2.67)$$

where α_D is written as

$$\alpha_D = \frac{\mu c_g}{(\mu c_g)_i} \frac{(\mu c_g)_0}{(\mu c_g)_w}, \dots\dots\dots(2.68)$$

When $\alpha_D \approx 1$, which is often the case for slug tests,⁷¹ the diffusivity equation written in terms of adjusted pseudovariables is of the same form as that for a slightly compressible fluid. Consequently, the dimensionless pressure solutions are the same, $p_{aD} = p_D$, and log-log type curves developed for a slightly compressible fluid can be used to analyze slug tests with compressible fluids when plotted in terms of adjusted pseudopressure and adjusted pseudotime.

In terms of adjusted pseudovariables, transmissibility is calculated from a pressure type curve match point as

$$\frac{kh}{\mu} = \left(\frac{p_{wsD}(0)C_a [p_{a0} - p_{ai}]}{2\pi} \right) \left[\frac{p_{wD}(t_D / C_D)}{\int_0^t [p_{aw}(\tau) - p_{ai}] d\tau} \right]_{MP}, \dots\dots\dots (2.69)$$

or from the time match point as

$$\frac{kh}{\mu} = p_{wsD}(0)C_a \left[\frac{t_D / C_D}{t_a} \right]_{MP}, \dots\dots\dots (2.70)$$

and the skin can be calculated from the matching type curve as

$$S = \frac{1}{2} \ln \left(\left[C_D e^{2S} \right]_{MP} \left(\frac{2\pi\phi c_{ti} h r_w^2}{C_a} \right) \right) \dots\dots\dots (2.71)$$

The reference conditions in the adjusted pseudopressure and adjusted pseudotime definitions are arbitrary and different forms of the solution can be derived by simply changing the normalizing reference conditions.

2.3 Injection/Falloff Testing At Pressures Greater Than Fracture Initiation Pressure

Injection/falloff tests at pressures greater than the fracture initiation pressure will propagate a hydraulic fracture and are referred to as fracture-injection/falloff tests to distinguish them from injection/falloff tests at pressures less than the fracture initiation pressure. Fracture-injection/falloff tests are essentially breakdown or minifrac treatments where the pressure decline is recorded during a shut-in period.

The pressure decline following a diagnostic fracture-injection/falloff test is analyzed using three methods that result in pore pressure and permeability estimates and a qualitative leakoff-type identification.^{57-61,74} The before fracture closure pressure decline is analyzed using *G*-function derivative analysis⁷⁴ to identify the leakoff type and before-closure pressure transient analysis to estimate permeability and fracture face resistance.⁵⁷⁻⁵⁹ After fracture closure, transmissibility and average reservoir pressure can be estimated during the pseudoradial flow regime using after-closure analysis.⁶⁰⁻⁶¹ Each method is relatively new and can be used independently; however, combining all three methods into a single cohesive interpretation scheme provides a series of checks to ensure reasonable pore pressure and permeability estimates are obtained.

2.3.1 *G*-Function Derivative Analysis. Classical minifrac analysis using the *G*-function was first described by Nolte.⁷⁵ The Carter⁷⁶ equation for fluid leakoff velocity, v_L , is written as

$$v_L = \frac{C_L}{\sqrt{t}}, \dots\dots\dots (2.72)$$

where C_L is a constant leakoff coefficient. Multiplying by leakoff area, A_L , and integrating from 0 to t , results in

$$\int_0^t v_L A_L dt = \int_0^t \frac{C_L A_L}{\sqrt{t}} dt, \dots\dots\dots(2.73)$$

which after integration is written as

$$V_L = 2C_L A_L \sqrt{t} + S_p, \dots\dots\dots(2.74)$$

where S_p is a constant of integration called the "spurt loss coefficient."

For any differential surface element, dA , of a fracture that is exposed to fracturing fluid at time τ_N , the leakoff rate is written as

$$\partial V_L = \partial A \frac{C_L}{\sqrt{t - \tau_N}} \partial t. \dots\dots\dots(2.75)$$

The leakoff volume at the end of pumping through two fracture faces of one fracture wing is found by integrating the leakoff rate from 0 to A_e for each fracture face and integrating over each differential element from τ_N to t_e , that is,

$$V_{Le} = 2 \int_0^{A_e} \int_{\tau_N}^{t_e} \frac{C_L}{\sqrt{t - \tau_N}} \partial A \partial t, \dots\dots\dots(2.76)$$

where the subscript 'e' denotes the end of pumping.

Nolte pressure-decline analysis assumes fracture growth during an injection is modeled by a power law relationship⁷⁷

$$A_D = t_{DN}^{\alpha_N}, \dots\dots\dots(2.77)$$

where A_D is the dimensionless fracture area of one face of one fracture wing, $A_D = A(t)/A_e$, t_{DN} is the dimensionless time defined by Nolte, $t_{DN} = t/t_e$, and α_N is the fracture growth exponent, which lies between $1/2$ and 1. With the dimensionless variables, and defining τ_{ND} by

$$\tau_{ND} = \frac{\tau_N}{t_e} = A_D^{1/\alpha_N}, \dots\dots\dots(2.78)$$

the leakoff volume at the end of pumping can be written as

$$V_{Le} = 2C_L A_e \sqrt{t_e} \int_0^1 \int_{A_D^{1/\alpha_N}}^1 \frac{1}{\sqrt{t_{DN} - A_D^{1/\alpha_N}}} dt_D dA_D. \dots\dots\dots(2.79)$$

Defining the dimensionless loss-volume function at the end of the injection, $g_0(\alpha)$, as

$$g_0(\alpha_N) = \int_0^1 \int_{A_D^{1/\alpha_N}}^1 \frac{1}{\sqrt{t_{DN} - A_D^{1/\alpha_N}}} dt_D dA_D, \dots\dots\dots(2.80)$$

then

$$g_0(\alpha_N) = \frac{V_{Le}}{2C_L A_e \sqrt{t_e}} \dots \dots \dots (2.81)$$

The definition of the dimensionless loss-volume function can be integrated analytically and the result written as⁷⁷

$$g_0(\alpha_N) = \frac{\alpha_N \sqrt{\pi} \Gamma[\alpha_N]}{\Gamma\left[\frac{3}{2} + \alpha_N\right]} \dots \dots \dots (2.82)$$

where $\Gamma[\cdot]$ is the Euler gamma function.

Nolte⁷⁵ assumes a constant fracture area during the shut-in period prior to fracture closure, which allows the dimensionless loss-volume function to be defined beyond the end of an injection. Defining the Nolte dimensionless shut-in time as

$$\Delta t_{DN} = \frac{t - t_e}{t_e} \dots \dots \dots (2.83)$$

then an analogous derivation begins with the leakoff-volume integral written as

$$V_{L(t_e + \Delta t)} = 2 \int_0^{A_e} \int_{\tau_N}^{t_e + \Delta t} \frac{C_L}{\sqrt{t - \tau_N}} \partial A \partial t \dots \dots \dots (2.84)$$

With dimensionless variables, the leakoff-volume integral is written as

$$V_{L(t_e + \Delta t)} = 2C_L A_e \sqrt{t_e} \int_0^1 \int_{A_D^{1/\alpha_N}}^{1 + \Delta t_{DN}} \frac{1}{\sqrt{t_{DN} - A_D^{1/\alpha_N}}} dt_D dA_D \dots \dots \dots (2.85)$$

The dimensionless loss-volume function at any shut-in time after the injection is defined as

$$g(\Delta t, \alpha_N) = \frac{V_{L(t_e + \Delta t)}}{2C_L A_e \sqrt{t_e}} = \int_0^1 \int_{A_D^{1/\alpha_N}}^{1 + \Delta t_{DN}} \frac{1}{\sqrt{t_{DN} - A_D^{1/\alpha_N}}} dt_D dA_D \dots \dots \dots (2.86)$$

which has a closed-form solution written as⁷⁸

$$g(\Delta t, \alpha_N) = \frac{4\alpha_N \sqrt{\Delta t_{DN}} + [2\sqrt{1 + \Delta t_{DN}}] F\left[1/2, \alpha_N; 1 + \alpha_N; (1 + \Delta t_{DN})^{-1}\right]}{1 + 2\alpha_N} \dots \dots \dots (2.87)$$

where the hypergeometric function is defined as⁷⁹

$$F[a, b; c; d] = \sum_{n=0}^{\infty} \frac{(a)_n (b)_n}{(c)_n} \frac{d^n}{n!} \dots \dots \dots (2.88)$$

Nolte⁸⁰ observed that a material balance of one fracture wing during closure can be written as

$$q_{\ell}(t, A_e) = -\frac{dV_f}{dt} = -A_e \frac{d\hat{w}_f}{dt} \dots \dots \dots (2.89)$$

where \hat{w}_f is the average fracture width and A_e is the area of one fracture face. Average fracture width can also be related to fracture net pressure by

$$\hat{w}_f = \frac{(p_w - p_c)}{S_f} = \frac{p_n}{S_f}, \dots\dots\dots(2.90)$$

where p_w is the wellbore pressure, p_c is the fracture closure stress, and p_n is the fracture net pressure. Fracture stiffness, S_f , is defined as the reciprocal of fracture compliance and is written for the three common two-dimensional fracture models as⁸⁰

$$S_f = \frac{2E'}{\pi} \begin{cases} \frac{1}{h_f} & \text{Vertical Plane Strain - PKN} \\ \frac{1}{2L_f} & \text{Horizontal Plane Strain - GDK} \dots\dots\dots(2.91) \\ \frac{3\pi^2}{32R_f} & \text{Radial} \end{cases}$$

Assuming fracture compliance is constant, the material balance can be written as

$$-\frac{dV_f}{dt} = -\frac{A_e}{S_f} \frac{dp_n}{dt}, \dots\dots\dots(2.92)$$

and with definition of the leakoff volume at the end of pumping (Eq. 2.79), the material balance is written as

$$\frac{dp_n}{dt} = \frac{2C_L S_f}{\sqrt{t_e}} \int_0^1 \frac{dA_D}{\sqrt{t_{DN} - A_D^{1/\alpha_N}}}, \dots\dots\dots(2.93)$$

which can be integrated from the end of pumping to some later time during the shut-in and written as

$$\Delta p_n = 2C_L S_f \sqrt{t_e} \left[\int_0^1 \int_{A_D^{1/\alpha_N}}^{1+\Delta t_D} \frac{1}{\sqrt{t_{DN} - A_D^{1/\alpha_N}}} dt_D dA_D - \int_0^1 \int_{A_D^{1/\alpha_N}}^1 \frac{1}{\sqrt{t_{DN} - A_D^{1/\alpha_N}}} dt_D dA_D \right] \dots\dots\dots(2.94)$$

With the definition of the loss-volume function, the net pressure difference can also be written as

$$\Delta p_n = 2C_L S_f \sqrt{t_e} [g(\Delta t_D, \alpha_N) - g_0(\alpha_N)]. \dots\dots\dots(2.95)$$

Nolte defines the dimensionless difference function, i.e., the *G*-function, as⁷⁵

$$G(\Delta t_D, \alpha_N) = \frac{4}{\pi} [g(\Delta t_D, \alpha_N) - g_0(\alpha_N)]. \dots\dots\dots(2.96)$$

With the *G*-function definition, the net pressure difference can be written as

$$\Delta p_n = C_L E' \sqrt{t_e} G(\Delta t_D, \alpha_N) \begin{cases} h_f & \text{PKN} \\ 2L & \text{GDK} \\ (32/3\pi^2)R_f & \text{Radial} \end{cases} \dots\dots\dots(2.97)$$

Provided a reservoir is homogeneous and the fracture area is constant during a shut-in period, a graph of pressure versus the G -function will fall along a straight line before fracture closure, and the leakoff coefficient is proportional to the slope of the straight line. Fracture closure is interpreted as the point that the pressure data begin to deviate from the straight line.

Castillo⁸¹ observed that pressure decline data on a G -function plot will not fall along a straight line in a reservoir exhibiting pressure-dependent leakoff. Pressure-dependent leakoff, which can be indicative of naturally fractured reservoirs, can be identified by a Cartesian graph of the pressure derivative, dp_w/dG , versus the G -function. A constant pressure derivative before fracture closure indicates a homogeneous-acting reservoir, but a continuously changing pressure derivative can indicate pressure-dependent leakoff.

A comprehensive G -function graphical technique for qualitatively identifying the leakoff type was presented by Barree and Mukherjee.⁷⁴ G -function derivative analysis uses graphs of pressure, the pressure derivative, and a "superposition" derivative, Gdp_w/dG , versus the G -function to identify the leakoff type and provide a definitive indication of hydraulic fracture closure.

The leakoff type is identified using the characteristic shape of the pressure-derivative and superposition-derivative curves. **Fig. 2.3** contains the G -function derivative graphs for four common leakoff types observed in low permeability "hard rock" sandstones.⁸² The four common leakoff types in "hard rock" sandstone reservoirs are normal, pressure-dependent leakoff from dilated fractures/fissures, fracture-height recession during shut-in, and fracture-tip extension during shut-in.⁷⁴

Normal leakoff behavior occurs when fracture area is constant during shut-in and leakoff is through a homogeneous rock matrix. With G -function derivative analysis, normal leakoff is indicated by a constant derivative and when the superposition derivative data fall along a straight line that passes through the origin. Fracture closure is identified when the superposition derivative data deviate downward from the straight line.

Pressure-dependent leakoff from dilated fractures/fissures is indicated by a characteristic "hump" in the superposition derivative that lies above a straight line drawn from the origin and through the normal leakoff data. The fissure opening pressure is identified at the end of the hump when the superposition derivative data begin to fall along the straight line, and fracture closure is identified when the superposition derivative data deviate downward from the straight line.

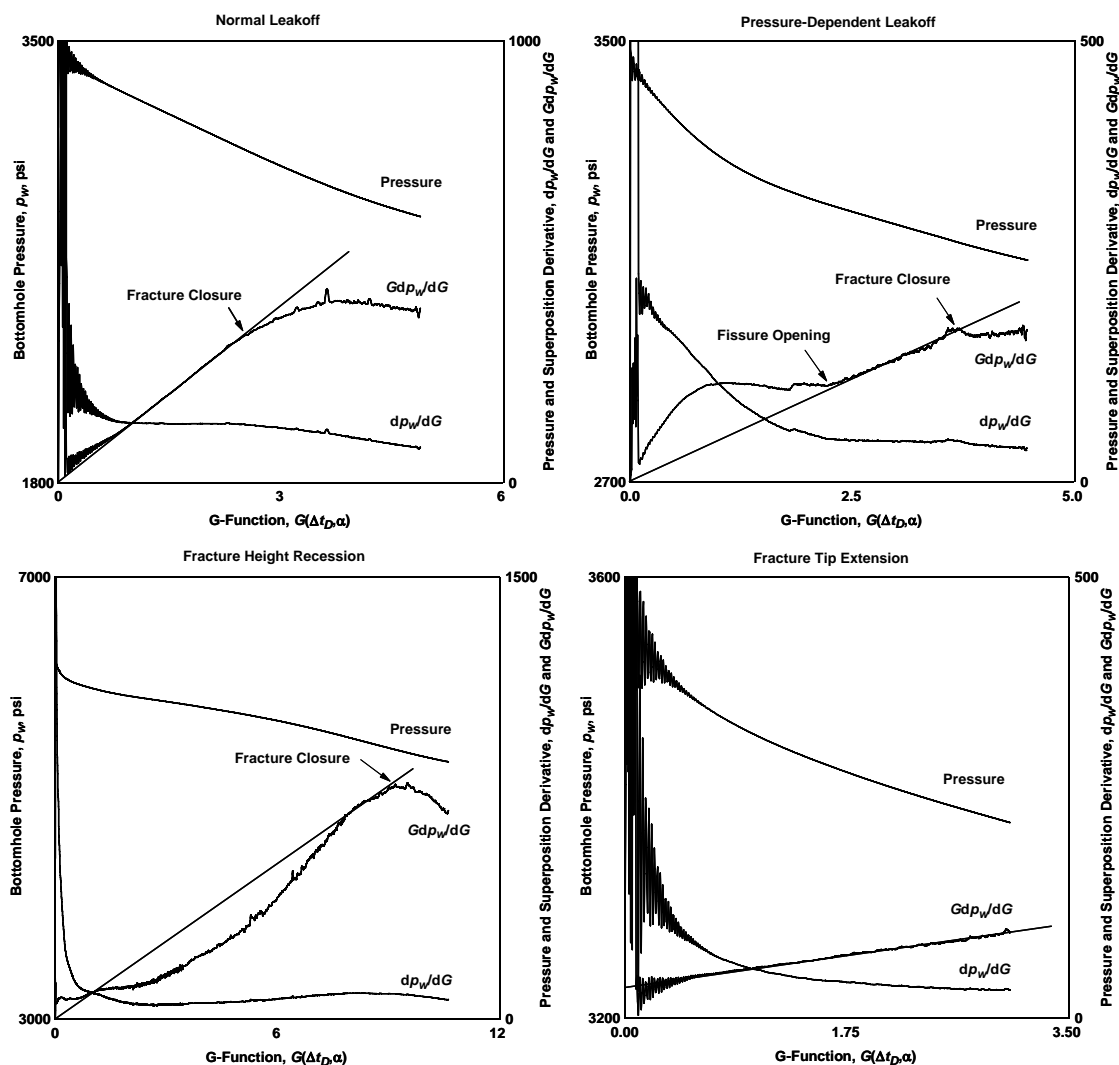


Fig. 2.3—G-function derivative analysis common leakoff types.⁸²

Fracture-height recession during shut-in is indicated when the superposition derivative data fall below a straight line drawn from the origin through the normal leakoff data. Fracture height recession is also indicated by a concave down pressure curve and an increasing pressure derivative. Hydraulic fracture closure is identified when the superposition derivative data deviate downward from a straight line drawn through the normal leakoff data.

Fracture-tip extension during shut-in occurs when the fracture continues to grow after the end of the injection. Tip extension is indicated when the superposition derivative data lie along a straight line that

extrapolates above the origin.

2.3.2 Before-Closure Pressure Transient Analysis. The pressure decline following a fracture-injection/falloff test can be divided into two distinct regions: before-fracture closure and after-fracture closure. Before-closure pressure transient analysis uses pressure transient methods to determine permeability from the before-fracture closure decline data. Mayerhofer and Economides⁵⁷ divide the pressure gradient between an open, infinite-conductivity fracture and the reservoir into four components written as

$$\Delta p(t) = \Delta p_r(t) + \Delta p_{cake}(t) + \Delta p_{piz}(t) + \Delta p_{fiz}(t) \quad (2.98)$$

The pressure drop in the polymer invaded zone, $\Delta p_{piz}(t)$, and the filtrate invaded zone, $\Delta p_{fiz}(t)$, are assumed to be negligibly small; thus, the pressure gradient consists of a reservoir component, $\Delta p_r(t)$, and a pressure drop across the filtercake, $\Delta p_{cake}(t)$, which is analogous to Cinco-Ley and Samaniego's fracture-face skin⁸³ defined as

$$S_{fs} = \frac{\pi b_{fs}}{2L_f} \left[\frac{k}{k_{fs}} - 1 \right], \quad (2.99)$$

where b_{fs} is the damage zone width and k_{fs} is the damage zone permeability. Mayerhofer and Economides⁵⁷ account for variable fracture-face skin by defining resistance as

$$R_{fs}(t) = \frac{b_{fs}(t)}{k_{fs}}, \quad (2.100)$$

and dimensionless resistance by⁵⁸

$$R_D(t) = \frac{R_{fs}(t)}{R_0} \approx \sqrt{\frac{t}{t_e}}, \quad (2.101)$$

where R_0 is the reference filtercake resistance at the end of the injection.⁵⁷

With the definition of resistance and dimensionless resistance, variable fracture-face resistance is written as

$$S_{fs} = \frac{\pi k R_0 R_D(t)}{2L_f} - \frac{\pi b_{fs}}{2L_f} \approx \frac{\pi k R_0 R_D(t)}{2L_f} \quad (2.102)$$

The pressure drop in the reservoir is modeled with the early-time vertical fracture infinite-conductivity solution, which in dimensionless form is written as⁸⁴

$$p_{fD}(t) = \sqrt{\pi t L_f D}, \quad (2.103)$$

where

$$p_{fD} = \frac{2\pi kh[p_r(t) - p_i]}{qB\mu}, \quad (2.104)$$

$$t_{LjD} = \frac{kt}{\phi\mu c_t L_f^2}, \dots\dots\dots (2.105)$$

and

$$q = 2q_\ell \dots\dots\dots (2.106)$$

Solving for the pressure difference, $\Delta p(t_j) = p_r(t_j) - p_i$, the early-time infinite-conductivity fracture solution can be written as

$$\Delta p(t_j) = \sqrt{\frac{B^2\mu}{4\pi k\phi c_t}} \frac{(q_\ell)_j}{(A)_j} \sqrt{t_j} \dots\dots\dots (2.107)$$

The pressure gradient at the end of pumping, $\Delta p(t_e)$, is obtained by applying the principle of superposition to account for the variable leakoff rates and fracture area during propagation. Note that $q_\ell = 0$ at $t_0 = 0$, and using superposition,

$$\Delta p_r(t_e) = \sqrt{\frac{B^2\mu}{4\pi k\phi c_t}} \sum_{j=1}^{ne} \left[\frac{(q_{\ell,inj})_j}{(A)_j} - \frac{(q_{\ell,inj})_{j-1}}{(A)_{j-1}} \right] \sqrt{t_{ne} - t_{j-1}}, \dots\dots\dots (2.108)$$

where 'ne' denotes the time index at the end of the injection. Similarly, the pressure drop from fracture-face resistance is written as

$$\Delta p_{sfs}(t) = \frac{qB\mu}{2\pi kh} \frac{\pi k R_0 R_D(t)}{2L_f}, \dots\dots\dots (2.109)$$

or

$$\Delta p_{sfs}(t) = \frac{B\mu R_0}{2} \frac{q_\ell(t)}{A(t)} R_D(t) \dots\dots\dots (2.110)$$

Mayerhofer and Economides⁵⁷ note that the rate-dependent skin is a steady-state pressure drop that is a function of the "current" leakoff rate and written as

$$\Delta p_{cake}(t_n) = \Delta p_{sfs}(t_n) = \frac{B\mu R_0}{2A} (R_D)_n (q_\ell)_n \dots\dots\dots (2.111)$$

The pressure difference at the end of the injection is written as

$$\Delta p(t_e) = \Delta p_r(t_e) + \Delta p_{cake}(t_e), \dots\dots\dots (2.112)$$

or

$$\begin{aligned} \Delta p(t_e) = & \sqrt{\frac{B^2\mu}{4\pi k\phi c_t}} \sum_{j=1}^{ne} \left[\frac{(q_{\ell,inj})_j}{(A)_j} - \frac{(q_{\ell,inj})_{j-1}}{(A)_{j-1}} \right] \sqrt{t_{ne} - t_{j-1}} \\ & + \frac{B\mu R_0}{2A_e} (R_D)_{ne} (q_{\ell,inj})_{ne} \dots\dots\dots (2.113) \end{aligned}$$

The pressure difference during the shut-in period is calculated by subtracting the pressure drop during the injection from the superposition of all pressure solutions corresponding to each leakoff rate from the beginning of the injection. The pressure difference is written as

$$\begin{aligned} \Delta p(t_n) &= [p_i - p_f(t_n)] - [p_i - p_f(t_{ne})] \\ &= p_f(t_{ne}) - p_f(t_n) \\ &= \sqrt{\frac{B^2 \mu}{4\pi k \phi c_t}} \left[\sum_{j=1}^{ne} \left[\frac{(q_{\ell, inj})_j}{(A)_j} - \frac{(q_{\ell, inj})_{j-1}}{(A)_{j-1}} \right] \sqrt{t_n - t_{j-1}} \right. \\ &\quad + \sum_{j=m+1}^n \left[\frac{(q_{\ell})_j}{(A)_j} - \frac{(q_{\ell})_{j-1}}{(A)_{j-1}} \right] \sqrt{t_n - t_{j-1}} \\ &\quad \left. - \sum_{j=1}^{ne} \left[\frac{(q_{\ell, inj})_j}{(A)_j} - \frac{(q_{\ell, inj})_{j-1}}{(A)_{j-1}} \right] \sqrt{t_{ne} - t_{j-1}} \right] \\ &\quad + \frac{B\mu R_0}{2A_e} [(R_D)_n (q_{\ell})_n - (R_D)_{ne} (q_{\ell, inj})_{ne}] \dots\dots\dots (2.114) \end{aligned}$$

Provided an estimate for the leakoff rate from one fracture wing, q_{ℓ} , is available, Eq. 2.114 models the pressure decline following a fracture-injection/falloff test before hydraulic fracture closure. The before-closure leakoff rate can be written as

$$(q_{\ell})_j = -\frac{A}{S_f} \frac{d(\Delta p)_j}{d(\Delta t)_j} \approx \frac{A}{S_f} \frac{(p_{j-1} - p_j)}{(t_j - t_{j-1})} \dots\dots\dots (2.115)$$

During fracture propagation, the leakoff rate is bound between upper and lower limits as demonstrated by Nolte.⁸⁰ The leakoff rate is written as

$$(q_{\ell})_j = \begin{cases} \frac{4C_L(A)_j}{\sqrt{t_j}} & \text{Upper Bound} \\ \frac{\pi C_L(A)_j}{\sqrt{t_j}} & \text{Lower Bound} \end{cases} \dots\dots\dots (2.116)$$

Eqs. 2.114 through 2.116 can be used to simulate and history-match a before-closure pressure decline following a fracture-injection/falloff test.

Valkó and Economides⁵⁹ modified the method by writing the reservoir pressure drop as

$$\Delta p_r(t_n) = \frac{B\mu}{\pi kh} \sum_{j=1}^n [(q_{\ell})_j - (q_{\ell})_{j-1}] p_{fD} [(t_n - t_{j-1})_{L_f D}] \dots\dots\dots (2.117)$$

and evaluating the dimensionless pressure function, p_{fD} , with respect to the fracture length, $(L_f)_n$, at time t_n as opposed to some other time t_j corresponding to $(A)_j$. Valkó and Economides⁵⁹ also assume that the first $ne + 1$ leakoff rates are equal; thus

$$(q_{\ell})_i = \text{Constant}, \quad 1 \leq i \leq ne+1, \dots\dots\dots (2.118)$$

where ne is the index corresponding to the end of the injection. The pressure gradient at a time t_n during the pressure decline can now be written as

$$p_f(t_n) - p_i = \frac{B\mu}{\pi kh} \left[\sum_{j=1}^n [(q_{\ell})_j - (q_{\ell})_{j-1}] p_{fD} [(t_n - t_{j-1})_{LjD}] \right] + \frac{B\mu R_0}{2A} (R_D)_n (q_{\ell})_n, \dots\dots\dots (2.119)$$

which can also be written as

$$p_f(t_n) - p_i = \frac{B\mu}{\pi kh} \left[(q_{\ell})_j p_{fD} [(t_n)_{LjD}] + [(q_{\ell})_{e+2} - (q_{\ell})_{ne+1}] p_{fD} [(t_n - t_{ne+1})_{LjD}] + \sum_{j=ne+3}^n [(q_{\ell})_j - (q_{\ell})_{j-1}] p_{fD} [(t_n - t_{j-1})_{LjD}] \right] + \frac{B\mu R_0}{2A} (R_D)_n (q_{\ell})_n, \dots\dots\dots (2.120)$$

With dimensions, the pressure difference is written as

$$p_f(t_n) - p_i = Bc_f \sqrt{\frac{\mu}{\pi \phi k c_t}} \left[\frac{(p_{ne} - p_{ne+1}) \sqrt{t_n}}{\Delta t_{ne+1}} + \left[\frac{(p_{ne+1} - p_{ne+2})}{\Delta t_{ne+2}} - \frac{(p_{ne} - p_{ne+1})}{\Delta t_{ne+1}} \right] \sqrt{t_n - t_{ne+1}} + \sum_{j=ne+3}^n \left[\frac{(p_{j-1} - p_j)}{\Delta t_j} - \frac{(p_{j-2} - p_{j-1})}{\Delta t_{j-1}} \right] \sqrt{t_n - t_{j-1}} \right] + \frac{B\mu c_f R_0}{2} \sqrt{\frac{t_n}{t_{ne}}} \frac{(p_{n-1} - p_n)}{\Delta t_n}, \dots\dots\dots (2.121)$$

A graphical method for estimating the permeability and fracture-face resistance from the pressure decline following a diagnostic fracture-injection/falloff test has been developed from Eqs. 2.114 and 2.121.⁵⁷⁻⁵⁹

Appendix A contains a new derivation of before-closure pressure-transient analysis in terms of adjusted pseudovariables, and demonstrates the development of the "specialized" Cartesian graph for determining permeability and fracture-face resistance. **Table A-2** contains the specialized graph plotting functions in terms of pressure and time and adjusted pseudopressure and time. Additionally, **Table A-3** contains the plotting functions in terms of pressure and time and adjusted pseudopressure and adjusted pseudotime for the specialized graph.

2.3.3 Before-Closure Pressure Transient Analysis in Dual-Porosity Reservoirs. Ehlig-Economides, Fan, and Economides⁸⁵ formulated the Mayerhofer and Economides⁵⁷ model for dual-porosity reservoirs using Cinco-Ley and Meng's⁸⁶ early-time solution for flow from an infinite conductivity fracture written as

$$p_{fD} = \sqrt{\frac{\pi t_{LjD}}{\omega}}, \dots\dots\dots (2.122)$$

where for dual-porosity reservoirs,

$$p_{fD} = \frac{2\pi k_{fb}h[p_r(t) - p_i]}{qB\mu}, \dots\dots\dots (2.123)$$

and

$$t_{LjD} = \frac{k_{fb}t}{\phi\mu c_t L_f^2}. \dots\dots\dots (2.124)$$

The early-time infinite-conductivity solution can be written as

$$\omega p_{LjD} = \sqrt{\pi\omega t_{LjD}}, \dots\dots\dots (2.125)$$

which with the definitions of dimensionless pressure and dimensionless time for a dual porosity reservoir can be written as

$$\Delta p(t_j) = \sqrt{\frac{B^2\mu}{4\pi\omega k_{fb}\phi c_t}} \frac{(q\ell)_j}{(A)_j} \sqrt{t_j}. \dots\dots\dots (2.126)$$

The reservoir pressure difference for a single porosity reservoir (Eq. 2.107) differs from the dual porosity reservoir pressure difference by the permeability, k , and the product of storativity ratio and bulk fracture permeability, ωk_{fb} . The fracture face pressure difference, Δp_{cake} , remains as defined in Eq. 2.111, and after applying the superposition principle, the pressure gradient at can be written as

$$\begin{aligned} \Delta p(t_n) &= [p_i - p_f(t_n)] - [p_i - p_f(t_{ne})] \\ &= p_f(t_{ne}) - p_f(t_n) \\ &= \sqrt{\frac{B^2\mu}{4\pi\omega k_{fb}\phi c_t}} \left[\sum_{j=1}^{ne} \left[\frac{(q\ell, inj)_j}{(A)_j} - \frac{(q\ell, inj)_{j-1}}{(A)_{j-1}} \right] \sqrt{t_n - t_{j-1}} \right. \\ &\quad + \sum_{j=ne+1}^n \left[\frac{(q\ell)_j}{(A)_j} - \frac{(q\ell)_{j-1}}{(A)_{j-1}} \right] \sqrt{t_n - t_{j-1}} \\ &\quad \left. - \sum_{j=1}^{ne} \left[\frac{(q\ell, inj)_j}{(A)_j} - \frac{(q\ell, inj)_{j-1}}{(A)_{j-1}} \right] \sqrt{t_{ne} - t_{j-1}} \right] \\ &\quad + \frac{B\mu R_0}{2A} [(R_D)_n (q\ell)_n - (R_D)_{ne} (q\ell, inj)_{ne}]. \dots\dots\dots (2.127) \end{aligned}$$

where the leakoff rate during closure is defined by Eq. 2.116, and the leakoff rate during the injection is defined by⁸⁵

$$(q\ell)_j = \frac{(V_{inj} - V_{Lc})}{2\sqrt{t_{ne}}\sqrt{t_j}}. \dots\dots\dots (2.128)$$

In a dual-porosity reservoir, therefore, before-closure pressure-transient analysis using the specialized Cartesian graph results in an estimate of fracture-face resistance and the product ωk_{fb} . Current methods only allow the product to be calculated, and estimating fracture storativity or bulk-fracture permeability requires additional testing. Additionally, the Ehlig-Economides, Fan, and Economides⁸⁵ model does not account for deformation during the injection, that is, the method assumes the fracture network does not dilate and contract during a fracture-injection/falloff test. Intuition suggests otherwise, and *G*-function derivative analysis confirms natural fracture dilation/contraction is common.⁵⁴

2.4 After-Closure Analysis

Concurrent with the development of before-closure analysis, Gu *et al.*⁶⁰ and Abousleiman *et al.*⁶¹ examined the pressure decline after fracture closure and presented after-closure analysis theory. Abousleiman *et al.*⁶¹ assume that a homogeneous reservoir with impervious bounding layers is penetrated completely by the wellbore, and assume that an injection induces a hydraulic fracture across the entire formation thickness. Additionally, they assume that the effect of hydraulic fracturing on the reservoir pressure can be modeled by fluid sources distributed along the fracture trajectory with the magnitude of each fluid source proportional to the fracturing fluid leakoff rate at that position during the injection.

Abousleiman, *et al.*⁶¹ state that the pressure response of a unit volume injection from a distribution of instantaneous point sources can be written as

$$\Delta p(x, y, t) = p(x, y, t) - p_i = \frac{\mu}{4\pi kh t} e^{-[(x-x')^2 + (y-y')^2] \phi \mu c_l / 4kt} \dots\dots\dots (2.129)$$

The fracture trajectory is along the *x*-axis with the fracture extending from $-L_e \leq x \leq L_e$. Additionally, since the fracture is closed, the fracture width is zero, and $y' = 0$. The exposure time of a point, x' , during the injection along the fracture trajectory lies between $\tau_a(x') \leq t' \leq \tau_d(x')$, and assuming a variable leakoff rate, and using the principle of superposition, the pressure response can be integrated and written as

$$\Delta p(0, 0, t) = \frac{\mu}{4\pi kh} \int_{-L_e}^{L_e} \int_{\tau_a(x')}^{\tau_d(x')} q_\ell(x', t') \frac{e^{-(x')^2 \phi \mu c_l / 4k(t-\tau)}}{t-\tau} d\tau dx' \dots\dots\dots (2.130)$$

As a mathematical convenience, the reference time in Eq. 2.130 can be adjusted to the closure time by defining⁶¹

$$\tau_0(x') = \tau_d(x') - \tau_a(x'), \dots\dots\dots (2.131)$$

$$t_1(x') = t - \tau_a(x'), \dots\dots\dots (2.132)$$

and

$$\Delta t_{ac} = t - t_c \dots\dots\dots (2.133)$$

Assuming the fracture is symmetric about the wellbore, then Eq. 2.130 can be written as

$$\Delta p(\Delta t_{ac}) = \frac{\mu}{2\pi kh} \int_0^{L_f} \int_0^{\tau_0(x')} q_\ell(t') \frac{e^{-(x')^2 \phi \mu c_t / 4k[t_1(x') - \tau]}}{t_1(x') - \tau} d\tau dx', \dots\dots\dots (2.134)$$

where

$$q_\ell(\tau) = \frac{2C_L}{\sqrt{\tau}} \dots\dots\dots (2.135)$$

The large-time asymptotic solution is developed by recognizing that as $t \rightarrow \infty$, $t_1 \approx \Delta t_{ac}$, and $\Delta t_{ac} \approx t_1 - \tau$; thus, the exponential term in Eq. 2.134 tends to one, that is,

$$\lim_{[t_1(x') - \tau] \rightarrow \infty} e^{-(x')^2 \phi \mu c_t / 4k[t_1(x') - \tau]} = 1, \dots\dots\dots (2.136)$$

and

$$\Delta p(\Delta t_{ac}) \cong \frac{\mu}{2\pi kh \Delta t_{ac}} \int_0^{L_e} \int_0^{\tau_0(x')} q_\ell(\tau) d\tau dx'. \dots\dots\dots (2.137)$$

At closure, the volume injected into one fracture wing, V_{inj} , can be written as

$$V_{inj} = \int_0^{L_f} \int_0^{\tau_0(x')} q_\ell(\tau) d\tau dx', \dots\dots\dots (2.138)$$

and the large-time asymptotic solution is written as

$$\Delta p(\Delta t_{ac}) \cong \frac{\mu V_{inj}}{2\pi kh} \frac{1}{\Delta t_{ac}} \dots\dots\dots (2.139)$$

Eq. 2.139 suggests a Cartesian graph of p_w versus $1/\Delta t_{ac}$ during pseudoradial flow will result in a straight line with transmissibility,

$$\frac{kh}{\mu} = \frac{V_{inj}}{4\pi m_{acpr}}, \dots\dots\dots (2.140)$$

where m_{acpr} is the slope of the line. A log-log graph of $p_w - p_i$ versus $1/\Delta t_{ac}$ will have a unit slope, and a log-log graph of the pressure derivative,

$$\frac{d\Delta p(\Delta t_{ac})}{d[\ln(1/\Delta t_{ac})]} = \frac{1}{\Delta t} \frac{d\Delta p(\Delta t_{ac})}{d(1/\Delta t_{ac})} = \frac{\mu V_{inj}}{4\pi kh} \frac{1}{\Delta t_{ac}}, \dots\dots\dots (2.141)$$

will also have a unit slope and overlay the pressure curve during pseudoradial flow. The implication of the model is that after "sufficient" time, the pressure behavior of the reservoir is not influenced by the fracture propagation or the final fracture dimensions created by the injection.

Nolte⁸⁷ also describes the after-closure pressure behavior during the pseudolinear flow period. Nolte states that the pressure behavior of a finite-length fracture subject to constant pressure leakoff and zero flux after closure or the pressure behavior of an incremental-length of a propagating fracture within the linear-flow regime can be written as

$$\Delta p = C_L \sqrt{\frac{\pi\mu}{k\phi c_t}} \left[\frac{2}{\pi} \sin^{-1} \sqrt{\frac{t_c}{\Delta t_{ac}}} \right] = C_L \sqrt{\frac{\pi\mu}{k\phi c_t}} \sqrt{F_L^2(\Delta t_{ac}, t_c)} \quad (2.142)$$

Eq. 2.142 suggests that a log-log graph of $p_w - p_i$ versus $F_L^2(\Delta t_{ac}, t_c)$ and a log-log graph of the pressure derivative versus $F_L^2(\Delta t_{ac}, t_c)$ will have a $1/2$ slope during pseudolinear flow, but the two curves will be offset by a factor of 2. A straight line drawn through the pseudolinear flow data on a Cartesian graph of p_w versus $F_L(\Delta t_{ac}, t_c)$ will have a slope equal to

$$m_{acpl} = C_L \sqrt{\frac{\pi\mu}{k\phi c_t}} \quad (2.143)$$

2.5 Discussion of Existing Injection/Falloff and Fracture-Injection/Falloff Test Analysis Methods

Injection/falloff test interpretation, including both impulse and slug tests, is fundamentally limited⁸⁸ by the requirement that average reservoir pressure must be known accurately to calculate transmissibility from the falloff data. Additionally, field implementation of a slug-test requires a finite time of injection, but the analysis method assumes an injection is instantaneous. Butler⁸⁹ notes that an injection can be considered instantaneous when the time of injection is short relative to the reservoir response. However, quantitative guidelines for when an injection can be considered as occurring instantaneously are not available.

Injection/falloff test theory used to analyze slug-test data also assumes that the pressure during an injection must remain below the fracture propagation pressure and assumes that if a fracture exists, it was created prior to the injection. Thus, when a fracture is initiated during an injection, the assumptions of existing slug-test solutions are violated.⁴⁹

Like an injection/falloff test, a fracture-injection/falloff test analysis requires an accurate average reservoir pressure to calculate transmissibility from the falloff data. Current before-closure models for fracture-injection/falloff tests are also highly idealized, and field tests routinely deviate from ideal behavior. For example, Craig *et al.*⁵⁴ have shown that only 15% of 994 tests analyzed in Rocky Mountain basins exhibited idealized "normal" leakoff behavior. Additionally, before-closure pressure-transient analysis fails to adequately model the pressure decline with nonideal leakoff behavior. For example, pressure-dependent leakoff can be indicative of a naturally fractured or dual-porosity reservoir, and although Ehlig-Economides *et al.*⁸⁵ formulated before-closure pressure-transient analysis for dual-porosity reservoirs, field examples demonstrate that the model fails when natural fractures deform (dilate and contract) during an injection/falloff test.⁸²

With existing models, only specific and small portions of the pressure decline during a fracture-injection/falloff test sequence can be analyzed. Before-closure data, which can extend from a few seconds to several hours, can be analyzed, and after-closure data can be analyzed provided pseudoradial flow is observed. However, in a low permeability reservoir or when a relatively long fracture is created during the

injection, an extended shut-in period—hours or possibly days—are required to observe pseudoradial flow. A quantitative transmissibility estimate from the remaining pressure falloff data, which represents the vast majority of the recorded pressure decline, is not possible with existing models.

A new fracture-injection/falloff model accounting for fracture creation, fracture closure, and after-closure diffusion is presented in Chapter III. Although the new model still requires an accurate estimate of reservoir pressure to calculate transmissibility from the pressure falloff data, the new model removes other before- and after-closure analysis limitations. Specifically, the new model can be used to demonstrate when a finite injection time can be considered as occurring instantaneously – which based on limiting-case solutions, allows the pressure difference recorded during the falloff to be transformed to an equivalent constant-rate pressure difference and analyzed using quantitative type-curve analysis. Consequently, all data recorded during a fracture-injection falloff test is used to construct a type-curve match to estimate transmissibility.

CHAPTER III

MODELING A FRACTURE-INJECTION/FALLOFF TEST IN A RESERVOIR WITHOUT A PRE-EXISTING FRACTURE

3.1 Introduction

When the injection time of a fracture-injection/falloff test is short relative to the reservoir response, the injection can be considered as occurring instantaneously, and slug-test analysis methods can be applied to the falloff data as though the created fracture were pre-existing.

The preferred slug-test analysis method converts variable-rate pressure falloff data to an equivalent constant-rate pressure difference by integration of the recorded pressure difference with respect to time. After conversion, constant-rate drawdown type curves are used for quantitative type-curve analysis. However, during the falloff period the created fracture closes, which creates a variable storage problem that requires new constant-rate drawdown solutions for type-curve matching.

Chapter III presents analytical constant-rate drawdown solutions for a well in an infinite slab reservoir containing a single dilated vertical fracture with the initial reservoir pressure above the minimum insitu or closure stress and with fracture storage and wellbore storage as follows:

- Constant before- and constant after-closure fracture and wellbore storage.
- Constant before- and constant after-closure fracture and wellbore storage with fracture-face and choked-fracture skin.
- Fracture flow during closure with constant before-closure fracture and wellbore storage and radial flow after closure with constant wellbore storage and skin.

A new fracture-injection/falloff model accounting for fracture creation, fracture closure, and after-closure diffusion is also presented to demonstrate when slug-test analysis methods are applicable. By considering fracture propagation as time-dependent storage, three new models are presented for a fracture-injection/falloff sequence for a well in an infinite slab reservoir with a single vertical fracture created during an injection with fracture and wellbore storage as follows:

- Equivalent propagating-fracture storage and before-closure storage with constant after-closure storage.
- Time-dependent propagating-fracture storage, constant before-closure storage, and constant after-closure storage.
- Time-dependent propagating-fracture storage and before-closure storage with linear flow from the fracture before closure and after-closure radial flow with constant wellbore storage and skin.

Limiting-case solutions of the fracture-injection/falloff models and numerical evaluations are also presented to demonstrate when a fracture-injection can be considered as occurring instantaneously and slug-test analysis methods can be applied to the falloff data for quantitative type-curve analysis.

3.2 Constant-Rate Drawdown Solutions With Variable Fracture Storage

Constant-rate drawdown solutions for a well in an infinite slab reservoir containing a single dilated vertical fracture with the initial reservoir pressure above the minimum in-situ or closure stress and with variable fracture and wellbore storage are derived in **Appendix B**. The drawdown solutions assume the reservoir and fracture are initially at a constant uniform pressure sufficient to keep the fracture open, but as the pressure declines during the drawdown, the fracture closes. Consequently, the new pressure-transient solution accounts for variable storage before- and after-closure during a constant-rate drawdown.

3.2.1 Constant-Rate Drawdown With Constant Before- and Constant After-Closure Storage. Correa and Ramey⁶²⁻⁶⁴ solved a changing storage problem by using the unit-step function written as

$$U_a = U(t-a) = \begin{cases} 0 & , t < a \\ 1 & , t > a \end{cases}, \dots\dots\dots(3.1)$$

and writing a material balance equation valid at all times during a drawdown. During a variable storage drawdown in a well with a closing fracture, the before-closure dimensionless material balance equation is written as

$$q_D = q_{wD} - C_{bcD} \frac{dp_{wD}}{dt_{LfD}}, \dots\dots\dots(3.2)$$

where the dimensionless sandface flow rate is defined as

$$q_D = \frac{q}{q_t}, \dots\dots\dots(3.3)$$

with q being the sandface flow rate and q_t being the well production rate. Dimensionless pressure is defined as

$$p_{wD} = \frac{2\pi kh(p_i - p_w(t))}{qB\mu}, \dots\dots\dots(3.4)$$

and dimensionless time is defined as

$$t_{LfD} = \frac{kt}{\phi\mu c_t L_f^2}, \dots\dots\dots(3.5)$$

A dimensionless before-closure storage coefficient is defined as

$$C_{bcD} = \frac{C_{bc}}{2\pi\phi c_t h L_f^2}, \dots\dots\dots(3.6)$$

where the before-closure storage coefficient is written as

$$C_{bc} = c_w V_w + 2c_f V_f + 2 \frac{dV_f}{dp_w}, \dots\dots\dots (3.7)$$

and V_f is the volume of one wing a fracture symmetrical about the wellbore.

An after-closure storage coefficient is written as

$$C_{ac} = c_w V_w + 2c_f V_{fr}, \dots\dots\dots (3.8)$$

where V_{fr} is the residual volume of one fracture wing, and the dimensionless after-closure storage coefficient is written as

$$C_{acD} = \frac{C_{ac}}{2\pi\phi c_t h L_f^2} \dots\dots\dots (3.9)$$

In terms of dimensionless variables, the after-closure material balance equation is written as

$$q_D = q_{wD} - C_{acD} \frac{dp_{wD}}{dt_{LfD}} \dots\dots\dots (3.10)$$

Using the technique of Correa and Ramey,⁶²⁻⁶⁴ a dimensionless material balance equation valid at all times during the drawdown is written as

$$q_D = \left(1 - U(t_c)_{LfD}\right) \left(q_{wD} - C_{bcD} \frac{dp_{wD}}{dt_{LfD}}\right) + U(t_c)_{LfD} \left(q_{wD} - C_{acD} \frac{dp_{wD}}{dt_{LfD}}\right), \dots\dots\dots (3.11)$$

where $(t_c)_{LfD}$ is the dimensionless fracture closure time.

A detailed derivation is contained in Appendix B, but in general the drawdown solution is developed by first transforming the material balance equation to the Laplace domain. Since the governing differential equations and boundary conditions are linear, the superposition principle can be applied by transforming the superposition integral to the Laplace domain and combining with the transformed material balance equation. After algebraic manipulation, the solution is obtained by inverting back to the time domain. Thus, for a well in an infinite slab reservoir with an open fracture supported by initial reservoir pressure that closes during the drawdown with constant before- and after-closure storage, the solution is written as

$$p_{wD}(t_{LfD}) = p_{acD}(t_{LfD}) - (C_{bcD} - C_{acD}) \int_0^{(t_c)_{LfD}} p'_{acD}(t_{LfD} - \tau_D) p'_{wD}(\tau_D) d\tau_D, \dots\dots\dots (3.12)$$

where p_{wD} denotes that the pressure solution is for a constant rate and p_{acD} is the dimensionless pressure solution for a constant-rate drawdown with constant after-closure storage, which is written in the Laplace domain as

$$\bar{p}_{acD} = \frac{\bar{p}_{fD}}{1 + s^2 C_{acD} \bar{p}_{fD}}, \dots\dots\dots (3.13)$$

and p_{fD} is the reservoir solution for a single vertical infinite- or finite-conductivity fracture.

3.2.2 Constant-Rate Drawdown With Constant Before- and Constant After-Closure Storage With Fracture-Face and Choked-Fracture Skin. Fracture volume before closure is greater than the residual fracture volume after closure, $V_f > V_{fr}$, and the change in fracture volume with respect to pressure is positive. Thus before-closure storage, when a fracture is open and closing, is greater than after-closure storage, which is written as

$$c_f V_f + \frac{dV_f}{dp_w} > c_f V_{fr} \dots\dots\dots (3.14)$$

Consequently, decreasing storage should be expected during a constant-rate drawdown with a closing fracture as has been demonstrated for a closing waterflood-induced fracture during a falloff period by Koning and Niko,⁹⁰ Koning,⁹¹ and van den Hoek.⁹²⁻⁹³

Can storage appear to increase during a constant-rate drawdown with a closing fracture? Spivey and Lee⁹⁴ describe a variable wellbore storage model for reservoirs with natural fractures of limited extent in communication with the wellbore. The variable storage model includes a natural fracture storage coefficient and natural fracture skin affecting communication with the reservoir, and a wellbore storage coefficient and a completion skin affecting communication between the natural fractures and the wellbore. The Spivey and Lee radial model with natural fractures of limited extent in communication with the wellbore demonstrates that storage can appear to increase when the completion skin is greater than zero.

The concept of Spivey and Lee⁹⁴ is easily extended to a constant-rate drawdown for a well with a vertical hydraulic fracture by incorporating fracture-face and choked fracture skin as described by Cinco-Ley and Samaniego.⁸³ The problem is formulated by first considering only wellbore storage and writing a dimensionless material balance equation as

$$q_D = q_{wD} - C_D \frac{dp_{wD}}{dt_{Lfd}} \dots\dots\dots (3.15)$$

where C_D is the dimensionless wellbore storage coefficient written as

$$C_D = \frac{C}{2\pi\phi c_t h L_f^2} \dots\dots\dots (3.16)$$

and C is the wellbore storage coefficient defined as

$$C = c_w V_w \dots\dots\dots (3.17)$$

The dimensionless material balance equation is combined with the superposition integral in the Laplace domain, and the wellbore solution is written as

$$\bar{p}_{wD} = \frac{s\bar{p}_{wfD} + (S_{fs})ch}{s \left[1 + sC_D \left[s\bar{p}_{wfD} + (S_{fs})ch \right] \right]} \dots\dots\dots (3.18)$$

where $(S_{fs})_{ch}$ is the choked fracture skin and p_{wfD} is the dimensionless pressure solution outside of the wellbore in the fracture. The solution outside of the wellbore accounts for variable fracture storage and is formulated by writing a before-closure dimensionless material balance equation as

$$q_D = q_{wD} - C_{fbcD} \frac{dp_{wfD}}{dt_{LjD}}, \dots\dots\dots(3.19)$$

where the dimensionless before-closure fracture storage is written as

$$C_{fbcD} = \frac{C_{fbc}}{2\pi\phi c_t h L_f^2}, \dots\dots\dots(3.20)$$

and the before-closure fracture storage coefficient is written as

$$C_{fbc} = 2c_f V_f + 2 \frac{dV_f}{dp_w}. \dots\dots\dots(3.21)$$

The after-closure dimensionless material balance equation is written as

$$q_D = q_{wD} - C_{facD} \frac{dp_{wfD}}{dt_{LjD}}, \dots\dots\dots(3.22)$$

where the dimensionless after-closure fracture storage is written as

$$C_{facD} = \frac{C_{fac}}{2\pi\phi c_t h L_f^2}, \dots\dots\dots(3.23)$$

and the after-closure fracture storage coefficient is written as

$$C_{fac} = 2c_f V_{fr}. \dots\dots\dots(3.24)$$

A dimensionless material balance equation written for flow outside of the wellbore in the fracture that is valid at all times during the drawdown is written as

$$q_D = \left(1 - U(t_c)_{LjD}\right) \left(q_{wD} - C_{fbcD} \frac{dp_{wfD}}{dt_{LjD}}\right) + U(t_c)_{LjD} \left(q_{wD} - C_{facD} \frac{dp_{wfD}}{dt_{LjD}}\right). \dots\dots\dots(3.25)$$

The drawdown solution outside of the wellbore in the fracture for a well in an infinite slab reservoir with an open fracture supported by initial reservoir pressure that closes during the drawdown with constant before- and after-closure storage is written as

$$p_{wfD}(t_{LjD}) = p_{facD}(t_{LjD}) - (C_{fbcD} - C_{facD}) \int_0^{(t_c)_{LjD}} p'_{facD}(t_{LjD} - \tau_D) p'_{wfD}(\tau_D) d\tau_D, \dots\dots\dots(3.26)$$

where p_{facD} is the dimensionless pressure solution in the fracture for a constant-rate drawdown with constant storage, which is written in the Laplace domain as

$$\bar{p}_{facD} = \frac{s\bar{p}_{fD} + S_{fs}}{s \left[1 + sC_{facD}(s\bar{p}_{fD} + S_{fs})\right]}, \dots\dots\dots(3.27)$$

and p_{fD} is the reservoir solution for a single vertical fracture and S_{fs} is the fracture-face skin.

The Laplace-domain drawdown solution outside of the wellbore in the fracture is written as

$$\bar{p}_{wfD} = \bar{p}_{facD} - (C_{fbcD} - C_{facD}) \bar{s} \bar{p}_{facD} \int_0^{(t_c)_{LfD}} e^{-st_{LfD}} p'_{wfD}(t_{LfD}) dt_{LfD} \dots\dots\dots (3.28)$$

3.2.3 Constant-Rate Drawdown With Constant Before-Closure Storage, Constant After-Closure Wellbore Storage, and After-Closure Radial Flow With Skin. When an open hydraulic fracture closes completely with little or no retained conductivity, the production can no longer be regarded as flowing from the fracture alone and the system can effectively convert to radial flow. The before-closure dimensionless material balance equation remains the same and is written as

$$q_{fD} = q_{wD} - C_{bcD} \frac{dp_{wD}}{dt_{LfD}}, \dots\dots\dots (3.29)$$

where q_{fD} denotes the flow rate is at the fracture sandface. With complete closure, the after-closure storage does not include the fracture volume and a material balance equation is written as

$$q_{rD} = q_{wD} - C_D \frac{dp_{wD}}{dt_{LfD}}, \dots\dots\dots (3.30)$$

where q_{rD} is the sandface flow rate of a radial system.

A drawdown solution can be developed using the unit-step function and writing the dimensionless wellbore pressure as a sum of superposition integrals reflecting flow from the fracture before closure and from a radial system after closure. The dimensionless wellbore pressure is written as

$$p_{wD} = \left[\int_0^{t_{LfD}} q_{fD}(\tau_D) \left[1 - U(t_c)_{LfD} \right] \frac{dp_{fD}(t_{LfD} - \tau_D)}{dt_{LfD}} d\tau_D \right] + \left[\int_0^{t_{LfD}} q_{rD}(\tau_D) U(t_c)_{LfD} \frac{dp_{sD}(t_{LfD} - \tau_D)}{dt_{LfD}} d\tau_D \right], \dots\dots\dots (3.31)$$

where p_{fD} is the dimensionless reservoir solution for a well with a fixed-length fracture, and the dimensionless reservoir solution for a radial system with skin effect is written as

$$p_{sD}(t_{LfD}) = p_{rD}(t_{LfD}) + S, \dots\dots\dots (3.32)$$

and p_{rD} is the dimensionless radial flow reservoir solution and S is the skin effect. Note that dimensionless time is defined in terms fracture half-length; thus, fracture half-length is the characteristic length used in the dimensionless radius definition, $r_{wD} = r_w/L_f$, and radial solution.

After converting the material balance equations and the superposition integrals to the Laplace domain, simplifying, and inverting back to the time domain, a drawdown solution for a well with an open fracture that closes during the drawdown with constant after-closure wellbore storage and after-closure radial flow is written as

$$p_{wcD}(t_{LjD}) = \left[\begin{array}{l} p_{fD}(t_{LjD}) - p_{fD} [t_{LjD} - (t_c)_{LjD}] + p_{sD} [t_{LjD} - (t_c)_{LjD}] \\ -C_{acD} \int_{(t_c)_{LjD}}^{t_{LjD}} p'_{sD}(t_{LjD} - \tau_D) p'_{wcD}(\tau_D) d\tau_D \\ -C_{bcD} \int_0^{(t_c)_{LjD}} p'_{fD}(t_{LjD} - \tau_D) p'_{wcD}(\tau_D) d\tau_D \end{array} \right] \dots\dots\dots (3.33)$$

3.3 Constant-Rate Drawdown Numerical Solutions With Variable Fracture Storage

3.3.1 Constant-Rate Drawdown With Constant Before- and Constant After-Closure Storage. The solution for a constant-rate drawdown in an infinite slab reservoir producing through a finite- or infinite-conductivity fracture with constant before- and after-closure storage is written as

$$p_{wcD}(t_{LjD}) = p_{acD}(t_{LjD}) - (C_{bcD} - C_{acD}) \int_0^{(t_c)_{LjD}} p'_{acD}(t_{LjD} - \tau_D) p'_{wcD}(\tau_D) d\tau_D \dots\dots\dots (3.34)$$

After integrating-by-parts, the solution is written as

$$p_{wcD}(t_{LjD}) = \left[\begin{array}{l} p_{acD}(t_{LjD}) + (C_{bcD} - C_{acD}) p_{acD} [t_{LjD} - (t_c)_{LjD}] p'_{wcD} [(t_c)_{LjD}] \\ - (C_{bcD} - C_{acD}) \int_0^{(t_c)_{LjD}} p''_{wcD}(\tau_D) p_{acD}(t_{LjD} - \tau_D) d\tau_D \end{array} \right] \dots\dots\dots (3.35)$$

and after discretizing the integral term, a numerical approximation is written as

$$p_{wcD}(t_{LjD})_n = \left[\begin{array}{l} p_{acD}(t_{LjD})_n + (C_{bcD} - C_{acD}) p_{acD} [(t_{LjD})_n - (t_{LjD})_j] p'_{wcD} [(t_{LjD})_j] \\ - (C_{bcD} - C_{acD}) \sum_{i=1}^j \left[\begin{array}{l} \left(\frac{p_{wcD}(t_{LjD})_i - p_{wcD}(t_{LjD})_{i-1}}{(t_{LjD})_i - (t_{LjD})_{i-1}} \right) \\ - \left(\frac{p_{wcD}(t_{LjD})_{i-1} - p_{wcD}(t_{LjD})_{i-2}}{(t_{LjD})_{i-1} - (t_{LjD})_{i-2}} \right) \right] \\ \times p_{acD} [(t_{LjD})_n - (t_{LjD})_{i-1}] \end{array} \right] \dots\dots\dots (3.36)$$

where j is the time index at closure. Note that for $n \leq j$, $p_{acD}[(t_{LjD})_n - (t_{LjD})_j] = 0$.

A drawdown in an infinite slab reservoir producing through an infinite-conductivity fracture with constant before-closure storage and decreasing after-closure storage is illustrated in **Fig. 3.1**, which is a log-log graph of dimensionless pressure versus dimensionless time for $C_{bcD} = 10$, $C_{acD} = 1$, and $(t_c)_{LjD} = \{10^{-5}, 10^{-4}, 10^{-3}, 10^{-2}\}$. A drawdown in an infinite slab reservoir producing through an infinite-conductivity fracture with constant before-closure storage and increasing after-closure storage is illustrated in **Fig. 3.2** with $C_{bcD} = 1$, $C_{acD} = 10$, and $(t_c)_{LjD} = \{10^{-5}, 10^{-4}, 10^{-3}, 10^{-2}\}$.

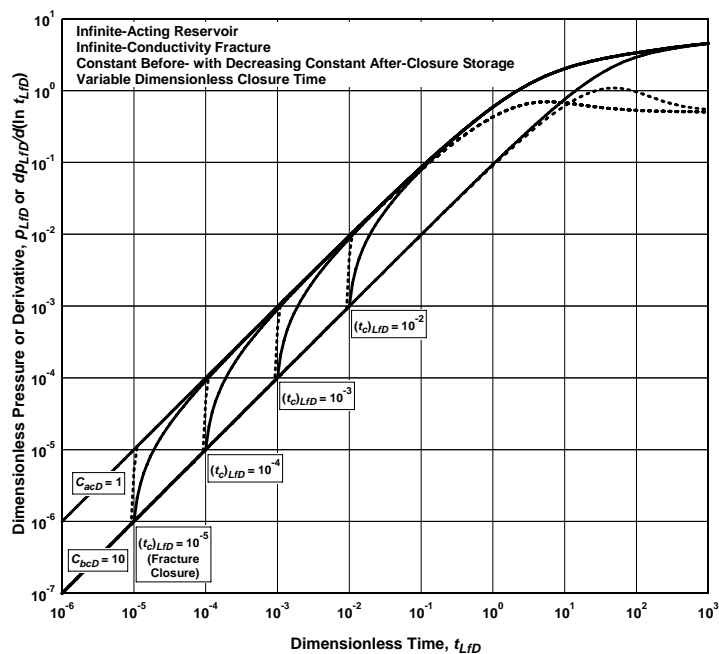


Fig. 3.1—Constant-rate drawdown in a reservoir with an open fracture with constant before-closure storage, decreasing constant after-closure storage, and variable dimensionless closure time.

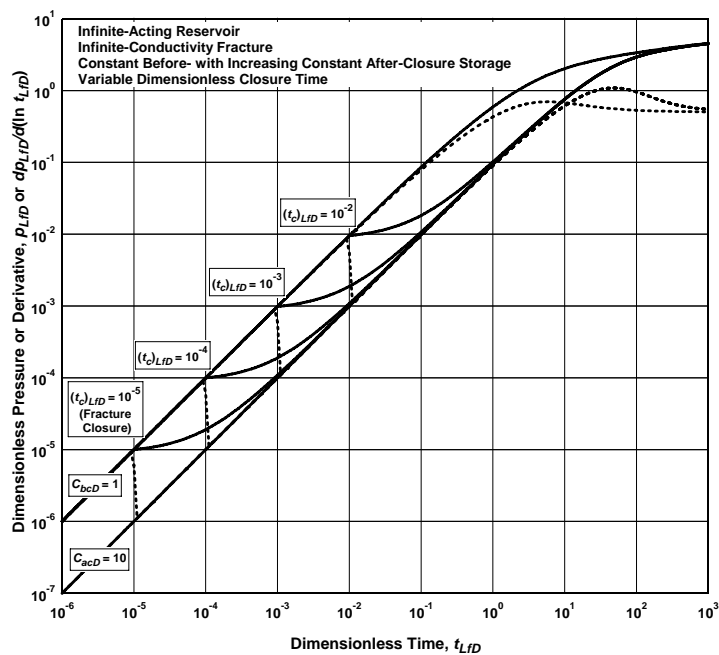


Fig. 3.2—Constant-rate drawdown in a reservoir with an open fracture with constant before-closure storage, increasing constant after-closure storage, and variable dimensionless closure time.

3.3.2 Constant-Rate Drawdown With Constant Before- and Constant After-Closure Storage With Fracture-Face and Choked-Fracture Skin. The dimensionless pressure outside of the wellbore in the fracture for a constant-rate drawdown with constant before-closure storage, after-closure storage, and fracture-face skin is written in the time domain as

$$p_{wfd}(t_{Lfd}) = p_{facD}(t_{Lfd}) - (C_{fbcD} - C_{facD}) \int_0^{(t_c)_{Lfd}} p'_{facD}(t_{Lfd} - \tau_D) p'_{wfd}(\tau_D) d\tau_D, \dots\dots\dots (3.37)$$

which is discretized as

$$p_{wfd}(t_{Lfd})_n = \left[\begin{array}{l} p_{facD}(t_{Lfd})_n + (C_{fbcD} - C_{facD}) p_{facD} \left[(t_{Lfd})_n - (t_{Lfd})_j \right] p'_{wfd} \left[(t_{Lfd})_j \right] \\ - (C_{fbcD} - C_{facD}) \sum_{i=1}^j \left[\begin{array}{l} \left[\left(\frac{p_{wfd}(t_{Lfd})_i - p_{wfd}(t_{Lfd})_{i-1}}{(t_{Lfd})_i - (t_{Lfd})_{i-1}} \right) \right] \\ - \left[\left(\frac{p_{wfd}(t_{Lfd})_{i-1} - p_{wfd}(t_{Lfd})_{i-2}}{(t_{Lfd})_{i-1} - (t_{Lfd})_{i-2}} \right) \right] \\ \times p_{facD} \left[(t_{Lfd})_n - (t_{Lfd})_{i-1} \right] \end{array} \right] \end{array} \right] \dots\dots\dots (3.38)$$

The dimensionless pressure outside of the wellbore in the fracture is written in the Laplace domain as

$$\bar{p}_{wfd} = \bar{p}_{facD} - (C_{fbcD} - C_{facD}) s \bar{p}_{facD} \int_0^{(t_c)_{Lfd}} e^{-st_{Lfd}} p'_{wfd}(t_{Lfd}) dt_{Lfd}, \dots\dots\dots (3.39)$$

and after integrating-by-parts is written as

$$\bar{p}_{wfd} = \bar{p}_{facD} \left[\begin{array}{l} 1 - (C_{fbcD} - C_{facD}) s e^{-s(t_c)_{Lfd}} p_{wfd} \left[(t_c)_{Lfd} \right] \\ - (C_{fbcD} - C_{facD}) s^2 \int_0^{(t_c)_{Lfd}} e^{-st_{Lfd}} p_{wfd}(t_{Lfd}) dt_{Lfd} \end{array} \right] \dots\dots\dots (3.40)$$

The Laplace domain wellbore pressure solution with wellbore storage and choked-fracture skin is written as

$$\bar{p}_{wD} = \frac{s \bar{p}_{wfd} + (S_{fs})_{ch}}{s \left[1 + s C_D \left[s \bar{p}_{wfd} + (S_{fs})_{ch} \right] \right]} \dots\dots\dots (3.41)$$

Before fracture closure, the dimensionless pressure in the fracture outside of the wellbore is simply a function of before-closure fracture storage and fracture-face skin and can be written in the Laplace domain as

$$\bar{p}_{wfd} = \frac{s \bar{p}_{fD} + S_{fs}}{s \left[1 + s C_{fbcD} \left[s \bar{p}_{fD} + S_{fs} \right] \right]} \dots\dots\dots (3.42)$$

The before-closure dimensionless wellbore pressure accounting for fracture-face skin, before-closure storage, choked-fracture skin, and wellbore storage is solved by numerically inverting⁶⁸ the Laplace domain solution, Eqs. 3.41 and 3.42.

After fracture closure, the dimensionless wellbore pressure solution is obtained by evaluating the time-domain discretized solution for the dimensionless pressure outside of the wellbore and in the fracture, Eq. 3.38, at each time $(t_{LFD})_n$. With the time-domain dimensionless pressure outside of the wellbore in the fracture known, the Laplace domain solution, Eq. 3.40, can be evaluated numerically and combined with the Laplace domain wellbore solution, Eq. 3.41, and numerically inverted to the time domain.⁶⁸

Fig. 3.3 compares log-log graphs of dimensionless pressure versus dimensionless time for two cases. The first case is a constant-rate drawdown in an infinite slab reservoir producing through an infinite-conductivity fracture with constant before-closure storage, $C_{bcD} = 10$, decreasing constant after-closure storage, $C_{acD} = 1$, and a dimensionless closure time of $(t_c)_{LFD} = 10^{-3}$. The second case includes wellbore storage, $C_D = 0.5$, before-closure fracture storage, $C_{fbcD} = 9.5$, after-closure fracture storage, $C_{facD} = 0.5$, no fracture-face or choked fracture skin, and a dimensionless closure time of $(t_c)_{LFD} = 10^{-3}$.

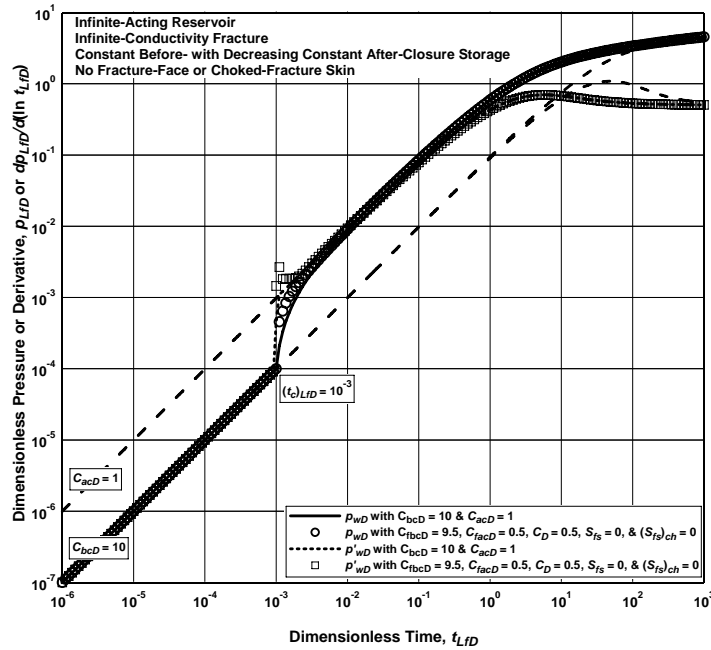


Fig. 3.3—Comparison of constant-rate drawdown numerical solutions formulated with and without fracture-face and choked-fracture skin.

With precise numerical evaluation, the two curves should overlay. However, the two curves during the transition from before- to after-closure storage separate at closure and converge over a log cycle. The separation is attributed to error in the numerical approximation of the integral in Eq. 3.40 and numerical inversion.⁶⁸ The integral was evaluated using 2-point (Trapezoid) and 4-point (Simpson's 3/8 Rule) approximations with near identical numerical inversion results.

Cases illustrating the effects of fracture-face and choked-fracture skin for $C_D = 1$, $C_{fbcD} = 10$, $C_{facD} = 9$, and $(t_c)_{LFD} = 10^{-3}$ are shown in **Figs. 3.4, 3.5, 3.6**. Fig. 3.4 shows a log-log graph of dimensionless pressure versus dimensionless time for variable fracture-face skin, $S_{fs} = \{0, 0.5, 1\}$, and no choked-fracture skin, $(S_{fs})_{ch} = 0$.

Fig. 3.5 contains a log-log graph of dimensionless pressure versus dimensionless time for no fracture-face skin, $S_{fs} = 0$, and variable choked-fracture skin, $(S_{fs})_{ch} = \{0.05, 1, 5\}$. Fig. 3.5 clearly demonstrates that storage appears to increase during a constant-rate drawdown in a well with a closing fracture and choked-fracture skin.

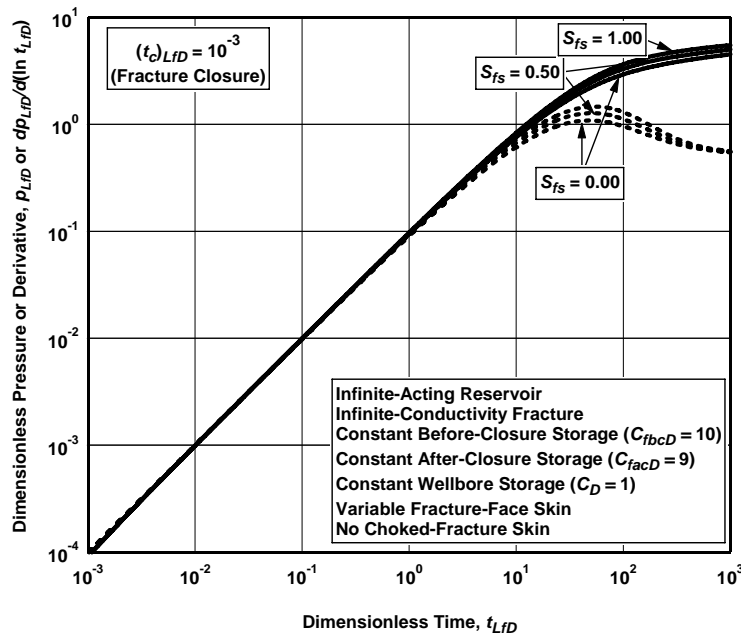


Fig. 3.4—Constant-rate drawdown in an infinite-slab reservoir with constant before- and decreasing constant after-closure storage with variable fracture-face and no choked-fracture skin.

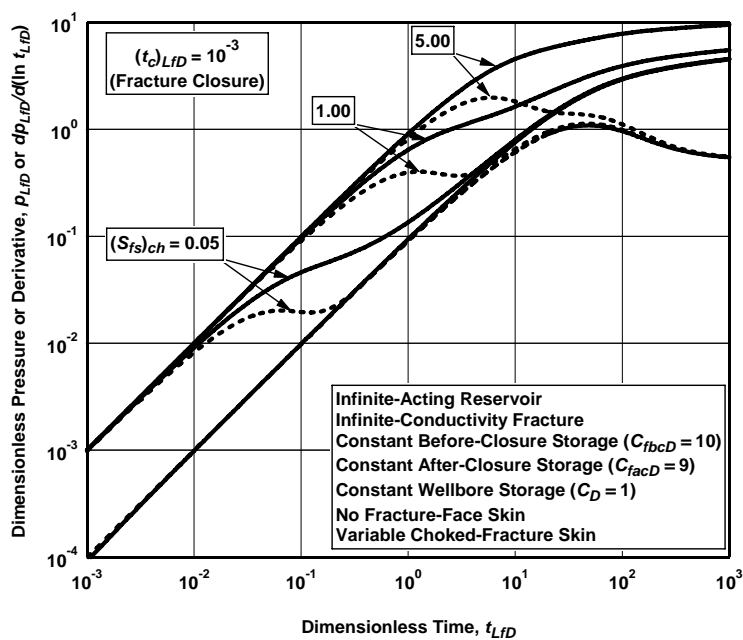


Fig. 3.5—Constant-rate drawdown in an infinite-slab reservoir with constant before- and decreasing constant after-closure storage with no fracture-face and variable choked-fracture skin.

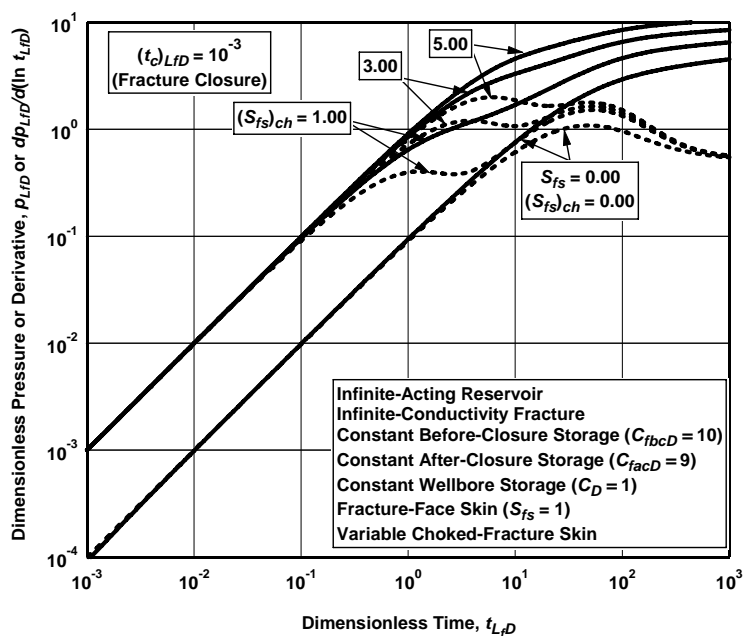


Fig. 3.6—Constant-rate drawdown in an infinite-slab reservoir with constant before- and decreasing constant after-closure storage with fracture-face and choked-fracture skin.

Fig. 3.6 contains a log-log graph of dimensionless pressure versus dimensionless time for fracture-face skin of $S_{fs} = 1$ and variable choked-fracture skin, $(S_{fs})_{ch} = \{1, 3, 5\}$. Fig. 3.6 also illustrates storage appearing to increase during a constant-rate drawdown in a well with a closing fracture with choked-fracture and fracture-face skin.

3.3.3 Constant-Rate Drawdown With Constant Before-Closure Storage, Constant After-Closure Wellbore Storage, and After-Closure Radial Flow With Skin. The constant-rate drawdown solution for a well with an open fracture that closes during the drawdown with fracture flow and fracture storage before closure and radial flow with wellbore storage and skin after closure is written as

$$p_{wcD}(t_{LjD}) = \left[\begin{array}{l} p_{fD}(t_{LjD}) - p_{fD} [t_{LjD} - (t_c)_{LjD}] + p_{sD} [t_{LjD} - (t_c)_{LjD}] \\ -C_{acD} \int_0^{t_{LjD}} p'_{wcD}(\tau_D) p'_{sD}(t_{LjD} - \tau_D) d\tau_D \\ -C_{acD} \int_0^{(t_c)_{LjD}} p'_{wcD}(\tau_D) p'_{sD}(t_{LjD} - \tau_D) d\tau_D \\ -C_{bcD} \int_0^{(t_c)_{LjD}} p'_{wcD}(\tau_D) p'_{fD}(t_{LjD} - \tau_D) d\tau_D \end{array} \right] \dots\dots\dots (3.43)$$

After integrating-by-parts, the solution is written as

$$p_{wcD}(t_{LjD}) = \left[\begin{array}{l} p_{fD}(t_{LjD}) - p_{fD} [t_{LjD} - (t_c)_{LjD}] + p_{sD} [t_{LjD} - (t_c)_{LjD}] \\ - \left(C_{acD} p_{sD} [t_{LjD} - (t_c)_{LjD}] - C_{bcD} p_{fD} [t_{LjD} - (t_c)_{LjD}] \right) p'_{wcD} [(t_c)_{LjD}] \\ -C_{acD} \int_0^{t_{LjD}} p''_{wcD}(\tau_D) p_{sD}(t_{LjD} - \tau_D) d\tau_D \\ -C_{acD} \int_0^{(t_c)_{LjD}} p''_{wcD}(\tau_D) p_{sD}(t_{LjD} - \tau_D) d\tau_D \\ -C_{bcD} \int_0^{(t_c)_{LjD}} p''_{wcD}(\tau_D) p_{fD}(t_{LjD} - \tau_D) d\tau_D \end{array} \right], \dots\dots\dots (3.44)$$

and after discretizing the integrals, a numerical approximation is written as

$$\begin{aligned}
p_{wcd}(t_{LjD})_n = & \left[\begin{aligned} & p_{jD}(t_{LjD})_n - p_{jD}[(t_{LjD})_n - (t_{LjD})_{ne}] + p_{sD}[(t_{LjD})_n - (t_{LjD})_{ne}] \\ & - \left(C_{acD} p_{sD} [(t_{LjD})_n - (t_{LjD})_{ne}] \right) \left(\frac{p_{wcd}(t_{LjD})_{ne} - p_{wcd}(t_{LjD})_{ne-1}}{(t_{LjD})_{ne} - (t_{LjD})_{ne-1}} \right) \\ & - C_{bcD} p_{jD} [(t_{LjD})_n - (t_{LjD})_{ne}] \left[\begin{aligned} & \left[\left(\frac{p_{wcd}(t_{LjD})_i - p_{wcd}(t_{LjD})_{i-1}}{(t_{LjD})_i - (t_{LjD})_{i-1}} \right) \right] \\ & - \left(\frac{p_{wcd}(t_{LjD})_{i-1} - p_{wcd}(t_{LjD})_{i-2}}{(t_{LjD})_{i-1} - (t_{LjD})_{i-2}} \right) \right] \\ & \times p_{sD} [(t_{LjD})_n - (t_{LjD})_{i-1}] \end{aligned} \right] \\ & + \sum_{i=1}^{ne} \left[\begin{aligned} & \left[\left(\frac{p_{wcd}(t_{LjD})_i - p_{wcd}(t_{LjD})_{i-1}}{(t_{LjD})_i - (t_{LjD})_{i-1}} \right) \right] \\ & - \left(\frac{p_{wcd}(t_{LjD})_{i-1} - p_{wcd}(t_{LjD})_{i-2}}{(t_{LjD})_{i-1} - (t_{LjD})_{i-2}} \right) \right] \\ & \times \left(C_{acD} p_{sD} [(t_{LjD})_n - (t_{LjD})_{i-1}] - C_{bcD} p_{jD} [(t_{LjD})_n - (t_{LjD})_{i-1}] \right) \end{aligned} \right] \end{aligned} \right] \dots (3.45)
\end{aligned}$$

Fig. 3.7 is a log-log graph of dimensionless pressure versus dimensionless time for before-closure fracture flow with constant before-closure storage, $C_{bcD} = 10$, and constant after-closure wellbore storage, $C_D = 1$ with radial flow and no skin, $S = 0$. Before closure, the reservoir produces through an infinite-conductivity fracture, which is modeled in the Laplace domain as⁹⁵

$$\bar{p}_{jD} = \frac{1}{2s\sqrt{u}} \left[\int_0^{\sqrt{u}(1+0.732)} K_0[z] dz + \int_0^{\sqrt{u}(1-0.732)} K_0[z] dz \right], \dots (3.46)$$

where K_0 is the modified Bessel function of order zero and $u = sf(s)$. For a single-porosity reservoir, $f(s) = 1$, and for dual-porosity reservoir with pseudosteady-state interporosity flow, $f(s)$ is written as⁹⁶

$$f(s) = \frac{\lambda + \omega(1-\omega)s}{\lambda + (1-\omega)s}, \dots (3.47)$$

for transient interporosity flow with slab matrix blocks,⁹⁷⁻⁹⁸

$$f(s) = \omega + \sqrt{\frac{\lambda(1-\omega)}{3s}} \tanh \sqrt{\frac{3(1-\omega)s}{\lambda}}, \dots (3.48)$$

and for transient interporosity flow with spherical matrix blocks,⁹⁷⁻⁹⁸

$$f(s) = \omega + \frac{\lambda}{5s} \left[\sqrt{\frac{15(1-\omega)s}{\lambda}} \coth \sqrt{\frac{15(1-\omega)s}{\lambda}} - 1 \right]. \dots (3.49)$$

The after-closure radial flow reservoir solution is calculated with the cylindrical-source solution with skin, S , which is written in the Laplace domain as⁶⁵

$$\bar{p}_{sD} = \frac{1}{s} \frac{K_0(r_{wD}\sqrt{s})}{\sqrt{s}K_1(\sqrt{s})} + \frac{S}{s}, \quad \dots\dots\dots(3.50)$$

where K_1 is the modified Bessel function of order one.

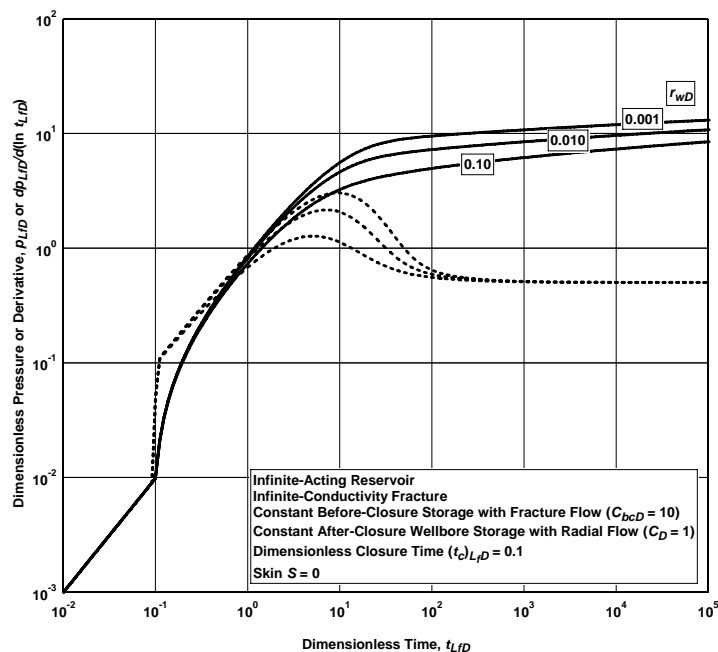


Fig. 3.7—Constant-rate drawdown in an infinite-slab reservoir with fracture flow before closure, constant before-closure storage, and radial flow after closure with wellbore storage and skin—variable dimensionless wellbore radius.

Dimensionless pressure and pressure derivative curves are presented for $r_{wD} = \{0.10, 0.010, 0.001\}$ and a dimensionless fracture closure time, $(t_c)_{LFD}$, of 0.10, which is clearly indicated by the rapid change in the derivative and dimensionless pressure values after closure. **Fig. 3.8** is a log-log graph of dimensionless pressure versus dimensionless time for $C_{bcD} = 10$, $C_D = 9$, $(t_c)_{LFD} = 0.10$, $r_{wD} = 0.005$, and variable after-closure skin. In both Figs. 3.7 and 3.8, the dimensionless pressure and pressure derivative curves after fracture closure have the distinctive shape of conventional drawdown type curves for an infinite-acting well with radial flow, wellbore storage, and skin.

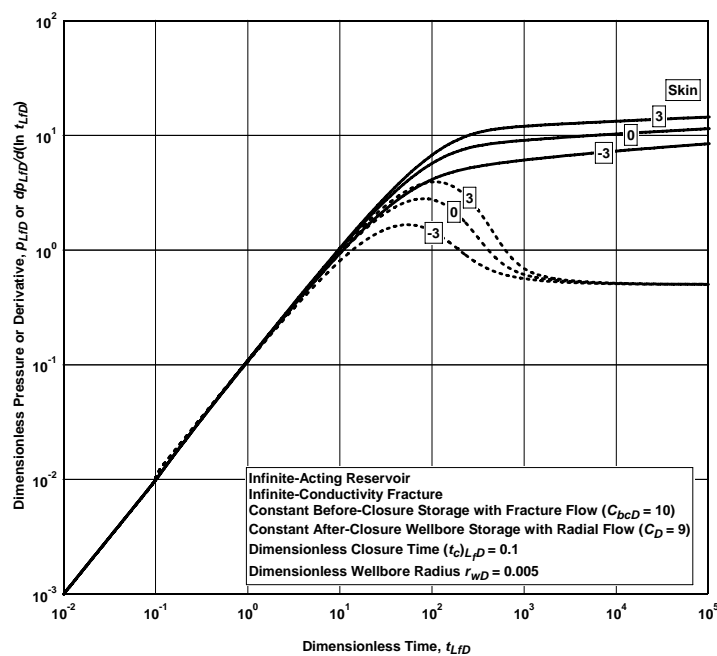


Fig. 3.8—Constant-rate drawdown in an infinite-slab reservoir with fracture flow before closure, constant before-closure storage, and radial flow after closure with wellbore storage and skin—variable skin.

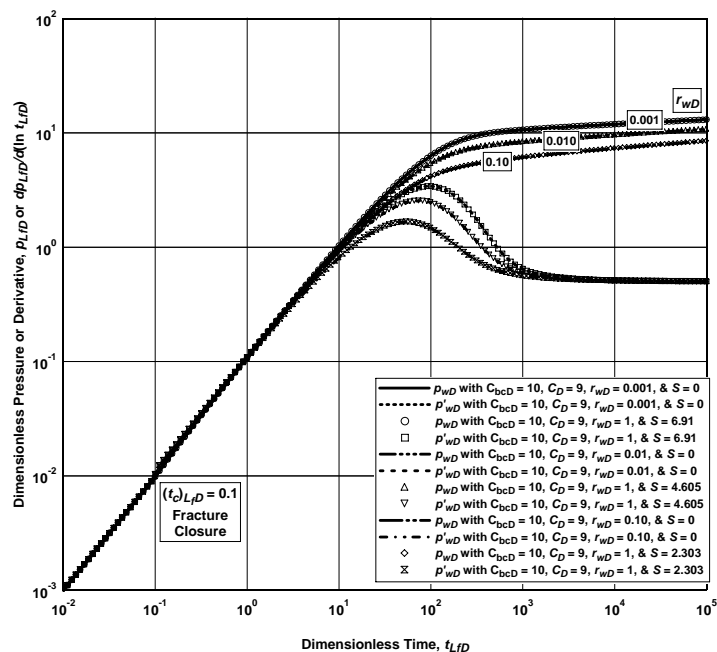


Fig. 3.9—Constant-rate drawdown in an infinite-slab reservoir with fracture flow before closure, constant before-closure storage, and radial flow after closure with wellbore storage and skin—variable dimensionless wellbore radius and approximation with $r_{wD} = 1$.

Fig. 3.9 is a log-log graph of dimensionless pressure versus dimensionless time for $C_{bcD} = 10$, $C_D = 9$, $(t_e)_{L_fD} = 0.10$, $S = 0$, and $r_{wD} = \{0.10, 0.010, 0.001\}$. From well test analysis, an effective wellbore radius is approximated as⁹⁹

$$r_{weD} = r_D e^{-S} \quad \dots\dots\dots (3.51)$$

Let $r_D = 1$ and for an effective dimensionless wellbore radius, r_{weD} , of 0.10, 0.010, and 0.001, the skin calculated from Eq. 3.46 is 2.303, 4.605 and 6.91, respectively. Fig. 3.9 also shows the dimensionless pressure and pressure derivative curves generated with $r_D = 1$ and $S = \{2.303, 4.905, 6.91\}$, which overlays the curves generated with $r_{wD} = \{0.10, 0.010, 0.001\}$ and $S = 0$. Fig. 3.9 demonstrates that when "true" skin damage is negligible, the dimensionless pressure curves can be generated with $r_D = 1$ and a skin factor determined by

$$S = -\ln(r_{wD}) \quad \dots\dots\dots (3.52)$$

Since the dimensionless radius is defined in terms of fracture half length, $r_{wD} = r_w/L_f$, Fig. 3.9 also suggests that the skin determined from a type-curve match can be used to calculate r_{wD} using Eq. 3.52 and fracture half length, L_f .

3.4 Fracture-Injection/Falloff Solutions

Current fracture-injection/falloff analysis methods⁵⁷⁻⁶¹ are based on limiting-case models of specific and small portions of the pressure response during the falloff. **Fig. 3.10** is a graph of pressure versus time for a typical field fracture-injection/falloff test in a moderate permeability gas reservoir. The injection consisted of 60.5 bbl of 2% KCl water pumped at an average rate of 6.20 bbl/min over an injection period of 9.8 minutes, and the falloff period was recorded for approximately 3.5 hours. Before-closure pressure-transient analysis⁵⁷⁻⁵⁹ for determining permeability and fracture-face resistance is applicable to the pressure data recored before hydraulic fracture closure, which for the data from the field test in Fig. 3.10 consists of only the first 5 minutes of shut-in data.

Permeability and reservoir pressure can be determined using after-closure analysis⁶⁰⁻⁶¹ provided pseudoradial flow is observed after fracture closure, but observing pseudoradial flow can require an excessive shut-in time. **Fig. 3.11**, for example, is a graph of pressure versus time for the field example, but the shut-in pressure data are extrapolated from 3.5 hr to 60 hr, which corresponds to the calculated beginning of pseudoradial flow.

With only before-closure and after-closure analysis methods available, only the data in those specific flow regimes can be analyzed, and the vast majority of the shut-in data cannot be analyzed quantitatively. Analyzing the entire pressure falloff dataset requires a new model that accounts for fracture creation, fracture closure, and after-closure pressure diffusion.

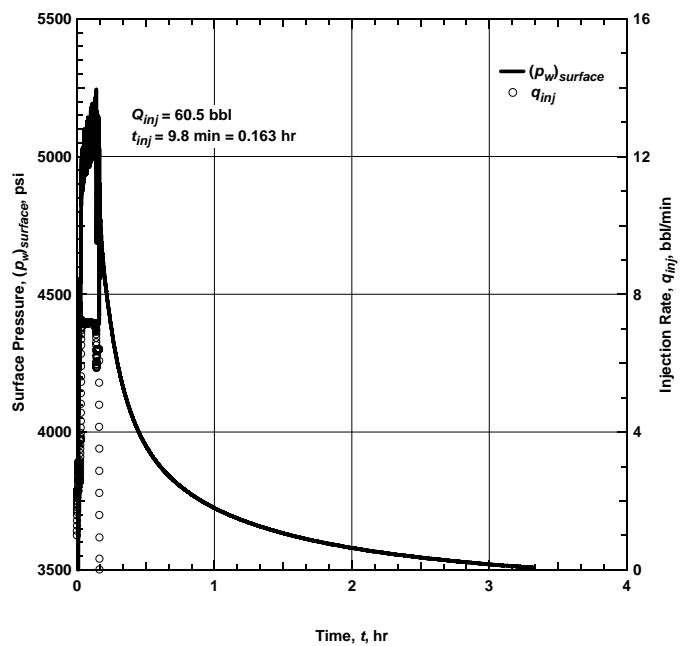


Fig. 3.10—A typical fracture-injection/falloff sequence in a moderate-permeability gas reservoir.

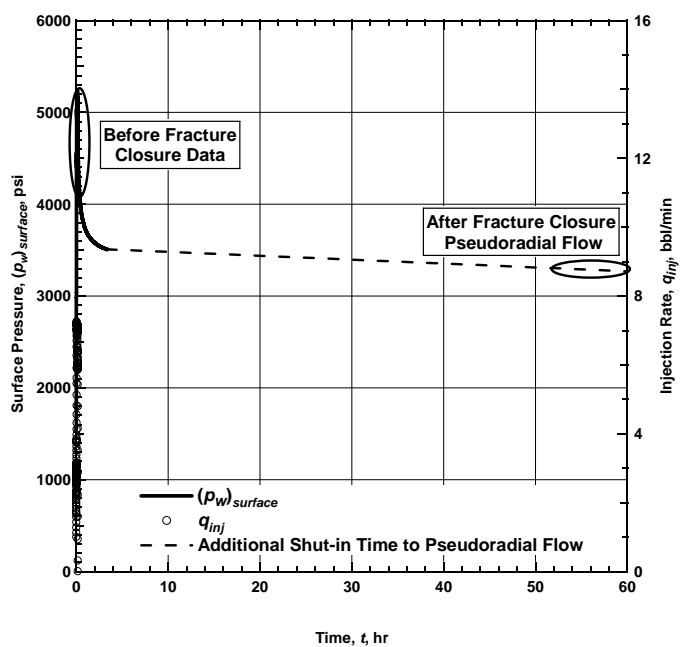


Fig. 3.11—Pressure extrapolated to beginning of pseudoradial flow.

3.4.1 Solution Accounting for a Dilating Fracture, Before-Closure Storage, and After-Closure Storage. Consider a fracture-injection/falloff test with the entire fracture length developed instantaneously when the injection begins. The injection is at a pressure in excess of the minimum in-situ stress, and fracture volume changes are a function of fracture width, which is a function of pressure during the injection and before-closure pressure falloff. Fracture dilation is modeled as time-dependent storage in the dimensionless pressure solution development, which is derived in detail in **Appendix C**.

During a constant-rate injection with a constant fracture length, the fracture volume of one wing is written as

$$V_f = h_f L_f \hat{w}_f(p_w(t)) = A_f \hat{w}_f(p_w(t)) \quad (3.53)$$

The average fracture width, $\hat{w}_f(p_w(t))$, is a function of net pressure, $p_n = p_w(t) - p_c$, and written as^{75,80}

$$\hat{w}_f = \frac{p_n}{S_f} = \frac{p_w(t) - p_c}{S_f}, \quad (3.54)$$

where S_f is the fracture "stiffness" and p_c is the fracture closure stress. Fracture stiffness, or the inverse of fracture compliance, is defined by the elastic energy or "strain energy" created by an open fracture in a rock assuming linear elastic theory is applicable. **Table 3.1** contains the fracture stiffness definitions for three common 2D fracture models.^{80,100} In Table 3.1, E' is the plane-strain modulus, R_f is the fracture radius of a radial fracture, and h_f is the gross fracture height.

Table 3.1—Fracture stiffness for common two-dimensional fracture models.^{80,100}

Radial	Perkins-Kern-Nordgren Vertical Plane Strain	Geertsma-deKlerk Horizontal Plane Strain
$(S_f)_{RAD} = \frac{3\pi E'}{16R_f}$	$(S_f)_{PKN} = \frac{2E'}{\pi h_f}$	$(S_f)_{GDK} = \frac{E'}{\pi L_f}$

The derivative of average fracture width with respect to pressure is written as

$$\frac{d\hat{w}_f}{dp_w} = \frac{1}{S_f} \quad (3.55)$$

A propagating-fracture storage coefficient is defined as

$$C_{pf} = c_w V_w + 2c_f V_f(p_w(t)) + 2 \frac{dV_f(p_w(t))}{dp_w}, \quad (3.56)$$

and a dilating-fracture storage coefficient can be written as

$$C_{fd} = c_w V_w + 2 \frac{A_f}{S_f} (c_f p_n + 1) \quad (3.57)$$

Typically, $c_f p_n(t) \ll 1$,^{90-93,101} and the dilating-fracture storage coefficient can be written as

$$C_{fd} = c_w V_w + 2 \frac{A_f}{S_f} \quad (3.58)$$

The dimensionless dilating-fracture storage coefficient can be written as

$$C_{fdD} = \frac{C_{fd}}{2\pi\phi c_l h L_f^2} \quad (3.59)$$

and the dimensionless material balance equation during a fracture injection with a dilating fixed-length fracture is written as

$$q_D = q_{wD} - C_{fdD} \frac{dp_{wD}}{dt_{LfD}} \quad (3.60)$$

where dimensionless wellbore pressure for a fracture-injection falloff is defined as

$$p_{wsD}(t_{LfD}) = \frac{p_w(t_{LfD}) - p_i}{p_0 - p_i} \quad (3.61)$$

where p_i is the initial reservoir pressure and p_0 is an arbitrary reference pressure. At time zero, the wellbore pressure is increased to the “opening” pressure, p_{w0} , which is generally set equal to p_0 , and the dimensionless wellbore pressure at time zero is written as

$$p_{wsD}(0) = \frac{p_{w0} - p_i}{p_0 - p_i} \quad (3.62)$$

In the material balance equation, dimensionless sandface flow rate is written as

$$q_D = \frac{q_{sf} B \mu}{2\pi k h (p_0 - p_i)} \quad (3.63)$$

and the dimensionless well flow rate is defined as

$$q_{wD} = \frac{q_w B \mu}{2\pi k h (p_0 - p_i)} \quad (3.64)$$

Following the injection, the falloff portion of the test begins, and a dimensionless before-closure material balance is written as

$$q_D = -C_{bcD} \frac{dp_{wsD}}{dt_{LfD}} \quad (3.65)$$

where the dimensionless before-closure storage coefficient is written as

$$C_{bcD} = \frac{C_{bc}}{2\pi\phi c_t h L_f^2}, \dots\dots\dots(3.66)$$

and the before-closure storage coefficient is equivalent to the dilating-fracture storage coefficient and written as

$$C_{bc} = c_w V_w + 2 \frac{A_f}{S_f} = C_{fd}. \dots\dots\dots(3.67)$$

After fracture closure a constant after-closure storage coefficient is written as

$$C_{ac} = c_w V_w + 2c_f V_{fr}, \dots\dots\dots(3.68)$$

where V_{fr} is the residual fracture volume at closure. In some cases, no residual volume will remain after-closure, and $C_{ac} = c_w V_w$. The dimensionless after-closure wellbore storage coefficient is written as

$$C_{acD} = \frac{C_{ac}}{2\pi\phi c_t h L_f^2}, \dots\dots\dots(3.69)$$

and the after-closure pressure falloff dimensionless material balance equation is written as

$$q_D = -C_{acD} \frac{dp_{wsD}}{dt_{Lfd}}. \dots\dots\dots(3.70)$$

Following the method of Correa and Ramey,⁶²⁻⁶⁴ and as shown in Appendix C, the dimensionless pressure solution for a fracture-injection/falloff with a dilating fracture during the injection and a constant dimensionless after-closure storage coefficient is written as

$$p_{wsD}(t_{Lfd}) = \left[q_{wD} \left[p_{acD}(t_{Lfd}) - p_{acD}(t_{Lfd} - (t_e)_{Lfd}) \right] + p_{wsD}(0) C_{acD} p'_{acD}(t_{Lfd}) \right] \left[- (C_{bcd} - C_{acD}) \int_0^{(t_c)_{Lfd}} p'_{acD}(t_{Lfd} - \tau_D) p'_{wsD}(\tau_D) d\tau_D \right], \dots\dots\dots(3.71)$$

where the Laplace domain dimensionless fracture solution for a well produced at a constant rate with constant after-closure storage is written as

$$\bar{p}_{acD} = \frac{\bar{p}_{fd}}{1 + s^2 C_{acD} \bar{p}_{fd}}, \dots\dots\dots(3.72)$$

and the dimensionless reservoir pressure solution is for a fixed-length finite- or infinite-conductivity fracture.

3.4.2 Solution Accounting for a Propagating Fracture, Constant Before-Closure Storage, and Constant After-Closure Storage. A new fracture-injection/falloff model accounting for fracture propagation, closure, and after-closure diffusion is developed that includes a time-dependent storage term during fracture extension in addition to a constant before-closure storage coefficient and a constant after-closure storage coefficient. A dimensionless material balance equation applicable during the injection and fracture creation is derived in **Appendix C** and is written as

$$q_{sD} = q_{wsD} - C_{pfD}(p_{wD}(t_{LFD})) \frac{dp_{wD}}{dt_{LFD}} \dots\dots\dots (3.73)$$

Utilizing the superposition principle to develop a dimensionless pressure solution requires that the dimensionless propagating fracture storage coefficient be written as a function of time only. The storage coefficient can be written as a function of time by incorporating a power model for fracture growth.^{75,77} Power-model fracture propagation is written as

$$\frac{A(t)}{A_f(t_e)} = \frac{h_f L(t)}{h_f L_f} = \left(\frac{t}{t_e} \right)^{\alpha N} \dots\dots\dots (3.74)$$

With power-model propagation, fracture volume as a function of time is written as

$$V_f(p_w(t)) = h_f L(t) \hat{w}_f(t) = h_f L_f \frac{(p_w(t) - p_c)}{S_f} \left(\frac{t}{t_e} \right)^{\alpha N}, \dots\dots\dots (3.75)$$

and the derivative with respect to wellbore pressure is written as

$$\frac{dV_f(p_w(t))}{dp_w} = \frac{h_f L_f}{S_f} \left(\frac{t}{t_e} \right)^{\alpha N} \dots\dots\dots (3.76)$$

A propagating-fracture storage coefficient is written as

$$C_{pf}(p_w(t)) = c_w V_w + 2c_f V_f(p_w(t)) + 2 \frac{dV_f(p_w(t))}{dp_w}, \dots\dots\dots (3.77)$$

which with power-model fracture propagation can be written as

$$C_{pf}(p_w(t)) = c_w V_w + 2 \frac{h_f L_f}{S_f} \left(\frac{t}{t_e} \right)^{\alpha N} (c_f p_n + 1). \dots\dots\dots (3.78)$$

As previously noted, $c_{pn}(t) \ll 1$,^{90-93,101} and the propagating-fracture storage coefficient is written as a function of dimensionless time only as

$$C_{pf}(t_{LFD}) = c_w V_w + 2 \frac{A_f}{S_f} \left(\frac{t_{LFD}}{(t_e)_{LFD}} \right)^{\alpha N}, \dots\dots\dots (3.79)$$

and the dimensionless propagating-fracture storage coefficient is written as a function of time only as

$$C_{pfD}(t_{LFD}) = \frac{C_{pf}(t_{LFD})}{2\pi\phi c_t h L_f^2} \dots\dots\dots (3.80)$$

The material balance equation during the injection of a fracture-injection/falloff can now be written as

$$q_{sD} = q_{wsD} - C_{pfD}(t_{LFD}) \frac{dp_{wD}}{dt_{LFD}}, \dots\dots\dots (3.81)$$

and a material balance equation valid at all times for a fracture-injection/falloff test with a propagating fracture, constant before-closure storage, and constant after-closure storage is written as

$$q_{sD} = \begin{bmatrix} q_{wsD} - U(t_e)_{LjD} q_{wsD} - C_{pfd}(t_{LjD}) \frac{dp_{wsD}}{dt_{LjD}} \\ +U(t_e)_{LjD} [C_{pfd}(t_{LjD}) - C_{bcD}] \frac{dp_{wsD}}{dt_{LjD}} \\ +U(t_c)_{LjD} [C_{bcD} - C_{acD}] \frac{dp_{wsD}}{dt_{LjD}} \end{bmatrix} \dots\dots\dots (3.82)$$

Developing a solution requires an approach similar to the dilated fracture case, but with the fracture half-length increasing during the injection, a dimensionless pressure solution is required for both a propagating and fixed-length fracture half-length. The dimensionless material balance equation can be split into injection and falloff parts by writing as

$$q_{sD} = q_{pfd} + q_{fd}, \dots\dots\dots (3.83)$$

where the dimensionless material balance equation describing the injection, but valid for all time, is written as

$$q_{pfd} = \left(1 - U(t_e)_{LjD}\right) \left(q_{wsD} - C_{pfd}(t_{LjD}) \frac{dp_{wsD}}{dt_{LjD}} \right), \dots\dots\dots (3.84)$$

and the dimensionless material balance equation valid for all time and describing the falloff is written as

$$q_{fd} = U(t_c)_{LjD} (C_{bcD} - C_{acD}) \frac{dp_{wsD}}{dt_{LjD}} - U(t_e)_{LjD} C_{bcD} \frac{dp_{wsD}}{dt_{LjD}}. \dots\dots\dots (3.85)$$

A dimensionless pressure solution is derived in Appendix C for a propagating fracture, $p_{pfd}(t_{LjD})$, and the propagating-fracture solution for a single vertical fracture is written as

$$p_{pfd}(t_{LjD}) = \begin{cases} p_{pfd}(t_{LjD}) & t_{LjD} < (t_e)_{LjD} \\ p_{fd}(t_{LjD}) & t_{LjD} > (t_e)_{LjD} \end{cases}, \dots\dots\dots (3.86)$$

or using the unit-step function written as

$$p_{pfd}(t_{LjD}) = \left(1 - U(t_e)_{LjD}\right) p_{pfd}(t_{LjD}) + U(t_e)_{LjD} p_{fd}(t_{LjD}). \dots\dots\dots (3.87)$$

A quasi-static solution during fracture propagation is written in the Laplace domain as

$$\bar{p}_{pfd} = \frac{1}{L_{jD}(t_{LjD})} \frac{1}{2s\sqrt{u}} \left[\int_0^{\sqrt{u}L_{jD}(t_{LjD})(1+0.732)} K_0[z] dz + \int_0^{\sqrt{u}L_{jD}(t_{LjD})(1-0.732)} K_0[z] dz \right], \dots\dots (3.88)$$

where the dimensionless fracture half-length is defined as

$$L_{jD}(t_{LjD}) = \begin{cases} \left(\frac{t_{LjD}}{(t_e)_{LjD}} \right)^{\alpha_N} & t_{LjD} < (t_e)_{LjD} \\ 1 & t_{LjD} \geq (t_e)_{LjD} \end{cases}, \dots\dots\dots (3.89)$$

Appendix C describes the development of the quasi-static solution.

The reservoir solution with a constant fracture half length, $p_{pD}(t_{LFD})$, results when $t_{LFD} \geq (t_e)_{LFD}$ or when the fracture-growth exponent is set equal to zero, $\alpha_N = 0$. The two different reservoir models can be superposed¹⁰² to develop a dimensionless wellbore pressure solution by writing the superposition integrals as

$$p_{wsD} = \int_0^{t_{LFD}} q_{pFD}(\tau_D) \frac{dp_{pFD}(t_{LFD} - \tau_D)}{dt_{LFD}} d\tau_D + \int_0^{t_{LFD}} q_{fD}(\tau_D) \frac{dp_{fD}(t_{LFD} - \tau_D)}{dt_{LFD}} d\tau_D \dots\dots\dots (3.90)$$

The solution for a fracture-injection/falloff with a propagating fracture with constant before- and after-closure storage is developed in the Laplace domain, and after inverting to the time domain is written as

$$p_{wsD}(t_{LFD}) = \left[\begin{array}{l} q_{wsD} [p_{pFD}(t_{LFD}) - p_{pFD}(t_{LFD} - (t_e)_{LFD})] \\ -C_{acD} \int_0^{t_{LFD}} p'_{fD}(t_{LFD} - \tau_D) p'_{wsD}(\tau_D) d\tau_D \\ - \int_0^{(t_e)_{LFD}} p'_{pFD}(t_{LFD} - \tau_D) C_{pFD}(\tau_D) p'_{wsD}(\tau_D) d\tau_D \\ + C_{bcD} \int_0^{(t_e)_{LFD}} p'_{fD}(t_{LFD} - \tau_D) p'_{wsD}(\tau_D) d\tau_D \\ - (C_{bcD} - C_{acD}) \int_0^{(t_c)_{LFD}} p'_{fD}(t_{LFD} - \tau_D) p'_{wsD}(\tau_D) d\tau_D \end{array} \right] \dots\dots\dots (3.91)$$

3.4.3 Solution Accounting for a Propagating Fracture, Before-Closure Storage, Constant After-Closure Storage, and After-Closure Radial Flow. All solutions presented thus far assume flow at the sandface is through a hydraulic fracture, but after fracture closure with little or no fracture conductivity remaining, the effect of the induced fracture can be negligible and the reservoir should be modeled as a radial system. While the material balance for all time for a case with a propagating fracture, constant before-closure storage, and constant after-closure storage is unchanged, the pressure solution requires the introduction of a radial reservoir flow model after fracture closure. The dimensionless wellbore pressure is the sum of superposition integrals for each reservoir model and is written as

$$p_{wsD} = \sum_{j=1}^3 \int_0^{t_{LFD}} q_{Dj} p'_{Dj}(t_{LFD} - \tau_D) d\tau_D, \dots\dots\dots (3.92)$$

or expanded and written as

$$p_{wsD} = \left[\begin{array}{l} \int_0^{t_{LFD}} q_{pFD} p'_{pFD}(t_{LFD} - \tau_D) d\tau_D \\ + \int_0^{t_{LFD}} q_{fD} p'_{fD}(t_{LFD} - \tau_D) d\tau_D \\ + \int_0^{t_{LFD}} q_{rD} p'_{sD}(t_{LFD} - \tau_D) d\tau_D \end{array} \right], \dots\dots\dots (3.93)$$

where q_{rD} is the after-closure dimensionless flow rate for the radial system and the radial flow pressure solution with skin, p_{sD} , is written as

$$p_{sD}(t_{LfD}) = p_{rD}(t_{LfD}) + S \dots\dots\dots (3.94)$$

Note that dimensionless time is defined in terms of the fracture half-length; thus, fracture half-length is the characteristic length used in the dimensionless radius definition and radial solution.

A solution is obtained by transforming the dimensionless wellbore pressure equation to the Laplace domain and combining with the dimensionless flow rate equations valid for each flow model. The dimensionless flow rate equation for the fracture injection (propagation model) is written as

$$q_{pfD} = \left(1 - U(t_e)_{LfD}\right) \left(q_{wsD} - C_{pfD}(t_{LfD}) \frac{dp_{wsD}}{dt_{LfD}} \right), \dots\dots\dots (3.95)$$

and the flow rate equation for a fixed-length closing fracture is written as

$$q_{fD} = - \left(U(t_e)_{LfD} - U(t_c)_{LfD} \right) C_{bcD} \frac{dp_{wsD}}{dt_{LfD}} \dots\dots\dots (3.96)$$

The dimensionless after-closure radial flow rate is written as

$$q_{rD} = -U(t_c)_{LfD} C_D \frac{dp_{wsD}}{dt_{LfD}}, \dots\dots\dots (3.97)$$

where the dimensionless after-closure wellbore storage coefficient is defined as

$$C_D = \frac{c_w V_w}{2\pi\phi c_t h L_f^2} \dots\dots\dots (3.98)$$

After transforming to the Laplace domain, simplifying, and inverting to the time domain, the dimensionless wellbore pressure solution for a fracture-injection/falloff test with a propagating fracture during the injection, constant before-closure storage, constant after-closure wellbore storage, and after-closure radial flow with skin is written as

$$p_{wsD} = \left[\begin{array}{l} q_{wsD} \left[p_{pfD}(t_{LfD}) - p_{pfD}(t_{LfD} - (t_e)_{LfD}) \right] \\ - C_D \int_0^{t_{LfD}} p'_{sD}(t_{LfD} - \tau_D) p'_{wsD}(\tau_D) d\tau_D \\ - \int_0^{(t_e)_{LfD}} p'_{pfD}(t_{LfD} - \tau_D) C_{pfD}(\tau_D) p'_{wsD}(\tau_D) d\tau_D \\ + C_{bcD} \int_0^{(t_e)_{LfD}} p'_{fD}(t_{LfD} - \tau_D) p'_{wsD}(\tau_D) d\tau_D \\ + C_D \int_0^{(t_c)_{LfD}} p'_{sD}(t_{LfD} - \tau_D) p'_{wsD}(\tau_D) d\tau_D \\ - C_{bcD} \int_0^{(t_c)_{LfD}} p'_{fD}(t_{LfD} - \tau_D) p'_{wsD}(\tau_D) d\tau_D \end{array} \right] \dots\dots\dots (3.99)$$

3.5 Fracture-Injection/Falloff Limiting Solutions

3.5.1 Limiting-Case Solutions With a Dilating Fracture, Before-Closure Storage, and After-Closure Storage. The dimensionless wellbore pressure solution for a fracture-injection/falloff with a dilating fracture during the injection, constant before-closure storage, and constant after-closure storage is written as

$$p_{wsD}(t_{LjD}) = \left[q_{wD} \left[p_{acD}(t_{LjD}) - p_{acD}(t_{LjD} - (t_e)_{LjD}) \right] + p_{wsD}(0) C_{acD} p'_{acD}(t_{LjD}) \right. \\ \left. - (C_{bcD} - C_{acD}) \int_0^{(t_c)_{LjD}} p'_{acD}(t_{LjD} - \tau_D) p'_{wsD}(\tau_D) d\tau_D \right], \dots\dots\dots (3.100)$$

where the Laplace domain dimensionless fracture solution for a well produced at a constant rate with constant after-closure storage is written as

$$\bar{p}_{acD} = \frac{\bar{p}_{jD}}{1 + s^2 C_{acD} \bar{p}_{jD}} \dots\dots\dots (3.101)$$

Consider a limiting case where $t_{LjD} > (t_e)_{LjD}$ such that $p_{acD}(t_{LjD}) - p_{acD}(t_{LjD} - (t_e)_{LjD}) \approx 0$, and the dimensionless wellbore pressure solution can be written as

$$p_{wsD}(t_{LjD}) = \left[p_{wsD}(0) C_{acD} p'_{acD}(t_{LjD}) \right. \\ \left. - (C_{bcD} - C_{acD}) \int_0^{(t_c)_{LjD}} p'_{acD}(t_{LjD} - \tau_D) p'_{wsD}(\tau_D) d\tau_D \right] \dots\dots\dots (3.102)$$

When $C_{bcD} = C_{acD}$, the solution reduces to

$$p_{wsD}(t_{LjD}) = p_{wsD}(0) C_{acD} p'_{acD}(t_{LjD}), \dots\dots\dots (3.103)$$

which is the slug-test solution for a hydraulically fractured well with constant storage as defined by Rushing *et al.*⁶⁷

When $C_{bcD} \neq C_{acD}$ and $t_{LjD} < (t_c)_{LjD}$, the dimensionless wellbore pressure solution can be written as

$$p_{wsD}(t_{LjD}) = \left[p_{wsD}(0) C_{acD} p'_{acD}(t_{LjD}) \right. \\ \left. - (C_{bcD} - C_{acD}) \int_0^{t_{LjD}} p'_{acD}(t_{LjD} - \tau_D) p'_{wsD}(\tau_D) d\tau_D \right], \dots\dots\dots (3.104)$$

which after transforming to the Laplace domain is written as

$$\bar{p}_{wsD} = \left[p_{wsD}(0) C_{acD} \bar{s} \bar{p}_{acD} \right. \\ \left. - (C_{bcD} - C_{acD}) \left[\bar{s} \bar{p}_{acD} (s \bar{p}_{wsD} - p_{wsD}(0)) \right] \right] \dots\dots\dots (3.105)$$

After expanding the terms and simplifying, the solution can be written as

$$\bar{p}_{wsD} = p_{wsD}(0) C_{bcD} s \left(\frac{\bar{p}_{acD}}{1 + s^2 (C_{bcD} - C_{acD}) \bar{p}_{acD}} \right), \dots\dots\dots (3.106)$$

but with the Laplace domain dimensionless fracture solution for a well produced at a constant rate with constant after-closure storage given in Eq. 3.101, the pressure solution can be simplified and written as

$$\bar{p}_{wsD} = p_{wsD}(0)C_{bcD}s \left(\frac{\bar{p}_{fD}}{1+s^2C_{bcD}\bar{p}_{fD}} \right) \dots\dots\dots (3.107)$$

Define a Laplace domain dimensionless fracture solution for a well produced at a constant rate with constant before-closure storage as

$$\bar{p}_{bcD} = \frac{\bar{p}_{fD}}{1+s^2C_{bcD}\bar{p}_{fD}}, \dots\dots\dots (3.108)$$

and the before-closure limiting-case dimensionless wellbore pressure solution is written in the Laplace domain as

$$\bar{p}_{wsD} = p_{wsD}(0)C_{bcD}s\bar{p}_{bcD} \dots\dots\dots (3.109)$$

After inverting to the time domain, the solution is written as

$$p_{wsD}(t_{LjD}) = p_{wsD}(0)C_{bcD}p'_{bcD}(t_{LjD}), \dots\dots\dots (3.110)$$

which is the slug-test solution for a hydraulically fractured well with constant before-closure storage.

When $C_{bcD} \neq C_{acD}$ and $t_{LjD} \gg (t_c)_{LjD} > (t_e)_{LjD}$, the dimensionless wellbore pressure solution can be written as

$$p_{wsD}(t_{LjD}) = \left[\begin{array}{l} p_{wsD}(0)C_{acD}p'_{acD}(t_{LjD}) \\ -(C_{bcD} - C_{acD}) \int_0^{(t_c)_{LjD}} p'_{acD}(t_{LjD} - \tau_D) p'_{wsD}(\tau_D) d\tau_D \end{array} \right], \dots\dots\dots (3.111)$$

but with $t_{LjD} \gg (t_c)_{LjD}$, $p'_{acD}(t_{LjD} - \tau_D) \approx p'_{acD}(t_{LjD})$, and the pressure solution can be written as

$$p_{wsD}(t_{LjD}) = \left[\begin{array}{l} p_{wsD}(0)C_{acD}p'_{acD}(t_{LjD}) \\ -(C_{bcD} - C_{acD})p'_{acD}(t_{LjD}) \left[p_{wsD}((t_c)_{LjD}) - p_{wsD}(0) \right] \end{array} \right] \dots\dots\dots (3.112)$$

After expanding the terms and simplifying, the dimensionless wellbore pressure solution can be written as

$$p_{wsD}(t_{LjD}) = \left[p_{wsD}(0)C_{bcD} - p_{wsD}((t_c)_{LjD})(C_{bcD} - C_{acD}) \right] p'_{acD}(t_{LjD}), \dots\dots\dots (3.113)$$

which is a slug-test solution for a hydraulically fractured well with variable storage – constant before-closure storage and constant after-closure storage.

3.5.2 Limiting-Case Solutions With a Propagating Fracture, Before-Closure Storage, and After-Closure Storage. The dimensionless wellbore pressure solution for a fracture-injection/falloff with a propagating fracture during the injection, constant before-closure storage, and constant after-closure storage is written as

$$p_{wsD}(t_{LjD}) = \begin{bmatrix} q_{wsD} [p_{pFD}(t_{LjD}) - p_{pFD}(t_{LjD} - (t_e)_{LjD})] \\ -C_{acD} \int_0^{t_{LjD}} p'_{jD}(t_{LjD} - \tau_D) p'_{wsD}(\tau_D) d\tau_D \\ - \int_0^{(t_e)_{LjD}} p'_{pFD}(t_{LjD} - \tau_D) C_{pFD}(\tau_D) p'_{wsD}(\tau_D) d\tau_D \\ + C_{bcD} \int_0^{(t_e)_{LjD}} p'_{jD}(t_{LjD} - \tau_D) p'_{wsD}(\tau_D) d\tau_D \\ - (C_{bcD} - C_{acD}) \int_0^{(t_c)_{LjD}} p'_{jD}(t_{LjD} - \tau_D) p'_{wsD}(\tau_D) d\tau_D \end{bmatrix}, \dots\dots\dots (3.114)$$

which can also be written as

$$p_{wsD}(t_{LjD}) = \begin{bmatrix} q_{wsD} [p_{pFD}(t_{LjD}) - p_{pFD}(t_{LjD} - (t_e)_{LjD})] \\ -C_{acD} \int_0^{t_{LjD}} p'_{jD}(t_{LjD} - \tau_D) p'_{wsD}(\tau_D) d\tau_D \\ + \int_0^{(t_e)_{LjD}} [C_{bcD} p'_{jD}(t_{LjD} - \tau_D) - C_{pFD}(\tau_D) p'_{pFD}(t_{LjD} - \tau_D)] p'_{wsD}(\tau_D) d\tau_D \\ - (C_{bcD} - C_{acD}) \int_0^{(t_c)_{LjD}} p'_{jD}(t_{LjD} - \tau_D) p'_{wsD}(\tau_D) d\tau_D \end{bmatrix}. \quad (3.115)$$

When the fracture is pre-existing or the fracture half-length is created instantaneously, $C_{bcD} = C_{jD}(t_{LjD})$, and when $t_{LjD} \gg (t_e)_{LjD}$, the dimensionless wellbore pressure solution reduces to

$$p_{wsD}(t_{LjD}) = \begin{bmatrix} p_{wsD}(0) C_{acD} p'_{acD} \\ - (C_{bcD} - C_{acD}) \int_0^{(t_c)_{LjD}} p'_{acD}(t_{LjD} - \tau_D) p'_{wsD}(\tau_D) d\tau_D \end{bmatrix}, \dots\dots\dots (3.116)$$

which leads to the same limiting-case solutions as existed for a fracture-injection/falloff with a dilating fracture, constant before-closure storage, and constant after-closure storage.

Consider the integral term containing propagating-fracture storage, which is written as

$$I = \int_0^{(t_e)_{LjD}} [C_{bcD} p'_{jD}(t_{LjD} - \tau_D) - C_{pFD}(\tau_D) p'_{pFD}(t_{LjD} - \tau_D)] p'_{wsD}(\tau_D) d\tau_D. \quad \dots\dots\dots (3.117)$$

When $t_{LjD} \gg (t_e)_{LjD}$, the propagating-fracture solution derivative can be written as

$$p'_{pFD}(t_{LjD} - \tau_D) \cong p'_{pFD}(t_{LjD}), \quad \dots\dots\dots (3.118)$$

and the fracture solution derivative can also be approximated as

$$p'_{jD}(t_{LjD} - \tau_D) \cong p'_{jD}(t_{LjD}). \quad \dots\dots\dots (3.119)$$

The definition of the dimensionless propagating-fracture solution states that when $t_{LjD} > (t_e)_{LjD}$, the propagating-fracture and fracture solution are equal, and $p'_{pFD}(t_{LjD}) = p'_{jD}(t_{LjD})$. Consequently, the integral term containing the propagating-fracture storage for $t_{LjD} \gg (t_e)_{LjD}$ can be written as

$$I = p'_{jD}(t_{LjD}) \int_0^{(t_e)_{LjD}} [C_{bcD} - C_{pFD}(\tau_D)] p'_{wsD}(\tau_D) d\tau_D, \quad \dots\dots\dots (3.120)$$

and the dimensionless wellbore pressure solution can be written as

$$p_{wsD}(t_{LjD}) = \left[\begin{array}{l} p'_{fD}(t_{LjD}) \int_0^{(t_e)_{LjD}} [C_{bcD} - C_{pfD}(\tau_D)] p'_{wsD}(\tau_D) d\tau_D \\ -C_{acD} \int_0^{t_{LjD}} p'_{fD}(t_{LjD} - \tau_D) p'_{wsD}(\tau_D) d\tau_D \\ -(C_{bcD} - C_{acD}) \int_0^{(t_c)_{LjD}} p'_{fD}(t_{LjD} - \tau_D) p'_{wsD}(\tau_D) d\tau_D \end{array} \right] \dots\dots\dots (3.121)$$

The before-closure storage coefficient is by definition always greater than the propagating-fracture storage coefficient, and the difference of the two coefficients cannot be zero unless the fracture half-length is created instantaneously. However, the difference is also relatively small when compared to C_{bcD} or C_{acD} , and when the dimensionless time of injection is short and $t_{LjD} > (t_e)_{LjD}$, the integral term containing the propagating-fracture storage coefficient becomes negligibly small, which is written as

$$\left| \begin{array}{l} p'_{fD}(t_{LjD}) \int_0^{(t_e)_{LjD}} [C_{bcD} - C_{pfD}(\tau_D)] p'_{wsD}(\tau_D) d\tau_D \\ \ll \left[\begin{array}{l} -C_{acD} \int_0^{t_{LjD}} p'_{fD}(t_{LjD} - \tau_D) p'_{wsD}(\tau_D) d\tau_D \\ -(C_{bcD} - C_{acD}) \int_0^{(t_c)_{LjD}} p'_{fD}(t_{LjD} - \tau_D) p'_{wsD}(\tau_D) d\tau_D \end{array} \right] \end{array} \right| \dots\dots\dots (3.122)$$

Thus, with a short dimensionless time of injection and $(t_e)_{LjD} \ll t_{LjD} < (t_c)_{LjD}$, the limiting-case before-closure dimensionless wellbore pressure solution can be written as

$$p_{wsD}(t_{LjD}) = \left[\begin{array}{l} -C_{acD} \int_0^{t_{LjD}} p'_{fD}(t_{LjD} - \tau_D) p'_{wsD}(\tau_D) d\tau_D \\ -(C_{bcD} - C_{acD}) \int_0^{(t_c)_{LjD}} p'_{fD}(t_{LjD} - \tau_D) p'_{wsD}(\tau_D) d\tau_D \end{array} \right], \dots\dots\dots (3.123)$$

which after simplifying in the Laplace domain and inverting back to the time domain can be written as

$$p_{wsD}(t_{LjD}) = \left[\begin{array}{l} p_{wsD}(0) C_{acD} p'_{acD}(t_{LjD}) \\ -(C_{bcD} - C_{acD}) \int_0^{(t_c)_{LjD}} p'_{acD}(t_{LjD} - \tau_D) p'_{wsD}(\tau_D) d\tau_D \end{array} \right] \dots\dots\dots (3.124)$$

When $t_{LjD} < (t_c)_{LjD}$, the dimensionless wellbore pressure solution can be written as

$$p_{wsD}(t_{LjD}) = \left[\begin{array}{l} p_{wsD}(0) C_{acD} p'_{acD}(t_{LjD}) \\ -(C_{bcD} - C_{acD}) \int_0^{t_{LjD}} p'_{acD}(t_{LjD} - \tau_D) p'_{wsD}(\tau_D) d\tau_D \end{array} \right], \dots\dots\dots (3.125)$$

and as previously shown, the solution can be simplified in the Laplace domain and inverted back to the time domain to obtain the before-closure limiting-case dimensionless wellbore pressure solution written as

$$p_{wsD}(t_{LjD}) = p_{wsD}(0) C_{bcD} p'_{bcD}(t_{LjD}), \dots\dots\dots (3.126)$$

which is the slug test solution for a hydraulically fractured well with constant before-closure storage.

When the dimensionless time of injection is short and $t_{LjD} \gg (t_c)_{LjD} > (t_e)_{LjD}$, the fracture solution derivative can be approximated as

$$p'_{fD}(t_{LjD} - \tau_D) \cong p'_{fD}(t_{LjD}), \quad \dots\dots\dots (3.127)$$

and the dimensionless wellbore pressure solution can be written as

$$p_{wsD}(t_{LjD}) = \left[\begin{array}{l} p_{wsD}(0)C_{acD}p'_{acD}(t_{LjD}) \\ -(C_{bcD} - C_{acD}) \int_0^{(t_c)_{LjD}} p'_{acD}(t_{LjD} - \tau_D)p'_{wsD}(\tau_D)d\tau_D \end{array} \right], \quad \dots\dots\dots (3.128)$$

but with $t_{LjD} \gg (t_c)_{LjD}$, $p'_{acD}(t_{LjD} - \tau_D) \approx p'_{acD}(t_{LjD})$, and the dimensionless wellbore pressure solution can be written as

$$p_{wsD}(t_{LjD}) = \left[\begin{array}{l} p_{wsD}(0)C_{acD}p'_{acD}(t_{LjD}) \\ -(C_{bcD} - C_{acD})p'_{acD}(t_{LjD}) \left[p_{wsD}((t_c)_{LjD}) - p_{wsD}(0) \right] \end{array} \right] \dots\dots\dots (3.129)$$

After expanding the terms and simplifying, the dimensionless wellbore pressure solution is written as

$$p_{wsD}(t_{LjD}) = \left[p_{wsD}(0)C_{bcD} - p_{wsD}((t_c)_{LjD})(C_{bcD} - C_{acD}) \right] p'_{acD}(t_{LjD}), \quad \dots\dots\dots (3.130)$$

which is also a slug-test solution and the same as the dimensionless wellbore pressure solution for a fracture-injection/falloff with a dilating fracture, constant before-closure storage, and constant after-closure storage.

3.5.3 Limiting-Case Solutions With a Propagating Fracture, Before-Closure Storage, Constant After-Closure Storage, and After-Closure Radial Flow. The dimensionless wellbore pressure solution for a fracture-injection/falloff with a propagating fracture during the injection, constant before-closure storage, constant after-closure wellbore storage, and after-closure radial flow with skin is written as

$$p_{wsD} = \left[\begin{array}{l} q_{wsD} \left[p_{pfD}(t_{LjD}) - p_{pfD}(t_{LjD} - (t_e)_{LjD}) \right] \\ -C_D \int_0^{t_{LjD}} p'_{sD}(t_{LjD} - \tau_D)p'_{wsD}(\tau_D)d\tau_D \\ - \int_0^{(t_e)_{LjD}} p'_{pfD}(t_{LjD} - \tau_D)C_{pfD}(\tau_D)p'_{wsD}(\tau_D)d\tau_D \\ +C_{bcD} \int_0^{(t_e)_{LjD}} p'_{fD}(t_{LjD} - \tau_D)p'_{wsD}(\tau_D)d\tau_D \\ +C_D \int_0^{(t_c)_{LjD}} p'_{sD}(t_{LjD} - \tau_D)p'_{wsD}(\tau_D)d\tau_D \\ -C_{bcD} \int_0^{(t_c)_{LjD}} p'_{fD}(t_{LjD} - \tau_D)p'_{wsD}(\tau_D)d\tau_D \end{array} \right] \dots\dots\dots (3.131)$$

Consider a case with $t_{LjD} > (t_e)_{LjD}$, $p_{acD}(t_{LjD}) - p_{acD}(t_{LjD} - (t_e)_{LjD}) \approx 0$, and with a short dimensionless time of injection such that the dimensionless wellbore pressure solution can be written as

$$p_{wsD}(t_{LjD}) = \begin{bmatrix} +C_D \int_0^{(t_c)_{LjD}} p'_{sD}(t_{LjD} - \tau_D) p'_{wsD}(\tau_D) d\tau_D \\ -C_D \int_0^{t_{LjD}} p'_{sD}(t_{LjD} - \tau_D) p'_{wsD}(\tau_D) d\tau_D \\ -C_{bcD} \int_0^{(t_c)_{LjD}} p'_{fD}(t_{LjD} - \tau_D) p'_{wsD}(\tau_D) d\tau_D \end{bmatrix} \dots \dots \dots (3.132)$$

When $(t_e)_{LjD} \ll t_{LjD} < (t_c)_{LjD}$, the dimensionless wellbore pressure solution can be written as

$$p_{wsD}(t_{LjD}) = -C_{bcD} \int_0^{t_{LjD}} p'_{fD}(t_{LjD} - \tau_D) p'_{wsD}(\tau_D) d\tau_D, \dots \dots \dots (3.133)$$

which can be transformed to the Laplace domain, simplified, and inverted back to the time domain as

$$p_{wsD}(t_{LjD}) = p_{wsD}(0) C_{bcD} p'_{bcD}(t_{LjD}). \dots \dots \dots (3.134)$$

When the dimensionless time of injection is short and $t_{LjD} \gg (t_c)_{LjD} > (t_e)_{LjD}$, the fracture solution derivative can be approximated as

$$p'_{fD}(t_{LjD} - \tau_D) \cong p'_{fD}(t_{LjD}), \dots \dots \dots (3.135)$$

and the radial-flow solution derivative is similarly approximated as

$$p'_{sD}(t_{LjD} - \tau_D) \cong p'_{sD}(t_{LjD}), \dots \dots \dots (3.136)$$

which allows the dimensionless wellbore pressure solution to be written as

$$p_{wsD}(t_{LjD}) = \begin{bmatrix} +C_D p'_{sD}(t_{LjD}) \left[p_{wsD}((t_c)_{LjD}) - p_{wsD}(0) \right] \\ -C_D \int_0^{t_{LjD}} p'_{sD}(t_{LjD} - \tau_D) p'_{wsD}(\tau_D) d\tau_D \\ -C_{bcD} p'_{fD}(t_{LjD}) \left[p_{wsD}((t_c)_{LjD}) - p_{wsD}(0) \right] \end{bmatrix} \dots \dots \dots (3.137)$$

After transforming the solution to the Laplace domain, simplifying, and inverting back to the time domain, the dimensionless wellbore pressure solution is written as

$$p_{wsD}(t_{LjD}) = \begin{bmatrix} p_{wsD}(0) C_D p'_{sacD}(t_{LjD}) \\ - \left[p_{wsD}((t_c)_{LjD}) - p_{wsD}(0) \right] \left(C_{bcD} p'_{facD}(t_{LjD}) - C_D p'_{sacD}(t_{LjD}) \right) \end{bmatrix} \dots \dots \dots (3.138)$$

where the radial flow solution with skin and constant after-closure wellbore storage is written in the Laplace domain as

$$\bar{p}_{sacD} = \frac{\bar{p}_{sD}}{1 + s^2 C_D \bar{p}_{sD}}, \dots \dots \dots (3.139)$$

and a hybrid fracture-flow solution with constant storage is written in the Laplace domain as

$$\bar{p}_{facD} = \frac{\bar{p}_{fD}}{1 + s^2 C_D \bar{p}_{sD}} \dots \dots \dots (3.140)$$

As dimensionless time becomes large, the influence of wellbore storage on the dimensionless pressure diminishes such that $p_{sacD}(t_{LjD}) \approx p_{sD}(t_{LjD})$, $p_{facD}(t_{LjD}) \approx p_{fD}(t_{LjD})$. Additionally, the derivative of the solutions at large dimensionless times are equal, which allows the dimensionless wellbore pressure solution to be written as

$$p_{wsD}(t_{LjD}) = \left[\begin{array}{l} p_{wsD}(0)C_D p'_{sacD}(t_{LjD}) \\ -(C_{bcD} - C_D) p'_{sacD}(t_{LjD}) \left[p_{wsD}(t_c)_{LjD} - p_{wsD}(0) \right] \end{array} \right] \dots \dots \dots (3.141)$$

After expanding the terms and simplifying, the dimensionless wellbore pressure solution is written as

$$p_{wsD}(t_{LjD}) = \left[p_{wsD}(0)C_{bcD} - p_{wsD}(t_c)_{LjD} \right] (C_{bcD} - C_D) p'_{sacD}(t_{LjD}), \dots \dots \dots (3.142)$$

which is also a slug-test solution.

3.5.4 Limiting-Case Solutions With a Large Dimensionless Time of Injection. All previous limiting-case solutions have assumed the dimensionless time of injection is small, but in many cases, for example, a pressure falloff test with waterflood-induced fractures, the dimensionless time of injection can be quite large. Consider a fracture-injection/falloff with a dilating fracture during the injection, constant before-closure storage, and constant after-closure storage. The dimensionless wellbore pressure solution is written as

$$p_{wsD}(t_{LjD}) = \left[\begin{array}{l} q_{wD} \left[p_{acD}(t_{LjD}) - p_{acD}(t_{LjD} - (t_e)_{LjD}) \right] + p_{wsD}(0)C_{acD} p'_{acD}(t_{LjD}) \\ -(C_{bcD} - C_{acD}) \int_0^{(t_c)_{LjD}} p'_{acD}(t_{LjD} - \tau_D) p'_{wsD}(\tau_D) d\tau_D \end{array} \right] \dots \dots \dots (3.143)$$

With a large dimensionless time of injection and $t_{LjD} \gg (t_e)_{LjD}$, $p'_{acD}(t_{LjD} - \tau_D) \approx p'_{acD}(t_{LjD})$ and the solution can be written as

$$p_{wsD}(t_{LjD}) = \left[\begin{array}{l} q_{wD} \left[p_{acD}(t_{LjD}) - p_{acD}(t_{LjD} - (t_e)_{LjD}) \right] + p_{wsD}(0)C_{acD} p'_{acD}(t_{LjD}) \\ - \left[p_{wsD}(t_c)_{LjD} - p_{wsD}(0) \right] (C_{bcD} - C_{acD}) p'_{acD}(t_{LjD}) \end{array} \right] \dots \dots \dots (3.144)$$

Following the logic of Correa and Ramey,⁶² a long-time approximation for the dimensionless wellbore pressure is developed by recognizing that as dimensionless time increases, the effect of after-closure storage becomes minimal and $p_{facD}(t_{LjD}) \approx p_{fD}(t_{LjD})$. A long-time approximation for the dimensionless fracture-flow solution is written as⁸⁴

$$p_{fD}(t_{LjD}) = \frac{1}{2} (\ln t_{LjD} + 2.80907), \dots \dots \dots (3.145)$$

with a derivative with respect to time defined as

$$p'_{fD}(t_{LjD}) = \frac{1}{2t_{LjD}} \dots \dots \dots (3.146)$$

With the fracture-flow solution, derivative, and as dimensionless time increases, the terms containing storage tend to zero, and the dimensionless wellbore pressure solution can be written as

$$p_{wsD}(t_{Lfd}) = \frac{q_{wD}}{2} \ln \left(\frac{t_{Lfd}}{t_{Lfd} - (t_e)_{Lfd}} \right), \dots\dots\dots (3.147)$$

which is equivalent to the traditional long-time solution for a pressure buildup with the dimensionless time of production, $(t_p)_{Lfd}$, used in place of the dimensionless time of injection, $(t_e)_{Lfd}$.

3.6 Numerical Evaluation of a Fracture-Injection/Falloff Analytical Solution

Numerical evaluations of a fracture-injection/falloff solution are provided to quantify a "small" dimensionless time of injection and to establish when the time of a fracture-injection can be considered short relative to the reservoir response.

The dimensionless wellbore pressure solution for a fracture-injection/falloff with a dilating fracture during the injection, constant before-closure storage, and constant after-closure storage is written as

$$p_{wsD}(t_{Lfd}) = \left[\begin{aligned} & q_{wD} [p_{acD}(t_{Lfd}) - p_{acD}(t_{Lfd} - (t_e)_{Lfd})] + p_{wsD}(0) C_{acD} p'_{acD}(t_{Lfd}) \\ & - (C_{bcD} - C_{acD}) \int_0^{(t_c)_{Lfd}} p'_{acD}(t_{Lfd} - \tau_D) p'_{wsD}(\tau_D) d\tau_D \end{aligned} \right] \dots\dots\dots (3.148)$$

After integrating-by-parts the solution is written as

$$p_{wsD}(t_{Lfd}) = \left[\begin{aligned} & q_{wD} [p_{acD}(t_{Lfd}) - p_{acD}(t_{Lfd} - (t_e)_{Lfd})] + p_{wsD}(0) C_{acD} p'_{acD}(t_{Lfd}) \\ & + (C_{bcD} - C_{acD}) p'_{wsD} [(t_c)_{Lfd}] p_{acD} [t_{Lfd} - (t_c)_{Lfd}] \\ & - (C_{bcD} - C_{acD}) \int_0^{(t_c)_{Lfd}} p''_{wsD}(\tau_D) p_{acD}(t_{Lfd} - \tau_D) d\tau_D \end{aligned} \right] \dots\dots\dots (3.149)$$

and a discretized form of the solution can be written with $p_{wsD}(0) = 1$ as

$$p_{wsD}(t_{Lfd})_n = \left[\begin{aligned} & q_{wD} [p_{acD}(t_{Lfd})_n - p_{acD} [(t_{Lfd})_n - (t_{Lfd})_{ne}]] \\ & + C_{acD} p'_{acD}(t_{Lfd})_n \\ & + (C_{bcD} - C_{acD}) \left(\frac{p_{wsD}(t_{Lfd})_{ne} - p_{wsD}(t_{Lfd})_{ne-1}}{(t_{Lfd})_{ne} - (t_{Lfd})_{ne-1}} \right) p_{acD} [(t_{Lfd})_n - (t_{Lfd})_{ne}] \\ & - (C_{bcD} - C_{acD}) \sum_{i=1}^{ne} \left[\begin{aligned} & \left(\frac{p_{wsD}(t_{Lfd})_i - p_{wsD}(t_{Lfd})_{i-1}}{(t_{Lfd})_i - (t_{Lfd})_{i-1}} \right) \\ & - \left(\frac{p_{wsD}(t_{Lfd})_{i-1} - p_{wsD}(t_{Lfd})_{i-2}}{(t_{Lfd})_{i-1} - (t_{Lfd})_{i-2}} \right) \end{aligned} \right] \\ & \times p_{acD} [(t_{Lfd})_n - (t_{Lfd})_{i-1}] \end{aligned} \right] \dots\dots\dots (3.150)$$

where the subscript 'ne' corresponds to the time index at the end of the injection.

Consider a case where $C_{bcD} = C_{acD}$, which allows the dimensionless wellbore pressure solution to be written with $p_{wsD}(0) = 1$ as

$$p_{wsD}(t_{Lfd}) = q_{wD} \left[p_{bcD}(t_{Lfd}) - p_{bcD}(t_{Lfd} - (t_e)_{Lfd}) \right] + C_{bcD} p'_{bcD}(t_{Lfd}) \dots (3.151)$$

When the injection term is negligibly small, the dimensionless wellbore pressure solution reverts to a fractured-well slug-test solution. The magnitude of the slug-test term is a strong function of the the dimensionless before-closure storage coefficient, and as the storage coefficient decreases, the dimensionless time of injection must also decrease for the injection term to be negligibly small. Recall the dimensionless before-closure storage coefficient is written as

$$C_{bcD} = \frac{C_{bc}}{2\pi\phi c_t h L_f^2} \dots (3.152)$$

and the before-closure storage coefficient is defined as

$$C_{bc} = c_w V_w + 2 \frac{A_f}{S_f} \dots (3.153)$$

Since the definition of the dimensionless before-closure storage coefficient is defined in terms of the fracture half-length, the coefficient decreases as the fracture length increases. Alternatively, if the wellbore storage term is assumed to be negligibly small and assuming the dilating fracture is modeled by a horizontal plane strain condition, the fracture stiffness (Table 3.1) is defined as

$$S_f = \frac{E'}{\pi L_f} \dots (3.154)$$

and the dimensionless before-closure storage coefficient can be written as

$$C_{bcD} = \frac{1}{\phi c_t E'} \dots (3.155)$$

which suggests a small dimensionless before-closure storage coefficient for "hard" rock, i.e., $E' \approx 10^6$ psi and a somewhat larger coefficient for softer rock. A reasonable range for the before-closure storage coefficient is written as

$$0.001 \leq C_{bcD} \leq 0.10 \dots (3.156)$$

The after-closure storage coefficient is defined as

$$C_{ac} = c_w V_w + c_f V_{f0} \dots (3.157)$$

and is generally smaller. If closure is complete, $V_{f0} = 0$, with wellbore storage being negligibly small, the dimensionless after-closure storage coefficient is zero, $C_{acD} = 0$. Therefore, a reasonable range of the dimensionless after-closure storage coefficient is written as

$$0 \leq C_{acD} \leq C_{bcD} \dots (3.158)$$

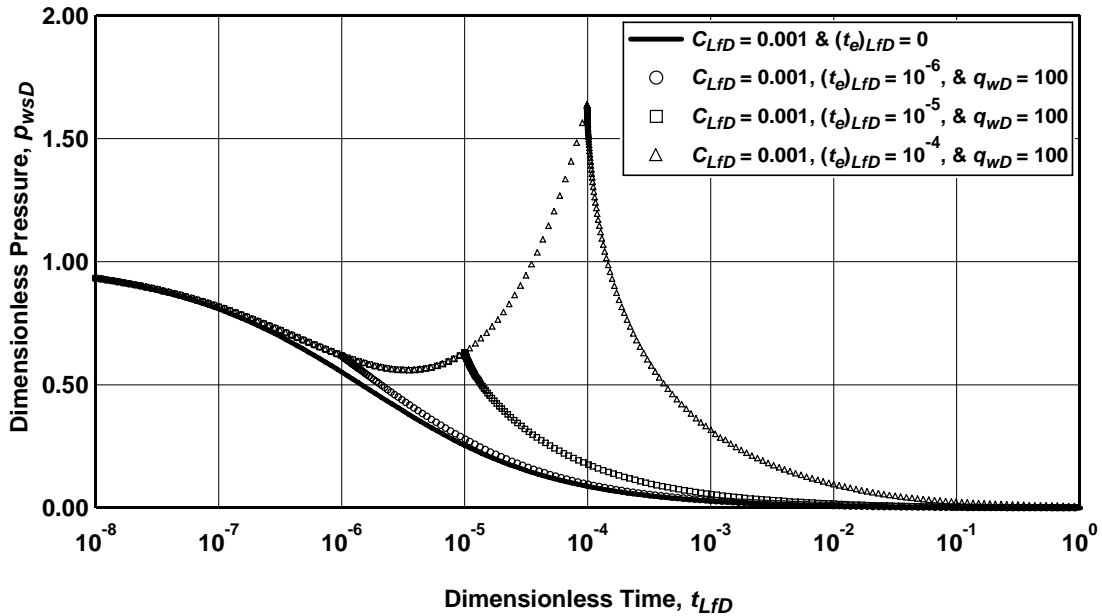


Fig. 3.12—Comparison of a slug-test solution for $C_{LfD} = 0.001$ with the dimensionless wellbore pressure from an injection/falloff sequence with $q_{wD} = 100$ and $(t_e)_{LfD} = \{10^{-4}, 10^{-5}, 10^{-6}\}$.

A series of numerical evaluations were completed assuming $C_{bcd} = C_{acd} = C_{LfD}$, which models an injection/falloff sequence in a well with a vertical hydraulic fracture created instantaneously during the injection or with a pre-existing fracture. **Fig. 3.12** is a semilog graph of dimensionless wellbore pressure versus dimensionless time and shows that the dimensionless wellbore pressure for a slug-test [$(t_e)_{LfD} = 0$] with $C_{LfD} = 0.001$ and for three injection/falloff sequences with $q_{wD} = 100$ and $(t_e)_{LfD} = \{10^{-4}, 10^{-5}, 10^{-6}\}$. All injection/falloff sequences shown in **Fig. 3.12** result in dimensionless wellbore pressure deviation from the slug-test solution with the smallest deviation observed for the shortest dimensionless time of injection, $(t_e)_{LfD} = 10^{-6}$. Similarly, semilog graphs shown in **Figs. 3.13 and 3.14** illustrate the deviation of the dimensionless wellbore pressure during an injection/falloff sequence from a slug test solution for $C_{LfD} = 0.01$ and $C_{LfD} = 0.10$, respectively. Collectively, **Figs. 3.12 through 3.14** illustrate that the dimensionless wellbore pressure deviation from a slug test solution is reduced as the dimensionless time of injection becomes smaller and as the storage coefficient increases.

Semilog graphs of dimensionless wellbore pressure versus dimensionless time are also shown for injection/falloff sequences with $q_{wD} = 10$ in **Figs. 3.15 through 3.17**. The smaller dimensionless injection rate results in less deviation of the dimensionless wellbore pressure from the slug-test solution when compared to equivalent dimensionless injection times in **Figs. 3.12 through 3.14**.

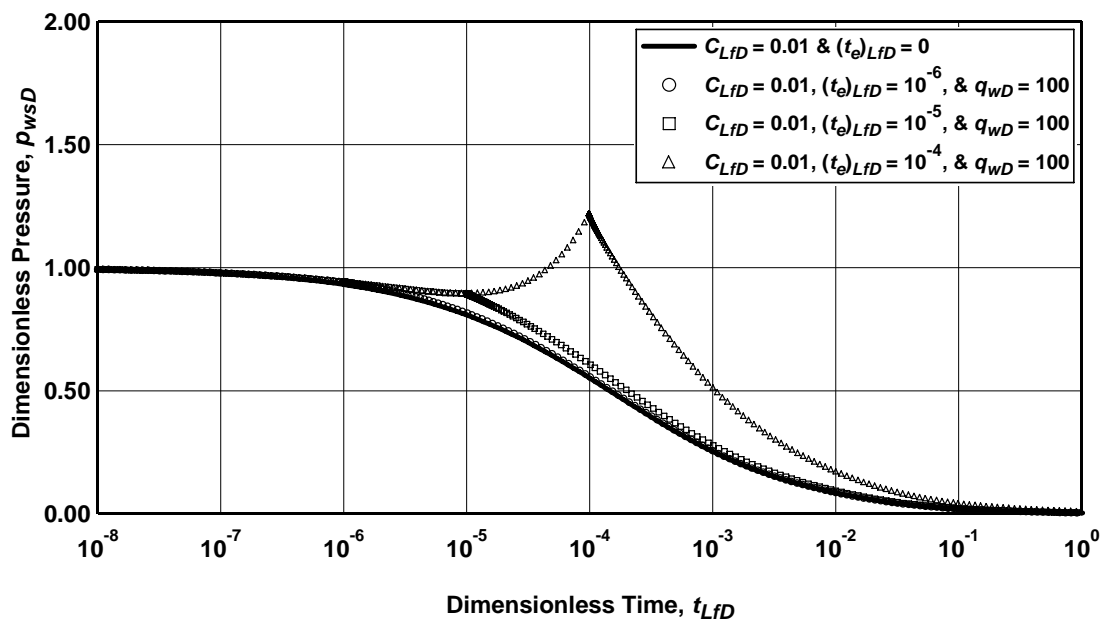


Fig. 3.13—Comparison of a slug-test solution for $C_{LfD} = 0.01$ with the dimensionless wellbore pressure from an injection/falloff sequence with $q_{wD} = 100$ and $(t_e)_{LfD} = \{10^{-4}, 10^{-5}, 10^{-6}\}$.

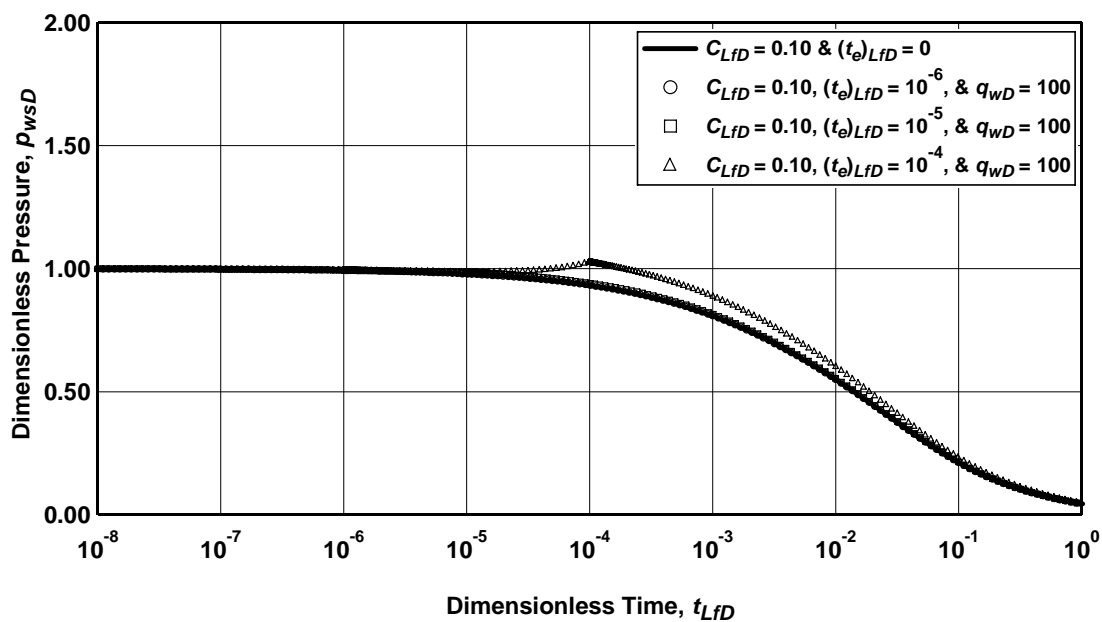


Fig. 3.14—Comparison of a slug-test solution for $C_{LfD} = 0.10$ with the dimensionless wellbore pressure from an injection/falloff sequence with $q_{wD} = 100$ and $(t_e)_{LfD} = \{10^{-4}, 10^{-5}, 10^{-6}\}$.

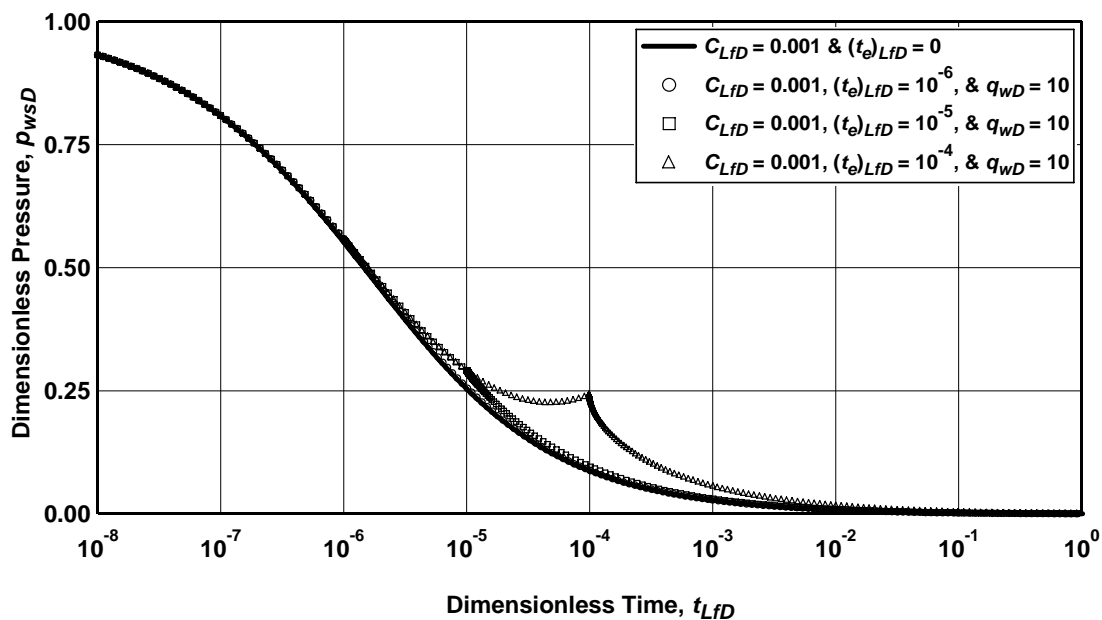


Fig. 3.15—Comparison of a slug-test solution for $C_{Lfd} = 0.001$ with the dimensionless wellbore pressure from an injection/falloff sequence with $q_{wD} = 10$ and $(t_e)_{Lfd} = \{10^{-4}, 10^{-5}, 10^{-6}\}$.

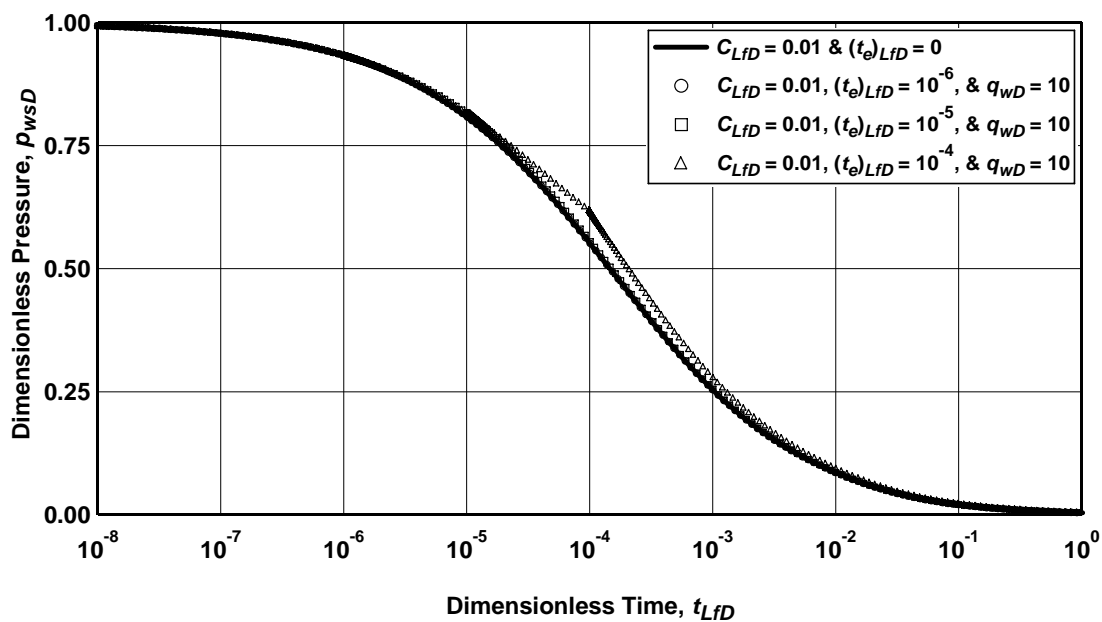


Fig. 3.16—Comparison of a slug-test solution for $C_{Lfd} = 0.01$ with the dimensionless wellbore pressure from an injection/falloff sequence with $q_{wD} = 10$ and $(t_e)_{Lfd} = \{10^{-4}, 10^{-5}, 10^{-6}\}$.

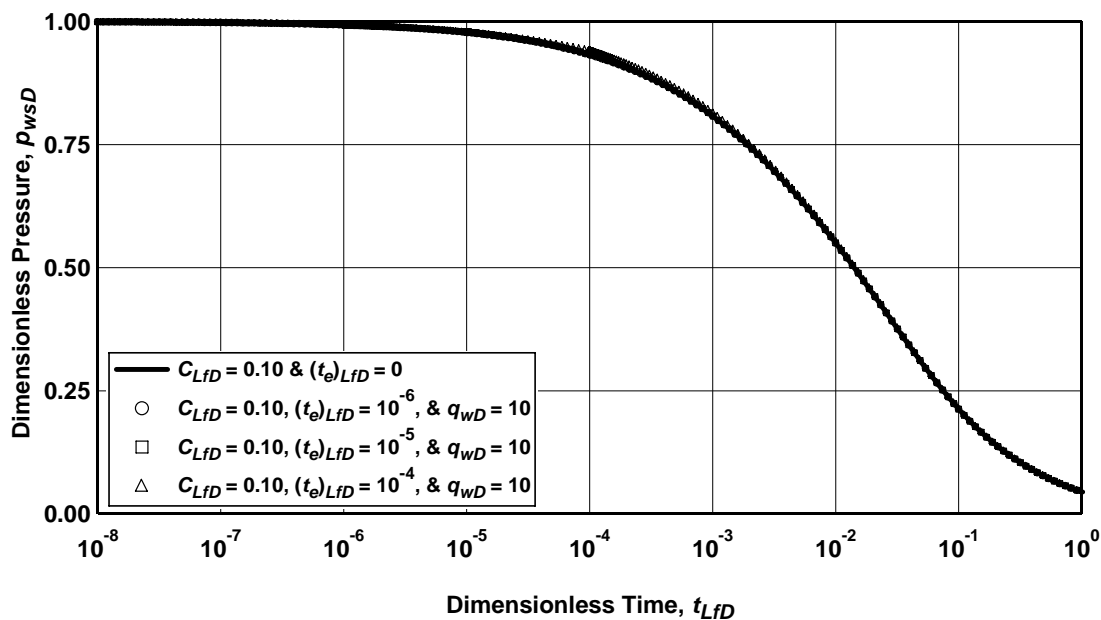


Fig. 3.17—Comparison of a slug-test solution for $C_{LfD} = 0.10$ with the dimensionless wellbore pressure from an injection/falloff sequence with $q_{wD} = 10$ and $(t_e)_{LfD} = \{10^{-4}, 10^{-5}, 10^{-6}\}$.

The numerical evaluations graphically shown in Figs. 3.12 through 3.17 clearly suggest that as fracture half-length increases, the time of injection must decrease to minimize the deviation between the dimensionless wellbore pressure during an injection/falloff sequence and a slug-test solution. However, the evaluations do not suggest a definitive rule for when an injection/falloff sequence can be modeled as a slug test. It appears that a dimensionless injection time on the order of 10^{-5} with $q_{wD} < 100$ is a reasonable rule of thumb that will result in minimal deviation from the slug-test solution.

Fig. 3.18 shows a semilog graph of dimensionless wellbore pressure versus dimensionless time for a variable-storage dilating-fracture injection/falloff sequence with $C_{bcD} = 0.01$, $C_{acD} = 0.005$, $q_{wD} = 10$, $(t_e)_{LfD} = \{0, 10^{-5}\}$, and $(t_c)_{LfD} = \{2(10)^{-5}, 2(10)^{-4}\}$. Recall that Fig. 3.16 demonstrated the dimensionless wellbore pressure from a fracture-injection/falloff sequence with $C_{LfD} = 0.01$, $q_{wD} = 10$, and $(t_e)_{LfD} = 10^{-5}$ would show very little deviation from the constant-storage slug-test solution with $(t_e)_{LfD} = 0$. Similarly, Fig. 3.18 demonstrates minimal deviation is observed between the dimensionless wellbore pressure calculated using the new variable-storage fracture-injection/falloff model and the variable-storage slug-test solutions that result when $(t_e)_{LfD} = 0$.

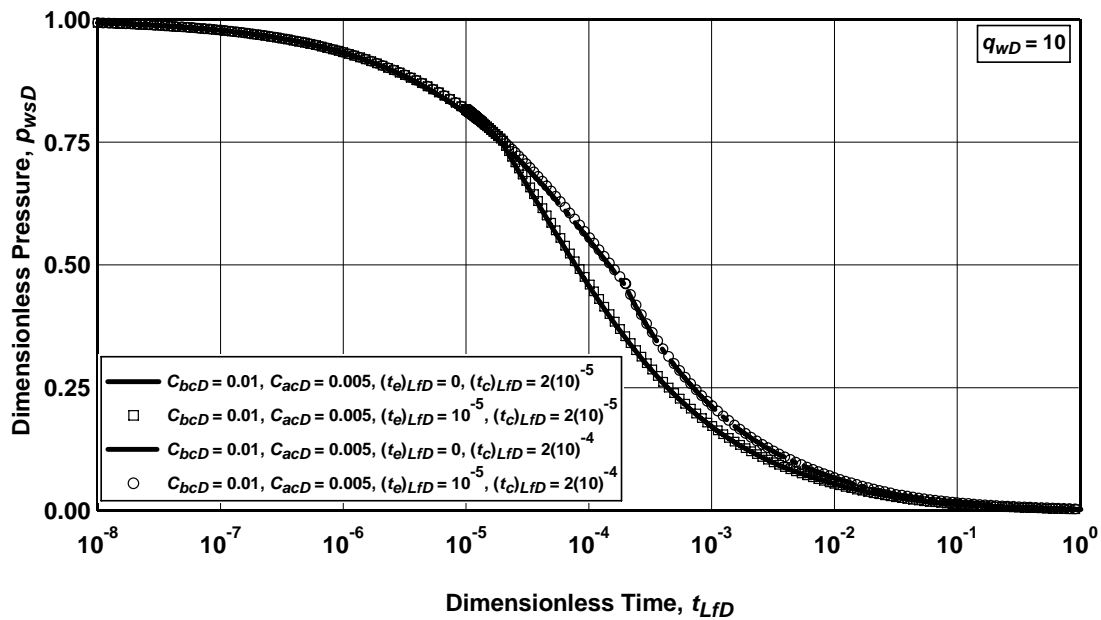


Fig. 3.18—Comparison of a dilating fracture slug-test solution for $C_{bcD} = 0.01$, $C_{acD} = 0.005$, and $(t_c)_{LfD} = \{2(10)^{-5}, 2(10)^{-4}\}$ with the dimensionless wellbore pressure from a fracture-injection/falloff sequence with $q_{wD} = 10$, $(t_e)_{LfD} = 10^{-5}$, and $(t_c)_{LfD} = \{2(10)^{-5}, 2(10)^{-4}\}$.

CHAPTER IV

MODELING A FRACTURE-INJECTION/FALLOFF TEST IN A RESERVOIR WITH A PRE-EXISTING FRACTURE

4.1 Introduction

A fracture-injection/falloff sequence in a well containing a pre-existing conductive fracture will either dilate the existing fracture or induce a secondary fracture(s). When the injection time of a fracture-injection/falloff sequence in a reservoir with a pre-existing conductive fracture is short relative to the reservoir response, the injection can be considered as occurring instantaneously, and the variable-rate pressure falloff data can be converted to an equivalent constant-rate pressure difference by integration of the recorded pressure difference with respect to time. After conversion, constant-rate drawdown type curves are used for quantitative type-curve analysis. However, during the falloff the dilated or induced secondary fracture(s) contract to closure, which results in variable storage and requires new constant-rate drawdown solutions for type-curve matching.

In Chapter III, the new analytical pressure-transient solutions for a fracture-injection/falloff sequence used the infinite-slab reservoir solution for production through a single vertical finite- or infinite-conductivity fracture. However, a fracture-injection/falloff sequence in a reservoir with a pre-existing fracture that also induces and propagates a secondary vertical fracture, requires a new pressure-transient solution for production through multiple arbitrarily-oriented finite- or infinite-conductivity fractures in an infinite-slab reservoir.

Chapter IV presents new analytical pressure-transient solutions for a well in an infinite-slab reservoir producing through multiple uniform-flux, infinite-conductivity, or finite-conductivity arbitrarily-oriented vertical fractures. The multiple-fracture reservoir solution is then used in the development of a new analytical pressure-transient solution for a constant-rate drawdown in a well in an infinite-slab reservoir containing two arbitrarily-oriented vertical fractures with the initial reservoir pressure above the minimum insitu or closure stress of the secondary fracture and with constant storage before- and constant storage after secondary fracture closure.

Chapter IV also presents a new fracture-injection/falloff model for a well with a pre-existing conductive fracture that accounts for primary fracture dilation, secondary fracture creation, multiple fracture closures, and after-closure diffusion. Limiting-case solutions of the fracture-injection/falloff model with constant primary fracture volume and secondary fracture creation are also presented to demonstrate when a fracture-injection/falloff sequence in a well with a pre-existing conductive fracture can be considered as occurring instantaneously and slug-test analysis methods can be applied to the falloff data for quantitative type-curve analysis.

4.2 Multiple Arbitrarily-Oriented Vertical Fracture Pressure Transient Solution

The new pressure-transient solutions for a well producing through multiple arbitrarily-oriented uniform-flux or infinite-conductivity vertical fractures in an infinite slab reservoir are derived in **Appendix D**, and the new pressure-transient solution for a well producing through multiple arbitrarily-oriented finite-conductivity vertical fractures is derived in **Appendix E**. All new solutions allow for variable fracture half-length and an arbitrary angle between each hydraulic fracture. The finite-conductivity multiple-fracture solution also allows for constant conductivity within each fracture, but conductivity can vary among fractures.

4.2.1 Uniform Flux. Multiple fracture pressure-transient solutions require writing a general uniform-flux solution for a single vertical fracture at any arbitrary angle, which as developed in **Appendix D** and written in the Laplace domain for a fracture rotated by an angle θ_f from a point (r_D, θ_r) as

$$\bar{p}_D = \frac{q_D}{L_{fD}} \frac{1}{2s} \int_{-L_{fD}}^{L_{fD}} K_0 \left[\sqrt{u} \sqrt{\left[r_D \cos(\theta_r - \theta_f) - \alpha \right]^2 + r_D^2 \sin^2(\theta_r - \theta_f)} \right] d\alpha, \quad (4.1)$$

where dimensionless variables are defined as

$$\bar{p}_D = \frac{2\pi kh\Delta\bar{p}}{\bar{q}\mu}, \quad (4.2)$$

$$L_{fD} = \frac{L_f}{L_c}, \quad (4.3)$$

$$q_D = \frac{q}{q_t}, \quad (4.4)$$

$$u = sf(s), \quad (4.5)$$

$$r_D = \sqrt{x_D^2 + y_D^2}, \quad (4.6)$$

$$x_D = r_D \cos \theta_r, \quad (4.7)$$

$$y_D = r_D \sin \theta_r, \quad (4.8)$$

L_c is the characteristic length, θ_f is the angle between the fracture and the x_D -axis, (r_D, θ_r) are the polar coordinates of a point (x_D, y_D) , and (α, θ_f) are the polar coordinates of a point along the fracture.¹⁰³

For a single-porosity reservoir, $f(s) = 1$, and for dual-porosity reservoir with pseudosteady-state interporosity flow, $f(s)$ is written as⁹⁶

$$f(s) = \frac{\lambda + \omega(1-\omega)s}{\lambda + (1-\omega)s}, \quad (4.9)$$

for transient interporosity flow with slab matrix blocks,⁹⁷⁻⁹⁸

$$f(s) = \omega + \sqrt{\frac{\lambda(1-\omega)}{3s}} \tanh \sqrt{\frac{3(1-\omega)s}{\lambda}} \dots\dots\dots(4.10)$$

and for transient interporosity flow with spherical matrix blocks,⁹⁷⁻⁹⁸

$$f(s) = \omega + \frac{\lambda}{5s} \left[\sqrt{\frac{15(1-\omega)s}{\lambda}} \coth \sqrt{\frac{15(1-\omega)s}{\lambda}} - 1 \right] \dots\dots\dots(4.11)$$

For a well containing n_f fractures connected at the wellbore, the total flow rate from the well assuming all production is through the fractures is written as

$$\sum_{i=1}^{n_f} q_{iD} = 1, \dots\dots\dots(4.12)$$

where q_{iD} is the dimensionless flow rate for the i^{th} -fracture defined as

$$q_{iD} = \frac{q_i}{q_w} = \frac{q_i}{\sum_{k=1}^{n_f} q_k} \dots\dots\dots(4.13)$$

and q_i is the flow rate from the i^{th} -fracture.

For all fractures intersecting the wellbore, the wellbore pressure is the same and written as

$$p_{LjD} = (p_{wD})_\ell \quad , \quad \ell = 1, 2, \dots, n_f \dots\dots\dots(4.14)$$

The uniform-flux dimensionless pressure solution is obtained by superposing all fractures¹⁰² and written in the Laplace domain as

$$\begin{aligned} \bar{p}_{LjD} = (\bar{p}_{wD})_\ell = \sum_{i=1}^{n_f} \frac{\bar{q}_{iD}}{2L_{fiD}} \int_{-L_{fiD}}^{L_{fiD}} K_0 \left[\sqrt{u} \sqrt{[r_D \cos(\theta_\ell - \theta_i) - \alpha]^2 + r_D^2 \sin^2(\theta_\ell - \theta_i)} \right] d\alpha \\ \ell = 1, 2, \dots, n_f \dots\dots\dots(4.15) \end{aligned}$$

Defining the normalized fracture length as

$$\delta_i = \frac{L_{fi}}{L_{f1}} \quad , \quad i = 1, 2, \dots, n_f, \dots\dots\dots(4.16)$$

and assuming the fracture height is the same for all fractures, allows the dimensionless flow rate to be written as

$$q_{iD} = \frac{q_i}{q_w} = \frac{\delta_i}{\sum_{k=1}^{n_f} \delta_k} \dots\dots\dots(4.17)$$

With the definition of dimensionless flow rate, the uniform-flux multiple arbitrarily-oriented vertical fracture pressure-transient solution is written in the Laplace domain as

$$(\bar{p}_{wD})_\ell = \sum_{i=1}^{n_f} \frac{\delta_i}{\sum_{k=1}^{n_f} \delta_k} \frac{1}{2sL_{f1D}} \int_{-L_{f1D}}^{L_{f1D}} K_0 \left[\sqrt{u} \sqrt{[r_D \cos(\theta_\ell - \theta_i) - \alpha]^2 + r_D^2 \sin^2(\theta_\ell - \theta_i)} \right] d\alpha \dots\dots\dots(4.18)$$

Fig. 4.1 shows a log-log graph of dimensionless pressure versus dimensionless time for a cruciform uniform-flux vertical fracture. The inset graphics in Fig. 4.1 illustrate a cruciform fracture with primary fracture half length, L_{f1D} , and the secondary fracture half length is defined by the ratio of secondary to primary fracture half length, $\delta_L = L_{f2D}/L_{f1D}$, where in Fig. 4.1, $\delta_L = \{0, 0.001, 0.01, 0.1, 1\}$. As shown in **Appendix D**, the cruciform-fracture uniform-flux solution is equivalent to the single-fracture uniform-flux solution, $\delta_L = 0$, when the primary and secondary fracture half-lengths are the same $\delta_L = 1$. For small dimensionless times and as δ_L approaches zero, the dimensionless pressure for a cruciform-fracture approaches twice the dimensionless pressure of a single uniform-flux fracture, but as dimensionless time increases, all solutions for $\delta_L \leq 1$ converge to the single-fracture uniform-flux solution.

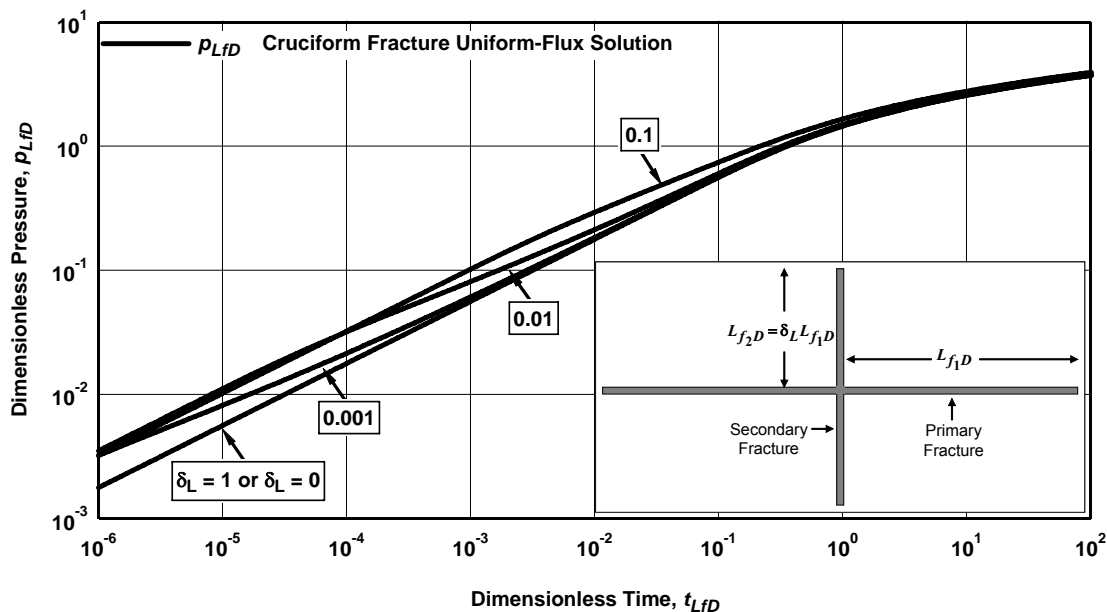


Fig. 4.1—Cruciform uniform-flux vertical fracture pressure transient solution for $\delta_L = 0.001, 0.01, 0.1, \text{ and } 1$.

4.2.2 Infinite Conductivity. For a single vertical fracture, an approximate infinite-conductivity solution is obtained by evaluating the uniform-flux solution at an equivalent average pressure point, ($x_D = 0.732, y_D = 0$). However, the equivalent average pressure point is dependent on the system geometry and must be determined numerically for each multi-fracture system.¹⁰⁴

Kuchuk *et al.*¹⁰⁴ encountered a similar problem when deriving the infinite-conductivity solution for horizontal wells and elected to use the pressure-averaging technique proposed by Wilkinson and Hammond.¹⁰⁵ The pressure-averaging technique approximates the infinite-conductivity horizontal well solution by averaging the pressure along the flowpath using the uniform-flux solution, which according to Wilkinson and Hammond approaches the exact solution as a horizontal wellbore radius tends to zero.

As shown in **Appendix D**, a pressure-averaging approximate infinite-conductivity solution is written as a system of equations with the dimensionless pressure in Laplace space for the ℓ^{th} -fracture written as

$$\begin{aligned} \widehat{(\bar{p}_{LjD})}_\ell &= \sum_{j=1}^{n_f} \frac{\bar{q}_{jD}}{2L_{f\ell D}L_{jD}} \frac{1}{2s} \int_{-L_{f\ell D}}^{L_{f\ell D}} \int_{-L_{jD}}^{L_{jD}} K_0 \left[\sqrt{u} \sqrt{r_D \cos(\theta_\ell - \theta_j) - \alpha}^2 + r_D^2 \sin^2(\theta_\ell - \theta_j) \right] d\alpha dr_D \\ \ell &= 1, 2, \dots, n_f, \dots \end{aligned} \quad (4.19)$$

and the dimensionless flow rate for all fractures in Laplace space written as

$$\sum_{j=1}^{n_f} \bar{q}_{jD} = \frac{1}{s} \dots \dots \dots (4.20)$$

The system of equations is formed by recognizing that for infinite-conductivity fractures, the Laplace domain dimensionless pressure in each fracture is the same, which is written as

$$\widehat{(\bar{p}_{LjD})}_1 = \widehat{(\bar{p}_{LjD})}_2 = \dots = \widehat{(\bar{p}_{LjD})}_{n_f} = \widehat{\bar{p}_{LjD}}, \dots \dots \dots (4.21)$$

and the system of equations can be written as

$$\begin{bmatrix} 1 & A_{11} & A_{12} & \dots & A_{1n_f} \\ 1 & A_{21} & A_{22} & \dots & A_{2n_f} \\ \vdots & \vdots & \vdots & \dots & \vdots \\ 1 & A_{n_f 1} & A_{n_f 2} & \vdots & A_{n_f n_f} \\ 0 & 1 & 1 & \dots & 1 \end{bmatrix} \begin{bmatrix} \widehat{\bar{p}_{LjD}} \\ \bar{q}_{1D} \\ \bar{q}_{2D} \\ \vdots \\ \bar{q}_{n_f D} \end{bmatrix} = \begin{bmatrix} 0 \\ 0 \\ 0 \\ \vdots \\ \frac{1}{s} \end{bmatrix}, \dots \dots \dots (4.22)$$

where

$$A_{ij} = \frac{(-1)}{4sL_{jiD}L_{jD}} \int_{-L_{jiD}}^{L_{jiD}} \int_{-L_{jD}}^{L_{jD}} K_0 \left[\sqrt{u} \sqrt{r_D \cos(\theta_i - \theta_j) - \alpha}^2 + r_D^2 \sin^2(\theta_i - \theta_j) \right] d\alpha dr_D \dots \dots \dots (4.23)$$

A semianalytical multiple arbitrarily-oriented infinite-conductivity fracture solution can also be developed in the Laplace domain without resorting to the pressure-averaging technique. If flux is not uniform along

the fracture(s), a Laplace domain dimensionless pressure for a fracture ℓ at an arbitrary angle, θ_ℓ , accounting for the effect of a fracture(s) i at angle θ_i is written as

$$(\bar{p}_D)_{\ell i} = \frac{1}{2(L_{fD})_i} \int_{-(L_{fD})_i}^{(L_{fD})_i} (\bar{q}_D)_i(\alpha, s) K_0 \left[\sqrt{u} \sqrt{[r_{iD} \cos(\theta_\ell - \theta_i) - \alpha]^2 + r_{iD}^2 \sin^2(\theta_\ell - \theta_i)} \right] d\alpha, \dots\dots\dots (4.24)$$

where $i, \ell = 1, 2, \dots, n_f$. Note that $(q_D)_i = q_i/q_{wi}$, where q_{wi} is the flow rate from the i^{th} -fracture and $(L_{fD})_i = L_{fi}/L_{fi} = 1$. If a point (r_{iD}, θ_i) is restricted to a point along the i^{th} -fracture axis, then the reference and fracture axis are the same and the Laplace domain dimensionless pressure is written as

$$(\bar{p}_D)_{\ell i} = \frac{1}{2} \int_{-1}^1 (\bar{q}_D)_i(\alpha, s) K_0 \left[\sqrt{u} \sqrt{[\hat{x}_{iD} \cos(\theta_\ell - \theta_i) - \alpha]^2 + \hat{x}_{iD}^2 \sin^2(\theta_\ell - \theta_i)} \right] d\alpha, \\ i, \ell = 1, 2, \dots, n_f \dots\dots\dots (4.25)$$

Assuming each fracture is homogeneous and symmetric, that is, $(\bar{q}_D)_i(\alpha, s) = (\bar{q}_D)_i(-\alpha, s)$, the Laplace domain dimensionless pressure for an arbitrarily-oriented infinite-conductivity fracture ℓ in an isotropic reservoir accounting for the effects of an infinite-conductivity fracture i is written as

$$(\bar{p}_D)_{\ell i} = \frac{1}{2} \int_0^1 (\bar{q}_D)_i(x', s) \left[\begin{array}{l} K_0 \left[\sqrt{u} \sqrt{[\hat{x}_{iD} \cos(\theta_\ell - \theta_i) - x']^2 + \hat{x}_{iD}^2 \sin^2(\theta_\ell - \theta_i)} \right] \\ + K_0 \left[\sqrt{u} \sqrt{[\hat{x}_{iD} \cos(\theta_\ell - \theta_i) + x']^2 + \hat{x}_{iD}^2 \sin^2(\theta_\ell - \theta_i)} \right] \end{array} \right] dx', \\ i, \ell = 1, 2, \dots, n_f \dots\dots\dots (4.26)$$

A semianalytical solution for the multiple infinite-conductivity fractures is obtained by dividing each fracture into n_{fs} equal segments of length, $\Delta \hat{x}_{iD} = L_{fiD} / n_{fs}$, and assuming constant flux in each segment. Although the number of segments in each fracture is the same, the segment length can be different for each fracture, $\Delta \hat{x}_{iD} \neq \Delta \hat{x}_{jD}$. With the discretization, the Laplace domain dimensionless pressure for an arbitrarily-oriented infinite-conductivity fracture ℓ in an isotropic reservoir accounting for the effects of an infinite-conductivity fracture i is written as

$$(\bar{p}_D)_{\ell i}(s) = \sum_{m=1}^{n_{fs}} \frac{(\bar{q}_D)_{im}(s)}{2} \int_{[\hat{x}_{iD}]_m}^{[\hat{x}_{iD}]_{m+1}} \left[\begin{array}{l} K_0 \left[\sqrt{u} \sqrt{[(\hat{x}_{iD})_j \cos(\theta_\ell - \theta_i) - x']^2 + (\hat{x}_{iD})_j^2 \sin^2(\theta_\ell - \theta_i)} \right] \\ + K_0 \left[\sqrt{u} \sqrt{[(\hat{x}_{iD})_j \cos(\theta_\ell - \theta_i) + x']^2 + (\hat{x}_{iD})_j^2 \sin^2(\theta_\ell - \theta_i)} \right] \end{array} \right] dx', \\ i, \ell = 1, 2, \dots, n_f \text{ and } j, m = 1, 2, \dots, n_{fs} \dots\dots\dots (4.27)$$

The multiple infinite-conductivity fracture solution considering permeability anisotropy in an infinite slab reservoir is developed by defining the dimensionless distance variables as⁹⁵

$$x_D = \frac{x}{L_c} \sqrt{\frac{k}{k_x}}, \dots\dots\dots (4.28)$$

$$y_D = \frac{y}{L_c} \sqrt{\frac{k}{k_y}}, \dots\dots\dots (4.29)$$

and

$$k = \sqrt{k_x k_y} \dots\dots\dots (4.30)$$

The dimensionless variables rescale the anisotropic reservoir to an equivalent isotropic system. As a result of the rescaling, the dimensionless fracture half-length changes and must be redefined as¹⁰⁶

$$L'_{fD} = \frac{L_{fD}}{L_c} \sqrt{\frac{k}{k_x} \cos^2 \theta_f + \frac{k}{k_y} \sin^2 \theta_f}, \dots\dots\dots (4.31)$$

where the angle of the fracture with respect to the rescaled x_D -axis is written as

$$\theta'_f = \tan^{-1} \left(\sqrt{\frac{k_x}{k_y}} \tan \theta_f \right), \quad 0 < \theta_f < \frac{\pi}{2} \dots\dots\dots (4.32)$$

When $\theta_f = 0$ or $\theta_f = \pi/2$, the angle does not rescale and $\theta'_f = \theta_f$.

With the redefined dimensionless variables and after fracture discretization the Laplace domain dimensionless pressure for an arbitrarily-oriented infinite-conductivity fracture ℓ in an anisotropic reservoir accounting for the effects of an infinite-conductivity fracture i is written as

$$(\bar{p}_D)_{\ell i}(s) = \sum_{m=1}^{n_{fs}} \frac{(\bar{q}_D)_{im}(s)}{2} \int_{[\hat{x}'_{iD}]_m}^{[\hat{x}'_{iD}]_{m+1}} \left[K_0 \left[\sqrt{u} \sqrt{[(\hat{x}'_{iD})_j \cos(\theta'_\ell - \theta'_i) - x']^2 + (\hat{x}'_{iD})_j^2 \sin^2(\theta'_\ell - \theta'_i)} \right] \right. \\ \left. + K_0 \left[\sqrt{u} \sqrt{[(\hat{x}'_{iD})_j \cos(\theta'_\ell - \theta'_i) + x']^2 + (\hat{x}'_{iD})_j^2 \sin^2(\theta'_\ell - \theta'_i)} \right] \right] dx' \\ i, \ell = 1, 2, \dots, n_f \text{ and } j, m = 1, 2, \dots, n_{fs} \dots\dots\dots (4.33)$$

A semianalytical solution accounting for multiple arbitrarily-oriented infinite-conductivity fractures in an anisotropic reservoir is written in the Laplace domain using superposition as

$$(\bar{p}_{LjD})_{\ell}(s) = \sum_{i=1}^{n_f} s \bar{q}_{iD} \sum_{m=1}^{n_{fs}} \frac{(\bar{q}_D)_{im}(s)}{2} \int_{[\hat{x}'_{iD}]_m}^{[\hat{x}'_{iD}]_{m+1}} \left[K_0 \left[\sqrt{u} \sqrt{[(\hat{x}'_{iD})_j \cos(\theta'_\ell - \theta'_i) - x']^2 + (\hat{x}'_{iD})_j^2 \sin^2(\theta'_\ell - \theta'_i)} \right] \right. \\ \left. + K_0 \left[\sqrt{u} \sqrt{[(\hat{x}'_{iD})_j \cos(\theta'_\ell - \theta'_i) + x']^2 + (\hat{x}'_{iD})_j^2 \sin^2(\theta'_\ell - \theta'_i)} \right] \right] dx' \\ i, \ell = 1, 2, \dots, n_f \text{ and } j, m = 1, 2, \dots, n_{fs} \dots\dots\dots (4.34)$$

with the Laplace domain dimensionless flow rate for a single fracture defined by

$$\Delta \hat{x}'_{iD} \sum_{m=1}^{n_{fs}} (\bar{q}_D)_{im} = \frac{1}{s}, \dots\dots\dots (4.35)$$

and the Laplace domain dimensionless total flow rate for n_f fractures defined by

$$\sum_{i=1}^{n_f} \bar{q}_{iD} = \frac{1}{s} \dots\dots\dots(4.36)$$

For each fracture, an equation relating the dimensionless pressure is written in the Laplace domain as

$$(\bar{p}_D)_{\ell_i}|_{j=1} = (\bar{p}_D)_{\ell_i}|_{j=2} = \dots = (\bar{p}_D)_{\ell_i}|_{j=n_{fs}} = (\bar{p}_D)_{\ell_i}, \dots\dots\dots(4.37)$$

and for the entire multiple-fracture system, the dimensionless pressure at the wellbore is written in the Laplace domain as

$$(\bar{p}_{wD})_1 = (\bar{p}_{wD})_2 = \dots = (\bar{p}_{wD})_{n_f} = \bar{p}_{L_fD} \dots\dots\dots(4.38)$$

With each fracture divided into n_{fs} equal length uniform-flux segments, Eqs. 4.34 through 4.38 describe a system of $n_f(n_{fs} + n_f + 1) + 1$ equations and $n_f(n_{fs} + n_f + 1) + 1$ unknowns. The system of equations forms the Laplace domain solution for a well with multiple arbitrarily-oriented infinite-conductivity fractures in an infinite-slab anisotropic reservoir. The system is solved in the Laplace domain and inverted to the time domain to obtain the pressure-transient solution as described in **Appendix D**.

Fig. 4.2 shows a log-log graph of the dimensionless pressure and dimensionless pressure derivative versus dimensionless time for a cruciform fracture with $\delta_L = 1$. The solutions were generated using the semianalytical multiple-fracture infinite-conductivity solution, the pressure-averaging infinite-conductivity solution, and the uniform-flux solution. Several interesting features are noted. First, unlike a single-fracture solution,⁸⁴ the infinite-conductivity and uniform-flux solutions are not equivalent at dimensionless times as small as 10^{-6} , but the solutions converge as dimensionless time increases. Second, the semianalytical and pressure-averaging multiple-fracture infinite-conductivity solutions overlay at small dimensionless times, but the solutions diverge significantly at intermediate dimensionless times. Third, as pseudoradial flow develops, $t_{LD} \geq 3$, the semianalytical and pressure-averaging infinite-conductivity solutions converge again. Similar comparisons are shown in **Appendix D** for a cruciform infinite-conductivity fracture with $\delta_L = 3/4, 1/2$, and $1/4$.

Following the ideas of Raghavan *et al.*¹⁰² for comparing the pressure-transient solutions of a horizontal well intercepted by a single or multiple fractures, **Fig. 4.3** shows a log-log graph of the product of $(1 + \delta_L)$ and dimensionless pressure versus dimensionless time for a cruciform infinite-conductivity fracture with $\delta_L = 0, 1/4, 1/2, 3/4$, and 1. At early times, the cruciform-fracture solutions overlay the single-fracture solution, but as interference occurs, the multiple fracture solutions diverge from the single-fracture solution. The divergence occurs at an earlier time for a shorter secondary fracture half length, and the dimensionless time when divergence begins, which corresponds to the beginning of interference, also corresponds to the divergence of the semianalytical infinite-conductivity and pressure-averaging infinite-conductivity solutions shown in Fig 4.2.

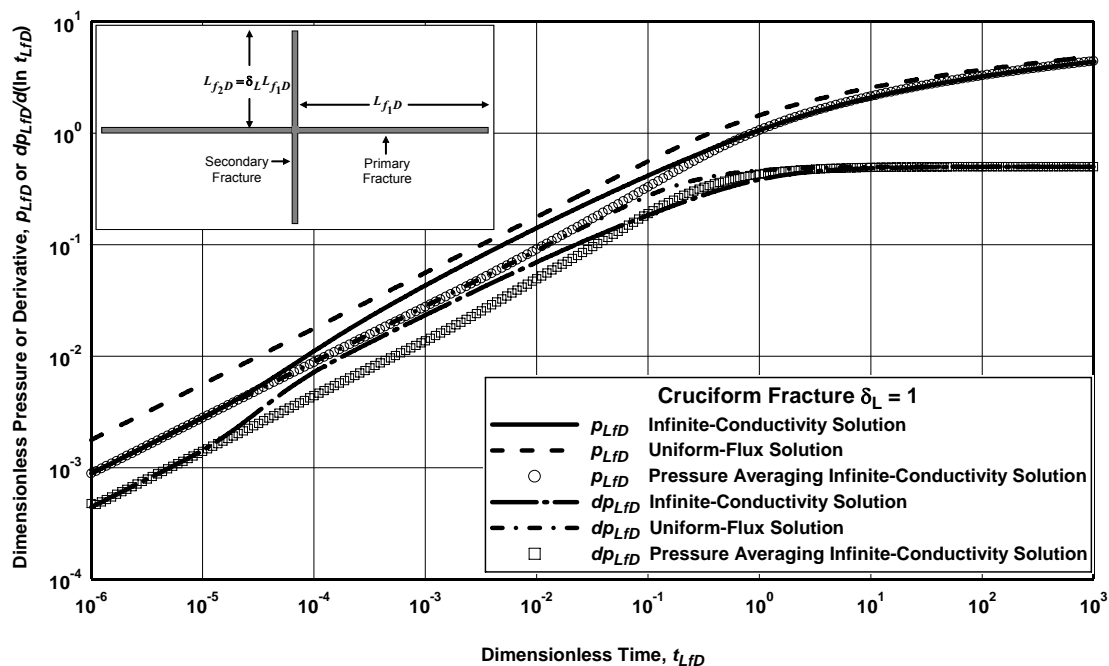


Fig. 4.2—A comparison of a pressure-averaging infinite-conductivity solution, the uniform-flux solution, and the semianalytical infinite-conductivity solution for a cruciform fracture with $\delta_L = 1$.

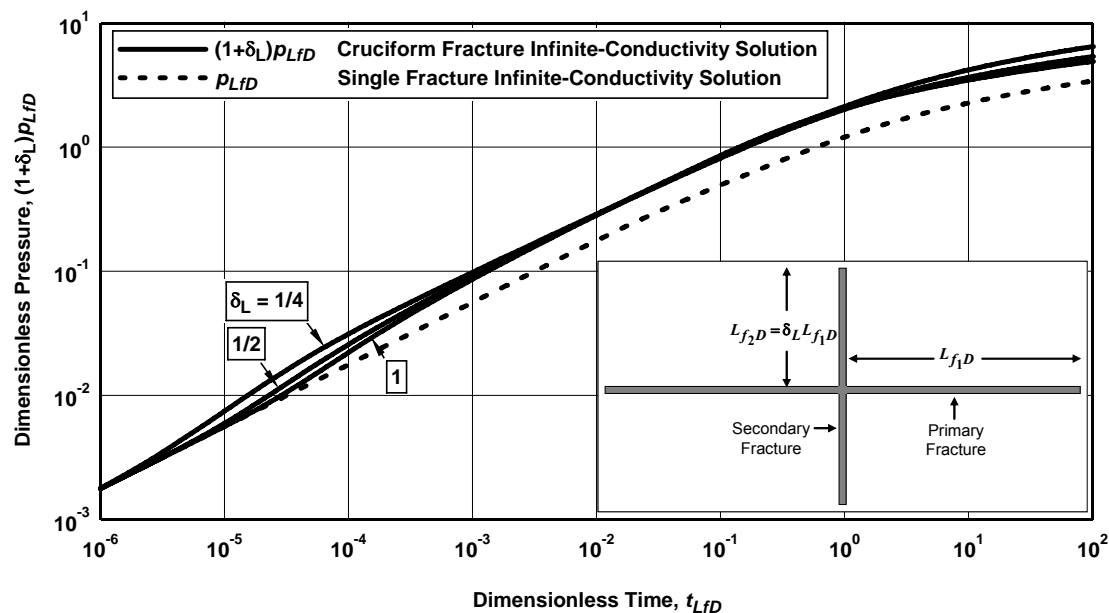


Fig. 4.3—Product of $(1 + \delta_L)$ and dimensionless pressure versus dimensionless time for a cruciform infinite-conductivity fracture with $\delta_L = 0, 1/4, 1/2, 3/4,$ and 1 .

Consequently, the pressure-averaging infinite-conductivity solution is *not* a good approximation of the cruciform semianalytical infinite-conductivity fracture solution when interference between the fractures is observed at intermediate dimensionless times. However, the pressure-averaging infinite-conductivity solution is a good approximation at very small dimensionless times and as pseudoradial flow develops. For example, the pressure-averaging infinite-conductivity solution can be used during fracture propagation in the numerical implementation of a fracture-injection/falloff model in a reservoir containing a constant-volume pre-existing conductive fracture with a secondary fracture induced and propagated during the injection.

4.2.3 Finite Conductivity. The development of a multiple finite-conductivity vertical fracture solution requires writing a general solution for a single finite-conductivity vertical fracture at any arbitrary angle, θ , from the x_D -axis. The multiple-fracture solution is then derived following the approach of Cinco-Ley *et al.*¹⁰⁷ for a single-fracture finite-conductivity fracture and of Cinco-Ley and Meng⁸⁶ for a single finite-conductivity fracture in a dual-porosity reservoir. The complete semianalytical multiple finite-conductivity vertical fracture solution is derived in **Appendix E**.

A finite-conductivity solution requires coupling reservoir and fracture-flow components, and the solution assumes the following for each fracture:

- The fracture is modeled as a homogeneous slab porous medium with fracture half-length, L_f , fracture width, w_f , and fully penetrating across the entire reservoir thickness, h .
- Fluid flow into the fracture is along the fracture length and no flow enters through the fracture tips.
- Fluid flow in the fracture is incompressible and steady by virtue of the limited pore volume of the fracture relative to the reservoir.
- The fracture centerline is aligned with the \hat{x}_D axis which is rotated by an angle, θ , from the x_D axis.

Cinco-Ley *et al.*¹⁰⁷ show that the Laplace domain pressure distribution in a single finite-conductivity fracture is written as

$$\bar{p}_{fD}(s) - \bar{p}_D(\hat{x}_D, s) = \frac{\pi \hat{x}_D}{s C_{fD}} - \frac{\pi}{C_{fD}} \int_0^{\hat{x}_D} \int_0^{x'} \bar{q}_D(x'', s) dx'' dx' \dots \dots \dots (4.39)$$

where $\bar{p}_D(\hat{x}_D, s)$ is a reservoir solution and the dimensionless fracture conductivity is defined as,

$$C_{fD} = \frac{k_f w_f}{k L_f}, \dots \dots \dots (4.40)$$

After discretizing the the reservoir and fracture flow component as shown in **Appendix E**, a semianalytical Laplace domain multiple arbitrarily-oriented finite-conductivity fracture solution in an anisotropic infinite-slab reservoir is written as

$$\begin{aligned}
(\bar{p}_{wD})_{\ell}(s) = & \left\{ \begin{aligned} & \sum_{i=1}^{n_f} s \bar{q}_{iD} \sum_{m=1}^{n_{fs}} \frac{(\bar{q}_D)_{im}(s)}{2} \int_{[\hat{x}'_{iD}]_m}^{[\hat{x}'_{iD}]_{m+1}} \left[\begin{aligned} & K_0 \left[\sqrt{u} \sqrt{[(\hat{x}'_{iD})_{j=1} \cos(\theta'_\ell - \theta'_i) - x']^2 + (\hat{x}'_{iD})_{j=1}^2 \sin^2(\theta'_\ell - \theta'_i)} \right] \\ & + K_0 \left[\sqrt{u} \sqrt{[(\hat{x}'_{iD})_{j=1} \cos(\theta'_\ell - \theta'_i) + x']^2 + (\hat{x}'_{iD})_{j=1}^2 \sin^2(\theta'_\ell - \theta'_i)} \right] \end{aligned} \right] dx' , \quad j=1 \\ & - \frac{\pi}{C_{fiD}} \frac{(\Delta \hat{x}'_{iD})^2}{8} (\bar{q}_D)_{ij=1}(s) + \frac{\pi (\hat{x}'_{iD})_{j=1}}{s C_{fiD}} \\ & \sum_{i=1}^{n_f} s \bar{q}_{iD} \sum_{m=1}^{n_{fs}} \frac{(\bar{q}_D)_{im}(s)}{2} \int_{[\hat{x}'_{iD}]_m}^{[\hat{x}'_{iD}]_{m+1}} \left[\begin{aligned} & K_0 \left[\sqrt{u} \sqrt{[(\hat{x}'_{iD})_j \cos(\theta'_\ell - \theta'_i) - x']^2 + (\hat{x}'_{iD})_j^2 \sin^2(\theta'_\ell - \theta'_i)} \right] \\ & + K_0 \left[\sqrt{u} \sqrt{[(\hat{x}'_{iD})_j \cos(\theta'_\ell - \theta'_i) + x']^2 + (\hat{x}'_{iD})_j^2 \sin^2(\theta'_\ell - \theta'_i)} \right] \end{aligned} \right] dx' , \quad j > 1 \\ & - \frac{\pi}{C_{fiD}} \left[\frac{(\Delta \hat{x}'_{iD})^2}{8} (\bar{q}_D)_{ij}(s) + \sum_{m=1}^{j-1} \left[\frac{(\Delta \hat{x}'_{iD})^2}{2} + (\Delta \hat{x}'_{iD}) [(\hat{x}'_{iD})_j - m \Delta \hat{x}'_{iD}] \right] (\bar{q}_D)_{im}(s) \right] + \frac{\pi (\hat{x}'_{iD})_j}{s C_{fiD}} \end{aligned} \right\} \dots (4.41)
\end{aligned}$$

for $i, \ell = 1, 2, \dots, n_f$ and $j, m = 1, 2, \dots, n_{fs}$.

The Laplace domain dimensionless flow rate for a single fracture is defined by

$$\Delta \hat{x}'_{iD} \sum_{m=1}^{n_{fs}} (\bar{q}_D)_{im} = \frac{1}{s}, \dots (4.42)$$

and the Laplace domain dimensionless total flow rate from n_f fractures is defined by

$$\sum_{i=1}^{n_f} \bar{q}_{iD} = \frac{1}{s}, \dots (4.43)$$

For each fracture, an equation relating the dimensionless pressure is written in the Laplace domain as

$$(\bar{p}_D)_{\ell i} \Big|_{j=1} = (\bar{p}_D)_{\ell i} \Big|_{j=2} = \dots = (\bar{p}_D)_{\ell i} \Big|_{j=n_{fs}} = (\bar{p}_D)_{\ell i}, \dots (4.44)$$

and for the entire multiple-fracture system, the dimensionless pressure at the wellbore is written in the Laplace domain as

$$(\bar{p}_{wD})_1 = (\bar{p}_{wD})_2 = \dots = (\bar{p}_{wD})_{n_f} = \bar{p}_{LFD}. \dots (4.45)$$

For each fracture divided into n_{fs} equal length uniform-flux segments, Eqs. 4.41 through 4.45 describe a system of $n_f(n_{fs} + n_f + 1) + 1$ equations and $n_f(n_{fs} + n_f + 1) + 1$ unknowns. Solving the system of equations requires writing an equation for each fracture *segment*, which is demonstrated in **Appendix E**. As was noted for the semianalytical multiple infinite-conductivity fracture solution, the system of equations are solved in the Laplace domain and then inverted to the time domain to obtain the dimensionless pressure.

Fig. 4.4 shows a log-log graph of dimensionless pressure and dimensionless pressure derivative versus dimensionless time for a cruciform fracture where the angle between the fractures is $\pi/2$. In Fig. 4.4, $\delta_L = 1$, and the inset graphic illustrates a cruciform fracture with primary fracture conductivity, C_{f1D} , and the secondary fracture conductivity is defined by the ratio of secondary to primary fracture conductivity, $\delta_C = C_{f2D} / C_{f1D}$ where in Fig. 4.4, $\delta_C = 1$.

In addition to allowing each fracture to have a different half length and conductivity, the multiple fracture solution also allows for an arbitrary angle between fractures. **Fig. 4.5** shows log-log type curves for equal primary and secondary fracture half length, $\delta_L = 1$ and equal primary and secondary conductivity, $\delta_C = 1$, where $C_{f1D} = 100\pi$. The type curves illustrate the effects of decreasing the angle between the fractures as shown by type curves for $\theta_{f2} = \pi/2, \pi/4$, and $\pi/8$.

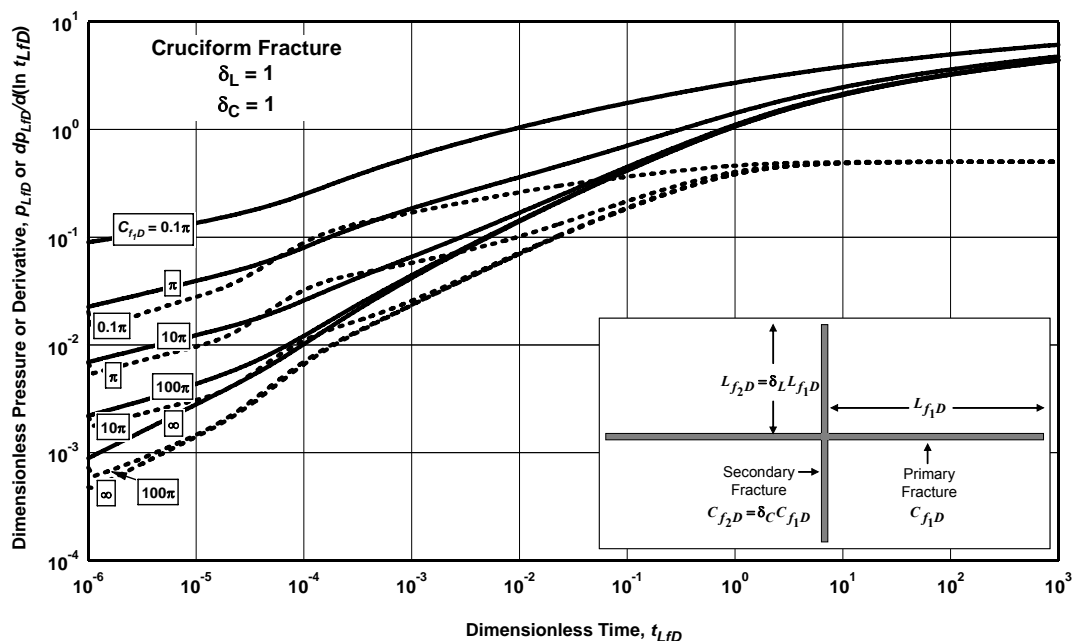


Fig. 4.4—Cruciform fracture log-log type curve with variable conductivity, $\delta_L = 1$ and $\delta_C = 1$.

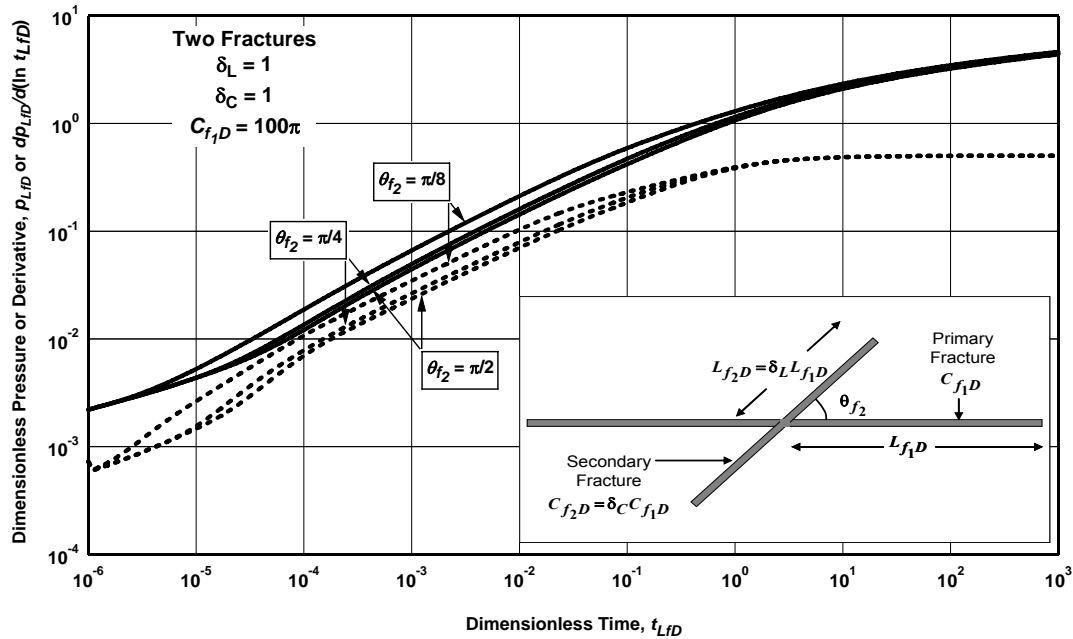


Fig. 4.5—Log-log type curves for oblique fractures with $\delta_L = 1$, $\delta_C = 1$, $C_{f1D} = 100\pi$ and $\theta_{f_2} = \pi/2$, $\pi/4$, and $\pi/8$.

4.3 Multiple Vertical Fracture Constant-Rate Drawdown Pressure Transient Solution With Variable Fracture Storage

Two scenarios can be considered for a constant-rate drawdown of a well in an infinite slab reservoir containing multiple vertical fractures with the initial reservoir pressure above the minimum in-situ or closure stress. First, isotropic stress results in all fractures dilating and closing simultaneously as the pressure declines below the closure stress. Second, an anisotropic stress condition results in a different closure stress for each fracture and different closure times for each open vertical fracture. However, not all fractures are required to be open in an anisotropic stress case since the initial reservoir pressure must be greater than the closure stress of each open fracture that subsequently closes during a drawdown.

The drawdown solution presented assumes an anisotropic stress condition with the reservoir and two fractures initially at a constant uniform pressure sufficient to keep the secondary fracture open, but the initial reservoir pressure is insufficient to dilate the primary fracture. As the pressure declines during the drawdown, the secondary fracture closes. The anisotropic stress scenario selected for modeling is based on field data indicating secondary hydraulic fracture reorientation.²⁰⁻²⁴ Reorientation occurs during refracturing because production from the primary fracture depletes the pore volume adjacent to the fracture. As the pore volume is depleted, the pressure and in-situ stress are reduced. Consequently, the

original reservoir stress condition is altered and the direction of minimum insitu stress will change. A subsequent fracture treatment in a well with altered stress will propagate a fracture(s) in a plane different than the primary fracture. Other isotropic or anisotropic stress scenarios can be modeled with a similar approach, but are not developed in Chapter IV.

The derivation for a constant-rate drawdown for a well in an infinite-acting slab reservoir with multiple vertical hydraulic fractures and the initial reservoir pressure above the closure stress of the secondary fracture but below the closure stress of the primary fracture is identical to the constant-rate drawdown with constant before- and after-closure storage for a well with a single vertical fracture derived in **Appendix B**. However, the nomenclature changes somewhat to reflect the new multiple fracture storage coefficient definitions and the reservoir solution accounting for multiple hydraulic fractures. The solution is written as

$$p_{wCD}(t_{LFD}) = p_{LfacD}(t_{LFD}) - (C_{LfbCD} - C_{LfacD}) \int_0^{(t_c)_{LFD}} p'_{LfacD}(t_{LFD} - \tau_D) p'_{wCD}(\tau_D) d\tau_D, \dots (4.46)$$

where p_{LfacD} is the dimensionless pressure solution for a constant-rate drawdown in a well producing from multiple finite- or infinite conductivity vertical fractures with constant after-closure storage, which is written in the Laplace domain as

$$\bar{p}_{LfacD} = \frac{\bar{p}_{LFD}}{1 + s^2 C_{LfacD} \bar{p}_{LFD}}, \dots (4.47)$$

and \bar{p}_{LFD} is the Laplace domain reservoir solution for production from multiple arbitrarily-oriented finite- or infinite-conductivity fractures.

The dimensionless before-closure storage is defined as

$$C_{LfbCD} = \frac{C_{LfbC}}{2\pi\phi c_t h L_{f1}^2}, \dots (4.48)$$

and the before-closure storage coefficient is written as

$$C_{LfbC} = c_w V_w + 2c_f V_{f1} + 2 \frac{A_{f2}}{S_{f2}}. \dots (4.49)$$

The before-closure storage coefficient consists of constant wellbore storage, $c_w V_w$, constant primary fracture storage, $2c_f V_{f1}$, and constant secondary fracture storage where A_{f2} is the area of one wing of the secondary fracture and S_{f2} is the secondary fracture stiffness, which is defined for a single fracture in **Appendix B**.

The dimensionless after-closure storage is defined as

$$C_{LfacD} = \frac{C_{Lfac}}{2\pi\phi c_t h L_{f1}^2}, \dots (4.50)$$

where the dimensionless after-closure storage is defined as

$$C_{Lfac} = c_w V_w + 2c_f (V_{f1} + V_{f2}) \dots\dots\dots(4.51)$$

4.3.1 Numerical Evaluation of a Multiple Vertical Fracture Constant-Rate Drawdown Pressure Transient Solution With Variable Fracture Storage. The constant-rate drawdown solution for a well in an infinite-acting slab reservoir with multiple vertical hydraulic fractures and the initial reservoir pressure above the closure stress of the secondary fracture but below the closure stress of the primary fracture is written as

$$p_{wcD}(t_{Lfd}) = p_{LfacD}(t_{Lfd}) - (C_{Lfbcd} - C_{LfacD}) \int_0^{(t_c)_{Lfd}} p'_{LfacD}(t_{Lfd} - \tau_D) p'_{wcD}(\tau_D) d\tau_D \dots\dots(4.52)$$

After integrating-by-parts, the solution is written as

$$p_{wcD}(t_{Lfd}) = \left[\begin{array}{l} p_{LfacD}(t_{Lfd}) + (C_{Lfbcd} - C_{LfacD}) p_{acD} [t_{Lfd} - (t_c)_{Lfd}] p'_{wcD} [(t_c)_{Lfd}] \\ - (C_{Lfbcd} - C_{LfacD}) \int_0^{(t_c)_{Lfd}} p''_{wcD}(\tau_D) p_{LfacD}(t_{Lfd} - \tau_D) d\tau_D \end{array} \right] \dots\dots(4.53)$$

and after discretizing the integral term, a numerical approximation is written as

$$p_{wcD}(t_{Lfd})_n = \left[\begin{array}{l} p_{LfacD}(t_{Lfd})_n + (C_{Lfbcd} - C_{LfacD}) p_{LfacD} [(t_{Lfd})_n - (t_{Lfd})_j] p'_{wcD} [(t_{Lfd})_j] \\ - (C_{Lfbcd} - C_{LfacD}) \sum_{i=1}^j \left[\begin{array}{l} \left(\frac{p_{wcD}(t_{Lfd})_i - p_{wcD}(t_{Lfd})_{i-1}}{(t_{Lfd})_i - (t_{Lfd})_{i-1}} \right) \\ - \left(\frac{p_{wcD}(t_{Lfd})_{i-1} - p_{wcD}(t_{Lfd})_{i-2}}{(t_{Lfd})_{i-1} - (t_{Lfd})_{i-2}} \right) \right] \\ \times p_{LfacD} [(t_{Lfd})_n - (t_{Lfd})_{i-1}] \end{array} \right] \end{array} \right] \dots\dots(4.54)$$

where j is the time index at closure. Note that for $n \leq j$, $p_{LfacD}[(t_{Lfd})_n - (t_{Lfd})_j] = 0$.

Fig. 4.6 shows a log-log graph of dimensionless pressure and dimensionless pressure derivative versus dimensionless time for a cruciform fracture where the angle between two infinite-conductivity fractures is $\pi/2$ and the before- and after-closure storage is constant, $C_{Lfbcd} = C_{LfacD} = \{0.005, 0.010\}$. Similarly, **Fig. 4.7** shows a log-log constant-rate drawdown type curve for an infinite-conductivity cruciform fracture with $C_{Lfbcd} = 0.010$, $C_{LfacD} = 0.005$, and $(t_c)_{Lfd} = 10^{-4}$. Note that the variable storage solution overlays the constant storage type curve before and after closure.

The semianalytical multiple arbitrarily-oriented infinite-conductivity fracture solution with constant storage is "expensive" to evaluate in terms of computer time. For example, the constant storage evaluation for $C_{Lfbcd} = 0.010$ – with the solution programmed in Mathematica 5.2 – required 27 hours of CPU time to calculate 200 data points across 9 log cycles. However, if the constant storage solution is expensive, the variable storage solution is exorbitant. The 50 data points across 5 log cycles shown in Fig. 4.7 required 168 hours (seven *days*) of CPU time.

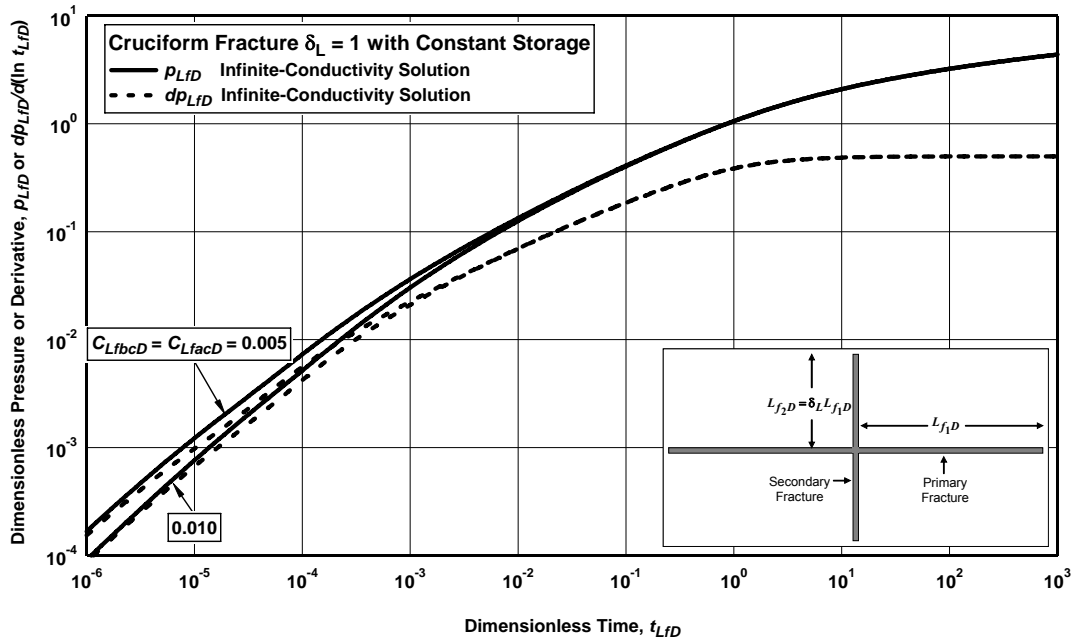


Fig. 4.6—Cruciform fracture log-log type curve with infinite-conductivity fractures and constant storage, $C_{LfbcD} = C_{LfacD} = \{0.005, 0.010\}$.

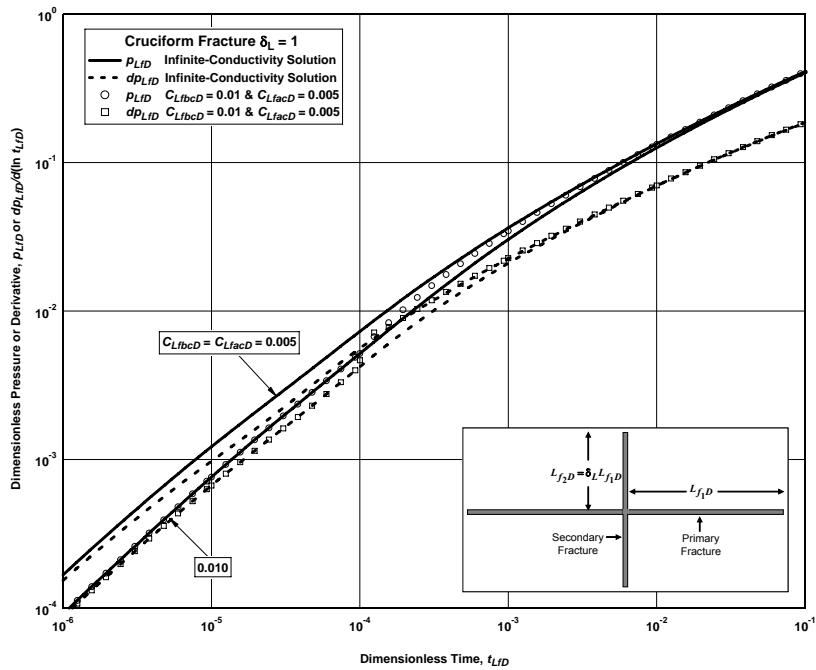


Fig. 4.7—Cruciform fracture log-log constant storage type curve with infinite-conductivity fractures and variable storage, $C_{LfbcD} = 0.005$ and $C_{LfacD} = 0.010$.

Obviously, more efficient algorithms and custom software will improve the CPU time required to evaluate either the constant or variable storage solutions, but with the variable storage solution overlaying the constant storage solution before- and after-closure, it may not necessary to calculate the variable storage solution for routine type curve matching. Matching observed variable-storage data to constant-storage type curves and ignoring the transition from one curve to another should be sufficient in most cases.

4.4 Fracture-Injection/Falloff Solution With a Pre-Existing Fracture

Several scenarios can occur during a fracture-injection/falloff sequence in a well with a pre-existing hydraulic fracture. If the local stress field has not been altered by production, an existing fracture can dilate during the injection and close as the pressure declines below the closure stress during the falloff. However, if the local stress field has been altered, the existing fracture may dilate during the injection with a new fracture induced and propagated in an adjacent plane. Alternatively, the injection may induce a new fracture in a plane other than the pre-existing fracture, but the pressure during the injection is insufficient to dilate the pre-existing fracture.

When a pre-existing fracture dilates during an injection and closes during the falloff without inducing an additional fracture, a fracture-injection/falloff sequence is modeled as shown in Chapter III with fracture length considered to be created instantaneously. When a new fracture is induced in a plane other than the existing fracture *without* pre-existing fracture dilation, the propagating- and existing-fracture dimensionless storage coefficient is defined as

$$C_{pLfD} = \frac{C_{pLf}(p_w(t))}{2\pi\phi c_t h L_{f1}^2}, \dots\dots\dots(4.55)$$

where the propagating- and existing-fracture storage coefficient is defined as

$$C_{pLf}(p_w(t)) = c_w V_w + 2c_f [V_{f1} + V_{f2}(p_w(t))] + 2 \frac{dV_{f2}(p_w(t))}{dp_w} \dots\dots\dots(4.56)$$

Assuming as shown in **Appendix C** that a power model can be used for fracture propagation; assuming $c_{fn2} \ll 1$; and assuming linear-elastic fracture mechanics are applicable; the propagating- and existing-fracture storage coefficient is written as

$$C_{pLf}(t_{LfD}) = c_w V_w + 2c_f V_{f1} + 2 \frac{A_{f2}}{S_{f2}} \left(\frac{t_{LfD}}{(t_e)_{LfD}} \right)^\alpha, \dots\dots\dots(4.57)$$

which is not a function of pressure and allows the superposition principle to be used to develop a fracture-injection/falloff solution in a well with a pre-existing fracture.

During the falloff, the induced fracture closes, and the before-closure storage coefficient is the same as previously defined for a closing secondary fracture during a drawdown in a reservoir with multiple fractures. The before-secondary fracture closure storage coefficient is written as

$$C_{Lfbc} = c_w V_w + 2c_f V_{f1} + 2 \frac{A_{f2}}{S_{f2}} \dots (4.58)$$

Similarly, the after-closure storage coefficient is written as

$$C_{Lfac} = c_w V_w + 2c_f (V_{f1} + V_{f2}) \dots (4.59)$$

The model for a fracture-injection/falloff sequence in a well with a constant-volume pre-existing vertical fracture that induces a secondary fracture is a simple modification of the fracture-injection/falloff model without an existing fracture developed in **Appendix C**. However, the nomenclature and storage coefficient definitions change somewhat to reflect the new propagating- and existing fracture storage coefficient definition, and the reservoir solution changes to account for multiple hydraulic fractures. The solution is written as

$$p_{wsD}(t_{LjD}) = \left[\begin{array}{l} q_{wsD} \left[p_{pLjD}(t_{LjD}) - p_{pLjD}(t_{LjD} - (t_e)_{LjD}) \right] \\ - \int_0^{(t_e)_{LjD}} p'_{pLjD}(t_{LjD} - \tau_D) C_{pLjD}(\tau_D) p'_{wsD}(\tau_D) d\tau_D \\ + C_{LfbcD} \int_0^{(t_e)_{LjD}} p'_{LjD}(t_{LjD} - \tau_D) p'_{wsD}(\tau_D) d\tau_D \\ - (C_{LfbcD} - C_{LfacD}) \int_0^{(t_c)_{LjD}} p'_{LjD}(t_{LjD} - \tau_D) p'_{wsD}(\tau_D) d\tau_D \\ - C_{LfacD} \int_0^{t_{LjD}} p'_{LjD}(t_{LjD} - \tau_D) p'_{wsD}(\tau_D) d\tau_D \end{array} \right] \dots (4.60)$$

where p_{pLjD} is the propagating-fracture solution with multiple constant-length fractures and a single induced fracture, and p_{LjD} is the multiple arbitrarily-oriented finite- or infinite-conductivity fracture solution.

With secondary fracture propagation, the before-closure limiting-case solution for $(t_e)_{LjD} \ll t_{LjD} < (t_c)_{LjD}$ is written as

$$p_{wsD}(t_{LjD}) = p_{wsD}(0) C_{LfbcD} p'_{LfbcD}(t_{LjD}) \dots (4.61)$$

where p_{LfbcD} is the dimensionless pressure solution for a constant-rate drawdown in a well producing from multiple fractures with constant before-closure storage, which is written in the Laplace domain as

$$\bar{p}_{LfbcD} = \frac{\bar{p}_{LjD}}{1 + s^2 C_{LfbcD} \bar{p}_{LjD}} \dots (4.62)$$

and \bar{p}_{LjD} is the Laplace domain reservoir solution for production from multiple arbitrarily-oriented finite- or infinite-conductivity fractures.

The after-closure limiting-case solution with secondary fracture propagation when $t_{LjD} \gg (t_e)_{LjD} \gg (t_c)_{LjD}$ is written as

$$p_{wsD}(t_{LjD}) = \left[p_{wsD}(0)C_{LjbcD} - p_{wsD}\left((t_c)_{LjD}\right)(C_{LjbcD} - C_{LjacD}) \right] p'_{LjacD}(t_{LjD}) \dots\dots\dots(4.63)$$

where p_{LjacD} is the dimensionless pressure solution for a constant-rate drawdown in a well producing from multiple fractures with constant after-closure storage, which is written in the Laplace domain as

$$\bar{p}_{LjbcD} = \frac{\bar{p}_{LjD}}{1 + s^2 C_{LjacD} \bar{p}_{LjD}} \dots\dots\dots(4.64)$$

The limiting-case solutions are slug-test solutions, which suggest that a fracture-injection/falloff sequence in a well with a pre-existing fracture and a secondary fracture induced during an injection can be analyzed as a slug test provided the injection time is short relative to the reservoir response.

A fracture-injection/falloff model is more complicated when existing fractures dilate and a new fracture is induced during an injection. For example, during an injection, an induced fracture will begin to propagate in the direction of maximum stress. When the injection pressure exceeds the closure stress in the existing fractures, the existing fractures will begin to dilate. During the falloff, multiple closure times will be observed as the pressure declines below the closure stress of each dilated existing fracture and the induced fracture. A fracture-injection/falloff model developed using the unit-step function must account for each fracture opening and closing through the use of multiple storage coefficients and fracture closure times. Consider a relatively simple case with a single existing fracture dilated and a single fracture induced during the injection. The dimensionless propagating- and existing-fracture storage coefficient is written as

$$C_{pLf}(t_{LjD}) = c_w V_w + 2c_f V_{f1} + 2 \frac{A_{f2}}{S_{f2}} \left(\frac{t_{LjD}}{(t_e)_{LjD}} \right)^\alpha \dots\dots\dots(4.65)$$

When the existing fracture begins to dilate, $(t_d)_{LjD} < t_{LjD} \leq (t_e)_{LjD}$, a new propagating- and dilating-fracture storage coefficient is defined as

$$C_{pdLf}(t_{LjD}) = c_w V_w + 2 \frac{A_{f1}}{S_{f1}} + 2 \frac{A_{f2}}{S_{f2}} \left(\frac{t_{LjD}}{(t_e)_{LjD}} \right)^\alpha \dots\dots\dots(4.66)$$

During the falloff when $(t_e)_{LjD} < t_{LjD} \leq (t_{c1})_{LjD}$, a primary-fracture before-closure storage coefficient is defined as

$$C_{Ljbc1}(t_{LjD}) = c_w V_w + 2 \left[\frac{A_{f1}}{S_{f1}} + \frac{A_{f2}}{S_{f2}} \right] \dots\dots\dots(4.67)$$

and a secondary-fracture before-closure storage coefficient is defined for $(t_{c1})_{LjD} < t_{LjD} \leq (t_{c2})_{LjD}$ as

$$C_{Lfbc2} = c_w V_w + 2c_f V_{f1} + 2 \frac{A_{f2}}{S_{f2}} \dots (4.68)$$

After primary- and secondary-fracture closure, $t_{LjD} > (t_{c2})_{LjD}$, the after-closure storage coefficient is defined as

$$C_{Lfac} = c_w V_w + 2c_f (V_{f1} + V_{f2}) \dots (4.69)$$

Following the derivation method described in **Appendix C**, a material balance equation is developed that is applicable at all times during the fracture-injection/falloff sequence, and using the unit-step function, a fracture-injection/falloff model for a well with an existing fracture dilated and a secondary fracture induced during the injection is written as

$$p_{wsD}(t_{LjD}) = \left[\begin{aligned} & q_{wsD} [p_{pLjD}(t_{LjD}) - p_{pLjD}(t_{LjD} - (t_e)_{LjD})] \\ & - \int_0^{(t_d)_{LjD}} p'_{pLjD}(t_{LjD} - \tau_D) [C_{pLjD}(\tau_D) - C_{pdLjD}(\tau_D)] p'_{wsD}(\tau_D) d\tau_D \\ & - \int_0^{(t_e)_{LjD}} p'_{pLjD}(t_{LjD} - \tau_D) C_{pdLjD}(\tau_D) p'_{wsD}(\tau_D) d\tau_D \\ & + C_{LfbclD} \int_0^{(t_e)_{LjD}} p'_{LjD}(t_{LjD} - \tau_D) p'_{wsD}(\tau_D) d\tau_D \\ & - (C_{LfbclD} - C_{Lfbcl2D}) \int_0^{(t_{c1})_{LjD}} p'_{LjD}(t_{LjD} - \tau_D) p'_{wsD}(\tau_D) d\tau_D \\ & - (C_{Lfbcl2D} - C_{LfacD}) \int_0^{(t_{c2})_{LjD}} p'_{LjD}(t_{LjD} - \tau_D) p'_{wsD}(\tau_D) d\tau_D \\ & - C_{LfacD} \int_0^{t_{LjD}} p'_{LjD}(t_{LjD} - \tau_D) p'_{wsD}(\tau_D) d\tau_D \end{aligned} \right] \dots (4.70)$$

Similar to the propagating-fracture solution for a single vertical fracture described in Chapter III, the propagating-fracture solution, $p_{pLjD}(t_{LjD})$, with multiple constant-length fractures and a single induced fracture can be written as

$$p_{pLjD}(t_{LjD}) = \begin{cases} p_{prLjD}(t_{LjD}) & t_{LjD} < (t_e)_{LjD} \\ p_{LjD}(t_{LjD}) & t_{LjD} > (t_e)_{LjD} \end{cases} \dots (4.71)$$

or using the unit-step function written as

$$p_{pLjD}(t_{LjD}) = (1 - U_{(t_e)_{LjD}}) p_{prLjD}(t_{LjD}) + U_{(t_e)_{LjD}} p_{LjD}(t_{LjD}) \dots (4.72)$$

The propagating-fracture solution with multiple constant-length fractures and a single induced fracture can be written in terms of the semianalytical multiple arbitrarily-oriented finite- or infinite-conductivity fracture solution by writing a quasi-static form as

$$\begin{aligned}
 (\bar{P}_{prLjD})_{\ell}(s) = & \\
 & \left\{ \begin{aligned}
 & \sum_{i=1}^{n_f} s \bar{q}_{iD} \sum_{m=1}^{n_{fs}} \frac{(\bar{q}_D)_{im}(s)}{2} \int_{[\hat{x}'_{iD}(t_{LjD})]_m}^{[\hat{x}'_{iD}(t_{LjD})]_{m+1}} \left[\begin{aligned}
 & K_0 \left[\sqrt{u} \sqrt{[(\hat{x}'_{iD})_{j=1} \cos(\theta'_\ell - \theta'_i) - x']^2 + (\hat{x}'_{iD})_{j=1}^2 \sin^2(\theta'_\ell - \theta'_i)} \right] \\
 & + K_0 \left[\sqrt{u} \sqrt{[(\hat{x}'_{iD})_{j=1} \cos(\theta'_\ell - \theta'_i) + x']^2 + (\hat{x}'_{iD})_{j=1}^2 \sin^2(\theta'_\ell - \theta'_i)} \right]
 \end{aligned} \right] dx' \quad , j = 1 \\
 & - \frac{\pi}{C_{fjD}} \frac{(\Delta \hat{x}'_{iD})^2}{8} (\bar{q}_D)_{ij=1}(s) + \frac{\pi (\hat{x}'_{iD})_{j=1}}{s C_{fjD}} \\
 & \sum_{i=1}^{n_f} s \bar{q}_{iD} \sum_{m=1}^{n_{fs}} \frac{(\bar{q}_D)_{im}(s)}{2} \int_{[\hat{x}'_{iD}(t_{LjD})]_m}^{[\hat{x}'_{iD}(t_{LjD})]_{m+1}} \left[\begin{aligned}
 & K_0 \left[\sqrt{u} \sqrt{[(\hat{x}'_{iD})_j \cos(\theta'_\ell - \theta'_i) - x']^2 + (\hat{x}'_{iD})_j^2 \sin^2(\theta'_\ell - \theta'_i)} \right] \\
 & + K_0 \left[\sqrt{u} \sqrt{[(\hat{x}'_{iD})_j \cos(\theta'_\ell - \theta'_i) + x']^2 + (\hat{x}'_{iD})_j^2 \sin^2(\theta'_\ell - \theta'_i)} \right]
 \end{aligned} \right] dx' \quad , j > 1 \\
 & - \frac{\pi}{C_{fjD}} \left[\frac{(\Delta \hat{x}'_{iD})^2}{8} (\bar{q}_D)_{ij}(s) + \sum_{m=1}^{j-1} \left[\frac{(\Delta \hat{x}'_{iD})^2}{2} + (\Delta \hat{x}'_{iD}) [(\hat{x}'_{iD})_j - m \Delta \hat{x}'_{iD}] \right] (\bar{q}_D)_{im}(s) \right] + \frac{\pi (\hat{x}'_{iD})_j}{s C_{fjD}}
 \end{aligned} \right\} \dots \dots \dots (4.73)
 \end{aligned}$$

for $i, \ell = 1, 2, \dots, n_f$ and $j, m = 1, 2, \dots, n_{fs}$. The Laplace domain dimensionless flow rate for a single fracture is defined by

$$\Delta \hat{x}'_{iD} \sum_{m=1}^{n_{fs}} (\bar{q}_D)_{im} = \frac{1}{s}, \dots \dots \dots (4.74)$$

and the Laplace domain dimensionless total flow rate from n_f fractures is defined by

$$\sum_{i=1}^{n_f} \bar{q}_{iD} = \frac{1}{s}, \dots \dots \dots (4.75)$$

For each fracture, an equation relating the dimensionless pressure is written in the Laplace domain as

$$(\bar{P}_D)_{\ell i} |_{j=1} = (\bar{P}_D)_{\ell i} |_{j=2} = \dots = (\bar{P}_D)_{\ell i} |_{j=n_{fs}} = (\bar{P}_D)_{\ell i}, \dots \dots \dots (4.76)$$

and for the entire multiple-fracture system, the dimensionless pressure at the wellbore is written in the Laplace domain as

$$(\bar{P}_{prLjD})_1 = (\bar{P}_{prLjD})_2 = \dots = (\bar{P}_{prLjD})_{n_f} = \bar{P}_{prLjD} \dots \dots \dots (4.77)$$

Note that the propagating fracture half length changes during the injection, which can be modeled using a power model approximation and written as

$$L_{fjD}(t_{LjD}) = \begin{cases} \left(\frac{t_{LjD}}{(t_e)_{LjD}} \right)^{\alpha_{iN}} & t_{LjD} < (t_e)_{LjD} \\ 1 & t_{LjD} \geq (t_e)_{LjD} \end{cases} \dots \dots \dots (4.78)$$

where α_{iN} is the fracture-growth exponent, which varies between $\frac{1}{2}$ and 1 for low-and high-efficiency fracture growth, respectively, and where $(t_e)_{LjD}$ is the dimensionless time at the end of fracture

propagation. With $L'_{fiD}(t_{LfD})$ a function of dimensionless time, $\Delta\hat{x}'_{iD} = L'_{fiD}(t_{LfD}) / n_{fs}$ and the dimensionless distances, $[\hat{x}'_{iD}]_j$ and $[\hat{x}'_{iD}(t_{LfD})]_m$, are also functions of dimensionless time.

With infinite-conductivity fractures and a small dimensionless injection time, the pressure-averaging solution described in Section 4.2.2 can be used to numerically evaluate the solution provided the dimensionless injection time is on the order of 10^{-5} . The computational difficulty of the semianalytical solution versus the relative speed and simplicity of the pressure-averaging solution makes the pressure-averaging solution the preferred solution at small dimensionless times. With a propagating fracture during the injection, the pressure-averaging solution can be written as

$$\begin{bmatrix} 1 & A_{11} & A_{12} & \cdots & A_{1n_f} \\ 1 & A_{21} & A_{22} & \cdots & A_{2n_f} \\ \vdots & \vdots & \vdots & \cdots & \vdots \\ 1 & A_{n_f 1} & A_{n_f 2} & \vdots & A_{n_f n_f} \\ 0 & 1 & 1 & \cdots & 1 \end{bmatrix} \begin{bmatrix} \overline{p_{prLfD}} \\ \bar{q}_{1D} \\ \bar{q}_{2D} \\ \vdots \\ \bar{q}_{n_f D} \end{bmatrix} = \begin{bmatrix} 0 \\ 0 \\ 0 \\ \vdots \\ \frac{1}{s} \end{bmatrix}, \dots\dots\dots(4.79)$$

where

$$A_{ij} = \frac{(-1)}{4sL_{fiD}(t_{LfD})L_{fjD}(t_{LfD})} \int_{-L_{fiD}(t_{LfD})}^{L_{fiD}(t_{LfD})} \int_{-L_{fjD}(t_{LfD})}^{L_{fjD}(t_{LfD})} K_0 \left[\sqrt{u} \frac{\left[r_D \cos(\theta_i - \theta_j) - \alpha \right]^2}{\sqrt{r_D^2 \sin^2(\theta_i - \theta_j)}} \right] d\alpha dr_D \dots\dots\dots(4.80)$$

4.4.1 Limiting-Case Fracture-Injection/Falloff Solutions With a Dilating Pre-Existing Fracture, a Propagating Induced Fracture, Multiple Closures, and Constant After-Closure Storage. The dimensionless wellbore pressure solution for a fracture-injection/falloff with a dilating pre-existing fracture, a propagating induced fracture during the injection, multiple closure times, and constant after-closure storage is written as

$$p_{wsD}(t_{LfD}) = \begin{bmatrix} q_{wsD} \left[p_{pLfD}(t_{LfD}) - p_{pLfD}(t_{LfD} - (t_e)_{LfD}) \right] \\ - \int_0^{(t_d)_{LfD}} p'_{pLfD}(t_{LfD} - \tau_D) \left[C_{pLfD}(\tau_D) - C_{pdLfD}(\tau_D) \right] p'_{wsD}(\tau_D) d\tau_D \\ - \int_0^{(t_e)_{LfD}} p'_{pLfD}(t_{LfD} - \tau_D) C_{pdLfD}(\tau_D) p'_{wsD}(\tau_D) d\tau_D \\ + C_{LfbclD} \int_0^{(t_e)_{LfD}} p'_{LfD}(t_{LfD} - \tau_D) p'_{wsD}(\tau_D) d\tau_D \\ - \left(C_{LfbclD} - C_{Lfbcl2D} \right) \int_0^{(t_{c1})_{LfD}} p'_{LfD}(t_{LfD} - \tau_D) p'_{wsD}(\tau_D) d\tau_D \\ - \left(C_{Lfbcl2D} - C_{LfacD} \right) \int_0^{(t_{c2})_{LfD}} p'_{LfD}(t_{LfD} - \tau_D) p'_{wsD}(\tau_D) d\tau_D \\ - C_{LfacD} \int_0^{t_{LfD}} p'_{LfD}(t_{LfD} - \tau_D) p'_{wsD}(\tau_D) d\tau_D \end{bmatrix}, \dots\dots\dots(4.81)$$

which can also be written as

$$p_{wsD}(t_{LjD}) = \left[\begin{aligned} & q_{wsD} \left[p_{pLjD}(t_{LjD}) - p_{pLjD}(t_{LjD} - (t_e)_{LjD}) \right] \\ & - \int_0^{(t_d)_{LjD}} p'_{pLjD}(t_{LjD} - \tau_D) \left[C_{pLjD}(\tau_D) - C_{pdLjD}(\tau_D) \right] p'_{wsD}(\tau_D) d\tau_D \\ & - \int_0^{(t_e)_{LjD}} p'_{pLjD}(t_{LjD} - \tau_D) \left[C_{pdLjD}(\tau_D) - C_{Ljbc1D} \right] p'_{wsD}(\tau_D) d\tau_D \\ & - \left(C_{Ljbc1D} - C_{Ljbc2D} \right) \int_0^{(t_{c1})_{LjD}} p'_{LjD}(t_{LjD} - \tau_D) p'_{wsD}(\tau_D) d\tau_D \\ & - \left(C_{Ljbc2D} - C_{LfacD} \right) \int_0^{(t_{c2})_{LjD}} p'_{LjD}(t_{LjD} - \tau_D) p'_{wsD}(\tau_D) d\tau_D \\ & - C_{LfacD} \int_0^{t_{LjD}} p'_{LjD}(t_{LjD} - \tau_D) p'_{wsD}(\tau_D) d\tau_D \end{aligned} \right] \dots\dots\dots (4.82)$$

Assume the secondary fracture half-length is created instantaneously such that $C_{pLjD} = C_{Ljbc2D}$ and $C_{pdLjD} = C_{Ljbc1D}$. A limiting-case solution can be written as

$$p_{wsD}(t_{LjD}) = \left[\begin{aligned} & q_{wsD} \left[p_{LjD}(t_{LjD}) - p_{LjD}(t_{LjD} - (t_e)_{LjD}) \right] \\ & + \left(C_{Ljbc1D} - C_{Ljbc2D} \right) \int_0^{(t_d)_{LjD}} p'_{LjD}(t_{LjD} - \tau_D) p'_{wsD}(\tau_D) d\tau_D \\ & - \left(C_{Ljbc1D} - C_{Ljbc2D} \right) \int_0^{(t_{c1})_{LjD}} p'_{LjD}(t_{LjD} - \tau_D) p'_{wsD}(\tau_D) d\tau_D \\ & - \left(C_{Ljbc2D} - C_{LfacD} \right) \int_0^{(t_{c2})_{LjD}} p'_{LjD}(t_{LjD} - \tau_D) p'_{wsD}(\tau_D) d\tau_D \\ & - C_{LfacD} \int_0^{t_{LjD}} p'_{LjD}(t_{LjD} - \tau_D) p'_{wsD}(\tau_D) d\tau_D \end{aligned} \right] \dots\dots\dots (4.83)$$

Consider a case when $(t_d)_{LjD} < (t_e)_{LjD} \ll t_{LjD} < (t_{c1})_{LjD}$, which allows the solution to be written as

$$p_{wsD}(t_{LjD}) = \left[\begin{aligned} & \left(C_{Ljbc1D} - C_{Ljbc2D} \right) \int_0^{(t_d)_{LjD}} p'_{LjD}(t_{LjD} - \tau_D) p'_{wsD}(\tau_D) d\tau_D \\ & - C_{Ljbc1D} \int_0^{t_{LjD}} p'_{LjD}(t_{LjD} - \tau_D) p'_{wsD}(\tau_D) d\tau_D \end{aligned} \right] \dots\dots\dots (4.84)$$

When the injection time is short, $(t_e)_{LjD} \rightarrow 0$, and recognizing that $(t_e)_{LjD} > (t_d)_{LjD}$, the solution can be written as

$$p_{wsD}(t_{LjD}) = -C_{Ljbc1D} \int_0^{t_{LjD}} p'_{LjD}(t_{LjD} - \tau_D) p'_{wsD}(\tau_D) d\tau_D, \dots\dots\dots (4.85)$$

which after transforming to the Laplace domain, simplifying, and inverting back to the time domain is written as

$$p_{wsD}(t_{LjD}) = p_{wsD}(0) C_{Ljbc1D} p'_{Ljbc1D}(t_{LjD}), \dots\dots\dots (4.86)$$

where the Laplace domain dimensionless multiple-fracture solution for a well produced at a constant rate with constant primary-fracture before-closure storage is written in the Laplace domain as

$$\bar{p}_{Ljbc1D} = \frac{\bar{p}_{LjD}}{1 + s^2 C_{Ljbc1D} \bar{p}_{LjD}} \dots\dots\dots(4.87)$$

Consequently, the limiting-case solution for an instantaneous injection, $(t_e)_{LjD} \rightarrow 0$, with $(t_d)_{LjD} < (t_e)_{LjD} \ll t_{LjD} < (t_{c1})_{LjD}$ is a slug-test solution.

Consider a case with an instantaneous injection, $(t_e)_{LjD} \rightarrow 0$, when $(t_d)_{LjD} < (t_e)_{LjD} \ll (t_{c1})_{LjD} \ll t_{LjD} < (t_{c2})_{LjD}$, which allows the solution to be written as

$$p_{wsD}(t_{LjD}) = \left[\begin{array}{l} -(C_{Ljbc1D} - C_{Ljbc2D}) \int_0^{(t_{c1})_{LjD}} p'_{LjD}(t_{LjD} - \tau_D) p'_{wsD}(\tau_D) d\tau_D \\ -C_{Ljbc2D} \int_0^{t_{LjD}} p'_{LjD}(t_{LjD} - \tau_D) p'_{wsD}(\tau_D) d\tau_D \end{array} \right] \dots\dots\dots(4.88)$$

After transforming to the Laplace domain, simplifying, and inverting back to the time domain, the limiting-case solution is written as

$$p_{wsD}(t_{LjD}) = \left[p_{wsD}(0) C_{Ljbc1D} - p_{wsD}((t_{c1})_{LjD}) (C_{Ljbc1D} - C_{Ljbc2D}) \right] p'_{Ljbc2D}(t_{LjD}), \dots\dots\dots(4.89)$$

where the Laplace domain dimensionless multiple-fracture solution for a well produced at a constant rate with constant secondary-fracture before-closure storage is written in the Laplace domain as

$$\bar{p}_{Ljbc2D} = \frac{\bar{p}_{LjD}}{1 + s^2 C_{Ljbc2D} \bar{p}_{LjD}} \dots\dots\dots(4.90)$$

Consequently, the limiting-case solution for an instantaneous injection, $(t_e)_{LjD} \rightarrow 0$, with $(t_d)_{LjD} < (t_e)_{LjD} \ll (t_{c1})_{LjD} \ll t_{LjD} < (t_{c2})_{LjD}$ is also a slug-test solution.

Finally, consider the case of an instantaneous injection, $(t_e)_{LjD} \rightarrow 0$, when $(t_d)_{LjD} < (t_e)_{LjD} \ll (t_{c1})_{LjD} < (t_{c2})_{LjD} \ll t_{LjD}$, which allows the solution to be written as

$$p_{wsD}(t_{LjD}) = \left[\begin{array}{l} -(C_{Ljbc1D} - C_{Ljbc2D}) \int_0^{(t_{c1})_{LjD}} p'_{LjD}(t_{LjD} - \tau_D) p'_{wsD}(\tau_D) d\tau_D \\ -(C_{Ljbc2D} - C_{LjfacD}) \int_0^{(t_{c2})_{LjD}} p'_{LjD}(t_{LjD} - \tau_D) p'_{wsD}(\tau_D) d\tau_D \\ -C_{LjfacD} \int_0^{t_{LjD}} p'_{LjD}(t_{LjD} - \tau_D) p'_{wsD}(\tau_D) d\tau_D \end{array} \right] \dots\dots\dots(4.91)$$

After transforming to the Laplace domain, simplifying, and inverting back to the time domain, the limiting-case solution is written as

$$p_{wsD}(t_{LjD}) = \left[\begin{array}{l} p_{wsD}(0) C_{Ljbc1D} - p_{wsD}((t_{c1})_{LjD}) (C_{Ljbc1D} - C_{Ljbc2D}) \\ -p_{wsD}((t_{c2})_{LjD}) (C_{Ljbc2D} - C_{LjfacD}) \end{array} \right] p'_{LjfacD}(t_{LjD}), \dots\dots\dots(4.92)$$

where the Laplace domain dimensionless multiple-fracture solution for a well produced at a constant rate with constant after-closure storage is written in the Laplace domain as

$$\bar{p}_{LfacD} = \frac{\bar{p}_{LjD}}{1 + s^2 C_{LfacD} \bar{p}_{LjD}} \dots\dots\dots(4.93)$$

Consequently, the limiting-case solution for an instantaneous injection, $(t_e)_{LjD} \rightarrow 0$, with $(t_d)_{LjD} < (t_e)_{LjD} \ll (t_{c1})_{LjD} < (t_{c2})_{LjD} \ll t_{LjD}$ is also a slug-test solution.

The limiting-case slug-test solutions are applicable provided that a fracture-injection can be considered to occur instantaneously. From the analytical solution, a fracture-injection with a dilating pre-existing fracture, a propagating induced fracture, multiple closure times, and constant after-closure storage can be considered to occur instantaneously when the inequality written as

$$\left| \begin{aligned} & p'_{LjD}(t_{LjD}) \int_0^{(t_d)_{LjD}} [C_{pdLjD} - C_{pLjD}(\tau_D)] p'_{wsD}(\tau_D) d\tau_D \\ & + p'_{LjD}(t_{LjD}) \int_0^{(t_e)_{LjD}} [C_{Ljbc1D} - C_{pdLjD}(\tau_D)] p'_{wsD}(\tau_D) d\tau_D \\ & - C_{LfacD} \int_0^{t_{LjD}} p'_{LjD}(t_{LjD} - \tau_D) p'_{wsD}(\tau_D) d\tau_D \\ & \ll - (C_{Ljbc1D} - C_{Ljbc2D}) \int_0^{(t_{c1})_{LjD}} p'_{LjD}(t_{LjD} - \tau_D) p'_{wsD}(\tau_D) d\tau_D \\ & - (C_{Ljbc2D} - C_{LfacD}) \int_0^{(t_{c2})_{LjD}} p'_{LjD}(t_{LjD} - \tau_D) p'_{wsD}(\tau_D) d\tau_D \end{aligned} \right|, \dots\dots\dots(4.94)$$

holds for a finite, but short relative to the reservoir response, time of injection.

CHAPTER V

A REFRACTURE-CANDIDATE DIAGNOSTIC AND EXAMPLE FIELD APPLICATIONS

5.1 Introduction

The new refracture-candidate diagnostic requires isolating a layer to be tested and completing a fracture-injection/falloff sequence where the time of injection is short relative to the reservoir response. The new analytical pressure-transient solutions that were developed in Chapter III for cases without a pre-existing fracture and in Chapter IV for cases with a pre-existing fracture(s) suggest that with a short time of injection, the pressure difference recorded during the falloff period can be transformed to an equivalent pressure difference if the rate were constant, plotted, and matched to variable-storage, constant-rate drawdown type curves. The limiting-case solutions presented in Chapters III and IV also form the basis for quantitative interpretation of the observed pressure falloff recorded during the new refracture-candidate diagnostic test.

The new refracture-candidate diagnostic is used prior to a refracture treatment to achieve the following objectives.

- To determine if:
 - A fracture retaining residual width exists.
 - A pre-existing fracture is damaged.
- To estimate:
 - Effective fracture half-length of a pre-existing fracture.
 - Fracture conductivity of a pre-existing fracture.
 - Reservoir transmissibility.
 - Average reservoir pressure.

When the diagnostic objectives are achieved, the benefits of refracturing can be easily evaluated, and the incremental production from a refracture treatment can be predicted.

Chapter V describes the new refracture-candidate diagnostic and the interpretation method for oil and gas reservoirs. With oil reservoirs—or liquid-filled reservoirs like water saturated coals—the analysis is performed in terms of pressure and time. With gas reservoirs—or a reservoir containing compressible fluid modeled as a real gas—the analysis is performed in terms of adjusted pseudopressure and adjusted pseudotime. A unique quantitative interpretation may not be possible when insufficient falloff data are recorded, but qualitative analysis of variable storage behavior is useful for identification of a pre-existing

fracture and flow regime identification is useful for selecting before- and after-closure data for specialized analysis. The focus of Chapter V is applications, and, as such, all equations in Chapter V are written in field units.

Chapter V also contains field examples to illustrate the interpretation of a fracture-injection/falloff sequence for the following cases.

- Without a pre-existing fracture:
 - Pseudoradial flow observed after closure.
 - Pseudolinear flow observed after closure.
- With a pre-existing Fracture
 - A pre-existing conductive hydraulic fracture with choked-fracture skin damage.

5.2 Refracture-Candidate Diagnostic Test

The new refracture-candidate diagnostic test is a fracture-injection/falloff sequence where the time of injection is short relative to the reservoir response and where the pressure during the injection is sufficient to initiate, dilate, or propagate a fracture(s). The test was developed by recognizing that an existing fracture retaining residual width has associated storage, and a new induced fracture creates additional storage. Consequently, a fracture-injection/falloff test in a layer with a pre-existing fracture will exhibit variable storage during the pressure falloff, and the change in storage is observed at hydraulic fracture closure. In essence the test induces a fracture to rapidly identify a pre-existing fracture retaining residual width.

Both qualitative and quantitative interpretations are possible provided sufficient pressure data are recorded during the falloff. Qualitative interpretation to identify a pre-existing fracture and pre-existing fracture damage requires determining hydraulic fracture closure using existing methods and characterizing the observed variable-storage behavior. Quantitative interpretation of transmissibility requires developing a type-curve match, or when sufficient data are recorded to observe the pseudoradial flow regime, the transmissibility can be calculated from the impulse solution.^{55,60-61} Initial reservoir pressure can also be estimated from the pressure observed during pseudoradial flow, and fracture half-length and fracture conductivity can be estimated from the type-curve match.

The new refracture-candidate diagnostic test requires the following.

- Isolate a layer to be tested.
- Inject liquid or gas at a pressure exceeding fracture initiation and propagation pressure. The injected volume should be roughly equivalent to the proppant-pack pore volume of an existing fracture if known or suspected to exist, but the injection time should be limited to a few minutes.

- Shut-in and record a pressure falloff period of several hours. A bottomhole gauge and bottomhole shut-in are preferable to minimize wellbore storage.

Both qualitative and quantitative interpretation require the following steps:

- Identify hydraulic fracture closure during the pressure falloff using existing methods.^{54,74}
- For a reservoir containing a slightly-compressible liquid, transform the recorded variable-rate pressure falloff data to an equivalent pressure difference if the rate were constant by integrating the pressure difference with respect to time, which is written in field units as

$$I(\Delta p) = \int_0^{t_e + \Delta t} [p_w(\tau) - p_i] d\tau, \dots\dots\dots(5.1)$$

where $\Delta t = t - t_e$, t [hr] is the time, t_e [hr] is the time at the end of the injection, p_w [psi] is the observed wellbore pressure, and p_i [hr] is the initial reservoir pressure.

Calculate the well testing pressure derivative of the pressure observed during the falloff by evaluating the pressure derivative function written in field units as

$$\Delta p' = \frac{dI(\Delta p)}{d(\ln(t_e + \Delta t))} = (t_e + \Delta t)[p_w(t) - p_i], \dots\dots\dots(5.2)$$

Prepare a log-log graph of $I(\Delta p)$ versus $t_e + \Delta t$ and $\Delta p'$ versus $t_e + \Delta t$.

- For a reservoir containing a compressible fluid (real gas), calculate adjusted pseudotime in field units as

$$t_a = (\mu c_t)_i \int_0^t \frac{dt}{(\mu c_t)_w}, \dots\dots\dots(5.3)$$

where μ [cp] is the viscosity, c_t [1/psi] is the total compressibility, the subscript i denotes the variables are evaluated at the initial reservoir pressure, and the subscript w denotes the variables are evaluated at the observed wellbore pressure.

Calculate adjusted pseudopressure in field units as

$$p_a = \left(\frac{\mu z}{p}\right)_i \int_0^p \frac{p dp}{\mu z}, \dots\dots\dots(5.4)$$

where z is the gas deviation factor.

Transform the observed adjusted pseudopressure data to an equivalent adjusted pseudopressure difference if the rate were constant by integrating the adjusted pseudopressure difference with respect to time, which is written in field units as

$$I(\Delta p_a) = \int_0^{((t_e)_a + \Delta t_a)} [p_{aw}(\tau) - p_{ai}] d\tau, \dots\dots\dots(5.5)$$

where $\Delta t_a = t_a - (t_e)_a$.

Calculate the well testing adjusted pseudopressure derivative observed during the falloff by evaluating the derivative written in field units as

$$\Delta p'_a = \frac{dI(\Delta p_a)}{d[\ln((t_e)_a + \Delta t_a)]} = ((t_e)_a + \Delta t_a) [p_{aw}(t_a) - p_{ai}] \dots\dots\dots(5.6)$$

Prepare a log-log graph of $I(\Delta p_a)$ versus $(t_e)_a + \Delta t_a$ and $\Delta p'_a$ versus $(t_e)_a + \Delta t_a$.

5.2.1 Qualitative Analysis. A fracture-injection/falloff sequence in a reservoir either with or without a pre-existing fracture can result in variable storage behavior. In an ideal case without a pre-existing fracture prior to the injection and no wellbore storage, the fracture created during the injection will close completely during the falloff period. With complete closure, storage after closure goes to zero. Conversely, in an ideal case with a pre-existing fracture that retains residual width prior to the injection and no wellbore storage, a fracture induced by the injection, or existing fracture dilation as a result of the injection, will close during the falloff period. However, with complete closure of the induced- or dilated-fracture, storage does not tend to zero because the pre-existing fracture retains residual width and remains open.

Variable-storage behavior is illustrated in **Figs. 5-1 through 5-3**. Fig. 5-1 shows a log-log graph of dimensionless pressure and pressure derivative versus dimensionless time for a variable-storage drawdown. During the falloff of an ideal fracture-injection/falloff sequence in a reservoir without an existing fracture, the transformed equivalent constant-rate pressure difference and derivative fall along the curve corresponding to $C_{bcD} = 0.1$. After complete fracture closure, the storage goes to zero, $C_{acD} = 0$, which creates an abrupt increase in both the dimensionless pressure and the derivative. Van den Hoek⁹²⁻⁹³ presented field data showing similar pressure and derivative changes observed during falloff testing of a well with a waterflood-induced fracture.

Fig. 5-2 also shows a log-log graph of dimensionless pressure and pressure derivative versus dimensionless time for a variable-storage drawdown. However, Fig. 5-2 illustrates the falloff of an ideal fracture-injection/falloff sequence in a reservoir with an existing fracture. With an existing fracture, the storage after closure is greater than zero provided the existing fracture retains residual width. Consequently, the transformed equivalent constant-rate pressure difference and derivative would fall along the curve corresponding to $C_{bcD} = 0.1$, and after fracture closure, the storage decreases, $C_{acD} = 0.05$, which creates a more subtle increase in both the dimensionless pressure and the derivative.

Fig. 5-3 illustrates a case with apparent increasing storage, and shows a log-log graph of dimensionless pressure and pressure derivative versus dimensionless time for a variable-storage drawdown with choked-fracture skin. With a pre-existing fracture that is damaged at the wellbore, the storage appears to increase

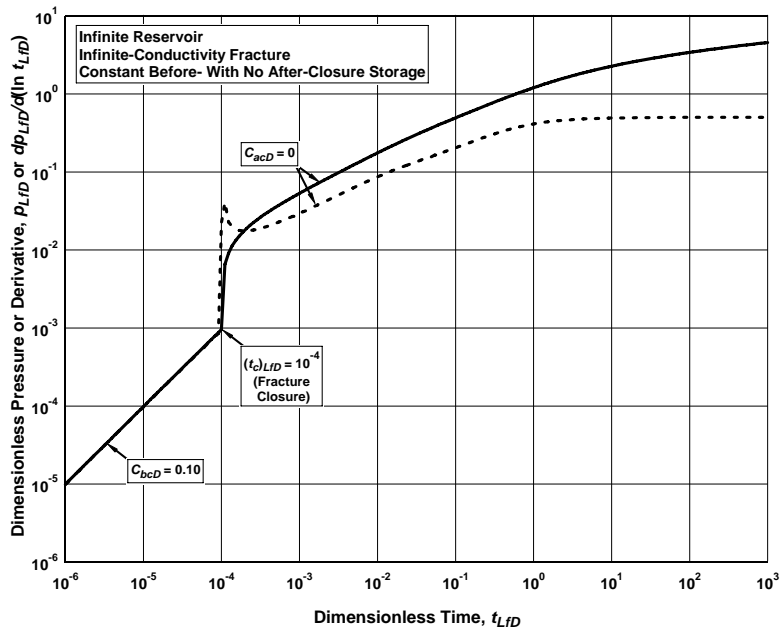


Fig. 5.1—Variable storage drawdown type curve with closure at $(t_c)_{LFD} = 0.0001$, $C_{bcd} = 0.10$, and $C_{acd} = 0$.

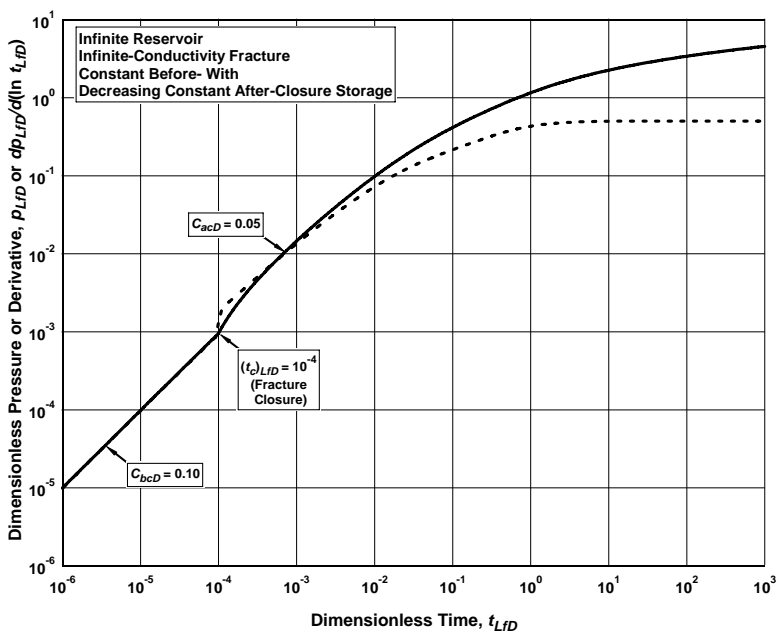


Fig. 5.2—Variable storage drawdown type curve with closure at $(t_c)_{LFD} = 0.0001$, $C_{bcd} = 0.10$, and $C_{acd} = 0.05$.

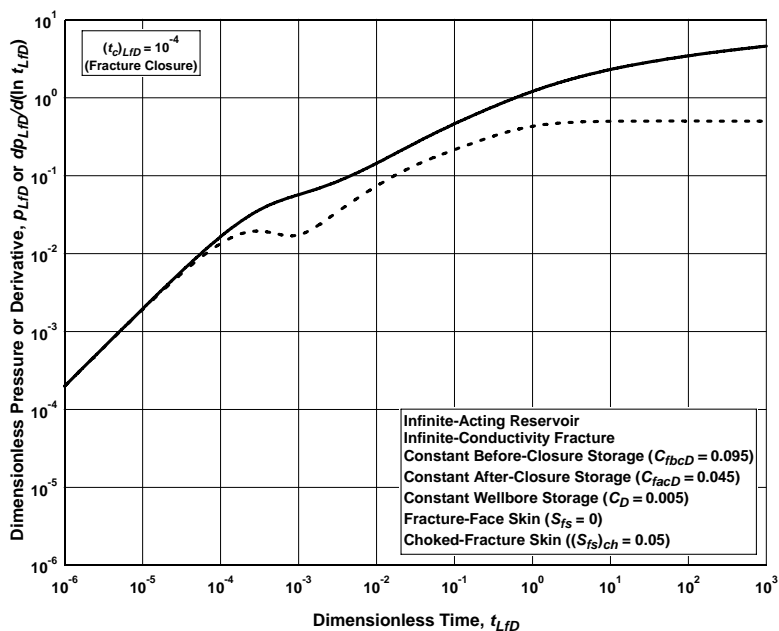


Fig. 5.3—Variable storage drawdown type curve with closure at $(t_c)_{LFD} = 0.0001$, $C_{bcD} = 0.095$, $C_{acD} = 0.045$, $C_D = 0.005$, and choked-fracture skin, $(S_{fs})_{ch} = 0.05$.

because of the choked-fracture skin. The pressure and derivative curves in Fig. 5-3 were generated with before-closure fracture storage, $C_{fbcD} = 0.095$, after-closure fracture storage, $C_{facD} = 0.045$, wellbore storage, $C_D = 0.005$, choked-fracture skin, $(S_{fs})_{ch} = 0.001$, and fracture closure at $(t_c)_{LFD} = 0.0001$. Consequently, the transformed equivalent constant-rate pressure difference and derivative appear to decrease during and after fracture closure to the curve corresponding to $C_{acD} = 0.05$.

Provided the storage does not tend to zero, a change in the magnitude of storage at fracture closure suggests a fracture retaining residual width exists. When storage decreases to a constant value greater than zero, an existing fracture is nondamaged. Conversely, a damaged fracture, or a fracture exhibiting choked-fracture skin, is indicated by apparent increase in the storage coefficient.

In addition to identifying an existing fracture, qualitative analysis is useful for identifying the flow regimes observed during a fracture-injection/falloff sequence and for identifying the observed data to be used with quantitative special analysis, including traditional before- and after-closure methods.⁵⁷⁻⁶¹ **Fig. 5-4** shows a log-log graph of dimensionless pressure and pressure derivative versus dimensionless time for a variable-storage drawdown with $C_{bcD} = 0.01$, $C_{acD} = 0.009$, and $(t_c)_{LFD} = 10^{-5}$.

The data observed during storage-dominated flow, which is indicated by the unit slope line, correspond to both wellbore and fracture storage. When fracture storage is much greater than wellbore storage and the

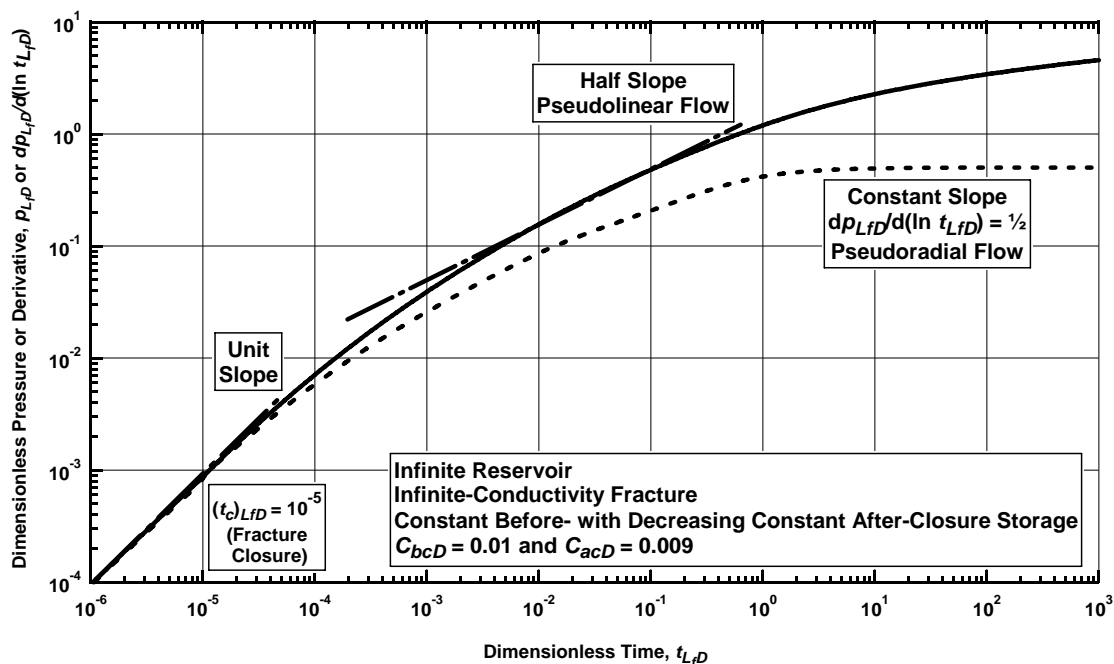


Fig. 5.4—Variable storage drawdown type curve with closure at $(t_c)_{LFD} = 0.00001$, $C_{bcD} = 0.01$, and $C_{acD} = 0.009$.

data fall along a unit slope line, the fracture is open, and a change in storage indicates hydraulic fracture closure has been observed. However, in many field cases, wellbore storage will be much greater than fracture storage, and the transition from storage-dominated flow may not be a reliable indicator of fracture closure. For example, in Fig. 5-4, fracture closure occurs at $(t_c)_{LFD} = 10^{-5}$, but storage-dominated flow continues for a period of time because of wellbore storage.

Before-closure pressure-transient analysis⁵⁷⁻⁵⁹ is applicable to the storage-dominated flow data. When a shut-in period following a fracture-injection only extends to the end of or slightly beyond closure, the equivalent constant-rate pressure difference and derivative data will remain in storage-dominated flow during the entire pressure falloff. Consequently, before-closure pressure-transient analysis is the only quantitative interpretation method that can provide estimates of permeability and fracture-face resistance.

Pseudolinear flow will be observed after closure when sufficient fracture half-length was created during the injection and provided the fracture after closure has essentially infinite conductivity. In very low-permeability reservoirs, pseudolinear flow is often observed.⁵⁴ Pseudolinear flow is indicated by a $1/2$ slope of the pressure and derivative curves.

Pseudoradial flow can be observed when the shut-in period is sufficient, and pseudoradial flow is indicated by a constant pressure derivative function equal to $\frac{1}{2}$ as shown in Fig. 5-4. When pseudoradial flow is indicated, after-closure analysis based on the impulse solution will provide an estimate of transmissibility, and with transmissibility known, a type-curve match point will provide an estimate of storage and the created fracture half-length.

It is also noteworthy that with complete fracture closure, or when the created fracture half-length is very short, a log-log graph of equivalent constant-rate pressure difference and the pressure derivative will transition immediately from storage-dominated flow during fracture closure to radial flow. When radial flow is indicated immediately after closure, the equivalent constant-rate pressure and derivative data will fit on a radial flow with wellbore storage and skin type curve. Recall an analytical solution for the case was presented in Chapter III.

5.2.2 Quantitative Analysis – Before-Closure Pressure-Transient Analysis. Quantitative analysis of a refracture-candidate diagnostic involves both type-curve matching and specialized analysis of data in specific flow regimes. Without a pre-existing fracture, specialized analysis includes before- and after-closure methods. Before-closure pressure-transient analysis does not account for a pre-existing fracture, so when a pre-existing fracture is indicated by type-curve analysis, before-closure analysis is invalid.

Before-closure pressure-transient analysis⁵⁷⁻⁵⁹ was described in Chapter II for reservoirs containing a slightly-compressible liquid, and **Appendix A** extends before-closure analysis to reservoirs containing compressible fluids by formulating in terms of adjusted pseudopressure and adjusted pseudotime. **Table A-2** contains the equations formulated in pressure and time and adjusted pseudopressure and time, and **Table A-3** contains the equations formulated in pressure and time and adjusted pseudopressure and adjusted pseudotime required for completing before-closure pressure-transient analysis.

Completing before-closure analysis in a reservoir containing a slightly-compressible fluid requires the following.

- Calculate the constant c_1 , which is written in field units as

$$c_1 = \sqrt{\frac{\mu}{\phi c_t}}, \dots\dots\dots (5.7)$$

and c_2 , which is written in field units as

$$c_2 = \frac{5.615}{24} S_f w_L \sqrt{\frac{\mu}{\phi c_t}}, \dots\dots\dots (5.8)$$

where S_f [psi/ft] is the fracture "stiffness" and w_L [ft] is the fracture lost width corresponding to fluid leak-off volume.⁵⁹ Fracture stiffness, or the inverse of fracture compliance, is defined by the elastic energy or "strain energy" created by an open fracture in a rock assuming linear elastic

theory is applicable. **Table 5-1** contains the fracture stiffness definitions for three common 2D fracture models.^{80,100} In field units, E' [psi] is the plane-strain modulus, R_f [ft] is the radius of a radial fracture, h_f [ft] is the gross fracture height, and L_f [ft] is the fracture half length.

Table 5-1—Fracture stiffness for 2D fracture models.^{80,100}

Radial	Perkins-Kern-Nordgren Vertical Plane Strain	Geertsma-deKlerk Horizontal Plane Strain
$(S_f)_{RAD} = \frac{3\pi E'}{16R_f}$	$(S_f)_{PKN} = \frac{2E'}{\pi h_f}$	$(S_f)_{GDK} = \frac{E'}{\pi L_f}$

Estimating fracture stiffness using the 2D idealizations requires determining one fracture dimension consisting of fracture radius, fracture height, or fracture half-length. With a vertical plane strain assumption (PKN), fracture height is required for calculating stiffness. In most cases, fracture height is assumed based on lithology interpreted from log analysis. However, fracture-imaging methods can also provide an estimate of fracture height when available.²⁷

Imaging methods may also be beneficial for estimating fracture half length or radius, but in most cases, a relatively simple fracture model is used. One method for determining fracture radius or half-length was described by Valkó and Economides⁵⁹ and assumes no spurt loss, which is an instantaneous fluid loss as the fracturing fluid contacts "new" rock during fracture propagation. Without spurt loss and assuming ideal leakoff behavior, the pressure recorded during the before-closure shut-in period will fall along a straight line on a graph of bottomhole pressure versus the dimensionless loss-volume function, $g(\Delta t, \alpha_N)$, which was described in Chapter II.

Assuming $\alpha_N = 8/9$ for a radial fracture, the radius can be calculated from the intercept, b_N [psi], of a line drawn through the observed data, as⁵⁹

$$R_f = \sqrt[3]{\frac{3(5.615)}{8} \frac{E'V_{inj}}{(b_N - p_c)}}, \dots\dots\dots(5.9)$$

where V_{inj} [bbl] is the volume of fluid injected in one fracture wing, $V_{inj} = Q_t/2$, and Q_t [bbl] is the total volume injected. Assuming $\alpha_N = 2/3$ for a horizontal plane-strain (GDK) idealization, fracture half-length can be calculated as⁵⁹

$$L_f = \sqrt{\frac{(5.615)E'V_{inj}}{\pi h_f(b_N - p_c)}} \dots\dots\dots(5.10)$$

With a characteristic fracture dimension determined for each 2D idealization, fracture lost width is estimated from the slope of a line, m_N [psi], drawn through the observed data. For a vertical plane strain assumption, $\alpha_N = 4/5$, the fracture lost-width is written in field units as⁵⁹

$$w_L = \frac{0.7075(12)\pi h_f}{E'} (-m_N), \dots\dots\dots(5.11)$$

and for a horizontal plane strain assumption, $\alpha_N = 2/3$, the fracture lost-width is written in field units as⁵⁹

$$w_L = \frac{1.478(12)\pi L_f}{E'} (-m_N) . \dots\dots\dots(5.12)$$

Assuming a radial fracture geometry, the fracture lost-width is written in field units as

$$w_L = \frac{7.343(12)R_f}{\pi E'} (-m_N) . \dots\dots\dots(5.13)$$

- Preparing the specialized graph for a reservoir containing a slightly-compressible fluid requires calculating the dimensionless plotting function, y_n , for each timestep, n . The plotting function is written as

$$y_n = \frac{(p_w)_n - p_i}{d_n \sqrt{t_n} \sqrt{t_{ne}}}, \dots\dots\dots(5.14)$$

where $(p_w)_n$ [psi] is the observed pressure at time index n , p_i [psi] is the initial reservoir pressure, t [hr] is the time, the subscript 'ne' denotes the index corresponding to the end of pumping, the variable d_n [psi/hr] is written as

$$d_j = \frac{p_{j-1} - p_j}{t_j - t_{j-1}}, \dots\dots\dots(5.15)$$

and $j=n$.

- The dimensionless plotting function, x_n , for each timestep is calculated as

$$x_n = \left[\begin{array}{l} \left[\frac{d_{ne+2}}{d_n} \left(\frac{t_n - t_{ne+1}}{t_n t_{ne}} \right)^{1/2} \right. \\ \left. + \sum_{j=ne+3}^n \frac{[d_j - d_{j-1}]}{d_n} \left(\frac{t_n - t_{j-1}}{t_n t_{ne}} \right)^{1/2} \right] \\ \left. + \frac{c_2}{d_n t_{ne}^{3/2}} \left[1 - \left(1 - \frac{t_{ne+1}}{t_n} \right)^{1/2} \right] \right] \dots\dots\dots(5.16)$$

- Prepare a Cartesian graph of the plotting functions, y_n vs. x_n , and draw a straight line through the data points. Fracture-face resistance, R_0 [cp/ft] is calculated from the intercept of the straight line, b_M , as

$$R_0 = \frac{5.615}{\pi(141.2)(24)} r_p S_f t_{ne} b_M, \dots\dots\dots (5.17)$$

where r_p is the ratio of permeable to gross fracture height. Permeability is calculated in field units from the slope of a straight line, m_M , drawn through the data points as

$$k = \left[\frac{2(141.2)(0.02878)(24)}{5.615} \frac{1}{r_p S_f m_M} \right]^2 \dots\dots\dots (5.18)$$

In many cases, nonideal leakoff behavior will not result in a straight line on the specialized graph,⁸² and the cause and effect of nonideal leakoff behavior on the permeability estimate have been examined by Craig *et al.*⁸²

In a reservoir containing a compressible reservoir fluid that can be modeled as a real gas, before-closure pressure-transient analysis requires the following.

- Calculate the constant c_{ap1} , which is written in field units as

$$c_{ap1} = \sqrt{\frac{\mu_{gi}}{\phi c_{ti}}}, \dots\dots\dots (5.19)$$

where μ_{gi} [cp] is the gas viscosity at initial reservoir pressure and c_{ti} [1/psi] is the total compressibility at initial reservoir pressure.

Calculate the constant c_{ap2} , which is written in field units as

$$c_{ap2} = \frac{5.615}{24} S_f w_L \frac{B_i}{B_e} \sqrt{\frac{\mu_{gi}}{\phi c_{ti}}}, \dots\dots\dots (5.20)$$

where B_i [bbl/Mscf] is the gas formation volume factor evaluated at initial reservoir pressure and B_e [bbl/Mscf] is the gas formation volume factor evaluated at the pressure at the end of the injection.

- Preparing the specialized graph for a reservoir containing a slightly-compressible fluid requires calculating the dimensionless plotting function, $(y_{ap})_n$, for each timestep, n . The plotting function is written as

$$(y_{ap})_n = \frac{(p_{aw})_n - p_{ai}}{(d_{ap})_n \sqrt{t_n} \sqrt{t_{ne}}}, \dots\dots\dots (5.21)$$

where $(p_{aw})_n$ [psi] is the observed adjusted pseudopressure at time index n , p_{ai} [psi] is the initial adjusted pseudopressure, t [hr] is the time, the subscript 'ne' denotes the index corresponding to the end of pumping, the variable $(d_{ap})_n$ [psi/hr] is written as

$$(d_{ap})_j = \frac{c_{ti}}{(c_t)_j} \left[\frac{(p_a)_{j-1} - (p_a)_j}{(t_a)_j - (t_a)_{j-1}} \right], \dots\dots\dots(5.22)$$

and $j=n$.

- The dimensionless adjusted plotting function, $(x_{ap})_n$, for each timestep is calculated as

$$(x_{ap})_n = \left[\begin{aligned} & \frac{(d_{ap})_{ne+2} \left[\frac{(t_a)_n - (t_a)_{ne+1}}{t_n t_{ne}} \right]^{1/2}}{(d_{ap})_n} \\ & + \sum_{j=ne+3}^n \frac{[(d_{ap})_j - (d_{ap})_{j-1}] \left(\frac{(t_a)_n - (t_a)_{j-1}}{t_n t_{ne}} \right)^{1/2}}{(d_{ap})_n} \\ & + \frac{c_{ap1} (t_a)_n^{1/2}}{(d_{ap})_n t_n^{1/2} t_{ne}^{3/2}} \left[1 - \left(1 - \frac{(t_a)_{ne+1}}{(t_a)_n} \right)^{1/2} \right] \end{aligned} \right] \dots\dots\dots(5.23)$$

- Prepare a Cartesian graph of the plotting functions, $(y_{ap})_n$ vs. $(x_{ap})_n$, and draw a straight line through the data points. Fracture-face resistance, R_0 [cp/ft] is calculated from the intercept of the straight line, b_M , as

$$R_0 = \frac{5.615}{\pi(141.2)(24)} r_p S_f t_{ne} b_M \dots\dots\dots(5.24)$$

Permeability is calculated from the slope of a straight line, m_M , drawn through the data points as

$$k = \left[\frac{2(141.2)(0.02878)(24)}{5.615} \frac{1}{r_p S_f m_M} \right]^2 \dots\dots\dots(5.25)$$

5.2.3 Quantitative Analysis – After-Closure Analysis. When pseudoradial flow is observed, which is indicated by a constant derivative on a log-log graph of equivalent constant-rate pressure difference and derivative versus time, after-closure analysis based on the impulse solution provides an estimate of transmissibility *independent* of fracture half length(s).^{55,60-61,108} Consequently, after-closure pseudoradial flow analysis can also be applied to refracture-candidate diagnostic data generated with a pre-existing fracture.

As shown by Gu *et al.*⁶⁰ and Abousleiman *et al.*,⁶¹ the impulse solution forming the basis of after-closure pseudoradial flow analysis is written for a slightly-compressible liquid in field units as

$$p_w - p_i = \frac{141.2(24)}{2} \frac{Q_i \mu}{kh} \frac{1}{\Delta t_{ac}}, \dots\dots\dots(5.26)$$

where Q_i is the total fluid volume injected during the impulse. The definition of elapsed time, Δt_{ac} , is defined differently by Gu *et al.*⁶⁰ and Abousleiman *et al.*⁶¹ The authors reason that the injection continues during fracture closure, and the total injection time should include at least a portion of the time to closure.

Consequently, Gu *et al.* defined elapsed time as $\Delta t_{ac} = t - 0.5t_c$, while Abousleiman *et al.* define elapsed time as $\Delta t_{ac} = t - t_c$.

Recently, Soliman *et al.*¹⁰⁸ suggested that the elapsed time should be the total time including the injection and falloff periods defined as $\Delta t_{ac} = t_e + \Delta t = t$, which the authors base partly on the results published by Soliman¹⁰⁹ for a buildup test following a short producing time. Soliman *et al.*¹⁰⁸ argue that when the time to the end of injection is short, fracture propagation during the injection can be ignored, and the after-closure falloff data can be analyzed as an injection/falloff (or drawdown/buildup) using conventional pressure transient solutions. Ayoub *et al.*,⁵⁵ also noted for a impulse test without fracture propagation that the elapsed time for the impulse solution should be defined as, $\Delta t_{ac} = t_e + \Delta t$, and the product $\Delta t_{ac}(p_w - p_i)$ when plotted versus Δt_{ac} on a log-log graph will overlay the well-testing pressure derivative of the appropriate constant-rate type curve for the reservoir/system.

The pseudoradial flow impulse solutions are essentially the same, but the time function is defined differently in each special case. To provide consistency and reconcile the differences, the analytical solutions presented in Chapters III and IV can be used to write the complete impulse solution. To illustrate the solution, consider the case of a dilating existing fracture or a fracture created instantaneously with equivalent before- and after-closure storage. The analytical solution developed in Chapter III is written as

$$p_{wsD}(t_{LjD}) = \left[q_{wD} \left[p_{acD}(t_{LjD}) - p_{acD}(t_{LjD} - (t_e)_{LjD}) \right] + p_{wsD}(0) C_{acD} p'_{acD}(t_{LjD}) \right] - (C_{bcd} - C_{acD}) \int_0^{(t_c)_{LjD}} p'_{acD}(t_{LjD} - \tau_D) p'_{wsD}(\tau_D) d\tau_D, \dots\dots\dots(5.27)$$

where the Laplace domain dimensionless fracture solution for a well produced at a constant rate with constant after-closure storage is written as

$$\bar{p}_{acD} = \frac{\bar{p}_{jD}}{1 + s^2 C_{acD} \bar{p}_{jD}}, \dots\dots\dots(5.28)$$

and the dimensionless reservoir pressure solution is for a fixed-length finite- or infinite-conductivity fracture. With $C_{bcd} = C_{acD}$, the solution is written as

$$p_{wsD}(t_{LjD}) = q_{wD} \left[p_{acD}(t_{LjD}) - p_{acD}(t_{LjD} - (t_e)_{LjD}) \right] + p_{wsD}(0) C_{acD} p'_{acD}(t_{LjD}). \dots\dots\dots(5.29)$$

As time increases and storage effects dissipate, the reservoir solution can be written as $p_{acD}(t_{LjD}) = p_{jD}(t_{LjD})$, which results in

$$p_{wsD}(t_{LjD}) = q_{wD} \left[p_{jD}(t_{LjD}) - p_{jD}(t_{LjD} - (t_e)_{LjD}) \right] + p_{wsD}(0) C_{acD} p'_{jD}(t_{LjD}). \dots\dots\dots(5.30)$$

The dimensionless well injection rate can be written as

$$q_{wD} = \frac{141.2 q_w B \mu}{kh(p_0 - p_i)} = \frac{141.2 \mu}{kh(p_0 - p_i)} \frac{q_w B t_e}{t_e} = \frac{141.2(24) \mu}{kh(p_0 - p_i)} \frac{Q_t}{(t_e)_{LjD}} \frac{0.0002637k}{\phi \mu c_t L_f^2}, \dots\dots\dots(5.31)$$

and the solution can be written as

$$p_{wsD}(t_{LjD}) = \left[\frac{Q_t}{(t_e)_{LjD}} \left[p_{fD}(t_{LjD}) - p_{fD}(t_{LjD} - (t_e)_{LjD}) \right] \frac{141.2(24)\mu}{kh(p_0 - p_i)} \frac{0.0002637k}{\phi\mu c_t L_f^2} \right] + p_{wsD}(0)C_{acD}p'_{fD}(t_{LjD}) \dots\dots\dots(5.32)$$

As $(t_e)_{LjD} \rightarrow 0$, the derivative of pressure is written as

$$\lim_{(t_e)_{LjD} \rightarrow 0} \frac{p_{fD}(t_{LjD}) - p_{fD}(t_{LjD} - (t_e)_{LjD})}{(t_e)_{LjD}} = \frac{dp_{fD}(t_{LjD})}{dt_{LjD}} = p'_{fD}(t_{LjD}), \dots\dots\dots(5.33)$$

and the solution can be written as

$$p_{wsD}(t_{LjD})t_{LjD} = \left[\frac{Q_t t_{LjD} p'_{fD}(t_{LjD})}{kh(p_0 - p_i)} \frac{141.2(24)\mu}{\phi\mu c_t L_f^2} \frac{0.0002637k}{\phi\mu c_t L_f^2} \right] + p_{wsD}(0)C_{acD}t_{LjD}p'_{fD}(t_{LjD}) \dots\dots\dots(5.34)$$

During pseudoradial flow, the well-testing pressure derivative is written as

$$t_{LjD}p'_{fD}(t_{LjD}) = \frac{1}{2}, \dots\dots\dots(5.35)$$

and the solution is written as

$$p_{wsD}(t_{LjD})t_{LjD} = \left[\frac{Q_t}{2} \frac{141.2(24)\mu}{kh(p_0 - p_i)} \frac{0.0002637k}{\phi\mu c_t L_f^2} \right] + p_{wsD}(0)\frac{C_{acD}}{2} \dots\dots\dots(5.36)$$

Define dimensionless time as

$$t_{LjD} = \frac{0.0002637k(t_e + \Delta t)}{\phi\mu c_t L_f^2}, \dots\dots\dots(5.37)$$

and the complete impulse-fracture solution is written as

$$p_w - p_i = \frac{141.2(24)}{2} \frac{\mu}{kh} (Q_t + p_{wsD}(0)C_{ac}(p_0 - p_i)) \frac{1}{t_e + \Delta t} \dots\dots\dots(5.38)$$

The difference between the solution of Soliman, *et al.*¹⁰⁸ and the impulse-fracture solution is the term containing the initial pressure difference and storage. When the injection begins without applying an instantaneous pressure difference, $p_{wsD}(0) = 0$, the impulse solution of Soliman, *et al.*¹⁰⁸ results. However, in low permeability reservoirs, beginning the injection at a rate sufficient to create, propagate, or dilate an existing fracture essentially results in $p_{wsD}(0) = 1$. Thus, ignoring the pressure-difference and storage term will create some error in the estimation of transmissibility.

Transmissibility is estimated from the slope of a line through the pseudoradial flow data on a graph of bottomhole pressure versus reciprocal elapsed time, and the initial reservoir pressure is estimated from the intercept of the line. The complete impulse-fracture solution also suggests a plot for diagnosing pseudoradial flow is prepared by a log-log graph of the well-testing pressure derivative written as

$$\frac{1}{t_e + \Delta t} \frac{dp_w}{d(1/(t_e + \Delta t))} = \frac{141.2(24)}{2} \frac{\mu}{kh} (Q_t + p_{wsD}(0)C_{ac}(p_0 - p_i)) \frac{1}{t_e + \Delta t}, \dots\dots\dots(5.39)$$

versus reciprocal elapsed time. Pseudoradial flow is indicated when the well-testing derivative data fall along a unit slope. Additionally, the correct initial reservoir pressure is known when a log-log graph of the pressure difference, $p_w - p_i$, versus reciprocal elapsed time overlays the well-testing derivative curve during pseudoradial flow. As shown by the complete impulse-fracture solution, the appropriate time function is $t_e + \Delta t$. However, in many low-permeability cases, the shut-in time required to observe pseudoradial flow is such that $t_e + \Delta t \approx \Delta t$.

The pseudolinear flow impulse-fracture solution is developed by considering the impulse-fracture solution written as

$$p_{wsD}(t_{Lfd}) = \left[\begin{array}{l} Q_t p'_{fD}(t_{Lfd}) \frac{141.2(24)\mu}{kh(p_0 - p_i)} \frac{0.0002637k}{\phi\mu c_t L_f^2} \\ + p_{wsD}(0)C_{ac} D p'_{fD}(t_{Lfd}) \end{array} \right] \dots\dots\dots(5.40)$$

Assuming linear flow, the dimensionless pressure solution is written as

$$p_{fD}(t_{Lfd}) = \sqrt{\pi t_{Lfd}}, \dots\dots\dots(5.41)$$

and the derivative with respect to dimensionless time is written as

$$p'_{fD}(t_{Lfd}) = \frac{\sqrt{\pi}}{2} \frac{1}{\sqrt{t_{Lfd}}}. \dots\dots\dots(5.42)$$

With the derivative of pressure, the pseudolinear flow impulse-fracture solution can be written as

$$p_{wsD}(t_{Lfd}) = \left[\begin{array}{l} \frac{141.2(24)\sqrt{\pi}}{2} \frac{Q_t \mu}{kh(p_0 - p_i)} \frac{0.0002637k}{\phi\mu c_t L_f^2} \\ + \frac{\sqrt{\pi}}{2} p_{wsD}(0)C_{ac} D \end{array} \right] \frac{1}{\sqrt{t_{Lfd}}}. \dots\dots\dots(5.43)$$

With the definition of the dimensionless terms, the pseudolinear flow complete impulse-fracture solution is written as

$$p_w - p_i = \frac{141.2(24)\sqrt{\pi}\sqrt{0.0002637}}{2} \frac{1}{hL_f} \left(\frac{\mu}{\phi c_t k} \right)^{1/2} (Q_t + p_{wsD}(0)C_{ac}(p_0 - p_i)) \left(\frac{1}{t_e + \Delta t} \right)^{1/2}. \dots\dots\dots(5.44)$$

The solution presented by Soliman¹⁰⁹ and Soliman *et al.*¹⁰⁸ is written as

$$p_w - p_i = \frac{141.2(24)\sqrt{0.0002637}}{\sqrt{\pi}} \frac{Q_t}{hL_f} \left(\frac{\mu}{\phi c_t k} \right)^{1/2} \left(\frac{1}{t_e + \Delta t} \right)^{1/2}, \dots\dots\dots(5-45)$$

which differs from the complete impulse-fracture solution by the pressure-difference and storage term *and* the constant term. In terms of dimensionless variables, Soliman¹⁰⁹ wrote the linear-flow impulse-solution as

$$p_{wD}(t_{LjD}) = \frac{(t_e)_{LjD}}{\sqrt{\pi t_{LjD}}}, \dots\dots\dots(5-46)$$

which is incorrect. As shown by the the complete pseudolinear-flow impulse solution, assuming $p_{wsD}(0) = 0$, the solution can be written in dimensionless terms as

$$p_{wD}(t_{LjD}) = \frac{\sqrt{\pi} (t_e)_{LjD}}{2 \sqrt{t_{LjD}}}. \dots\dots\dots(5-47)$$

The complete pseudolinear-flow impulse-fracture solution suggests that a graph of bottomhole pressure versus the square root of reciprocal elapsed time will yield an initial reservoir pressure estimate from the intercept of a line through the pseudolinear flow data. Additionally, if the fracture half-length is known, permeability can be estimated from the slope of the line. The complete pseudolinear-flow impulse-fracture solution also suggests a plot for diagnosing pseudolinear flow is prepared by a log-log graph of the well-testing pressure derivative written as

$$\frac{1}{t_e + \Delta t} \frac{dp_w}{d(1/(t_e + \Delta t))} = \frac{141.2(24)\sqrt{\pi}\sqrt{0.0002637}}{4} \frac{1}{hL_f} \left(\frac{\mu}{\phi c_t k}\right)^{1/2} (Q_t + p_{wsD}(0)C_{ac}(p_0 - p_i)) \left(\frac{1}{t_e + \Delta t}\right)^{1/2}, \dots\dots(5.48)$$

versus reciprocal elapsed time. Pseudolinear flow is indicated when the well-testing derivative data fall along a half-slope line. Additionally, the correct initial reservoir pressure is known when a log-log graph of the pressure difference, $p_w - p_i$, versus reciprocal elapsed time offsets the well-testing derivative curve by a factor of two with a half-slope during pseudolinear flow.

After-closure analysis requires the following for a reservoir containing a slightly-compressible fluid.

- Prepare a log-log graph of pressure difference, $p_w - p_i$, versus the reciprocal of elapsed time, $1/(t_e + \Delta t)$.
- Identify the pseudolinear (1/2 slope) and pseudoradial (unit slope) flow regimes if they exist. Pseudolinear flow may not be observed unless the created fracture retains essentially infinite conductivity after closure. Additionally, pseudoradial flow may not be observed without very long shut-in periods when the permeability is low and the created fracture half-length is relatively long.

Estimating the permeability during pseudolinear flow in a reservoir containing a slightly-compressible liquid requires the following.

- Prepare a Cartesian graph of bottomhole pressure, p_w , versus the square root of the reciprocal of elapsed time, $(1/(t_e + \Delta t))^{1/2}$.
- The data points on the graph during pseudolinear flow will fall along a line. The intercept of the line is the initial reservoir pressure, p_i .

- Permeability is calculated from the slope of the line, m_{acpl} [psi·(hr)^{1/2}], through the data points during pseudoradial flow and is written in field units as

$$k = \left[\frac{141.2(24)\sqrt{\pi}\sqrt{0.0002637}}{2} \frac{1}{hL_f m_{acpl}} \left(\frac{\mu}{\phi c_t} \right)^{1/2} (Q_t + p_{wsD}(0)C_{ac}(p_0 - p_i)) \right]^2 \dots\dots\dots(5.49)$$

Calculating the permeability requires knowing the fracture half length which may not be known. When the after-closure storage coefficient, C_{ac} , is unknown, and $p_{wsD}(0) \neq 0$, the permeability can be estimated by assuming $C_{ac} = 0$.

Estimating the transmissibility during pseudoradial flow in a reservoir containing a slightly-compressible liquid requires the following.

- Prepare a graph of bottomhole pressure, p_w , versus the reciprocal of elapsed time, $1/(t_e + \Delta t)$.
- The data points on the graph during pseudoradial flow will fall along a line. The intercept of the line is the initial reservoir pressure, p_i .
- Transmissibility is calculated from the slope of the line, m_{acpr} [psi·hr], through the data points during pseudoradial flow and is written in field units as

$$\frac{kh}{\mu} = \frac{141.2(24)}{2} \frac{(Q_t + p_{wsD}(0)C_{ac}(p_0 - p_i))}{m_{acpr}} \dots\dots\dots(5-50)$$

When the after-closure storage coefficient, C_{ac} , is unknown, and $p_{wsD}(0) \neq 0$, the transmissibility can be estimated by assuming $C_{ac} = 0$.

Gu *et al.*⁶⁰ examined the effects of a water injection in a gas reservoir using a numerical simulation of a radial model and found that the impulse solution remained valid for pseudoradial flow analysis. However, after-closure pseudoradial flow analysis in a reservoir containing a compressible fluid modeled as a real gas was not addressed theoretically by either Gu *et al.*⁶⁰ or Abousleiman *et al.*⁶¹

The impulse solution can be derived in terms of adjusted pseudopressure and adjusted pseudotime as follows. Assume the wellbore, fracture, and reservoir contain a real gas and that fracture propagation can be modeled as occurring instantaneously during an injection. With no storage, a material balance equation can be written for all time as

$$q_{rD} = (1 - U_{(t_e)_{aLjD}})q_D, \dots\dots\dots(5-51)$$

where q_{rD} is the dimensionless sandface injection rate, q_D is the wellbore injection rate, and U is the unit-step function defined as⁶²

$$U_a = \begin{cases} 0 & , t < a \\ 1 & , t > a \end{cases} \dots\dots\dots(5-52)$$

A solution to the injection/falloff problem is obtained using superposition, which is written in terms of adjusted pseudopressure and adjusted pseudotime as

$$p_{awD} = \int_0^{t_{aLfD}} q_{rD}(\tau_{aD}) \frac{dp_{aD}(t_{aLfD} - \tau_{aD})}{dt_{aLfD}} d\tau_{aD} \dots\dots\dots(5-53)$$

where dimensionless adjusted pseudopressure is defined as

$$p_{aD} = \frac{kh(p_a - p_{ai})}{141.2q(B\mu)_i} \dots\dots\dots(5-54)$$

The superposition integral and the material balance equation valid at all time can be transformed to the Laplace domain and written as

$$\bar{p}_{awD} = q_D \bar{p}_{aD} - q_D \bar{p}_{aD} e^{-s(t_e)_{aLfD}}, \dots\dots\dots(5-55)$$

which can be inverted to the time domain and written as

$$p_{awD}(t_{aLfD}) = q_D (p_{aD}(t_{aLfD}) - p_{aD}(t_{aLfD} - (t_e)_{aLfD})) \dots\dots\dots(5-56)$$

where p_{aD} is a general reservoir solution written in terms of adjusted pseudotime.

During an impulse, the cumulative volume injected is written as $Q_t = qBt_e/24$, where q [Mscf/D] is the gas injection rate, which allows the dimensionless injection rate to be written as

$$q_D = \frac{qBt_e}{qBt_e} = \frac{qB(t_e)_{aLfD}}{qB(t_e)_{aLfD}} = \frac{24Q_t}{qB(t_e)_{aLfD}} \frac{0.0002637k}{\phi(\mu c_t)_i L_f^2} \dots\dots\dots(5-57)$$

With the dimensionless injection rate, the solution can be written as

$$p_{awD}(t_{aLfD}) = \frac{24Q_t}{(t_e)_{aLfD}} (p_{aD}(t_{aLfD}) - p_{aD}(t_{aLfD} - (t_e)_{aLfD})) \frac{0.0002637k}{qB\phi(\mu c_t)_i L_f^2} \dots\dots\dots(5-58)$$

In the limit as $(t_e)_{aLfD}$ goes to 0, that is, as the injection becomes instantaneous for a constant Q_t , the instantaneous source solution is written as

$$p_{awD}(t_{aLfD}) = 24Q_t \frac{dp_{aD}(t_{aLfD})}{dt_{aLfD}} \frac{0.0002637k}{qB\phi(\mu c_t)_i L_f^2} \dots\dots\dots(5-59)$$

The derivative of dimensionless adjusted pseudopressure with respect to the natural logarithm of adjusted pseudotime is written as

$$\frac{dp_{aD}(t_{aLfD})}{d(\ln t_{aLfD})} = t_{aLfD} \frac{dp_{aD}(t_{aLfD})}{dt_{aLfD}}, \dots\dots\dots(5-60)$$

which during pseudoradial flow is equal to 1/2. Consequently, the instantaneous source solution during pseudoradial flow can be written as

$$p_{awD}(t_{aLfD}) t_{aLfD} = \frac{24(0.0002637)Q_t k}{qB\phi(\mu c_t)_i L_f^2} t_{aLfD} \frac{dp_{aD}(t_{aLfD})}{dt_{aLfD}}, \dots\dots\dots(5-61)$$

or written as

$$p_{awD}((t_e)_a + \Delta t_a) = \frac{24 Q_t}{2 qB} \dots\dots\dots(5-62)$$

With the definition of adjusted pseudopressure, the impulse solution is written in terms of adjusted pseudovariables as

$$p_{aw} - p_{ai} = \frac{141.2(24) Q_{at} \mu_i}{2 kh} \frac{1}{((t_e)_a + \Delta t_a)} \dots\dots\dots(5-63)$$

where Q_{at} [bbl] is the total volume injected, $Q_{at} = qB_i t_e / 24$, and $\Delta t_a = t_a - (t_e)_a$. Similarly, the complete impulse-fracture solution is written as

$$p_{aw} - p_{ai} = \frac{141.2(24) \mu_i}{2 kh} (Q_t + P_{wsD}(0)C_{aac}(P_{a0} - P_{ai})) \frac{1}{((t_e)_a + \Delta t_a)} \dots\dots\dots(5.64)$$

The pseudolinear flow impulse-fracture solution is written in terms of adjusted pseudopressure and adjusted pseudotime as

$$p_{aw} - p_{ai} = \frac{141.2(24)\sqrt{\pi}\sqrt{0.0002637}}{2} \frac{1}{hL_f} \left(\frac{\mu_i}{\phi c_t k}\right)^{1/2} (Q_t + P_{wsD}(0)C_{aac}(P_{a0} - P_{ai})) \left(\frac{1}{((t_e)_a + \Delta t_a)}\right)^{1/2} \dots\dots(5.65)$$

The impulse-fracture solutions written in terms of pressure and time and adjusted pseudopressure and pseudotime are of the same form, and after-closure analysis requires the following.

- Prepare a log-log graph of adjusted pseudopressure difference, $p_{aw} - p_{ai}$, versus the reciprocal of elapsed adjusted pseudotime, $1/((t_e)_a + \Delta t_a)$.
- Identify the pseudolinear (1/2 slope) and pseudoradial (unit slope) flow regimes if they exist. Pseudolinear flow may not be observed unless the created fracture retains essentially infinite conductivity after closure. Additionally, pseudoradial flow may not be observed without very long shut-in periods when the permeability is low and the created fracture half-length is relatively long.

Estimating the permeability during pseudolinear flow in a reservoir containing a compressible fluid requires the following.

- Prepare a Cartesian graph of bottomhole adjusted pseudopressure, p_{aw} , versus the square root of the reciprocal of elapsed adjusted pseudotime, $(1/((t_e)_a + \Delta t_a))^{1/2}$.
- The data points on the graph during pseudolinear flow will fall along a line. The intercept of the line is the initial reservoir adjusted pseudopressure, p_{ai} .
- Permeability is calculated from the slope of the line, m_{acpl} [psi·(hr)^{1/2}], through the data points during pseudoradial flow and is written in field units as

$$k = \left[\frac{141.2(24)\sqrt{\pi}\sqrt{0.0002637}}{2} \frac{1}{hL_f m_{acpl}} \left(\frac{\mu_i}{\phi c_{ti}}\right)^{1/2} (Q_{at} + P_{awsD}(0)C_{aac}(P_{a0} - P_{ai})) \right]^2 \dots\dots\dots(5.66)$$

Calculating the permeability requires knowing the fracture half length which may not be known. When the after-closure storage coefficient, C_{aac} , is unknown, and $p_{awsD}(0) \neq 0$, the permeability can be estimated by assuming $C_{ac} = 0$.

Estimating the transmissibility during pseudoradial flow in a reservoir containing a compressible fluid requires the following.

- Prepare a graph of bottomhole adjusted pseudopressure, p_{aw} , versus the reciprocal of elapsed adjusted pseudotime, $1/((t_e)_a + \Delta t_a)$.
- The data points on the graph during pseudoradial flow will fall along a line. The intercept of the line is the initial reservoir adjusted pseudopressure, p_{ai} .
- Transmissibility is calculated from the slope of the line, m_{acpr} [psi·hr], through the data points during pseudoradial flow and is written in field units as

$$\frac{kh}{\mu_i} = \frac{141.2(24) (Q_{at} + p_{awsD}(0)C_{aac}(p_{a0} - p_{ai}))}{2 m_{acpr}} \dots\dots\dots(5-67)$$

When the after-closure storage coefficient, C_{aac} , is unknown, and $p_{awsD}(0) \neq 0$, the transmissibility can be estimated by assuming $C_{aac} = 0$.

5.2.4 Quantitative Analysis – Type-Curve Analysis. Quantitative type-curve matching is applicable when the equivalent constant-rate pressure difference and derivative extend beyond the end of storage-dominated flow. In the absence of pseudolinear or pseudoradial flow, before-closure pressure-transient analysis and type-curve analysis are the only methods for determining transmissibility from a fracture-injection/falloff sequence.

Quantitative type-curve analysis is based on the limiting-case solutions for a fracture-injection/falloff sequence where the fracture-injection can be considered as occurring instantaneously. The solutions were developed in Chapter III for a fracture-injection/falloff sequence without a pre-existing fracture and in Chapter IV for cases with a pre-existing fracture. The limiting-case solutions are summarized as follows.

- Before-Closure [$t_{LFD} < (t_c)_{LFD}$] Limiting Case Solutions for a Fracture-Injection Sequence With a Dilating or Propagating Fracture

- Slightly-Compressible Liquid

$$p_{wsD}(t_{LFD}) = p_{wsD}(0)C_{bcD}p'_{bcD}(t_{LFD}), \dots\dots\dots(5.68)$$

where the Laplace domain dimensionless fracture solution for a well produced at a constant rate with constant before-closure storage is written as

$$\bar{p}_{bcD} = \frac{\bar{p}_{fD}}{1 + s^2 C_{bcD} \bar{p}_{fD}} \dots\dots\dots(5.69)$$

The limiting-case solution is a slug-test solution, and as shown by Peres *et al.*,⁶⁹ a slug-test solution can be integrated with respect to t_{LjD} and written as

$$\frac{1}{p_{wsD}(0)C_{bcD}} \int_0^{t_{LjD}} p_{wsD}(t_{LjD}) dt_{LjD} = p_{bcD}(t_{LjD}) \dots (5.70)$$

The before-closure storage coefficient is defined in field units as

$$C_{bcD} = \frac{5.615}{2\pi} \frac{C_{bc}}{\phi c_t h L_f^2} = \frac{0.8936 C_{bc}}{\phi c_t h L_f^2}, \dots (5.71)$$

where C_{bc} [bbl/psi] is the before-closure storage coefficient defined as

$$C_{bc} = c_w V_w + \frac{2}{5.615} \frac{A_f}{S_f}, \dots (5.72)$$

with c_w [1/psi] defined as the compressibility of the wellbore fluid, V_w [bbl] defined as the volume of the wellbore, and A_f [ft²] is the area of one fracture wing.

Dimensionless wellbore pressure is defined in field units as

$$p_{wsD}(t_{LjD}) = \frac{p_w(t_{LjD}) - p_i}{p_0 - p_i}, \dots (5.73)$$

which allows the solution for transmissibility to be written in field units as

$$\frac{kh}{\mu} = (141.2)(24) p_{wsD}(0)(p_0 - p_i) C_{bc} \left[\frac{p_{bcD}(t_{LjD})}{\int_0^t (p_w(t) - p_i) dt} \right]_{MP}, \dots (5.74)$$

where the subscript 'MP' denotes a matchpoint of the before-closure integrated pressure difference and the constant-rate, constant before-closure storage solution.

- Compressible Fluid

$$p_{awsD}(t_{aLjD}) = p_{awsD}(0) C_{abcD} p'_{bcD}(t_{aLjD}), \dots (5.75)$$

where the adjusted before-closure storage is used in the Laplace domain dimensionless fracture solution for a well produced at a constant rate with constant before-closure storage and is written as

$$\bar{p}_{bcD} = \frac{\bar{p}_{jD}}{1 + s^2 C_{abcD} \bar{p}_{jD}} \dots (5.76)$$

The dimensionless adjusted before-closure storage coefficient is defined in field units as

$$C_{abcD} = C_{aD} + C_{jD} = \frac{5.615}{2\pi} \left[\frac{C_a}{\phi c_{ti} h L_f^2} + \frac{C_{jbc}}{\phi \bar{c}_{tbc} h L_f^2} \right] \frac{T_i}{T_w}, \dots (5.77)$$

where C_a [bbl/psi] is the adjusted wellbore-storage coefficient defined as

$$C_a = c_{gi} V_w, \dots\dots\dots (5.78)$$

and C_{fbc} [bbl/psi] is the dilated/before-closure storage coefficient written as

$$C_{fbc} = \frac{2}{5.615} \frac{A_f}{S_f} \dots\dots\dots (5.79)$$

The dimensionless adjusted before-closure storage coefficient can also be written as

$$C_{abcD} = C_{aD} + C_{fbcD} = \frac{5.615}{2\pi} \frac{C_{abc}}{\phi c_{ti} h L_f^2} \frac{T_i}{T_w}, \dots\dots\dots (5.80)$$

where the adjusted before-closure storage coefficient is defined as

$$C_{abc} = C_a + \frac{c_{ti}}{c_{tbc}} C_{fbc}, \dots\dots\dots (5.81)$$

with c_{tbc} [1/psi] defined as the before-closure average total compressibility written as

$$c_{tbc} = \frac{c_{t0} + c_{tc}}{2}, \quad p_w > p_c, \dots\dots\dots (5.82)$$

where c_{t0} [1/psi] is the total compressibility evaluated at the pressure at the end of the injection and c_{tc} [1/psi] is the total compressibility evaluated at fracture closure pressure.

With the dimensionless adjusted before-closure storage coefficient definition, transmissibility can be calculated as

$$\frac{kh}{\mu_i} = (141.2)(24) p_{awsD}(0) (p_{a0} - p_{ai}) C_{abc} \frac{T_i}{T_w} \left[\frac{p_{bcD}(t_{aL}fD)}{\int_0^{t_a} (p_{aw}(t) - p_{ai}) dt_a} \right]_{MP} \dots\dots\dots (5.83)$$

- After-Closure [$t_{LFD} \gg (t_c)_{LFD}$] Limiting Case Solutions for a Fracture-Injection Sequence With a Dilating or Propagating Fracture

- Slightly-Compressible Liquid

$$p_{wsD}(t_{LFD}) = \left[p_{wsD}(0) C_{bcD} - p_{wsD}((t_c)_{LFD}) (C_{bcD} - C_{acD}) \right] p'_{acD}(t_{LFD}), \dots\dots\dots (5.84)$$

where the Laplace domain dimensionless fracture solution for a well produced at a constant rate with constant after-closure storage is written as

$$\bar{p}_{acD} = \frac{\bar{p}_{fD}}{1 + s^2 C_{acD} \bar{p}_{fD}} \dots\dots\dots (5.85)$$

The after-closure limiting-case solution is also a slug-test solution, and can be integrated with respect to t_{LFD} and written as

$$\frac{1}{p_{wsD}(0) C_{bcD} - p_{wsD}((t_c)_{LFD}) (C_{bcD} - C_{acD})} \int_0^{t_{LFD}} p_{wsD}(t_{LFD}) dt_{LFD} = p_{bcD}(t_{LFD}) \dots\dots\dots (5.86)$$

The after-closure storage coefficient is defined in field units as

$$C_{acD} = \frac{5.615}{2\pi} \frac{C_{ac}}{\phi c_f h L_f^2} = \frac{0.8936 C_{ac}}{\phi c_f h L_f^2}, \dots\dots\dots(5.87)$$

where C_{ac} [bbl/psi] is the after-closure storage coefficient defined as

$$C_{ac} = c_w V_w + 2c_f V_{fr}, \dots\dots\dots(5.88)$$

where c_f [1/psi] is the compressibility of the fluid in the fracture and V_{fr} [bbl] is the residual fracture volume at closure.

With the dimensionless before- and after-closure storage coefficient definitions, transmissibility can be calculated in field units as

$$\frac{kh}{\mu} = (141.2)(24)(p_0 - p_i) \left[p_{wsD}(0)C_{bc} - p_{wsD}\left((t_c)_{LFD}\right)(C_{bc} - C_{ac}) \right] \left[\frac{p_{acD}(t_{LFD})}{\int_0^t (p_w(t) - p_i) dt} \right]_{MP} \dots\dots(5.89)$$

- Compressible Fluid

$$p_{awsD}(t_{aLFD}) = \left[p_{awsD}(0)C_{abcD} - p_{awsD}\left((t_c)_{aLFD}\right)(C_{abcD} - C_{aacD}) \right] p'_{acD}(t_{aLFD}), \dots\dots(5.90)$$

The dimensionless adjusted after-closure storage coefficient is defined in field units as

$$C_{aacD} = \frac{5.615}{2\pi} \frac{C_a + C_{aac}}{\phi c_{gi} h L_f^2} \frac{T_i}{T_w}, \dots\dots\dots(5.91)$$

where C_{aac} [bbl/psi] is the adjusted after-closure storage coefficient defined as

$$C_{aac} = 2c_{gi} V_{fr}, \dots\dots\dots(5.92)$$

and c_{gi} [1/psi] is the gas compressibility evaluated at initial reservoir pressure.

With the dimensionless adjusted after-closure storage coefficient definition, transmissibility can be calculated as

$$\frac{kh}{\mu_i} = (141.2)(24)(p_{a0} - p_{ai}) \left[\begin{matrix} p_{awsD}(0)C_{abc} \\ -p_{awsD}\left((t_c)_{aLFD}\right)(C_{abc} - C_{aac}) \end{matrix} \right] \frac{T_i}{T_w} \left[\frac{p_{bcD}(t_{aLFD})}{\int_0^{t_a} (p_{aw}(t) - p_{ai}) dt_a} \right]_{MP} \dots\dots(5.93)$$

- Before-Closure [$t_{LFD} < (t_c)_{LFD}$] Limiting Case Solutions for a Fracture-Injection Sequence With a Dilating or Propagating Fracture, Fracture Flow During Closure, and Radial Flow With Wellbore Storage and Skin After Closure

- Slightly-Compressible Liquid

$$p_{wsD}(t_{LFD}) = p_{wsD}(0)C_{bcD} p'_{bcD}(t_{LFD}) \dots\dots\dots(5.94)$$

The before-closure limiting-case solution is identical to the before-closure solution for a fracture-injection/falloff sequence with a dilating or propagating fracture during the injection, and transmissibility is calculated in field units as

$$\frac{kh}{\mu} = (141.2)(24)p_{wsD}(0)(p_0 - p_i)C_{bc} \left[\frac{p_{bcD}(t_{Lfd})}{\int_0^t (p_w(t) - p_i)dt} \right]_{MP} \dots\dots\dots(5.95)$$

- Compressible Fluid

$$p_{awsD}(t_{aLfd}) = p_{awsD}(0)C_{abcD}p'_{bcD}(t_{aLfd}) \dots\dots\dots(5.96)$$

Similarly, for a compressible fluid, transmissibility is calculated in field units as

$$\frac{kh}{\mu_i} = (141.2)(24)p_{awsD}(0)(p_{a0} - p_{ai})C_{abc} \frac{T_i}{T_w} \left[\frac{p_{bcD}(t_{aLfd})}{\int_0^{t_a} (p_{aw}(t) - p_{ai})dt_a} \right]_{MP} \dots\dots\dots(5.97)$$

- After-Closure [$t_{Lfd} \gg (t_c)_{Lfd}$] Limiting Case Solutions for a Fracture-Injection Sequence With a Dilating or Propagating Fracture, Fracture Flow During Closure, and Radial Flow With Wellbore Storage and Skin After Closure

- Slightly-Compressible Liquid

$$p_{wsD}(t_{Lfd}) = \left[p_{wsD}(0)C_{bcD} - p_{wsD}((t_c)_{Lfd})(C_{bcD} - C_D) \right] p'_{sacD}(t_{Lfd}), \dots\dots\dots(5.98)$$

where the Laplace domain dimensionless radial flow solution with skin and constant after-closure wellbore storage is written in the Laplace domain as

$$\bar{p}_{sacD} = \frac{\bar{p}_{sD}}{1 + s^2 C_D \bar{p}_{sD}}, \dots\dots\dots(5.99)$$

The cylindrical-source reservoir solution with skin, S , is written in the Laplace domain as⁶⁵

$$\bar{p}_{sD} = \frac{1}{s} \frac{K_0(r_{wD}\sqrt{s})}{\sqrt{s}K_1(\sqrt{s})} + \frac{S}{s}, \dots\dots\dots(5.100)$$

where the dimensionless radius is defined in terms of the created fracture half length written as

$$r_{wD} = \frac{r_w}{L_f} \dots\dots\dots(5.101)$$

After fracture closure no residual volume remains, and the dimensionless wellbore-storage coefficient is defined in field units as

$$C_D = \frac{5.615}{2\pi} \frac{C}{\phi c_t h L_f^2} = \frac{0.8936C}{\phi c_t h L_f^2}, \dots\dots\dots(5.102)$$

where C [bbl/psi] is the wellbore storage coefficient defined as

$$C = c_w V_w \dots\dots\dots(5.103)$$

With the dimensionless storage definitions, transmissibility is calculated in field units as

$$\frac{kh}{\mu} = (141.2)(24)(p_0 - p_i) \left[p_{wsD}(0)C_{bc} - p_{wsD}((t_c)_{Lfd})(C_{bc} - C) \right] \left[\frac{p_{sD}(t_{Lfd})}{\int_0^t (p_w(t) - p_i)dt} \right]_{MP} \dots\dots\dots(5.104)$$

Note that the integrated pressure difference is matched with a constant-rate type curve for production from an infinite slab reservoir with wellbore storage and skin. Additionally, the before-closure storage coefficient is a function of fracture half length, which for previous solutions was estimated from fracture imaging²⁷ or other methods.⁵⁹ However, as shown in Chapter III, an immediate transition to radial flow after closure allows the fracture half length to be calculated from skin estimated from the type curve match provided the "true" skin damage is negligible. Recall from Chapter III that assuming $r_D = 1$, a skin factor is calculated as

$$r_{wD} = \frac{r_w}{L_f} = r_D e^{-S}, \dots\dots\dots (5.105)$$

which allows fracture half-length to be calculated in field units as

$$L_f = \frac{r_w}{e^{-S}}, \dots\dots\dots (5.106)$$

where r_w [ft] is the wellbore radius.

- Compressible Fluid

$$p_{awsD}(t_{aLfD}) = \left[p_{awsD}^{(0)} C_{abcD} - p_{awsD} \left((t_c)_{aLfD} \right) (C_{abcD} - C_{aD}) \right] p'_{sacD}(t_{aLfD}), \dots\dots\dots (5.107)$$

After fracture closure no residual volume remains, and the dimensionless wellbore-storage coefficient is defined in field units as

$$C_{aD} = \frac{5.615}{2\pi} \frac{C_a}{\phi c_t h L_f^2} \frac{T_i}{T_w} = \frac{0.8936 C_a}{\phi c_t h L_f^2} \frac{T_i}{T_w}, \dots\dots\dots (5.108)$$

where C_a [bbl/psi] is the wellbore storage coefficient defined as

$$C_a = c_{gi} V_w \dots\dots\dots (5.109)$$

With the dimensionless storage definitions, transmissibility is calculated in field units as

$$\frac{kh}{\mu_i} = (141.2)(24)(p_{a0} - p_{ai}) \frac{T_i}{T_w} \left[\frac{p_{awsD}^{(0)} C_{abc}}{-p_{awsD} \left((t_c)_{aLfD} \right) (C_{abc} - C_a)} \right] \left[\frac{p_{sD}(t_{aLfD})}{\int_0^{t_a} (p_{aw}(t_a) - p_{ai}) dt_a} \right]_{MP} \dots\dots (5.110)$$

Once again note that the integrated pressure difference is matched with a constant-rate type curve for production from an infinite slab reservoir with wellbore storage and skin. As was true for the slightly-compressible fluid case, fracture half length can be calculated from the skin factor match as

$$L_f = \frac{r_w}{e^{-S}} \dots\dots\dots (5.111)$$

- Before-Closure [$t_{LFD} < (t_c)_{LFD}$] Limiting Case Solutions for a Fracture-Injection Sequence With a Constant-Volume Pre-Existing Fracture With Secondary Fracture Propagation

- Slightly-Compressible Liquid

$$p_{wsD}(t_{LjD}) = p_{wsD}(0)C_{LjbcD}P'_{LjbcD}(t_{LjD}), \dots\dots\dots(5.112)$$

where the Laplace domain dimensionless fracture solution for a well producing at a constant rate in an infinite slab reservoir through multiple fractures with constant before-closure storage is written as

$$\bar{P}_{LjbcD} = \frac{\bar{p}_{LjD}}{1 + s^2 C_{LjbcD} \bar{P}_{LjD}} \dots\dots\dots(5.113)$$

The limiting-case solution with multiple fractures is also a slug-test solution, and the solution can be integrated with respect to t_{LjD} and written as

$$\frac{1}{p_{wsD}(0)C_{LjbcD}} \int_0^{t_{LjD}} p_{wsD}(t_{LjD}) dt_{LjD} = P_{LjbcD}(t_{LjD}) \dots\dots\dots(5.114)$$

The dimensionless secondary-fracture before-closure storage coefficient is defined in field units as

$$C_{LjbcD} = \frac{5.615}{2\pi} \frac{C_{Ljbc}}{\phi c_t h L_f^2} = \frac{0.8936 C_{Ljbc}}{\phi c_t h L_f^2}, \dots\dots\dots(5.115)$$

where C_{Ljbc} [bbl/psi] is the secondary-fracture before-closure storage coefficient defined as

$$C_{Ljbc} = c_w V_w + 2c_f V_{f1} + \frac{2}{5.615} \frac{A_{f2}}{S_{f2}}, \dots\dots\dots(5.116)$$

with V_{f1} [bbl] defined as the volume of the primary fracture, A_{f2} [ft²] is the area of one wing of the secondary fracture, and S_{f2} [psi/ft] is the fracture stiffness of the secondary fracture.

The solution for transmissibility is written in field units as

$$\frac{kh}{\mu} = (141.2)(24) p_{wsD}(0)(p_0 - p_i) C_{Ljbc} \left[\frac{P_{LjbcD}(t_{LjD})}{\int_0^t (p_w(t) - p_i) dt} \right]_{MP} \dots\dots\dots(5.117)$$

Note that calculating transmissibility requires knowing both primary and secondary fracture half lengths. The multiple-fracture type-curve match provides a length ratio defined as

$$\delta_L = \frac{L_{f2}}{L_{f1}}, \dots\dots\dots(5.118)$$

where L_{f1} [ft] is the primary fracture half length and L_{f2} [ft] is the secondary fracture half length. When the primary fracture half length is known from prior well test interpretations or production data analysis, the secondary fracture half length can be calculated. When the primary fracture half length is unknown, the secondary fracture half length can be estimated by fracture imaging.²⁷ Assuming no spurt loss and using the method of Valkó and Economides⁵⁹ will not provide an accurate estimate of fracture half-length because leakoff is through two fractures. However, if either the primary or secondary fracture half length is known, or can be determined, the other

fracture half-length can be calculated from the type curve match, and the secondary-fracture before-closure storage coefficients can be calculated and the transmissibility estimated.

- Compressible Fluid

$$p_{awsD}(t_{aLfd}) = p_{awsD}(0)C_{aLfbcd}p'_{Lfbcd}(t_{aLfd}) \dots\dots\dots (5.119)$$

The dimensionless adjusted secondary-fracture before-closure storage coefficient is defined in field units as

$$C_{aLfbcd} = \frac{5.615}{2\pi} \frac{C_{aLfbcd}}{\phi c_{ti} h L_f^2} \frac{T_i}{T_w}, \dots\dots\dots (5.120)$$

where C_{Lfbcd} [bbl/psi] is the adjusted secondary-fracture before-closure storage coefficient defined as

$$C_{aLfbcd} = C_a + C_{aac1} + C_{fbc1}, \dots\dots\dots (5.121)$$

the adjusted primary-fracture after-closure storage coefficient is written as

$$C_{aac1} = 2c_{gi} V_{f1}, \dots\dots\dots (5.122)$$

and the adjusted secondary-fracture before-closure storage coefficient is written as

$$C_{fbc1} = \frac{2}{5.615} \frac{c_{ti}}{c_{tbc}} \frac{A_f}{S_f} \dots\dots\dots (5.123)$$

With the storage coefficients defined, transmissibility can be calculated in field units as

$$\frac{kh}{\mu_i} = (141.2)(24)p_{awsD}(0)(p_{a0} - p_{ai})C_{aLfbcd} \frac{T_i}{T_w} \left[\frac{p_{Lfbcd}(t_{aLfd})}{\int_0^{t_a} (p_{aw}(t) - p_{ai}) dt_a} \right]_{MP} \dots\dots\dots (5.124)$$

- After-Closure [$t_{Lfd} \gg (t_c)_{Lfd}$] Limiting Case Solutions for a Fracture-Injection Sequence With a Constant-Volume Pre-Existing Fracture With Secondary Fracture Propagation

- Slightly-Compressible Liquid

$$p_{wsD}(t_{Lfd}) = [p_{wsD}(0)C_{Lfbcd} - p_{wsD}((t_c)_{Lfd})(C_{Lfbcd} - C_{LfacD})] p'_{LfacD}(t_{Lfd}), \dots\dots\dots (5.125)$$

where the Laplace domain dimensionless fracture solution for a well producing at a constant rate through multiple fractures with constant after-closure storage is written as

$$\bar{p}_{LfacD} = \frac{\bar{p}_{Lfd}}{1 + s^2 C_{LfacD} \bar{p}_{Lfd}} \dots\dots\dots (5.126)$$

The dimensionless multiple-fracture after-closure storage coefficient is defined in field units as

$$C_{LfacD} = \frac{5.615}{2\pi} \frac{C_{Lfac}}{\phi c_t h L_f^2} = \frac{0.8936 C_{Lfac}}{\phi c_t h L_f^2}, \dots\dots\dots (5.127)$$

where C_{Lfac} [bbl/psi] is the multiple-fracture after-closure storage coefficient defined as

$$C_{ac} = c_w V_w + 2c_f V_{f1} + 2c_f V_{f2}, \dots\dots\dots (5.128)$$

where V_{f2} [bbl] defined as the volume of the primary fracture.

With the storage coefficient definitions, transmissibility can be calculated in field units as

$$\frac{kh}{\mu} = (141.2)(24)(p_0 - p_i) \left[\begin{matrix} p_{wsD}(0)C_{Lfac} \\ -p_{wsD}(t_c)_{LjD}(C_{Lfac} - C_{Lfac}) \end{matrix} \right] \left[\frac{p_{LfacD}(t_{LjD})}{\int_0^t (p_w(t) - p_i) dt} \right]_{MP} \dots\dots\dots (5.129)$$

▪ Compressible Fluid

$$p_{awsD}(t_{aLjD}) = \left[\begin{matrix} p_{awsD}(0)C_{aLfacD} \\ -p_{awsD}(t_c)_{aLjD}(C_{aLfacD} - C_{aLfacD}) \end{matrix} \right] p'_{LfacD}(t_{aLjD}) \dots\dots\dots (5.130)$$

The dimensionless adjusted secondary-fracture after-closure storage coefficient is defined in field units as

$$C_{aLfacD} = \frac{5.615}{2\pi} \frac{C_{aLfac}}{\phi c_{ti} h L_f^2} \frac{T_i}{T_w}, \dots\dots\dots (5.131)$$

where C_{aLfac} [bbl/psi] is the adjusted secondary-fracture before-closure storage coefficient defined as

$$C_{aLfac} = C_a + C_{aac1} + C_{aac2}, \dots\dots\dots (5.132)$$

the adjusted primary-fracture after-closure storage coefficient is written as

$$C_{aac1} = 2c_{gi} V_{f1}, \dots\dots\dots (5.133)$$

and the adjusted secondary-fracture after-closure storage coefficient is written as

$$C_{aac2} = 2c_{gi} V_{f2} \dots\dots\dots (5.134)$$

With the storage coefficients defined, transmissibility can be calculated in field units as

$$\frac{kh}{\mu_i} = (141.2)(24)(p_{a0} - p_{ai}) \left[\begin{matrix} p_{awsD}(0)C_{aLfac} \\ -p_{awsD}(t_c)_{aLjD}(C_{aLfac} - C_{aLfac}) \end{matrix} \right] \times \frac{T_i}{T_w} \left[\frac{p_{LfacD}(t_{aLjD})}{\int_0^{t_a} (p_{aw}(t_a) - p_{ai}) dt_a} \right]_{MP} \dots\dots\dots (5.135)$$

- Primary-Fracture Before-Closure [$t_{LjD} < (t_c)_{LjD}$] Limiting Case Solutions for a Fracture-Injection Sequence With a Dilating Pre-Existing Fracture, Secondary Fracture Propagation, Multiple Fracture Closures, and Constant After-Closure Storage

▪ Slightly-Compressible Liquid

$$p_{wsD}(t_{LjD}) = p_{wsD}(0)C_{Lfac1D} p'_{Lfac1D}(t_{LjD}) \dots\dots\dots (5.136)$$

where the Laplace domain dimensionless fracture solution for a well producing at a constant rate with constant primary-fracture before-closure storage is written in the Laplace domain as

$$\bar{p}_{LfbclD} = \frac{\bar{p}_{LfD}}{1 + s^2 C_{LfbclD} \bar{p}_{LfD}} \dots\dots\dots (5.137)$$

The dimensionless primary-fracture before-closure storage coefficient is defined in field units as

$$C_{LfbclD} = \frac{5.615}{2\pi} \frac{C_{Lfbcl}}{\phi c_t h L_f^2} = \frac{0.8936 C_{Lfbcl}}{\phi c_t h L_f^2}, \dots\dots\dots (5.138)$$

where C_{Lfbcl} [bbl/psi] is the primary-fracture before-closure storage coefficient defined as

$$C_{Lfbcl} = c_w V_w + \frac{2}{5.615} \left[\frac{A_{f1}}{S_{f1}} + \frac{A_{f2}}{S_{f2}} \right], \dots\dots\dots (5.139)$$

with A_{fj} [ft²] is the area of one wing of the primary fracture, and S_{fj} [psi/ft] is the fracture stiffness of the primary fracture.

The solution for transmissibility is written in field units as

$$\frac{kh}{\mu} = (141.2)(24) p_{wsD}(0)(p_0 - p_i) C_{Lfbcl} \left[\frac{p_{LfbclD}(t_{LfD})}{\int_0^t (p_w(t) - p_i) dt} \right]_{MP} \dots\dots\dots (5.140)$$

Note that calculating transmissibility requires knowing both primary and secondary fracture half lengths. The multiple-fracture type-curve match provides a length ratio defined as

$$\delta_L = \frac{L_{f2}}{L_{f1}}, \dots\dots\dots (5.141)$$

where L_{f1} [ft] is the primary fracture half length and L_{f2} [ft] is the secondary fracture half length. When the primary fracture half length is unknown, the secondary fracture half length can be estimated by fracture imaging.²⁷ Assuming no spurt loss and using the method of Valkó and Economides⁵⁹ to estimate fracture half length cannot provide an accurate estimate because leakoff is through two fractures. However, if either the primary or secondary fracture half length is known or can be determined, the other fracture half length can be calculated from the type curve match, and the secondary-fracture before-closure storage coefficient can be calculated and the transmissibility estimated.

- Compressible Fluid

$$p_{awsD}(t_{aLfD}) = p_{awsD}(0) C_{aLfbclD} p'_{LfbclD}(t_{aLfD}) \dots\dots\dots (5.142)$$

The dimensionless adjusted primary-fracture before-closure storage coefficient is defined in field units as

$$C_{aLfbc1D} = \frac{5.615 C_{aLfbc1} T_i}{2\pi \phi c_{ti} h L_f^2 T_w} = \frac{0.8936 C_{aLfbc1} T_i}{\phi c_{ti} h L_f^2 T_w}, \dots\dots\dots (5.143)$$

where C_{aLfbc1} [bbl/psi] is the adjusted primary-fracture before-closure storage coefficient defined as

$$C_{aLfbc1} = c_w V_w + \frac{2}{5.615} \frac{c_{ti}}{c_{tbc1}} \left[\frac{A_{f1}}{S_{f1}} + \frac{A_{f2}}{S_{f2}} \right], \dots\dots\dots (5.144)$$

with c_{tbc1} [1/psi] defined as the primary-fracture before-closure average total compressibility written as

$$c_{tbc1} = \frac{c_{t0} + c_{tc1}}{2}, \quad P_w > P_{c1}, \dots\dots\dots (5.145)$$

where c_{tc1} [1/psi] is the total compressibility evaluated at the primary-fracture closure pressure, P_{c1} .

The solution for transmissibility is written in field units as

$$\frac{kh}{\mu_i} = (141.2)(24) p_{awsD}(0)(p_{a0} - p_{ai}) C_{aLfbc1} \frac{T_i}{T_w} \left[\frac{PLfbc1D(t_{aLfd})}{\int_0^{\Delta t_a} (p_{aw}(t) - p_{ai}) dt_a} \right]_{MP} \dots\dots\dots (5.146)$$

- Secondary-Fracture Before-Closure $[(t_{c1})_{Lfd} \ll t_{Lfd} < (t_{c2})_{Lfd}]$ Limiting Case Solutions for a Fracture-Injection Sequence With a Dilating Pre-Existing Fracture, Secondary Fracture Propagation, Multiple Fracture Closures, and Constant After-Closure Storage

- Slightly-Compressible Liquid

$$p_{wsD}(t_{Lfd}) = \left[p_{wsD}(0) C_{Lfbc1D} - p_{wsD}((t_{c1})_{Lfd}) (C_{Lfbc1D} - C_{Lfbc2D}) \right] p'_{Lfbc2D}(t_{Lfd}) \dots\dots (5.147)$$

where the Laplace domain dimensionless fracture solution for a well producing at a constant rate with constant secondary-fracture before-closure storage is written in the Laplace domain as

$$\bar{p}_{Lfbc2D} = \frac{\bar{p}_{Lfd}}{1 + s^2 C_{Lfbc2D} \bar{p}_{Lfd}} \dots\dots\dots (5.148)$$

The dimensionless primary-fracture before-closure storage coefficient is defined in field units as

$$C_{Lfbc2D} = \frac{5.615 C_{Lfbc2}}{2\pi \phi c_t h L_f^2} = \frac{0.8936 C_{Lfbc2}}{\phi c_t h L_f^2}, \dots\dots\dots (5.149)$$

where C_{Lfbc2} [bbl/psi] is the primary-fracture before-closure storage coefficient defined as

$$C_{Lfbc2} = c_{gi} V_w + 2c_f V_{f1} + \frac{2}{5.615} \frac{A_{f2}}{S_{f2}} \dots\dots\dots (5.150)$$

The solution for transmissibility is written in field units as

$$\frac{kh}{\mu} = (141.2)(24)(p_0 - p_i) \left[\begin{array}{l} p_{wsD}(0) C_{Lfbc1} \\ -p_{wsD}((t_{c1})_{Lfd}) (C_{Lfbc1} - C_{Lfbc2}) \end{array} \right] \left[\frac{PLfbc2D(t_{Lfd})}{\int_0^t (p_w(t) - p_i) dt} \right]_{MP} \dots\dots\dots (5.151)$$

- Compressible Fluid

$$p_{awsD}(t_{aLFD}) = \left[\begin{array}{l} p_{awsD}(0)C_{aLfbclD} \\ -p_{awsD}((t_{c1})_{aLFD})(C_{aLfbclD} - C_{aLfbcl2D}) \end{array} \right] p'_{Lfbcl2D}(t_{aLFD}) \dots (5.152)$$

The dimensionless adjusted primary-fracture before-closure storage coefficient is defined in field units as

$$C_{aLfbcl2D} = \frac{5.615 C_{aLfbcl2} T_i}{2\pi \phi c_{ti} h L_f^2 T_w} \dots (5.153)$$

where $C_{aLfbcl2}$ [bbl/psi] is the adjusted secondary-fracture before-closure storage coefficient defined as

$$C_{aLfbcl2} = c_{gi}V_w + 2c_fV_{f1} + \frac{2}{5.615} \frac{c_{ti} A_f 2}{c_{tbc2} S_f 2} \dots (5.154)$$

with c_{tbc2} [1/psi] defined as the secondary-fracture before-closure average total compressibility written as

$$c_{tbc2} = \frac{c_{tc1} + c_{tc2}}{2} \dots (5.155)$$

where c_{tc2} [1/psi] is the total compressibility evaluated at the secondary-fracture closure pressure, p_{e2} .

With the storage coefficients defined, transmissibility can be calculated in field units as

$$\frac{kh}{\mu_i} = (141.2)(24)(p_{a0} - p_{ai}) \left[\begin{array}{l} p_{awsD}(0)C_{aLfbcl} \\ -p_{awsD}((t_{c1})_{aLFD})(C_{aLfbcl} - C_{aLfbcl2}) \end{array} \right] \dots (5.156)$$

$$\times \frac{T_i}{T_w} \left[\begin{array}{l} p_{Lfbcl2D}(t_{aLFD}) \\ \int_0^{t_a} (p_{aw}(t_a) - p_{ai}) dt_a \end{array} \right]_{MP}$$

- After-Closure [$t_{LFD} \gg (t_{c2})_{LFD} > (t_{c1})_{LFD}$] Limiting Case Solutions for a Fracture-Injection Sequence

With a Dilating Pre-Existing Fracture, Secondary Fracture Propagation, Multiple Fracture Closures, and Constant After-Closure Storage

- Slightly-Compressible Liquid

$$p_{wsD}(t_{LFD}) = \left[\begin{array}{l} p_{wsD}(0)C_{LfbclD} - p_{wsD}((t_{c1})_{LFD})(C_{LfbclD} - C_{Lfbcl2D}) \\ -p_{wsD}((t_{c2})_{LFD})(C_{Lfbcl2D} - C_{LfacD}) \end{array} \right] p'_{LfacD}(t_{LFD}) \dots (5.157)$$

The solution for transmissibility is written in field units as

$$\frac{kh}{\mu} = (141.2)(24)(p_0 - p_i) \left[\begin{array}{l} p_{wsD}(0)C_{Lfbc1} - p_{wsD}((t_{c1})_{LjD})(C_{Lfbc1} - C_{Lfbc2}) \\ -p_{wsD}((t_{c2})_{LjD})(C_{Lfbc2} - C_{Lfac}) \end{array} \right] \dots\dots\dots (5.158)$$

$$\times \left[\frac{p_{LfacD}(t_{LjD})}{\int_0^t (p_w(t) - p_i) dt} \right]_{MP}$$

- Compressible Fluid

$$p_{awsD}(t_{aLjD}) = \left[\begin{array}{l} p_{awsD}(0)C_{aLfbc1D} - p_{awsD}((t_{c1})_{aLjD})(C_{aLfbc1D} - C_{aLfbc2D}) \\ -p_{awsD}((t_{c2})_{aLjD})(C_{aLfbc2D} - C_{aLfacD}) \end{array} \right] p'_{LfacD}(t_{aLjD}) \dots\dots\dots (5.159)$$

From the limiting-case solution, transmissibility can be calculated in field units as

$$\frac{kh}{\mu_i} = (141.2)(24)(p_{a0} - p_{ai}) \left[\begin{array}{l} p_{awsD}(0)C_{aLfbc1} \\ -p_{awsD}((t_{c1})_{aLjD})(C_{aLfbc1} - C_{aLfbc2}) \\ -p_{awsD}((t_{c2})_{aLjD})(C_{aLfbc2} - C_{aLfac}) \end{array} \right] \dots\dots\dots (5.160)$$

$$\times \frac{T_i}{T_w} \left[\frac{p_{LfacD}(t_{aLjD})}{\int_0^{t_a} (p_{aw}(t_a) - p_{ai}) dt_a} \right]_{MP}$$

5.3 Field Examples

Chapter V also contains field examples to illustrate the interpretation of a fracture-injection/falloff sequence for the following cases.

- Without a pre-existing fracture:
 - Pseudoradial flow observed after closure.
 - Pseudolinear flow observed after closure.
- With a pre-existing fracture:
 - A pre-existing conductive hydraulic fracture with choked-fracture skin damage.

5.3.1 Pseudoradial Flow Observed After Closure. A fracture-injection/falloff sequence was completed in a relatively thin sandstone reservoir between 10,159- to 10,177 feet. The fracture-injection was pumped via 3-1/2 inch tubing landed at 10,091 feet, and the fracture-injection consisted of 67.9 bbl of KCl treated water, which was pumped at an average rate of 10.7 bbl/min during the 6.32 minute injection.

The entire fracture-injection/falloff sequence is shown in **Fig. 5-5**, which is a graph of bottomhole pressure and surface injection rate versus time. The falloff period shown in Fig. 5.5 extended for 1.70 hours beyond the end of the fracture-injection. The fracture-injection/falloff sequence is analyzed as follows. **Table 5-2** contains the time, pressure, and rate data recorded during the injection.

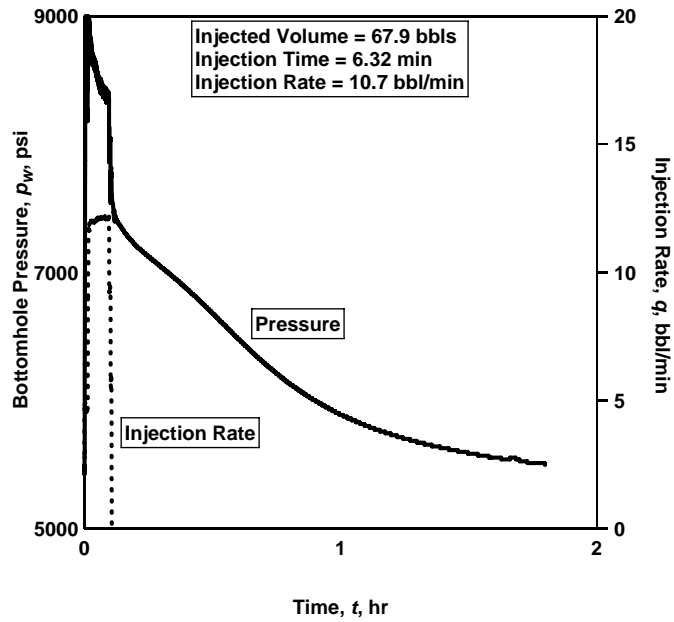


Fig. 5.5—Fracture-injection/falloff sequence.

Table 5-2—Fracture-injection time, pressure, and rate data.

t, s	p _w , psi	q _i , bbl/min	t, s	p _w , psi	q _i , bbl/min	t, s	p _w , psi	q _i , bbl/min	t, s	p _w , psi	q _i , bbl/min	t, s	p _w , psi	q _i , bbl/min
0	5496.93	2.893	76	8832.80	11.951	152	8600.74	12.076	228	8513.72	12.076	304	8397.69	12.139
1	5424.41	4.466	77	8905.32	11.951	153	8644.25	12.076	229	8470.20	12.076	305	8325.17	12.139
2	5482.43	4.906	78	8861.81	11.951	154	8600.74	12.076	230	8412.19	12.076	306	8412.19	12.139
3	5554.95	4.780	79	8789.29	11.951	155	8571.73	12.076	231	8499.21	12.076	307	8397.69	12.139
4	5598.46	4.780	80	8818.29	11.951	156	8644.25	12.014	232	8455.70	12.139	308	8339.67	12.139
5	6280.13	4.843	81	8847.30	11.951	157	8600.74	12.014	233	8397.69	12.139	309	8412.19	12.139
6	6526.70	4.969	82	8803.79	11.951	158	8571.73	12.076	234	8499.21	12.076	310	8368.68	12.139
7	6700.74	4.906	83	8774.78	11.951	159	8644.25	12.076	235	8441.20	12.139	311	8368.68	12.076
8	6860.28	4.906	84	8832.80	12.014	160	8600.74	12.076	236	8426.69	12.076	312	8426.69	12.076
9	7251.89	4.780	85	8818.29	11.951	161	8557.23	12.076	237	8484.71	12.139	313	8368.68	12.076
10	7599.98	4.843	86	8731.27	11.951	162	8629.75	12.014	238	8441.20	12.139	314	8383.18	12.076
11	7875.55	4.906	87	8818.29	11.951	163	8600.74	12.014	239	8412.19	12.139	315	8397.69	12.139
12	8020.59	4.906	88	8818.29	11.951	164	8542.72	12.076	240	8455.70	12.202	316	8339.67	12.139
13	8339.67	4.843	89	8731.27	11.951	165	8615.24	12.014	241	8412.19	12.202	317	8383.18	12.139
14	8615.24	4.780	90	8774.78	11.951	166	8600.74	12.014	242	8397.69	12.139	318	8397.69	12.139
15	8977.84	4.717	91	8803.79	12.014	167	8528.22	12.076	243	8470.20	12.139	319	8339.67	12.076
16	9180.89	4.717	92	8760.28	11.951	168	8600.74	12.076	244	8426.69	12.139	320	8412.19	12.076
17	9369.44	4.654	93	8731.27	11.951	169	8600.74	12.076	245	8397.69	12.139	321	8383.18	12.139
18	9572.49	4.654	94	8803.79	11.951	170	8528.22	12.014	246	8470.20	12.139	322	8339.67	12.076
19	9601.50	4.592	95	8774.78	11.951	171	8586.23	12.014	247	8426.69	12.139	323	8397.69	12.139
20	9732.03	4.592	96	8687.76	12.014	172	8586.23	12.076	248	8412.19	12.139	324	8383.18	12.076
21	9630.51	4.654	97	8774.78	12.014	173	8528.22	12.076	249	8470.20	12.139	325	8354.17	12.076
22	9659.51	4.529	98	8745.78	12.014	174	8586.23	12.014	250	8412.19	12.139	326	8397.69	12.139
23	9412.95	4.529	99	8687.76	12.014	175	8586.23	12.076	251	8426.69	12.076	327	8354.17	12.139
24	9180.89	4.529	100	8745.78	11.951	176	8528.22	12.014	252	8470.20	12.139	328	8339.67	12.139
25	8847.30	4.654	101	8760.28	11.951	177	8571.73	12.076	253	8412.19	12.076	329	8397.69	12.139
26	8702.26	4.592	102	8702.26	12.014	178	8571.73	12.076	254	8426.69	12.076	330	8339.67	12.139
27	8499.21	4.529	103	8687.76	11.951	179	8499.21	12.139	255	8455.70	12.139	331	8368.68	12.139
28	8426.69	4.592	104	8745.78	11.951	180	8528.22	12.139	256	8397.69	12.139	332	8383.18	12.139
29	8354.17	4.529	105	8716.77	11.951	181	8571.73	12.076	257	8426.69	12.076	333	8325.17	12.076
30	8223.64	4.654	106	8673.26	11.951	182	8499.21	12.139	258	8455.70	12.139	334	8397.69	12.076
31	8281.65	4.529	107	8716.77	12.014	183	8542.72	12.076	259	8383.18	12.139	335	8383.18	12.139
32	8194.63	4.654	108	8702.26	12.014	184	8557.23	12.076	260	8426.69	12.139	336	8325.17	12.076
33	8281.65	4.529	109	8644.25	12.014	185	8499.21	12.076	261	8441.20	12.139	337	8412.19	12.076
34	8194.63	4.654	110	8702.26	11.951	186	8513.72	12.139	262	8368.68	12.139	338	8368.68	12.139
35	8252.65	4.592	111	8716.77	11.951	187	8557.23	12.076	263	8441.20	12.139	339	8325.17	12.139
36	8223.64	4.654	112	8658.75	12.014	188	8499.21	12.076	264	8441.20	12.139	340	8397.69	12.139
37	8267.15	4.654	113	8658.75	11.951	189	8513.72	12.076	265	8368.68	12.139	341	8354.17	12.076
38	8238.14	4.654	114	8687.76	12.014	190	8542.72	12.076	266	8441.20	12.139	342	8354.17	12.139
39	8252.65	4.654	115	8658.75	12.014	191	8484.71	12.076	267	8426.69	12.139	343	8397.69	12.139
40	8281.65	4.654	116	8615.24	12.014	192	8499.21	12.076	268	8368.68	12.139	344	8310.66	12.139
41	8180.13	4.654	117	8702.26	11.951	193	8542.72	12.076	269	8441.20	12.139	345	8354.17	12.202
42	8267.15	4.654	118	8687.76	11.951	194	8484.71	12.076	270	8441.20	12.076	346	7861.05	12.139
43	8194.63	4.654	119	8615.24	11.951	195	8499.21	12.076	271	8383.18	12.076	347	8006.08	10.693
44	8252.65	4.654	120	8658.75	12.014	196	8528.22	12.139	272	8441.20	12.139	348	8136.62	9.372
45	8180.13	4.654	121	8687.76	11.951	197	8484.71	12.076	273	8412.19	12.139	349	8006.08	9.435
46	8252.65	4.654	122	8629.75	11.951	198	8499.21	12.076	274	8383.18	12.139	350	8035.09	9.246
47	8426.69	4.717	123	8658.75	11.951	199	8528.22	12.076	275	8441.20	12.139	351	8006.08	9.246
48	8600.74	5.032	124	8673.26	12.014	200	8455.70	12.139	276	8397.69	12.139	352	8020.59	9.246
49	8745.78	5.661	125	8644.25	12.014	201	8484.71	12.139	277	8397.69	12.139	353	8020.59	9.246
50	8760.28	7.736	126	8615.24	12.076	202	8528.22	12.076	278	8441.20	12.139	354	8020.59	9.246
51	8455.70	8.994	127	8687.76	11.951	203	8470.20	12.076	279	8383.18	12.139	355	8035.09	9.183
52	8977.84	8.806	128	8673.26	11.951	204	8484.71	12.139	280	8397.69	12.139	356	8035.09	9.183
53	9108.37	9.498	129	8615.24	11.951	205	8513.72	12.139	281	8426.69	12.139	357	8020.59	9.246
54	8992.34	10.567	130	8673.26	12.014	206	8455.70	12.139	282	8368.68	12.139	358	8020.59	9.246
55	8992.34	11.699	131	8673.26	12.014	207	8470.20	12.139	283	8412.19	12.139	359	8035.09	9.183
56	8963.33	11.888	132	8615.24	12.014	208	8513.72	12.076	284	8426.69	12.139	360	8035.09	9.183
57	8745.78	11.825	133	8644.25	12.014	209	8441.20	12.139	285	8354.17	12.139	361	8049.59	9.246
58	8977.84	11.699	134	8673.26	12.014	210	8484.71	12.076	286	8441.20	12.076	362	8049.59	9.246
59	8934.32	11.636	135	8644.25	11.951	211	8499.21	12.139	287	8426.69	12.139	363	8020.59	9.435
60	8774.78	11.762	136	8615.24	12.014	212	8441.20	12.139	288	8354.17	12.139	364	8049.59	9.372
61	8934.32	11.825	137	8673.26	12.014	213	8499.21	12.076	289	8412.19	12.202	365	8049.59	9.372
62	8919.82	11.825	138	8644.25	12.014	214	8499.21	12.139	290	8397.69	12.139	366	8049.59	9.372
63	8818.29	11.825	139	8586.23	12.014	215	8426.69	12.139	291	8354.17	12.139	367	8049.59	9.372
64	8948.83	11.825	140	8658.75	12.076	216	8484.71	12.139	292	8441.20	12.076	368	7570.97	9.246
65	8934.32	11.825	141	8658.75	11.951	217	8484.71	12.139	293	8397.69	12.139	369	7541.96	8.428
66	8861.81	11.762	142	8586.23	12.014	218	8426.69	12.139	294	8368.68	12.139	370	7788.53	5.975
67	8977.84	11.762	143	8658.75	12.014	219	8484.71	12.139	295	8441.20	12.076	371	7759.52	5.472
68	8977.84	11.825	144	8658.75	12.014	220	8484.71	12.139	296	8383.18	12.139	372	7672.50	5.661
69	8876.31	11.951	145	8600.74	11.951	221	8412.19	12.139	297	8368.68	12.139	373	7716.01	5.975
70	8861.81	11.951	146	8629.75	12.014	222	8513.72	12.076	298	8441.20	12.076	374	7788.53	5.975
71	8948.83	11.951	147	8644.25	12.014	223	8470.20	12.139	299	8354.17	12.139	375	7803.03	5.975
72	8861.81	11.888	148	8586.23	12.076	224	8412.19	12.139	300	8397.69	12.139	376	7817.53	5.975
73	8847.30	11.888	149	8615.24	12.076	225	8499.21	12.076	301	8412.19	12.139	377	7774.02	6.038
74	8934.32	11.888	150	8644.25	12.076	226	8470.20	12.139	302	8354.17	12.076	378	7745.02	6.038
75	8890.81	11.951	151	8600.74	12.076	227	8397.69	12.139	303	8412.19	12.139	379	7774.02	6.038

1. Calculate the function $G(g(\Delta t, \alpha_N))$ for each time and pressure recorded during the falloff period where the function is calculated as⁷⁵

$$G(\Delta t_D, \alpha_N) = \frac{4}{\pi} [g(\Delta t_D, \alpha_N) - g_0(\alpha_N)]. \dots\dots\dots (5.161)$$

The function $g(\Delta t, \alpha_N)$ can be calculated from the closed-form solution⁷⁸ noted in Chapter II, or it can be calculated from correlations, like those provided by Ispas *et al.*¹¹⁰ **Table 5-3** contains the tabulated values of time, pressure, $g(\Delta t, \alpha_N)$, and $G(g(\Delta t, \alpha_N))$.

2. Prepare a Cartesian graph of bottomhole pressure, p_w , versus the function $G(g(\Delta t, \alpha_N))$, the derivative of pressure, dp_w/dG , and the "superposition" derivative, Gdp_w/dG .

3. Identify the leakoff type⁷⁴ and hydraulic fracture closure using the G -function plot. **Fig. 5-6** contains the G -function plot for the fracture-injection/falloff sequence. The leakoff type is fracture height recession during shut-in, which is indicated by the characteristic dip in the superposition derivative below a straight line from the origin through the "normal" leakoff data. Fracture closure is observed at $G_c = 4.33$, and the closure stress is 6,382 psi.

4. Initial reservoir pressure can be estimated from the closure stress and the uniaxial strain relationship, which is written as

$$p_i = \frac{\sigma_{\min} - \left(\frac{\nu}{1-\nu}\right)\sigma_z}{1 - \left(\frac{\nu}{1-\nu}\right)}. \dots\dots\dots (5.162)$$

Assuming Poisson's ratio, $\nu = 0.20$, and an overburden stress, $\sigma_z = 10,150$ psi (1 psi/ft overburden gradient), the initial reservoir pressure estimate is $p_i = 5,126$ psi. The estimated initial reservoir pressure from closure stress should be considered as a guide only—the pressure may or may not be accurate depending on additional factors, including tectonic stress.

5. Before-closure analysis⁵⁹ requires an estimate of fracture half-length and lost fracture width because of fluid leakoff, w_L . Fracture half-length and lost width are estimated from a graph of bottomhole pressure versus the loss-volume function, $g(\Delta t, \alpha_N)$, which is shown in **Fig. 5.7** assuming the fracture grows under horizontal plane strain conditions (GDK). The slope of the line through the before-closure data is $(m_N)_{GDK} = -323$ psia and the intercept is $(b_N)_{GDK} = 8003$ psia. Fracture half length is calculated from the intercept assuming Young's modulus, $E = 5(10)^6$ psi, and fracture height, $h_f = 6$ ft, as⁵⁹

Table 5-3—Variables required for before- and after-closure analysis.

t, s	p _w , psi	g(Δt, α _N)	G(g(Δt, α _N))	t _a , hr	p _{av} , psi	B _g , bbl/Mscf	c _i , psi ⁻¹	t, s	p _w , psi	g(Δt, α _N)	G(g(Δt, α _N))	t _a , hr	p _{av} , psi	B _g , bbl/Mscf	c _i , psi ⁻¹
385	7599.98	1.478	0.0000	0.10694	6135.57	0.5338	5.012E-05	2081	6526.70	4.473	3.8125	0.54164	5083.26	0.5750	6.344E-05
394	7541.96	1.516	0.0474	0.10944	6079.18	0.5357	5.070E-05	2106	6512.19	4.502	3.8494	0.54765	5068.92	0.5756	6.366E-05
403	7527.46	1.550	0.0917	0.11192	6065.08	0.5362	5.085E-05	2131	6497.69	4.530	3.8861	0.55365	5054.57	0.5763	6.389E-05
410	7469.44	1.576	0.1248	0.11384	6008.61	0.5381	5.144E-05	2161	6483.19	4.565	3.9298	0.56083	5040.22	0.5770	6.411E-05
416	7425.93	1.598	0.1524	0.11547	5966.23	0.5396	5.190E-05	2186	6468.68	4.593	3.9659	0.56680	5025.87	0.5776	6.434E-05
421	7483.95	1.616	0.1749	0.11684	6022.73	0.5376	5.129E-05	2211	6454.18	4.621	4.0019	0.57275	5011.51	0.5783	6.457E-05
426	7396.92	1.633	0.1971	0.11820	5937.96	0.5406	5.221E-05	2241	6439.68	4.655	4.0447	0.57989	4997.15	0.5790	6.481E-05
436	7440.44	1.667	0.2404	0.12092	5980.36	0.5391	5.175E-05	2266	6425.17	4.683	4.0802	0.58582	4982.79	0.5797	6.504E-05
441	7411.43	1.684	0.2615	0.12228	5952.09	0.5401	5.206E-05	2296	6410.67	4.716	4.1224	0.59292	4968.42	0.5804	6.527E-05
446	7425.93	1.700	0.2824	0.12364	5966.23	0.5396	5.190E-05	2321	6396.16	4.744	4.1574	0.59882	4954.06	0.5811	6.551E-05
451	7396.92	1.716	0.3030	0.12499	5937.96	0.5406	5.221E-05	2351	6381.66	4.776	4.1992	0.60589	4939.69	0.5818	6.575E-05
456	7411.43	1.732	0.3233	0.12635	5952.09	0.5401	5.206E-05	2376	6367.16	4.804	4.2337	0.61177	4925.31	0.5825	6.599E-05
466	7396.92	1.764	0.3633	0.12906	5937.96	0.5406	5.221E-05	2406	6352.65	4.836	4.2749	0.61880	4910.94	0.5832	6.623E-05
481	7382.42	1.809	0.4216	0.13312	5923.81	0.5411	5.237E-05	2431	6338.15	4.863	4.3091	0.62466	4896.56	0.5839	6.647E-05
501	7367.92	1.868	0.4966	0.13853	5909.67	0.5416	5.252E-05	2461	6323.65	4.895	4.3498	0.63166	4882.18	0.5846	6.672E-05
516	7353.41	1.911	0.5511	0.14257	5895.52	0.5421	5.268E-05	2491	6309.14	4.926	4.3902	0.63865	4867.79	0.5853	6.696E-05
531	7338.91	1.953	0.6042	0.14661	5881.36	0.5426	5.284E-05	2521	6294.64	4.958	4.4304	0.64563	4853.41	0.5860	6.721E-05
551	7324.41	2.007	0.6730	0.15199	5867.21	0.5431	5.300E-05	2551	6280.13	4.989	4.4704	0.65258	4839.02	0.5867	6.746E-05
566	7309.90	2.046	0.7232	0.15601	5853.05	0.5436	5.316E-05	2586	6265.63	5.026	4.5167	0.66068	4824.63	0.5875	6.771E-05
591	7295.40	2.110	0.8046	0.16271	5838.88	0.5441	5.332E-05	2616	6251.13	5.057	4.5561	0.66761	4810.23	0.5882	6.796E-05
606	7280.89	2.148	0.8522	0.16672	5824.71	0.5446	5.348E-05	2646	6236.62	5.087	4.5952	0.67452	4795.83	0.5889	6.822E-05
631	7266.39	2.208	0.9296	0.17339	5810.54	0.5451	5.365E-05	2676	6222.12	5.118	4.6342	0.68141	4781.43	0.5897	6.847E-05
656	7251.89	2.267	1.0047	0.18005	5796.37	0.5457	5.381E-05	2711	6207.62	5.153	4.6793	0.68944	4767.03	0.5904	6.873E-05
681	7237.38	2.325	1.0778	0.18669	5782.19	0.5462	5.398E-05	2746	6193.11	5.189	4.7241	0.69745	4752.62	0.5912	6.899E-05
701	7222.88	2.370	1.1349	0.19200	5768.01	0.5467	5.414E-05	2776	6178.61	5.219	4.7623	0.70429	4738.22	0.5919	6.925E-05
726	7208.38	2.425	1.2048	0.19862	5753.82	0.5472	5.431E-05	2811	6164.10	5.253	4.8066	0.71226	4723.81	0.5927	6.951E-05
756	7193.87	2.489	1.2864	0.20655	5739.63	0.5477	5.448E-05	2841	6149.60	5.283	4.8443	0.71908	4709.39	0.5934	6.978E-05
786	7179.37	2.551	1.3660	0.21447	5725.44	0.5483	5.465E-05	2876	6135.10	5.317	4.8881	0.72701	4694.98	0.5942	7.004E-05
816	7164.86	2.612	1.4435	0.22237	5711.24	0.5488	5.482E-05	2916	6120.59	5.356	4.9377	0.73605	4680.56	0.5949	7.031E-05
846	7150.36	2.672	1.5193	0.23025	5697.04	0.5493	5.499E-05	2951	6106.09	5.390	4.9809	0.74395	4666.14	0.5957	7.058E-05
876	7135.86	2.730	1.5933	0.23812	5682.84	0.5499	5.516E-05	2986	6091.59	5.424	5.0237	0.75182	4651.72	0.5965	7.085E-05
906	7121.35	2.787	1.6657	0.24598	5668.63	0.5504	5.534E-05	3026	6077.08	5.462	5.0724	0.76080	4637.29	0.5973	7.113E-05
936	7106.85	2.842	1.7367	0.25382	5654.42	0.5510	5.551E-05	3066	6062.58	5.500	5.1208	0.76976	4622.87	0.5981	7.140E-05
971	7092.35	2.906	1.8177	0.26295	5640.21	0.5515	5.569E-05	3106	6048.07	5.538	5.1688	0.77870	4608.44	0.5989	7.168E-05
1001	7077.84	2.959	1.8857	0.27076	5626.99	0.5521	5.586E-05	3146	6033.57	5.575	5.2165	0.78761	4594.00	0.5996	7.196E-05
1036	7063.34	3.020	1.9635	0.27985	5611.77	0.5526	5.604E-05	3186	6019.07	5.613	5.2639	0.79651	4579.57	0.6004	7.224E-05
1066	7048.83	3.072	2.0289	0.28763	5597.55	0.5532	5.622E-05	3226	6004.56	5.650	5.3110	0.80538	4565.14	0.6012	7.252E-05
1096	7034.33	3.122	2.0933	0.29540	5583.32	0.5537	5.640E-05	3271	5990.06	5.691	5.3636	0.81534	4550.70	0.6021	7.281E-05
1126	7019.83	3.172	2.1566	0.30315	5569.09	0.5543	5.658E-05	3311	5975.55	5.732	5.4159	0.82527	4536.26	0.6029	7.310E-05
1161	7005.32	3.229	2.2292	0.31217	5554.88	0.5548	5.676E-05	3361	5961.05	5.773	5.4678	0.83518	4521.81	0.6037	7.338E-05
1196	6990.82	3.285	2.3005	0.32118	5540.61	0.5554	5.694E-05	3411	5946.55	5.818	5.5250	0.84616	4507.37	0.6045	7.366E-05
1221	6976.32	3.325	2.3507	0.32760	5526.37	0.5560	5.713E-05	3461	5932.04	5.862	5.5818	0.85712	4492.92	0.6053	7.397E-05
1251	6961.81	3.371	2.4102	0.33529	5512.13	0.5565	5.731E-05	3506	5917.54	5.902	5.6326	0.86695	4478.47	0.6062	7.426E-05
1286	6947.31	3.425	2.4785	0.34424	5497.88	0.5571	5.750E-05	3556	5903.04	5.946	5.6886	0.87785	4464.02	0.6070	7.456E-05
1316	6932.80	3.470	2.5362	0.35190	5483.63	0.5577	5.769E-05	3611	5888.53	5.994	5.7498	0.88982	4449.57	0.6078	7.486E-05
1346	6918.30	3.515	2.5932	0.35954	5469.37	0.5583	5.788E-05	3666	5874.03	6.042	5.8105	0.90175	4435.11	0.6087	7.516E-05
1376	6903.80	3.559	2.6494	0.36717	5455.12	0.5588	5.807E-05	3726	5859.52	6.093	5.8762	0.91474	4420.66	0.6095	7.546E-05
1406	6889.29	3.603	2.7050	0.37478	5440.85	0.5594	5.826E-05	3786	5845.02	6.145	5.9414	0.92769	4406.20	0.6104	7.577E-05
1436	6874.79	3.646	2.7598	0.38238	5426.59	0.5600	5.845E-05	3846	5830.52	6.195	6.0060	0.94061	4391.74	0.6113	7.608E-05
1461	6860.28	3.681	2.8051	0.38870	5412.32	0.5606	5.864E-05	3906	5816.01	6.246	6.0702	0.95350	4377.27	0.6121	7.639E-05
1491	6845.78	3.724	2.8588	0.39627	5398.05	0.5612	5.884E-05	3971	5801.51	6.300	6.1392	0.96742	4362.81	0.6130	7.670E-05
1521	6831.28	3.765	2.9119	0.40382	5383.77	0.5618	5.903E-05	4041	5787.01	6.358	6.2128	0.98239	4348.34	0.6139	7.701E-05
1546	6816.77	3.800	2.9557	0.41010	5369.50	0.5624	5.923E-05	4116	5772.50	6.419	6.2911	0.99837	4333.87	0.6147	7.733E-05
1576	6802.27	3.841	3.0077	0.41762	5355.21	0.5630	5.943E-05	4191	5758.00	6.480	6.3686	1.01432	4319.40	0.6156	7.764E-05
1606	6787.77	3.881	3.0592	0.42513	5340.93	0.5636	5.963E-05	4266	5743.49	6.541	6.4455	1.03023	4304.93	0.6165	7.797E-05
1631	6773.26	3.914	3.1017	0.43137	5326.64	0.5642	5.983E-05	4351	5728.99	6.608	6.5319	1.04821	4290.46	0.6174	7.829E-05
1661	6758.76	3.954	3.1523	0.43884	5312.35	0.5648	6.003E-05	4436	5714.49	6.676	6.6174	1.06615	4275.99	0.6183	7.861E-05
1686	6744.25	3.987	3.1940	0.44506	5298.06	0.5654	6.023E-05	4526	5699.98	6.746	6.7072	1.08509	4261.51	0.6192	7.894E-05
1711	6729.75	4.019	3.2353	0.45126	5283.76	0.5660	6.044E-05	4626	5685.48	6.824	6.8060	1.10608	4247.03	0.6201	7.927E-05
1741	6715.25	4.058	3.2846	0.45869	5269.46	0.5666	6.064E-05	4726	5670.98	6.901	6.9038	1.12702	4232.55	0.6211	7.960E-05
1766	6700.74	4.090	3.3252	0.46487	5255.15	0.5673	6.085E-05	4831	5656.47	6.980	7.0054	1.14895	4218.07	0.6220	7.994E-05
1791	6686.24	4.122	3.3656	0.47103	5240.85	0.5679	6.106E-05	4931	5641.96	7.063	7.1148	1.17199	4203.59	0.6229	8.028E-05
1816	6671.74	4.153	3.4056	0.47719	5226.53	0.5685	6.127E-05	5036	5627.45	7.153	7.2248	1.19679	4189.11	0.6239	8.061E-05
1846	6657.23	4.190	3.4532	0.48455	5212.22	0.5691	6.148E-05	5136	5612.94	7.245	7.3422	1.22269	4174.62	0.6248	8.095E-05
1871	6642.73	4.221	3.4926	0.49068	5										

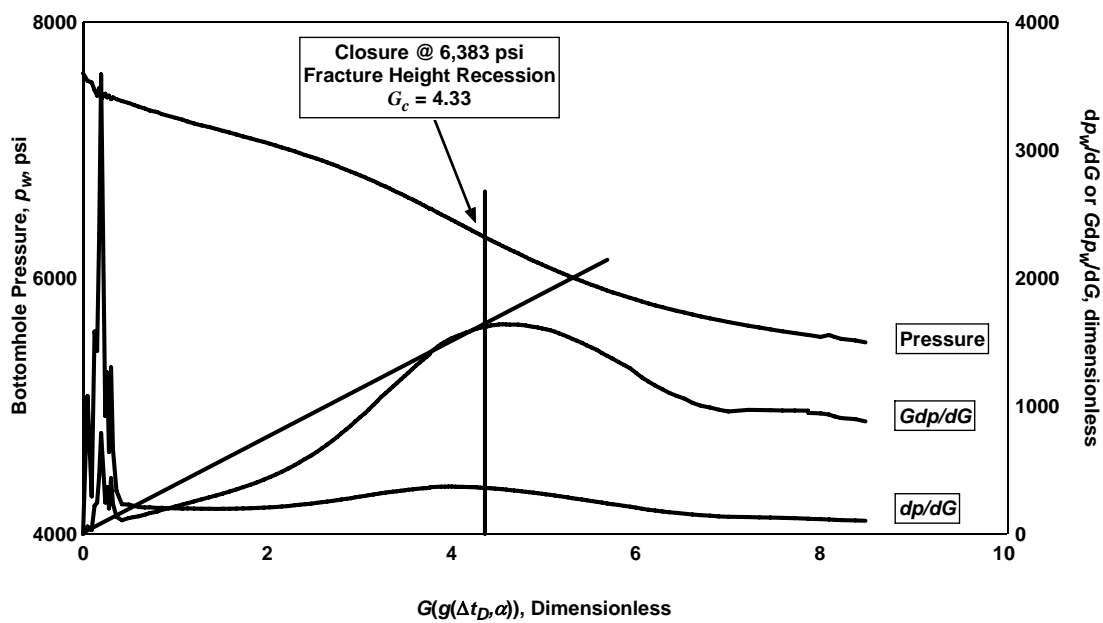


Fig. 5.6—Fracture-injection/falloff sequence G -function derivative analysis.

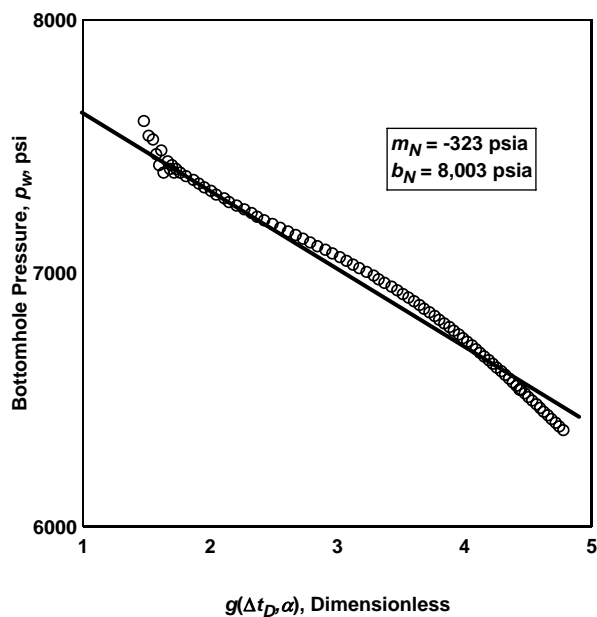


Fig. 5.7—Fracture-injection/falloff sequence before-closure pressure versus the dimensionless loss-volume function.

$$(L_f)_{GDK} = \sqrt{\frac{(5.615)(5,208,333.3)(67.9/2)}{\pi(6)(8003 - 6382)}} = 180.3 \text{ ft},$$

and lost width is calculated from the slope as

$$(w_L)_{GDK} = \frac{1.478(12)\pi(180.3)}{5,208,333.3}(323) = 0.62 \text{ in.}$$

For a radial fracture geometry, $(m_N)_{RAD} = -317.6$ psi and the intercept is $(b_N)_{RAD} = 7964$ psi. Fracture radius is calculated as

$$R_f = \sqrt[3]{\frac{3(5.615)(5,208,333.3)(67.9/2)}{8(7,964 - 6,382)}} = 61.7 \text{ ft},$$

and the lost width is calculated as

$$(w_L)_{RAD} = \frac{7.343(12)(61.7)}{\pi(5208333.3)}(317.6) = 0.11 \text{ in.}$$

6. Calculate the adjusted pseudotime, adjusted pseudopressure, gas formation volume factor, and total compressibility for each recorded time and pressure after the end of the injection. Scale time to zero at the beginning of the shut-in period for calculating adjusted pseudotime. Assume the initial reservoir pressure is 5,126 psi, which was estimated from the observed closure stress. The reservoir temperature is 205°F and the gas gravity is 0.70. **Table 5-4** contains the tabulated values for the Kakwa 07-24 fracture-injection/falloff sequence.

7. Note the following variables required for the analysis.

$$p_{ai} = 3,686.9 \text{ psia}$$

$$p_{a0} = 6,135.57 \text{ psia}$$

$$B_{gi} = 0.660313 \text{ bbl/Mscf}$$

$$B_{ge} = 0.533824 \text{ bbl/Mscf}$$

$$\mu_{gi} = 0.0280152 \text{ cp}$$

$$c_{ti} = 9.40285(10)^{-5} \text{ psi}^{-1}$$

$$c_w = 4.52135(10)^{-6} \text{ psi}^{-1}$$

8. Calculate and graph $(y_{ap})_n$ versus $(x_{ap})_n$ for each recorded time and pressure before fracture closure. Table 5-4 contains the tabulated values that are graphed in **Fig. 5.8**. Under normal leakoff conditions, the data on the specialized graph will fall along a straight line, but nonideal leakoff, like fracture-height recession during closure causes the data to fan across the page.⁸² Fracture-height recession during closure indicates a changing fracture area during the falloff period, which violates the assumptions of before-closure pressure-transient analysis. Consequently, the permeability and fracture-face resistance estimated will contain error. Drawing a line from the origin through the last few data

Table 5-4—Variables required for before-closure pressure transient analysis.

t, s	t_a, hr	p_{aw}, psi	$B_g, bbl/Mscf$	c_t, psi^{-1}	$(x_{ap})_n$	$(y_{ap})_n$	t, s	t_a, hr	p_{aw}, psi	$B_g, bbl/Mscf$	c_t, psi^{-1}	$(x_{ap})_n$	$(y_{ap})_n$
385	0.00000	6135.57	0.5338	5.012E-05									
394	0.00249	6079.18	0.5357	5.070E-05			1286	0.23729	5497.88	0.5571	5.750E-05	187.9971	3.5605
403	0.00497	6065.08	0.5362	5.085E-05			1316	0.24495	5483.63	0.5577	5.769E-05	163.2005	2.9961
410	0.00689	6008.61	0.5381	5.144E-05	24.0547	0.3916	1346	0.25260	5469.37	0.5583	5.788E-05	163.5288	2.9421
416	0.00853	5966.23	0.5396	5.190E-05	32.8346	0.4369	1376	0.26023	5455.12	0.5588	5.807E-05	163.6744	2.8895
421	0.00989	6022.73	0.5376	5.129E-05	6.1500	—	1406	0.26784	5440.85	0.5594	5.826E-05	163.7626	2.8385
426	0.01126	5937.96	0.5406	5.221E-05	19.4855	0.1785	1436	0.27544	5426.59	0.5600	5.845E-05	163.8124	2.7888
436	0.01397	5980.36	0.5391	5.175E-05	-4.9332	—	1461	0.28175	5412.32	0.5606	5.864E-05	140.0193	2.2875
441	0.01533	5952.09	0.5401	5.206E-05	27.6168	0.5271	1491	0.28932	5398.05	0.5612	5.884E-05	165.4812	2.6977
446	0.01669	5966.23	0.5396	5.190E-05	-17.0092	—	1521	0.29687	5383.77	0.5618	5.903E-05	165.0903	2.6514
451	0.01805	5937.96	0.5406	5.221E-05	29.0252	0.5184	1546	0.30315	5369.50	0.5624	5.923E-05	140.8235	2.1755
456	0.01941	5952.09	0.5401	5.206E-05	-19.3170	—	1576	0.31068	5355.21	0.5630	5.943E-05	166.3640	2.5664
466	0.02212	5937.96	0.5406	5.221E-05	72.2688	2.0380	1606	0.31818	5340.93	0.5636	5.963E-05	165.8772	2.5232
481	0.02618	5923.81	0.5411	5.237E-05	104.5844	2.9929	1631	0.32442	5326.64	0.5642	5.983E-05	141.3283	2.0708
501	0.03158	5909.67	0.5416	5.252E-05	130.7354	3.8888	1661	0.33190	5312.35	0.5648	6.003E-05	166.9778	2.4434
516	0.03563	5895.52	0.5421	5.268E-05	104.0959	2.8583	1686	0.33811	5298.06	0.5654	6.023E-05	142.0026	2.0055
531	0.03967	5881.36	0.5426	5.284E-05	106.5143	2.8021	1711	0.34432	5283.76	0.5660	6.044E-05	143.0818	1.9753
551	0.04505	5867.21	0.5431	5.300E-05	135.0873	3.6476	1741	0.35175	5269.46	0.5666	6.064E-05	168.6777	2.3313
566	0.04907	5853.05	0.5436	5.316E-05	107.3828	2.6842	1766	0.35792	5255.15	0.5673	6.085E-05	143.1735	1.9137
591	0.05576	5838.88	0.5441	5.332E-05	162.7713	4.3534	1791	0.36409	5240.85	0.5679	6.106E-05	144.1008	1.8849
606	0.05977	5824.71	0.5446	5.348E-05	106.4305	2.5650	1816	0.37024	5226.53	0.5685	6.127E-05	144.8157	1.8568
631	0.06644	5810.54	0.5451	5.365E-05	163.3161	4.1655	1846	0.37761	5212.22	0.5691	6.148E-05	170.5956	2.1919
656	0.07310	5796.37	0.5457	5.381E-05	160.2104	4.0622	1871	0.38373	5197.90	0.5698	6.169E-05	144.5468	1.7992
681	0.07975	5782.19	0.5462	5.398E-05	158.4452	3.9639	1896	0.38985	5183.58	0.5704	6.190E-05	145.3550	1.7724
701	0.08506	5768.01	0.5467	5.414E-05	131.5366	3.1072	1926	0.39717	5169.26	0.5711	6.212E-05	171.3402	2.0924
726	0.09168	5753.82	0.5472	5.431E-05	159.3154	3.7944	1951	0.40325	5154.94	0.5717	6.233E-05	145.1162	1.7177
756	0.09961	5739.63	0.5477	5.448E-05	183.0094	4.4355	1976	0.40933	5140.61	0.5723	6.255E-05	145.8882	1.6920
786	0.10752	5725.44	0.5483	5.465E-05	179.5933	4.3243	2001	0.41539	5126.27	0.5730	6.277E-05	146.4633	1.6667
816	0.11542	5711.24	0.5488	5.482E-05	177.2222	4.2186	2026	0.42144	5111.94	0.5737	6.299E-05	146.9561	1.6418
846	0.12331	5697.04	0.5493	5.499E-05	175.4250	4.1179	2046	0.42626	5097.60	0.5743	6.321E-05	120.9402	1.2953
876	0.13118	5682.84	0.5499	5.516E-05	174.0180	4.0223	2051	0.42747	5097.60	0.5743	6.321E-05	0.0000	—
906	0.13903	5668.63	0.5504	5.534E-05	172.8680	3.9307	2056	0.42868	5097.60	0.5743	6.321E-05	0.0000	—
936	0.14687	5654.42	0.5510	5.551E-05	171.9267	3.8434	2081	0.43470	5083.26	0.5750	6.344E-05	145.9733	1.5910
971	0.15600	5640.21	0.5515	5.569E-05	194.3686	4.3750	2106	0.44071	5068.92	0.5756	6.366E-05	146.8988	1.5671
1001	0.16381	5625.99	0.5521	5.586E-05	168.4366	3.6700	2131	0.44670	5054.57	0.5763	6.389E-05	147.4764	1.5435
1036	0.17291	5611.77	0.5526	5.604E-05	191.3621	4.1822	2161	0.45388	5040.22	0.5770	6.411E-05	173.9394	1.8222
1066	0.18069	5597.55	0.5532	5.622E-05	166.1740	3.5112	2186	0.45985	5025.87	0.5776	6.434E-05	147.0343	1.4954
1096	0.18845	5583.32	0.5537	5.640E-05	166.3411	3.4406	2211	0.46581	5011.51	0.5783	6.457E-05	147.6890	1.4728
1126	0.19620	5569.09	0.5543	5.658E-05	166.3093	3.3724	2241	0.47294	4997.15	0.5790	6.481E-05	174.2920	1.7385
1161	0.20523	5554.85	0.5548	5.676E-05	189.2106	3.8492	2266	0.47887	4982.79	0.5797	6.504E-05	147.2964	1.4266
1196	0.21423	5540.61	0.5554	5.694E-05	187.2035	3.7675	2296	0.48597	4968.42	0.5804	6.527E-05	174.0966	1.6839
1221	0.22065	5526.37	0.5560	5.713E-05	139.5048	2.6455	2321	0.49188	4954.06	0.5811	6.551E-05	147.1746	1.3816
1251	0.22834	5512.13	0.5565	5.731E-05	165.1360	3.1153	2351	0.49894	4939.69	0.5818	6.575E-05	174.0459	1.6307

points recorded before closure results in $(m_M)_{GDK} = 0.009350$. The created fracture height is assumed to be confined to the permeable fracture height, $r_p = h_p/h_f = 1$, and the permeability is estimated as

$$(k)_{GDK} = \left[\frac{2(141.2)(0.02878)(24)}{5.615} \frac{1}{(1)(9199.7)(0.009350)} \right]^2 = 0.163 \text{ md} .$$

There is no fracture face resistance since the straight line is drawn from the origin.

Assuming the opposite extreme of radial fracture geometry, the specialized graph results in $(b_M)_{RAD} = 0$ and $(m_M)_{RAD} = 0.009233$. The ratio of permeable to total fracture height for a radial fracture is written as⁵⁹

$$(r_p)_{RAD} = \frac{2}{\pi} \left[\frac{h_p}{2R_f} \sqrt{1 - \left(\frac{h_p}{2R_f} \right)^2} + \sin^{-1} \frac{h_p}{2R_f} \right], \dots\dots\dots (5.163)$$

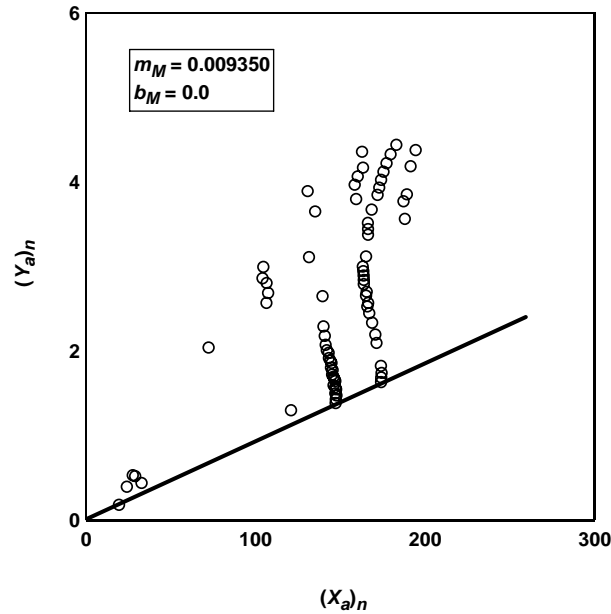


Fig. 5.8—Fracture-injection/falloff sequence before-closure pressure-transient analysis.

and is calculated as

$$(r_p)_{RAD} = \frac{2}{\pi} \left[\frac{6}{2(61.7)} \sqrt{1 - \left(\frac{6}{2(61.7)} \right)^2} + \sin^{-1} \frac{6}{2(61.7)} \right] = 0.063 .$$

The permeability assuming radial fracture geometry is estimated as

$$(k)_{RAD} = \left[\frac{2(141.2)(0.02878)(24)}{5.615} \frac{1}{(1)(50330.7)(0.009233)} \right]^2 = 1.408 \text{ md} .$$

An order of magnitude change in the estimated permeability results by assuming an unconfined radial fracture versus a confined fracture. With fracture-height recession observed during the before-closure falloff, which suggests the fracture grew into higher stress, low permeability layers adjacent to the permeable layer, a radial fracture seems more plausible. However, without fracture imaging the true fracture geometry is unknown and before-closure pressure-transient analysis can only bracket the estimated permeability, that is, $0.163 \text{ md} \leq k \leq 1.408 \text{ md}$.

9. After-closure analysis requires a log-log graph of the adjusted pseudopressure difference, $p_{aw} - p_{ai}$, and the well testing pressure derivative versus the reciprocal elapsed adjusted pseudotime, which is shown in **Fig. 5.9**. The elapsed time and corresponding adjusted pseudotime used in after-

closure analysis is calculated relative to the time since the beginning of the injection, and the points in Fig 5.9 were calculated and graphed using the adjusted pseudopressure and pseudotime values tabulated in Table 5-3.

The derivative curve is not a function of initial reservoir pressure and should be used to identify the flow regimes. In Fig. 5.9, the derivative data fall along a unit slope line, which indicates pseudoradial flow was observed. Additionally, the adjusted pseudopressure difference data overlay the derivative data on the unit slope line, which suggests that the estimated initial reservoir pressure is correct. In most cases, the determination of initial reservoir pressure is an iterative process, and the adjusted pseudopressure difference and derivative curves will not overlay during pseudoradial flow until the initial reservoir pressure is correct.

10. Since pseudoradial flow was indicated in Fig. 5.9, a Cartesian graph of adjusted pseudopressure versus the reciprocal elapsed adjusted pseudotime is prepared, which is shown in Fig. 5.10. A straight line is drawn through the data corresponding to pseudoradial flow, and the initial adjusted pseudopressure corresponds to the intercept of the straight line, $b_{acpr} = p_{ai} = 3,684$ psia, which indicates the initial reservoir pressure is 5,125 psia. The slope of the straight line, $m_{acpr} = 449.082$ psia·hr, and the

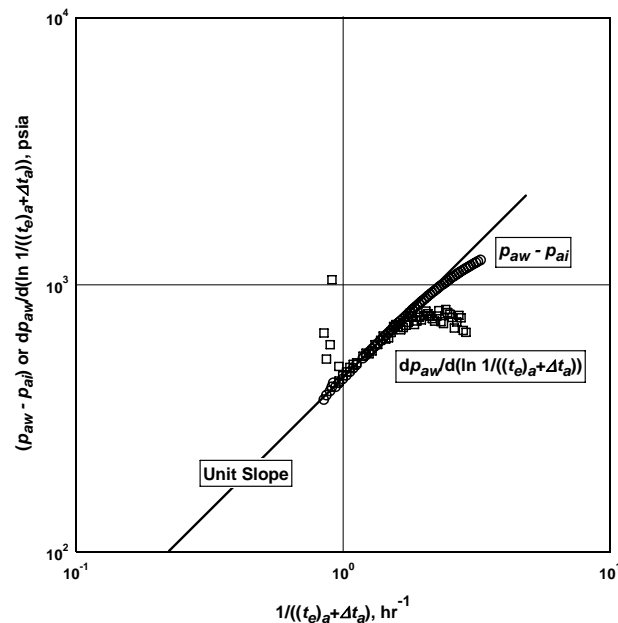


Fig. 5.9—Fracture-injection/falloff sequence after-closure analysis diagnostic graph.

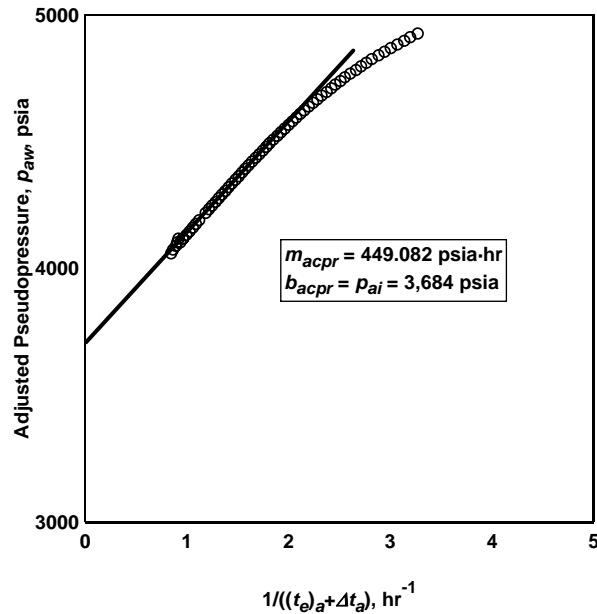


Fig. 5.10—Fracture-injection/falloff sequence Cartesian after-closure analysis graph.

transmissibility is calculated as

$$\frac{kh}{\mu_i} = \frac{141.2(24)}{2} \frac{67.9}{449.082} = 256.117 \frac{\text{md} \cdot \text{ft}}{\text{cp}},$$

which corresponds to a permeability-thickness product of $kh = 7.173 \text{ md} \cdot \text{ft}$.

Since pseudoradial flow was observed during the Kakwa 07-24 Bluesky fracture-injection/falloff sequence, type-curve analysis is unnecessary; however, type-curve analysis can be used to calculate the effective fracture half length created during the fracture-injection.

11. Prepare a log-log graph of $I(\Delta p_a)$ versus $(t_e)_a + \Delta t_a$ and $\Delta p'_a$ versus $(t_e)_a + \Delta t_a$ and overlay the appropriate constant-rate, drawdown type curve for the reservoir/system. **Fig 5.11** shows a non-unique type-curve match obtained with the observed data and a type curve for production through and infinite-conductivity fracture in an infinite slab reservoir. The equivalent constant-rate pressure difference and derivative points plotted in Fig. 5.11 are also tabulated in **Table 5-5**.

Note that the type curve match indicates variable storage during fracture closure, that is, the early-time data fall along the solution with $C_{bcD} = 3.0$, and the late-time data overlay the solution with $C_{acD} = 2.0$. A before-closure match point is as follows.

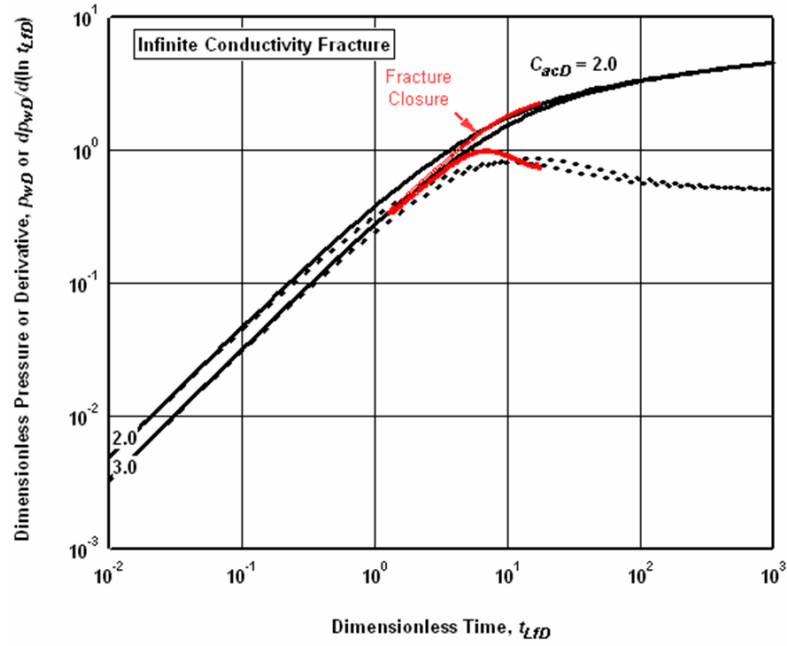


Fig. 5.11—Fracture-injection/falloff sequence variable-storage type-curve match.

$$t_{aLfD} = 2.090752 \rightarrow (t_e)_a + \Delta t_a = 0.173389 \text{ hr}$$

$$p_{acD} = 0.512268 \rightarrow I(\Delta p_a) = 409.8144 \text{ psia} \cdot \text{hr}$$

and an after-closure match point is

$$t_{aLfD} = 10 \rightarrow (t_e)_a + \Delta t_a = 0.83518 \text{ hr}$$

$$p_{acD} = 1.757406 \rightarrow I(\Delta p_a) = 1,383.963 \text{ psia} \cdot \text{hr}$$

12. The before-closure match point is used with the transmissibility calculated from after-closure analysis to calculate the adjusted before-closure storage coefficient, C_{abc} . Assume $T_i = T_w$, let $p_{awsD}(0) = 1$, and C_{abc} is calculated as

$$C_{abc} = \frac{\frac{kh}{\mu_i}}{(141.2)(24)(p_{a0} - p_{ai})} p_{awsD}(0) \frac{T_i}{T_w} \left[\frac{\int_0^{((t_e)_a + \Delta t_a)} (p_{aw}(t) - p_{ai}) dt_a}{p_{bcD}(t_{aLfD})} \right]_{MP}$$

$$= \frac{256.117}{(141.2)(24)(6135.37 - 3686.9)(1)} \left[\frac{409.8144}{0.512268} \right] = 0.024694 \frac{\text{bbl}}{\text{psia}}$$

Table 5-5—Variables required for type-curve match.

t_a , hr	p_{aw} , psi	$I(\Delta p_a)$, psi-hr	$dp_a/d(\ln t_a)$, psi-hr	t_a , hr	p_{aw} , psi	$I(\Delta p_a)$, psi-hr	$dp_a/d(\ln t_a)$, psi-hr
0.10694	6135.57	261.8867	261.8867				
0.10944	6079.18	267.9172	261.8166	0.54164	5083.26	1063.0632	756.3933
0.11192	6065.08	273.8341	266.1723	0.54765	5068.92	1071.4115	756.9289
0.11384	6008.61	278.3482	264.3131	0.55365	5054.57	1079.6555	757.2724
0.11547	5966.23	282.1125	263.2178	0.56083	5040.22	1089.4238	759.0442
0.11684	6022.73	285.2619	272.9306	0.56680	5025.87	1097.4606	758.9882
0.11820	5937.96	288.3864	266.0918	0.57275	5011.51	1105.3942	758.7420
0.12092	5980.36	294.5611	277.3365	0.57989	4997.15	1114.7912	759.8637
0.12228	5952.09	297.6608	276.9990	0.58582	4982.79	1122.5196	759.2209
0.12364	5966.23	300.7482	281.8245	0.59292	4968.42	1131.6711	759.9063
0.12499	5937.96	303.8232	281.3844	0.59882	4954.06	1139.1956	758.8692
0.12635	5952.09	306.8858	286.2240	0.60589	4939.69	1148.1033	759.1209
0.12906	5937.96	313.0111	290.5436	0.61177	4925.31	1155.4253	757.6920
0.13312	5923.81	322.1250	297.8035	0.61880	4910.94	1164.0908	757.5118
0.13853	5909.67	334.1784	307.9355	0.62466	4896.56	1171.2118	755.6930
0.14257	5895.52	343.1449	314.9131	0.63166	4882.18	1179.6368	755.0838
0.14661	5881.36	352.0378	321.7595	0.63865	4867.79	1187.9423	754.2531
0.15199	5867.21	363.7974	331.4053	0.64563	4853.41	1196.1286	753.2009
0.15601	5853.05	372.5439	337.9711	0.65258	4839.02	1204.1962	751.9277
0.16271	5838.88	386.9999	350.1697	0.66068	4824.63	1213.4702	751.7513
0.16672	5824.71	395.6007	356.4368	0.66761	4810.23	1221.3016	750.0218
0.17339	5810.54	409.8144	368.2405	0.67452	4795.83	1229.0154	748.0738
0.18005	5796.37	423.9074	379.8285	0.68141	4781.43	1236.6121	745.9077
0.18669	5782.19	437.8799	391.2011	0.68944	4767.03	1245.3390	744.7621
0.19200	5768.01	448.9619	399.5975	0.69745	4752.62	1253.9302	743.3640
0.19862	5753.82	462.6945	410.5595	0.70429	4738.22	1261.1784	740.5137
0.20655	5739.63	479.0303	424.0206	0.71226	4723.81	1269.5000	738.6288
0.21447	5725.44	495.2229	437.2255	0.71908	4709.39	1276.5180	735.3318
0.22237	5711.24	511.2729	450.1748	0.72701	4694.98	1284.5720	732.9625
0.23025	5697.04	527.1805	462.8687	0.73605	4680.56	1293.6245	731.4679
0.23812	5682.84	542.9461	475.3080	0.74395	4666.14	1301.4129	728.5850
0.24598	5668.63	558.5701	487.4931	0.75182	4651.72	1309.0693	725.4550
0.25382	5654.42	574.0528	499.4247	0.76080	4637.29	1317.6692	723.1450
0.26295	5640.21	591.9517	513.6509	0.76976	4622.87	1326.1193	720.5537
0.27076	5625.99	607.1530	525.0581	0.77870	4608.44	1334.4202	717.6828
0.27985	5611.77	624.7243	538.7143	0.78761	4594.00	1342.5726	714.5324
0.28763	5597.55	639.6457	549.5995	0.79651	4579.57	1350.5770	711.1040
0.29540	5583.32	654.4277	560.2338	0.80538	4565.14	1358.4341	707.3983
0.30315	5569.09	669.0706	570.6177	0.81534	4550.70	1367.1080	704.3714
0.31217	5554.85	685.9921	583.1597	0.82527	4536.26	1375.6175	701.0350
0.32118	5540.61	702.7524	595.4111	0.83518	4521.81	1383.9632	697.3893
0.32760	5526.37	714.6090	602.6478	0.84616	4507.37	1393.0549	694.3374
0.33529	5512.13	728.6994	612.0168	0.85712	4492.92	1401.9660	690.9448
0.34424	5497.88	744.9782	623.4546	0.86695	4478.47	1409.8242	686.3467
0.35190	5483.63	758.7947	632.3103	0.87785	4464.02	1418.3764	682.2916
0.35954	5469.37	772.4747	640.9194	0.88982	4449.57	1427.5877	678.7281
0.36717	5455.12	786.0186	649.2823	0.90175	4435.11	1436.6037	674.7953
0.37478	5440.85	799.4269	657.3998	0.91474	4420.66	1446.2271	671.2880
0.38238	5426.59	812.6999	665.2723	0.92769	4406.20	1455.6392	667.3797
0.38870	5412.32	823.6483	670.7194	0.94061	4391.74	1464.8409	663.0727
0.39627	5398.05	836.6519	678.1215	0.95350	4377.27	1473.8331	658.3673
0.40382	5383.77	849.5214	685.2801	0.96742	4362.81	1483.3487	653.9901
0.41010	5369.50	860.1344	690.0825	0.98239	4348.34	1493.3539	649.8920
0.41762	5355.21	872.7368	696.7742	0.99837	4333.87	1503.8154	646.0239
0.42513	5340.93	885.2061	703.2241	1.01432	4319.40	1514.0195	641.6662
0.43137	5326.64	895.4868	707.3859	1.03023	4304.93	1523.9674	636.8196
0.43884	5312.35	907.6914	713.3720	1.04821	4290.46	1534.9526	632.7639
0.44506	5298.06	917.7520	717.1150	1.06615	4275.99	1545.6500	628.1589
0.45126	5283.76	927.7031	720.6585	1.08509	4261.51	1556.6733	623.6105
0.45869	5269.46	939.5135	725.9618	1.10608	4247.03	1568.5859	619.6613
0.46487	5255.15	949.2466	729.0895	1.12702	4232.55	1580.1645	615.0723
0.47103	5240.85	958.8711	732.0187	1.14895	4218.07	1591.9730	610.4017
0.47719	5226.53	968.3875	734.7503	1.19679	4189.11	1616.6987	601.1534
0.48455	5212.22	979.6777	739.1575	1.22269	4174.62	1629.5212	596.4527
0.49068	5197.90	988.9787	741.4771	1.24956	4160.13	1642.4323	591.4561
0.49679	5183.58	998.1724	743.6005	1.27841	4145.65	1655.8818	586.5935
0.50411	5169.26	1009.0767	747.3366	1.30925	4131.16	1669.8073	581.7728
0.51020	5154.94	1018.0571	749.0514	1.34205	4116.67	1684.1463	576.9022
0.51627	5140.61	1026.9312	750.5713	1.34308	4116.67	1684.5864	577.3423
0.52233	5126.27	1035.6995	751.8965	1.37375	4102.18	1697.5490	570.6199
0.52838	5111.94	1044.3623	753.0282	1.39420	4116.67	1706.1908	599.3170
0.53321	5097.60	1051.2084	752.2632	1.40851	4102.18	1712.2400	585.0590
0.53442	5097.60	1052.9094	753.9643	1.42483	4087.69	1718.8985	571.1860
0.53562	5097.60	1054.6105	755.6653	1.46144	4073.19	1733.3095	564.6811

13. Fracture half length can be estimated from the before-closure storage coefficient with $\phi = 0.10$ as

$$L_f = \sqrt{\frac{0.8936C_{bc}}{\phi c_{ti} h C_{bcD}}} = \sqrt{\frac{0.8936(0.024694)}{(0.10)(0.00009402)(6)(3)}} = 11.4 \text{ ft}$$

Recall from before-closure analysis that the created fracture half-length estimates varied from 61 feet for a radial fracture to 180 feet for a confined-height fracture, which suggests either (1) the type-curve match is incorrect, (2) the before-closure estimates of fracture half-length are incorrect or (3) fracture half length decreases during closure. The before-closure estimate of fracture half length assumes no spurt loss, and with the permeability of the formation, it seems unlikely spurt loss is negligible. Consequently, it's likely that the before-closure fracture half length estimate is incorrect. However, a better type-curve match might have been obtained with additional shut-in data. The observed data plotted in Fig. 5.11 "match" many variable-storage type-curve combinations, but additional pseudoradial flow data would improve the match by limiting the number of possibilities.

From the type curve match, the dimensionless after-closure storage coefficient can be written as

$$C_{aacD} = \frac{2}{3}C_{abcD} \rightarrow C_{aac} = \frac{2}{3}C_{abc},$$

which is reasonable considering the tubular volume is 87.8 bbl and the injected volume was 67.9 bbl. In other words, the fracture storage is of the same magnitude as wellbore storage and a closing fracture will create a measureable change in the dimensionless storage coefficient.

14. Recall that transmissibility is estimated from an after-closure type-curve match point as

$$\frac{kh}{\mu_i} = (141.2)(24)(p_{a0} - p_{ai}) \left[\frac{P_{awsD}^{(0)} C_{abc}}{-P_{awsD}((t_c)_{aLFD})(C_{abc} - C_{aac})} \right] \frac{T_i}{T_w} \left[\frac{P_{acD}(t_{aLFD})}{\int_0^{\Delta t_a} (p_{aw}(t) - p_{ai}) dt_a} \right]_{MP} \dots (5.164)$$

The dimensionless wellbore adjusted pseudopressure observed at hydraulic fracture closure is calculated as

$$P_{awsD}((t_c)_{aLFD}) = \frac{p_{aw} - p_{ai}}{p_{a0} - p_{ai}} = \frac{4939.69 - 3686.9}{6135.37 - 3686.9} = 0.5117,$$

and the transmissibility is calculated from the after-closure type-curve match as

$$\begin{aligned} \frac{kh}{\mu_i} &= (141.2)(24)(p_{a0} - p_{ai}) C_{abc} \left(1 - \frac{P_{awsD}((t_c)_{aLFD})}{3} \right) \left[\frac{P_{acD}(t_{aLFD})}{\int_0^{\Delta t_a} (p_{aw}(t) - p_{ai}) dt_a} \right]_{MP} \\ &= (141.2)(24)(6135.37 - 3686.7)(0.024694) \left(1 - \frac{0.5117}{3} \right) \left[\frac{1.757406}{1383.963} \right]_{MP} \\ &= 215.8 \frac{\text{md} \cdot \text{ft}}{\text{cp}} \end{aligned}$$

The permeability-thickness from the after-closure type-curve match is $kh = 6.05$ md-ft, which compares with 7.17 md-ft from the pseudoradial flow after-closure analysis. A subsequent post-frac pressure buildup

test was also completed in the formation with a nonunique interpretation concluding the initial reservoir pressure was $p_i = 5,265$ psia and the permeability-thickness product was $kh = 6.77$ md·ft. Thus the results from type-curve analysis, after-closure pseudoradial flow analysis, and the post-frac pressure buildup are all in general agreement.

5.3.2 Pseudolinear Flow Observed After Closure. The shut-in period of a fracture-injection/falloff sequence in a low permeability reservoir is often insufficient to observe pseudoradial flow, and most interpretations must rely on before-closure pressure transient analysis or after-closure pseudolinear flow analysis when it is observed.⁵⁴ The GM 543-33 is a well producing from 20 low permeability Mesaverde sands. Prior to hydraulic fracturing the sandstone reservoir perforated at 4,954 feet, an isolated-layer fracture-injection/falloff sequence was completed. A total of 17.69 bbls of 1% KCl treated water was pumped at an average rate of 3.30 bbl/min during a 5.30 minute fracture injection. At the end of the fracture-injection, a bottomhole plug was seated, and the pressure falloff was recorded for 16.10 hours. **Table 5-6** contains the time, pressure, and rate data recorded during the fracture injection, and **Table 5-7** contains the time and pressure recorded during the pressure falloff.

After the falloff period, the plug was removed, and the layer was produced for 168 hours prior to seating the plug and beginning a 15 day pressure buildup. With both a fracture-injection/falloff and drawdown/buildup sequences completed sequentially, a direct comparison of the buildup and falloff interpretations is possible.

The porosity of the Mesaverde formation is 10%, the gas saturation is 50%, and the gross and net thicknesses are 14 feet and 12 feet, respectively, where net thickness is defined as porosity greater than 6%. Gas gravity is 0.63, and the bottomhole temperature is 160°F. Before-closure analysis assumes a Young's modulus of 5,000,000 psi and a Poisson's ration of 0.20, which results in a plane-strain modulus of 5,208,333.3 psi. The Mesaverde formation is separated from adjacent sandstone reservoirs by impermeable and high stress shale and mudstone formations.

Table 5-6—GM 543-33 fracture-injection time, bottomhole pressure, and injection rate.

<i>t</i> , s	<i>p_w</i> , psi	<i>q_i</i> , bbl/min	<i>t</i> , s	<i>p_w</i> , psi	<i>q_i</i> , bbl/min	<i>t</i> , s	<i>p_w</i> , psi	<i>q_i</i> , bbl/min	<i>t</i> , s	<i>p_w</i> , psi	<i>q_i</i> , bbl/min	<i>t</i> , s	<i>p_w</i> , psi	<i>q_i</i> , bbl/min
0	1808.60	3.17				127	3672.87	3.10				254	3513.45	3.10
1	1827.54	3.17	64	3656.96	3.09	128	3675.05	3.10	191	3919.13	4.50	255	3518.10	3.09
2	1846.67	3.17	65	3663.33	3.09	129	3689.54	3.10	192	3911.73	4.50	256	3525.30	3.09
3	1866.34	3.17	66	3665.12	3.09	130	3696.94	3.10	193	3910.42	4.50	257	3526.18	3.09
4	1887.04	3.17	67	3669.00	3.09	131	3661.73	3.10	194	3914.85	4.50	258	3526.45	3.09
5	1907.99	3.17	68	3674.00	3.09	132	3624.31	3.10	195	3907.45	4.49	259	3534.10	3.09
6	1929.38	3.17	69	3678.84	3.09	133	3599.31	3.10	196	3916.91	4.49	260	3531.31	3.09
7	1951.74	3.17	70	3685.89	3.09	134	3576.70	3.10	197	3909.34	4.49	261	3520.45	3.09
8	1974.34	3.17	71	3691.09	3.09	135	3566.36	3.10	198	3910.74	4.49	262	3532.21	3.09
9	1997.26	3.17	72	3698.48	3.09	136	3544.72	3.10	199	3909.97	4.49	263	3523.55	3.09
10	2021.12	3.16	73	3700.23	3.09	137	3546.16	3.10	200	3907.54	4.49	264	3527.47	3.09
11	2045.71	3.16	74	3705.37	3.09	138	3559.77	3.10	201	3919.06	4.49	265	3520.63	3.09
12	2070.20	3.16	75	3707.30	3.09	139	3565.21	3.10	202	3913.36	4.49	266	3522.72	3.09
13	2096.91	3.16	76	3708.65	3.09	140	3576.05	3.10	203	3913.76	4.49	267	3530.56	3.09
14	2123.28	3.16	77	3710.46	3.09	141	3592.27	3.10	204	3912.08	4.49	268	3534.07	3.09
15	2150.83	3.16	78	3704.93	3.09	142	3581.60	3.10	205	3903.85	4.49	269	3521.92	3.09
16	2179.71	3.16	79	3681.73	3.09	143	3602.08	3.10	206	3920.60	4.49	270	3535.23	3.09
17	2208.64	3.16	80	3633.14	3.09	144	3595.58	3.10	207	3914.60	4.50	271	3529.66	3.09
18	2238.54	3.15	81	3569.66	3.09	145	3592.15	3.10	208	3912.96	4.49	272	3531.47	3.09
19	2269.82	3.15	82	3521.56	3.09	146	3592.72	3.10	209	3911.79	4.50	273	3528.96	3.09
20	2301.28	3.15	83	3485.97	3.10	147	3586.38	3.10	210	3905.70	4.50	274	3528.07	3.09
21	2334.11	3.15	84	3456.68	3.10	148	3588.87	3.10	211	3922.70	4.50	275	3523.20	3.09
22	2368.44	3.15	85	3432.63	3.10	149	3595.71	3.10	212	3916.79	4.49	276	3519.49	3.09
23	2404.23	3.14	86	3413.65	3.10	150	3602.03	3.10	213	3915.12	4.50	277	3528.54	3.09
24	2441.06	3.15	87	3396.13	3.10	151	3588.55	3.10	214	3917.10	4.50	278	3526.11	3.08
25	2478.64	3.15	88	3380.58	3.10	152	3604.51	3.10	215	3908.02	4.50	279	3530.59	3.07
26	2519.03	3.14	89	3368.48	3.11	153	3601.07	3.10	216	3923.78	4.50	280	3522.83	3.06
27	2558.40	3.14	90	3357.52	3.11	154	3602.40	3.17	217	3918.42	4.50	281	3519.56	3.05
28	2599.40	3.14	91	3346.23	3.11	155	3597.20	3.31	218	3914.13	4.50	282	3518.14	3.02
29	2643.53	3.14	92	3336.37	3.11	156	3597.63	3.45	219	3915.92	4.50	283	3509.06	2.99
30	2687.07	3.14	93	3329.36	3.11	157	3800.62	3.59	220	3901.36	4.50	284	3496.03	2.96
31	2733.67	3.14	94	3321.78	3.11	158	3863.26	3.73	221	3914.87	4.49	285	3485.85	2.92
32	2785.49	3.13	95	3311.74	3.11	159	3897.01	3.87	222	3908.74	4.50	286	3479.63	2.87
33	2835.77	3.13	96	3306.68	3.11	160	3908.88	4.01	223	3902.82	4.49	287	3465.81	2.81
34	2885.17	3.13	97	3302.11	3.11	161	3927.83	4.15	224	3903.72	4.49	288	3446.68	2.74
35	2943.31	3.13	98	3293.85	3.11	162	3932.71	4.29	225	3894.30	4.49	289	3414.93	2.66
36	2998.80	3.13	99	3284.51	3.11	163	3937.08	4.43	226	3904.34	4.49	290	3397.62	2.58
37	3055.56	3.12	100	3284.20	3.11	164	3935.31	4.50	227	3898.28	4.49	291	3370.21	2.48
38	3113.04	3.12	101	3278.58	3.11	165	3928.13	4.50	228	3893.50	4.49	292	3372.54	2.37
39	3152.43	3.12	102	3268.82	3.11	166	3932.35	4.50	229	3899.20	4.49	293	3353.54	2.27
40	3248.57	3.12	103	3268.54	3.11	167	3925.58	4.49	230	3889.46	4.49	294	3306.88	2.19
41	3318.83	3.11	104	3265.65	3.11	168	3928.29	4.50	231	3900.10	4.49	295	3299.01	2.12
42	3372.58	3.11	105	3258.07	3.11	169	3927.70	4.50	232	3893.05	4.49	296	3311.82	2.06
43	3436.21	3.11	106	3255.33	3.11	170	3921.19	4.50	233	3890.50	4.49	297	3322.79	2.01
44	3482.22	3.11	107	3258.84	3.12	171	3926.76	4.50	234	3898.11	4.49	298	3329.09	1.98
45	3507.17	3.10	108	3262.80	3.11	172	3923.44	4.50	235	3885.90	4.49	299	3332.32	1.95
46	3520.89	3.10	109	3284.60	3.11	173	3930.33	4.49	236	3894.74	4.49	300	3324.64	1.93
47	3531.07	3.10	110	3314.79	3.11	174	3930.00	4.49	237	3889.33	4.44	301	3312.85	1.94
48	3539.44	3.10	111	3334.94	3.11	175	3925.43	4.49	238	3880.79	4.30	302	3315.07	1.96
49	3546.97	3.10	112	3347.70	3.11	176	3926.93	4.49	239	3894.42	4.16	303	3312.69	1.98
50	3556.64	3.10	113	3412.31	3.11	177	3920.71	4.49	240	3680.62	4.02	304	3305.18	1.99
51	3564.52	3.10	114	3502.43	3.11	178	3925.18	4.49	241	3608.07	3.88	305	3313.14	1.99
52	3570.44	3.10	115	3550.31	3.11	179	3926.64	4.49	242	3571.49	3.74	306	3209.97	1.98
53	3578.42	3.10	116	3605.56	3.11	180	3919.12	4.49	243	3549.66	3.60	307	3158.20	1.96
54	3591.63	3.10	117	3610.88	3.10	181	3923.64	4.49	244	3540.96	3.46	308	3151.38	1.80
55	3604.07	3.10	118	3636.67	3.10	182	3916.15	4.49	245	3546.53	3.32	309	3146.82	1.60
56	3612.86	3.09	119	3649.53	3.10	183	3918.15	4.49	246	3525.54	3.18	310	3143.15	1.40
57	3621.89	3.09	120	3647.31	3.10	184	3924.11	4.49	247	3537.59	3.09	311	3139.89	1.20
58	3630.28	3.09	121	3648.77	3.10	185	3914.19	4.49	248	3533.63	3.09	312	3137.01	1.00
59	3635.23	3.09	122	3660.82	3.10	186	3919.90	4.50	249	3530.60	3.09	313	3134.23	0.80
60	3640.80	3.09	123	3651.79	3.10	187	3911.97	4.50	250	3527.56	3.09	314	3131.80	0.60
61	3647.62	3.09	124	3666.57	3.10	188	3916.05	4.50	251	3528.90	3.09	315	3129.47	0.40
62	3650.58	3.09	125	3646.61	3.10	189	3923.56	4.49	252	3521.62	3.09	316	3127.25	0.22
63	3654.16	3.09	126	3659.89	3.10	190	3910.34	4.49	253	3527.79	3.09	317	3125.04	0.04

Table 5-7—GM 543-33 time and bottomhole pressure recorded during the pressure falloff.

t, s	p _w , psi	t, s	p _w , psi	t, s	p _w , psi	t, s	p _w , psi	t, s	p _w , psi	t, s	p _w , psi	t, s	p _w , psi	t, s	p _w , psi
318	3123.09	1323	2849.67	2328	2767.22	3333	2715.22	4758	2667.20	6768	2622.85	10038	2574.89	18918	2509.64
333	3098.72	1338	2848.07	2343	2766.22	3348	2714.48	4788	2666.40	6798	2622.09	10098	2574.11	19518	2506.93
348	3080.28	1353	2846.55	2358	2765.21	3363	2713.85	4818	2665.50	6828	2621.61	10158	2573.42	20118	2504.25
363	3065.26	1368	2844.90	2373	2764.35	3378	2713.33	4848	2664.81	6858	2621.03	10218	2572.85	20718	2501.64
378	3052.42	1383	2843.36	2388	2763.40	3393	2712.69	4878	2663.97	6888	2620.53	10278	2572.07	21318	2499.29
393	3040.86	1398	2841.89	2403	2762.53	3408	2711.96	4908	2663.20	6918	2619.88	10338	2571.33	21918	2496.92
408	3030.73	1413	2840.39	2418	2761.54	3423	2711.40	4938	2662.32	6948	2619.56	10398	2570.70	22518	2494.66
423	3021.44	1428	2839.02	2433	2760.60	3438	2710.89	4968	2661.54	6978	2619.03	10458	2569.99	23118	2492.54
438	3012.94	1443	2837.40	2448	2759.80	3453	2710.18	4998	2660.80	7008	2618.36	10518	2569.43	23718	2489.98
453	3005.09	1458	2836.07	2463	2758.74	3468	2709.55	5028	2660.13	7038	2617.91	10578	2568.69	24318	2488.24
468	2997.89	1473	2834.49	2478	2758.03	3483	2709.02	5058	2659.28	7068	2617.45	10638	2567.96	24918	2487.05
483	2991.38	1488	2833.11	2493	2757.08	3498	2708.40	5088	2658.58	7098	2616.88	10698	2567.50	25518	2485.46
498	2985.36	1503	2831.66	2508	2756.22	3513	2707.76	5118	2657.66	7128	2616.41	10758	2566.72	26118	2484.00
513	2979.83	1518	2830.30	2523	2755.21	3528	2707.13	5148	2656.94	7158	2615.88	10818	2566.08	26718	2483.16
528	2974.66	1533	2828.87	2538	2754.39	3543	2706.71	5178	2656.28	7188	2615.35	10878	2565.44	27318	2481.56
543	2969.80	1548	2827.60	2553	2753.57	3558	2706.04	5208	2655.63	7218	2614.90	10938	2564.79	27918	2479.80
558	2965.31	1563	2826.21	2568	2752.65	3573	2705.39	5238	2654.80	7248	2614.27	10998	2564.28	28518	2478.45
573	2961.19	1578	2824.76	2583	2751.79	3588	2705.02	5268	2654.07	7278	2613.73	11058	2563.69	29118	2477.21
588	2957.39	1593	2823.41	2598	2750.88	3603	2704.40	5298	2653.41	7308	2613.24	11118	2563.00	29718	2476.04
603	2953.69	1608	2822.17	2613	2750.16	3618	2703.71	5328	2652.62	7338	2612.68	11178	2562.41	30318	2474.69
618	2950.18	1623	2820.88	2628	2749.18	3633	2703.08	5358	2651.92	7368	2612.18	11238	2561.83	30918	2473.33
633	2946.91	1638	2819.58	2643	2748.39	3648	2702.51	5388	2651.28	7398	2611.68	11298	2561.31	31518	2471.82
648	2943.63	1653	2818.22	2658	2747.55	3663	2702.16	5418	2650.34	7428	2611.20	11358	2560.67	32118	2470.38
663	2940.51	1668	2816.82	2673	2746.76	3678	2701.42	5448	2649.75	7458	2610.74	11418	2560.15	32718	2469.03
678	2937.56	1683	2815.62	2688	2746.04	3693	2700.93	5478	2649.06	7488	2610.19	11478	2559.60	33318	2468.32
693	2934.61	1698	2814.37	2703	2745.23	3708	2700.27	5508	2648.41	7518	2609.69	11538	2559.01	33918	2467.72
708	2931.86	1713	2813.12	2718	2744.39	3723	2699.77	5538	2647.71	7548	2609.70	11598	2558.53	34518	2467.03
723	2929.15	1728	2811.77	2733	2743.61	3738	2699.14	5568	2647.05	7578	2609.72	11658	2558.33	35118	2466.31
738	2926.45	1743	2810.58	2748	2742.73	3753	2698.66	5598	2646.32	7608	2609.69	11718	2557.41	35718	2465.62
753	2923.97	1758	2809.31	2763	2742.10	3768	2698.17	5628	2645.67	7758	2609.78	11778	2556.83	36318	2464.97
768	2921.17	1773	2808.06	2778	2741.29	3783	2697.55	5658	2644.91	7818	2609.84	11838	2556.29	36918	2464.20
783	2918.83	1788	2806.77	2793	2740.39	3798	2697.15	5688	2644.32	7878	2609.98	11898	2555.72	37518	2463.56
798	2916.29	1803	2805.53	2808	2739.68	3813	2696.50	5718	2643.61	7938	2609.00	11958	2555.18	38118	2462.82
813	2913.98	1818	2804.31	2823	2738.82	3828	2696.05	5748	2642.92	7998	2609.98	12018	2554.61	38718	2462.19
828	2911.65	1833	2803.19	2838	2738.14	3843	2695.40	5778	2642.28	8058	2609.27	12078	2554.02	39318	2461.53
843	2909.41	1848	2801.85	2853	2737.40	3858	2694.80	5808	2641.65	8118	2609.23	12138	2553.56	39918	2461.00
858	2907.03	1863	2800.62	2868	2736.54	3873	2694.33	5838	2641.04	8178	2599.38	12198	2553.06	40518	2460.32
873	2904.76	1878	2799.50	2883	2735.93	3888	2693.78	5868	2640.33	8238	2599.49	12258	2552.54	41118	2459.54
888	2902.63	1893	2798.24	2898	2735.09	3903	2693.32	5898	2639.66	8298	2599.66	12318	2551.97	41718	2459.05
903	2900.59	1908	2796.94	2913	2734.34	3918	2692.79	5928	2639.00	8358	2599.77	12378	2551.38	42318	2458.43
918	2898.42	1923	2795.83	2928	2733.61	3948	2691.72	5958	2638.44	8418	2599.86	12438	2550.79	42918	2457.62
933	2896.35	1938	2794.63	2943	2732.87	3978	2690.72	5988	2637.73	8478	2599.21	12498	2550.27	43518	2456.92
948	2894.24	1953	2793.45	2958	2732.25	4008	2689.64	6018	2637.20	8538	2599.26	12558	2549.72	44118	2456.51
963	2892.34	1968	2792.27	2973	2731.43	4038	2688.81	6048	2636.48	8598	2599.33	12618	2549.35	44718	2455.96
978	2890.50	1983	2791.13	2988	2730.71	4068	2687.75	6078	2635.89	8658	2599.43	12678	2548.77	45318	2455.31
993	2888.39	1998	2790.01	3003	2729.99	4098	2686.64	6108	2635.22	8718	2599.67	12738	2548.17	45918	2454.57
1008	2886.43	2013	2788.82	3018	2729.22	4128	2685.73	6138	2634.66	8778	2599.95	12798	2547.75	46518	2454.15
1023	2884.50	2028	2787.74	3033	2728.54	4158	2684.89	6168	2634.14	8838	2599.02	12858	2547.24	47118	2453.50
1038	2882.64	2043	2786.63	3048	2727.89	4188	2683.95	6198	2633.51	8898	2599.35	12918	2546.72	47718	2452.99
1053	2880.74	2058	2785.55	3063	2727.12	4218	2682.86	6228	2632.84	8958	2599.38	13218	2544.31	48318	2452.49
1068	2878.77	2073	2784.49	3078	2726.51	4248	2682.02	6258	2632.20	9018	2587.56	13518	2542.02	48918	2451.84
1083	2877.09	2088	2783.26	3093	2725.64	4278	2681.06	6288	2631.75	9078	2587.77	13818	2539.76	49518	2451.42
1098	2875.16	2103	2782.21	3108	2724.97	4308	2680.19	6318	2631.20	9138	2586.83	14118	2537.47	50118	2450.92
1113	2873.43	2118	2781.16	3123	2724.35	4338	2679.33	6348	2630.54	9198	2586.17	14418	2535.33	50718	2450.41
1128	2871.64	2133	2780.04	3138	2723.65	4368	2678.36	6378	2630.03	9258	2584.52	14718	2533.29	51318	2449.81
1143	2869.80	2148	2779.14	3153	2722.94	4398	2677.36	6408	2629.35	9318	2583.56	15018	2531.25	51918	2449.39
1158	2868.05	2163	2778.07	3168	2722.19	4428	2676.55	6438	2628.79	9378	2582.66	15318	2529.39	52518	2448.96
1173	2866.27	2178	2777.08	3183	2721.71	4458	2675.70	6468	2628.28	9438	2582.09	15618	2527.33	53118	2448.40
1188	2864.61	2193	2775.93	3198	2721.02	4488	2674.81	6498	2627.71	9498	2581.27	15918	2525.58	53718	2448.04
1203	2862.76	2208	2775.07	3213	2720.34	4518	2674.02	6528	2627.08	9558	2580.49	16218	2523.82	54318	2447.42
1218	2861.14	2223	2773.97	3228	2719.56	4548	2673.12	6558	2626.55	9618	2579.69	16518	2522.09	54918	2447.04
1233	2859.40	2238	2773.02	3243	2718.96	4578	2672.14	6588	2626.01	9678	2579.03	16818	2520.34	55518	2446.54
1248	2857.76	2253	2772.01	3258	2718.32	4608	2671.41	6618	2625.47	9738	2578.36	17118	2518.61	56118	2446.05
1263	2856.05	2268	2771.08	3273	2717.76	4638	2670.54	6648	2624.86	9798	2577.62	17418	2516.98	56718	2445.72
1278	2854.45	2283	2770.04	3288	2717.09	4668	2669.70	6678	2624.34	9858	2576.82	17718	2515.59	57318	2445.39
1293	2852.79	2298	2769.14	3303	2716.44	4698	2668.78	6708	2623.75	9918	2576.17	18018	2514.07	57918	2444.79
1308	2851.25	2313	2768.07	3318	2715.71	4728	2668.05	6738	2623.19	9978	2575.52	18318	2512.62	58518	2444.34

The entire fracture-injection/falloff sequence is shown in **Fig. 5.12**, which contains a graph of bottomhole pressure and injection rate versus time. Note that relative to the shut-in period, the fracture-injection is very short and might reasonably be considered as occurring instantaneously.

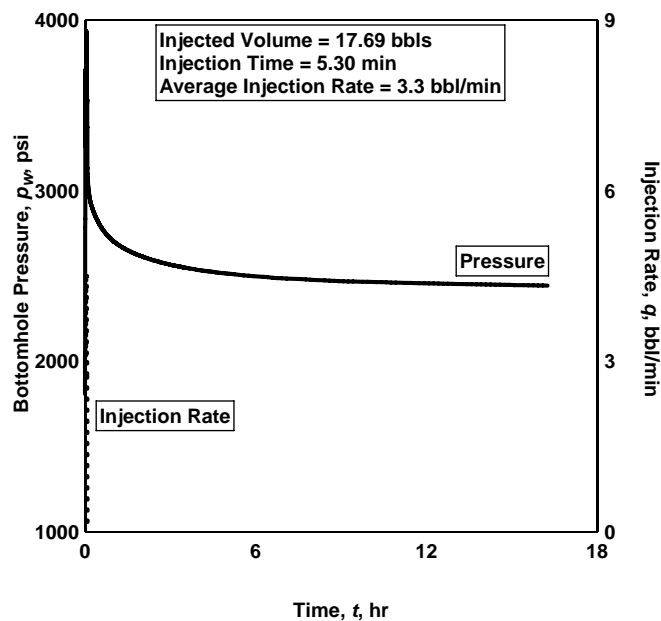


Fig. 5.12—GM 543-33 Mesaverde formation fracture-injection/falloff sequence.

1. Calculate the function $G(g(\Delta t, \alpha_N))$ for each time and pressure recorded during the falloff period and prepare a Cartesian graph of bottomhole pressure, p_w , the derivative of pressure, dp_w/dG , and the "superposition" derivative, Gdp_w/dG versus the function $G(g(\Delta t, \alpha_N))$.

Identify the leakoff type⁷⁴ and hydraulic fracture closure using the G -function plot. Fig. 5.13 contains the G -function plot for the fracture-injection/falloff sequence. The leakoff type is pressure-dependent leakoff, which is indicated by the characteristic hump in the superposition derivative above a straight line drawn from the origin through the "normal" leakoff data. Fracture closure is observed at $G_c = 4.42$, and the closure stress is 2,790 psi.

2. Initial reservoir pressure can be estimated from the closure stress and the uniaxial strain relationship. Assuming an overburden stress, $\sigma_z = 4,954$ psi (1 psi/ft overburden gradient), the initial reservoir pressure estimate is $p_i = 2,069$ psi. The estimated initial reservoir pressure from closure stress should be considered as a guide only—the pressure may or may not be accurate depending on additional factors, including tectonic stress.

Before-closure analysis⁵⁹ requires an estimate of fracture half-length and lost fracture width, w_L , because of fluid leakoff. Fracture half-length and lost width are estimated from a graph of bottomhole pressure versus the loss-volume function, $g(\Delta t, \alpha_N)$, which is shown in Fig. 5.14 assuming the fracture grows under

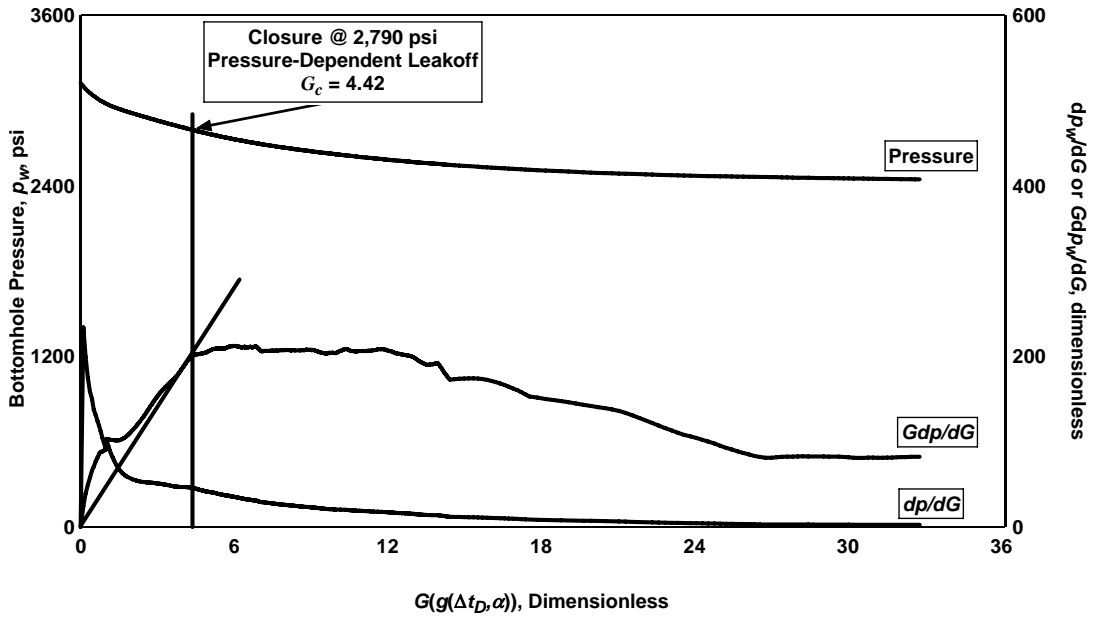


Fig. 5.13—GM 543-33 Mesaverde formation fracture-injection/falloff sequence G -function derivative analysis.

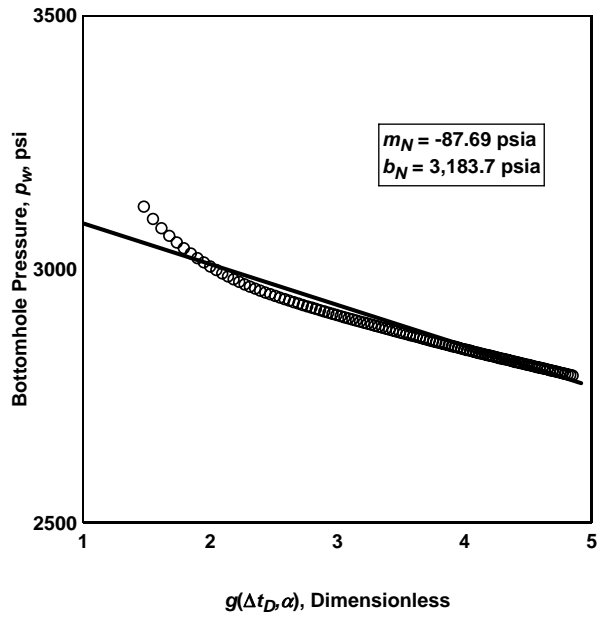


Fig. 5.14—GM 543-33 Mesaverde formation fracture-injection/falloff sequence before-closure pressure versus the dimensionless loss-volume function.

horizontal plane strain conditions (GDK). The slope of the line through the before-closure data is $(m_N)_{GDK} = -87.69$ psia and the intercept is $(b_N)_{GDK} = 3183.69$ psia. Fracture half-length is calculated from the intercept as

$$(L_f)_{GDK} = \sqrt{\frac{(5.615)(5,208,333.3)(17.69/2)}{\pi(14)(3183.69 - 2790)}} = 122.2 \text{ ft},$$

and lost width is calculated from the slope as

$$(w_L)_{GDK} = \frac{1.478(12)\pi(122.2)}{5,208,333.3}(87.69) = 0.11 \text{ in}.$$

Fracture stiffness assuming horizontal plane strain conditions is calculated as

$$(S_f)_{GDK} = \frac{5,208,333.3}{\pi(122.2)} = 13,566.8 \frac{\text{psi}}{\text{ft}}.$$

Microseismic imaging of fracture growth in Piceance basin Mesaverde formation suggests a fracture created during an injection with water is "contained" by the bounding shale and mudstone formations.¹¹¹⁻¹¹² Consequently, radial fracture growth is not anticipated, but the radial fracture calculations are included for completeness. For a radial fracture geometry, $(m_N)_{RAD} = -86.855$ psi and the intercept is $(b_N)_{RAD} = 3177.3$ psi. Fracture radius is calculated as

$$R_f = \sqrt[3]{\frac{3(5.615)(5,208,333.3)(17.69/2)}{8(3,177.3 - 2,790)}} = 63.0 \text{ ft},$$

and the lost width is calculated as

$$(w_L)_{RAD} = \frac{7.343(12)(63.0)}{\pi(5208333.3)}(86.855) = 0.03 \text{ in}.$$

Fracture stiffness assuming radial fracture geometry is calculated as

$$(S_f)_{GDK} = \frac{3\pi(5,208,333.3)}{16(63.0)} = 48,697.8 \frac{\text{psi}}{\text{ft}}.$$

3. Calculate adjusted pseudotime, adjusted pseudopressure, gas formation volume factor, and total compressibility for each recorded time and pressure after the end of the injection. For before-closure pressure-transient analysis, scale time to zero at the beginning of the shut-in period for calculating adjusted pseudotime. An estimate of reservoir pressure is needed for a first iteration. The reservoir pressure estimated from the observed closure stress, 2,069 psi, could be used, or an estimate of reservoir pressure from other data. For the GM 543-33, assume the reservoir pressure is 2,332 psi.

4. Note the following variables required for the analysis.

$$p_{ai} = 1,300.69 \text{ psia}$$

$$p_{a0} = 2,154.88 \text{ psia}$$

$$B_{gi} = 1.16107 \text{ bbl/Mscf}$$

$$B_{ge} = 0.87974 \text{ bbl/Mscf}$$

$$\mu_{gi} = 0.0177 \text{ cp}$$

$$c_{ti} = 2.26(10)^{-4} \text{ psi}^{-1}$$

5. Calculate and graph $(y_{ap})_n$ versus $(x_{ap})_n$ for each recorded time and pressure before fracture closure, which is shown in **Fig. 5.15**. Under normal leakoff conditions, the data on the specialized graph will fall along a straight line, but nonideal leakoff, like pressure-dependent leakoff causes the data to fan across the page.⁸² Drawing a line from the origin through the last few data points recorded before closure results in $(m_M)_{\text{GDK}} = 0.0337$. The created fracture height is assumed to extend across the total thickness of the Mesaverde formation, but the net or permeable fracture height is less than the total height. The ratio of permeable to total fracture height is $r_p = 12/14 = 0.86$, and the permeability is estimated as

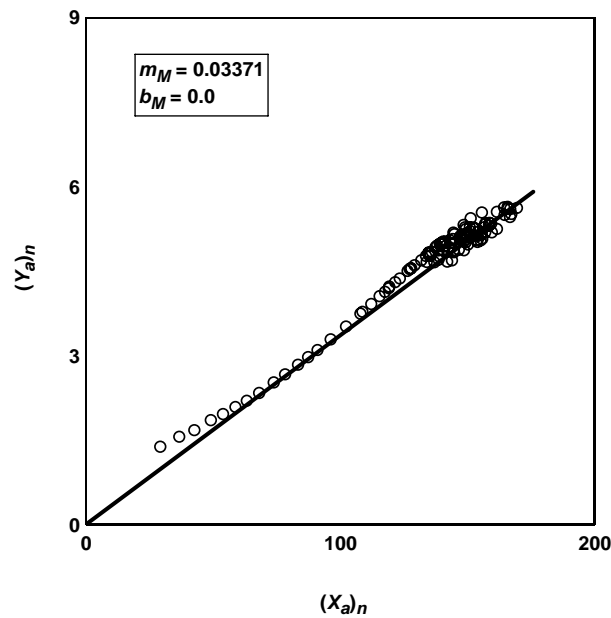


Fig. 5.15—GM 543-33 Mesaverde formation fracture-injection/falloff sequence before-closure pressure-transient analysis.

$$(k)_{\text{GDK}} = \left[\frac{2(141.2)(0.02878)(24)}{5.615} \frac{1}{(1)(0.87)(13566.8)(0.0337)} \right]^2 = 0.008 \text{ md}.$$

There is no fracture face resistance since the straight line is drawn from the origin.

With radial fracture geometry, the specialized graph results in $(b_M)_{\text{RAD}} = 0$ and $(m_M)_{\text{RAD}} = 0.03273$. The ratio of permeable to total fracture height for a radial fracture is calculated as⁵⁹

$$(r_p)_{\text{RAD}} = \frac{2}{\pi} \left[\frac{12}{2(63.0)} \sqrt{1 - \left(\frac{12}{2(63.0)} \right)^2} + \sin^{-1} \frac{12}{2(63.0)} \right] = 0.121.$$

The permeability assuming radial fracture geometry is estimated as

$$(k)_{\text{RAD}} = \left[\frac{2(141.2)(0.02878)(24)}{5.615} \frac{1}{(1)(0.121)(48697.8)(0.03273)} \right]^2 = 0.032 \text{ md}.$$

There is a factor of 4 difference in the estimated permeability that results by assuming an unconfined radial fracture versus a confined fracture. However, as noted above, water injections in Mesaverde formations are typically confined, and the lower permeability estimate is more realistic. However, without fracture imaging the true fracture geometry is unknown and before-closure pressure-transient analysis can only bracket the estimated permeability, that is, $0.008 \text{ md} \leq k \leq 0.032 \text{ md}$.

6. After-closure analysis requires a log-log graph of the adjusted pseudopressure difference, $p_{aw} - p_{ai}$, and well testing pressure derivative versus the reciprocal elapsed adjusted pseudotime, which is shown in **Fig. 5.16**. The elapsed time and corresponding adjusted pseudotime used in after-closure analysis is calculated relative to the time since the beginning of the injection.

The derivative curve is not a function of initial reservoir pressure and should be used to identify the flow regime(s). In Fig. 5.16, a portion of the derivative data fall along a $\frac{1}{2}$ -slope line, which indicates pseudolinear flow was observed. Additionally, the adjusted pseudopressure difference data are offset by a factor of 2 and also fall along a $\frac{1}{2}$ -slope line, which seems to confirm pseudolinear flow is observed for a portion of the data and suggests that the estimated initial reservoir pressure is correct. In most cases, the determination of initial reservoir pressure is an iterative process, and the adjusted pseudopressure difference will not follow a $\frac{1}{2}$ -slope line with a factor of 2 offset until the initial reservoir pressure is correct. Note that as the shut-in progresses, the late-time data diverge from the $\frac{1}{2}$ -slope line.

7. Since pseudolinear flow was indicated in Fig. 5.16, a Cartesian graph of adjusted pseudopressure versus the square root of reciprocal elapsed adjusted pseudotime is prepared, which is shown in **Fig. 5.17**. A straight line is drawn through the data corresponding to pseudolinear flow, and the initial adjusted pseudopressure corresponds to the intercept of the straight line, $b_{acpl} = p_{ai} = 1,300$ psia, which corresponds to an initial reservoir pressure of $p_i = 2,332$ psia.

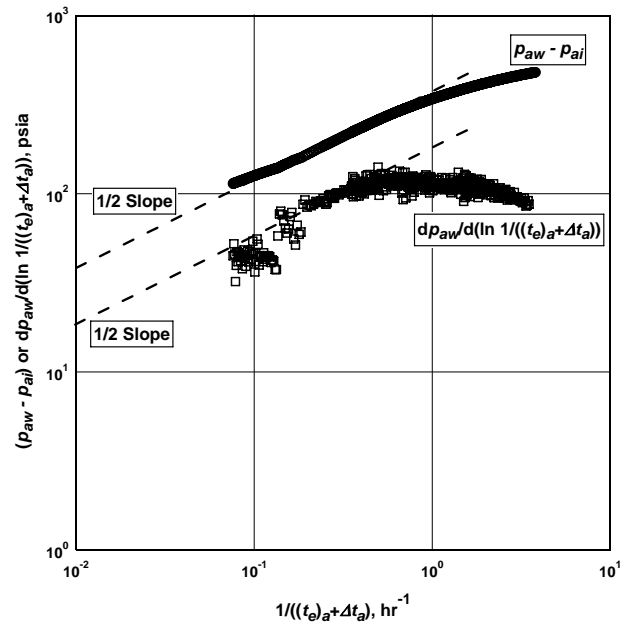


Fig. 5.16—GM 543-33 Mesaverde formation fracture-injection/falloff sequence after-closure analysis diagnostic graph.

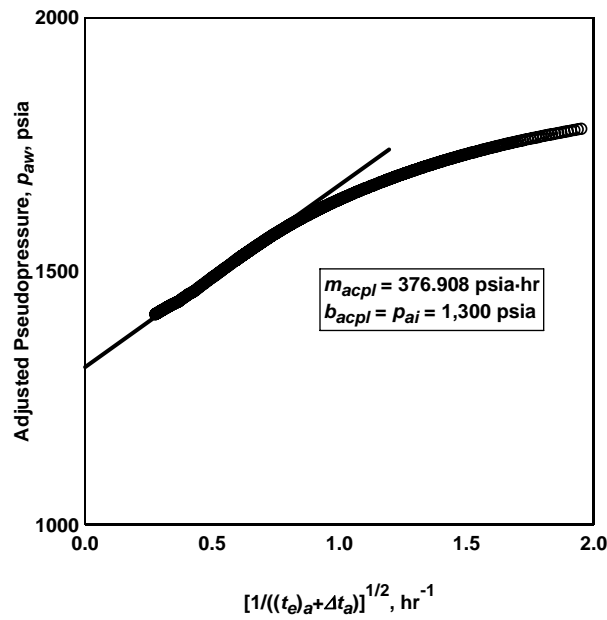


Fig. 5.17—GM 543-33 Mesaverde formation fracture-injection/falloff sequence after-closure pseudolinear flow graph.

The permeability cannot be calculated from the slope of the straight line, $m_{acpl} = 376.908$ psia-hr on the pseudolinear flow graph unless fracture half-length is known. Assuming the fracture half-length from before-closure analysis with a confined height fracture and horizontal plane strain, $L_f = 122$ feet, and assuming $p_{awsD}(0) = 0$, the permeability is calculated as

$$k = \left[\frac{141.2(24)\sqrt{\pi}\sqrt{0.0002637}}{2} \frac{1}{12(122)(376.908)} \left(\frac{0.0177}{0.10(2.256)(10)^{-4}} \right)^{1/2} (17.69) \right]^2 = 0.002 \text{ md} .$$

which corresponds to a permeability-thickness product of $kh = 0.024$ md·ft.

The difference between the permeability calculated from before-closure pressure-transient analysis and after-closure pseudolinear flow analysis is factor of 4. A complete and satisfactory analysis of the data requires that before-closure analysis, after-closure analysis, and type-curve analysis are consistent and provide comparable permeability estimates.

8. Prepare a log-log graph of $I(\Delta p_a)$ versus $(t_e)_a + \Delta t_a$ and $\Delta p'_a$ versus $(t_e)_a + \Delta t_a$ and overlay the appropriate constant-rate, drawdown type curve for the reservoir/system. **Fig 5.18** shows a type-curve match obtained with the observed data and a type curve for production through and finite-conductivity fracture in an infinite slab reservoir.

Note that the type curve match indicates minimal storage change during fracture closure, and the before- and after-closure storage can be considered equivalent, $C_{abcd} = C_{aacD}$. A match point is as follows.

$$\begin{aligned} t_a L_f D &= 0.002091 \rightarrow (t_e)_a + \Delta t_a = 3.046213 \text{ hr} \\ p_{acD} &= 0.060911 \rightarrow I(\Delta p_a) = 1108.66 \text{ psia} \cdot \text{hr} \end{aligned}$$

From the type-curve match, $C_{aacD} = 0.01$, and the storage coefficient is calculated as

$$C_a + C_{aac} = \frac{\phi c_i h L_f^2 C_{aacD}}{0.8936} = \frac{(0.10)(2.256)(10)^{-4} (12)(122)^2 (0.01)}{0.8936} = 0.04509 \frac{\text{bbl}}{\text{psi}}$$

The transmissibility is calculated assuming $T_i = T_w$ as

$$\frac{kh}{\mu_i} = (141.2)(24)(1)(2154.88 - 1300.69)(0.04509) \left[\frac{0.060911}{1108.66} \right]_{MP} = 7.17 \frac{\text{md} \cdot \text{ft}}{\text{cp}}$$

The permeability-thickness product is 0.127 md·ft, and the permeability is 0.011 md.

The type-curve match and calculated permeability are in general agreement with before-closure pressure transient analysis, but the calculated permeability from after-closure pseudolinear flow differs by a factor of four. With the storage coefficient determined from type-curve analysis, $C_a + C_{aac} = 0.04509$ bbl/psi, the complete pseudolinear flow impulse solution is used to calculate permeability as

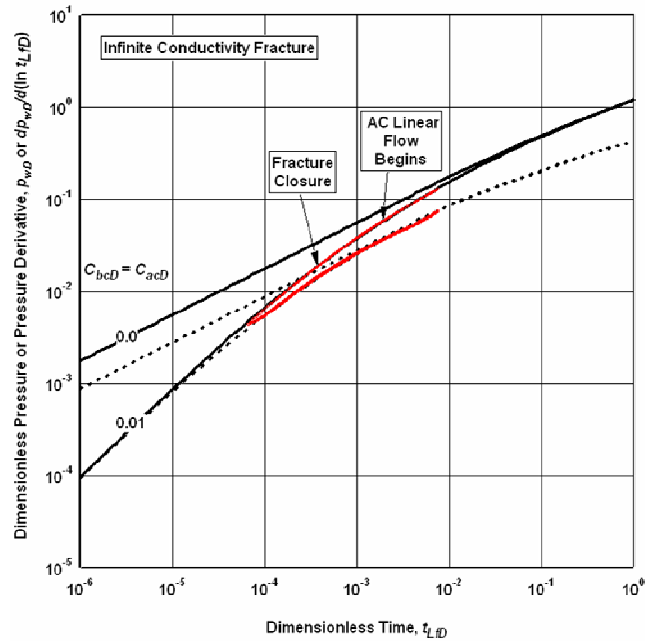


Fig. 5.18—GM 543-33 Mesaverde formation fracture-injection/falloff sequence infinite-conductivity fracture type-curve match.

$$k = \left[\frac{141.2(24)\sqrt{\pi}\sqrt{0.0002637}}{2} \frac{1}{12(122)(376.908)} \left(\frac{0.0177}{0.10(2.256)(10)^{-4}} \right)^{1/2} \right]^2 = 0.019 \text{ md},$$

$$\times (17.69 + .04509(2154.88 - 1300.69))$$

which is closer to the results of before-closure and type-curve analysis, but still differs. The type curve in Fig. 5.18 illustrates that fully developed linear flow was never established. The annotation marks the estimated beginning of pseudolinear flow as interpreted from the after-closure diagnostic graph, but the type curve shows that storage distorts the linear flow data as the transition to pseudolinear flow begins. Thus some difference between the results of before-closure, after-closure pseudolinear flow, and type-curve analysis should be expected with the match selected. The example does illustrate the importance of using the complete pseudolinear flow impulse solution.

None of the methods used for the analysis of the fracture-injection falloff allow for a unique interpretation of the data, and the agreement between the results of before-closure, after-closure pseudolinear flow, and type-curve analysis might be improved with another iteration using a slightly different initial reservoir pressure. However, the results are comparable and reasonably consistent, and iterating is probably unnecessary.

Note that the calculated storage coefficient is about four times greater than the maximum estimated storage coefficient. The tubular configuration resulted in a wellbore volume of 4.65 bbl, and assuming the residual fracture volume is the same as the created fracture volume, that is, assuming the fracture width did not change during closure, the fracture volume for one wing of a symmetrical fracture is 8.845 bbl. Using the gas compressibility in the calculation of storage, the storage coefficient is estimated to be

$$C_a + C_{aac} = c_{gi}V_w + 2c_{gi}V_{fr} = (4.312)(10)^{-4}(4.65 + 2(8.845)) = 0.0096 \frac{\text{bbl}}{\text{psi}}$$

The reservoir is believed to contain natural fractures, which is supported by the pressure-dependent leakoff observed during before-closure G -function analysis, so it is possible that the additional storage volume represents natural fractures that were dilated during the fracture injection.

Immediately following the fracture-injection/falloff, a drawdown/buildup sequence was completed on the GM 543-33 Mesaverde formation. During the drawdown, the layer was produced at a constant rate of 100 Mscf/D for 141.7 hours, but the rate decreased to 98 Mscf/D for the next 24.3 hours. During the slickline work required to seat the plug, the rate decreased to 60 Mscf/D for 0.6 hours, and finally 50 Mscf/D for the final 0.1 hours of the drawdown. After seating the plug, the pressure buildup was recorded for 14.95 days. A type curve match for the buildup data is shown in **Fig. 5.19**, and the buildup data are tabulated in **Table 5-8**.

Table 5-9 contains a summary of the results from the fracture-injection/falloff and drawdown/buildup interpretations. None of the interpretations are unique, but the results from the fracture-injection/falloff sequence are consistent and comparable to the results from the drawdown/buildup sequence, which increases the confidence that the interpretations are correct.

Two additional observations are noteworthy. First, the wellbore storage coefficient from the drawdown/buildup interpretation, $C = 0.001978$ bbl/psi, is comparable to the calculated storage coefficient based on the wellbore volume, $C_a = (4.65 \text{ bbl})(0.000431 \text{ psi}^{-1}) = 0.002$ bbl/psi. Recall from the fracture-injection/falloff sequence that the storage coefficient from the type-curve match was four times the calculated storage coefficient based on wellbore and injected fluid volume. Consequently, if natural fractures were dilated by the fracture-injection and increase the system storage, then the natural fractures must have closed during the drawdown to not affect the wellbore storage during the buildup.

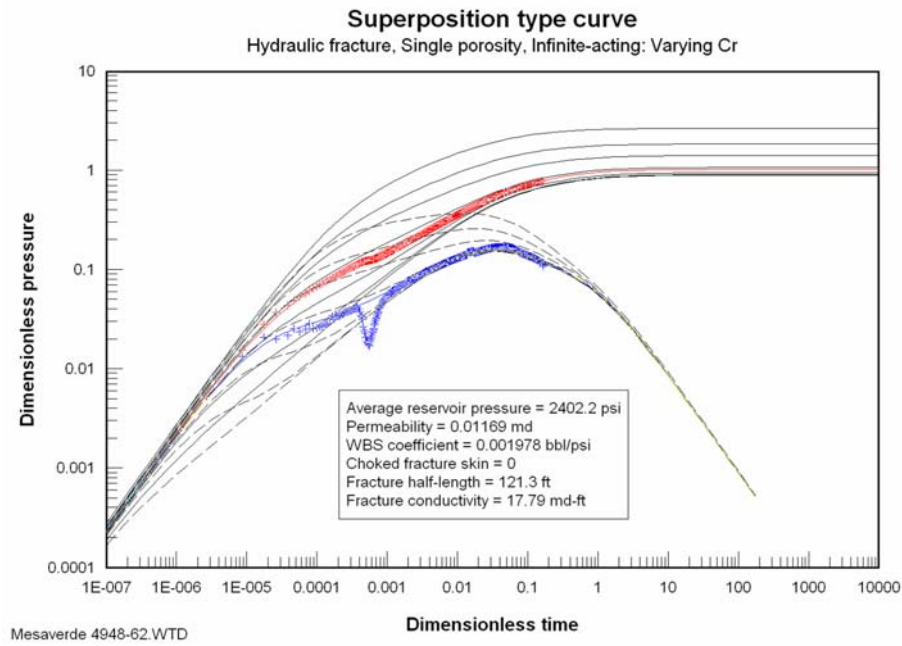


Fig. 5.19—GM 543-33 Mesaverde formation fracture-injection/falloff sequence infinite-conductivity fracture type-curve match.

Second, the fracture-injection/falloff data were matched to a type curve for an infinite-conductivity fracture, and data from the drawdown/buildup sequence was matched to a type curve for a finite-conductivity fracture, $C_f = 17.79$ md-ft, which corresponds to a dimensionless fracture conductivity of $C_{fD} = 12.5$. Thus, a small volume water injection without proppant in a low permeability Mesaverde formation created a fracture of significant length and surprisingly high dimensionless conductivity—which may partly explain the success of "slickwater" fracturing treatments in tight-gas sands.

Table 5-8—GM 543-33 time and bottomhole pressure recorded during the pressure buildup.

t, hr	p _{ws} , psi	t, hr	p _{ws} , psi	t, hr	p _{ws} , psi	t, hr	p _{ws} , psi	t, hr	p _{ws} , psi	t, hr	p _{ws} , psi	t, hr	p _{ws} , psi	t, hr	p _{ws} , psi	t, hr	p _{ws} , psi
1.03	1040.81	3.31	1258.43			23.18	1569.14			65.57	1794.14			226.91	2060.12		
1.06	1066.84	3.38	1260.55	12.18	1449.62	23.34	1570.49	43.57	1703.12	65.91	1795.32	119.91	1932.80	228.91	2061.59		
1.09	1084.31	3.44	1262.53	12.34	1452.01	23.51	1571.85	43.91	1704.78	66.24	1796.60	120.91	1934.58	230.91	2063.13		
1.13	1097.22	3.51	1264.56	12.51	1454.30	23.68	1573.33	44.24	1706.41	66.57	1797.59	121.91	1936.54	232.91	2064.50		
1.16	1107.35	3.58	1266.70	12.68	1456.68	23.84	1574.87	44.57	1707.99	66.91	1798.87	122.91	1938.19	234.91	2066.08		
1.19	1116.23	3.64	1268.84	12.84	1458.99	24.01	1576.15	44.91	1709.58	67.24	1800.05	123.91	1940.10	236.91	2067.59		
1.23	1123.85	3.71	1271.06	13.01	1461.09	24.18	1577.53	45.24	1711.25	67.57	1801.11	124.91	1941.79	238.91	2069.11		
1.26	1130.72	3.78	1273.06	13.18	1463.37	24.34	1578.85	45.57	1712.94	67.91	1802.22	125.91	1943.64	240.91	2070.36		
1.29	1136.66	3.84	1275.26	13.34	1465.54	24.51	1580.34	45.91	1714.49	68.24	1803.27	126.91	1945.36	242.91	2071.80		
1.33	1142.20	3.91	1277.40	13.51	1467.73	24.68	1581.56	46.24	1715.93	68.57	1804.51	127.91	1947.08	244.91	2073.23		
1.36	1147.44	3.98	1279.60	13.68	1470.02	24.84	1583.05	46.57	1717.61	68.91	1805.51	128.91	1948.79	246.91	2074.50		
1.39	1152.21	4.04	1281.70	13.84	1472.16	25.18	1585.76	46.91	1719.21	69.24	1806.67	129.91	1950.55	248.91	2075.91		
1.43	1156.76	4.11	1283.74	14.01	1474.35	25.51	1588.29	47.24	1720.70	69.57	1807.71	130.91	1952.03	250.91	2077.21		
1.46	1160.99	4.18	1285.82	14.18	1476.46	25.84	1590.85	47.57	1722.29	69.91	1808.80	131.91	1953.80	252.91	2078.64		
1.49	1165.00	4.24	1287.86	14.34	1478.52	26.18	1593.49	47.91	1723.85	70.24	1809.98	132.91	1955.47	254.91	2079.88		
1.53	1168.94	4.31	1290.10	14.51	1480.50	26.51	1596.08	48.24	1725.23	70.57	1811.10	133.91	1956.92	256.91	2081.29		
1.56	1172.68	4.38	1292.09	14.68	1482.71	26.84	1598.59	48.57	1726.93	70.91	1812.15	134.91	1958.68	258.91	2082.36		
1.59	1176.48	4.44	1294.08	14.84	1484.70	27.18	1601.07	48.91	1728.27	71.24	1813.26	135.91	1960.24	260.91	2083.77		
1.63	1180.02	4.51	1296.15	15.01	1486.65	27.51	1603.68	49.24	1729.91	71.57	1814.28	136.91	1961.81	262.91	2085.04		
1.66	1183.50	4.58	1298.09	15.18	1488.70	27.84	1606.18	49.57	1731.30	71.91	1815.38	137.91	1963.35	264.91	2086.25		
1.69	1186.84	4.64	1300.08	15.34	1490.58	28.18	1608.53	49.91	1732.91	72.24	1816.49	138.91	1964.99	266.91	2087.55		
1.73	1190.05	4.71	1302.01	15.51	1492.65	28.51	1610.88	50.24	1734.32	73.91	1821.60	139.91	1966.36	268.91	2088.74		
1.76	1193.17	4.78	1303.95	15.68	1494.55	28.84	1613.48	50.57	1735.82	74.91	1824.82	140.91	1967.98	270.91	2090.00		
1.79	1196.10	4.84	1305.73	15.84	1496.59	29.18	1615.71	50.91	1737.22	75.91	1827.81	141.91	1969.57	272.91	2091.20		
1.83	1198.76	5.01	1310.49	16.01	1498.46	29.51	1618.06	51.24	1738.64	76.91	1830.89	142.91	1970.98	274.91	2092.44		
1.86	1201.78	5.18	1315.05	16.18	1500.24	29.84	1620.49	51.57	1740.09	77.91	1833.78	143.91	1972.55	276.91	2093.63		
1.89	1204.42	5.34	1319.56	16.34	1502.03	30.18	1622.61	51.91	1741.55	78.91	1836.79	144.91	1973.91	278.91	2094.68		
1.93	1207.04	5.51	1323.91	16.51	1503.97	30.51	1624.93	52.24	1742.94	79.91	1839.81	146.91	1976.92	280.91	2095.88		
1.96	1209.47	5.68	1328.16	16.68	1505.94	30.84	1627.29	52.57	1744.36	80.91	1842.59	148.91	1979.81	282.91	2097.03		
1.99	1211.95	5.84	1332.29	16.84	1507.76	31.18	1629.61	52.91	1745.75	81.91	1845.31	150.91	1982.50	284.91	2098.01		
2.03	1214.32	6.01	1336.42	17.01	1509.63	31.51	1631.89	53.24	1747.10	82.91	1848.20	152.91	1985.29	286.91	2099.17		
2.06	1216.72	6.18	1340.43	17.18	1511.28	31.84	1634.10	53.57	1748.50	83.91	1851.00	154.91	1987.98	288.91	2100.34		
2.09	1219.07	6.34	1344.46	17.34	1513.12	32.18	1636.15	53.91	1749.93	84.91	1853.70	156.91	1990.72	290.91	2101.34		
2.13	1221.38	6.51	1348.36	17.51	1515.00	32.51	1638.44	54.24	1751.31	85.91	1856.41	158.91	1993.39	292.91	2102.41		
2.16	1223.67	6.68	1352.08	17.68	1516.79	32.84	1640.54	54.57	1752.70	86.91	1859.13	160.91	1995.99	294.91	2103.46		
2.19	1225.76	6.84	1355.84	17.84	1518.47	33.18	1642.73	54.91	1754.05	87.91	1861.74	162.91	1998.38	296.91	2104.57		
2.23	1227.97	7.01	1359.49	18.01	1520.24	33.51	1644.77	55.24	1755.42	88.91	1864.34	164.91	2000.83	298.91	2105.68		
2.26	1229.95	7.18	1363.09	18.18	1522.11	33.84	1646.92	55.57	1756.78	89.91	1866.96	166.91	2003.12	300.91	2106.64		
2.29	1231.97	7.34	1366.79	18.34	1523.68	34.18	1648.94	55.91	1758.08	90.91	1869.62	168.91	2005.53	302.91	2107.77		
2.33	1233.73	7.51	1370.32	18.51	1525.46	34.51	1651.10	56.24	1759.32	91.91	1872.11	170.91	2007.88	304.91	2108.63		
2.36	1235.37	7.68	1373.69	18.68	1527.11	34.84	1653.12	56.57	1760.62	92.91	1874.64	172.91	2010.09	306.91	2109.56		
2.39	1236.76	7.84	1377.06	18.84	1528.86	35.18	1655.10	56.91	1762.04	93.91	1876.98	174.91	2012.70	308.91	2110.61		
2.43	1237.91	8.01	1380.22	19.01	1530.43	35.51	1657.14	57.24	1763.42	94.91	1879.42	176.91	2014.66	310.91	2111.64		
2.46	1238.79	8.18	1383.46	19.18	1532.27	35.84	1659.08	57.57	1764.68	95.91	1881.78	178.91	2016.84	312.91	2112.65		
2.49	1239.65	8.34	1386.83	19.34	1533.80	36.18	1661.15	57.91	1766.06	96.91	1884.20	180.91	2018.89	314.91	2113.54		
2.53	1240.74	8.51	1389.99	19.51	1535.55	36.51	1663.20	58.24	1767.26	97.91	1886.58	182.91	2020.89	316.91	2114.56		
2.56	1241.64	8.68	1392.98	19.68	1537.17	36.84	1664.91	58.57	1768.54	98.91	1888.87	184.91	2022.96	318.91	2115.39		
2.59	1241.97	8.84	1396.01	19.84	1538.80	37.18	1666.92	58.91	1769.86	99.91	1891.29	186.91	2024.92	320.91	2116.40		
2.63	1242.53	9.01	1399.07	20.01	1540.30	37.51	1668.77	59.24	1771.12	100.91	1893.52	188.91	2027.00	322.91	2117.33		
2.66	1243.12	9.18	1401.96	20.18	1541.87	37.84	1670.89	59.57	1772.50	101.91	1895.81	190.91	2028.84	324.91	2118.27		
2.69	1243.80	9.34	1405.02	20.34	1543.63	38.18	1672.69	59.91	1773.75	102.91	1898.08	192.91	2030.73	326.91	2119.18		
2.73	1244.59	9.51	1407.83	20.51	1545.06	38.51	1674.63	60.24	1774.98	103.91	1900.15	194.91	2032.70	328.91	2120.04		
2.76	1245.24	9.68	1410.78	20.68	1546.63	38.84	1676.38	60.57	1776.18	104.91	1902.47	196.91	2034.69	330.91	2120.96		
2.79	1245.92	9.84	1413.45	20.84	1548.25	39.18	1678.16	60.91	1777.53	105.91	1904.71	198.91	2036.50	332.91	2121.74		
2.83	1246.41	10.01	1416.25	21.01	1549.83	39.51	1680.02	61.24	1778.68	106.91	1906.84	200.91	2038.22	334.91	2122.66		
2.86	1246.99	10.18	1418.99	21.18	1551.32	39.84	1681.82	61.57	1779.96	107.91	1908.96	202.91	2040.13	336.91	2123.63		
2.89	1247.41	10.34	1421.55	21.34	1552.83	40.18	1683.83	61.91	1781.11	108.91	1910.92	204.91	2041.86	338.91	2124.44		
2.93	1248.26	10.51	1424.37	21.51	1554.39	40.51	1685.45	62.24	1782.20	109.91	1913.05	206.91	2043.67	340.91	2125.28		
2.96	1249.12	10.68	1427.09	21.68	1555.89	40.84	1686.33	62.57	1783.48	110.91	1915.16	208.91	2045.40	342.91	2126.06		
2.99	1249.87	10.84	1429.67	21.84	1557.48	41.18	1688.68	62.91	1784.67	111.91	1917.10	210.91	2047.04	344.91	2126.83		
3.03	1250.61	11.01	1432.37	22.01	1558.88	41.51	1691.29	63.24	1785.99	112.91	1919.18	212.91	2048.80	346.91	2127.72		
3.06	1251.47	11.18	1434.81	22.18	1560.43	41.84	1693.09	63.57	1787.13	113.91	1921.17	214.91	2050.46	348.91	2128.46		
3.09	1252.40	11.34	1437.28	22.34	1561.95	42.18	1694.69	63.91	1788.26	114.91	1923.20	216.91	2052.22	350.91	2129.34		
3.13	1253.25	11.51	1439.89	22.51	1563.37	42.51	1696.39	64.24	1789.46	115.91	1925.18	218.91	2053.76				

Table 5-9—GM 543-33 summary of results from the interpretation of the fracture-injection/falloff and drawdown/buildup sequences in the Mesaverde formation between 4,948- and 4,962-feet.

	Fracture-Injection/Falloff				Buildup
	Before-Closure	After-Closure Q_{at} Only	After-Closure $Q_{at} + \text{Storage}$	Type Curve	Type Curve
p_i	2,096 psi	2332 psi	2332 psi	2,332	2,402 psi
k	0.008 md	0.002 md	0.019 md	0.011 md	0.012 md
kh	0.096 md·ft	0.024 md·ft	0.228 md·ft	0.132 md·ft	0.144 md·ft
L_f	122 ft	122 ft	122 ft	122 ft	121.3 ft
C_{fD}	∞	∞	∞	∞	12.5

5.3.3 Pre-Existing Conductive Hydraulic Fracture With Choked-Fracture Skin Damage. The final example illustrates a refracture-candidate diagnostic test in an isolated low-permeability Mesaverde sandstone formation. Unlike the previous examples, a propped-fracture treatment placing 250,000 lb of 20/40 mesh sand had been pumped, and the well had been produced *prior* to the fracture-injection/falloff sequence. Post-frac well performance was below expectations, and the objective of the test was to verify the presence of an open hydraulic fracture and to look for evidence of "damage."

The test consisted of 75.8 bbl of 1% KCl treated water that was injected at an average rate of 4.10 bbl/min during an 18.5 minute injection period. Following the fracture-injection, the pressure falloff was recorded for 4 hours. **Fig. 5.20** shows a graph of surface pressure and injection rate recorded during the entire fracture-injection/falloff sequence. As shown in Fig. 5.19, the pressure during the injection exceeded the fracture closure stress significantly, and the instantaneous shut-in pressure indicates that about 500 psi of pressure in excess of the fracture closure stress was observed during the fracture injection.

Fig. 5.21 shows a log-log graph of the integrated adjusted pseudopressure difference and derivative versus adjusted pseudotime. Dual unit slope (storage-dominated flow) periods were observed during the falloff period. The first unit-slope period corresponds to a constant storage coefficient during closure, and the second unit slope period—which is clearly shown by the derivative curve—is observed after fracture closure. The apparent increase in storage is the characteristic response of a damaged fracture with choked-fracture skin, and the curves suggest a fracture retaining residual width exists, but the fracture is damaged. Consequently, the refracture-candidate diagnostic test qualitatively verified an existing damaged fracture, but since the data did not extend beyond the end of storage-dominated flow, quantitative analysis is not possible.

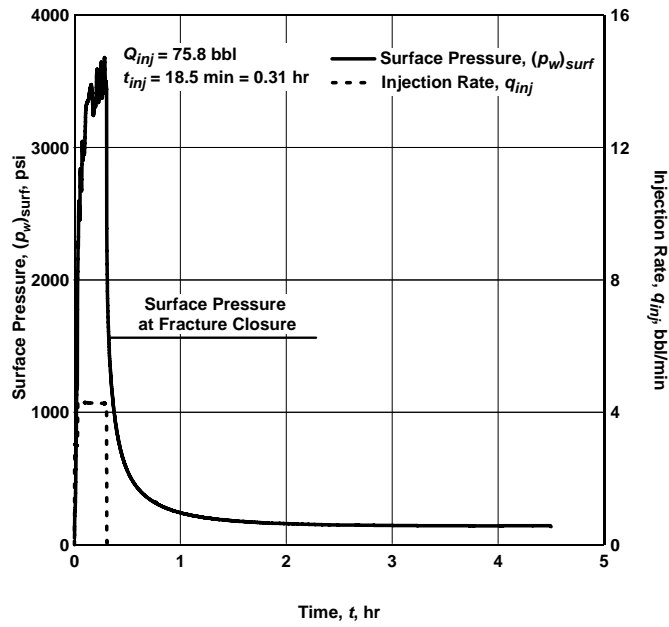


Fig. 5.20—Mesaverde formation refracture-candidate diagnostic test pressure and injection rate recorded versus time.

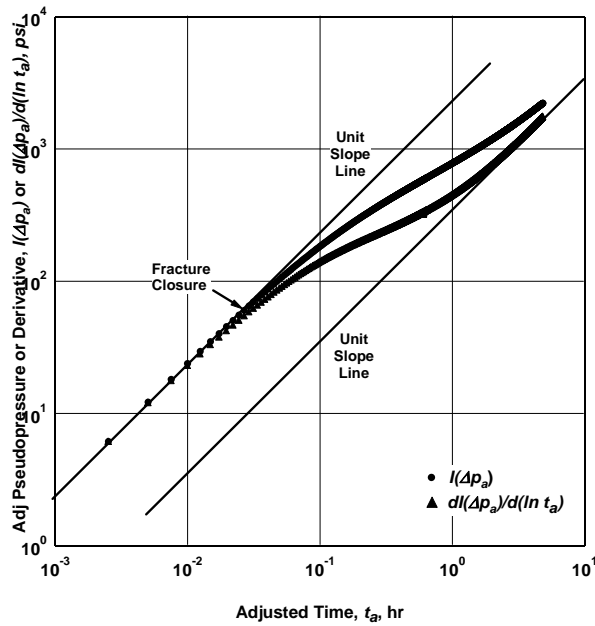


Fig. 5.21—Mesaverde formation refracture-candidate diagnostic equivalent constant-rate adjusted pseudopressure difference and derivative versus adjusted pseudotime.

CHAPTER VI

SUMMARY, CONCLUSIONS, AND RECOMMENDATIONS

6.1 Summary and Conclusions

The goal of the research was to develop a new pressure-transient test for refracture-candidate identification, and it was asserted that a fracture-injection/falloff sequence with the time of injection short relative to the reservoir response could be a viable refracture-candidate diagnostic.

Achieving the research goal required several modifications to existing theory, a new theoretical approach to a fracture-injection/falloff sequence, and new ancillary, but important, pressure-transient solutions. For example, current fracture-injection/falloff analysis methods were modified by formulating before-closure pressure-transient analysis and after-closure analysis methods in terms of adjusted pseudopressure and adjusted pseudotime to account for pressure-dependent reservoir fluid properties. Additionally, after-closure analysis was modified by redefining the time plotting function for consistency with Soliman's¹⁰⁹ method for the analysis of a buildup test with a short producing time, and Soliman's¹⁰⁹ and Soliman *et al.*'s¹⁰⁸ pseudolinear flow solution was corrected.

The new theoretical approach to modeling a fracture-injection/falloff sequence utilized throughout the dissertation considers fracture creation, propagation, and closure to be storage phenomena. Fracture propagation is modeled as time-dependent storage, and fracture closure and after-closure diffusion are modeled as having constant, but possibly different, storage. As a result, the pressure-transient solution for a fracture-injection/falloff sequence includes variable storage to account for fracture propagation, fracture closure, and after-closure diffusion. Since each storage coefficient is derived from fundamental principles, properties of the system can be interpreted from the storage coefficient(s), or, more specifically, from the changes observed in the storage coefficients.

New analytical fracture-injection/falloff solutions were developed for the following cases.

- Equivalent propagating-fracture storage and before-closure storage with constant after-closure storage.
- Time-dependent propagating-fracture storage, constant before-closure storage, and constant after-closure storage.
- Time-dependent propagating-fracture storage and before-closure storage with linear flow from the fracture before closure and after-closure radial flow with constant wellbore storage and skin.

Additionally, limiting-case solutions were developed for each case, and the limiting-case solutions demonstrated that when the time of injection is short relative to the reservoir response, the observed pressure difference between the wellbore and average reservoir pressure during the variable-rate falloff can be integrated and converted to an equivalent "constant-rate" pressure difference. A log-log graph of

the equivalent pressure difference versus time will overlay a constant-rate type curve for the appropriate reservoir/system, which allows for type-curve analysis of fracture-injection/falloff data.

Since the fracture-injection/falloff model developed includes variable storage, new constant-rate, variable-storage drawdown solutions were developed for a well producing from an infinite-slab reservoir containing a single dilated vertical fracture with the initial reservoir pressure above the minimum insitu or closure stress and with fracture and wellbore storage as follows:

- Constant before-closure and constant after-closure storage.
- Constant before- and constant after-closure storage with fracture-face and choked-fracture skin.
- Fracture flow during closure with constant before-closure storage and radial flow after closure with constant wellbore storage and skin.

With the new fracture-injection/falloff theory, a new refracture-candidate diagnostic was developed by recognizing that a fracture-injection/falloff sequence in an isolated layer with an existing conductive fracture will have a falloff response with characteristic variable-storage behavior. The variable-storage behavior is used to qualitatively identify the following.

- A pre-existing conductive fracture.
- A pre-existing fracture with damage.

Both apparent increasing and decreasing storage at fracture closure can indicate an existing conductive fracture, but apparent increasing storage indicates the existing fracture is damaged in the form of choked-fracture skin.

Developing a quantitative type curve analysis method for the refracture-candidate diagnostic required the most important ancillary development in the dissertation: a semianalytical pressure-transient solution for a well producing from an infinite-slab reservoir through multiple, arbitrarily-oriented uniform-flux, infinite-conductivity, or finite-conductivity fractures. The new multiple-fracture reservoir solutions were combined with variable storage models to develop constant-rate drawdown type curves for a well producing through multiple fractures. With the new type curves and after extending the fracture-injection/falloff theory to cases with multiple fractures and anisotropic stress conditions, a quantitative type-curve analysis method was developed for the refracture-candidate diagnostic.

The new solutions allow for determining the primary and secondary fracture half-length, the primary and secondary fracture conductivity, and reservoir transmissibility from the pressure falloff of a refracture candidate diagnostic after converting the observed pressure difference to an equivalent constant-rate pressure difference and matching with log-log type curves for a well producing from an infinite slab reservoir with multiple, arbitrarily-oriented fractures. Additionally, when pseudoradial flow is observed, a

refracture-candidate diagnostic can provide an estimate of average reservoir pressure using the after-closure impulse solution.

Completing the method required developing solutions in terms of adjusted pseudopressure and adjusted pseudotime to account for reservoir fluid compressibility. Before-closure, after-closure, and the limiting-case solutions that allow type-curve analysis of a fracture-injection-falloff analysis were all derived in terms of adjusted pseudovariabes. Thus, a complete analysis "package" for a fracture-injection/falloff sequence or refracture-candidate diagnostic is available and correct for reservoirs containing oil, gas, or water (coal).

Field fracture-injection/falloff examples and interpretations were provided for a moderate- and a low-permeability gas reservoir without a pre-existing conductive fracture, and the results of both fracture-injection/falloff interpretations were compared and validated with conventional pressure-transient tests. Additionally, a qualitative interpretation of a refracture-candidate diagnostic in a low-permeability gas reservoir with an existing fracture identified a damaged fracture based on apparent increasing storage behavior after fracture closure, which validates the new refracture-candidate diagnostic theory.

Modifications of current fracture-injection/falloff analysis methods; the development of new fracture-injection/falloff models; the ancillary development of new pressure-transient solutions; and validation with field cases demonstrates that the the new refracture-candidate diagnostic presented in the dissertation achieves the goal of developing a new pressure-transient test for refracture-candidate identification.

6.2 Recommendations for Future Research

The new solutions presented in the dissertation provide numerous opportunities for additional research—some of which are as follows.

- The analytical solutions developed within the dissertation need thorough numerical evaluation. The dissertation focused on deriving the solutions and provided minimal numerical evaluations of the new solutions. A more exhaustive examination is warranted. For example, numerical evaluations could quantify the error created by assuming an instantaneous injection when a finite injection time is required, that is, quantify the error when $(t_e)_{LD} = \{10^{-6}, 10^{-5}, 10^{-4}, 10^{-3}\}$.
- Similarly, the theory is derived to account for dual porosity reservoirs. Numerical evaluation of the dual porosity solutions should be compared to single porosity examples. On a more fundamental level, the numerical evaluations of the dual porosity solutions should be used to identify when, and if, dual porosity behavior can be observed from the falloff of a fracture-injection/falloff sequence.
- The approach used to derive the pressure-transient solution for a well producing from an infinite-slab reservoir through multiple, arbitrarily-oriented uniform-flux, infinite-conductivity, or finite-conductivity fractures is general. The same approach could be used to derive solutions for more complex fracture patterns. For example, microseismic fracture imaging from the Barnett shale

indicates hydraulic fracturing dilates an entire macro-scale fracture network. Pressure-transient solutions with parallel fractures connected through a perpendicular fracture could be derived following the same approach. The derivation method and solutions could be used to determine how pressure-transient tests in reservoirs with complex-fracture patterns differ from the single, planar fracture case.

- The pressure-transient solution for a well producing from an infinite-slab reservoir through multiple, arbitrarily-oriented uniform-flux, infinite-conductivity, or finite-conductivity fractures also needs to be derived for bounded reservoirs.

NOMENCLATURE

<i>a</i>	=..... variable of substitution, dimensionless
<i>A</i>	=..... fracture area during propagation, L^2 , m^2
<i>A_L</i>	=..... fracture leakoff area, L^2 , m^2
<i>A_{ij}</i>	=..... matrix element, dimensionless
<i>b</i>	=..... variable of substitution, dimensionless
<i>b_M</i>	=..... intercept from special before-closure pressure-transient graph, dimensionless
<i>b_N</i>	=..... intercept from Nolte-Shlyapobersky graph, m/Lt^2 , Pa
<i>b_{fs}</i>	=..... damage zone width, L, m
<i>B</i>	=..... formation volume factor, dimensionless
<i>c</i>	=..... variable of substitution, dimensionless
<i>c₁</i>	=..... before-closure pressure-transient analysis function, $m/Lt^{3/2}$, $Pa \cdot s^{1/2}$
<i>c₂</i>	=..... before-closure pressure-transient analysis function, m^2/L^2t^3 , $Pa^2 \cdot s^{1/2}$
<i>c_{ap1}</i>	=..... adjusted before-closure pressure-transient analysis function, $m/Lt^{3/2}$, $Pa \cdot s^{1/2}$
<i>c_{ap2}</i>	=..... adjusted before-closure pressure-transient analysis function, m^2/L^2t^3 , $Pa^2 \cdot s^{1/2}$
<i>c_f</i>	=..... compressibility of fluid in fracture, Lt^2/m , Pa^{-1}
<i>c_g</i>	=..... gas compressibility, Lt^2/m , Pa^{-1}
<i>c_{gw}</i>	=..... wellbore gas compressibility, Lt^2/m , Pa^{-1}
<i>c_t</i>	=..... total compressibility, Lt^2/m , Pa^{-1}
<i>c_{ti}</i>	=..... total compressibility at initial conditions, Lt^2/m , Pa^{-1}
<i>c_{tbc}</i>	=..... average before-closure total compressibility, Lt^2/m , Pa^{-1}
<i>c_w</i>	=..... compressibility of fluid in wellbore, Lt^2/m , Pa^{-1}
<i>C</i>	=..... wellbore storage, L^4t^2/m , m^3/Pa
<i>C_a</i>	=..... adjusted wellbore storage, L^4t^2/m , m^3/Pa
<i>C_{ac}</i>	=..... after-closure storage, L^4t^2/m , m^3/Pa
<i>C_{aac}</i>	=..... adjusted after-closure storage, L^4t^2/m , m^3/Pa
<i>C_{bc}</i>	=..... before-closure storage, L^4t^2/m , m^3/Pa
<i>C_{fbc}</i>	=..... before-closure storage, L^4t^2/m , m^3/Pa
<i>C_f</i>	=..... fracture conductivity, m^3 , m^3
<i>C_{fd}</i>	=..... dilating fracture storage, L^4t^2/m , m^3/Pa
<i>C_{fac}</i>	=..... after-closure fracture storage, L^4t^2/m , m^3/Pa
<i>C_{fbc}</i>	=..... before-closure fracture storage, L^4t^2/m , m^3/Pa
<i>C_L</i>	=..... leakoff coefficient, $L/m^{1/2}$, $m/s^{1/2}$
<i>C_{Lf}</i>	=..... wellbore storage in well with hydraulic fracture, L^4t^2/m , m^3/Pa
<i>C_{pf}</i>	=..... propagating-fracture storage, L^4t^2/m , m^3/Pa

C_{fac}	= after-closure fracture storage, $L^4t^2/m, m^3/Pa$
C_{f1D}	= primary fracture conductivity, m^3, m^3
C_{f2D}	= secondary fracture conductivity, m^3, m^3
C_{fbc}	= before-closure fracture storage, $L^4t^2/m, m^3/Pa$
C_{plf}	= propagating-fracture storage with multiple fractures, $L^4t^2/m, m^3/Pa$
C_{pdlf}	= propagating- and dilating-fracture storage with multiple fractures, $L^4t^2/m, m^3/Pa$
C_{Lfac}	= after-closure multiple fracture storage, $L^4t^2/m, m^3/Pa$
C_{Lfbc}	= before-closure multiple fracture storage, $L^4t^2/m, m^3/Pa$
d	= variable of substitution, dimensionless
d_j	= before-closure pressure-transient analysis variable, $m/Lt^3, Pa/s$
$(d_{ap})_j$	= adjusted before-closure pressure-transient analysis variable, $m/Lt^3, Pa/s$
E'	= plane-strain modulus, $m/Lt^2, Pa$
F	= hypergeometric function, dimensionless
F_L	= linear-flow time function, dimensionless
g	= loss-volume function, dimensionless
G	= G-function, dimensionless
h	= height, L, m
h_f	= fracture height, L, m
I	= integral, $m/Lt, Pa \cdot s$
k	= permeability, L^2, m^2
k_f	= fracture permeability, L^2, m^2
k_x	= permeability in x -direction, L^2, m^2
k_y	= permeability in y -direction, L^2, m^2
k_{fb}	= dual-porosity bulk-fracture permeability, L^2, m^2
k_{fs}	= fracture-face damage-zone permeability, L^2, m^2
K_0	= modified Bessel function of the second kind (order zero), dimensionless
K_1	= modified Bessel function of the second kind (order one), dimensionless
L	= propagating fracture half length, L, m
L_c	= characteristic length, L, m
L_e	= fracture half length at end of pumping, L, m
L_f	= fracture half length at end of pumping, L, m
L_{fi}	= fracture half length of fracture i at end of pumping, L, m
L'_{fi}	= fracture half length of fracture i at end of pumping rescaled for anisotropy, L, m
m	= mass, m, kg
M	= molecular weight, moles

m_M	=..... slope from special before-closure pressure-transient graph, dimensionless
m_N	=..... slope from Nolte-Shlyapobersky graph, m/Lt^2 , Pa
m_{acpl}	=..... slope of data on after-closure pseudolinear flow Cartesian graph, m/Lt^2 , Pa
m_{acpr}	=..... slope of data on after-closure pseudoradial flow Cartesian graph, m/Lt , Pa·s
n_f	=..... number of fractures, dimensionless
n_{fs}	=..... number of fracture segments, dimensionless
p	=..... pressure, m/Lt^2 , Pa
p_a	=..... adjusted pressure, m/Lt^2 , Pa
p_{ac}	=..... pressure with constant after-closure storage, m/Lt^2 , Pa
p_{ar}	=..... adjusted reservoir pressure, m/Lt^2 , Pa
p_{bc}	=..... pressure with constant before-closure storage, m/Lt^2 , Pa
p_{aac}	=..... adjusted pressure with constant after-closure storage, m/Lt^2 , Pa
p_{aws}	=..... injection/falloff wellbore adjusted pressure, m/Lt^2 , Pa
p_{cake}	=..... filter-cake pressure, m/Lt^2 , Pa
p_f	=..... pressure with production from a single fracture, m/Lt^2 , Pa
p_{fs}	=..... pressure at fracture face with fracture-face skin, m/Lt^2 , Pa
p_{fac}	=..... fracture pressure with constant after-closure fracture storage, m/Lt^2 , Pa
p_{fiz}	=..... filtrate-invaded zone pressure, m/Lt^2 , Pa
p_{face}	=..... pressure at fracture face, m/Lt^2 , Pa
p_{ls}	=..... line-source pressure, m/Lt^2 , Pa
p_{Lf}	=..... pressure with production from multiple fractures, m/Lt^2 , Pa
p_{Lfac}	=..... pressure with production from multiple fractures and constant after-closure storage, m/Lt^2 , Pa
p_{Lfbc}	=..... pressure with production from multiple fractures and constant before-closure storage, m/Lt^2 , Pa
p_n	=..... fracture net pressure, m/Lt^2 , Pa
p_{pf}	=..... pressure with a propagating fracture, m/Lt^2 , Pa
p_{ps}	=..... point-source pressure, m/Lt^2 , Pa
p_{piz}	=..... polymer-invaded zone pressure, m/Lt^2 , Pa
p_{pLf}	=..... pressure with a propagating secondary fracture, m/Lt^2 , Pa
p_{prf}	=..... pressure during fracture propagation, m/Lt^2 , Pa
p_{prLf}	=..... pressure during secondary fracture propagation, m/Lt^2 , Pa
p_{sac}	=..... pressure with radial flow and skin with constant after-closure fracture storage, m/Lt^2 , Pa
p_s	=..... pressure in radial system with skin, m/Lt^2 , Pa

$p_{sf\dot{s}}$	=pressure from fracture-face resistance, m/Lt^2 , Pa
p_{wc}	=wellbore pressure with constant flow rate, m/Lt^2 , Pa
$p_{w\dot{f}}$	=pressure outside wellbore in fracture, m/Lt^2 , Pa
p_{ws}	=injection/falloff wellbore pressure, m/Lt^2 , Pa
q	= flow rate, L^3/t , m^3/s
\tilde{q}	= fracture-face flux, L^3/t , m^3/s
q_i	= flow rate for the i^{th} -fracture, L^3/t , m^3/s
q_ℓ	= fluid leakoff rate, L^3/t , m^3/s
q_s	=sandface flow rate, L^3/t , m^3/s
q_t	= total flow rate, L^3/t , m^3/s
q_{as}	= adjusted sandface flow rate, L^3/t , m^3/s
q_{pf}	= propagating-fracture flow rate, L^3/t , m^3/s
q_{sf}	= sand-face flow rate, L^3/t , m^3/s
q_{ws}	=injection/falloff wellbore flow rate, L^3/t , m^3/s
q_{aws}	= adjusted injection/falloff wellbore flow rate, L^3/t , m^3/s
Q_t	=total injection volume, L^3 , m^3
Q_{at}	=total injected gas volume, L^3 , m^3
r	= radius, L, m
R_f	= radial fracture radius, L, m
r_p	=ratio of permeable to total fracture area, dimensionless
r_{we}	=effective wellbore radius, L, m
R	=resistance, L^{-1} , m/m^2
R_0	=reference filtercake resistance at the end of the injection, L^{-1} , m/m^2
R_{fs}	= filtercake resistance, L^{-1} , m/m^2
s	= Laplace transform variable, dimensionless
S	= skin, dimensionless
S_f	= fracture stiffness, m/L^2t^2 , Pa/m
S_p	= spurt-loss coefficient, L^3 , m^3
S_{fs}	= fracture-face skin, dimensionless
$(S_{fs})_{ch}$	= choked-fracture skin, dimensionless
t	= time, t, s
t_l	= reference time, t, s
t_a	=adjusted time, t, s
t_e	= time at the end of an injection, t, s
t_c	= time at hydraulic fracture closure, t, s

t_{ac}	= time after-closure, t, s
t_{DN}	= Nolte dimensionless time, dimensionless
t_{LFD}	= dimensionless time, dimensionless
T	= temperature, °K
u	= variable of substitution, dimensionless
U	= unit-step function, dimensionless
v_L	= fracture fluid leakoff velocity, L/t, m/s
V	= volume, L ³ , m ³
V_L	= leakoff volume, L ³ , m ³
V_{fr}	= residual fracture volume of one wing, L ³ , m ³
V_{Lc}	= fluid volume lost from one wing of a hydraulic fracture during the time of closure, L ³ , m ³
w	= width, L, m
w_L	= lost width, L, m
\hat{w}_f	= average fracture width, L, m
x	= coordinate of point along x-axis, L, m
x_n	= before-closure pressure-transient analysis plotting function, dimensionless
$(x_{ap})_n$	= adjusted before-closure pressure-transient analysis plotting function, dimensionless
x'	= variable of integration, L, m
x''	= variable of integration, L, m
\hat{x}	= coordinate of point along \hat{x} -axis, L, m
x_w	= wellbore position along x-axis, L, m
y	= coordinate of point along y-axis, L, m
y_n	= before-closure pressure-transient analysis plotting function, dimensionless
$(y_{ap})_n$	= adjusted before-closure pressure-transient analysis plotting function, dimensionless
y'	= variable of integration, L, m
\hat{y}	= coordinate of point along \hat{y} -axis, L, m
y_w	= wellbore position along y-axis, L, m
z	= gas deviation factor, dimensionless
Z_i	= matrix element, dimensionless
Greek		
α	= variable of integration, dimensionless
α_D	= viscosity-compressibility function, dimensionless
α_N	= fracture growth exponent, dimensionless

δ_i	=	ratio of fracture i to primary fracture conductivity, dimensionless
δ_C	=	ratio of secondary to primary fracture conductivity, dimensionless
δ_L	=	ratio of secondary to primary fracture half length, dimensionless
ε	=	dual-porosity variable in point-source solution, dimensionless
Γ	=	Gamma function, dimensionless
Δ	=	difference, dimensionless
ζ	=	variable of substitution, dimensionless
η	=	variable of substitution, dimensionless
η_f	=	fracture diffusivity, L^2/t , m^2/s
η_r	=	reservoir diffusivity, L^2/t , m^2/s
η_{fD}	=	dimensionless diffusivity, dimensionless
θ'	=	angle rescaled for permeability anisotropy, radians
θ	=	angle, radians
λ	=	interporosity flow coefficient, dimensionless
μ	=	viscosity, m/Lt , $Pa \cdot s$
ξ	=	variable of substitution, dimensionless
ρ	=	density, m/L^3 , kg/m^3
ρ_f	=	density of fluid filling a fracture, m/L^3 , lbm/ft^3
ρ_g	=	gas density, m/L^3 , lbm/ft^3
ρ_{wb}	=	density of wellbore fluid, m/L^3 , lbm/ft^3
σ_{min}	=	minimum or closure stress, m/Lt^2 , Pa
σ_z	=	overburden stress, m/Lt^2 , Pa
τ	=	variable of substitution, dimensionless
τ_0	=	reference time, t , s
τ_a	=	time at the beginning of an injection, t , s
τ_d	=	a shut-in time following an injection, t , s
τ_N	=	time at exposure, t , s
τ_{ND}	=	dimensionless time at exposure, dimensionless
ν	=	Poisson's ratio, dimensionless
ϕ	=	porosity, dimensionless
χ	=	variable of substitution, dimensionless
ψ	=	variable of substitution, dimensionless
ω	=	fracture storativity ratio

Subscripts

0	=	reference time zero
-----	---------	---------------------

<i>a</i>	=	adjusted
<i>c</i>	=	closure
<i>D</i>	=	dimensionless
<i>e</i>	=	end of injection
<i>f</i>	=	fracture
<i>g</i>	=	gas
<i>i</i>	=	initial conditions
<i>inj</i>	=	injection
<i>j</i>	=	index
<i>ℓ</i>	=	fracture index
<i>m</i>	=	index
MP	=	match point
<i>n</i>	=	index
<i>ne</i>	=	index at the end of injection
<i>r</i>	=	reservoir
<i>re</i>	=	reference
sc	=	standard conditions
<i>w</i>	=	wellbore

Superscripts

'	=	denotes derivative with respect to time
"	=	denotes second derivative with respect to time

Character Symbols

—	=	denotes Laplace transform
^	=	denotes average

REFERENCES

1. Howard, G.C. and Fast, C.R.: "Results of Hydraulic Fracturing," *Hydraulic Fracturing*, Monograph Series, SPE, Richardson, Texas (1970) **2**, 172-176.
2. Green, J.: "Study of Refracturing Results in the Clinton Sand Formation," paper SPE 6361 presented at the 1976 SPE Eastern Regional Meeting, Columbus, Ohio, 18-19 November.
3. Branch, G.A. and Drennan, K.M.: "Refracture Stimulations in the Norge Marchand Unit: A Case Study," paper SPE 21642 presented at the 1991 Production Operations Symposium, Oklahoma City, Oklahoma, 7-9 April.
4. Olson, K.E.: "A Case Study of Hydraulically Refractured Wells in the Devonian Formation, Crane County, Texas," paper SPE 22834 presented at the SPE 1991 Annual Technical Conference and Exhibition of the Society of Petroleum Engineers, Dallas, Texas, 6-9 October.
5. Fleming, M.E.: "Successful Refracturing in the North Westbrook Unit," paper SPE 24011 presented at the 1992 SPE Permian Basin Oil and Gas Recovery Conference, Midland, Texas, 18-20 March.
6. McGowen, H.E., III and Krauhs, J.: "Development and Application of an Integrated Petroleum Engineering and Geologic Information System in the Giddings Austin Chalk Field," paper SPE 24441 presented at the 1992 Seventh SPE Petroleum Computer Conference, Houston, Texas, 19-22 July.
7. Pospisii, G., Lynch, K.W., Pearson, C.M., and Rugen, J.A.: "Results of a Large-Scale Refracture Stimulation Program, Kuparuk River Unit, Alaska," paper SPE 24857 presented at the 1992 SPE Annual Technical Conference and Exhibition of the Society of Petroleum Engineers, Washington, DC, 4-7 October.
8. Parrot, D.I. and Long, M.G.: "A Case History of Massive Hydraulic Refracturing in the Tight Muddy "J" Formation," paper SPE 7936 presented at the 1979 SPE Symposium on Low Permeability Gas Reservoirs, Denver, Colorado, 20-22 May.
9. Hunter, J.C.: "A Case History of Refracs in the Oak Hill (Cotton Valley) Field," paper SPE 14655 presented at the 1986 East Texas Regional Meeting of the Society of Petroleum Engineers, Tyler, Texas, 21-22 April.
10. Ennis, B.K.: "Case History of Restimulations in Western Oklahoma," paper SPE 18861 presented at the 1989 SPE Production Operations Symposium, Oklahoma City, Oklahoma, 13-14 March.

11. Durrani, A.J., Escovedo, B.M., Ordemann, B., Bickley, J.A., Tepper, B.J., *et al.*: "The Rejuvenation of the 30-Year-Old McAllen Ranch Field: An Application of Cross-Functional Team Management," SPE 24872 presented at the 1992 SPE Annual Technical Conference and Exhibition of the Society of Petroleum Engineers, Washington, DC, 4-7 October.
12. Fairchild, N.R., Jr. and Wood, D.D.: "Optimization of Clinton Restimulation Program in Stark-Summitt Gas Storage Field: A Field Case Study," paper SPE 39220 presented at the 1997 SPE Eastern Regional Meeting, Lexington, Kentucky, 22-24 October.
13. Reeves, S.R.: "Assessment of Technology Barriers and Potential Benefits of Restimulation R&D for Natural Gas Wells," final report, Report No. GRI-96/0267, Gas Research Institute, Chicago, Illinois, July 1996.
14. Williams, P.: "The Barnett Shale," *Oil & Gas Investor* (March 2002) **22**, No. 3, 34.
15. Williams, P.: "Wattenberg Revival," *Oil & Gas Investor* (March 1999) **19**, No. 3, 22.
16. Moritis, G.: "Diagnosing Underperforming Wells," *Oil & Gas Journal* (4 December 2000) **98**, No. 49, 23.
17. Williams, P.: "Value in the Vicksburg," *Oil & Gas Investor* (August 2004) **24**, No. 8, 49.
18. Conway, M.W., McMechan, D.E., McGowen, J.M., Brown, D., Chisholm, P.T., *et al.*: "Expanding Recoverable Reserves Through Refracturing," paper SPE 14376 presented at the 1985 SPE Annual Technical Conference and Exhibition of the Society of Petroleum Engineers, Las Vegas, Nevada, 22-25 September.
19. Voneiff, G.W., Robinson, B.M., and Holditch, S.A.: "The Effects of Unbroken Fracture Fluid on Gas Well Performance," SPE 26664 available from SPE, Richardson, Texas (1994).
20. Elbel, J.L. and Mack, M.G.: "Refracturing: Observations and Theories," paper SPE 25464 presented at the 1993 SPE Production Operations Symposium, Oklahoma City, Oklahoma, 21-23 March.
21. Wright, C.A., Stewart, D.W., Emanuele, M.A., and Wright, W.W.: "Reorientation of Propped Refracture Treatments in the Lost Hills Field," paper SPE 27896 presented at the 1994 SPE Western Regional Meeting, Long Beach, California, 23-25 March.
22. Wright, C.A., Conant, R.A., Stewart, D.W., and Byerly, P.M.: "Reorientation of Propped Refracture Treatments," paper SPE 28078 presented at the 1994 SPE/ISRM Rock Mechanics in Petroleum Engineering Conference, Delft, The Netherlands, 29-31 August.
23. Wright, C.A. and Conant, R.A.: "Hydraulic Fracture Reorientation in Primary and Secondary Recovery from Low-Permeability Reservoirs," paper SPE 30484 presented at the 1995 SPE Annual Technical Conference and Exhibition, Dallas, Texas, 22-25 October.

24. Siebrits, E., Elbel, J.L., Hoover, R.S., Diyashev, I.R., Griffin, L.G., *et al.*: "Refracture Reorientation Enhances Gas Production in Barnett Shale Tight Gas Wells," SPE 63030 presented at the 2000 SPE Annual Technical Conference and Exhibition, Dallas, Texas, 1-4 October.
25. Esphahanian, C. and Storhaug, D.G.: "A Statistical Approach to Pay Identification in the Tight, Fractured, Heterogeneous Reservoirs of the Piceance Basin," paper SPE 38366 presented at the 1997 Rocky Mountain Regional Meeting, Casper, Wyoming, 18-21 May.
26. Eberhard, M. and Mullen, M.: "The Effect of Completion Methodologies on Production in the Jonah Field," *SPEPF* (August 2003) 145.
27. Barree, R.D., Fisher, M.K., and Woodroof, R.A.: "A Practical Guide to Hydraulic Fracture Diagnostic Technologies," paper SPE 77442 presented at the 2002 SPE Annual Technical Conference and Exhibition, San Antonio, Texas, 29 September – 2 October.
28. Fisher, K., Robinson, B.M., and Voneiff, G.W.: "A Comprehensive Study of the Analysis and Economic Benefit of Radioactive Tracer Engineered Stimulation Procedures," paper SPE 30794 presented at the 1995 SPE Annual Technical Conference and Exhibition, Dallas, Texas, 22-25 October.
29. Reese, J.L., Britt, L.K., and Jones, J.R.: "Selecting Economic Refracturing Candidates," paper SPE 28490 presented at the 1994 SPE Annual Technical Conference and Exhibition, New Orleans, Louisiana, 25-28 September.
30. Crowell, R.F. and Jennings, A.R.: "A Diagnostic Technique for Restimulation Candidate Selection," paper SPE 7556 presented at the 1978 SPE Annual Fall Technical Conference and Exhibition, Houston, Texas, 1-3 October.
31. Kuuskraa, V.A., Reeves, S.R., Schraufnagel, R.A., and Spafford, S.D.: "Economic and Technical Rationale for Remediating Inefficiently Producing Eastern Gas Shale and Coalbed Methane Wells," paper SPE 26894 presented at the 1993 SPE Eastern Regional Conference & Exhibition, Pittsburgh, Pennsylvania, 2-4 November.
32. Hower, T.L. and Decker, M.K.: "Identifying Recompletion Candidates in Stratified Gas Reservoirs," paper SPE 24307 presented at the 1992 SPE Mid-Continent Gas Symposium, Amarillo, Texas, 13-14 April.
33. Fetkovich, M.J., Bradley, M.D., Works, A.M., and Thrasher, T.S.: "Depletion Performance of Layered Reservoirs Without Crossflow," *SPEFE* (September 1990) 310.

34. Fetkovich, M.J.: "Advanced Decline Curve Analysis Identifies Fracture Stimulation Potential," paper SPE 38903 presented at the 1997 SPE Annual Technical Conference and Exhibition, San Antonio, Texas, 5-8 October.
35. McCoy, T.F., Reese, D.E., and Johnson, P.G.: "Depletion Performance of Poorly Stimulated Layered Reservoirs Without Crossflow," paper SPE 59757 presented at the 2000 SPE/CERI Gas Technology Symposium, Calgary, Alberta, Canada, 3-5 April.
36. Mohaghegh, S.: "Performance Drivers in Restimulation of Gas-Storage Wells," *SPEREE* (December 2001) 536.
37. Shelley, R.F.: "Artificial Neural Networks Identify Restimulation Candidates in the Red Oak Field," paper SPE 52190 presented at the 1999 SPE Mid-Continent Operations Symposium, Oklahoma City, Oklahoma, 28-31 March.
38. Oberwinkler, C. and Economides, M.J.: "The Definitive Identification of Candidate Wells for Refracturing," paper SPE 84211 presented at the 2003 SPE Annual Technical Conference and Exhibition, Denver, Colorado, 5-8 October.
39. Reeves, S.R., Hill, D.G., Tiner, R.L., Bastian, P.A., Conway, M.W., *et al.*: "Restimulation of Tight Gas Sand Wells in the Rocky Mountain Region," paper SPE 55627 presented at the 1999 SPE Rocky Mountain Regional Meeting, Gillette, Wyoming, 15-18 May.
40. Reeves, S.R., Hill, D.G., Hopkins, C.W., Conway, M.W., Tiner, R.L., *et al.*: "Restimulation Technology for Tight Gas Sand Wells," paper SPE 56482 presented at the 1999 SPE Annual Technical Conference and Exhibition, Houston, Texas, 3-6 October.
41. Reeves, S. and Wolhart, S.: "Study Looks at Tight-Gas Restimulation Candidate Wells," *Oil & Gas Journal* (8 October 2001) **99**, No. 41, 37.
42. McCain, W.D., Voneiff, S.A., Hunt, E.R., and Semmelbeck, M.E.: "A Tight Gas Field Study: Carthage (Cotton Valley) Field," paper SPE 26141 presented at the 1993 SPE Gas Technology Symposium, Calgary, Alberta, Canada, 28-30 June.
43. Voneiff, G.W. and Cipolla, C.: "A New Approach to Large-Scale Infill Evaluations Applied to the OZONA (Canyon) Gas Sands," paper SPE 35203 presented at the 1996 SPE Permian Basin Oil & Gas Recovery Conference, Midland, Texas, 27-29 March.
44. Cox, D.O., Kuuskraa, V.A., and Hansen, J.T.: "Advanced Type Curve Analysis for Low Permeability Gas Reservoirs," paper SPE 35595 presented at the 1996 SPE Gas Technology Conference, Calgary, Alberta, Canada, 28 April – 1 May.
45. Reeves, S.R.: "Natural Gas Production Enhancement via Restimulation," final report, Contract No. 5097-210-4090, Gas Research Institute, Chicago, Illinois (June 2001).

46. Reeves, S. and Wolhart, S.: "Insights Into Restimulation Candidate Selection," *GasTIPS* (Fall 2001) **7**, No. 4, 15.
47. Ely, J.W., Tiner, R., Rothenberg, M., Krupa, A., McDougal, F., *et al.*: "Restimulation Program Finds Success in Enhancing Recoverable Reserves," paper SPE 63241 presented at the 2000 SPE Annual Technical Conference and Exhibition, Dallas, Texas, 1-4 October.
48. Ehlig-Economides, C.A. and Joseph, J.: "A New Test for Determination of Individual Layer Properties in a Multilayered Reservoir," *SPEFE* (September 1987) 261.
49. Jochen, J.E., Hopkins, C.W., and Frantz, J.H., Jr.: "Quantifying Layered Reservoir Properties With a Novel Permeability Test," paper SPE 25864 presented at the 1993 SPE Rocky Mountain Regional/Low Permeability Symposium, Denver, Colorado, 12-14 April.
50. Hopkins, C.W., Lancaster, D.E., Foster, J.M., and Graham, R.L.: "The Use of Injection/Falloff Tests and Pressure Buildup Tests to Evaluate Fracture Geometry and Post-Stimulation Well Performance in the Devonian Shales," paper SPE 23433 presented at the 1991 SPE Eastern Regional Meeting, Lexington, Kentucky, 22-25 October.
51. Hopkins, C.W., Frantz, J.H., Jr., Tatum, C.L., and Hill, D.G.: "Screening Restimulation Candidates in the Antrim Shale," paper SPE 29172 presented at the 1994 SPE Eastern Regional Conference & Exhibition, Charleston, West Virginia, 8-10 November.
52. Huang, H., Bastian, P.A., Hopkins, C.W., and Wolhart, S.: "A Short Shut-In Time Testing Method for Determining Stimulation Effectiveness in Low Permeability Gas Reservoirs," *GAStips* (Fall 2000), **6**, No. 4, 28.
53. Frantz, J.H., Jr., Shannon, P.M., Moody, C.E., Glaser, T., Wawyer, W.K., *et al.*: "Novel Well Testing Procedures Prove Successful in Dakota Formation Infill Program, San Juan Basin," paper SPE 71519 presented at the 2001 SPE Annual Technical Conference and Exhibition, New Orleans, Louisiana, 30 September – 3 October.
54. Craig, D.P., Eberhard, M.J., Ramurthy, M., Odegard, C.E., and Mullen, R.: "Permeability, Pore Pressure, and Leakoff-Type Distributions in Rocky Mountain Basins," *SPEPF* (February 2005) 48.
55. Ayoub, J.A., Bourdet, D.P., and Chauvel, Y.L.: "Impulse Testing," *SPEFE* (September 1988) 534.
56. Ramey, H.J., Jr., Agarwal, R.G., and Martin, I.: "Analysis of 'Slug Test' or DST Flow Period Data," *J. Cdn. Pet. Tech.* (July-September 1975) 37.

57. Mayerhofer, M.J. and Economides, M.J.: "Permeability Estimation From Fracture Calibration Treatments," paper SPE 26039 presented at the 1993 Western Regional Meeting, Anchorage, Alaska, 26-28 May.
58. Mayerhofer, M.J., Ehlig-Economides, C.A., and Economides, M.J.: "Pressure-Transient Analysis of Fracture-Calibration Tests," *JPT* (March 1995) 229.
59. Valkó, P. and Economides, M.J.: "Fluid-Leakoff Delineation in High-Permeability Fracturing," *SPEPF* (May 1999) 117.
60. Gu, H., Elbel, J.L., Nolte, K.G., Cheng, A.H-D., and Abousleiman, Y.: "Formation Permeability Determination Using Impulse-Fracture Injection," paper SPE 25425 presented at the 1993 SPE Production Operations Symposium, Oklahoma City, Oklahoma, 21-23 March.
61. Abousleiman, Y., Cheng, A. H-D., and Gu, H.: "Formation Permeability Determination by Micro or Mini-Hydraulic Fracturing," *J. of Energy Resources Technology* (June 1994) 116, No. 6, 104.
62. Correa, A.C. and Ramey, H.J., Jr.: "Combined Effects of Shut-In and Production: Solution With a New Inner Boundary Condition," paper SPE 15579 presented at the 1986 SPE Annual Technical Conference and Exhibition, New Orleans, Louisiana, 05-08 October.
63. Correa, A.C. and Ramey, H.J., Jr.: "A Method for Pressure Buildup Analysis of Drillstem Tests," paper SPE 16802 presented at the 1987 SPE Annual Technical Conference and Exhibition, Dallas, Texas, 27-30 September.
64. Correa, A.C. and Ramey, H.J., Jr.: "Application of the Unit Step Function to Unusual Well Test Problems," paper SPE 18156 presented at the 1988 SPE Annual Technical Conference and Exhibition, Houston, Texas, 02-05 October.
65. van Everdingen, A.F. and Hurst, W.: "The Application of the Laplace Transformation to Flow Problems in Reservoirs," *Trans. AIME* (1949) **186**, 305-324.
66. Ramey, H.J., Jr. and Agarwal, R.G.: "Annulus Unloading Rates As Influenced by Wellbore Storage and Skin Effect," *SPEJ* (October 1972) 453; *Trans. AIME* (1972) **253**.
67. Rushing, J.A., Blasingame, T.A., Poe, B.D., Jr., Brimhall, R.M., and Lee, W.J.: "Analysis of Slug Test Data From Hydraulically Fractured Coalbed Methan Wells," paper SPE 21492 presented at the 1991 SPE Gas Technology Symposium, Houston, Texas, 23-25 January.
68. Stehfest, H.: "Numerical Inversion of Laplace Transforms," *Communications of the ACM* (January 1970), 13, No. 1, 47-49.
69. Peres, A.M.M., Onur, M., and Reynolds, A.C.: "A New Genral Pressure-Analysis Procedure for Slug Tests," *SPEFE* (December 1993) 292.

70. Ramey, H.J. Jr. and Gringarten, A.C.: "Effect of High Volume Vertical Fractures on Geothermal Steam Well Behavior," *Proc.*, Second United Nations Symposium on the Use and Development of Geothermal Energy, San Francisco, California (20-29 May 1975).
71. Xiao, J.J. and Reynolds, A.C.: "A Pseudopressure-Pseudotime Transformation for the Analysis of Gas Well Closed Chamber Tests," paper SPE 25879 presented at the 1993 SPE Rocky Mountain Regional/Low-Permeability Reservoirs Symposium, Denver, Colorado, 12-14 April.
72. Lee, W.J. and Holditch, S.A.: "Application of Pseudotime to Buildup Test Analysis of Low-Permeability Gas Wells With Long-Duration Wellbore Storage Distortion," *JPT* (December 1982) 2877.
73. Meunier, D.F., Kabir, C.S., and Wittmann, M.J.: "Gas Well Test Analysis: Use of Normalized Pseudovariates," *SPEFE* (December 1987) 529.
74. Barree, R.D. and Mukherjee, H.: "Determination of Pressure Dependent Leakoff and Its Effect on Fracture Geometry," paper SPE 36424 presented at the 1996 SPE Annual Technical Conference and Exhibition, Denver, Colorado, 6-9 October.
75. Nolte, K.G.: "Determination of Fracture Parameters From Fracturing Pressure Decline," paper SPE 8341 presented at the 1979 SPE Annual Technical Conference and Exhibition, Dallas, Texas, 23-25 September.
76. Howard, G.C. and Fast, C.R.: "Optimum Fluid Characteristics for Fracture Extension, *Drilling and Production Practices* (1957), API, 261-270.
77. Valkó, P. and Economides, M.J.: "Material Balance," *Hydraulic Fracture Mechanics*, John Wiley & Sons, New York City (1997) Chap. 8, 165-188.
78. Valkó, P. and Economides, M.J.: "Fracture Height Containment With Continuum Damage Mechanics," paper SPE 26598 presented at the 1993 SPE Annual Technical Conference and Exhibition, Houston, Texas, 3-6 October.
79. Oberhettinger, F.: "Hypergeometric Functions," *Handbook of Mathematical Functions*, Milton Abramowitz and Irene A. Stegun (eds.), Dover Publications, New York City (1965), Chap. 15, 555-566.
80. Nolte, K.G.: "A General Analysis of Fracturing Pressure Decline With Application to Three Models," *SPEFE* (December 1986) 57.
81. Castillo, J.L.: "Modified Fracture Pressure Decline Analysis Including Pressure-Dependent Leakoff," paper SPE 16417 presented at the 1987 SPE/DOE Low Permeability Reservoirs Symposium, Denver, Colorado, 18-19 May.

82. Craig, D.P., Eberhard, M.J., and Barree, R.D.: "Adapting High Permeability Leakoff Analysis to Low Permeability Sands for Estimating Reservoir Engineering Parameters," paper SPE 60291 presented at the 2000 SPE Rocky Mountain Regional/Low Permeability Reservoirs Symposium, Denver, Colorado, 12-15 March.
83. Cinco-Ley, H. and Samaniego-V., F.: "Transient Pressure Analysis: Finite Conductivity Fracture Case Versus Damage Fracture Case," paper SPE 10179 presented at the 1981 SPE Annual Technical Conference and Exhibition, San Antonio, Texas, 5-7 October.
84. Gringarten, A.C., Ramey, H.J., Jr., Raghavan, R.: "Unsteady-State Pressure Distributions Created by a Well With a Single Infinite-Conductivity Vertical Fracture," *SPEJ* (August 1974) 347.
85. Ehlig-Economides, C.A., Fan, Y., and Economides, M.J.: "Interpretation Model for Fracture Calibration Tests in Naturally Fractured Reservoirs," paper SPE 28690 presented at the 1994 SPE International Petroleum Conference and Exhibition of Mexico, Veracruz, Mexico, 10-13 October.
86. Cinco-Ley, H. and Meng, H.-Z.: "Pressure Transient Analysis of Wells With Finite Conductivity Vertical Fractures in Dual Porosity Reservoirs," paper SPE 18172 presented at the 1988 SPE Annual Technical Conference and Exhibition, Houston, Texas, 2-5 October.
87. Nolte, K.G.: "Background for After-Closure Analysis of Fracture Calibration Tests," unsolicited paper SPE 39407 available from SPE, Richardson, Texas (1997).
88. Bourdet, D.: "Special Tests," *Well Test Analysis: The Use of Advanced Interpretation Models*, Elsevier, New York (2002), Chap. 9, 335.
89. Butler, J.J., Jr.: "The Performance of Slug Tests," *The Design, Performance, and Analysis of Slug Tests*, Lewis Publishers, Boca Raton (1997), 33.
90. Koning, E.J.L. and Niko, H.: "Fractured Water-Injection Wells: A Pressure Falloff Test for Determining Fracturing Dimensions," paper SPE 14458 presented at the 1985 Annual Technical Conference and Exhibition of the Society of Petroleum Engineers, Las Vegas, NV, 22-25 September.
91. Koning, E.J.L.: "Waterflooding Under Fracturing Conditions," PhD Thesis, Delft Technical University, Delft, The Netherlands (1988).
92. van den Hoek, P.J.: "Pressure Transient Analysis in Fractured Produced Water Injection Wells," paper SPE 77946 presented at the 2002 SPE Asia Pacific Oil & Gas Conference, Melbourne, Australia, 8-10 October.

93. van den Hoek, P.J.: "A Novel Methodology to Derive the Dimensions and Degree of Containment of Waterflood-Induced Fractures From Pressure Transient Analysis," paper SPE 84289 presented at the 2003 SPE Annual Technical Conference and Exhibition, Denver, Colorado, 5-8 October.
94. Spivey, J.P. and Lee, W.J.: "Variable Wellbore Storage Models for a Dual-Volume Wellbore," paper SPE 56615 presented at the 1999 SPE Annual Technical Conference and Exhibition, Houston, Texas, 3-6 October.
95. Ozkan, E. and Raghavan, R.: "New Solutions for Well-Test-Analysis Problems: Part 1—Analytical Considerations," *SPEFE* (September 1991), 359.
96. Warren, J.E. and Root, P.J.: "The Behavior of Naturally Fractured Reservoirs," *SPEJ* (September 1963) 245.
97. de Swaan, A.: "Analytic Solutions for Determining Naturally Fractured Reservoir Properties by Well Testing," *SPEJ* (June 1976) 117.
98. Bourdet, D. and Gringarten, A.C.: "Determination of Fissure Volume and Block Size in Fractured Reservoirs by Type-Curve Analysis," paper SPE 9293 presented at the 1980 SPE Annual Fall Technical Conference and Exhibition, Dallas, Texas, 21-24 September 1980.
99. Hawkins, M.F., Jr.: "A Note on the Skin Effect," *Trans.*, AIME (1956) **207**, 356.
100. Valkó, P. and Economides, M.J.: "Coupling of Elasticity, Flow, and Material Balance," *Hydraulic Fracture Mechanics*, John Wiley & Sons, New York City (1997) Chap. 9, 189.
101. Hagoort, J.: "Waterflood-induced hydraulic fracturing," PhD Thesis, Delft Technical University, 1981.
102. Raghavan, R., Chen, C-C, and Agarwal, B.: "An Analysis of Horizontal Wells Intercepted by Multiple Fractures," *SPEJ* (September 1997) 235.
103. Ozkan, E., Yildiz, T., and Kuchuk, F.J.: "Transient Pressure Behavior of Duallateral Wells," SPE 38670 presented at the 1997 SPE Annual Technical Conference and Exhibition, San Antonio, Texas, 05-08 October.
104. Kuchuk, F.J., Goode, P.A., Wilkinson, D.J., and Thambynayagam, R.K.M.: "Pressure-Transient Behavior of Horizontal Wells With and Without Gas Cap or Aquifer," *SPEFE* (March 1991) 86.
105. Wilkinson, D. and Hammond, P.S.: "A Perturbation Method for Mixed Boundary-Value Problems in Pressure Transient Testing," *Transport in Porous Media* (1990) **5**, 609-636.

106. Spivey, J.P. and Lee, W.J.: "Estimating the Pressure-Transient Response for a Horizontal or a Hydraulically Fractured Well at an Arbitrary Orientation in an Anisotropic Reservoir," *SPEREE* (October 1999) 462.
107. Cinco-L., H., Samaniego-V, F., and Dominguez-A, F.: "Transient Pressure Behavior for a Well With a Finite-Conductivity Vertical Fracture," *SPEJ* (August 1978) 253
108. Soliman, M.Y., Craig, D., Bartko, K., Rahim, Z., and Adams, D.: "After-Closure Analysis to Determine Formation Permeability, Reservoir Pressure, and Residual Fracture Properties, SPE 93419 presented at the 2005 SPE Middle East Oil and Exhibition, Manama, Bahrain, 12-15 March.
109. Soliman, M.Y.: "Analysis of Buildup Tests With Short Producing Time," *SPEFE* (August 1986) 363.
110. Ispas, I.N., Britt, L.K, Diab, D., Valkó, P., and Economides, M.J.:"Methodology of Fluid Leakoff Analysis in High-Permeability Fracturing," paper SPE 39476 presented at the 1998 SPE International Symposium on Formation Damage Control, Lafayette, Louisiana, 18-19 February.
111. Warpinski, N.R., Wright, T.B., Uhl, J.E., Drozda, P.M., Peterson, R.E., *et al.*:"Microseismic Monitoring of the B-Sand Hydraulic Fracture Experiment at the DOE/GRI Multi-Site Project," paper SPE 36450 presented at the 1996 SPE Annual Technical Conference and Exhibition, Denver, Colorado, 6-9 October.
112. Wolhart, S.L., Odegard, C.E., Warpinski, N.R., Waltman, C.K., and Machovoe, S.R.:"Microseismic Fracture Mapping Optimizes Development of Low-Permeability Sands of the Williams Fork Formation in the Piceance Basin," paper SPE 95637 presented at the 2005 SPE Annual Technical Conference and Exhibition, Dallas, Texas, 9-12 October.
113. Larsen, L. and Bratvold, R.B.: "Effects of Propagating Fractures on Pressure-Transient Injection and Falloff Data," paper SPE 20580 presented at the 1990 SPE Annual Technical Conference and Exhibition, New Orleans, Louisiana, 23-26 September.
114. Ozkan, E. and Raghavan, R.: "New Solutions for Well-Test-Analysis Problems: Part 2—Computational Considerations and Applications," *SPEFE* (September 1991), 369.
115. Yildiz, T.: "Multilateral Pressure-Transient Response," *SPEJ* (March 2003) 5.
116. Bennett, C.O., Reynolds, A.C., Raghavan, R., and Elbel, J.L.: "Performance of Finite-Conductivity, Vertically Fractured Wells in Single-Layer Reservoirs," *SPEFE* (August 1986) 399.

APPENDIX A

**BEFORE-CLOSURE PRESSURE-TRANSIENT ANALYSIS WITH
PRESSURE-DEPENDENT RESERVOIR FLUID PROPERTIES**

The methods of Mayerhofer *et al.*⁵⁸ and Valkó and Economides⁵⁹ for analyzing the before-closure pressure decline following a fracture-injection/falloff test do not consider a compressible mobile reservoir fluid. Accounting for pressure-dependent reservoir fluid properties is accomplished by using pseudovari-ables, or for convenience, adjusted pseudovari-ables.

The pressure difference between the created fracture and a point in the reservoir at initial reservoir pressure is written as

$$\Delta p(t) = \Delta p_r(t) + \Delta p_{cake}(t) + \Delta p_{piz}(t) + \Delta p_{fiz}(t) \dots\dots\dots(A-1)$$

Writing the pressure difference across the filtercake, Δp_{cake} , polymer-invaded zone, Δp_{piz} , and filtrate-invaded zone, Δp_{fiz} , as a single fracture-face pressure difference, Δp_{face} , allows the total pressure difference to be written as

$$\Delta p(t) = \Delta p_r(t) + \Delta p_{face}(t) \dots\dots\dots(A-2)$$

where Δp_r is the reservoir pressure difference. Dividing the total pressure difference by the difference at the end of the injection, $p_0 - p_i$, allows the dimensionless pressure to be written as

$$p_{wD}(t_{LFD}) = p_{rD}(t_{LFD}) + p_{fD}(t_{LFD}) \dots\dots\dots(A-3)$$

where the dimensionless wellbore pressure is defined as

$$p_{wD}(t_{LFD}) = \frac{p_w(t_{LFD}) - p_i}{p_0 - p_i} \dots\dots\dots(A-4)$$

the dimensionless reservoir pressure is defined as

$$p_{rD}(t_{LFD}) = \frac{p_r(t_{LFD}) - p_i}{p_0 - p_i} \dots\dots\dots(A-5)$$

and the dimensionless fracture-face pressure is written as

$$p_{fD}(t_{LFD}) = \frac{p_f(t_{LFD}) - p_i}{p_0 - p_i} \dots\dots\dots(A-6)$$

The reservoir pressure difference in a formation containing a slightly compressible fluid is modeled using Gringarten *et al.*'s⁸⁴ early-time solution for the flow from an infinite-conductivity fracture which is written as

$$p_D = \sqrt{\pi t_{LFD}} \dots\dots\dots(A-7)$$

where dimensionless time is defined as

$$t_{LFD} = \frac{kt}{\phi\mu c_t L_f^2}, \dots\dots\dots(A-8)$$

and k is the permeability, ϕ is the porosity (fraction), μ is the reservoir fluid viscosity, c_t is the total compressibility, and L_f is the fracture half-length.

When the injected fluid is a liquid in a gas reservoir, a moving interface exists between the leakoff liquid and the mobile reservoir gas. Provided the injected volume is relatively small and assuming piston-like displacement, the depth of filtrate invasion is typically less than a few inches beyond the fracture face. When the fracture and the expanding invaded region are small relative to the investigated depth in the reservoir, the filtrate invaded region has negligible influence on the pressure behavior and a single-phase model is appropriate for the transient falloff analysis.¹¹³

For a compressible reservoir gas, a single-phase model can be formulated using adjusted pseudopressure and adjusted pseudotime. Adjusted pseudopressure is defined as

$$p_a = \left(\frac{\mu z}{p} \right)_{re} \int_0^p \frac{p dp}{\mu z}, \dots\dots\dots(A-9)$$

where the subscript 're' denotes a reference pressure. With the reference pressure defined as initial reservoir pressure, dimensionless adjusted pseudopressure is written as

$$p_{aD} = \frac{2\pi kh}{q_g B_g \mu_i} \Delta p_a(p), \dots\dots\dots(A-10)$$

where z is the real-gas deviation factor, h is the formation thickness, Δp_a is the adjusted pseudopressure difference, $p_{ar}(t_{aLD}) - p_{ai}$, q_g is the gas injection rate, B_g is the gas formation volume factor, and the subscript 'i' denotes the property is evaluated at initial reservoir pressure.

Similarly, adjusted pseudotime is defined as

$$t_a = (\mu c_t)_{re} \int_0^t \frac{dt}{\mu c_t}, \dots\dots\dots(A-11)$$

and with the reference pressure defined as initial reservoir pressure, dimensionless adjusted pseudotime is written as

$$t_{aLD} = \frac{kt_a}{\phi\mu_i c_{ti} L_f^2}. \dots\dots\dots(A-12)$$

Lee and Holditch⁷² demonstrated that the governing differential equation for a reservoir containing a compressible fluid can be effectively linearized by the writing in terms of pseudopressure and pseudotime. Meunier *et al.*⁷³ extended the concept by normalizing the transforms, which results in adjusted pseudopressure and adjusted pseudotime. With adjusted pseudovariabes, flow solutions developed for a

reservoir with slightly compressible fluid can be used directly in a reservoir containing a compressible fluid. Consequently, the dimensionless wellbore adjusted pseudopressure, p_{awD} , is written as

$$p_{awD}(t_{aLfD}) = p_{arD}(t_{aLfD}) + p_{afD}(t_{aLfD}) \dots\dots\dots(A-13)$$

Reservoir Adjusted Pseudopressure Difference

The early-time dimensionless reservoir adjusted pseudopressure solution for an infinite-conductivity fracture can be written as

$$p_{aD} = \sqrt{\pi t_{aLfD}} \dots\dots\dots(A-14)$$

The dimensionless reservoir adjusted pseudopressure is obtained by applying superposition, which is written as

$$p_{arD}(t_{aLfD}) = \int_0^{t_{aLfD}} q'_{aD}(\tau_{LfD}) p_{aD}(t_{aLfD} - \tau_{LfD}) d\tau_{LfD} \dots\dots\dots(A-15)$$

where dimensionless injection rate is defined as

$$q_{aD} = \frac{q_g B_{gi} \mu_i}{2\pi kh(p_{a0} - p_{ai})} \dots\dots\dots(A-16)$$

and p_{a0} is the adjusted pseudopressure at the end of the injection. The total injected gas rate, q_g , is divided between two fracture wings, which is written as

$$q_g = 2 \frac{q_{lg}}{B_g} \dots\dots\dots(A-17)$$

where q_{lg} is the gas leakoff rate at reservoir conditions.

A discretized form of the superposition integral is written as

$$p_{arD}(t_{aLfD})_n = \sum_{j=1}^n [(q_{aD})_j - (q_{aD})_{j-1}] p_{aD}[(t_{aLfD})_n - (t_{aLfD})_{j-1}] \dots\dots\dots(A-18)$$

where the subscript 'n' denotes the timestep and the subscript 'j' is a timestep index. With the dimensionless variable definitions, the discretized reservoir pseudopressure difference is written as

$$(\Delta p_{ar})_n = \frac{B_{gi}}{hL_f} \sqrt{\frac{\mu_i}{\pi\phi k c_{ti}}} \sum_{j=1}^n \left[\left(\frac{q_{lg}}{B_g} \right)_j - \left(\frac{q_{lg}}{B_g} \right)_{j-1} \right] \sqrt{(t_a)_n - (t_a)_{j-1}} \dots\dots\dots(A-19)$$

Nolte⁸⁰ defines the before-closure fracture leakoff rate as

$$q_l = -\frac{A_e}{S_f} \frac{d(p(t) - p_c)}{dt} = -\frac{A_e}{S_f} \frac{dp(t)}{dt} \dots\dots\dots(A-20)$$

where A_e is the area of one wing of a fracture symmetric about the wellbore, p_c is the fracture closure stress, and S_f is the fracture "stiffness." Fracture stiffness, or the inverse of fracture compliance, is defined by the elastic energy or "strain energy" created by an open fracture in a rock assuming linear elastic theory

is applicable. **Table A-1** contains the fracture stiffness definitions for three common 2D fracture models.^{80,100} In Table A-1, E' is the plane-strain modulus, R_f is the fracture radius of a radial fracture, and h_f is the gross fracture height.

Table A-1—Fracture stiffness for 2D fracture models.^{80,100}

Radial	Perkins-Kern-Nordgren Vertical Plane Strain	Geertsma-deKlerk Horizontal Plane Strain
$(S_f)_{RAD} = \frac{3\pi E'}{16R_f}$	$(S_f)_{PKN} = \frac{2E'}{\pi h_f}$	$(S_f)_{GDK} = \frac{E'}{\pi L_f}$

The before-closure fracture leakoff rate can also be written for a compressible fluid in terms of adjusted pseudopressure and adjusted pseudotime as

$$q_{lg} = -\frac{A_f B_g}{S_f c_t} \left(\frac{c_t}{B_g} \right)_i \frac{dp_a}{dt_a} \dots\dots\dots (A-21)$$

or written in a discretized form as

$$(q_{lg})_j = \frac{A_f}{S_f} \left(\frac{c_t}{B_g} \right)_i \left(\frac{B_g}{c_t} \right)_j \left[\frac{(p_a)_{j-1} - (p_a)_j}{(t_a)_j - (t_a)_{j-1}} \right] \dots\dots\dots (A-22)$$

The discretized reservoir pseudopressure difference can now be written as

$$(\Delta p_{ar})_n = \frac{1}{\sqrt{\pi}} \frac{1}{r_p S_f \sqrt{k}} \sqrt{\frac{\mu_i}{\phi c_{ti}}} \sum_{j=1}^n [(d_{ap})_j - (d_{ap})_{j-1}] \sqrt{(t_a)_n - (t_a)_{j-1}}, \dots\dots\dots (A-23)$$

where the discretized differential, $(d_{ap})_j$, is defined as

$$(d_{ap})_j = \frac{c_{ti}}{(c_t)_j} \left(\frac{(p_a)_{j-1} - (p_a)_j}{(t_a)_j - (t_a)_{j-1}} \right), \dots\dots\dots (A-24)$$

and the ratio of permeable fracture area to total fracture area is defined as

$$r_p = \frac{hL_f}{A_f} \dots\dots\dots (A-25)$$

Valkó and Economides⁵⁹ assume that the leakoff rates are constant during the fracture injection, and the assumption is modified such that the first $ne + 1$ leakoff rates are constant at *standard conditions*, which is written as

$$\left(\frac{q_{lg}}{B_g}\right)_j = \text{Constant} \quad 1 \leq j \leq ne+1, \dots\dots\dots(\text{A-26})$$

where 'ne' is the timestep index at the end of the injection. The assumption implies that the pressure in the fracture during the injection is approximately constant, and allows the discretized reservoir pseudopressure difference to be written as

$$(\Delta p_{ar})_n = \frac{1}{\sqrt{\pi}} \frac{1}{r_p S_f \sqrt{k}} \sqrt{\frac{\mu_i}{\phi c_{ti}}} \left[\begin{aligned} &+(d_{ap})_{ne+1} \sqrt{(t_a)_n} \left[1 - \sqrt{1 - \frac{(t_a)_{ne+1}}{(t_a)_n}} \right] \\ &(d_{ap})_{ne+2} \sqrt{(t_a)_n - (t_a)_{ne-1}} \\ &+ \sum_{j=ne+3}^n [(d_{ap})_j - (d_{ap})_{j-1}] \sqrt{(t_a)_n - (t_a)_{j-1}} \end{aligned} \right] \dots\dots\dots(\text{A-27})$$

Fracture-Face Adjusted Pseudopressure Difference

Cinco-Ley and Samaniego,⁸³ suggested a fracture-face skin defined by

$$S_{fs} = \frac{\pi b_{fs}}{2L_f} \left[\frac{k}{k_{fs}} - 1 \right], \dots\dots\dots(\text{A-28})$$

where b_{fs} is the width and k_{fs} is the permeability of the damaged zone. Mayerhofer and Economides⁵⁷ use the fracture-face skin concept to model a rate-dependent skin created by fluid leakoff by defining fracture-face resistance as

$$R_{fs}(t) = \frac{b_{fs}(t)}{k_{fs}}, \dots\dots\dots(\text{A-29})$$

and dimensionless resistance as⁵⁸

$$R_D(t) = \frac{R_{fs}(t)}{R'_0} \approx \sqrt{\frac{t}{t_{ne}}}, \dots\dots\dots(\text{A-30})$$

where R'_0 is a reference resistance. With the definition of fracture-face resistance and dimensionless resistance, fracture-face skin can be written as

$$S_{fs} = \frac{\pi k R'_0 R_D(t)}{2L_f} - \frac{\pi b_{fs}}{2L_f} \approx \frac{\pi k R'_0 R_D(t)}{2L_f}, \dots\dots\dots(\text{A-31})$$

or written as

$$S_{fs} = \frac{\pi k R'_0}{2L_f} \sqrt{\frac{t}{t_{ne}}}. \dots\dots\dots(\text{A-32})$$

Fracture-face skin can be written as a dimensionless pseudopressure across the fracture face as

$$p_{afsD} = S_{fs} = \frac{2\pi kh \Delta p_{af}}{q_g B_{gi} \mu_i}, \dots\dots\dots(\text{A-33})$$

or with the fracture-face skin definition, written as

$$\Delta p_{af} = \frac{B_{gi} \mu_{gi}}{hL_f} \frac{R'_0}{2\pi} \frac{q_g}{2} \sqrt{\frac{t}{t_{ne}}} \dots\dots\dots (A-34)$$

With the fracture symmetrical about the wellbore, the fracture-face pseudopressure difference can be written as

$$\Delta p_{af} = \frac{B_{gi} \mu_i}{hL_f} \frac{R'_0}{2\pi} \frac{q_{lg}}{B_g} \sqrt{\frac{t}{t_{ne}}} \dots\dots\dots (A-35)$$

Assuming the fracture-face skin is a steady-state skin,⁵⁷⁻⁵⁸ the fracture-face pseudopressure difference at any timestep n is written as

$$(\Delta p_{af})_n = \frac{B_{gi} \mu_i}{hL_f} \frac{R'_0}{2\pi} \left(\frac{q_{lg}}{B_g} \right)_n \sqrt{\frac{t_n}{t_{ne}}}, \dots\dots\dots (A-36)$$

or with the definition of before-closure fracture leakoff in terms of adjusted pseudopressure and pseudotime, the fracture-face pseudopressure difference can be written as

$$(\Delta p_{af})_n = \frac{1}{2\pi} \frac{R_0}{r_p S_f} (d_{ap})_n \sqrt{\frac{t_n}{t_{ne}}}, \dots\dots\dots (A-37)$$

where R_0 is the fracture-face resistance product defined as the product of gas viscosity at initial reservoir pressure and the reference fracture-face resistance, that is, $R_0 = \mu_i R'_0$.

Specialized Cartesian Graph for Determining Permeability and Fracture-Face Resistance

The dimensionless wellbore adjusted pseudopressure was defined as

$$p_{awD}(t_{aLjD}) = p_{arD}(t_{aLjD}) + p_{afD}(t_{aLjD}), \dots\dots\dots (A-38)$$

which can also be written in dimensional form as

$$(\Delta p_{aw})_n = (\Delta p_{ar})_n + (\Delta p_{af})_n \dots\dots\dots (A-39)$$

With the definitions of reservoir and fracture-face adjusted pseudopressure difference, the wellbore adjusted pseudopressure difference can be written as

$$(\Delta p_{aw})_n = \frac{1}{\sqrt{\pi}} \frac{1}{r_p S_f} \sqrt{\frac{\mu_i}{\phi c_{ti}}} \left[\begin{aligned} &+(d_{ap})_{ne+1} \sqrt{(t_a)_n} \left[1 - \sqrt{1 - \frac{(t_a)_{ne+1}}{(t_a)_n}} \right] \\ &(d_{ap})_{ne+2} \sqrt{(t_a)_n - (t_a)_{ne-1}} \\ &+ \sum_{j=ne+3}^n [(d_{ap})_j - (d_{ap})_{j-1}] \sqrt{(t_a)_n - (t_a)_{j-1}} \end{aligned} \right] + \frac{1}{2\pi} \frac{R_0}{r_p S_f} (d_{ap})_n \sqrt{\frac{t_n}{t_{ne}}} \dots\dots\dots (A-40)$$

Algebraic manipulation allows the wellbore adjusted pseudopressure difference to be written as

$$\frac{(\Delta p_{aw})_n}{(d_{ap})_n \sqrt{t_n} \sqrt{t_{ne}}} = \frac{1}{\sqrt{\pi}} \frac{1}{r_p S_f \sqrt{k}} \sqrt{\frac{\mu_i}{\phi c_{ti}}} \left[\frac{(d_{ap})_{ne+2} \left(\frac{(t_a)_n - (t_a)_{ne+1}}{t_n t_{ne}} \right)^{1/2}}{(d_{ap})_n} + \sum_{j=ne+3}^n \frac{[(d_a)_j - (d_a)_{j-1}]}{(d_a)_n} \left(\frac{(t_a)_n - (t_a)_{j-1}}{t_n t_{ne}} \right)^{1/2} + \frac{(d_{ap})_{ne+1} \sqrt{(t_a)_n}}{(d_{ap})_n \sqrt{t_n} \sqrt{t_{ne}}} \left[1 - \left(1 - \frac{(t_a)_{ne+1}}{(t_a)_n} \right)^{1/2} \right] \right] + \frac{1}{2\pi} \frac{R_0}{r_p S_f} \frac{1}{t_{ne}} \dots \dots \dots (A-41)$$

The term $(d_{ap})_{ne+1}$ can be written in an alternative form as

$$(d_{ap})_{ne+1} = \frac{S_f}{A_f} \frac{B_{gi}}{(B_g)_{ne+1}} \frac{A_f}{S_f} \frac{(B_g)_{ne+1}}{B_{gi}} (d_{ap})_{ne+1} = \frac{S_f}{A_f} \frac{B_{gi}}{(B_g)_{ne+1}} (q_{lg})_{ne+1}, \dots \dots \dots (A-42)$$

but recognizing that $[q_{lg}/B_g]_{ne} = [q_{lg}/B_g]_{ne+1}$ and $(V_L)_{ne} = (q_{lg})_{ne} t_{ne}$ allows the term $(d_{ap})_{ne+1}$ to be written as

$$(d_{ap})_{ne+1} = \frac{S_f}{t_{ne}} \frac{(B_g)_i}{(B_g)_{ne}} \frac{(V_L)_{ne}}{A_f}, \dots \dots \dots (A-43)$$

where $(V_L)_{ne}$ is the leakoff volume at the end of the injection. Define lost width due to leakoff at the end of the injection as

$$w_L = \frac{(V_L)_{ne}}{A_f}, \dots \dots \dots (A-44)$$

and the term $(d_{ap})_{ne+1}$ can be written as

$$(d_{ap})_{ne+1} = S_f w_L \frac{B_{gi}}{(B_g)_{ne}} \frac{1}{t_{ne}}, \dots \dots \dots (A-45)$$

Define

$$(y_{ap})_n = \frac{(\Delta p_{aw})_n}{(d_{ap})_n \sqrt{t_n} \sqrt{t_{ne}}}, \dots \dots \dots (A-46)$$

$$c_{ap1} = \sqrt{\frac{\mu_i}{\phi c_{ti}}}, \dots \dots \dots (A-47)$$

$$c_{ap2} = S_f w_L \frac{B_{gi}}{(B_g)_{ne}} \sqrt{\frac{\mu_i}{\phi c_{ti}}}, \dots \dots \dots (A-48)$$

$$(x_{ap})_n = \left[\begin{aligned} & c_{ap1} \left[\frac{(d_{ap})_{ne+2}}{(d_{ap})_n} \left(\frac{(t_a)_n - (t_a)_{ne+1}}{t_n t_{ne}} \right)^{1/2} \right. \\ & \left. + \sum_{j=ne+3}^n \frac{[(d_{ap})_j - (d_{ap})_{j-1}]}{(d_{ap})_n} \left(\frac{(t_a)_n - (t_a)_{j-1}}{t_n t_{ne}} \right)^{1/2} \right] \\ & \left. + \frac{c_{ap2} \sqrt{(t_a)_n}}{(d_{ap})_n \sqrt{t_n t_{ne}^{3/2}}} \left[1 - \left(1 - \frac{(t_a)_{ne+1}}{(t_a)_n} \right)^{1/2} \right] \right], \dots\dots\dots(A-49) \end{aligned} \right]$$

$$m_M = \frac{1}{\sqrt{\pi}} \frac{1}{r_p S_f \sqrt{k}}, \dots\dots\dots(A-50)$$

and

$$b_M = \frac{1}{2\pi} \frac{R_0}{r_p S_f t_{ne}}. \dots\dots\dots(A-51)$$

Combining Eq. A-41 and Eqs. A-46 through A-51 results in

$$(y_{ap})_n = m_M (x_{ap})_n + b_M, \dots\dots\dots(A-52)$$

which suggests a graph of $(y_{ap})_n$ versus $(x_{ap})_n$ using the observed fracture-injection/falloff before-closure data will result in a straight line with the slope a function of permeability and the intercept a function of fracture-face resistance. Eqs. A-50 and A-51 are used to determine permeability and fracture-face resistance from the slope and intercept of a straight-line through the observed data.

Table A-2 contains the variable definitions and plotting functions for before-closure pressure-transient analysis in terms of pressure and time and adjusted pseudopressure and time. Table A-3 contains the variable definitions and plotting functions in terms of pressure and time and adjusted pseudopressure and adjusted pseudotime.

The pressure and time and adjusted pseudopressure and time formulations require that $t_{ne} > 0$; thus, the time at shut-in cannot be scaled to zero. Time should vary from $t = 0$ to the end of the injection, $t = t_{ne}$, and to a point during the shut-in period, $t = t_n$. Adjusted pseudotime can be scaled to zero, that is $(t_a)_{ne} = 0$, in the adjusted pseudopressure and adjusted pseudotime formulation because only differences in t_a are used in the equations and $(t_a)_{ne}$ does not appear in a denominator.

Table A-2—Before-closure pressure-transient fracture-injection/falloff analysis in terms of pressure and time and adjusted pseudopressure and time.

Description	Pressure and Time	Adjusted Pseudopressure and Time
Basic Equation	$y_n = b_M + m_M x_n$	$(y_a)_n = b_M + m_M (x_a)_n$
y_n or $(y_a)_n$	$y_n = \frac{(p_w)_n - p_i}{d_n \sqrt{t_n} \sqrt{t_{ne}}}$	$(y_a)_n = \frac{(p_{aw})_n - p_{ai}}{(d_a)_n \sqrt{t_n} \sqrt{t_{ne}}}$
x_n or $(x_a)_n$	$x_n = \left[\begin{aligned} & \frac{d_{ne+2} \left(\frac{t_n - t_{ne+1}}{t_n t_{ne}} \right)^{1/2}}{d_n} \\ & + \sum_{j=ne+3}^n \frac{[d_j - d_{j-1}] \left(\frac{t_n - t_{j-1}}{t_n t_{ne}} \right)^{1/2}}{d_n} \\ & + \frac{c_2}{d_n t_{ne}^{3/2}} \left[1 - \left(\frac{t_{ne+1}}{t_n} \right)^{1/2} \right] \end{aligned} \right]$	$(x_a)_n = \left[\begin{aligned} & \frac{(d_a)_{ne+2} \left(\frac{t_n - t_{ne+1}}{t_n t_{ne}} \right)^{1/2}}{(d_a)_n} \\ & + \sum_{j=ne+3}^n \frac{[(d_a)_j - (d_a)_{j-1}] \left(\frac{t_n - t_{j-1}}{t_n t_{ne}} \right)^{1/2}}{(d_a)_n} \\ & + \frac{c_{a2}}{(d_a)_n t_{ne}^{3/2}} \left[1 - \left(\frac{t_{ne+1}}{t_n} \right)^{1/2} \right] \end{aligned} \right]$
d_j or $(d_a)_j$	$d_j = \frac{p_{j-1} - p_j}{t_j - t_{j-1}}$	$(d_a)_j = \frac{(\mu_g)_j}{(\mu_g)_i} \left[\frac{(p_a)_{j-1} - (p_a)_j}{t_j - t_{j-1}} \right]$
c_1 or c_{a1}	$c_1 = \sqrt{\frac{\mu}{\phi c_t}}$	$c_{a1} = \sqrt{\frac{\mu_i}{\phi c_{ti}}}$
c_2 or c_{a2}	$c_2 = S_f w_L \sqrt{\frac{\mu}{\phi c_t}}$	$c_{a2} = S_f w_L \frac{B_{gi}}{(B_g)_{ne}} \sqrt{\frac{\mu_i}{\phi c_{ti}}}$
b_M	$b_M = \frac{1}{2\pi} \frac{R_0}{r_p S_f} \frac{1}{t_{ne}}$	$b_M = \frac{1}{2\pi} \frac{R_0}{r_p S_f} \frac{1}{t_{ne}}$
m_M	$m_M = \frac{1}{\sqrt{\pi}} \frac{1}{r_p S_f \sqrt{k}}$	$m_M = \frac{1}{\sqrt{\pi}} \frac{1}{r_p S_f \sqrt{k}}$

Table A-3—Before-closure pressure-transient fracture-injection/falloff analysis in terms of pressure and time and adjusted pseudopressure and adjusted pseudotime.

Description	Pressure and Time	Adjusted Pseudopressure and Adjusted Pseudotime
Basic Equation	$y_n = b_M + m_M x_n$	$(y_{ap})_n = b_M + m_M (x_{ap})_n$
y_n or $(y_{ap})_n$	$y_n = \frac{(p_w)_n - p_i}{d_n \sqrt{t_n} \sqrt{t_{ne}}}$	$(y_{ap})_n = \frac{(p_{aw})_n - p_{ai}}{(d_{ap})_n \sqrt{t_n} \sqrt{t_{ne}}}$
x_n or $(x_{ap})_n$	$x_n = \left[\begin{array}{l} \frac{d_{ne+2} (t_n - t_{ne+1})^{1/2}}{d_n (t_n t_{ne})} \\ + \sum_{j=ne+3}^n \frac{[d_j - d_{j-1}] (t_n - t_{j-1})^{1/2}}{d_n (t_n t_{ne})} \\ + \frac{c_2}{d_n t_{ne}^{3/2}} \left[1 - \left(1 - \frac{t_{ne+1}}{t_n} \right)^{1/2} \right] \end{array} \right]$	$(x_{ap})_n = \left[\begin{array}{l} \frac{(d_{ap})_{ne+2} [(t_a)_n - (t_a)_{ne+1}]^{1/2}}{(d_{ap})_n (t_n t_{ne})} \\ + \sum_{j=ne+3}^n \frac{[(d_{ap})_j - (d_{ap})_{j-1}] [(t_a)_n - (t_a)_{j-1}]^{1/2}}{(d_{ap})_n (t_n t_{ne})} \\ + \frac{c_{ap2} (t_a)_n^{1/2}}{(d_{ap})_n t_{ne}^{3/2}} \left[1 - \left(1 - \frac{(t_a)_{ne+1}}{(t_a)_n} \right)^{1/2} \right] \end{array} \right]$
d_j or $(d_{ap})_j$	$d_j = \frac{p_{j-1} - p_j}{t_j - t_{j-1}}$	$(d_{ap})_j = \frac{(c_t)_i}{(c_t)_j} \left[\frac{(p_a)_{j-1} - (p_a)_j}{(t_a)_j - (t_a)_{j-1}} \right]$
c_1 or c_{ap1}	$c_1 = \sqrt{\frac{\mu}{\phi c_t}}$	$c_{ap1} = \sqrt{\frac{\mu_i}{\phi c_{ti}}}$
c_2 or c_{ap2}	$c_2 = S_f w_L \sqrt{\frac{\mu}{\phi c_t}}$	$c_{ap2} = S_f w_L \frac{B_{gi}}{(B_g)_{ne}} \sqrt{\frac{\mu_i}{\phi c_{ti}}}$
b_M	$b_M = \frac{1}{2\pi} \frac{R_0}{r_p S_f} \frac{1}{t_{ne}}$	$b_M = \frac{1}{2\pi} \frac{R_0}{r_p S_f} \frac{1}{t_{ne}}$
m_M	$m_M = \frac{1}{\sqrt{\pi}} \frac{1}{r_p S_f \sqrt{k}}$	$m_M = \frac{1}{\sqrt{\pi}} \frac{1}{r_p S_f \sqrt{k}}$

APPENDIX B

CONSTANT-RATE DRAWDOWN SOLUTIONS ACCOUNTING FOR BEFORE- AND AFTER-CLOSURE FRACTURE STORAGE

Assume a slightly compressible fluid fills the wellbore and a fracture in an infinite-slab reservoir and the initial reservoir pressure is constant throughout the reservoir and sufficient for fracture dilation. As a drawdown begins, the fracture will contract until closure. A mass balance equation is written for the before-closure drawdown as

$$\underbrace{q_{sf} B_r \rho_r}_{m_{in}} - \underbrace{q_w B \rho}_{m_{out}} = \overbrace{V_w \frac{d\rho_w}{dt} + 2 \frac{d(V_f \rho_f)}{dt}}^{\text{Storage}}, \dots \dots \dots (B-1)$$

where q_{sf} is the sandface flow rate into the fracture from the reservoir, and V_f is the fracture volume.

The material balance equation can be expanded using the product rule and written as

$$q_{sf} B_r \rho_r - q_w B \rho = V_w \frac{d\rho_w}{dt} + 2V_f \frac{d\rho_f}{dt} + 2\rho_f \frac{dV_f}{dt}. \dots \dots \dots (B-2)$$

The derivative with respect to time of the wellbore fluid density is written using the chain rule as

$$\frac{d\rho_w}{dt} = \rho_w \frac{1}{\rho_w} \frac{d\rho_w}{dp_w} \frac{dp_w}{dt} = \rho_w c_w \frac{dp_w}{dt}, \dots \dots \dots (B-3)$$

where c_w is the isothermal wellbore fluid compressibility. Assuming the wellbore and fracture pressure are equal, $p_w = p_f$, the derivative with respect to time of the density of the fluid filling the fracture is written as

$$\frac{d\rho_f}{dt} = \rho_f c_f \frac{dp_w}{dt}, \dots \dots \dots (B-4)$$

where c_f is the isothermal compressibility of the fluid filling the fracture.

The material balance equation can now be written as

$$q_{sf} B_r \rho_r - q_w B \rho = \left(\rho_w c_w V_w + 2\rho_f c_f V_f + 2\rho_f \frac{dV_f}{dp_w} \right) \frac{dp_w}{dt}, \dots \dots \dots (B-5)$$

or assuming a constant density, $\rho = \rho_w = \rho_f = \rho_r$, and a constant formation volume factor, $B = B_r$, the material balance equation is written as

$$q_{sf} = q_w + \frac{1}{B} \left(c_w V_w + 2c_f V_f + 2 \frac{dV_f}{dp_w} \right) \frac{dp_w}{dt}. \dots \dots \dots (B-6)$$

Define dimensionless pressure as

$$p_{wD} = \frac{2\pi kh(p_i - p_w(t))}{qB\mu}, \dots \dots \dots (B-7)$$

dimensionless time as

$$t_{L_f D} = \frac{kt}{\phi \mu c_t L_f^2}, \dots\dots\dots (B-8)$$

and dimensionless flow rate as

$$q_D = \frac{q_{sf}}{q_w}, \dots\dots\dots (B-9)$$

where q_w is the well production rate. With the dimensionless variables, the material balance equation during the before-closure drawdown is written as

$$q_D = q_{wD} - \frac{C_{bc}}{2\pi\phi c_t h L_f^2} \frac{dp_{wD}}{dt_{L_f D}}, \dots\dots\dots (B-10)$$

where the before-closure fracture storage coefficient is written as

$$C_{bc} = c_w V_w + 2c_f V_f + 2 \frac{dV_f}{dp_w}. \dots\dots\dots (B-11)$$

Define a dimensionless before-closure fracture storage coefficient as

$$C_{bcD} = \frac{C_{bc}}{2\pi\phi c_t h L_f^2}, \dots\dots\dots (B-12)$$

and the dimensionless material balance equation during a drawdown with a closing hydraulic fracture is written as

$$q_D = q_{wD} - C_{bcD} \frac{dp_{wD}}{dt_{L_f D}}. \dots\dots\dots (B-13)$$

Constant-Rate Drawdown With Constant Before- and Constant After-Closure Storage

During a constant-rate drawdown with a constant fracture half-length, the fracture volume is written as

$$V_f = h_f L_f \hat{w}_f(p_w(t)) = A_f \hat{w}_f(p_w(t)). \dots\dots\dots (B-14)$$

The average fracture width, \hat{w}_f , is a function of net pressure, $p_n = p_w(t) - p_c$, and is written as

$$\hat{w}_f = \frac{p_n}{S_f} = \frac{p_w(t) - p_c}{S_f}, \dots\dots\dots (B-15)$$

where p_c is the fracture closure stress and S_f is the fracture "stiffness." Fracture stiffness, or the inverse of fracture compliance, is defined by the elastic energy or "strain energy" created by an open fracture in a rock assuming linear elastic theory is applicable. **Table B-1** contains the fracture stiffness definitions for three common 2D fracture models.^{80,100} In Table B-1, E' is the plane-strain modulus, R_f is the fracture radius of a radial fracture, h_f is the gross fracture height, and L_f is the fracture half-length.

The derivative of average fracture width with respect to pressure is written as

$$\frac{d\hat{w}_f}{dp_w} = \frac{1}{S_f} \dots\dots\dots (B-16)$$

Table A-1—Fracture stiffness for 2D fracture models.^{80,100}

Radial	Perkins-Kern-Nordgren Vertical Plane Strain	Geertsma-deKlerk Horizontal Plane Strain
$(S_f)_{RAD} = \frac{3\pi E'}{16R_f}$	$(S_f)_{PKN} = \frac{2E'}{\pi h_f}$	$(S_f)_{GDK} = \frac{E'}{\pi L_f}$

A before-closure dilating-fracture storage coefficient can now be written as

$$C_{fd} = c_w V_w + 2 \frac{A_f}{S_f} (c_f p_n + 1) \dots\dots\dots (B-17)$$

Hagoort,¹⁰¹ and other investigators of waterflood induced fractures that followed,⁹⁰⁻⁹³ assume that

$$c_f p_n(t) + 1 \cong 1, \dots\dots\dots (B-18)$$

and the before-closure fracture storage coefficient can be written as

$$C_{bc} = c_w V_w + 2 \frac{A_f}{S_f} \dots\dots\dots (B-19)$$

After fracture closure, and assuming the fracture closes to a constant residual width, the material balance equation is again written as

$$\frac{m_{in}}{q_{sf} B_r \rho_r} - \frac{m_{out}}{q B \rho} = V_w \frac{d\rho_w}{dt} + \overbrace{2 \frac{d(V_f \rho_f)}{dt}}^{\text{Storage}}, \dots\dots\dots (B-20)$$

which is simplified and written as

$$q_{sf} = q + \frac{1}{B} \left(c_w V_w + 2c_f V_f + 2 \frac{dV_f}{dp_w} \right) \frac{dp_w}{dt}, \dots\dots\dots (B-21)$$

but the fracture volume is constant, and an after-closure constant storage coefficient is written as

$$C_{ac} = c_w V_w + 2c_f V_{fr}, \dots\dots\dots (B-22)$$

where V_{fr} is the residual fracture volume at closure. In some cases, no residual volume will remain after-closure, and $C_{ac} = c_w V_w$. After converting to dimensionless variables, the material balance equation is written as

$$q_D = q_{wD} - C_{acD} \frac{dp_{wD}}{dt_{LjD}}, \dots\dots\dots (B-23)$$

where the dimensionless after-closure wellbore storage coefficient is written as

$$C_{acD} = \frac{C_{ac}}{2\pi\phi c_t h L_f^2} \dots\dots\dots (B-24)$$

A material balance equation valid at all times for a constant-rate drawdown with a closing fracture and constant after-closure storage is written using the unit-step function,⁶² which is defined as

$$U_a = \begin{cases} 0 & , t < a \\ 1 & , t > a \end{cases} \dots\dots\dots (B-25)$$

Following the technique of Correa and Ramey,⁶²⁻⁶⁴ a dimensionless material balance equation is written as

$$q_D = \left(1 - U(t_c)_{LjD}\right) \left(q_{wD} - C_{bcD} \frac{dp_{wD}}{dt_{LjD}}\right) + U(t_c)_{LjD} \left(q_{wD} - C_{acD} \frac{dp_{wD}}{dt_{LjD}}\right), \dots\dots\dots (B-26)$$

where $(t_c)_{LjD}$ is the dimensionless fracture closure time. The material balance equation can be expanded and written as

$$q_D = q_{wD} - C_{bcD} \frac{dp_{wD}}{dt_{LjD}} + U(t_c)_{LjD} (C_{bcD} - C_{acD}) \frac{dp_{wD}}{dt_{LjD}} \dots\dots\dots (B-27)$$

With the identities of Correa and Ramey,⁶² the Laplace transform of the material balance equation is written as

$$\bar{q}_D = \frac{q_{wD}}{s} - s C_{acD} \bar{p}_{wD} - (C_{bcD} - C_{acD}) \int_0^{(t_c)_{LjD}} e^{-st_{LjD}} p'_{wD}(t_{LjD}) dt_{LjD} \dots\dots\dots (B-28)$$

A solution is developed by applying the superposition principle, which is written as

$$p_{wD} = \int_0^{t_{LjD}} q_D(\tau_D) \frac{dp_D(t_{LjD} - \tau_D)}{dt_{LjD}} d\tau_D \dots\dots\dots (B-29)$$

The initial condition in the fracture and reservoir requires a constant initial pressure, $p_D(t_{LjD}) = 0$, and with the initial condition, the Laplace transform of the superposition integral is written as

$$\bar{p}_{wD} = \bar{q}_D s \bar{p}_D \Leftrightarrow \bar{q}_D = \frac{\bar{p}_{wD}}{s \bar{p}_D} \dots\dots\dots (B-30)$$

Combining the transformed material balance equation and superposition integral results in

$$\bar{p}_{wD} \left(1 + s^2 C_{acD} \bar{p}_D\right) = q_{wD} \bar{p}_D - (C_{bcD} - C_{acD}) s \bar{p}_D \int_0^{(t_c)_{LjD}} e^{-st_{LjD}} p'_{wD}(t_{LjD}) dt_{LjD} \dots\dots\dots (B-31)$$

Let the Laplace domain dimensionless solution for a well produced through a fracture at a constant rate with constant after-closure storage be written as

$$\bar{p}_{acD} = \frac{\bar{p}_{fD}}{1 + s^2 C_{acD} \bar{p}_{fD}}, \dots\dots\dots(B-32)$$

where p_{fD} is either the infinite- or finite-conductivity fracture solution. The wellbore solution is written in the Laplace domain solution as

$$\bar{p}_{wD} = q_{wD} \bar{p}_{acD} - (C_{bcD} - C_{acD}) s \bar{p}_{acD} \int_0^{(t_c)_{LjD}} e^{-st_{LjD}} p'_{wD}(t_{LjD}) dt_{LjD} \dots\dots\dots(B-33)$$

Inverting the Laplace domain solution back to the time domain with $q_{wD} = 1$ results in the constant-rate drawdown solution with constant before-closure and constant after-closure storage written as

$$p_{wcD}(t_{LjD}) = p_{acD}(t_{LjD}) - (C_{bcD} - C_{acD}) \int_0^{(t_c)_{LjD}} p'_{acD}(t_{LjD} - \tau_D) p'_{wcD}(\tau_D) d\tau_D \dots\dots\dots(B-34)$$

where p_{wcD} denotes that the pressure solution is for a constant rate.

Constant-Rate Drawdown With Constant Before- and Constant After-Closure Storage With Fracture-Face and Choked-Fracture Skin

Consider a constant-rate drawdown in a reservoir with a damaged hydraulic fracture where the initial reservoir pressure is constant throughout and sufficient for fracture dilation. The drawdown is modeled with constant before-closure storage, constant after-closure storage, choked-fracture skin, and fracture-face skin. Developing a dimensionless pressure solution requires solving the problem in a serial fashion⁹⁴ – the wellbore solution with choked-fracture skin is formulated and coupled to the solution in the fracture outside of the wellbore with fracture-face skin.

The dimensionless material balance equation considering wellbore storage is written as

$$q_D = q_{wD} - C_D \frac{dp_{wD}}{dt_{LjD}} \dots\dots\dots(B-35)$$

The superposition integral is written as

$$p_{wD} = \int_0^{t_{LjD}} q_D(\tau_D) \frac{dp_D(t_{LjD} - \tau_D)}{dt_{LjD}} d\tau_D \dots\dots\dots(B-36)$$

and a “reservoir” pressure solution, $p_D(t_{LjD})$, is written as

$$p_D(t_{LjD}) = p_{wfD}(t_{LjD}) + (S_{fs})_{ch} \dots\dots\dots(B-37)$$

where p_{wfD} is the solution in the fracture outside of the wellbore considering before- and after-closure storage, and $(S_{fs})_{ch}$ is the choked-fracture skin.

The superposition integral is written in the Laplace domain as

$$\bar{p}_{wD} = \bar{q}_D s \bar{p}_D \dots\dots\dots(B-38)$$

and the Laplace domain reservoir pressure solution is written as

$$\bar{p}_D = \bar{p}_{wfD} + \frac{(S_{fs})ch}{s} \dots\dots\dots(B-39)$$

The transformed material balance equation is written as

$$\bar{q}_D = \frac{q_{wD}}{s} - sC_D \bar{p}_{wD} \dots\dots\dots(B-40)$$

Combining the superposition integral, the reservoir pressure solution, and the material balance equation in the Laplace domain results in

$$\bar{p}_{wD} = q_{wD} \bar{p}_D - s^2 C_{acD} \bar{p}_{wD} \bar{p}_D, \dots\dots\dots(B-41)$$

which with $q_{wD} = 1$, is written as

$$\bar{p}_{wD} = \frac{s\bar{p}_{wfD} + (S_{fs})ch}{s \left[1 + sC_D \left[s\bar{p}_{wfD} + (S_{fs})ch \right] \right]} \dots\dots\dots(B-42)$$

The solution outside of the wellbore in the fracture accounting for before- and after-closure storage and fracture-face skin is developed using the unit-step function. The dimensionless before-closure material balance equation is written as

$$q_D = q_{wD} - C_{fbcD} \frac{dp_{wfD}}{dt_{LfD}}, \dots\dots\dots(B-43)$$

and the dimensionless after-closure material balance equation is written as

$$q_D = q_{wD} - C_{facD} \frac{dp_{wfD}}{dt_{LfD}}, \dots\dots\dots(B-44)$$

where the dimensionless before-closure fracture storage is written as

$$C_{fbcD} = \frac{C_{fbc}}{2\pi\phi_c h L_f^2}, \dots\dots\dots(B-45)$$

and the before-closure fracture storage is defined as

$$C_{fbc} = 2c_f V_f + 2 \frac{A_f}{S_f} \dots\dots\dots(B-46)$$

The after-closure fracture storage is defined as

$$C_{fac} = 2c_f V_{fr}, \dots\dots\dots(B-47)$$

and the dimensionless after-closure fracture storage is written as

$$C_{facD} = \frac{C_{fac}}{2\pi\phi_c h L_f^2} \dots\dots\dots(B-48)$$

A dimensionless material balance equation valid at all times is written as

$$q_D = \left(1 - U(t_c)_{LjD}\right) \left(q_{wD} - C_{fbcD} \frac{dp_{wfD}}{dt_{LjD}} \right) + U(t_c)_{LjD} \left(q_{wD} - C_{facD} \frac{dp_{wfD}}{dt_{LjD}} \right), \dots\dots\dots(B-49)$$

or written as

$$q_D = q_{wD} - C_{fbcD} \frac{dp_{wfD}}{dt_{LjD}} + U(t_c)_{LjD} \left(C_{fbcD} - C_{facD} \right) \frac{dp_{wfD}}{dt_{LjD}}, \dots\dots\dots(B-50)$$

The Laplace transform of the dimensionless material balance equation is written as

$$\bar{q}_D = \left[\begin{aligned} &\frac{q_{wD}}{s} - C_{fbcD} s \bar{p}_{wfD} + C_{fbcD} p_{wfD}(0) + (C_{fbcD} - C_{facD}) \left[s \bar{p}_{wfD} - p_{wfD}(0) \right] \\ &- (C_{fbcD} - C_{facD}) \int_0^{(t_c)_{LjD}} e^{-st_{LjD}} p'_{wfD}(t_{LjD}) dt_{LjD} \end{aligned} \right] \dots\dots\dots(B-51)$$

With $p_{wfD}(0) = 0$, the dimensionless material balance equation is written as

$$\bar{q}_D = \frac{q_{wD}}{s} - C_{facD} s \bar{p}_{wfD} - (C_{fbcD} - C_{facD}) \int_0^{(t_c)_{LjD}} e^{-st_{LjD}} p'_{wfD}(t_{LjD}) dt_{LjD} \dots\dots\dots(B-52)$$

Combining the transformed material balance equation with the Laplace domain superposition integral results in

$$\bar{p}_{wfD} = \left[\begin{aligned} &q_{wD} \bar{p}_{fsD} - s^2 C_{facD} \bar{p}_{fsD} \bar{p}_{wfD} \\ &- (C_{fbcD} - C_{facD}) s \bar{p}_{fsD} \int_0^{(t_c)_{LjD}} e^{-st_{LjD}} p'_{wfD}(t_{LjD}) dt_{LjD} \end{aligned} \right], \dots\dots\dots(B-53)$$

which can be written as

$$\bar{p}_{wfD} = q_{wD} \bar{p}_{facD} - (C_{fbcD} - C_{facD}) s \bar{p}_{facD} \int_0^{(t_c)_{LjD}} e^{-st_{LjD}} p'_{wfD}(t_{LjD}) dt_{LjD}, \dots\dots\dots(B-54)$$

where p_{facD} is the solution for a finite- or infinite-conductivity fracture with fracture-face skin and constant after-closure storage, which is written in the Laplace domain as

$$\bar{p}_{facD} = \frac{\bar{p}_{fsD}}{1 + s^2 C_{facD} \bar{p}_{fsD}} \dots\dots\dots(B-55)$$

With fracture-face skin, the Laplace domain dimensionless fracture-sandface pressure solution is written as

$$\bar{p}_{fsD} = \bar{p}_{fD} + \frac{S_{fs}}{s}, \dots\dots\dots(B-56)$$

and the dimensionless fracture-sandface pressure with fracture-face skin and constant after-closure storage is written in the Laplace domain as

$$\bar{p}_{facD} = \frac{s \bar{p}_{fD} + S_{fs}}{s \left[1 + s C_{facD} \left[s \bar{p}_{fD} + S_{fs} \right] \right]} \dots\dots\dots(B-57)$$

Inverting the dimensionless pressure solution outside of the wellbore in the fracture to the time domain with $q_{wD} = 1$ results in

$$p_{wfD}(t_{LfD}) = p_{facD}(t_{LfD}) - (C_{fbcD} - C_{facD}) \int_0^{(t_c)_{LfD}} p'_{facD}(t_{LfD} - \tau_D) p'_{wfD}(\tau_D) d\tau_D \dots\dots\dots (B-58)$$

The dimensionless pressure solution for a constant-rate drawdown with constant before-closure storage, constant after-closure storage, fracture-face skin, and choked-fracture skin requires solving the time domain solution first for pressure in the fracture outside of the wellbore (Eq. B-58). With the time domain solution, the Laplace domain solutions, Eqs. B-42 and B-54, can be evaluated and numerically inverted to the time domain to obtain the dimensionless wellbore pressure.

Constant-Rate Drawdown With Constant Before-Closure Storage, Constant After-Closure Wellbore Storage, and After-Closure Radial Flow With Skin

Consider a constant-rate drawdown in a well with an open hydraulic fracture that closes with little or no remaining conductivity where the before-closure reservoir response during a drawdown is modeled as a hydraulically fractured system, but the after-closure reservoir response is modeled as a radial system.

The dimensionless material balance equation with constant before- and constant after-closure storage is written as

$$q_D = \left[\begin{array}{l} q_{wD} - U(t_c)_{LfD} q_{wD} - C_{bcD} \frac{dp_{wD}}{dt_{LfD}} + U(t_c)_{LfD} C_{bcD} \frac{dp_{wD}}{dt_{LfD}} \\ + U(t_c)_{LfD} q_{wD} - U(t_c)_{LfD} C_{acD} \frac{dp_{wD}}{dt_{LfD}} \end{array} \right], \dots\dots\dots (B-59)$$

but the fracture has negligible volume after fracture closure and the dimensionless after-closure wellbore storage coefficient is written as

$$C_{acD} = \frac{c_w V_w}{2\pi\phi c_t h L_f^2} = C_D \dots\dots\dots (B-60)$$

The dimensionless wellbore pressure is written as the sum of the effects of both reservoir models,¹⁰² that is, the solution is written as

$$p_{wD} = \int_0^{t_{LfD}} q_{fD}(\tau_D) \frac{dp_{fD}(t_{LfD} - \tau_D)}{dt_{LfD}} d\tau_D + \int_0^{t_{LfD}} q_{rD}(\tau_D) \frac{dp_{sD}(t_{LfD} - \tau_D)}{dt_{LfD}} d\tau_D, \dots\dots\dots (B-61)$$

where q_{fD} is the before-closure dimensionless flow rate for the hydraulically fractured system, and p_{fD} is the dimensionless reservoir solution for a well with a fixed-length fracture. The after-closure dimensionless flow rate, q_{rD} , is for the radial system, and the dimensionless radial flow reservoir solution with skin, p_{sD} , is written as

$$p_{sD}(t_{LfD}) = p_{rD}(t_{LfD}) + S, \dots\dots\dots (B-62)$$

where p_{rD} is the dimensionless reservoir solution, and S is the skin effect. Note that dimensionless time is defined in terms fracture half-length; thus, fracture half-length is the characteristic length used in the dimensionless radius definition and radial solution.

The dimensionless material balance can also be written in terms of before-closure and after-closure components as

$$q_D = q_{fD} + q_{rD}, \dots\dots\dots(B-63)$$

where the flow rate for a fixed-length closing fracture is written as

$$q_{fD} = q_{wD} - U_{(t_c)_{LjD}} q_{wD} - C_{bcD} \frac{dp_{wD}}{dt_{LjD}} + U_{(t_c)_{LjD}} C_{bcD} \frac{dp_{wD}}{dt_{LjD}}, \dots\dots\dots(B-64)$$

and the dimensionless after-closure radial flow rate is written as

$$q_{rD} = U_{(t_c)_{LjD}} q_{wD} - U_{(t_c)_{LjD}} C_{acD} \frac{dp_{wD}}{dt_{LjD}}. \dots\dots\dots(B-65)$$

However, the components of the material balance equation are also valid for all time for the specific flow models, and the sum of the superposition integrals and dimensionless flow rate equations can be transformed to the Laplace domain and combined as

$$\bar{p}_{wD} = \left[\begin{array}{l} q_{wD} \bar{p}_{fD} - q_{wD} \bar{p}_{fD} e^{-s(t_c)_{LjD}} + q_{wD} \bar{p}_{sD} e^{-s(t_c)_{LjD}} \\ -C_{acD} s^2 \bar{p}_{rD} \bar{p}_{wD} \\ -C_{bcD} s \bar{p}_{fD} \int_0^{(t_c)_{LjD}} e^{-st_{LjD}} p'_{wD}(t_{LjD}) dt_{LjD} \\ +C_{acD} s \bar{p}_{sD} \int_0^{(t_c)_{LjD}} e^{-st_{LjD}} p'_{wD}(t_{LjD}) dt_{LjD} \end{array} \right] \dots\dots\dots(B-66)$$

After inverting to the time domain, the dimensionless pressure solution is written as

$$p_{wcD}(t_{LjD}) = \left[\begin{array}{l} q_{wD} \left[p_{fD}(t_{LjD}) - p_{fD}(t_{LjD} - (t_c)_{LjD}) + p_{sD}(t_{LjD} - (t_c)_{LjD}) \right] \\ -C_{acD} \int_0^{t_{LjD}} p'_{sD}(t_{LjD} - \tau_D) p'_{wcD}(\tau_D) d\tau_D \\ -C_{bcD} \int_0^{(t_c)_{LjD}} p'_{fD}(t_{LjD} - \tau_D) p'_{wcD}(\tau_D) d\tau_D \\ +C_{acD} \int_0^{(t_c)_{LjD}} p'_{sD}(t_{LjD} - \tau_D) p'_{wcD}(\tau_D) d\tau_D \end{array} \right], \dots\dots\dots(B-67)$$

and after simplifying, the pressure solution for a constant-rate drawdown with $q_{wD} = 1$, constant before-closure fracture storage, constant after-closure wellbore storage, and after-closure radial flow is written as

$$p_{wcD}(t_{LjD}) = \left[\begin{array}{l} p_{fD}(t_{LjD}) - p_{fD}(t_{LjD} - (t_c)_{LjD}) + p_{sD}(t_{LjD} - (t_c)_{LjD}) \\ -C_{acD} \int_{(t_c)_{LjD}}^{t_{LjD}} p'_{sD}(t_{LjD} - \tau_D) p'_{wcD}(\tau_D) d\tau_D \\ -C_{bcD} \int_0^{(t_c)_{LjD}} p'_{fD}(t_{LjD} - \tau_D) p'_{wcD}(\tau_D) d\tau_D \end{array} \right] \dots\dots\dots (B-68)$$

APPENDIX C

FRACTURE-INJECTION/FALLOFF SOLUTIONS IN A RESERVOIR WITHOUT A PRE-EXISTING FRACTURE

Assume a slightly compressible fluid fills the wellbore and a fracture and is injected at a constant rate and at a pressure sufficient to create a new hydraulic fracture or dilate an existing fracture. A mass balance during a fracture injection is written as

$$\underbrace{q_w B \rho}_{m_{in}} - \underbrace{q_\ell B_r \rho_r}_{m_{out}} = \overbrace{V_w \frac{d\rho_w}{dt} + 2 \frac{d(V_f \rho_f)}{dt}}^{\text{Storage}}, \dots\dots\dots (C-1)$$

where q_ℓ is the fluid leakoff rate into the reservoir from the fracture, $q_\ell = q_{sf}$, and V_f is the fracture volume.

The material balance equation can be expanded using the product rule and written as

$$q_w B \rho - q_{sf} B_r \rho_r = V_w \frac{d\rho_w}{dt} + 2V_f \frac{d\rho_f}{dt} + 2\rho_f \frac{dV_f}{dt}. \dots\dots\dots (C-2)$$

The derivative with respect to time of the wellbore fluid density is written using the chain rule as

$$\frac{d\rho_w}{dt} = \rho_w \frac{1}{\rho_w} \frac{d\rho_w}{dp_w} \frac{dp_w}{dt} = \rho_w c_w \frac{dp_w}{dt}, \dots\dots\dots (C-3)$$

where c_w is the isothermal wellbore fluid compressibility. Assuming the wellbore and fracture pressure are equal, $p_w = p_f$, the derivative with respect to time of the density of the fluid filling the fracture is written as

$$\frac{d\rho_f}{dt} = \rho_f c_f \frac{dp_w}{dt}, \dots\dots\dots (C-4)$$

where c_f is the isothermal compressibility of the fluid filling the fracture.

The material balance equation can now be written as

$$q_w B \rho - q_{sf} B_r \rho_r = \left(\rho_w c_w V_w + 2\rho_f c_f V_f + 2\rho_f \frac{dV_f}{dp_w} \right) \frac{dp_w}{dt}, \dots\dots\dots (C-5)$$

or assuming a constant density, $\rho = \rho_w = \rho_f = \rho_r$, and a constant formation volume factor, $B = B_r$, the material balance equation is written as

$$q_{sf} = q_w - \frac{1}{B} \left(c_w V_w + 2c_f V_f + 2 \frac{dV_f}{dp_w} \right) \frac{dp_w}{dt}. \dots\dots\dots (C-6)$$

The dimensionless wellbore pressure for a fracture-injection/falloff is written as

$$p_{wsD}(t_{LFD}) = \frac{p_w(t_{LFD}) - p_i}{p_0 - p_i}, \dots\dots\dots (C-7)$$

where p_i is the initial reservoir pressure and p_0 is an arbitrary reference pressure. At time zero, the wellbore pressure is increased to the “opening” pressure, p_{w0} , which is generally set equal to p_0 , and the dimensionless wellbore pressure at time zero is written as

$$p_{wsD}(0) = \frac{p_{w0} - p_i}{p_0 - p_i} \dots\dots\dots (C-8)$$

Define dimensionless time as

$$t_{LjD} = \frac{kt}{\phi\mu c_t L_f^2}, \dots\dots\dots (C-9)$$

where L_f is the fracture half-length at the end of pumping. The dimensionless reservoir flow rate is defined as

$$q_{sD} = \frac{q_{sf} B\mu}{2\pi kh(p_0 - p_i)}, \dots\dots\dots (C-10)$$

and the dimensionless well flow rate is defined as

$$q_{wsD} = \frac{q_w B\mu}{2\pi kh(p_0 - p_i)}, \dots\dots\dots (C-11)$$

where q_w is the well injection rate. With the dimensionless variables, the material balance equation during an injection is written as

$$q_{sD} = q_{wsD} - \frac{C_{pf}}{2\pi\phi c_t h L_f^2} \frac{dp_{wsD}}{dt_{LjD}}, \dots\dots\dots (C-12)$$

where the propagating-fracture storage coefficient is written as

$$C_{pf} = c_w V_w + 2c_f V_f + 2 \frac{dV_f}{dp_w} \dots\dots\dots (C-13)$$

Define a dimensionless propagating-fracture storage coefficient as

$$C_{pfD} = \frac{C_{pf}}{2\pi\phi c_t h L_f^2}, \dots\dots\dots (C-14)$$

and the dimensionless material balance equation during an injection at a pressure sufficient to create or dilate a hydraulic fracture is written as

$$q_{sD} = q_{wsD} - C_{pfD} \frac{dp_{wsD}}{dt_{LjD}} \dots\dots\dots (C-15)$$

Solution Accounting for a Dilating Fracture, Before-Closure Storage, and After-Closure Storage

Consider a fracture-injection/falloff test with the entire fracture length developed instantaneously when the injection begins or with a pre-existing fracture. The injection is at a pressure in excess of the minimum in-

situ stress, and fracture volume changes are a function of fracture width – which is a function of pressure during the injection and before-closure pressure falloff.

During a constant rate injection with a constant fracture length, the fracture volume is written as

$$V_f = h_f L_f \hat{w}_f(p_w(t)) = A_f \hat{w}_f(p_w(t)) \dots\dots\dots (C-16)$$

The average fracture width, $\hat{w}_f(p_w(t))$, is a function of net pressure,⁸⁰ $p_n = p_w(t) - p_c$, and is written as

$$\hat{w}_f = \frac{p_n}{S_f} = \frac{p_w(t) - p_c}{S_f}, \dots\dots\dots (C-17)$$

where p_c is the fracture closure stress and S_f is the fracture "stiffness." Fracture stiffness, or the inverse of fracture compliance, is defined by the elastic energy or "strain energy" created by an open fracture in a rock assuming linear elastic theory is applicable. **Table C-1** contains the fracture stiffness definitions for three common 2D fracture models.^{80,100} In Table C-1, E' is the plane-strain modulus, R_f is the fracture radius of a radial fracture, h_f is the gross fracture height, and L_f is the fracture half-length.

Table C-1—Fracture stiffness for 2D fracture models.^{80,100}

Radial	Perkins-Kern-Nordgren Vertical Plane Strain	Geertsma-deKlerk Horizontal Plane Strain
$(S_f)_{RAD} = \frac{3\pi E'}{16R_f}$	$(S_f)_{PKN} = \frac{2E'}{\pi h_f}$	$(S_f)_{GDK} = \frac{E'}{\pi L_f}$

The derivative of average fracture width with respect to pressure is written as

$$\frac{d\hat{w}_f}{dp_w} = \frac{1}{S_f} \dots\dots\dots (C-18)$$

A dilated-fracture storage coefficient can now be written as

$$C_{fd} = c_w V_w + 2 \frac{A_f}{S_f} (c_f p_n + 1) \dots\dots\dots (C-19)$$

Hagoort,¹⁰¹ and other investigators of waterflood induced fractures that followed,⁹⁰⁻⁹³ assume that

$$c_f p_n(t) + 1 \cong 1, \dots\dots\dots (C-20)$$

which is also a reasonable approximation for a fracture-injection/falloff test, and the dilating-fracture storage coefficient can be written as

$$C_{fd} = c_w V_w + 2 \frac{A_f}{S_f}, \dots\dots\dots (C-21)$$

which is constant and no longer a function of pressure. The dilating-fracture storage coefficient can be written in dimensionless form as

$$C_{fdD} = \frac{C_{fd}}{2\pi\phi c_t h L_f^2}, \dots\dots\dots (C-22)$$

and the dimensionless material balance during an injection with a dilating fracture of fixed length is written as

$$q_{sD} = q_{wsD} - C_{fdD} \frac{dp_{wsD}}{dt L_f D}. \dots\dots\dots (C-23)$$

Following the injection, the falloff portion of the test begins, and a before-closure mass balance is written as

$$\underbrace{m_{in}}_{q_w B \rho} - \underbrace{m_{out}}_{q_\ell B_r \rho_r} = \overbrace{V_w \frac{d\rho_w}{dt} + 2 \frac{d(V_f \rho_f)}{dt}}^{\text{Storage}}, \dots\dots\dots (C-24)$$

which is the same as the dilating-fracture mass balance. Assuming the fracture length remains constant during the before-closure falloff, fracture volume changes are a function of fracture width, and the before-closure storage coefficient is equivalent to the dilating-fracture storage coefficient and written as

$$C_{bc} = c_w V_w + 2 \frac{A_f}{S_f} = C_{fd}. \dots\dots\dots (C-25)$$

The dimensionless before-closure storage coefficient is written as

$$C_{bcD} = \frac{C_{bc}}{2\pi\phi c_t h L_f^2}, \dots\dots\dots (C-26)$$

and the dimensionless before-closure pressure falloff material balance is written as

$$q_{sD} = q_{wsD} - C_{bcD} \frac{dp_{wsD}}{dt L_f D}. \dots\dots\dots (C-27)$$

However, during the falloff portion of the test, $q_{wD} = 0$, and the before-closure pressure falloff dimensionless material balance equation becomes

$$q_{sD} = -C_{bcD} \frac{dp_{wsD}}{dt L_f D}. \dots\dots\dots (C-28)$$

After fracture closure a constant after-closure storage coefficient is written as

$$C_{ac} = c_w V_w + 2c_f V_{fr}, \dots\dots\dots (C-29)$$

where V_{fr} is the residual fracture volume at closure. In some cases, no residual volume will remain after-closure, and $C_{ac} = c_w V_w$. The dimensionless after-closure wellbore storage coefficient is written as

$$C_{acD} = \frac{C_{ac}}{2\pi\phi c_t h L_f^2}, \dots\dots\dots (C-30)$$

and the after-closure pressure falloff dimensionless material balance equation is written as

$$q_{sD} = -C_{acD} \frac{dp_{wsD}}{dt_{Lfd}} \dots\dots\dots (C-31)$$

The Heaviside unit-step function,⁶² is defined as

$$U_a = \begin{cases} 0 & , t < a \\ 1 & , t > a \end{cases} \dots\dots\dots (C-32)$$

and following the technique of Correa and Ramey,⁶²⁻⁶⁴ a material balance equation valid at all times for a fracture-injection/falloff test with a dilating fracture and constant after-closure storage is written as

$$q_{sD} = \left[\begin{array}{l} \left(1 - U(t_e)_{Lfd}\right) \left(q_{wsD} - C_{fdD} \frac{dp_{wsD}}{dt_{Lfd}} \right) \\ - \left(U(t_e)_{Lfd} - U(t_c)_{Lfd} \right) C_{bcD} \frac{dp_{wsD}}{dt_{Lfd}} \\ - U(t_c)_{Lfd} C_{acD} \frac{dp_{wsD}}{dt_{Lfd}} \end{array} \right] \dots\dots\dots (C-33)$$

where $(t_e)_{Lfd}$ is the dimensionless time at the end of pumping and $(t_c)_{Lfd}$ is the dimensionless fracture closure time. The material balance equation can be expanded and written as

$$q_{sD} = \left[\begin{array}{l} q_{wsD} - U(t_e)_{Lfd} q_{wsD} - C_{fdD} \frac{dp_{wsD}}{dt_{Lfd}} + U(t_e)_{Lfd} C_{fdD} \frac{dp_{wsD}}{dt_{Lfd}} \\ - U(t_e)_{Lfd} C_{bcD} \frac{dp_{wsD}}{dt_{Lfd}} + U(t_c)_{Lfd} C_{bcD} \frac{dp_{wsD}}{dt_{Lfd}} \\ - U(t_c)_{Lfd} C_{acD} \frac{dp_{wsD}}{dt_{Lfd}} \end{array} \right] \dots\dots\dots (C-34)$$

but for a dilating fracture $C_{fdD} = C_{bcD}$, and the material balance equation can be simplified and written as

$$q_{sD} = \left(1 - U(t_e)_{Lfd}\right) q_{wsD} - C_{bcD} \frac{dp_{wsD}}{dt_{Lfd}} + U(t_c)_{Lfd} (C_{bcD} - C_{acD}) \frac{dp_{wsD}}{dt_{Lfd}} \dots\dots\dots (C-35)$$

The Laplace transform of the material balance equation⁶² is written as

$$\bar{q}_{sD} = \left[\begin{array}{l} \frac{q_{wsD}}{s} - \frac{q_{wsD}}{s} e^{-s(t_e)_{Lfd}} - C_{bcD} [s\bar{p}_{wsD} - p_{wsD}(0)] \\ + (C_{bcD} - C_{acD}) \left(s\bar{p}_{wsD} - p_{wsD}(0) - \int_0^{(t_c)_{Lfd}} e^{-st_{Lfd}} p'_{wsD}(t_{Lfd}) dt_{Lfd} \right) \end{array} \right] \dots\dots\dots (C-36)$$

or after canceling terms and simplifying the equation, written as

$$\bar{q}_{sD} = \left[\begin{aligned} & \frac{q_{wsD}}{s} - \frac{q_{wsD}}{s} e^{-s(t_e)LfD} - C_{acD}s\bar{p}_{wsD} + p_{wsD}(0)C_{acD} \\ & - (C_{bcD} - C_{acD}) \int_0^{(t_c)LfD} e^{-stLfD} p'_{wsD}(tLfD) dtLfD \end{aligned} \right] \dots\dots\dots (C-37)$$

A solution is developed by applying the superposition principle, which is written as

$$p_{wsD} = \int_0^{tLfD} q_{sD}(\tau_D) \frac{dp_D(tLfD - \tau_D)}{dtLfD} d\tau_D \dots\dots\dots (C-38)$$

The initial condition in the fracture and reservoir requires a constant initial pressure, $p_D(t_{LfD}) = 0$, and with the initial condition, the Laplace transform of the superposition integral is written as

$$\bar{p}_{wsD} = \bar{q}_{sD}s\bar{p}_D \Leftrightarrow \bar{q}_{sD} = \frac{\bar{p}_{wsD}}{s\bar{p}_D} \dots\dots\dots (C-39)$$

Combining the transformed material balance equation and superposition integral results in

$$\bar{p}_{wsD} \left(1 + s^2 C_{acD} \bar{p}_D \right) = \left[\begin{aligned} & q_{wsD} \bar{p}_D - q_{wsD} \bar{p}_D e^{-s(t_e)LfD} + p_{wsD}(0)C_{acD}s\bar{p}_D \\ & - (C_{bcD} - C_{acD})s\bar{p}_D \int_0^{(t_c)LfD} e^{-stLfD} p'_{wsD}(tLfD) dtLfD \end{aligned} \right] \dots\dots\dots (C-40)$$

Let the Laplace domain dimensionless fracture solution for a well produced at a constant rate with after-closure storage be written as

$$\bar{p}_{acD} = \frac{\bar{p}_{fD}}{1 + s^2 C_{acD} \bar{p}_{fD}} \dots\dots\dots (C-41)$$

and the Laplace domain fracture-injection/falloff solution is written as

$$\bar{p}_{wsD} = \left[\begin{aligned} & q_{wsD} \bar{p}_{acD} - q_{wsD} \bar{p}_{acD} e^{-s(t_e)LfD} + p_{wsD}(0)C_{acD}s\bar{p}_{acD} \\ & - (C_{bcD} - C_{acD})s\bar{p}_{acD} \int_0^{(t_c)LfD} e^{-stLfD} p'_{wsD}(tLfD) dtLfD \end{aligned} \right] \dots\dots\dots (C-42)$$

Inverting the Laplace domain solution results in the time domain dilated-fracture injection/falloff solution written as

$$p_{wsD}(tLfD) = \left[\begin{aligned} & q_{wsD} \left[p_{acD}(tLfD) - p_{acD}(tLfD - (t_e)LfD) \right] + p_{wsD}(0)C_{acD}p'_{acD}(tLfD) \\ & - (C_{bcD} - C_{acD}) \int_0^{(t_c)LfD} p'_{acD}(tLfD - \tau_D) p'_{wsD}(\tau_D) d\tau_D \end{aligned} \right] \dots\dots\dots (C-43)$$

Solution Accounting for a Propagating Fracture, Constant Before-Closure Storage, and Constant After-Closure Storage

Consider a fracture-injection/falloff test with fracture length and width developed during the injection. During a constant rate injection with changing fracture length and width, the fracture volume is written as

$$V_f(p_w(t)) = h_f L(p_w(t)) \hat{w}_f(p_w(t)) \dots\dots\dots (C-44)$$

and the propagating-fracture storage coefficient is written as

$$C_{pf}(p_w(t)) = c_w V_w + 2c_f V_f(p_w(t)) + 2 \frac{dV_f(p_w(t))}{dp_w} \dots\dots\dots(C-45)$$

With dimensionless variables, the material balance equation for a propagating fracture during injection is written as

$$q_{sD} = q_{wsD} - \frac{C_{pf}(p_w(t))}{2\pi\phi c_t h L_f^2} \frac{dp_{wsD}}{dt_{LjD}} \dots\dots\dots(C-46)$$

Define a dimensionless fracture storage coefficient as

$$C_{pfD} = \frac{C_{pf}(p_w(t))}{2\pi\phi c_t h L_f^2} \dots\dots\dots(C-47)$$

and the dimensionless material balance equation during an injection at a pressure sufficient to create and extend a hydraulic fracture is written as

$$q_{sD} = q_{wsD} - C_{pfD}(p_{wsD}(t_{LjD})) \frac{dp_{wsD}}{dt_{LjD}} \dots\dots\dots(C-48)$$

Using the technique of Correa and Ramey,⁶²⁻⁶⁴ a material balance equation valid at all times for a fracture-injection/falloff test with fracture creation and extension and constant after-closure wellbore storage is written as

$$q_{sD} = \left[\begin{array}{l} \left(1 - U(t_e)_{LjD}\right) \left(q_{wsD} - C_{pfD}(p_{wsD}(t_{LjD})) \frac{dp_{wsD}}{dt_{LjD}} \right) \\ - \left(U(t_e)_{LjD} - U(t_c)_{LjD} \right) C_{bcD} \frac{dp_{wsD}}{dt_{LjD}} \\ - U(t_c)_{LjD} C_{acD} \frac{dp_{wsD}}{dt_{LjD}} \end{array} \right] \dots\dots\dots(C-49)$$

or expanded and written as

$$q_{sD} = \left[\begin{array}{l} q_{wsD} - U(t_e)_{LjD} \left[q_{wsD} - C_{pfD}(p_{wsD}(t_{LjD})) \frac{dp_{wsD}}{dt_{LjD}} \right] \\ + U(t_e)_{LjD} \left[C_{pfD}(p_{wsD}(t_{LjD})) - C_{bcD} \right] \frac{dp_{wsD}}{dt_{LjD}} \\ + U(t_c)_{LjD} \left[C_{bcD} - C_{acD} \right] \frac{dp_{wsD}}{dt_{LjD}} \end{array} \right] \dots\dots\dots(C-50)$$

The Laplace transform of the material balance for an injection with fracture creation and extension is written as

$$\bar{q}_{sD} = \left[\begin{aligned} & \frac{q_{wsD}}{s} - q_{wsD} \frac{e^{-s(t_e)L_{fD}}}{s} - \int_0^\infty e^{-stL_{fD}} C_{pfD}(p_{wsD}(t_{LfD})) p'_{wsD}(t_{LfD}) dt_{LfD} \\ & + \int_0^\infty e^{-stL_{fD}} C_{pfD}(p_{wsD}(t_{LfD})) p'_{wsD}(t_{LfD}) dt_{LfD} \\ & - \int_0^{(t_e)L_{fD}} e^{-stL_{fD}} C_{pfD}(p_{wsD}(t_{LfD})) p'_{wsD}(t_{LfD}) dt_{LfD} \\ & - \int_0^\infty e^{-stL_{fD}} C_{bcD} p'_{wsD}(t_{LfD}) dt_{LfD} \\ & + \int_0^{(t_e)L_{fD}} e^{-stL_{fD}} C_{bcD} p'_{wsD}(t_{LfD}) dt_{LfD} \\ & + (C_{bcD} - C_{acD}) \left[s\bar{p}_{wsD} - p_{wsD}(0) - \int_0^{(t_c)L_{fD}} e^{-stL_{fD}} p'_{wsD}(t_{LfD}) dt_{LfD} \right] \end{aligned} \right] \dots\dots\dots (C-51)$$

After expanding and simplifying, the material balance equation is written as

$$\bar{q}_{sD} = \left[\begin{aligned} & \frac{q_{wsD}}{s} - q_{wsD} \frac{e^{-s(t_e)L_{fD}}}{s} - \int_0^{(t_e)L_{fD}} e^{-stL_{fD}} C_{pfD}(p_{wsD}(t_{LfD})) p'_{wsD}(t_{LfD}) dt_{LfD} \\ & - sC_{acD}\bar{p}_{wsD} + p_{wsD}(0)C_{acD} \\ & + \int_0^{(t_e)L_{fD}} e^{-stL_{fD}} C_{bcD} p'_{wsD}(t_{LfD}) dt_{LfD} \\ & - (C_{bcD} - C_{acD}) \int_0^{(t_c)L_{fD}} e^{-stL_{fD}} p'_{wsD}(t_{LfD}) dt_{LfD} \end{aligned} \right] \dots\dots\dots (C-52)$$

Developing a solution requires an approach similar to the dilated fracture case, but with the fracture half-length increasing during the injection, a dimensionless pressure solution is required for both a propagating and fixed fracture half-length. A quasi-static dimensionless pressure solution assumes the fracture half-length is constant for each instant in time, and a quasi-static dimensionless pressure solution is developed by integrating the line-source solution, which is written as⁹⁵

$$\bar{\Delta p}_{ls} = \frac{\tilde{q}\mu}{2\pi ks} K_0(r_D\sqrt{u}), \dots\dots\dots (C-53)$$

from $x_w - L(t_{LfD})$ and $x_w + L(t_{LfD})$ with respect to x'_w where $L(t_{LfD})$ is the fracture half-length during propagation. In terms of dimensionless variables, $x'_{wD} = x'_w/L_f$ and $dx'_w = L_f dx'_{wD}$, where L_f is the fracture half-length at the end of propagation, a quasi-static solution is developed by integrating the line-source solution from $x_{wD} - L_{fD}(t_{LfD})$ to $x_{wD} + L_{fD}(t_{LfD})$, which is written as

$$\bar{\Delta p} = \frac{\tilde{q}\mu L_f}{2\pi ks} \int_{x_{wD} - L_{fD}(t_{LfD})}^{x_{wD} + L_{fD}(t_{LfD})} K_0 \left[\sqrt{u} \sqrt{(x_D - x'_{wD})^2 + (y_D - y_{wD})^2} \right] dx'_{wD} \dots\dots\dots (C-54)$$

Assuming that the well center is at the origin, $x_{wD} = y_{wD} = 0$,

$$\frac{\bar{\Delta p}}{2\pi k_s} = \frac{\tilde{q}\mu L_f}{2\pi k_s} \int_{-L_{fD}(t_{LfD})}^{L_{fD}(t_{LfD})} K_0 \left[\sqrt{u} \sqrt{(x_D - x'_{wD})^2 + (y_D)^2} \right] dx'_{wD} \dots\dots\dots (C-55)$$

Assuming uniform flux, the flow rate is written as

$$q = \tilde{q}2hL(t_{LfD}), \dots\dots\dots (C-56)$$

and the plane-source solution can be written in dimensionless terms as

$$\bar{p}_D = \frac{q_D}{L_{fD}(t_{LfD})} \frac{1}{2s} \int_{-L_{fD}(t_{LfD})}^{L_{fD}(t_{LfD})} K_0 \left[\sqrt{u} \sqrt{(x_D - \alpha)^2 + (y_D)^2} \right] d\alpha, \dots\dots\dots (C-57)$$

where

$$\bar{p}_D = \frac{2\pi kh\bar{\Delta p}}{q_t \mu}, \dots\dots\dots (C-58)$$

$$L_{fD}(t_{LfD}) = \frac{L(t_{LfD})}{L_f}, \dots\dots\dots (C-59)$$

and defining the total flow rate in the time domain as $q_t(t)$, the dimensionless flow rate is written as

$$q_D(t_{LfD}) = \frac{q}{q_t} = 1, \dots\dots\dots (C-60)$$

where it is assumed that the flow rate is equivalent to the constant total flow rate at each point in time during fracture propagation such that $q_D(t_{LfD}) = 1$. The solution is evaluated in the plane of the fracture, and after simplifying the integral using the identity of Ozkan and Raghavan,¹¹⁴ a quasi-static dimensionless uniform-flux solution in the Laplace domain for a variable fracture half-length is written as

$$\bar{p}_{prfD} = \frac{1}{L_{fD}(t_{LfD})} \frac{1}{2s\sqrt{u}} \left[\int_0^{\sqrt{u}(L_{fD}(t_{LfD})+x_D)} K_0[z] dz + \int_0^{\sqrt{u}(L_{fD}(t_{LfD})-x_D)} K_0[z] dz \right], \dots\dots\dots (C-61)$$

and the infinite-conductivity solution is obtained by evaluating the uniform-flux solution at $L_{fD}x_D = 0.732$ and is written as

$$\bar{p}_{prfD} = \frac{1}{L_{fD}(t_{LfD})} \frac{1}{2s\sqrt{u}} \left[\int_0^{\sqrt{u}L_{fD}(t_{LfD})(1+0.732)} K_0[z] dz + \int_0^{\sqrt{u}L_{fD}(t_{LfD})(1-0.732)} K_0[z] dz \right] \dots (C-62)$$

The dimensionless fracture half-length varies between 0 and 1 during fracture propagation, and using a power-model approximation,⁸⁰ a dimensionless fracture half-length can be written during propagation and closure as

$$L_{fD}(t_{LfD}) = \begin{cases} \frac{L(t_{LfD})}{L_f} = \left(\frac{t_{LfD}}{(t_e)_{LfD}} \right)^{\alpha_N} & t_{LfD} < (t_e)_{LfD}, \dots\dots\dots (C-63) \\ 1 & t_{LfD} \geq (t_e)_{LfD} \end{cases}$$

where the power-model exponent ranges from $\alpha_N = 1/2$ and for a low efficiency (high leakoff) fracture and $\alpha_N = 1$ for a high efficiency (low leakoff) fracture.

Valkó and Economides⁵⁹ approximate dimensionless pressure during fracture propagation using an early-time approximation for the infinite-conductivity fixed-length fracture solution written as

$$(p_{fD})_n \cong \sqrt{\pi(t_{LfD})_n}, \dots\dots\dots(C-64)$$

where the dimensionless time, t_{LfD} , is defined in terms of the fracture length at time $(t)_n$ and written as

$$(t_{LfD})_n = \frac{k(t)_n}{\phi\mu c_t(L^2)_n} \dots\dots\dots(C-65)$$

Fig. C-1 is a graph of dimensionless pressure versus dimensionless fracture half-length for the propagating fracture solution (Eq. C-62) and the early-time approximation of a high efficiency fracture with $\alpha_N = 1$. The early-time approximation with dimensionless time as a function of fracture half-length at time $(t)_n$ generally overlays the propagating-fracture solution after about 5% of the fracture half-length is created. For a low efficiency fracture with $\alpha_N = 1/2$ the approximation is exact during the entire fracture propagation period.

During the before- and after-closure period when the fracture half-length is unchanging, the dimensionless pressure solution for an infinite-conductivity fracture results,⁸⁴ which is written in the Laplace domain as⁹⁵

$$\bar{p}_{fD} = \frac{1}{2s\sqrt{u}} \left[\int_0^{\sqrt{u}(1+0.732)} K_0[z] dz + \int_0^{\sqrt{u}(1-0.732)} K_0[z] dz \right] \dots\dots\dots(C-66)$$

The two different reservoir models, one for a propagating fracture and one for a fixed-length fracture, can be superposed¹⁰² to develop a dimensionless wellbore pressure solution by writing the superposition integrals as

$$p_{wsD} = \int_0^{t_{LfD}} q_{pfD}(\tau_D) \frac{dp_{pfD}(t_{LfD} - \tau_D)}{dt_{LfD}} d\tau_D + \int_0^{t_{LfD}} q_{fD}(\tau_D) \frac{dp_{fD}(t_{LfD} - \tau_D)}{dt_{LfD}} d\tau_D, \dots\dots\dots(C-67)$$

where $q_{pfD}(t_{LfD})$ is the dimensionless flow rate for the propagating fracture model with propagating-fracture solution, $p_{pfD}(t_{LfD})$, and $q_{fD}(t_{LfD})$ is the dimensionless flow rate with a fixed fracture half-length model used during the before- and after-closure falloff period. The initial condition in the fracture and reservoir is a constant initial pressure, $p_D(t_{LfD}) = p_{pfD}(t_{LfD}) = p_{fD}(t_{LfD}) = 0$, and with the initial condition, the Laplace transform of the superposition integral is written as

$$\bar{p}_{wsD} = \bar{q}_{pfD} s \bar{p}_{pfD} + \bar{q}_{fD} s \bar{p}_{fD} \dots\dots\dots(C-68)$$

The Laplace domain dimensionless material balance equation can be split into injection and falloff parts by writing as

$$\bar{q}_{sD} = \bar{q}_{pfD} + \bar{q}_{fD}, \dots\dots\dots(C-69)$$

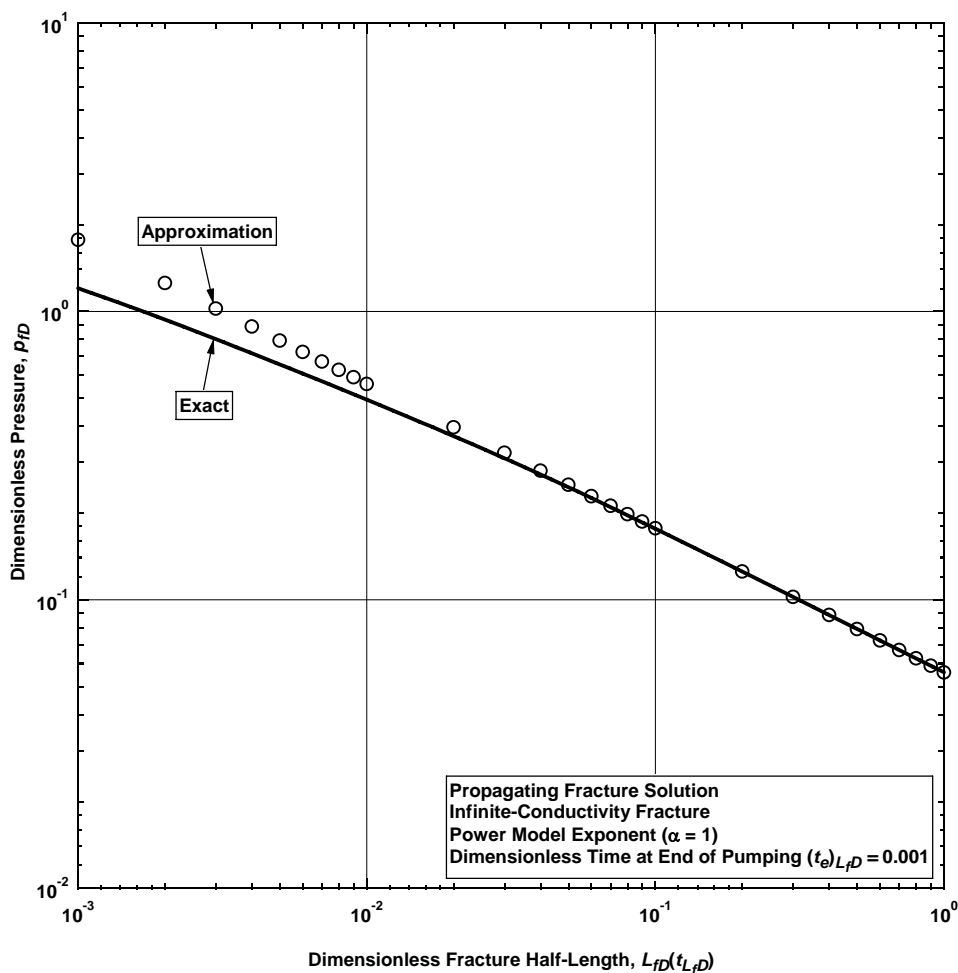


Fig. C-1—Comparison of Laplace Domain propagating fracture solution with early-time infinite-conductivity fracture approximation with dimensionless time as a function of fracture half-length at time $(t)_n$.

where the dimensionless reservoir flow rate during fracture propagation is written as

$$\bar{q}_{pFD} = \frac{q_{wsD}}{s} - q_{wsD} \frac{e^{-s(t_e)_{L,D}}}{s} - \int_0^{(t_e)_{L,D}} e^{-st_{L,D}} C_{pFD}(p_{wsD}(t_{L,D})) p'_{wsD}(t_{L,D}) dt_{L,D}, \dots\dots\dots(C-70)$$

and the dimensionless before- and after-closure fracture flow rate is written as

$$\bar{q}_{fD} = \left[\begin{array}{l} p_{wD}(0)C_{acD} - sC_{acD}\bar{p}_{wsD} \\ +C_{bcD} \int_0^{(t_e)_{LjD}} e^{-st_{LjD}} p'_{wsD}(t_{LjD}) dt_{LjD} \\ -(C_{bcD} - C_{acD}) \int_0^{(t_c)_{LjD}} e^{-st_{LjD}} p'_{wsD}(t_{LjD}) dt_{LjD} \end{array} \right] \dots\dots\dots(C-71)$$

Utilizing the superposition principle to develop a solution requires that the pressure-dependent dimensionless propagating-fracture storage coefficient be written as a function of time only. Let fracture propagation be modeled by a power model and written as⁸⁰

$$\frac{A(t)}{A_f} = \frac{h_f L(t)}{h_f L_f} = \left(\frac{t}{t_e} \right)^{\alpha_N} \dots\dots\dots(C-72)$$

Fracture volume as a function of time is written as

$$V_f(p_w(t)) = h_f L(p_w(t)) \hat{w}_f(p_w(t)) \dots\dots\dots(C-73)$$

which, using the power model, can also be written as

$$V_f(p_w(t)) = h_f L_f \frac{(p_w(t) - p_c)}{S_f} \left(\frac{t}{t_e} \right)^{\alpha_N} \dots\dots\dots(C-74)$$

The derivative of fracture volume with respect to wellbore pressure is written as

$$\frac{dV_f(p_w(t))}{dp_w} = \frac{h_f L_f}{S_f} \left(\frac{t}{t_e} \right)^{\alpha_N} \dots\dots\dots(C-75)$$

Recall the propagating-fracture storage coefficient is written as

$$C_{pf}(p_w(t)) = c_w V_w + 2c_f V_f(p_w(t)) + 2 \frac{dV_f(p_w(t))}{dp_w} \dots\dots\dots(C-76)$$

which, with power-model fracture propagation included, is written as

$$C_{pf}(p_w(t)) = c_w V_w + 2 \frac{h_f L_f}{S_f} \left(\frac{t}{t_e} \right)^{\alpha_N} (c_f p_n + 1) \dots\dots\dots(C-77)$$

As previously noted, $c_p p_n(t) \ll 1$, and the propagating-fracture storage coefficient is written as

$$C_{pf}(t_{LjD}) = c_w V_w + 2 \frac{A_f}{S_f} \left(\frac{t_{LjD}}{(t_e)_{LjD}} \right)^{\alpha_N} \dots\dots\dots(C-78)$$

which is not a function of pressure and allows the superposition principle to be used to develop a solution.

Combining the material balance equations and superposition integrals results in

$$\bar{p}_{wsD} = \left[\begin{aligned} & q_{wsD} \bar{p}_{pfd} - q_{wsD} \bar{p}_{pfd} e^{-s(t_e)LfD} - C_{acD} \left[s \bar{p}_{fD} (s \bar{p}_{wsD} - p_{wD}(0)) \right] \\ & - s \bar{p}_{pfd} \int_0^{(t_e)LfD} e^{-stLfD} C_{pfd}(tLfD) p'_{wsD}(tLfD) dtLfD \\ & + s \bar{p}_{fD} C_{bcD} \int_0^{(t_e)LfD} e^{-stLfD} p'_{wsD}(tLfD) \\ & - s \bar{p}_{fD} \int_0^{(t_c)LfD} e^{-stLfD} [C_{bcD} - C_{acD}] p'_{wsD}(tLfD) dtLfD \end{aligned} \right], \dots\dots\dots(C-79)$$

and after inverting to the time domain, the fracture-injection/falloff solution for the case of a propagating fracture, constant before-closure storage, and constant after-closure storage is written as

$$p_{pfd}(tLfD) = \left[\begin{aligned} & q_{wsD} \left[p_{pfd}(tLfD) - p_{pfd}(tLfD - (t_e)LfD) \right] \\ & - C_{acD} \int_0^{tLfD} p'_{fD}(tLfD - \tau_D) p'_{wsD}(\tau_D) d\tau_D \\ & - \int_0^{(t_e)LfD} p'_{pfd}(tLfD - \tau_D) C_{pfd}(\tau_D) p'_{wsD}(\tau_D) d\tau_D \\ & + C_{bcD} \int_0^{(t_e)LfD} p'_{fD}(tLfD - \tau_D) p'_{wsD}(\tau_D) d\tau_D \\ & - (C_{bcD} - C_{acD}) \int_0^{(t_c)LfD} p'_{fD}(tLfD - \tau_D) p'_{wsD}(\tau_D) d\tau_D \end{aligned} \right] \dots\dots\dots(C-80)$$

The propagating-fracture solution for a single vertical fracture, $p_{pfd}(tLfD)$, can be written as

$$p_{pfd}(tLfD) = \begin{cases} p_{prfd}(tLfD) & tLfD < (t_e)LfD \\ p_{fD}(tLfD) & tLfD > (t_e)LfD \end{cases}, \dots\dots\dots(C-81)$$

or using the unit-step function written as

$$p_{pfd}(tLfD) = \left(1 - U_{(t_e)LfD} \right) p_{prfd}(tLfD) + U_{(t_e)LfD} p_{fD}(tLfD), \dots\dots\dots(C-82)$$

where the solution during fracture propagation is written as

$$\bar{p}_{prfd} = \frac{1}{LfD(tLfD)} \frac{1}{2s\sqrt{u}} \left[\int_0^{\sqrt{u}LfD(tLfD)(1+0.732)} K_0[z] dz + \int_0^{\sqrt{u}LfD(tLfD)(1-0.732)} K_0[z] dz \right], \dots(C-83)$$

with dimensionless fracture half-length defined in the Laplace domain as

$$L_{fD}(tLfD) = \begin{cases} \frac{L(tLfD)}{L_f} = \left(\frac{tLfD}{(t_e)LfD} \right)^{\alpha_N} & tLfD < (t_e)LfD \\ 1 & tLfD \geq (t_e)LfD \end{cases} \dots\dots\dots(C-84)$$

Solution Accounting for a Propagating Fracture Storage, Before-Closure Storage, Constant After-Closure Storage, and After-Closure Radial Flow

The previous fracture solutions assumed fracture flow after-closure, but it is also likely that after-closure radial flow occurs when little or no fracture conductivity remains after fracture closure. The dimensionless material balance remains the same for the after-closure radial flow case and is written as

$$q_{sD} = \begin{bmatrix} \left(1 - U(t_e)_{LjD}\right) \left(q_{wsD} - C_{pfD}(p_{wsD}(t_{LjD})) \frac{dp_{wsD}}{dt_{LjD}} \right) \\ - \left(U(t_e)_{LjD} - U(t_c)_{LjD} \right) C_{bcD} \frac{dp_{wsD}}{dt_{LjD}} \\ - U(t_c)_{LjD} C_{acD} \frac{dp_{wsD}}{dt_{LjD}} \end{bmatrix}, \dots\dots\dots (C-85)$$

where the dimensionless after-closure storage coefficient is defined as

$$C_{acD} = \frac{c_w V_w}{2\pi\phi c_t h L_f^2} = C_D \dots\dots\dots (C-86)$$

The dimensionless wellbore pressure solution for flow from a propagating fracture, a fixed-length fracture during closure, and a perforated (radial) interval after closure can be written by applying the superposition principle as

$$p_{wsD} = \sum_{j=1}^3 \int_0^{t_{LjD}} q_{sDj} p'_{Dj}(t_{LjD} - \tau_D) d\tau_D, \dots\dots\dots (C-87)$$

or by expanding the summation written as

$$p_{wsD} = \begin{bmatrix} \int_0^{t_{LjD}} q_{pfD} p'_{pfD}(t_{LjD} - \tau_D) d\tau_D \\ + \int_0^{t_{LjD}} q_{fD} p'_{fD}(t_{LjD} - \tau_D) d\tau_D \\ + \int_0^{t_{LjD}} q_{rD} p'_{sD}(t_{LjD} - \tau_D) d\tau_D \end{bmatrix}, \dots\dots\dots (C-88)$$

where q_{rD} is the after-closure dimensionless flow rate for the radial system and $p_{sD}(t_{LjD}) = p_{rD}(t_{LjD}) + S$ is the dimensionless radial flow reservoir solution, p_{rD} , with skin effect, S . Note that dimensionless time is defined in terms of the fracture half-length; thus, fracture half-length is the characteristic length used in the dimensionless radius definition and radial solution.

The dimensionless material balance can also be written in terms of before-closure and after-closure components as

$$q_{sD} = q_{pfD} + q_{fD} + q_{rD}, \dots\dots\dots (C-89)$$

where, utilizing the power model, the flow rate for a propagating fracture is written as

$$q_{pfD} = \left(1 - U(t_e)_{LjD}\right) \left(q_{wsD} - C_{pfD}(t_{LjD}) \frac{dp_{wsD}}{dt_{LjD}} \right) \dots\dots\dots (C-90)$$

The flow rate for a fixed-length closing fracture is written as

$$q_{fD} = - \left(U(t_e)_{LjD} - U(t_c)_{LjD} \right) C_{bcD} \frac{dp_{wsD}}{dt_{LjD}}, \dots\dots\dots (C-91)$$

and the dimensionless after-closure radial flow rate is written as

$$q_{rD} = -U_{(t_c)_{LjD}} C_D \frac{dp_{wsD}}{dt_{LjD}} \dots\dots\dots (C-92)$$

The solution is obtained by applying the superposition principle for the propagating fracture, fixed fracture half-length, and radial model, which when combined with the material balance equations in the Laplace domain can be written as

$$\bar{p}_{wsD} = \left[\begin{array}{l} q_{wsD} \bar{p}_{pfd} - q_{wsD} \bar{p}_{pfd} e^{-s(t_e)_{LjD}} \\ -C_D [s \bar{p}_{sD} (s \bar{p}_{wsD} + p_{wsD}(0))] \\ -s \bar{p}_{pfd} \int_0^{(t_e)_{LjD}} e^{-st_{LjD}} C_{pfd}(t_{LjD}) p'_{wsD}(t_{LjD}) dt_{LjD} \\ +C_{bcD} s \bar{p}_{fD} \int_0^{(t_e)_{LjD}} e^{-st_{LjD}} p'_{wsD}(t_{LjD}) dt_{LjD} \\ -C_{bcD} s \bar{p}_{fD} \int_0^{(t_c)_{LjD}} e^{-st_{LjD}} p'_{wsD}(t_{LjD}) dt_{LjD} \\ +C_D s \bar{p}_{sD} \int_0^{(t_c)_{LjD}} e^{-st_{LjD}} p'_{wsD}(t_{LjD}) dt_{LjD} \end{array} \right] \dots\dots\dots (C-93)$$

After inverting to the time domain, the dimensionless pressure solution accounting for a propagating fracture, before- and after-closure storage, and after-closure radial flow is written as

$$p_{wsD}(t_{LjD}) = \left[\begin{array}{l} q_{wsD} [p_{pfd}(t_{LjD}) - p_{pfd}(t_{LjD} - (t_e)_{LjD})] \\ -C_D \int_0^{t_{LjD}} p_{sD}(t_{LjD} - \tau_D) p'_{wsD}(\tau_D) d\tau_D \\ -\int_0^{(t_e)_{LjD}} p'_{pfd}(t_{LjD} - \tau_D) C_{pfd}(\tau_D) p'_{wsD}(\tau_D) d\tau_D \\ +C_{bcD} \int_0^{(t_e)_{LjD}} p'_{fD}(t_{LjD} - \tau_D) p'_{wsD}(\tau_D) d\tau_D \\ +C_D \int_0^{(t_c)_{LjD}} p_{sD}(t_{LjD} - \tau_D) p'_{wsD}(\tau_D) d\tau_D \\ -C_{bcD} \int_0^{(t_c)_{LjD}} p'_{fD}(t_{LjD} - \tau_D) p'_{wsD}(\tau_D) d\tau_D \end{array} \right] \dots\dots\dots (C-94)$$

APPENDIX D

ANALYTICAL PRESSURE-TRANSIENT SOLUTION FOR A WELL CONTAINING MULTIPLE INFINITE-CONDUCTIVITY VERTICAL FRACTURES IN AN INFINITE SLAB RESERVOIR

Ozkan and Raghavan⁹⁵ write the point source solution in the Laplace domain for an infinite-slab reservoir between impermeable boundaries at $z_D = 0$ and $z_D = h_D$ as

$$\Delta \bar{p}_{ps} = \frac{\tilde{q}\mu}{2\pi kLh_D s} \left[K_0(r_D \sqrt{u}) + 2 \sum_{n=1}^{\infty} K_0(r_D \varepsilon_n) \cos\left(n\pi \frac{z_D}{h_D}\right) \cos\left(n\pi \frac{z_{wD}}{h_D}\right) \right], \dots\dots\dots (D-1)$$

where L_c is a reference length for the system. Assuming permeability isotropy, the dimensionless variables are defined as

$$h_D = \frac{h}{L_c}, \dots\dots\dots (D-2)$$

$$z_D = \frac{z}{L_c}, \dots\dots\dots (D-3)$$

$$z_{wD} = \frac{z_w}{L_c}, \dots\dots\dots (D-4)$$

and

$$r_D = \sqrt{(x_D - x_{wD})^2 + (y_D - y_{wD})^2}. \dots\dots\dots (D-5)$$

The Laplace variable is denoted by s , and the point-source solution accounts for dual-porosity reservoirs with u defined as

$$u = sf(s), \dots\dots\dots (D-6)$$

and ε_n defined as

$$\varepsilon_n = \sqrt{u + \left(\frac{n\pi}{h_D}\right)^2}, \dots\dots\dots (D-7)$$

where for a single-porosity $f(s) = 1$. For a dual-porosity case with pseudosteady-state interporosity flow, $f(s)$ is written as⁹⁶

$$f(s) = \frac{\lambda + \omega(1-\omega)s}{\lambda + (1-\omega)s}, \dots\dots\dots (D-8)$$

for transient interporosity flow with slab matrix blocks,⁹⁷⁻⁹⁸

$$f(s) = \omega + \sqrt{\frac{\lambda(1-\omega)}{3s}} \tanh \sqrt{\frac{3(1-\omega)s}{\lambda}}, \dots\dots\dots (D-9)$$

and for transient interporosity flow with spherical matrix blocks,⁹⁷⁻⁹⁸

$$f(s) = \omega + \frac{\lambda}{5s} \left[\sqrt{\frac{15(1-\omega)s}{\lambda}} \coth \sqrt{\frac{15(1-\omega)s}{\lambda}} - 1 \right] \dots\dots\dots(D-10)$$

Assuming constant flux, \tilde{q} , the line-source solution for a fully penetrating wellbore is developed by integrating the right-hand-side of the point-source solution from 0 to h with respect to z'_w . In terms of dimensionless variables with $z'_{wD} = z'_w/L_c$, the point-source solution is integrated from 0 to h_D , which is written as

$$\Delta\bar{p}_{ls} = \frac{\tilde{q}\mu}{2\pi kh_D s} \left[\int_0^{h_D} K_0(r_D \sqrt{u}) dz'_{wD} + 2 \sum_{n=1}^{\infty} K_0(r_D \varepsilon_n) \cos\left(n\pi \frac{z_D}{h_D}\right) \int_0^{h_D} \cos\left(n\pi \frac{z'_{wD}}{h_D}\right) dz'_{wD} \right] \dots\dots\dots(D-11)$$

Only the first integral term is nonzero, and the fully-penetrating line-source solution for an isotropic reservoir is written as

$$\Delta\bar{p}_{ls} = \frac{\tilde{q}\mu}{2\pi ks} K_0(r_D \sqrt{u}) \dots\dots\dots(D-12)$$

The plane-source (vertically-fractured well) solution is obtained by integrating the right-hand-side of the line-source solution from $x_w - L_f$ and $x_w + L_f$ with respect to x'_w . In terms of dimensionless variables with $x'_{wD} = x'_w/L_c$, the line-source solution is integrated from $x_{wD} - L_{fD}$ to $x_{wD} + L_{fD}$, which is written as

$$\Delta\bar{p} = \frac{\tilde{q}\mu L_c}{2\pi ks} \int_{x_{wD} - L_{fD}}^{x_{wD} + L_{fD}} K_0 \left[\sqrt{u} \sqrt{(x_D - x'_{wD})^2 + (y_D - y_{wD})^2} \right] dx'_{wD} \dots\dots\dots(D-13)$$

Assuming that the well center is at the origin, $x_{wD} = y_{wD} = 0$, the plane-source solution is written as

$$\Delta\bar{p} = \frac{\tilde{q}\mu L_c}{2\pi ks} \int_{-L_{fD}}^{L_{fD}} K_0 \left[\sqrt{u} \sqrt{(x_D - x'_{wD})^2 + (y_D)^2} \right] dx'_{wD} \dots\dots\dots(D-14)$$

With uniform flux, the constant flow rate is written as

$$q = \tilde{q}2hL_f, \dots\dots\dots(D-15)$$

and plane-source solution can be written in the Laplace domain as

$$\bar{p}_D = \frac{q_D}{L_{fD}} \frac{1}{2s} \int_{-L_{fD}}^{L_{fD}} K_0 \left[\sqrt{u} \sqrt{(x_D - \alpha)^2 + (y_D)^2} \right] d\alpha, \dots\dots\dots(D-16)$$

where

$$\bar{p}_D = \frac{2\pi kh \Delta\bar{p}}{q_t \mu}, \dots\dots\dots(D-17)$$

$$L_{fD} = \frac{L_f}{L_c}, \dots\dots\dots(D-18)$$

and defining the total constant flow rate as q_t , the dimensionless flow rate is written as

$$q_D = \frac{q}{q_t} = 1. \dots\dots\dots(D-19)$$

General Solution for a Vertical Fracture at an Arbitrary Angle from the x_D -axis

Fig. D-1 illustrates a vertical fracture at an arbitrary angle, θ , from the x_D -axis. The uniform-flux plane-source solution assuming an isotropic reservoir is written in the Laplace domain as

$$\bar{p}_D = \frac{1}{2sL_{fD}} \int_{-L_{fD}}^{L_{fD}} K_0 \left[\sqrt{u} \sqrt{(\hat{x}_D - \alpha)^2 + (\hat{y}_D)^2} \right] d\alpha, \dots\dots\dots(D-20)$$

where dimensionless variables are defined as

$$r_D = \sqrt{x_D^2 + y_D^2}, \dots\dots\dots(D-21)$$

$$x_D = r_D \cos \theta_r, \dots\dots\dots(D-22)$$

$$y_D = r_D \sin \theta_r, \dots\dots\dots(D-23)$$

$$\hat{x}_D = x_D \cos \theta_f + y_D \sin \theta_f, \dots\dots\dots(D-24)$$

$$\hat{y}_D = y_D \cos \theta_f - x_D \sin \theta_f, \dots\dots\dots(D-25)$$

and θ_f is the angle between the fracture and the x_D -axis, (r_D, θ_r) are the polar coordinates of a point (x_D, y_D) , and (α, θ_f) are the polar coordinates of a point along the fracture.¹⁰³ Combining Eqs. D-22 through D-25 results in

$$\hat{x}_D = r_D \cos(\theta_r - \theta_f), \dots\dots\dots(D-26)$$

and

$$\hat{y}_D = r_D \sin(\theta_r - \theta_f). \dots\dots\dots(D-27)$$

Consequently, the Laplace domain plane-source solution for a fracture rotated by an angle θ_f from a point (r_D, θ_r) is written as

$$\bar{p}_D = \frac{1}{2sL_{fD}} \int_{-L_{fD}}^{L_{fD}} K_0 \left[\sqrt{u} \sqrt{\left[r_D \cos(\theta_r - \theta_f) - \alpha \right]^2 + r_D^2 \sin^2(\theta_r - \theta_f)} \right] d\alpha. \dots\dots\dots(D-28)$$

The single fracture Laplace domain solution has the fracture aligned with the x_D -axis, and the single fracture solution is a special case of the general plane-source solution. With $\theta_r = \theta_f$, which essentially aligns the fracture with a reference axis, the general Laplace domain solution reduces to the known single fracture plane-source fracture solution written as

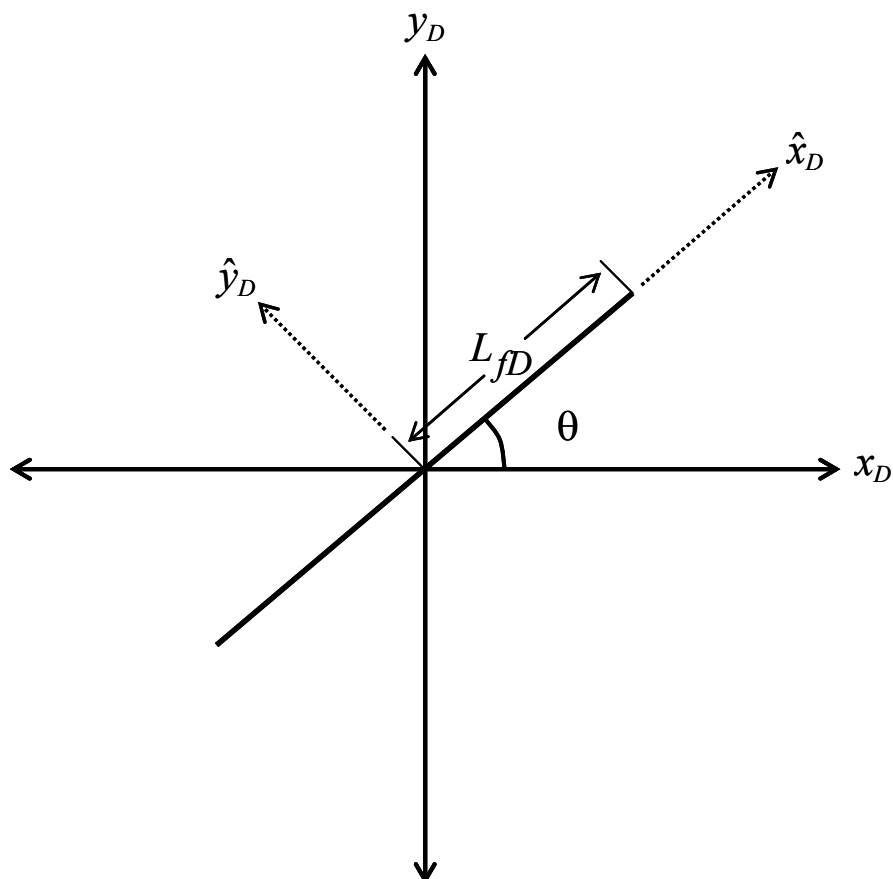


Fig. D-1—A vertical fracture at an arbitrary angle relative to the x_D -axis.

$$\bar{p}_D = \frac{1}{2sL_{fD}} \int_{-L_{fD}}^{L_{fD}} K_0 \left[\sqrt{u} \sqrt{(x_D - \alpha)^2 + (y_D)^2} \right] d\alpha \quad \text{.....(D-29)}$$

General Solution for Multiple Arbitrarily-Oriented Uniform-Flux Vertical Fractures

For a well containing n_f fractures connected at the wellbore, the total flow rate from the well assuming all production is through the fractures is written as

$$\sum_{i=1}^{n_f} q_{iD} = 1, \quad \text{.....(D-30)}$$

where q_{iD} is the dimensionless flow rate for the i^{th} -fracture defined as

$$q_{iD} = \frac{q_i}{q_w} = \frac{q_i}{\sum_{k=1}^{n_f} q_k}, \quad \text{.....(D-31)}$$

and q_i is the flow rate from the i^{th} -fracture.

For all fractures intersecting the wellbore, the wellbore pressure is the same and written as

$$p_{LjD} = (p_{wD})_{\ell} \quad , \quad \ell = 1, 2, \dots, n_f \quad \dots \dots \dots (D-32)$$

The dimensionless pressure solution is obtained by superposing all fractures¹⁰² and written using the superposition integral as

$$p_{LjD} = (p_{wD})_{\ell} = \sum_{i=1}^{n_f} \int_0^{t_{LjD}} q_{iD}(\tau_D) (p'_D)_{\ell i}(t_{LjD} - \tau_D) d\tau_D \quad , \quad \ell = 1, 2, \dots, n_f \quad \dots \dots \dots (D-33)$$

where the pressure derivative accounts for the effects of fracture ' i ' on fracture ' ℓ '.

The Laplace transform of the dimensionless rate equation is written as

$$\sum_{i=1}^{n_f} \bar{q}_{iD} = \frac{1}{s} \quad \dots \dots \dots (D-34)$$

and with the initial condition, $p_D(t_{LjD} = 0) = 0$, the Laplace transform of the dimensionless pressure solution is written as

$$(\bar{p}_{wD})_{\ell} = \sum_{i=1}^{n_f} s \bar{q}_{iD} (\bar{p}_D)_{\ell i} \quad , \quad \ell = 1, 2, \dots, n_f \quad \dots \dots \dots (D-35)$$

where $(\bar{p}_D)_{\ell i}$ is the Laplace domain uniform-flux solution for a single fracture written to account for the effects of multiple fractures as

$$(\bar{p}_D)_{\ell i} = \frac{1}{2sL_{fiD}} \int_{-L_{fiD}}^{L_{fiD}} K_0 \left[\sqrt{u} \sqrt{[r_D \cos(\theta_{\ell} - \theta_i) - \alpha]^2 + r_D^2 \sin^2(\theta_{\ell} - \theta_i)} \right] d\alpha \quad \dots \dots \dots (D-36)$$

The uniform-flux Laplace domain multiple fracture solution can now be written as

$$\begin{aligned} \bar{p}_{LjD} = (\bar{p}_{wD})_{\ell} &= \sum_{i=1}^{n_f} \frac{\bar{q}_{iD}}{2L_{fiD}} \int_{-L_{fiD}}^{L_{fiD}} K_0 \left[\sqrt{u} \sqrt{[r_D \cos(\theta_{\ell} - \theta_i) - \alpha]^2 + r_D^2 \sin^2(\theta_{\ell} - \theta_i)} \right] d\alpha \\ &\ell = 1, 2, \dots, n_f \quad \dots \dots \dots (D-37) \end{aligned}$$

For a uniform-flux fracture system, the flow rate from the primary fracture, L_{f1D} , is written as

$$q_1 = 2h_f L_{f1} \tilde{q} \quad \dots \dots \dots (D-38)$$

and the flow rate from the other fractures is written as

$$q_i = 2h_f \delta_i L_{fi} \tilde{q} \quad , \quad i = 2, 3, \dots, n_f \quad \dots \dots \dots (D-39)$$

where the normalized fracture length is written as

$$\delta_i = \frac{L_{fi}}{L_{f1}} \quad , \quad i = 1, 2, \dots, n_f \quad \dots \dots \dots (D-40)$$

The well flow rate is written as

$$q_w = 2h_f L_f \tilde{q} \sum_{k=1}^{n_f} \delta_k, \dots\dots\dots (D-41)$$

and the dimensionless flow rate is defined as

$$q_{iD} = \frac{q_i}{q_w} = \frac{\delta_i}{\sum_{k=1}^{n_f} \delta_k} \dots\dots\dots (D-42)$$

The Laplace transform of the constant dimensionless flow rate is written as

$$\bar{q}_{iD} = \frac{\delta_i}{s \sum_{k=1}^{n_f} \delta_k}, \dots\dots\dots (D-43)$$

and the Laplace domain uniform-flux multiple fracture solution is written as

$$\bar{p}_{LjD} = (\bar{p}_{wD})_\ell = \sum_{i=1}^{n_f} \frac{\delta_i}{\sum_{k=1}^{n_f} \delta_k} \frac{1}{2sL_{fiD}} \int_{-L_{fiD}}^{L_{fiD}} K_0 \left[\sqrt{u} \sqrt{\frac{[r_D \cos(\theta_\ell - \theta_i) - \alpha]^2}{+r_D^2 \sin^2(\theta_\ell - \theta_i)}} \right] d\alpha \dots\dots\dots (D-44)$$

For the special case of a cruciform fracture with $\theta_1 = 0$ and $\theta_2 = \pi/2$, the uniform-flux solution at the wellbore is written as

$$\bar{p}_{LjD} = \frac{1}{(1 + \delta_2)} \frac{1}{2sL_{f1D}} \left[\int_{-L_{f1D}}^{L_{f1D}} K_0 \left[\sqrt{u} \sqrt{\alpha^2} \right] d\alpha + \int_{-L_{f2D}}^{L_{f2D}} K_0 \left[\sqrt{u} \sqrt{\alpha^2} \right] d\alpha \right] \dots\dots\dots (D-45)$$

For $L_{f1D} = 1$ and $L_{f2D} = \delta_2$, the uniform-flux Laplace domain solution is written using the identity of Ozkan and Raghavan¹¹⁴ as

$$\bar{p}_{LjD} = \frac{1}{(1 + \delta_2)} \frac{1}{s\sqrt{u}} \left[\int_0^{\sqrt{u}} K_0 [z] dz + \int_0^{\delta_2 \sqrt{u}} K_0 [z] dz \right], \dots\dots\dots (D-46)$$

and for the special case when $L_{f1D} = L_{f2D}$, the Laplace domain uniform-flux pressure solution is written as

$$\bar{p}_{LjD} = \frac{1}{s\sqrt{u}} \int_0^{\sqrt{u}} K_0 [z] dz, \dots\dots\dots (D-47)$$

which is identically equal to a single planar fracture uniform-flux solution.

Solution for Multiple Arbitrarily-Oriented Infinite-Conductivity Vertical Fractures

For a single vertical fracture, an approximate infinite-conductivity solution is obtained by evaluating the uniform-flux solution at an equivalent average pressure point, ($x_D = 0.732$, $y_D = 0$). However, the equivalent average pressure point is dependent on the system geometry and must be determined numerically for each multi-fracture system.¹⁰⁴

Kuchuk *et al.*¹⁰⁴ encountered a similar problem when deriving the infinite-conductivity solution for horizontal wells and elected to use the pressure-averaging technique proposed by Wilkinson and Hammond.¹⁰⁵ The pressure-averaging technique approximates the infinite-conductivity solution by averaging the pressure along the flowpath using the uniform-flux solution, which according to Wilkinson and Hammond approaches the exact solution as the wellbore radius tends to zero.¹⁰⁴⁻¹⁰⁵ Pressure-averaging was utilized in developing the horizontal well solution of Kuchuk *et al.*,¹⁰⁴ the dual lateral solution of Ozkan *et al.*,¹⁰³ and the multi-lateral solution of Yildiz.¹¹⁵ However, it is unclear if the pressure averaging technique is appropriate for multiple intersecting vertical fractures.

For a *single* infinite-conductivity fracture, **Fig. D-2** contains a log-log graph of dimensionless pressure and dimensionless pressure derivative versus dimensionless time evaluated using the uniform-flux solution with an equivalent average pressure point, $x_D = 0.732$, and using a pressure-averaging approximation. The solutions overlay in the very early time, $t_{LD} \leq 10^{-5}$, and as pseudoradial flow develops when $t_{LD} \geq 3$, but diverge during the intermediate dimensionless times. However, the maximum deviation between the solution and pressure-averaging approximation is only 7.30% and is observed at $t_{LD} = 0.60$.

The pressure-averaging approximation for multiple infinite-conductivity fractures is developed from the definition of the average of a function, which is written as

$$\widehat{f(x)} = \frac{\int_a^b f(x) dx}{b-a}, \dots\dots\dots (D-48)$$

where for a pressure-averaging multiple infinite-conductivity Laplace-domain fracture solution, the function $f(x)$ is the pressure in the ℓ^{th} -fracture defined by the Laplace domain uniform-flux multiple-fracture solution (Eq. D-37) as

$$f(x) = (\bar{p}_{LjD})_\ell = \sum_{i=1}^{n_f} \frac{\bar{q}_{iD}}{2L_{fiD}} \int_{-L_{fiD}}^{L_{fiD}} K_0 \left[\sqrt{u} \sqrt{[r_D \cos(\theta_\ell - \theta_i) - \alpha]^2 + r_D^2 \sin^2(\theta_\ell - \theta_i)} \right] d\alpha \dots\dots (D-49)$$

With the definition of the average of a function, the pressure-averaging approximate infinite-conductivity solution is written as a system of equations with the dimensionless pressure in the Laplace domain for the ℓ^{th} -fracture written as

$$\begin{aligned} (\widehat{\bar{p}_{LjD}})_\ell &= \sum_{j=1}^{n_f} \frac{\bar{q}_{jD}}{2L_{f\ell D} L_{jD}} \frac{1}{2s} \int_{-L_{f\ell D}}^{L_{f\ell D}} \int_{-L_{jD}}^{L_{jD}} K_0 \left[\sqrt{u} \sqrt{[r_D \cos(\theta_\ell - \theta_j) - \alpha]^2 + r_D^2 \sin^2(\theta_\ell - \theta_j)} \right] d\alpha dr_D \\ &\ell = 1, 2, \dots, n_f, \dots\dots\dots (D-50) \end{aligned}$$

and the dimensionless flow rate for all fractures in Laplace space written as

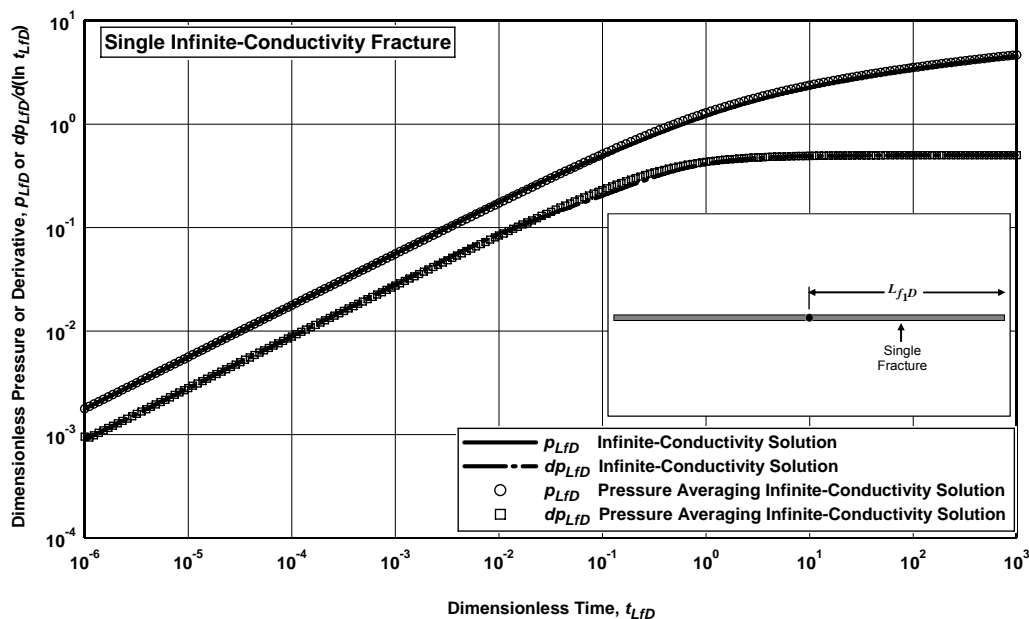


Fig. D-2—A comparison of the equivalent average pressure point infinite-conductivity solution with the pressure-averaging approximation for a single fracture.

$$\sum_{j=1}^{n_f} \bar{q}_{jD} = \frac{1}{s} \dots\dots\dots(D-51)$$

The system of equations is formed by recognizing that for infinite-conductivity fractures, the Laplace space dimensionless pressure in each fracture is the same, which is written as

$$(\widehat{\bar{p}}_{LjD})_1 = (\widehat{\bar{p}}_{LjD})_2 = \dots = (\widehat{\bar{p}}_{LjD})_{n_f} = \widehat{\bar{p}}_{LjD} \dots\dots\dots(D-52)$$

and the system of equations can be written as

$$\begin{bmatrix} 1 & A_{11} & A_{12} & \dots & A_{1n_f} \\ 1 & A_{21} & A_{22} & \dots & A_{2n_f} \\ \vdots & \vdots & \vdots & \dots & \vdots \\ 1 & A_{n_f1} & A_{n_f2} & \dots & A_{n_fn_f} \\ 0 & 1 & 1 & \dots & 1 \end{bmatrix} \begin{bmatrix} \widehat{\bar{p}}_{LjD} \\ \bar{q}_{1D} \\ \bar{q}_{2D} \\ \vdots \\ \bar{q}_{n_fD} \end{bmatrix} = \begin{bmatrix} 0 \\ 0 \\ 0 \\ \vdots \\ \frac{1}{s} \end{bmatrix} \dots\dots\dots(D-53)$$

where

$$A_{ij} = \frac{(-1)^{i+j}}{L_{fjD}L_{fiD}} \frac{1}{4s} \int_{-L_{fjD}}^{L_{fjD}} \int_{-L_{fiD}}^{L_{fiD}} K_0 \left[\sqrt{u} \sqrt{[r_D \cos(\theta_i - \theta_j) - \alpha]^2 + r_D^2 \sin^2(\theta_i - \theta_j)} \right] d\alpha dr_D \dots\dots\dots(D-54)$$

A semianalytical multiple arbitrarily-oriented infinite-conductivity fracture solution can also be developed in the Laplace domain without resorting to the pressure-averaging technique. Assume flux is not uniform along the fracture(s), and the dimensionless pressure for a fracture at an arbitrary angle, θ_i , accounting for the effect of a fracture(s) at angle θ_i is written as

$$(\bar{p}_D)_{li} = \frac{1}{2(L_{fD})_i} \int_{-(L_{fD})_i}^{(L_{fD})_i} (\bar{q}_D)_i(\alpha, s) K_0 \left[\sqrt{u} \sqrt{[r_{iD} \cos(\theta_\ell - \theta_i) - \alpha]^2 + r_{iD}^2 \sin^2(\theta_\ell - \theta_i)} \right] d\alpha, \dots\dots\dots(D-55)$$

where $i, \ell = 1, 2, \dots, n_f$. Note that the dimensionless flow rate for the i^{th} -fracture is defined as $(q_D)_i = q_i/q_{wi}$, where q_{wi} is the total flow rate assuming all production is from the i^{th} -fracture. Similarly, the dimensionless fracture half-length is defined relative to the i^{th} -fracture half-length, $(L_{fD})_i = L_{fi}/L_{fi} = 1$. If a point (r_{iD}, θ_i) is restricted to a point along the i^{th} -fracture axis, then the reference and fracture axis are the same and Eq. D-26 results in

$$\hat{x}_{iD} = r_{iD} \cos(\theta_i - \theta_i) = r_{iD}, \dots\dots\dots(D-56)$$

and the Laplace domain dimensionless pressure for fracture ℓ accounting for the effects of fracture i is written as

$$(\bar{p}_D)_{li} = \frac{1}{2} \int_{-1}^1 (\bar{q}_D)_i(\alpha, s) K_0 \left[\sqrt{u} \sqrt{[\hat{x}_{iD} \cos(\theta_\ell - \theta_i) - \alpha]^2 + \hat{x}_{iD}^2 \sin^2(\theta_\ell - \theta_i)} \right] d\alpha, \dots\dots\dots(D-57)$$

Assuming each fracture is homogeneous and symmetric, that is, $(q_D)_i(\alpha, t) = (q_D)_i(-\alpha, t)$, the reservoir component of the infinite-conductivity solution can be written as

$$\begin{aligned} & \int_{-1}^1 (\bar{q}_D)_i(\alpha, s) K_0 \left[\sqrt{u} \sqrt{[\hat{x}_{iD} \cos(\theta_\ell - \theta_i) - \alpha]^2 + \hat{x}_{iD}^2 \sin^2(\theta_\ell - \theta_i)} \right] d\alpha \\ &= \int_0^1 (\bar{q}_D)_i(\alpha, s) \left[\begin{array}{l} K_0 \left[\sqrt{u} \sqrt{[\hat{x}_{iD} \cos(\theta_\ell - \theta_i) - \alpha]^2 + \hat{x}_{iD}^2 \sin^2(\theta_\ell - \theta_i)} \right] \\ + K_0 \left[\sqrt{u} \sqrt{[\hat{x}_{iD} \cos(\theta_\ell - \theta_i) + \alpha]^2 + \hat{x}_{iD}^2 \sin^2(\theta_\ell - \theta_i)} \right] \end{array} \right] d\alpha, \dots\dots\dots(D-58) \end{aligned}$$

and the Laplace domain dimensionless pressure for an arbitrarily-oriented infinite-conductivity fracture ℓ in an isotropic reservoir accounting for the effects of an infinite-conductivity fracture i is written in the Laplace domain as

$$(\bar{p}_D)_{li} = \frac{1}{2} \int_0^1 (\bar{q}_D)_i(x', s) \left[\begin{array}{l} K_0 \left[\sqrt{u} \sqrt{[\hat{x}_{iD} \cos(\theta_\ell - \theta_i) - x']^2 + \hat{x}_{iD}^2 \sin^2(\theta_\ell - \theta_i)} \right] \\ + K_0 \left[\sqrt{u} \sqrt{[\hat{x}_{iD} \cos(\theta_\ell - \theta_i) + x']^2 + \hat{x}_{iD}^2 \sin^2(\theta_\ell - \theta_i)} \right] \end{array} \right] dx', \dots\dots\dots(D-59)$$

$i, \ell = 1, 2, \dots, n_f$

A semianalytical solution for the multiple infinite-conductivity fracture problem is obtained by dividing each fracture into n_{fs} equal segments of length, $\Delta\hat{x}_{iD} = L_{fjD} / n_{fs}$, and assuming constant flux in each segment. Note that $L_{fjD} = L_{fj} / L_{f1}$ where L_{f1} is the half-length of the primary fracture. Although the number of segments in each fracture is the same, the segment length can be different for each fracture, $\Delta\hat{x}_{iD} \neq \Delta\hat{x}_{jD}$. As shown in detail in Appendix E, the discretization allows the integral term to be written as

$$\begin{aligned} & \frac{1}{2} \int_0^1 (\bar{q}_D)_i(x', s) \left[K_0 \left[\sqrt{u} \sqrt{[\hat{x}_{iD} \cos(\theta_\ell - \theta_i) - x']^2 + \hat{x}_{iD}^2 \sin^2(\theta_\ell - \theta_i)} \right] \right. \\ & \left. + K_0 \left[\sqrt{u} \sqrt{[\hat{x}_{iD} \cos(\theta_\ell - \theta_i) + x']^2 + \hat{x}_{iD}^2 \sin^2(\theta_\ell - \theta_i)} \right] \right] dx' \\ & = \sum_{m=1}^{n_{fs}} \frac{(\bar{q}_D)_{im}(s)}{2} \int_{(\hat{x}_{iD})_m}^{(\hat{x}_{iD})_{m+1}} \left[K_0 \left[\sqrt{u} \sqrt{[(\hat{x}_{iD})_j \cos(\theta_\ell - \theta_i) - x']^2 + (\hat{x}_{iD})_j^2 \sin^2(\theta_\ell - \theta_i)} \right] \right. \\ & \left. + K_0 \left[\sqrt{u} \sqrt{[(\hat{x}_{iD})_j \cos(\theta_\ell - \theta_i) + x']^2 + (\hat{x}_{iD})_j^2 \sin^2(\theta_\ell - \theta_i)} \right] \right] dx', \dots \end{aligned} \quad (D-60)$$

and the Laplace domain dimensionless pressure for an arbitrarily-oriented infinite-conductivity fracture ℓ in an isotropic reservoir accounting for the effects of an infinite-conductivity fracture i is written in the Laplace domain as

$$\begin{aligned} (\bar{p}_D)_{\ell i}(s) &= \sum_{m=1}^{n_{fs}} \frac{(\bar{q}_D)_{im}(s)}{2} \int_{[\hat{x}_{iD}]_m}^{[\hat{x}_{iD}]_{m+1}} \left[K_0 \left[\sqrt{u} \sqrt{[(\hat{x}_{iD})_j \cos(\theta_\ell - \theta_i) - x']^2 + (\hat{x}_{iD})_j^2 \sin^2(\theta_\ell - \theta_i)} \right] \right. \\ & \left. + K_0 \left[\sqrt{u} \sqrt{[(\hat{x}_{iD})_j \cos(\theta_\ell - \theta_i) + x']^2 + (\hat{x}_{iD})_j^2 \sin^2(\theta_\ell - \theta_i)} \right] \right] dx', \\ & i, \ell = 1, 2, \dots, n_f \text{ and } j, m = 1, 2, \dots, n_{fs} \dots \end{aligned} \quad (D-61)$$

Solution for Multiple Arbitrarily-Oriented Infinite-Conductivity Vertical Fractures Considering Permeability Anisotropy

The multiple arbitrarily-oriented infinite-conductivity fracture solution considering permeability anisotropy in an infinite-slab reservoir is developed by defining the dimensionless distance variables as⁹⁵

$$x_D = \frac{x}{L_c} \sqrt{\frac{k}{k_x}}, \dots \quad (D-62)$$

$$y_D = \frac{y}{L_c} \sqrt{\frac{k}{k_y}}, \dots \quad (D-63)$$

and

$$k = \sqrt{k_x k_y} \dots \quad (D-64)$$

The dimensionless variables rescale the anisotropic reservoir to an equivalent isotropic system. As a result of the rescaling, the dimensionless fracture half-length changes and must be redefined as¹⁰⁶

$$L'_{fD} = \frac{L_f \hat{t}}{L_c} \sqrt{\frac{k}{k_x} \cos^2 \theta_f + \frac{k}{k_y} \sin^2 \theta_f}, \dots\dots\dots (D-65)$$

where the angle of the fracture with respect to the rescaled x_D -axis is written as

$$\theta'_f = \tan^{-1} \left(\sqrt{\frac{k_x}{k_y}} \tan \theta_f \right), \quad 0 < \theta_f < \frac{\pi}{2}. \dots\dots\dots (D-66)$$

When $\theta_f = 0$ or $\theta_f = \pi/2$, the angle does not rescale and $\theta'_f = \theta_f$.

The dimensionless fracture conductivity is defined in the original anisotropic system, which is written as,

$$C_{fD} = \frac{k_f w_f}{k L_f}, \dots\dots\dots (D-67)$$

but Spivey and Lee¹⁰⁶ note an equivalent dimensionless fracture conductivity can also be written in terms of the equivalent isotropic system.

With the redefined dimensionless variables, the Laplace domain dimensionless pressure for an arbitrarily-oriented infinite-conductivity fracture ℓ in an anisotropic reservoir accounting for the effects of an infinite-conductivity fracture i is written in the Laplace domain as

$$(\bar{p}_D)_{\ell i}(s) = \frac{1}{2} \int_0^1 (\bar{q}_D)_i(x', s) \left[\begin{array}{l} K_0 \left[\sqrt{u} \sqrt{[\hat{x}'_{iD} \cos(\theta'_\ell - \theta'_i) - x']^2 + \hat{x}'_{iD}{}^2 \sin^2(\theta'_\ell - \theta'_i)} \right] \\ + K_0 \left[\sqrt{u} \sqrt{[\hat{x}'_{iD} \cos(\theta'_\ell - \theta'_i) + x']^2 + \hat{x}'_{iD}{}^2 \sin^2(\theta'_\ell - \theta'_i)} \right] \end{array} \right] dx', \dots\dots\dots (D-68)$$

$i, \ell = 1, 2, \dots, n_f$

where the angle, θ' , is defined in the rescaled equivalent isotropic reservoir and is related to the anisotropic reservoir by

$$\theta' = \begin{cases} \theta & \theta = 0 \\ \tan^{-1} \left(\sqrt{\frac{k_x}{k_y}} \tan \theta \right) & 0 < \theta < \pi/2 \\ \theta & \theta = \pi/2 \end{cases} \dots\dots\dots (D-69)$$

After discretizing the integral term, the Laplace domain dimensionless pressure for an arbitrarily-oriented infinite-conductivity fracture ℓ in an anisotropic reservoir accounting for the effects of an infinite-conductivity fracture i is written in the Laplace domain as

$$(\bar{p}_D)_{\ell i}(s) = \sum_{m=1}^{n_{fs}} \frac{(\bar{q}_D)_{im}(s)}{2} \left[\begin{array}{c} [\hat{x}'_{iD}]_{m+1} \left[K_0 \left[\sqrt{u} \sqrt{[(\hat{x}'_{iD})_j \cos(\theta'_\ell - \theta'_i) - x']^2 + (\hat{x}'_{iD})_j^2 \sin^2(\theta'_\ell - \theta'_i)} \right] \right. \\ \left. + K_0 \left[\sqrt{u} \sqrt{[(\hat{x}'_{iD})_j \cos(\theta'_\ell - \theta'_i) + x']^2 + (\hat{x}'_{iD})_j^2 \sin^2(\theta'_\ell - \theta'_i)} \right] \right] \\ [\hat{x}'_{iD}]_m \end{array} \right] dx' \quad i, \ell = 1, 2, \dots, n_f \text{ and } j, m = 1, 2, \dots, n_{fs}, \dots \text{(D-70)}$$

where $\Delta \hat{x}'_{iD} = L'_{fiD} / n_{fs}$.

A semianalytical solution accounting for multiple arbitrarily-oriented infinite-conductivity fractures in an anisotropic reservoir is written in the Laplace domain using superposition as

$$(\bar{p}_{LFD})_\ell(s) = \sum_{i=1}^{n_f} s \bar{q}_{iD} (\bar{p}_D)_{\ell i}, \dots \text{(D-71)}$$

which can also be written as

$$(\bar{p}_{LFD})_\ell(s) = \sum_{i=1}^{n_f} s \bar{q}_{iD} \sum_{m=1}^{n_{fs}} \frac{(\bar{q}_D)_{im}(s)}{2} \left[\begin{array}{c} [\hat{x}'_{iD}]_{m+1} \left[K_0 \left[\sqrt{u} \sqrt{[(\hat{x}'_{iD})_j \cos(\theta'_\ell - \theta'_i) - x']^2 + (\hat{x}'_{iD})_j^2 \sin^2(\theta'_\ell - \theta'_i)} \right] \right. \\ \left. + K_0 \left[\sqrt{u} \sqrt{[(\hat{x}'_{iD})_j \cos(\theta'_\ell - \theta'_i) + x']^2 + (\hat{x}'_{iD})_j^2 \sin^2(\theta'_\ell - \theta'_i)} \right] \right] \\ [\hat{x}'_{iD}]_m \end{array} \right] dx' \quad i, \ell = 1, 2, \dots, n_f \text{ and } j, m = 1, 2, \dots, n_{fs}, \dots \text{(D-72)}$$

with the Laplace domain dimensionless flow rate for a single fracture defined by

$$\Delta \hat{x}'_{iD} \sum_{m=1}^{n_{fs}} (\bar{q}_D)_{im} = \frac{1}{s}, \dots \text{(D-73)}$$

and the Laplace domain dimensionless total flow rate for n_f fractures defined by

$$\sum_{i=1}^{n_f} \bar{q}_{iD} = \frac{1}{s}. \dots \text{(D-74)}$$

For each fracture, an equation relating the dimensionless pressure is written in the Laplace domain as

$$(\bar{p}_D)_{\ell i}|_{j=1} = (\bar{p}_D)_{\ell i}|_{j=2} = \dots = (\bar{p}_D)_{\ell i}|_{j=n_{fs}} = (\bar{p}_D)_{\ell i}, \dots \text{(D-75)}$$

and for the entire multiple-fracture system, the dimensionless pressure at the wellbore is written in the Laplace domain as

$$(\bar{p}_{wD})_1 = (\bar{p}_{wD})_2 = \dots = (\bar{p}_{wD})_{n_f} = \bar{p}_{LFD}. \dots \text{(D-76)}$$

Development of a Matrix Equation and Algorithm for Multiple Infinite-Conductivity Fracture Solution

For each fracture divided into n_{fs} equal length uniform-flux segments, Eqs. D-71 through D-76 describe a system of $n_f(n_{fs} + n_f + 1) + 1$ equations and $n_f(n_{fs} + n_f + 1) + 1$ unknowns. The solution algorithm is a three

step process. First, a system of equations is developed for each fracture where the reference axis and the fracture axis coincide, that is, a system of equations is written to solve for $(\bar{p}_D)_{ii}$ and $(\bar{q}_D)_{im}$ where $i = 1, 2, \dots, n_f$ and $m = 1, 2, \dots, n_{fs}$. Solving the system of equations for each fracture requires writing an equation for each fracture segment, $j = 1, 2, \dots, n_{fs}$, which is demonstrated in detail in **Appendix E**.

Recall the solution for $(\bar{p}_D)_{\ell i}$ is written as

$$(\bar{p}_D)_{\ell i}(s) = \sum_{m=1}^{n_{fs}} \frac{(\bar{q}_D)_{im}(s)}{2} \left[\begin{array}{c} [\hat{x}'_{iD}]_{m+1} \\ K_0 \left[\sqrt{u} \sqrt{[(\hat{x}'_{iD})_j \cos(\theta'_\ell - \theta'_i) - x']^2 + (\hat{x}'_{iD})_j^2 \sin^2(\theta'_\ell - \theta'_i)} \right] \\ + K_0 \left[\sqrt{u} \sqrt{[(\hat{x}'_{iD})_j \cos(\theta'_\ell - \theta'_i) + x']^2 + (\hat{x}'_{iD})_j^2 \sin^2(\theta'_\ell - \theta'_i)} \right] \\ [\hat{x}'_{iD}]_m \end{array} \right] dx' \quad i, \ell = 1, 2, \dots, n_f \text{ and } j, m = 1, 2, \dots, n_{fs} \dots \dots \dots (D-77)$$

Define a variable of substitution, $(\zeta_{ik})_{mj}$, as

$$(\zeta_{\ell i})_{mj} = \frac{1}{2} \left[\begin{array}{c} [\hat{x}'_{iD}]_{m+1} \\ K_0 \left[\sqrt{u} \sqrt{[(\hat{x}'_{iD})_j \cos(\theta'_\ell - \theta'_i) - x']^2 + (\hat{x}'_{iD})_j^2 \sin^2(\theta'_\ell - \theta'_i)} \right] \\ + K_0 \left[\sqrt{u} \sqrt{[(\hat{x}'_{iD})_j \cos(\theta'_\ell - \theta'_i) + x']^2 + (\hat{x}'_{iD})_j^2 \sin^2(\theta'_\ell - \theta'_i)} \right] \\ [\hat{x}'_{iD}]_m \end{array} \right] dx', \dots \dots \dots (D-78)$$

and a system of equations can be written as

$$\mathbf{A}_{ii} \mathbf{x}_i = \mathbf{b}_i, \dots \dots \dots (D-79)$$

where

$$\mathbf{A}_{ii} = \left[\begin{array}{cccccc} -(\zeta_{ii})_{11} & -(\zeta_{ii})_{21} & \dots & -(\zeta_{ii})_{n_{fs}1} & 1 \\ -(\zeta_{ii})_{12} & (\zeta_{ii})_{22} & \dots & -(\zeta_{ii})_{n_{fs}2} & 1 \\ -(\zeta_{ii})_{13} & (\zeta_{ii})_{23} & \dots & -(\zeta_{ii})_{n_{fs}3} & 1 \\ \vdots & \vdots & \ddots & \vdots & \vdots \\ -(\zeta_{ii})_{1n_{fs}-1} & -(\zeta_{ii})_{2n_{fs}-1} & \dots & -(\zeta_{ii})_{(n_{fs}n_{fs}-1)} & 1 \\ -(\zeta_{ii})_{1n_{fs}} & -(\zeta_{ii})_{2n_{fs}} & \dots & -(\zeta_{ii})_{n_{fs}n_{fs}} & 1 \\ \Delta \hat{x}'_{iD} & \Delta \hat{x}'_{iD} & \dots & \Delta \hat{x}'_{iD} & 0 \end{array} \right]_{n_{fs}+1 \times n_{fs}+1}, \quad i = 1, 2, \dots, n_f, \dots \dots \dots (D-80)$$

$$\mathbf{x}_i = \left[\begin{array}{c} (\bar{q}_D)_{i1} \\ (\bar{q}_D)_{i2} \\ \vdots \\ (\bar{q}_D)_{in_{fs}} \\ (\bar{p}_D)_{ik}(s) \end{array} \right]_{n_{fs}+1 \times 1}, \dots \dots \dots (D-81)$$

and

$$\mathbf{b}_i = \begin{bmatrix} 0 \\ \vdots \\ 0 \\ 1 \\ s \end{bmatrix}_{n_{fs}+1 \times 1} \dots \dots \dots (D-82)$$

Second, after solving the system of equations for $(\bar{p}_D)_{ii}$ and $(\bar{q}_D)_{im}$, the dimensionless pressure terms, $(\bar{p}_D)_{\ell i}$, with $i \neq \ell$ are easily evaluated for any j as

$$(\bar{p}_D)_{\ell i} = \sum_{m=1}^{n_{fs}} (\bar{q}_D)_{im} (\zeta_{\ell i})_{jm} \dots \dots \dots (D-83)$$

Third, the semianalytical solution for producing through n_f arbitrarily-oriented infinite-conductivity fractures in an infinite-slab anisotropic reservoir can be written as a system of equations in the Laplace domain as

$$\mathbf{Ax} = \mathbf{b} \dots \dots \dots (D-84)$$

where

$$\mathbf{A} = \begin{bmatrix} s(\bar{p}_D)_{11} & s(\bar{p}_D)_{12} & \dots & s(\bar{p}_D)_{1n_f} & -1 \\ s(\bar{p}_D)_{21} & s(\bar{p}_D)_{22} & \dots & s(\bar{p}_D)_{2n_f} & -1 \\ \vdots & \vdots & \ddots & \vdots & \vdots \\ s(\bar{p}_D)_{n_f 1} & s(\bar{p}_D)_{n_f 2} & \dots & s(\bar{p}_D)_{n_f n_f} & -1 \\ s & s & \dots & s & 0 \end{bmatrix}_{n_f+1 \times n_f+1} \dots \dots \dots (D-85)$$

$$\mathbf{x} = \begin{bmatrix} \bar{q}_{1D} \\ \bar{q}_{2D} \\ \vdots \\ \bar{q}_{n_f D} \\ \bar{p}_{LjD} \end{bmatrix}_{n_f+1 \times 1} \dots \dots \dots (D-86)$$

and

$$\mathbf{b} = \begin{bmatrix} 0 \\ 0 \\ \vdots \\ 0 \\ 1 \end{bmatrix}_{n_f+1 \times 1} \dots \dots \dots (D-87)$$

The system of equations, Eq. D-84, are solved in the Laplace domain and then inverted to the time domain to obtain the dimensionless pressure. The system of equations is solved within the Stehfest⁶⁸ algorithm, which is used for the Laplace to time domain inversion. With the Stehfest algorithm, s is calculated, and the \mathbf{A} and \mathbf{b} matrices are evaluated. Eq. D-84 is then solved as part of the numerical transformation from

the Laplace to the time domain. Since the system of equations is a function of s , the system must be solved N times during each Laplace to time domain inversion, where N is the number of Stehfest extrapolation coefficients.

Fig. D-3 shows a log-log graph of dimensionless pressure and dimensionless pressure derivative versus dimensionless time for a cruciform fracture where the angle between the fractures is $\pi/2$. In Fig. D-3, the inset graphic illustrates a cruciform fracture with primary fracture half length, L_{f1D} , and the secondary fracture half length is defined by the ratio of secondary to primary fracture half length, $\delta_L = L_{f2D}/L_{f1D}$, where in Fig. D-3, $\delta_L = 1$. The constant-rate type curves shown in Fig. D-3 illustrate that the pressure-averaging infinite-conductivity approximation and the semianalytical infinite-conductivity solution for a cruciform fracture are in agreement during the very early dimensionless times, $t_{LFD} \leq 10^{-5}$, and as pseudoradial flow develops when $t_{LFD} \geq 3$. However, the pressure-averaging approximation diverges significantly from the semianalytical solution at intermediate dimensionless times.

Similar comparisons result with decreasing secondary fracture half length as shown by the constant-rate type curves in **Figs. D-4 through D-6** for a cruciform infinite-conductivity fracture with $\delta_L = 3/4, 1/2$, and $1/4$. Consequently, the pressure-averaging method is *not* a good approximation of the cruciform infinite-conductivity fracture solution during intermediate dimensionless times, $\approx 10^{-5} \leq t_{LFD} \leq 3$.

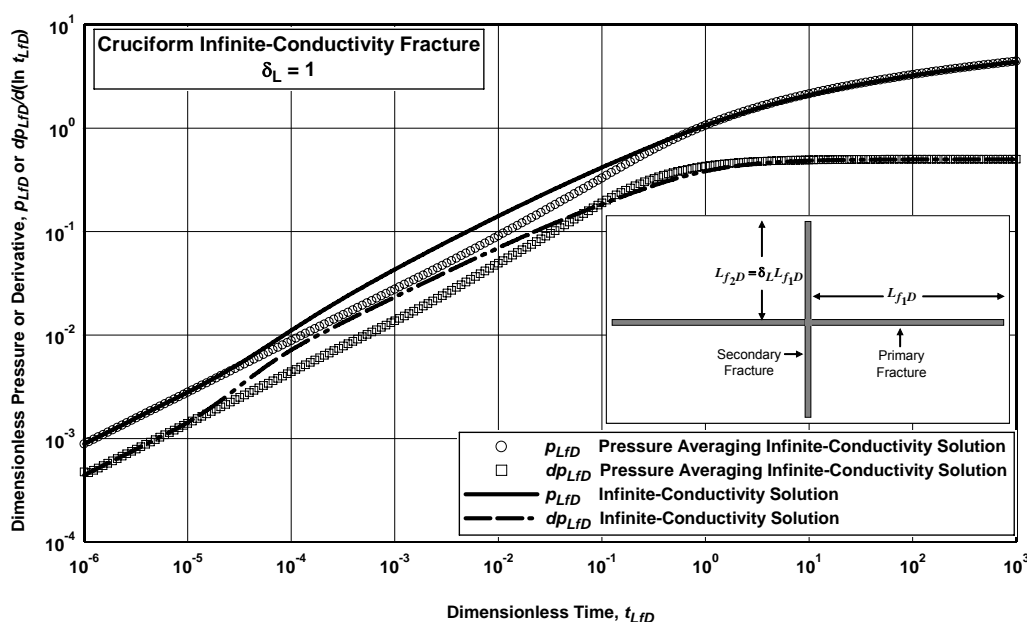


Fig. D-3—A comparison of a pressure-averaging infinite-conductivity solution and the semianalytical infinite-conductivity solution for a cruciform fracture with $\delta_L = 1$.

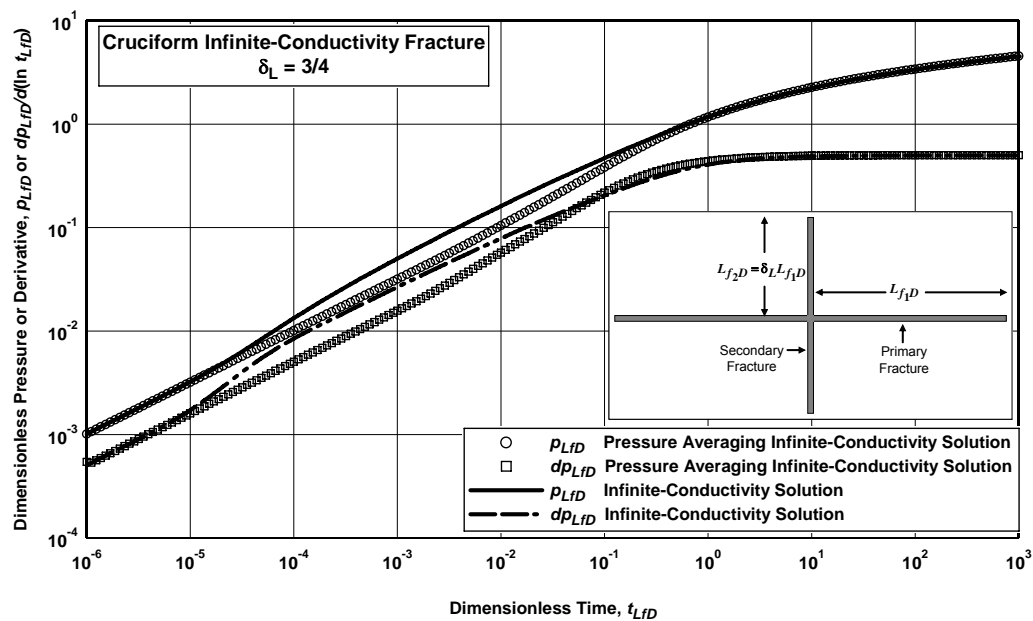


Fig. D-4—A comparison of a pressure-averaging infinite-conductivity solution and the semianalytical infinite-conductivity solution for a cruciform fracture with $\delta_L = 3/4$.

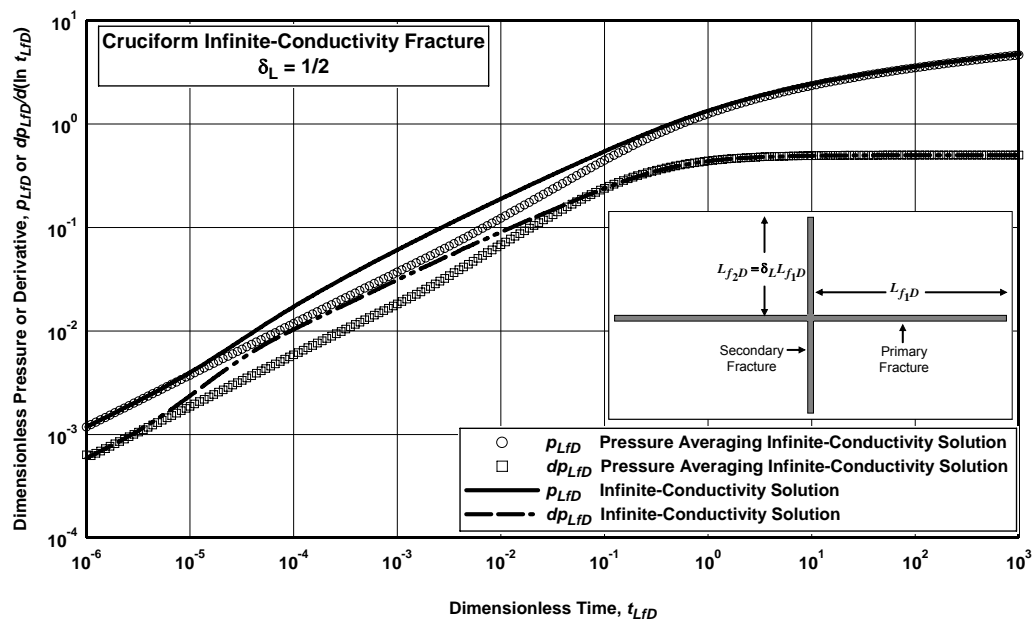


Fig. D-5—A comparison of a pressure-averaging infinite-conductivity solution and the semianalytical infinite-conductivity solution for a cruciform fracture with $\delta_L = 1/2$.

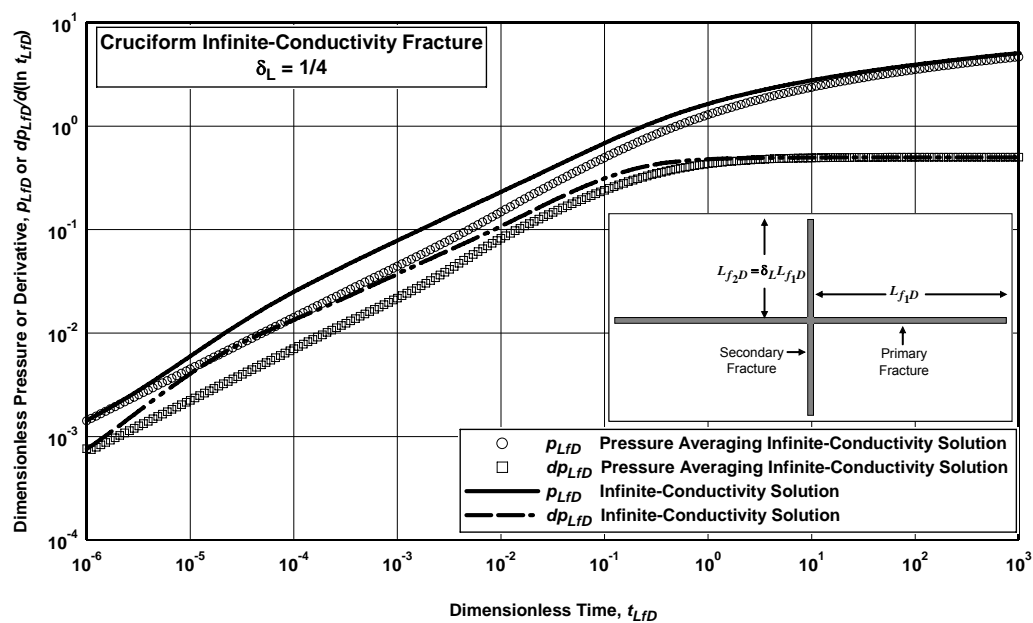


Fig. D-6—A comparison of a pressure-averaging infinite-conductivity solution and the semianalytical infinite-conductivity solution for a cruciform fracture with $\delta_L = 1/4$.

APPENDIX E

ANALYTICAL PRESSURE-TRANSIENT SOLUTION FOR A WELL CONTAINING MULTIPLE FINITE-CONDUCTIVITY VERTICAL FRACTURES IN AN INFINITE SLAB RESERVOIR

The development of a multiple finite-conductivity vertical fracture solution requires writing a general solution for a finite-conductivity vertical fracture at any arbitrary angle, θ , from the x_D -axis. The development follows from the finite-conductivity solutions of Cinco-Ley *et al.*¹⁰⁷ and, for the dual-porosity case, Cinco-Ley and Meng.⁸⁶ **Fig. E-1** illustrates a vertical finite-conductivity fracture at an angle, θ , from the x_D -axis in an isotropic reservoir.

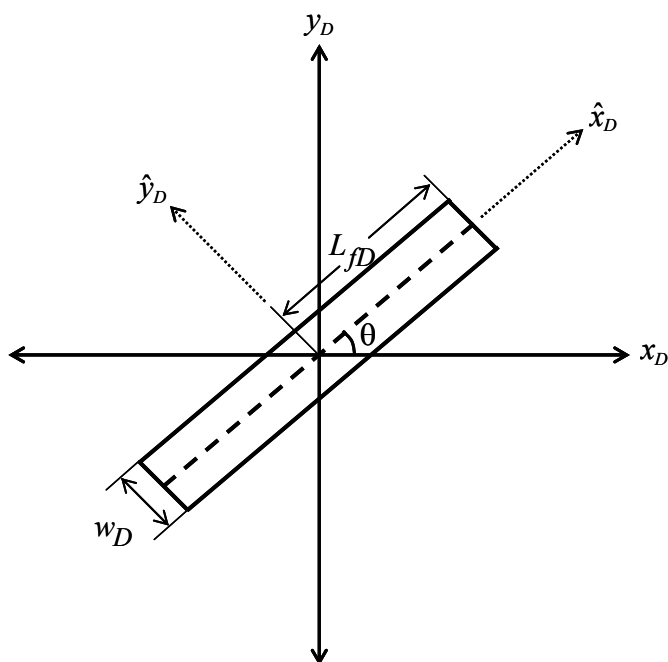


Fig. E-1—A vertical finite-conductivity fracture at an arbitrary angle to the x -axis.

A finite-conductivity solution requires coupling reservoir and fracture solutions, and as shown in **Appendix D**, a general plane-source constant-flux solution for a single arbitrarily-oriented fracture in an isotropic reservoir is written in the Laplace domain as

$$\bar{p}_D = \frac{q_D}{L_{fD}} \frac{1}{2s} \int_{-L_{fD}}^{L_{fD}} K_0 \left[\sqrt{u} \sqrt{(\hat{x}_D - \alpha)^2 + (\hat{y}_D)^2} \right] d\alpha, \dots\dots\dots (E-1)$$

where

$$\bar{p}_D = \frac{2\pi kh\Delta p}{q_t \mu}, \dots\dots\dots (E-2)$$

$$L_{fD} = \frac{L_f}{L_c}, \dots\dots\dots (E-3)$$

$$\hat{x}_D = x_D \cos \theta_f + y_D \sin \theta_f, \dots\dots\dots (E-4)$$

$$\hat{y}_D = y_D \cos \theta_f - x_D \sin \theta_f. \dots\dots\dots (E-5)$$

$$x_D = \frac{x}{L_c} \sqrt{\frac{k}{k_x}}, \dots\dots\dots (E-6)$$

$$y_D = \frac{y}{L_c} \sqrt{\frac{k}{k_y}}, \dots\dots\dots (E-7)$$

and defining the total constant flow rate as q_t , the dimensionless flow rate is written as

$$q_D = \frac{q}{q_t} = 1, \dots\dots\dots (E-8)$$

The fracture half-length, L_f , is the reference length for the system, and the horizontal permeability is written as $k = (k_x k_y)^{1/2}$, where for an isotropic reservoir, $k = k_x = k_y$. The Laplace variable is denoted by s , and the general solution accounts for dual-porosity reservoirs with u defined as

$$u = sf(s), \dots\dots\dots (E-9)$$

where for a single-porosity $f(s) = 1$. For a pseudosteady-state interporosity flow dual porosity case, $f(s)$ is written as⁹⁶

$$f(s) = \frac{\lambda + \omega(1-\omega)s}{\lambda + (1-\omega)s}, \dots\dots\dots (E-10)$$

for transient interporosity flow with slab matrix blocks,⁹⁷⁻⁹⁸

$$f(s) = \omega + \sqrt{\frac{\lambda(1-\omega)}{3s}} \tanh \sqrt{\frac{3(1-\omega)s}{\lambda}}, \dots\dots\dots (E-11)$$

and for transient interporosity flow with spherical matrix blocks,⁹⁷⁻⁹⁸

$$f(s) = \omega + \frac{\lambda}{5s} \left[\sqrt{\frac{15(1-\omega)s}{\lambda}} \coth \sqrt{\frac{15(1-\omega)s}{\lambda}} - 1 \right]. \dots\dots\dots (E-12)$$

For the finite-conductivity case, the flux is not constant and the Laplace domain plane-source solution for a reservoir containing an arbitrarily-oriented vertical fracture is modified and written as

$$\bar{p}_D = \frac{1}{2L_{fD}} \int_{-L_{fD}}^{L_{fD}} \bar{q}_D(\alpha, s) K_0 \left[\sqrt{u} \sqrt{(\hat{x}_D - \alpha)^2 + (\hat{y}_D)^2} \right] d\alpha, \dots\dots\dots (E-13)$$

A general fracture solution is developed by assuming

- The fracture is modeled as a homogeneous slab porous medium with fracture half-length, L_f , fracture width, w_f , and fully penetrating across the entire reservoir thickness, h .
- Fluid flow into the fracture is along the fracture length and no flow enters through the fracture tips.
- Fluid flow in the fracture is incompressible and steady by virtue of the limited pore volume of the fracture relative to the reservoir.
- The fracture centerline is aligned with the \hat{x}_D -axis which is rotated by an angle, θ , from the x_D -axis.

The dimensionless Laplace domain partial differential equation describing transient flow in a finite-conductivity fracture oriented along the \hat{x}_D -axis, is written as

$$\frac{\partial^2 \bar{p}_{LfD}}{\partial^2 \hat{x}_D} + \frac{2}{C_{fD}} \frac{\partial \bar{p}_D}{\partial \hat{y}_D} \bigg|_{\hat{y}_D=w_D/2} = 0, \dots\dots\dots (E-14)$$

for $-1 \leq \hat{x}_D \leq 1$. The dimensionless Laplace domain partial differential equation can also be written as

$$\frac{\partial^2 \bar{p}_{LfD}}{\partial^2 \hat{x}_D} - \frac{\pi}{C_{fD}} \bar{q}_D(\hat{x}_D) = 0, \dots\dots\dots (E-15)$$

where the dimensionless variables are defined as

$$\bar{q}_D(\hat{x}_D) = \frac{2L_f \bar{q}(\hat{x}, s)}{q_w} = \frac{-2}{\pi} \frac{\partial \bar{p}_D}{\partial \hat{y}_D} \bigg|_{\hat{y}_D=w_D/2}, \dots\dots\dots (E-16)$$

$$w_D = \frac{w_f}{L_f}, \dots\dots\dots (E-17)$$

$$C_{fD} = \frac{k_f w_f}{k L_f}, \dots\dots\dots (E-18)$$

and $\bar{q}(\hat{x}, s)$ is the Laplace domain flow rate per unit length into the fracture, q_w is the total well flow rate, and k_f is the fracture permeability.

The fracture-flow “wellbore” boundary condition for a constant rate is written in the Laplace domain as

$$\frac{\partial \bar{p}_{LfD}}{\partial \hat{x}_D} \bigg|_{\hat{x}_D=0} = -\frac{\pi}{s C_{fD}}, \dots\dots\dots (E-19)$$

and the boundary condition for no flow through the fracture tip is written in the Laplace domain as

$$\left. \frac{\partial \bar{p}_{LjD}}{\partial \hat{x}_D} \right|_{\hat{x}_D=\pm 1} = 0 \dots\dots\dots (E-20)$$

Eq. E-15 is integrated twice with respect to \hat{x}_D , and the general Laplace domain pressure distribution in a finite-conductivity fracture is written as

$$\bar{p}_{jD}(s) - \bar{p}_D(\hat{x}_D, s) = \frac{\pi \hat{x}_D}{s C_{jD}} - \frac{\pi}{C_{jD}} \int_0^{\hat{x}_D} \int_0^{x'} \bar{q}_D(x'', s) dx'' dx' \dots\dots\dots (E-21)$$

where $\bar{p}_D(\hat{x}_D, s)$ is the general reservoir solution defined in Eq. E-13. Adding the reservoir and fracture solutions results in the Laplace domain dimensionless pressure solution for a finite-conductivity fracture rotated by an angle θ_f from the x -axis, which is written as

$$\begin{aligned} \bar{p}_{jD}(s) = & \frac{1}{L_{jD}} \frac{1}{2} \int_{-L_{jD}}^{L_{jD}} \bar{q}_D(\alpha, s) K_0 \left[\sqrt{u} \sqrt{(\hat{x}_D - \alpha)^2 + (\hat{y}_D)^2} \right] d\alpha \\ & + \frac{\pi \hat{x}_D}{s C_{jD}} - \frac{\pi}{C_{jD}} \int_0^{\hat{x}_D} \int_0^{x'} \bar{q}_D(x'', s) dx'' dx', \dots\dots\dots (E-22) \end{aligned}$$

where dimensionless variables are defined as

$$r_D = \sqrt{x_D^2 + y_D^2}, \dots\dots\dots (E-23)$$

$$x_D = r_D \cos \theta_r, \dots\dots\dots (E-24)$$

$$y_D = r_D \sin \theta_r, \dots\dots\dots (E-25)$$

$$\hat{x}_D = x_D \cos \theta_f + y_D \sin \theta_f, \dots\dots\dots (E-26)$$

$$\hat{y}_D = y_D \cos \theta_f - x_D \sin \theta_f, \dots\dots\dots (E-27)$$

and θ_f is the angle between the fracture and the x_D -axis, (r_D, θ_r) are the polar coordinates of a point (x_D, y_D) , and (α, θ_f) are the polar coordinates of a point along the fracture. Combining Eqs. E-25 through E-27 results in

$$\hat{x}_D = r_D \cos(\theta_r - \theta_f), \dots\dots\dots (E-28)$$

and

$$\hat{y}_D = r_D \sin(\theta_r - \theta_f). \dots\dots\dots (E-29)$$

Consequently, the Laplace domain dimensionless pressure solution for a finite-conductivity fracture rotated by an angle θ_f from the x_D -axis is written as

$$\begin{aligned} \bar{p}_{fD}(s) = & \frac{1}{L_{fD}} \frac{1}{2} \int_{-L_{fD}}^{L_{fD}} \bar{q}_D(\alpha, s) K_0 \left[\sqrt{u} \sqrt{r_D \cos(\theta_r - \theta_f) - \alpha}^2 + r_D^2 \sin^2(\theta_r - \theta_f) \right] d\alpha \\ & + \frac{\pi \hat{x}_D}{s C_{fD}} - \frac{\pi}{C_{fD}} \int_0^{\hat{x}_D} \int_0^{x'} \bar{q}_D(x'', s) dx'' dx', \dots\dots\dots (E-30) \end{aligned}$$

where for a single fracture $\theta_r = \theta_f$, $\hat{x}_D = r_D$, $L_{fD} = 1$, and the single fracture solution is written as

$$\bar{p}_{fD}(s) = \frac{1}{2} \int_{-1}^1 \bar{q}_D(x', s) K_0 \left[\sqrt{u} \sqrt{\hat{x}_D - x'} \right] dx' + \frac{\pi \hat{x}_D}{s C_{fD}} - \frac{\pi}{C_{fD}} \int_0^{\hat{x}_D} \int_0^{x'} \bar{q}_D(x'', s) dx'' dx' \dots\dots\dots (E-31)$$

For a well in an infinite-slab reservoir producing through multiple finite-conductivity fractures, the Laplace domain dimensionless pressure for a fracture ℓ at an arbitrary angle, θ_ℓ , accounting for the effects of fracture i at an angle θ_i is written as

$$\begin{aligned} (\bar{p}_D)_{\ell i}(s) = & \frac{1}{2(L_{fD})_i} \int_{-(L_{fD})_i}^{(L_{fD})_i} (\bar{q}_D)_i(\alpha, s) K_0 \left[\sqrt{u} \sqrt{r_{iD} \cos(\theta_\ell - \theta_i) - \alpha}^2 + r_{iD}^2 \sin^2(\theta_\ell - \theta_i) \right] d\alpha \\ & + \frac{\pi \hat{x}_{iD}}{s C_{fiD}} - \frac{\pi}{C_{fiD}} \int_0^{\hat{x}_{iD}} \int_0^{x'} (\bar{q}_D)_i(x'', s) dx'' dx' \quad , \quad \ell = 1, 2, \dots, n_f, \dots\dots\dots (E-32) \end{aligned}$$

where $i, \ell = 1, 2, \dots, n_f$ and n_f is the number of fractures. Note that the dimensionless flow rate for the i^{th} -fracture is defined as $(q_D)_i = q_i/q_{wi}$, where q_{wi} is the well flow rate assuming all production is from the i^{th} -fracture. Similarly, the dimensionless fracture half-length is defined relative to the i^{th} -fracture half-length, $(L_{fD})_i = L_{fi}/L_{fi} = 1$. If a point (r_{iD}, θ_i) is restricted to a point along the i^{th} -fracture axis, then the reference and fracture axis are the same and Eq. E-28 results in

$$\hat{x}_{iD} = r_{iD} \cos(\theta_i - \theta_i) = r_{iD}, \dots\dots\dots (E-33)$$

and the Laplace domain finite-conductivity fracture dimensionless pressure can be written as

$$\begin{aligned} (\bar{p}_D)_{\ell i}(s) = & \frac{1}{2} \int_{-1}^1 (\bar{q}_D)_i(\alpha, s) K_0 \left[\sqrt{u} \sqrt{\hat{x}_{iD} \cos(\theta_\ell - \theta_i) - \alpha}^2 + \hat{x}_{iD}^2 \sin^2(\theta_\ell - \theta_i) \right] d\alpha \\ & + \frac{\pi \hat{x}_{iD}}{s C_{fiD}} - \frac{\pi}{C_{fiD}} \int_0^{\hat{x}_{iD}} \int_0^{x'} (\bar{q}_D)_i(x'', s) dx'' dx' \quad , \quad i, \ell = 1, 2, \dots, n_f \dots\dots\dots (E-34) \end{aligned}$$

Assuming each fracture is homogeneous and symmetric, that is, $(\bar{q}_D)_i(\alpha, s) = (\bar{q}_D)_i(-\alpha, s)$, the reservoir component of the Laplace domain dimensionless pressure can be written as

$$\int_{-1}^1 (\bar{q}_D)_i(\alpha, s) K_0 \left[\sqrt{u} \sqrt{[\hat{x}_{iD} \cos(\theta_\ell - \theta_i) - \alpha]^2 + \hat{x}_{iD}^2 \sin^2(\theta_\ell - \theta_i)} \right] d\alpha$$

$$= \int_0^1 (\bar{q}_D)_i(\alpha, s) \left[\begin{array}{l} K_0 \left[\sqrt{u} \sqrt{[\hat{x}_{iD} \cos(\theta_\ell - \theta_i) - \alpha]^2 + \hat{x}_{iD}^2 \sin^2(\theta_\ell - \theta_i)} \right] \\ + K_0 \left[\sqrt{u} \sqrt{[\hat{x}_{iD} \cos(\theta_\ell - \theta_i) + \alpha]^2 + \hat{x}_{iD}^2 \sin^2(\theta_\ell - \theta_i)} \right] \end{array} \right] d\alpha, \dots\dots\dots (E-35)$$

and the dimensionless pressure for a finite-conductivity fracture ℓ accounting for a finite-conductivity fracture i in an isotropic reservoir is written as

$$(\bar{p}_D)_{\ell i}(s) = \frac{1}{2} \int_0^1 (\bar{q}_D)_i(x', s) \left[\begin{array}{l} K_0 \left[\sqrt{u} \sqrt{[\hat{x}_{iD} \cos(\theta_\ell - \theta_i) - x']^2 + \hat{x}_{iD}^2 \sin^2(\theta_\ell - \theta_i)} \right] \\ + K_0 \left[\sqrt{u} \sqrt{[\hat{x}_{iD} \cos(\theta_\ell - \theta_i) + x']^2 + \hat{x}_{iD}^2 \sin^2(\theta_\ell - \theta_i)} \right] \end{array} \right] dx'$$

$$+ \frac{\pi \hat{x}_{iD}}{s C_{fjD}} - \frac{\pi}{C_{fjD}} \int_0^{\hat{x}_{iD}} \int_0^{x'} (\bar{q}_D)_i(x'', s) dx'' dx' \quad , \quad i, \ell = 1, 2, \dots, n_f \dots\dots\dots (E-36)$$

A semianalytical solution for the multiple finite-conductivity fracture problem is obtained by dividing each fracture into n_{fs} equal segments of length, $\Delta \hat{x}_{iD} = L_{fjD} / n_{fs}$, and assuming constant flux in each segment. Although the number of segments in each fracture is the same, the segment length can be different for each fracture, $\Delta \hat{x}_{iD} \neq \Delta \hat{x}_{jD}$. Note that $L_{fjD} = L_{fj} / L_{f1}$ where L_{f1} is the half-length of the primary fracture. With the discretization, the reservoir component of the Laplace domain dimensionless pressure can be written as

$$\frac{1}{2} \int_0^1 (\bar{q}_D)_i(x', s) \left[\begin{array}{l} K_0 \left[\sqrt{u} \sqrt{[\hat{x}_{iD} \cos(\theta_\ell - \theta_i) - x']^2 + \hat{x}_{iD}^2 \sin^2(\theta_\ell - \theta_i)} \right] \\ + K_0 \left[\sqrt{u} \sqrt{[\hat{x}_{iD} \cos(\theta_\ell - \theta_i) + x']^2 + \hat{x}_{iD}^2 \sin^2(\theta_\ell - \theta_i)} \right] \end{array} \right] dx'$$

$$= \sum_{m=1}^{n_{fs}} \frac{(\bar{q}_D)_{im}(s)}{2} \int_{(\hat{x}_{iD})_m}^{(\hat{x}_{iD})_{m+1}} \left[\begin{array}{l} K_0 \left[\sqrt{u} \sqrt{[(\hat{x}_{iD})_j \cos(\theta_\ell - \theta_i) - x']^2 + (\hat{x}_{iD})_j^2 \sin^2(\theta_\ell - \theta_i)} \right] \\ + K_0 \left[\sqrt{u} \sqrt{[(\hat{x}_{iD})_j \cos(\theta_\ell - \theta_i) + x']^2 + (\hat{x}_{iD})_j^2 \sin^2(\theta_\ell - \theta_i)} \right] \end{array} \right] dx' \dots\dots\dots (E-37)$$

The fracture component is approximated by dividing the fracture into equal length segments as shown in **Fig. E-2**. The double integral, which is written as

$$\Psi = \int_0^{\hat{x}_{iD}} \int_0^{x'} (\bar{q}_D)_i(x'', s) dx'' dx' \dots\dots\dots (E-38)$$

describes any point in the fracture, but the approximation assumes a point within any segment can be represented by the midpoint of the segment.

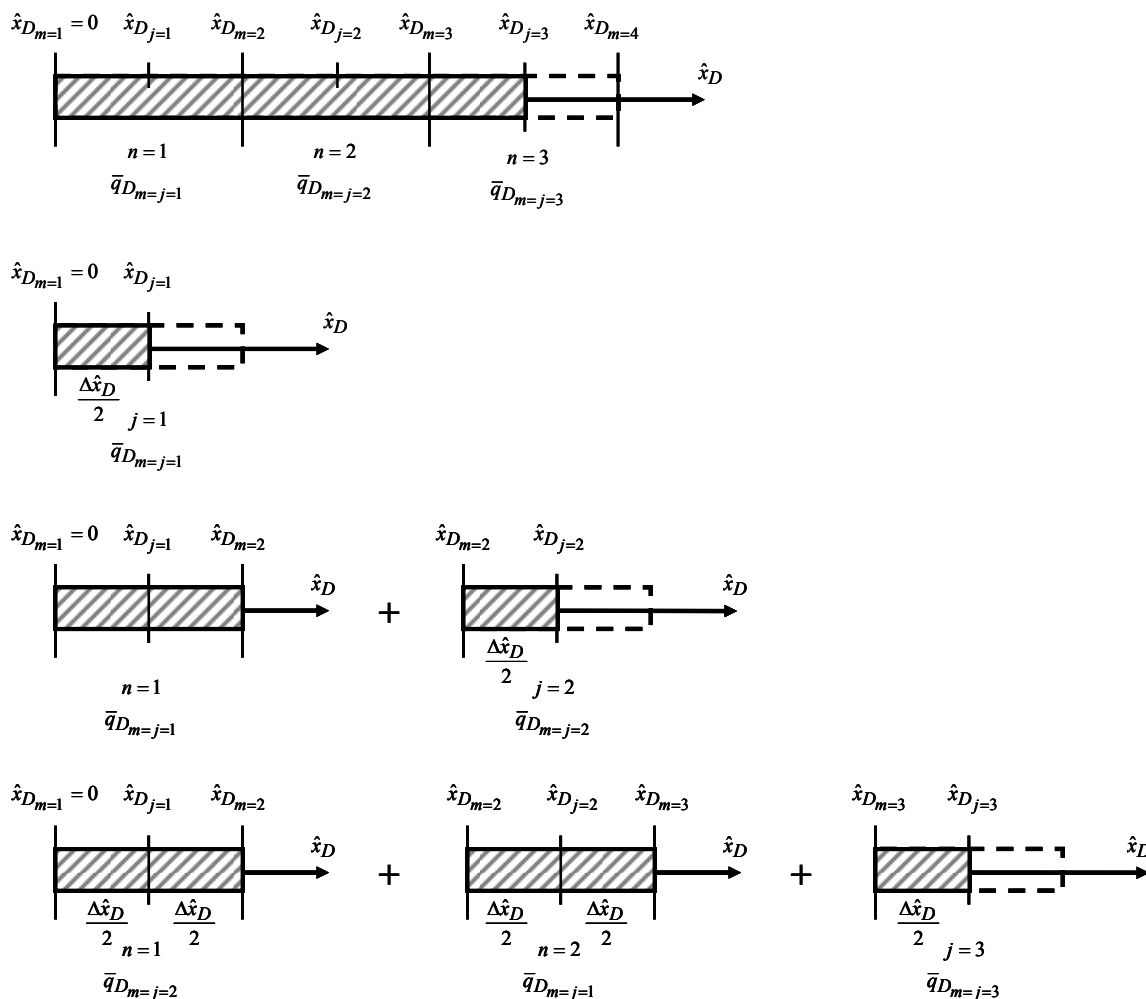


Fig. E-2. Fracture half-length discretization.

Let a point of interest be located in the first segment, $n = 1$, then $j = 1$ and the double integral can be written as

$$\Psi_{j=1} = \int_{(\hat{x}_{iD})_{m=1}}^{(\hat{x}_{iD})_{j=1}} \int_0^{x'} (\bar{q}_D)_i(x'', s) dx'' dx' \dots \dots \dots (E-39)$$

Assuming uniform flux within each fracture segment, $(\bar{q}_D)_i(x'', s) \equiv (\bar{q}_D)_{im=j}(s) = (\bar{q}_D)_{ij}$, and the double integral can now be written as

$$\Psi_{j=1} = \int_{(\hat{x}_{iD})_{m=1}}^{(\hat{x}_{iD})_{j=1}} (\bar{q}_D)_{ij=1}(s) \int_0^{x'} dx'' dx' = \int_{(\hat{x}_{iD})_{m=1}}^{(\hat{x}_{iD})_{j=1}} (\bar{q}_D)_{ij=1}(s) x' dx' \dots \dots \dots (E-40)$$

Referring to Fig. E-2 with $j = 1$ and $(\hat{x}_D)_{m=1}$, the limits of integration can also be written as

$$\Psi_{j=1} = \int_0^{\Delta \hat{x}_{iD}/2} (\bar{q}_D)_{ij=1} x' dx' = \frac{(\Delta \hat{x}_{iD})^2}{8} (\bar{q}_D)_{ij=1} \dots \dots \dots (E-41)$$

For the second segment, $j = 2$, the integration can be split into two parts (Fig. E-2), which is written as

$$\Psi_{j=2} = \int_{(\hat{x}_{iD})_{m=1}}^{(\hat{x}_{iD})_{m=2}} (\bar{q}_D)_{ij=1} \int_0^{x'} dx'' dx' + \int_{(\hat{x}_{iD})_{m=2}}^{(\hat{x}_{iD})_{j=2}} (\bar{q}_D)_{ij=2} \int_0^{x'} dx'' dx' \dots \dots \dots (E-42)$$

The uniform flux assumption for each equal length segment allows a local coordinate system to be used for integrating over any segment; thus,

$$\begin{aligned} \int_{(\hat{x}_{iD})_{m=2}}^{(\hat{x}_{iD})_{j=2}} (\bar{q}_D)_{ij=2} \int_0^{x'} dx'' dx' &= \int_{[(\hat{x}_{iD})_{m=2} - (\hat{x}_{iD})_{m=2}]^{[(\hat{x}_{iD})_{j=2} - (\hat{x}_{iD})_{m=2}]} (\bar{q}_D)_{ij=2} \int_0^{x'} dx'' dx' \\ &= \int_0^{\Delta \hat{x}_{iD}/2} (\bar{q}_D)_{ij=2} \int_0^{x'} dx'' dx', \dots \dots \dots (E-43) \end{aligned}$$

and after completing the integration, Eq. E-43 can be written as

$$\int_{(\hat{x}_{iD})_{m=2}}^{(\hat{x}_{iD})_{j=2}} (\bar{q}_D)_{ij=2} \int_0^{x'} dx'' dx' = \frac{(\Delta \hat{x}_{iD})^2}{8} (\bar{q}_D)_{ij=2} \dots \dots \dots (E-44)$$

The first integral of Eq. E-42 can also be evaluated using a local coordinate system, that is,

$$\int_{(\hat{x}_{iD})_{m=1}}^{(\hat{x}_{iD})_{m=2}} (\bar{q}_D)_{ij=1} \int_0^{x'} dx'' dx' = \int_0^{\Delta \hat{x}_{iD}} (\bar{q}_D)_{ij=1} \int_0^{x'} dx'' dx' = (\Delta \hat{x}_{iD})^2 (\bar{q}_D)_{ij=1} \dots \dots \dots (E-45)$$

Recognize that $(\Delta \hat{x}_D)^2$ can be written as

$$(\Delta \hat{x}_{iD})^2 = \Delta \hat{x}_{iD} (\Delta \hat{x}_{iD}) = (\Delta \hat{x}_{iD}) \left[\frac{\Delta \hat{x}_{iD}}{2} + \frac{\Delta \hat{x}_{iD}}{2} \right], \dots \dots \dots (E-46)$$

and Fig. E-2 shows that

$$\frac{\Delta \hat{x}_{iD}}{2} = (\hat{x}_{iD})_{j=2} - \Delta \hat{x}_{iD} \dots \dots \dots (E-47)$$

Consequently, the first integral of Eq. E-42 is written as

$$\int_{(\hat{x}_{iD})_{m=1}}^{(\hat{x}_{iD})_{m=2}} (\bar{q}_D)_{ij=1} \int_0^{x'} dx'' dx' = (\Delta \hat{x}_{iD}) \left[\frac{\Delta \hat{x}_{iD}}{2} + ((\hat{x}_{iD})_{j=2} - \Delta \hat{x}_{iD}) \right] (\bar{q}_D)_{ij=1}, \dots \dots \dots (E-48)$$

and $\Psi_{j=2}$ is written as

$$\Psi_{j=2} = \frac{(\Delta \hat{x}_{iD})^2}{8} (\bar{q}_D)_{ij=2} + \left[\frac{(\Delta \hat{x}_{iD})^2}{2} + (\Delta \hat{x}_{iD}) [(\hat{x}_{iD})_{j=2} - \Delta \hat{x}_{iD}] \right] (\bar{q}_D)_{ij=1} \dots \dots \dots (E-49)$$

The process can be repeated for $j = 3$ (Fig. E-2) by recognizing that each segment—and the integration over each segment—is independent, but over the same length. Consequently, the flux terms can be interchanged between blocks provided the sum of the integrations over each segment is equivalent to integrating over the entire fracture length. The resulting expression can be written as

$$\Psi_{j=3} = \frac{(\Delta\hat{x}_{iD})^2}{8}(\bar{q}_D)_{ij=3} + \left[\frac{(\Delta\hat{x}_{iD})^2}{2} + (\Delta\hat{x}_{iD})[(\hat{x}_{iD})_{j=3} - \Delta\hat{x}_{iD}] \right] (\bar{q}_D)_{ij=1} + \left[\frac{(\Delta\hat{x}_{iD})^2}{2} + (\Delta\hat{x}_{iD})[(\hat{x}_{iD})_{j=2} - 2\Delta\hat{x}_{iD}] \right] (\bar{q}_D)_{ij=2} \dots\dots\dots (E-50)$$

The pattern exhibited by Eqs. E-44, E-49, and E-50 suggests a general relationship can be written as

$$\Psi_j = \begin{cases} \frac{(\Delta\hat{x}_{iD})^2}{8}(\bar{q}_D)_{ij=1} & , \quad j = 1 \\ \frac{(\Delta\hat{x}_{iD})^2}{8}(\bar{q}_D)_{ij}(s) + \sum_{m=1}^{j-1} \left[\frac{(\Delta\hat{x}_{iD})^2}{2} + (\Delta\hat{x}_{iD})[(\hat{x}_{iD})_j - m\Delta\hat{x}_{iD}] \right] (\bar{q}_D)_{im}(s) & , \quad j > 1 \end{cases} \dots\dots\dots (E-51)$$

By combining the reservoir and fracture approximations, the Laplace domain dimensionless pressure for a finite-conductivity fracture ℓ accounting for a finite-conductivity fracture i in an isotropic infinite-slab reservoir with production through multiple finite-conductivity fractures is written as

$$(\bar{p}_D)_{\ell i} = \begin{cases} \sum_{m=1}^{n_{fs}} \frac{(\bar{q}_D)_{im}(s)}{2} \int_{[\hat{x}_{iD}]_m}^{[\hat{x}_{iD}]_{m+1}} \left[\begin{aligned} &K_0 \left[\sqrt{u} \sqrt{[(\hat{x}_{iD})_{j=1} \cos(\theta_\ell - \theta_i) - x']^2 + (\hat{x}_{iD})_{j=1}^2 \sin^2(\theta_\ell - \theta_i)} \right] \\ &+ K_0 \left[\sqrt{u} \sqrt{[(\hat{x}_{iD})_{j=1} \cos(\theta_\ell - \theta_i) + x']^2 + (\hat{x}_{iD})_{j=1}^2 \sin^2(\theta_\ell - \theta_i)} \right] \end{aligned} \right] dx' & , \quad j = 1 \\ -\frac{\pi}{C_{fiD}} \frac{(\Delta\hat{x}_{iD})^2}{8} (\bar{q}_D)_{ij=1}(s) + \frac{\pi(\hat{x}_{iD})_{j=1}}{sC_{fiD}} \\ \sum_{m=1}^{n_{fs}} \frac{(\bar{q}_D)_{im}(s)}{2} \int_{[\hat{x}_{iD}]_m}^{[\hat{x}_{iD}]_{m+1}} \left[\begin{aligned} &K_0 \left[\sqrt{u} \sqrt{[(\hat{x}_{iD})_j \cos(\theta_\ell - \theta_i) - x']^2 + (\hat{x}_{iD})_j^2 \sin^2(\theta_\ell - \theta_i)} \right] \\ &+ K_0 \left[\sqrt{u} \sqrt{[(\hat{x}_{iD})_j \cos(\theta_\ell - \theta_i) + x']^2 + (\hat{x}_{iD})_j^2 \sin^2(\theta_\ell - \theta_i)} \right] \end{aligned} \right] dx' & , \quad j > 1 \\ -\frac{\pi}{C_{fiD}} \left[\frac{(\Delta\hat{x}_{iD})^2}{8} (\bar{q}_D)_{ij}(s) + \sum_{m=1}^{j-1} \left[\frac{(\Delta\hat{x}_{iD})^2}{2} + (\Delta\hat{x}_{iD})[(\hat{x}_{iD})_j - m\Delta\hat{x}_{iD}] \right] (\bar{q}_D)_{im}(s) \right] + \frac{\pi(\hat{x}_{iD})_j}{sC_{fiD}} \end{cases} \dots\dots\dots (E-52)$$

where $i, \ell = 1, 2, \dots, n_f$ and $j, m = 1, 2, \dots, n_{fs}$.

A semianalytical solution accounting for multiple arbitrarily-oriented finite-conductivity fractures in an isotropic infinite-slab reservoir is written in the Laplace domain using superposition as

$$(\bar{p}_{LjD})_{\ell}(s) = \sum_{i=1}^{n_f} s\bar{q}_{iD}(\bar{p}_D)_{\ell i} \dots\dots\dots (E-53)$$

which can also be written as

$$(\bar{p}_{LFD})_\ell = \left\{ \begin{array}{l} \sum_{i=1}^{n_f} s \bar{q}_{iD} \sum_{m=1}^{n_{fs}} \frac{(\bar{q}_D)_{im}(s)}{2} \int_{[\hat{x}_{iD}]_m}^{[\hat{x}_{iD}]_{m+1}} \left[K_0 \sqrt{\sqrt{(\hat{x}_{iD})_{j=1} \cos(\theta_\ell - \theta_i) - x'}^2 + (\hat{x}_{iD})_{j=1}^2 \sin^2(\theta_\ell - \theta_i)}} + K_0 \sqrt{\sqrt{(\hat{x}_{iD})_{j=1} \cos(\theta_\ell - \theta_i) + x'}^2 + (\hat{x}_{iD})_{j=1}^2 \sin^2(\theta_\ell - \theta_i)}} \right] dx' , \quad j = 1 \\ -\frac{\pi}{C_{fiD}} \frac{(\Delta \hat{x}_{iD})^2}{8} (\bar{q}_D)_{ij=1}(s) + \frac{\pi (\hat{x}_{iD})_{j=1}}{s C_{fiD}} \\ \sum_{i=1}^{n_f} s \bar{q}_{iD} \sum_{m=1}^{n_{fs}} \frac{(\bar{q}_D)_{im}(s)}{2} \int_{[\hat{x}_{iD}]_m}^{[\hat{x}_{iD}]_{m+1}} \left[K_0 \sqrt{\sqrt{(\hat{x}_{iD})_{j=1} \cos(\theta_\ell - \theta_i) - x'}^2 + (\hat{x}_{iD})_{j=1}^2 \sin^2(\theta_\ell - \theta_i)}} + K_0 \sqrt{\sqrt{(\hat{x}_{iD})_{j=1} \cos(\theta_\ell - \theta_i) + x'}^2 + (\hat{x}_{iD})_{j=1}^2 \sin^2(\theta_\ell - \theta_i)}} \right] dx' , \quad j > 1 \\ -\frac{\pi}{C_{fiD}} \left[\frac{(\Delta \hat{x}_{iD})^2}{8} (\bar{q}_D)_{ij}(s) + \sum_{m=1}^{j-1} \left[\frac{(\Delta \hat{x}_{iD})^2}{2} + (\Delta \hat{x}_{iD}) [(\hat{x}_{iD})_j - m \Delta \hat{x}_{iD}] \right] (\bar{q}_D)_{im}(s) \right] + \frac{\pi (\hat{x}_{iD})_j}{s C_{fiD}} \end{array} \right. \dots \dots \dots (E-54)$$

where $i, \ell = 1, 2, \dots, n_f$ and $j, m = 1, 2, \dots, n_{fs}$. Note that $q_{iD} = q_i/q_t$ where q_t is the total production from all fractures, and $q_{iD} \neq (q_D)_i$.

The Laplace domain dimensionless flow rate for a single fracture is defined by

$$\Delta \hat{x}_{iD} \sum_{m=1}^{n_{fs}} (\bar{q}_D)_{im} = \frac{1}{s}, \dots \dots \dots (E-55)$$

and the Laplace domain dimensionless total flow rate for all fractures is defined by

$$\sum_{i=1}^{n_f} \bar{q}_{iD} = \frac{1}{s}, \dots \dots \dots (E-56)$$

For each fracture, an equation relating the dimensionless pressure is written in the Laplace domain as

$$(\bar{p}_D)_{\ell i} |_{j=1} = (\bar{p}_D)_{\ell i} |_{j=2} = \dots = (\bar{p}_D)_{\ell i} |_{j=n_{fs}} = (\bar{p}_D)_{\ell i}, \dots \dots \dots (E-57)$$

and for the entire multiple-fracture system, the dimensionless pressure at the wellbore is written in the Laplace domain as

$$(\bar{p}_{wD})_1 = (\bar{p}_{wD})_2 = \dots = (\bar{p}_{wD})_{n_f} = \bar{p}_{LFD} \dots \dots \dots (E-58)$$

Solution for Multiple Arbitrarily-Oriented Finite-Conductivity Vertical Fractures Considering Permeability Anisotropy

The multiple finite-conductivity fracture solution considering permeability anisotropy in an infinite-slab reservoir is developed by defining the dimensionless distance variables as⁹⁵

$$x_D = \frac{x}{L_c} \sqrt{\frac{k}{k_x}}, \dots \dots \dots (E-59)$$

$$y_D = \frac{y}{L_c} \sqrt{\frac{k}{k_y}}, \dots\dots\dots (E-60)$$

and

$$k = \sqrt{k_x k_y} \dots\dots\dots (E-61)$$

The dimensionless variables rescale the anisotropic reservoir to an equivalent isotropic system. As a result of the rescaling, the dimensionless fracture half-length changes and must be redefined as¹⁰⁶

$$L'_{fD} = \frac{L_{fI}}{L_c} \sqrt{\frac{k}{k_x} \cos^2 \theta_f + \frac{k}{k_y} \sin^2 \theta_f}, \dots\dots\dots (E-62)$$

where the angle of the fracture with respect to the rescaled x_D -axis is written as

$$\theta'_f = \tan^{-1} \left(\sqrt{\frac{k_x}{k_y}} \tan \theta_f \right), \quad 0 < \theta_f < \frac{\pi}{2} \dots\dots\dots (E-63)$$

When $\theta_f = 0$ or $\theta_f = \pi/2$, the angle does not rescale and $\theta'_f = \theta_f$.

The dimensionless fracture conductivity is defined in the original anisotropic system, which is written as,

$$C_{fD} = \frac{k_f w_f}{k L_f}, \dots\dots\dots (E-64)$$

but Spivey and Lee¹⁰⁶ note an equivalent dimensionless fracture conductivity can also be written in terms of the equivalent isotropic system.

With the redefined dimensionless variables, the Laplace domain dimensionless pressure for a finite-conductivity fracture ℓ accounting for a finite-conductivity fracture i considering permeability anisotropy is written as

$$(\bar{p}_D)_{\ell i}(s) = \frac{1}{2} \int_0^1 (\bar{q}_D)_i(x', s) \left[\begin{array}{l} K_0 \left[\sqrt{u} \sqrt{[\hat{x}'_{iD} \cos(\theta'_\ell - \theta'_i) - x']^2 + \hat{x}'_{iD}{}^2 \sin^2(\theta'_\ell - \theta'_i)} \right] \\ + K_0 \left[\sqrt{u} \sqrt{[\hat{x}'_{iD} \cos(\theta'_\ell - \theta'_i) + x']^2 + \hat{x}'_{iD}{}^2 \sin^2(\theta'_\ell - \theta'_i)} \right] \end{array} \right] dx' \\ + \frac{\pi \hat{x}'_{iD}}{s C_{fD}} - \frac{\pi}{C_{fD}} \int_0^{\hat{x}'_{iD}} \int_0^{x'} (\bar{q}_D)_i(x'', s) dx'' dx' \quad , \quad i, \ell = 1, 2, \dots, n_f \dots\dots\dots (E-65)$$

where the angle, θ' , is defined in the rescaled equivalent isotropic reservoir and is related to the anisotropic reservoir by

$$\theta' = \begin{cases} \theta & \theta = 0 \\ \tan^{-1} \left(\sqrt{\frac{k_x}{k_y}} \tan \theta \right) & 0 < \theta < \pi/2 \\ \theta & \theta = \pi/2 \end{cases} \dots\dots\dots (E-66)$$

A semianalytical multiple arbitrarily-oriented finite-conductivity fracture solution for an anisotropic infinite-slab reservoir is written in the Laplace domain as

$$\begin{aligned}
 (\bar{p}_{wD})_{\ell}(s) = & \left\{ \sum_{i=1}^{n_f} s \bar{q}_{iD} \sum_{m=1}^{n_{fs}} \frac{(\bar{q}_D)_{im}(s)}{2} \int_{[\hat{x}'_{iD}]_m}^{[\hat{x}'_{iD}]_{m+1}} \left[\begin{aligned} & K_0 \left[\sqrt{u} \sqrt{[(\hat{x}'_{iD})_{j=1} \cos(\theta'_\ell - \theta'_i) - x']^2 + (\hat{x}'_{iD})_{j=1}^2 \sin^2(\theta'_\ell - \theta'_i)} \right] \right. \\ & \left. + K_0 \left[\sqrt{u} \sqrt{[(\hat{x}'_{iD})_{j=1} \cos(\theta'_\ell - \theta'_i) + x']^2 + (\hat{x}'_{iD})_{j=1}^2 \sin^2(\theta'_\ell - \theta'_i)} \right] \right] dx' \right. \\ & \left. - \frac{\pi}{C_{fjD}} \frac{(\Delta \hat{x}'_{iD})^2}{8} (\bar{q}_D)_{ij=1}(s) + \frac{\pi(\hat{x}'_{iD})_{j=1}}{s C_{fjD}} \right. \\ & \left. \sum_{i=1}^{n_f} s \bar{q}_{iD} \sum_{m=1}^{n_{fs}} \frac{(\bar{q}_D)_{im}(s)}{2} \int_{[\hat{x}'_{iD}]_m}^{[\hat{x}'_{iD}]_{m+1}} \left[\begin{aligned} & K_0 \left[\sqrt{u} \sqrt{[(\hat{x}'_{iD})_j \cos(\theta'_\ell - \theta'_i) - x']^2 + (\hat{x}'_{iD})_j^2 \sin^2(\theta'_\ell - \theta'_i)} \right] \right. \\ & \left. + K_0 \left[\sqrt{u} \sqrt{[(\hat{x}'_{iD})_j \cos(\theta'_\ell - \theta'_i) + x']^2 + (\hat{x}'_{iD})_j^2 \sin^2(\theta'_\ell - \theta'_i)} \right] \right] dx' \right. \\ & \left. - \frac{\pi}{C_{fjD}} \left[\frac{(\Delta \hat{x}'_{iD})^2}{8} (\bar{q}_D)_{ij}(s) + \sum_{m=1}^{j-1} \left[\frac{(\Delta \hat{x}'_{iD})^2}{2} + (\Delta \hat{x}'_{iD}) [(\hat{x}'_{iD})_j - m \Delta \hat{x}'_{iD}] \right] (\bar{q}_D)_{im}(s) \right] + \frac{\pi(\hat{x}'_{iD})_j}{s C_{fjD}} \right. \\ & \left. \right\} \dots \dots \dots (E-67)
 \end{aligned}$$

for $i, \ell = 1, 2, \dots, n_f$ and $j, m = 1, 2, \dots, n_{fs}$.

The Laplace domain dimensionless flow rate for a single fracture is defined by

$$\Delta \hat{x}'_{iD} \sum_{m=1}^{n_{fs}} (\bar{q}_D)_{im} = \frac{1}{s}, \dots \dots \dots (E-68)$$

and the Laplace domain dimensionless total flow rate from n_f fractures is defined by

$$\sum_{i=1}^{n_f} \bar{q}_{iD} = \frac{1}{s}, \dots \dots \dots (E-69)$$

For each fracture, an equation relating the dimensionless pressure is written in the Laplace domain as

$$(\bar{p}_D)_{\ell i} |_{j=1} = (\bar{p}_D)_{\ell i} |_{j=2} = \dots = (\bar{p}_D)_{\ell i} |_{j=n_{fs}} = (\bar{p}_D)_{\ell i}, \dots \dots \dots (E-70)$$

and for the entire multiple-fracture system, the dimensionless pressure at the wellbore is written in the Laplace domain as

$$(\bar{p}_{wD})_1 = (\bar{p}_{wD})_2 = \dots = (\bar{p}_{wD})_{n_f} = \bar{p}_{LfD}. \dots \dots \dots (E-71)$$

Development of Matrix Equation and Algorithm for Multiple Finite-Conductivity Fracture Solution

For each fracture divided into n_{fs} equal length uniform-flux segments, Eqs. E-67 through E-71 describe a system of $n_f(n_{fs} + n_f + 1) + 1$ equations and $n_f(n_{fs} + n_f + 1) + 1$ unknowns. The solution algorithm is a three step process. First, a system of equations is developed for each fracture where the reference axis and the

fracture axis coincide, that is, a system of equations is written to solve for $(\bar{p}_D)_{ii}$ and $(\bar{q}_D)_{im}$ where $i = 1, 2, \dots, n_f$ and $m = 1, 2, \dots, n_{fs}$. Solving the system of equations for each fracture requires writing an equation for each fracture segment, $j = 1, 2, \dots, n_{fs}$. For example considered the discretized cruciform fracture with each fracture wing divided into three segments as shown in **Fig. E-3**. The system of equations will be written for the discretized fracture in Fig. E-3 and then generalized for n_f fractures divided into n_{fs} fracture segments.

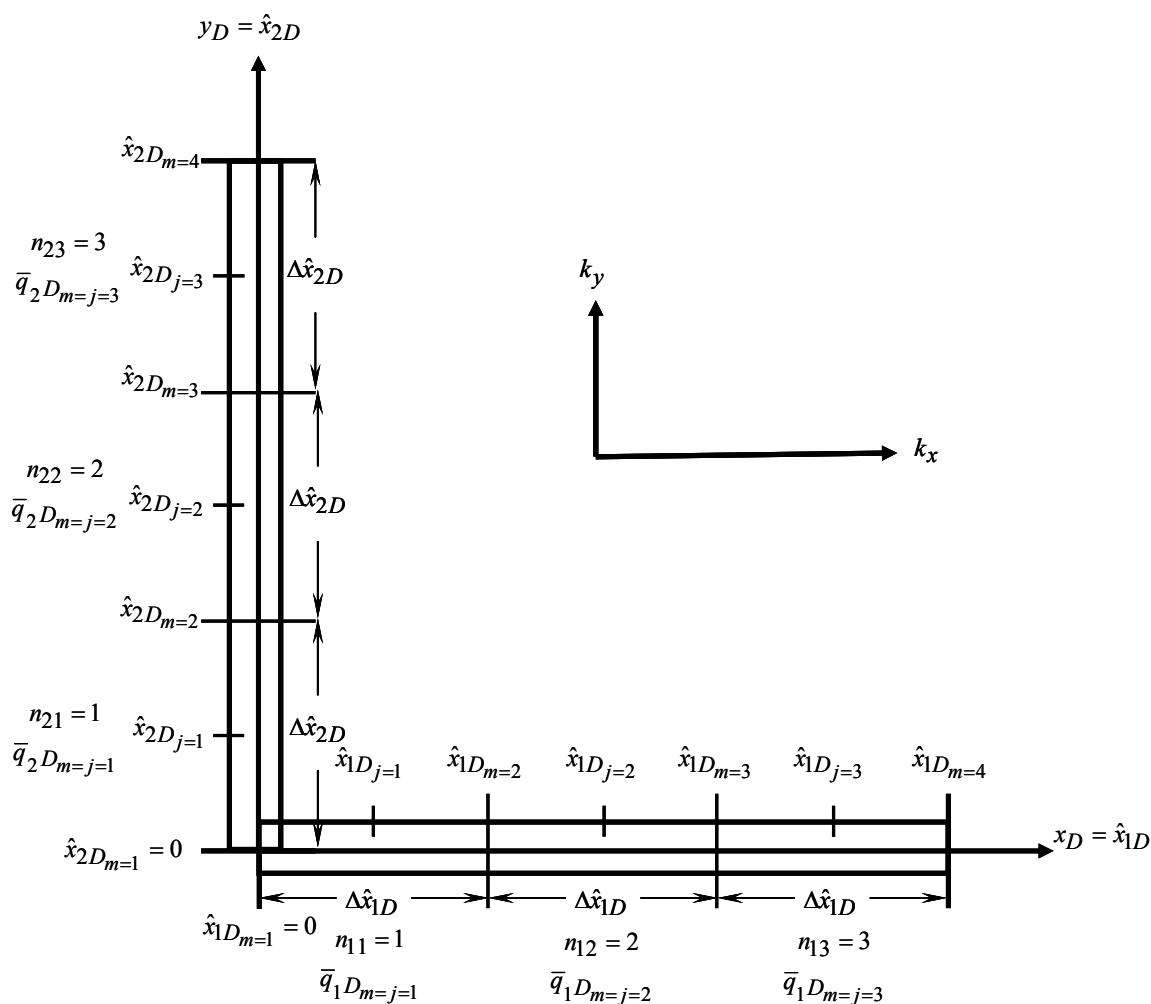


Figure E-3. Multiple fracture half-length discretization.

For the cruciform fracture in an anisotropic reservoir illustrated in Fig. E-3, the primary fracture is oriented at an angle $\theta_{f1} = \theta'_{f1} = \theta_{fr} = 0$ and the secondary fracture is oriented at an angle $\theta_{f2} = \theta'_{f2} = \pi/2$. Let the reference length be defined as $L_c = L'_{f1}$, and let the length of the secondary fracture be defined as $L'_{f2} = \delta_2 L'_{f1}$. Consequently, the dimensionless fracture half-lengths are defined as $L'_{f1} = 1$, and $L'_{f2D} = \delta_2 L'_{f1D} = \delta_2$.

Define the following variables of substitution as

$$(\zeta_{ik})_{mj} = \frac{1}{2} \int_{[\hat{x}'_{iD}]_m}^{[\hat{x}'_{iD}]_{m+1}} \left[K_0 \sqrt{u} \sqrt{[(\hat{x}'_{iD})_j \cos(\theta'_\ell - \theta'_i) - x']^2 + (\hat{x}'_{iD})_j^2 \sin^2(\theta'_\ell - \theta'_i)} + K_0 \sqrt{u} \sqrt{[(\hat{x}'_{iD})_j \cos(\theta'_\ell - \theta'_i) + x']^2 + (\hat{x}'_{iD})_j^2 \sin^2(\theta'_\ell - \theta'_i)} \right] dx' \dots\dots\dots (E-72)$$

$$(\chi_i)_{mj} = \frac{\pi}{C_{fiD}} \left[\frac{(\Delta \hat{x}'_{iD})^2}{2} + (\Delta \hat{x}'_{iD}) [(\hat{x}'_{iD})_j - m \Delta \hat{x}'_{iD}] \right] \dots\dots\dots (E-73)$$

$$\xi_i = \frac{\pi}{C_{fiD}} \frac{(\Delta \hat{x}'_{iD})^2}{8} \dots\dots\dots (E-74)$$

and

$$(\eta_i)_j = \frac{\pi (\hat{x}'_{iD})_j}{C_{fiD}} \dots\dots\dots (E-75)$$

With the variables of substitution, the dimensionless pressure equation for a single finite-conductivity fracture accounting for multiple finite-conductivity fractures is written as

$$(\bar{p}_D)_{\ell i}(s) = \begin{cases} \frac{(\eta_i)_{j=1}}{s} - \xi_i (\bar{q}_D)_{ij=1}(s) + \sum_{m=1}^{n_{fs}} (\bar{q}_D)_{im}(s) (\zeta_{\ell i})_{m1} & , \quad j=1 \\ \frac{(\eta_i)_j}{s} - \xi_i (\bar{q}_D)_{ij}(s) - \sum_{m=1}^{j-1} (\chi_i)_{mj} (\bar{q}_D)_{im}(s) + \sum_{m=1}^{n_{fs}} (\bar{q}_D)_{im}(s) (\zeta_{\ell i})_{mj} & , \quad j > 1 \end{cases} \dots\dots\dots (E-76)$$

The development follows from the finite-conductivity solutions of Cinco-Ley *et al.*¹⁰⁷ and, for the dual-porosity case, Cinco-Ley and Meng.⁸⁶ Let $j = 1$, and the dimensionless pressure equation for the primary fracture is written as

$$(\bar{p}_D)_{11}(s) \Big|_{j=1} = (\zeta_{11})_{11} (\bar{q}_D)_{11}(s) + (\zeta_{11})_{21} (\bar{q}_D)_{12}(s) + (\zeta_{11})_{31} (\bar{q}_D)_{13}(s) - \xi_1 (\bar{q}_D)_{11}(s) + \frac{(\eta_1)_1}{s} \dots\dots\dots (E-77)$$

For $j = 2$, the dimensionless pressure equation is written as

$$(\bar{p}_D)_{11}(s) \Big|_{j=2} = \begin{cases} (\zeta_{11})_{12} (\bar{q}_D)_{11}(s) + (\zeta_{11})_{22} (\bar{q}_D)_{12}(s) + (\zeta_{11})_{32} (\bar{q}_D)_{13}(s) \\ - \xi_1 (\bar{q}_D)_{12}(s) - (\chi_1)_{12} (\bar{q}_D)_{11}(s) + \frac{(\eta_1)_2}{s} \end{cases} \dots\dots\dots (E-78)$$

and for $j = 3$, the dimensionless pressure equation is written as

$$(\bar{p}_D)_{11}(s)|_{j=3} = \begin{cases} (\zeta_{11})_{13}(\bar{q}_D)_{11}(s) + (\zeta_{11})_{23}(\bar{q}_D)_{12}(s) + (\zeta_{11})_{33}(\bar{q}_D)_{13}(s) \\ -\xi_1(\bar{q}_D)_{13}(s) - (\chi_1)_{13}(\bar{q}_D)_{11}(s) - (\chi_1)_{23}(\bar{q}_D)_{12}(s) + \frac{(\eta_1)_3}{s} \end{cases}, \dots\dots\dots (E-79)$$

Collecting like terms and algebraically rearranging the equations for the primary fracture results in

$$(\bar{p}_D)_{11}|_{j=1} + [\xi_1 - (\zeta_{11})_{11}](\bar{q}_D)_{11} - (\zeta_{11})_{21}(\bar{q}_D)_{12} - (\zeta_{11})_{31}(\bar{q}_D)_{13} = \frac{(\eta_1)_1}{s}, \dots\dots\dots (E-80)$$

$$(\bar{p}_D)_{11}|_{j=2} + [(\chi_1)_{12} - (\zeta_{11})_{12}](\bar{q}_D)_{11} + [\xi_1 - (\zeta_{11})_{22}](\bar{q}_D)_{12} - (\zeta_{11})_{32}(\bar{q}_D)_{13} = \frac{(\eta_1)_2}{s}, \dots\dots\dots (E-81)$$

and

$$(\bar{p}_D)_{11}|_{j=3} + [(\chi_1)_{13} - (\zeta_{11})_{13}](\bar{q}_D)_{11} + [(\chi_1)_{23} - (\zeta_{11})_{23}](\bar{q}_D)_{12} + [\xi_1 - (\zeta_{11})_{33}](\bar{q}_D)_{13} = \frac{(\eta_1)_3}{s} \dots\dots\dots (E-82)$$

With the dimensionless rate equation for a single fracture (Eq. E-68) expanded and written as

$$\Delta\hat{\chi}'_{1D}(\bar{q}_D)_{11} + \Delta\hat{\chi}'_{1D}(\bar{q}_D)_{12} + \Delta\hat{\chi}'_{1D}(\bar{q}_D)_{13} = \frac{1}{s}, \dots\dots\dots (E-89)$$

and recognizing from Eq. E-70 that $(\bar{p}_D)_{11}|_{j=1} = (\bar{p}_D)_{11}|_{j=2} = (\bar{p}_D)_{11}|_{j=3} = (\bar{p}_D)_{11}$, a linear system of equations can be written in matrix form as

$$\mathbf{A}_{11}\mathbf{x}_1 = \mathbf{b}_1, \dots\dots\dots (E-90)$$

where

$$\mathbf{A}_{11} = \begin{bmatrix} [\xi_1 - (\zeta_{11})_{11}] & -(\zeta_{11})_{21} & -(\zeta_{11})_{31} & 1 \\ [(\chi_1)_{12} - (\zeta_{11})_{12}] & [\xi_1 - (\zeta_{11})_{22}] & -(\zeta_{11})_{32} & 1 \\ [(\chi_1)_{13} - (\zeta_{11})_{13}] & [(\chi_1)_{23} - (\zeta_{11})_{23}] & [\xi_1 - (\zeta_{11})_{33}] & 1 \\ \Delta\hat{\chi}'_{1D} & \Delta\hat{\chi}'_{1D} & \Delta\hat{\chi}'_{1D} & 0 \end{bmatrix}, \dots\dots\dots (E-91)$$

$$\mathbf{x}_1 = \begin{bmatrix} (\bar{q}_D)_{11} \\ (\bar{q}_D)_{12} \\ (\bar{q}_D)_{13} \\ (\bar{p}_D)_{11} \end{bmatrix}, \dots\dots\dots (E-92)$$

$$\mathbf{b}_1 = \begin{bmatrix} \frac{(\eta_1)_1}{s} \\ \frac{(\eta_1)_2}{s} \\ \frac{(\eta_1)_3}{s} \\ \frac{1}{s} \end{bmatrix} \dots\dots\dots (E-93)$$

Similarly, a linear system of equations for the secondary fracture is written as

$$\mathbf{A}_{22}\mathbf{x}_2 = \mathbf{b}_2, \dots\dots\dots (E-94)$$

where

$$\mathbf{A}_{22} = \begin{bmatrix} [\xi_2 - (\zeta_{22})_{11}] & -(\zeta_{22})_{21} & -(\zeta_{22})_{31} & 1 \\ [(\chi_2)_{12} - (\zeta_{22})_{12}] & [\xi_2 - (\zeta_{22})_{22}] & -(\zeta_{22})_{32} & 1 \\ [(\chi_2)_{13} - (\zeta_{22})_{13}] & [(\chi_2)_{23} - (\zeta_{22})_{23}] & [\xi_2 - (\zeta_{22})_{33}] & 1 \\ \Delta \hat{x}'_{2D} & \Delta \hat{x}'_{2D} & \Delta \hat{x}'_{2D} & 0 \end{bmatrix}, \dots\dots\dots (E-95)$$

$$\mathbf{x}_1 = \begin{bmatrix} (\bar{q}_D)_{21} \\ (\bar{q}_D)_{22} \\ (\bar{q}_D)_{23} \\ (\bar{p}_D)_{22} \end{bmatrix}, \dots\dots\dots (E-96)$$

$$\mathbf{b}_2 = \begin{bmatrix} \frac{(\eta_2)_1}{s} \\ \frac{(\eta_2)_2}{s} \\ \frac{(\eta_2)_3}{s} \\ \frac{1}{s} \end{bmatrix} \dots\dots\dots (E-97)$$

The system of equations are solved for for $(\bar{p}_D)_{11}$, $(\bar{p}_D)_{22}$, $(\bar{q}_D)_{1m}$, and $(\bar{q}_D)_{2m}$, where $m = 1,2,3$.

The second step in the solution algorithm for a cruciform fracture requires solving for $(\bar{p}_D)_{12}$ and $(\bar{p}_D)_{21}$. Since $(\bar{q}_D)_{1m}$ and $(\bar{q}_D)_{2m}$ are known, the dimensionless pressure terms $(\bar{p}_D)_{12}$ and $(\bar{p}_D)_{21}$ can be evaluated for any j , where for convenience $j = 1$ is arbitrarily selected, and the pressure terms are written as

$$(\bar{p}_D)_{12}|_{j=1} = \frac{(\eta_2)_1}{s} - \xi_2 (\bar{q}_D)_{21}(s) + (\bar{q}_D)_{21}(\zeta_{12})_{11} + (\bar{q}_D)_{22}(\zeta_{12})_{12} + (\bar{q}_D)_{23}(\zeta_{12})_{13}, \dots\dots\dots (E-98)$$

and

$$(\bar{p}_D)_{21}|_{j=1} = \frac{(\eta_1)_1}{s} - \xi_1 (\bar{q}_D)_{11}(s) + (\bar{q}_D)_{11}(\zeta_{21})_{11} + (\bar{q}_D)_{12}(\zeta_{21})_{12} + (\bar{q}_D)_{13}(\zeta_{21})_{13} \dots\dots\dots (E-99)$$

The third and final step in the solution algorithm requires writing a system of equations in the Laplace domain as

$$\mathbf{Ax} = \mathbf{b}, \dots\dots\dots (E-100)$$

where

$$\mathbf{A} = \begin{bmatrix} s(\bar{p}_D)_{11} & s(\bar{p}_D)_{12} & -1 \\ s(\bar{p}_D)_{21} & s(\bar{p}_D)_{22} & -1 \\ s & s & 0 \end{bmatrix}, \dots\dots\dots (E-101)$$

$$\mathbf{x} = \begin{bmatrix} \bar{q}_{1D} \\ \bar{q}_{2D} \\ \bar{p}_{LjD} \end{bmatrix}, \dots\dots\dots (E-102)$$

and

$$\mathbf{b} = \begin{bmatrix} 0 \\ 0 \\ 1 \end{bmatrix} \dots\dots\dots (E-103)$$

The system of equations, Eq. E-100, are solved in the Laplace domain and then inverted to the time domain to obtain the dimensionless pressure, p_{LjD} .

The algorithm can also be written for n_f fractures as follows. First, a system of equations is developed for each fracture where the reference axis and the fracture axis coincide, that is, a system of equations is written to solve for $(\bar{p}_D)_{ii}$ and $(\bar{q}_D)_{im}$ where $i = 1, 2, \dots, n_f$ and $m = 1, 2, \dots, n_{fs}$. A system of equations can be written for each fracture as

$$\mathbf{A}_{ii} \mathbf{x}_i = \mathbf{b}_i \text{ , } \dots\dots\dots (E-104)$$

where

$$\mathbf{A}_{ii} = \begin{bmatrix} [\xi_i - (\zeta_{ii})_{11}] & -(\zeta_{ii})_{21} & \dots & -(\zeta_{ii})_{n_{fs}1} & 1 \\ [(\chi_i)_{12} - (\zeta_{ii})_{12}] & [\xi_i - (\zeta_{ii})_{22}] & \dots & -(\zeta_{ii})_{n_{fs}2} & 1 \\ \vdots & \vdots & \ddots & \vdots & \vdots \\ [(\chi_i)_{13} - (\zeta_{ii})_{1n_{fs}}] & [(\chi_i)_{23} - (\zeta_{ii})_{2n_{fs}}] & & [\xi_i - (\zeta_{ii})_{n_{fs}n_{fs}}] & 1 \\ \Delta \hat{x}'_{iD} & \Delta \hat{x}'_{iD} & & \Delta \hat{x}'_{iD} & 0 \end{bmatrix} \dots\dots\dots (E-105)$$

$$\mathbf{x}_i = \begin{bmatrix} (\bar{q}_D)_{i1} \\ (\bar{q}_D)_{i2} \\ \vdots \\ (\bar{q}_D)_{in_{fs}} \\ (\bar{p}_D)_{ii} \end{bmatrix} \dots\dots\dots (E-106)$$

$$\mathbf{b}_i = \begin{bmatrix} \frac{(\eta_i)_1}{s} \\ \frac{(\eta_i)_2}{s} \\ \vdots \\ \frac{(\eta_i)_{n_{fs}}}{s} \\ \frac{1}{s} \end{bmatrix} \dots\dots\dots (E-107)$$

Solving the system of equations, Eq. E-104, provides values for $(\bar{p}_D)_{ii}$ and $(\bar{q}_D)_{im}$, where $m = 1, 2, \dots, n_{fs}$.

Second, the Laplace domain dimensionless pressure, $(\bar{p}_D)_{i\ell}$, with $\ell \neq i$ is calculated. Since $(\bar{q}_D)_{im}$ are known, the dimensionless pressure terms can be evaluated for any j , where for convenience $j = 1$ is arbitrarily selected, and the dimensionless pressure term is written as

$$(\bar{p}_D)_{li} \Big|_{j=1} = \frac{(\eta_i)_1}{s} - \xi_i (\bar{q}_D)_{i1}(s) + \sum_{m=1}^{n_{fs}} (\bar{q}_D)_{im} (\zeta_{li})_{m1} \cdot \dots \dots \dots (E-108)$$

Third, the semianalytical solution for producing through n_f arbitrarily-oriented finite-conductivity fractures in an infinite-slab anisotropic reservoir can be written as a system of equations in the Laplace domain as

$$\mathbf{Ax} = \mathbf{b} \ , \dots \dots \dots (E-109)$$

where

$$\mathbf{A} = \begin{bmatrix} s(\bar{p}_D)_{11} & s(\bar{p}_D)_{12} & \dots & s(\bar{p}_D)_{1n_f} & -1 \\ s(\bar{p}_D)_{21} & s(\bar{p}_D)_{22} & \dots & s(\bar{p}_D)_{2n_f} & -1 \\ \vdots & \vdots & \ddots & \vdots & \vdots \\ s(\bar{p}_D)_{n_f 1} & s(\bar{p}_D)_{n_f 2} & \dots & s(\bar{p}_D)_{n_f n_f} & -1 \\ s & s & \dots & s & 0 \end{bmatrix}_{n_f+1 \times n_f+1} \ , \dots \dots \dots (E-110)$$

$$\mathbf{x} = \begin{bmatrix} \bar{q}_{1D} \\ \bar{q}_{2D} \\ \vdots \\ \bar{q}_{n_f D} \\ \bar{p}_{LjD} \end{bmatrix}_{n_f+1 \times 1} \ , \dots \dots \dots (E-111)$$

and

$$\mathbf{b} = \begin{bmatrix} 0 \\ 0 \\ \vdots \\ 0 \\ 1 \end{bmatrix}_{n_f+1 \times 1} \ , \dots \dots \dots (E-112)$$

The system of equations, Eq. E-109, are solved in the Laplace domain and then inverted to the time domain to obtain the dimensionless pressure. The system of equations is solved within the Stehfest⁶⁸ algorithm, which is used for the Laplace to time domain inversion. With the Stehfest algorithm, s is calculated, and the \mathbf{A} and \mathbf{b} matrices are evaluated. Eq. E-109 is then solved as part of the numerical transformation from the Laplace domain to the time domain. Since the system of equations is a function of s , the system must be solved N times during each Laplace to time domain inversion where N is the number of Stehfest extrapolation coefficients.

Fig. E-4 contains a log-log graph of dimensionless pressure and dimensionless pressure derivative versus dimensionless time for a cruciform fracture where the angle between the fractures is $\pi/2$. In Fig. E-4, the inset graphic illustrates a cruciform fracture with primary fracture half length, L_{f1D} , and primary fracture conductivity, C_{f1D} . Secondary fracture half length is defined by the ratio of secondary to primary fracture half length, $\delta_L = L_{f2D}/L_{f1D}$, and secondary fracture conductivity is similarly defined by the ratio of

secondary to primary conductivity, $\delta_C = C_{f2D}/C_{f1D}$. The constant-rate type curves shown in Fig. E-4 were generated with $\delta_L = \delta_C = 1$ and the variable fracture conductivity noted on each curve. **Figs. E-5 through E-7** contain the constant-rate type curves for a cruciform fracture with variable fracture conductivity, $\delta_C = 1$, and $\delta_L = 3/4, 1/2$, and $1/4$. **Figs. E-8 and E-9** contain constant-rate type curves for a cruciform fracture with $\delta_L = 1$ and $\delta_C = 1/4$ with $\delta_C = 1, 0.10$, and 0.010 .

In addition to allowing each fracture to have a different half length and conductivity, the multiple fracture solution also allows for an arbitrary angle between fractures. Fig. **E-10** contains constant-rate type curves for equal primary and secondary fracture half length, $\delta_L = 1$, and equal primary and secondary conductivity, $\delta_C = 1$ where $C_{f1D} = 100\pi$. The type curves illustrate the effects of decreasing the angle between the fractures as shown by type curves for $\theta_p = \pi/2, \pi/4, \pi/8$. As the angle is further reduced, the type curve response approaches the solution for a single finite-conductivity fracture.

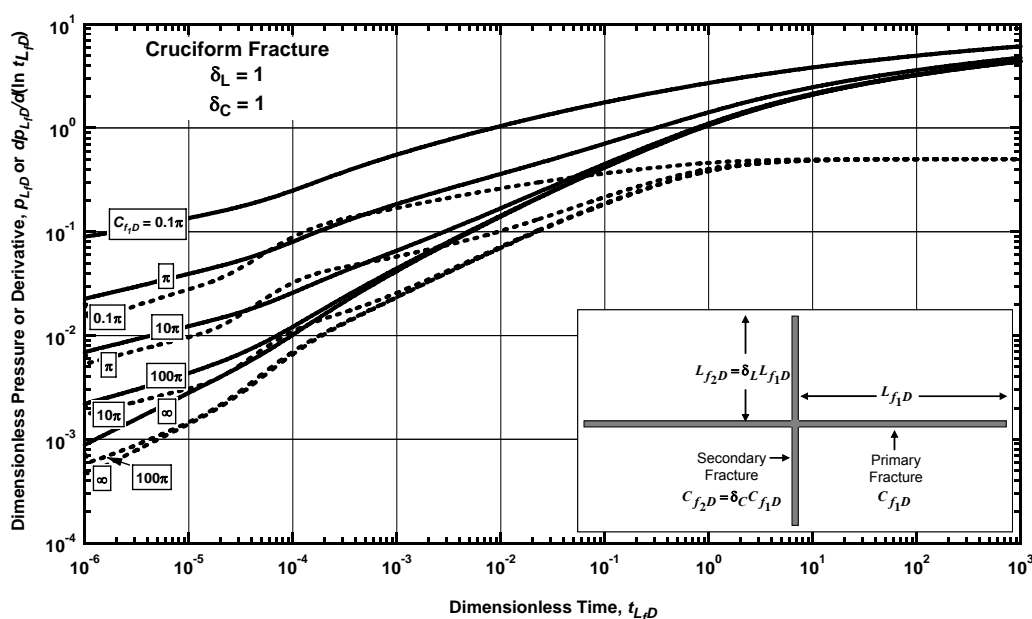


Fig. E-4—Cruciform fracture constant-rate type curve with variable conductivity, $\delta_L = 1$, and $\delta_C = 1$.

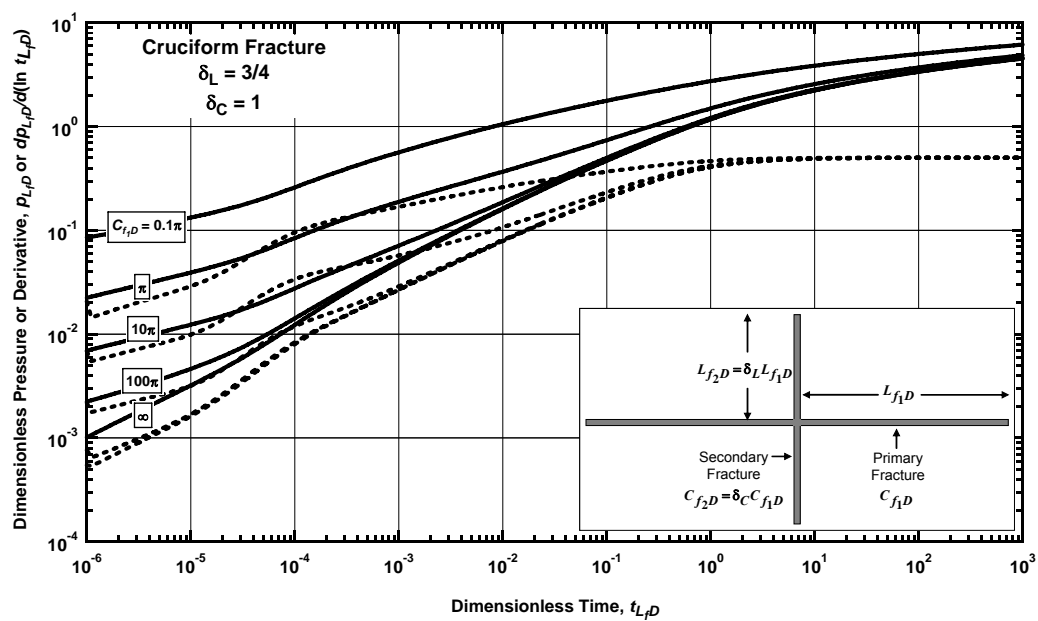


Fig. E-5—Cruciform fracture constant-rate type curve with variable conductivity, $\delta_L = 3/4$, and $\delta_C = 1$.

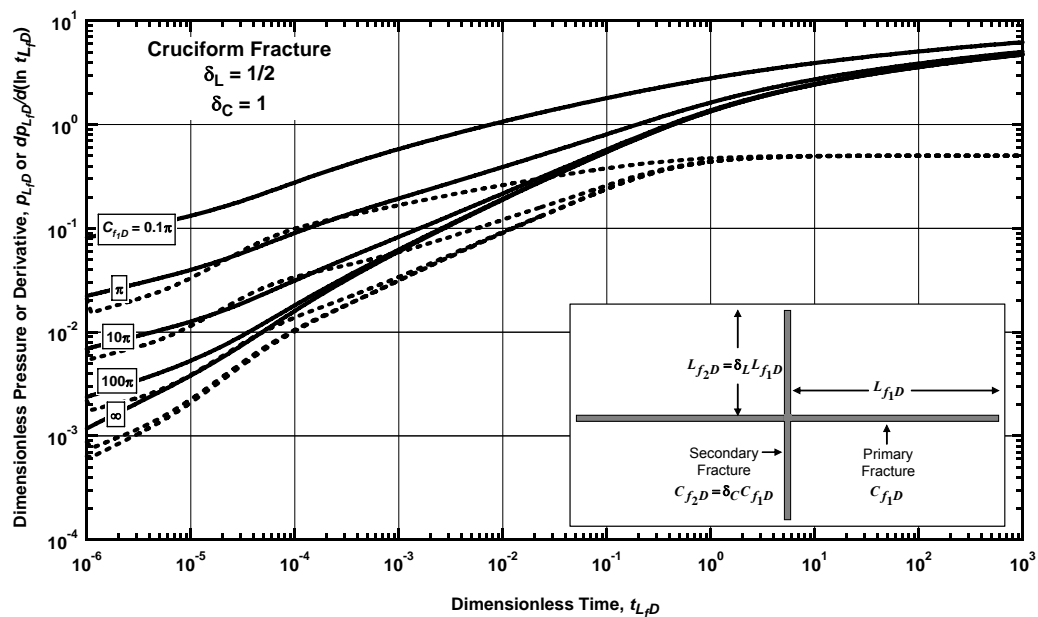


Fig. E-6—Cruciform fracture constant-rate type curve with variable conductivity, $\delta_L = 1/2$, and $\delta_C = 1$.

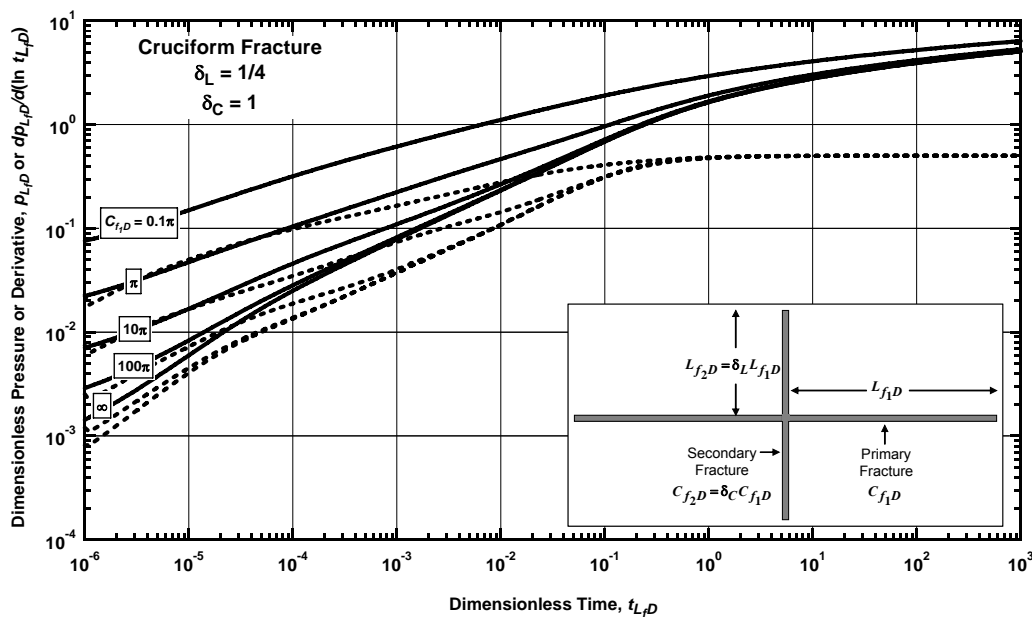


Fig. E-7—Cruciform fracture constant-rate type curve with variable conductivity, $\delta_L = 1/4$, and $\delta_C = 1$.

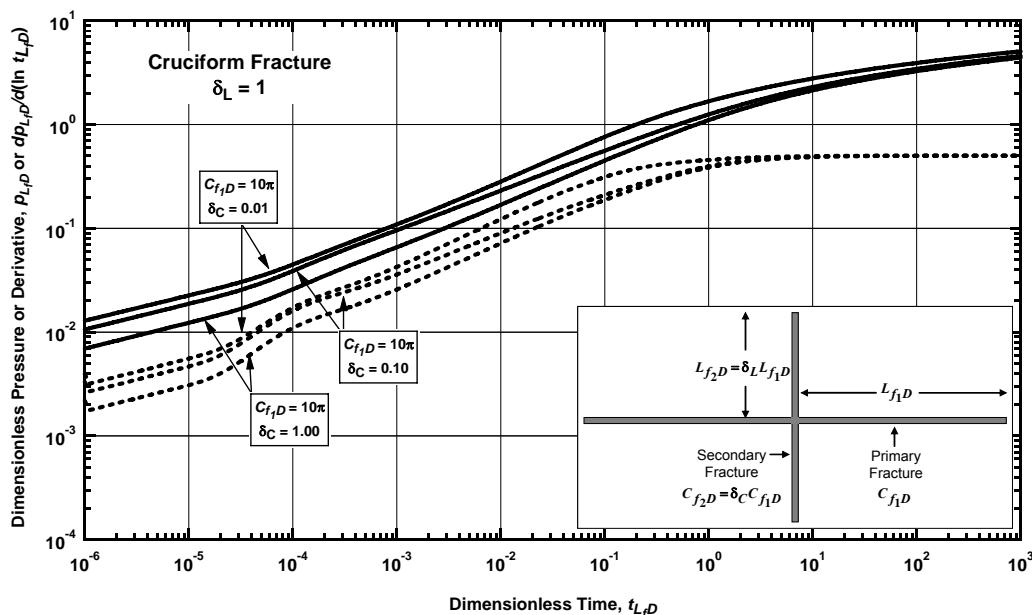


Fig. E-8—Cruciform fracture constant-rate type curve with $\delta_L = 1$, $C_{f1D} = 10\pi$, and $\delta_C = 0.01$, 0.1, and 1.

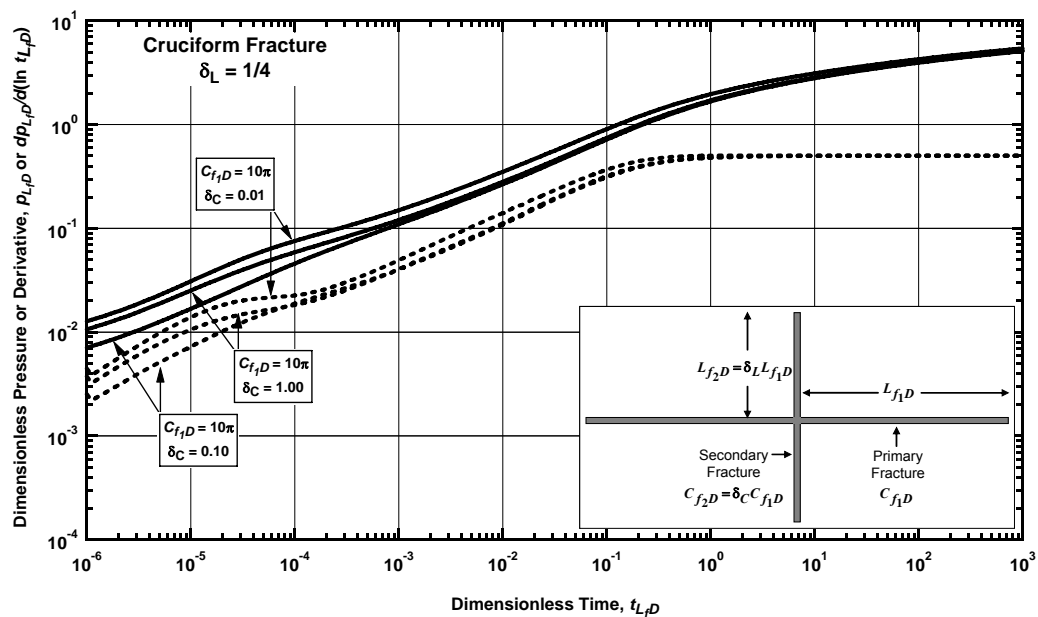


Fig. E-9—Cruciform fracture constant-rate type curve with $\delta_L = 1/4$, $C_{f1D} = 10\pi$, and $\delta_C = 0.01, 0.1$, and 1 .

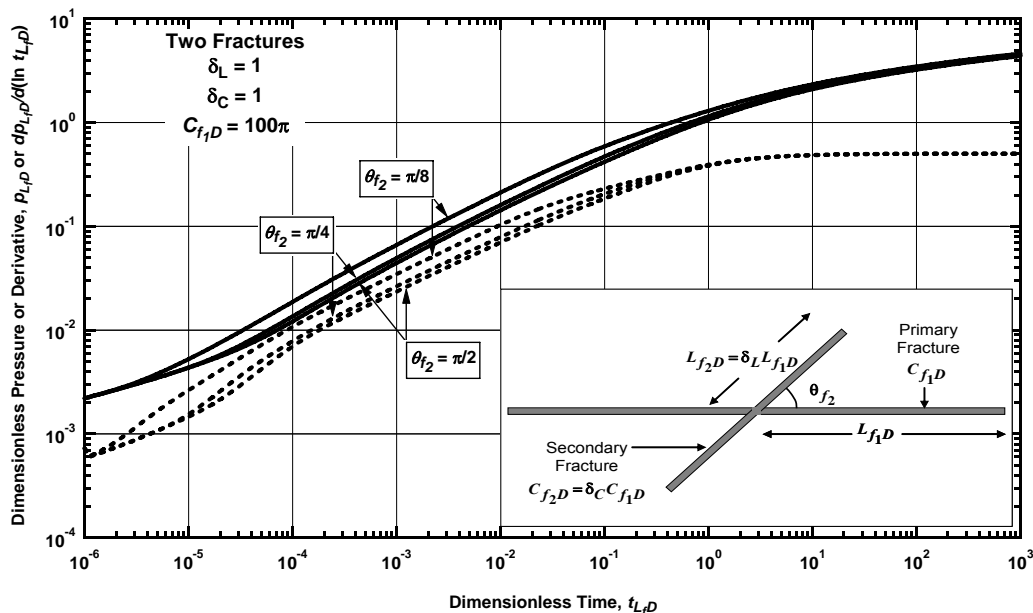


Fig. E-10—Constant-rate type curves for oblique fractures with $\delta_L = 1$, $\delta_C = 1$, $C_{f1D} = 100\pi$, and $\theta_{f_2} = \pi/2, \pi/4, \pi/8$.

APPENDIX F

FRACTURE-INJECTION/FALLOFF SOLUTIONS IN A RESERVOIR CONTAINING A COMPRESSIBLE FLUID

The fracture-injection/falloff solutions for a wellbore, fracture, and reservoir containing a slightly-compressible liquid are developed in Appendix C, but in many cases, a wellbore, fracture, and reservoir will contain a compressible fluid. In conventional pressure-transient testing, solutions developed for a reservoir containing a slightly compressible liquid can be used to interpret pressure-transient data in a reservoir containing a compressible fluid by transforming pressure and time into pseudopressure and pseudotime, or adjusted pseudopressure and adjusted pseudotime.⁷²⁻⁷³

Appendix F demonstrates that fracture-injection/falloff solutions developed for a reservoir containing a slightly compressible liquid can also be used to model pressure-transient data from a fracture-injection/falloff sequence in a well with the wellbore, fracture, and reservoir containing a compressible fluid (real gas) when pressure and time are transformed to adjusted pseudopressure and adjusted pseudotime.

Solution Accounting for a Dilating Fracture, Before-Closure Storage, and After-Closure Storage Formulated in Terms of Adjusted Pseudopressure and Adjusted Pseudotime

Consider a fracture-injection/falloff sequence with the entire fracture length developed instantaneously when the injection begins or with a pre-existing fracture. The wellbore, fracture, and reservoir contain a compressible fluid, and the injection is at a pressure in excess of the minimum in-situ stress. From Appendix C, a material balance equation during the fracture injection is written as

$$qB\rho - q_r B_r \rho_r = \rho_w c_{gw} V_w \frac{dp_w}{dt} + 2\rho_f \frac{A_f}{S_f} \frac{dp_w}{dt}, \dots\dots\dots (F-1)$$

where q is the well injection rate, q_r is the sandface flow (leakoff) rate, B is the well formation volume factor at injection conditions, B_r is the formation volume factor at reservoir conditions, ρ is the fluid density at injection conditions, ρ_r is the fluid density at reservoir conditions, ρ_w is the fluid density at wellbore conditions, ρ_f is the fluid density at fracture conditions, c_{gw} is the wellbore-gas compressibility, V_w is the wellbore volume, p_w is the wellbore pressure, t is the time, A_f is the fracture area, and S_f is the fracture "stiffness."

Fracture stiffness, or the inverse of fracture compliance, is defined by the elastic energy or "strain energy" created by an open fracture in a rock assuming linear elastic theory is applicable. **Table F-1** contains the fracture stiffness definitions for three common 2D fracture models.^{80,100} In Table F-1, E' is the plane-strain

modulus, R_f is the fracture radius of a radial fracture, h_f is the gross fracture height, and L_f is the fracture half-length.

Table F-1—Fracture stiffness for 2D fracture models.^{80,100}

Radial	Perkins-Kern-Nordgren Vertical Plane Strain	Geertsma-deKlerk Horizontal Plane Strain
$(S_f)_{RAD} = \frac{3\pi E'}{16R_f}$	$(S_f)_{PKN} = \frac{2E'}{\pi h_f}$	$(S_f)_{GDK} = \frac{E'}{\pi L_f}$

Define an adjusted wellbore storage coefficient as

$$C_a = c_{gi}V_w, \dots\dots\dots (F-2)$$

where c_{gi} is the gas compressibility at initial reservoir pressure, p_i , and define a before-closure storage coefficient as

$$C_{fbc} = 2 \frac{A_f}{S_f} \dots\dots\dots (F-3)$$

With the new definitions, the material balance equation can be written as

$$qB\rho - q_r B_r \rho_r = \rho_w C_a \frac{\mu_{gi} c_{gw}}{(\mu_g c_g)_i} \frac{dp_w}{dt} + \rho_f C_{fbc} \frac{dp_w}{dt} \dots\dots\dots (F-4)$$

Adjusted pseudopressure is defined as

$$p_a = \left(\frac{\mu z}{p} \right)_{re} \int_0^P \frac{p dp}{\mu z}, \dots\dots\dots (F-5)$$

and the derivative is written as

$$p_{aw} = \left(\frac{\mu z}{p} \right)_{re} \left(\frac{p}{\mu z} \right)_w dp_w \dots\dots\dots (F-6)$$

Adjusted pseudotime is defined as

$$t_a = (\mu c_t)_{re} \int_0^t \frac{dt}{(\mu c_t)_w}, \dots\dots\dots (F-7)$$

and the derivative can be written as

$$\frac{1}{dt} = \frac{(\mu c_t)_{re}}{(\mu z)_w} \frac{1}{dta} \dots\dots\dots (F-8)$$

With the definition of adjusted pseudopressure and adjusted pseudotime, the material balance equation can be written as

$$qB\rho - q_r B_r \rho_r = \left[\rho_w C_a \frac{\mu_{gi} c_{gw}}{(\mu_g c_g)_w} \frac{(\mu_g c_g)_{re}}{(\mu_g c_g)_i} \left(\frac{p}{\mu z}\right)_{re} \left(\frac{\mu z}{p}\right)_w \frac{dp_{aw}}{dt_a} + \rho_f C_{fbc} \frac{(\mu_g c_g)_{re}}{(\mu_g c_g)_i} \left(\frac{p}{\mu z}\right)_{re} \left(\frac{\mu z}{p}\right)_w \frac{dp_{aw}}{dt_a} \right] \dots \dots \dots (F-9)$$

Define the reference condition, subscript 're', as the initial reservoir pressure, p_i , and note that $c_g \cong c_i$. The reference condition allows the material balance equation to be written as

$$qB\rho - q_r B_r \rho_r = \left[\rho_w C_a + \rho_f C_{fbc} \frac{c_{ti}}{c_{tw}} \right] \left(\frac{p}{z}\right)_i \left(\frac{z}{p}\right)_w \frac{dp_{aw}}{dt_a} \dots \dots \dots (F-10)$$

Formation volume factor is defined for a real gas as

$$B = \frac{V}{V_{sc}} = \frac{zT}{p} \frac{p_{sc}}{z_{sc} T_{sc}}, \dots \dots \dots (F-11)$$

and the ratio of the formation volume factor at wellbore and initial conditions can be written as

$$\frac{B_w}{B_i} \frac{T_i}{T_w} = \left(\frac{p}{z}\right)_i \left(\frac{z}{p}\right)_w, \dots \dots \dots (F-12)$$

Gas density is defined as

$$\rho = \frac{Mp}{zRT}, \dots \dots \dots (F-13)$$

where M is the molecular weight of the gas and R is the gas constant. The ratio of reservoir-gas density to injected-gas density is written as

$$\frac{\rho_r}{\rho} = \frac{B}{B_r} \dots \dots \dots (F-14)$$

Similarly, the ratio of wellbore-gas density to injected-gas density is written as

$$\frac{\rho_w}{\rho} = \frac{B}{B_w}, \dots \dots \dots (F-15)$$

and the ratio of fracture-gas density to injected-gas density is written as

$$\frac{\rho_f}{\rho} = \frac{B}{B_f} \dots \dots \dots (F-16)$$

With the gas density and formation volume factor relationships, the material balance equation can be simplified and written as

$$qB_i - q_r B_i = \left[C_a + C_{fbc} \frac{B_w}{B_f} \frac{c_{ti}}{c_{tw}} \right] \frac{T_i}{T_w} \frac{dp_{aw}}{dt_a} \dots \dots \dots (F-17)$$

Define the dimensionless adjusted wellbore pressure as

$$p_{awsD} = \frac{(p_a)_w - (p_a)_i}{(p_a)_0 - (p_a)_i} = \frac{p_{aw} - p_{ai}}{p_{a0} - p_{ai}}, \dots\dots\dots (F-18)$$

and the dimensionless adjusted wellbore pressure derivative can be written as

$$dp_{aw} = (p_{a0} - p_{ai})p_{awsD} \dots\dots\dots (F-19)$$

Define the dimensionless adjusted pseudotime as

$$t_{aLfD} = \frac{kt_a}{\phi(\mu c_t)_i L_f^2}, \dots\dots\dots (F-20)$$

and the dimensionless adjusted pseudotime derivative can be written as

$$\frac{1}{dt_a} = \frac{k}{\phi(\mu c_t)_i L_f^2} \frac{1}{dt_{aLfD}} \dots\dots\dots (F-21)$$

With the definitions of dimensionless adjusted pseudovariables, the material balance equation can be written as

$$qB_i - q_r B_i = \left[C_a + C_{fbc} \frac{B_w c_{ti}}{B_f c_{tw}} \right] \frac{T_i}{T_w} \frac{2\pi kh(p_{a0} - p_{ai})}{\mu_i} \frac{1}{2\pi\phi c_{ti} L_f^2} \frac{dp_{awsD}}{dt_{aLfD}} \dots\dots\dots (F-22)$$

Define the dimensionless adjusted wellbore injection rate as

$$q_{awsD} = \frac{qB_i \mu_i}{2\pi kh(p_{a0} - p_{ai})}, \dots\dots\dots (F-23)$$

and the dimensionless adjusted sandface injection rate as

$$q_{asD} = \frac{q_r B_i \mu_i}{2\pi kh(p_{a0} - p_{ai})} \dots\dots\dots (F-24)$$

With the dimensionless rate definitions, the material balance equation can be written as

$$q_{asD} = q_{awsD} - \left[C_a + C_{fbc} \frac{B_w c_{ti}}{B_f c_{tw}} \right] \frac{T_i}{T_w} \frac{1}{2\pi\phi c_{ti} L_f^2} \frac{dp_{awsD}}{dt_{aLfD}} \dots\dots\dots (F-25)$$

Two assumptions and simplifications are required to develop the dimensionless material balance equation. First, assume that the fracture and wellbore formation volume factors are approximately equivalent, $B_f \cong B_w$. Second, assume the wellbore temperature, T_w , is constant and define a dimensionless adjusted wellbore storage coefficient as

$$C_{aD} = \frac{C_a}{2\pi\phi c_{ti} L_f^2} \frac{T_i}{T_w}, \dots\dots\dots (F-26)$$

and a dimensionless adjusted dilated/before-closure fracture storage coefficient as

$$C_{abcD} = \frac{C_{fbc}}{2\pi\phi c_{tw} L_f^2} \frac{T_i}{T_w} \dots\dots\dots (F-27)$$

At low pressures, the dimensionless adjusted dilated/before-closure fracture storage coefficient is not constant because of the total compressibility term. However, as the closure stress increases, the wellbore total compressibility approaches a constant value and can be approximated by the total compressibility at closure, $c_{tw} \approx c_{tc}$. Alternatively, recognize that the net pressure – the pressure in excess of fracture closure stress – generated during a fracture-injection/falloff test is minimal and typically on the order of a few hundred psi or less. Consequently, the average before-closure total compressibility is constant and approximately equal to the wellbore total compressibility where the average before-closure total compressibility is defined as

$$c_{tw} \equiv \bar{c}_{tbc} = \frac{c_{t0} + c_{tc}}{2}, \quad p_w > p_c \quad \text{..... (F-28)}$$

With the average before-closure total compressibility, the dimensionless adjusted dilated/before-closure fracture storage coefficient can be written as

$$C_{fbcD} = \frac{C_{fbc}}{2\pi\phi\bar{c}_{tbc}L_f^2} \frac{T_i}{T_w} \quad \text{..... (F-29)}$$

The dimensionless adjusted wellbore and dilated/before-closure storage definitions allow the material balance equation to be written as

$$q_{asD} = q_{awsD} - [C_{aD} + C_{fbcD}] \frac{dp_{awsD}}{dt_{aLFD}} \quad \text{..... (F-30)}$$

Provided the assumptions hold, the dimensionless adjusted wellbore and dilated/before-closure storage coefficients are constant and can be combined to create a single dimensionless adjusted before-closure storage coefficient written as

$$C_{abcD} = C_{aD} + C_{fbcD} \quad \text{..... (F-31)}$$

With the single dimensionless adjusted before-closure storage coefficient, the material balance equation during fracture-injection when the fracture dilates with the wellbore, fracture, and reservoir containing a real gas can be written as

$$q_{asD} = q_{awsD} - C_{abcD} \frac{dp_{awsD}}{dt_{aLFD}} \quad \text{..... (F-32)}$$

During the before-closure falloff of a fracture-injection/falloff sequence, the fracture contracts and the material balance equation can be written as

$$q_{asD} = -C_{abcD} \frac{dp_{awsD}}{dt_{aLFD}} \quad \text{..... (F-33)}$$

As shown in Appendix C, an after-closure material balance equation can be written as

$$qB\rho - q_r B_r \rho_r = (\rho_w c_{gw} V_w + 2\rho_f c_{gf} V_f) \frac{dp_w}{dt} \quad \text{..... (F-34)}$$

Define an adjusted after-closure storage coefficient as

$$C_{aac} = 2c_{gi}V_{fr}, \dots\dots\dots (F-35)$$

and with the definition of adjusted wellbore storage coefficient, a material balance equation can be written as

$$qB\rho - q_rB_r\rho_r = \left(\rho_w C_a \frac{\mu_{gi}c_{gw}}{(\mu_g c_g)_i} + \rho_f C_{aac} \frac{\mu_{gi}c_{gf}}{(\mu_g c_g)_i} \right) \frac{dp_w}{dt}. \dots\dots\dots (F-36)$$

With the definitions of adjusted pseudopressure and adjusted pseudotime (Eqs. F-5 through F-8) and with the reference condition, 're', defined as the initial pressure, p_i , the material balance equation can be written as

$$qB\rho - q_rB_r\rho_r = \left(\rho_w C_a + \rho_f C_{aac} \frac{\mu_{gw}c_{gf}}{(\mu_g c_g)_w} \right) \left(\frac{p}{z} \right)_i \left(\frac{z}{p} \right)_w \frac{dp_{aw}}{dt_a}. \dots\dots\dots (F-37)$$

Additionally, with the definitions of gas density, gas formation volume factor, and the relationships shown in Eqs. F-11 through F-16, the after-closure material balance equation can be written as

$$qB_i - q_rB_i = \left(C_a + C_{aac} \frac{\mu_{gw}c_{gf}}{(\mu_g c_g)_w} \frac{B_w}{B_f} \right) \frac{T_i}{T_w} \frac{dp_{aw}}{dt_a}. \dots\dots\dots (F-38)$$

The adjusted pseudovariation definitions, Eqs. F-18 through F-21, and the dimensionless rate equations, Eqs. F-23 and F-24, can be combined with the material balance equation, which is written as

$$q_{asD} = q_{awsD} - \left(C_a + C_{aac} \frac{\mu_{gw}c_{gf}}{(\mu_g c_g)_w} \frac{B_w}{B_f} \right) \frac{T_i}{T_w} \frac{1}{2\pi\phi c_{ti}hL_f^2} \frac{dp_{awsD}}{dt_a L_f D}. \dots\dots\dots (F-39)$$

Three assumptions and simplifications are required to develop the dimensionless material balance equation. First, assume that the fracture and wellbore formation volume factors are approximately equivalent, $B_f \cong B_w$. Second, assume the wellbore temperature, T_w , is constant, and third, assume the wellbore and fracture gas compressibility are equivalent. With the assumptions, and defining a dimensionless adjusted after-closure storage coefficient as

$$C_{aacD} = \frac{C_a + C_{aac}}{2\pi\phi c_{ti}hL_f^2} \frac{T_i}{T_w}, \dots\dots\dots (F-40)$$

the dimensionless after-closure material balance equation for a well with the wellbore, fracture, and reservoir containing a real gas can be written as

$$q_{asD} = q_{awsD} - C_{aacD} \frac{dp_{awsD}}{dt_a L_f D}. \dots\dots\dots (F-41)$$

However, during the after-closure period, there is no injected fluid, and the material balance equation can be simplified and written as

$$q_{asD} = -C_{aacD} \frac{dp_{awsD}}{dt_{aLfD}} \dots\dots\dots (F-42)$$

As shown in Appendix C, a material balance equation valid at all times can be written using the Heaviside unit-step function, which is defined as⁶²

$$U_a = \begin{cases} 0 & , t < a \\ 1 & , t > a \end{cases} \dots\dots\dots (F-43)$$

Following the technique of Correa and Ramey,⁶²⁻⁶⁴ a material balance equation valid at all times is written as

$$q_{asD} = \begin{bmatrix} \left(1 - U(t_e)_{aLfD}\right) \left(q_{awsD} - C_{abcD} \frac{dp_{awsD}}{dt_{aLfD}} \right) \\ - \left(U(t_e)_{aLfD} - U(t_c)_{LfD} \right) C_{abcD} \frac{dp_{awsD}}{dt_{aLfD}} \\ - U(t_c)_{aLfD} C_{aacD} \frac{dp_{awsD}}{dt_{aLfD}} \end{bmatrix} \dots\dots\dots (F-44)$$

where $(t_e)_{aLfD}$ is the dimensionless adjusted pseudotime at the end of pumping and $(t_c)_{aLfD}$ is the dimensionless adjusted pseudotime at fracture closure. After expanding and simplifying, the material balance equation for a fracture-injection/falloff sequence with the wellbore, fracture, and reservoir containing a real gas and with a dilating fracture and constant after-closure storage is written as

$$q_{asD} = \left(1 - U(t_e)_{LfD}\right) q_{awsD} - C_{abcD} \frac{dp_{awsD}}{dt_{aLfD}} + U(t_c)_{LfD} (C_{abcD} - C_{aacD}) \frac{dp_{awsD}}{dt_{aLfD}} \dots\dots\dots (F-45)$$

Following the derivation in Appendix C, the fracturing-injection/falloff solution in a well with the wellbore, fracture, and reservoir containing a real gas is written as

$$p_{awsD}(t_{aLfD}) = \begin{bmatrix} q_{awsD} \left[p_{aacD}(t_{aLfD}) - p_{aacD}(t_{aLfD} - (t_e)_{aLfD}) \right] \\ + p_{awsD}(0) C_{acD} p'_{aacD}(t_{aLfD}) \\ - (C_{abcD} - C_{aacD}) \int_0^{(t_c)_{aLfD}} p'_{aacD}(t_{aLfD} - \tau_D) p'_{awsD}(\tau_D) d\tau_D \end{bmatrix} \dots\dots\dots (F-46)$$

where p_{aacD} is defined in the Laplace domain as

$$\bar{p}_{aacD} = \frac{\bar{p}_{afD}}{1 + s^2 C_{aacD} \bar{p}_{afD}} \dots\dots\dots (F-47)$$

and p_{afD} is the finite- or infinite-conductivity fracture solution written in terms of adjusted pseudopressure and adjusted pseudotime.

Recall from Appendix C that the time-domain dilated-fracture injection/falloff solution in a well with the wellbore, fracture, and reservoir containing a slightly-compressible liquid is written as

$$p_{wsD}(t_{LjD}) = \left[\begin{array}{l} q_{wsD} [p_{acD}(t_{LjD}) - p_{acD}(t_{LjD} - (t_e)_{LjD})] \\ + p_{wsD} {}^{(0)}C_{acD} p'_{acD}(t_{LjD}) \\ - (C_{bcD} - C_{acD}) \int_0^{(t_c)_{LjD}} p'_{acD}(t_{LjD} - \tau_D) p'_{wsD}(\tau_D) d\tau_D \end{array} \right] \dots\dots\dots (F-48)$$

where p_{acD} is defined in the Laplace domain as

$$\bar{p}_{acD} = \frac{\bar{p}_{jD}}{1 + s^2 C_{acD} \bar{p}_{jD}}, \dots\dots\dots (F-49)$$

and p_{jD} is the finite- or infinite-conductivity fracture solution for a reservoir containing a slightly-compressible liquid.

Note that the two solutions, and limiting cases of the two solutions, have the same form. Consequently, the interpretation methods developed for a wellbore, fracture, and reservoir containing a slightly-compressible liquid can be applied when the wellbore, fracture, and reservoir contain a real gas provided that pressure and time are transformed to adjusted pseudopressure and adjusted pseudotime and provided that the reservoir pressure-transient solution written in terms of adjusted pseudovariabes, $p_{ajD}(t_{aLjD})$, is equivalent to the solution for a slightly-compressible fluid at the same dimensionless adjusted pseudotime, $p_{jD}(t_{aLjD})$.

Linearizing the Real-Gas Diffusivity Equation

Lee and Holditch⁷² demonstrated that the radial diffusivity equation for a real gas could be linearized under certain conditions by formulating in terms of pseudopressure and pseudotime. However, demonstrating the equivalence of $p_{ajD}(t_{aLjD})$ and $p_{jD}(t_{aLjD})$ requires formulating diffusivity equations in spherical and rectangular coordinates in terms of pseudopressure and pseudotime, or for convenience, adjusted pseudopressure and adjusted pseudotime. The spherical-flow diffusivity equation for a real gas is written in terms of adjusted pseudopressure with flow in the radial direction only as

$$\frac{1}{r^2} \frac{\partial}{\partial r} \left(r^2 \frac{\partial p_a}{\partial r} \right)_t = \frac{\phi \mu c_t}{k} \left(\frac{\partial p_a}{\partial t} \right)_r, \dots\dots\dots (F-50)$$

where $p_a = p_a(r, t)$ and $p_a = p_a(r, t_a)$. Following the derivation of Lee and Holditch,⁷² the spherical-flow real-gas diffusivity equation is effectively linearized by formulating in terms of adjusted pseudotime and adjusted pseudopressure when

$$\frac{1}{r^2} \frac{\partial}{\partial r} \left(r^2 \frac{\partial p_a}{\partial r} \right)_{t_a} \gg \left(\frac{\partial^2 p_a}{\partial t_a^2} \right)_r \left(\frac{\partial t_a}{\partial r} \right)_t^2 + 2 \left(\frac{\partial^2 p_a}{\partial t_a \partial r} \right)_{t_a, r} \left(\frac{\partial t_a}{\partial r} \right)_t + \frac{2}{r} \left(\frac{\partial p_a}{\partial r} \right)_r \left(\frac{\partial t_a}{\partial r} \right)_t, \dots\dots\dots (F-51)$$

and the linear spherical-flow real-gas diffusivity equation is written as

$$\frac{1}{r^2} \frac{\partial}{\partial r} \left(r^2 \frac{\partial p_a}{\partial r} \right) = \frac{\phi(\mu c_t)_i}{k} \left(\frac{\partial p_a}{\partial t_a} \right), \dots\dots\dots (F-52)$$

where the reference condition, 're', for the viscosity-compressibility product is the initial reservoir pressure, p_i .

Similarly, the real-gas diffusivity equation in a rectangular coordinate system is effectively linearized when

$$\begin{aligned} \left(\frac{\partial^2 p_a}{\partial x^2}\right)_{y,z,t_a} + \left(\frac{\partial^2 p_a}{\partial y^2}\right)_{x,z,t_a} + \left(\frac{\partial^2 p_a}{\partial z^2}\right)_{x,y,t_a} \gg & \left(\frac{\partial^2 p_a}{\partial t_a^2}\right)_{x,y,z} \left[\left(\frac{\partial t_a}{\partial x}\right)_{y,z,t}^2 + \left(\frac{\partial t_a}{\partial y}\right)_{x,z,t}^2 + \left(\frac{\partial t_a}{\partial z}\right)_{x,y,t}^2 \right] \\ & + 2 \frac{\partial}{\partial t_a} \left[\left(\frac{\partial p_a}{\partial x}\right)_{y,z,t_a} \right]_{x,y,z} \left(\frac{\partial t_a}{\partial x}\right)_{y,z,t} \\ & + 2 \frac{\partial}{\partial t_a} \left[\left(\frac{\partial p_a}{\partial y}\right)_{x,z,t_a} \right]_{x,y,z} \left(\frac{\partial t_a}{\partial y}\right)_{x,z,t} \\ & + 2 \frac{\partial}{\partial t_a} \left[\left(\frac{\partial p_a}{\partial z}\right)_{x,y,t_a} \right]_{x,y,z} \left(\frac{\partial t_a}{\partial z}\right)_{x,y,t} \end{aligned} \quad , \text{ (F-53)}$$

and linear diffusivity equation for a reservoir containing a real gas can be written in rectangular coordinates as

$$\frac{\partial^2 p_a}{\partial x^2} + \frac{\partial^2 p_a}{\partial y^2} + \frac{\partial^2 p_a}{\partial z^2} = \frac{\phi(\mu c_t)_i}{k} \left(\frac{\partial p_a}{\partial t_a}\right) \quad \dots \text{ (F-54)}$$

Partial Differential Equation for a Reservoir Producing Through a Finite-Conductivity Fracture

Consider a reservoir and fracture model as shown in **Fig. F-1**. Assume linear flow in the reservoir, which is written as

$$\frac{\partial p_a}{\partial x} = \frac{\partial p_{aD}}{\partial x_D} = 0, \quad \dots \text{ (F-55)}$$

where $x_D = x/L_f$ and the derivative of dimensionless pressure is defined as

$$\partial p_{aD} = \frac{2\pi kh}{qB_i \mu_i} \partial p_a \quad \dots \text{ (F-56)}$$

The partial differential equation describing flow in the reservoir is written as

$$\frac{\partial^2 p_{aD}}{\partial y_D^2} = \frac{1}{\eta_r} \frac{\partial p_{aD}}{\partial t_{aLfD}}, \quad \dots \text{ (F-57)}$$

where $y_D = y/L_f$, the diffusivity is defined as

$$\eta_r = \frac{k}{\phi(\mu c_t)_i}, \quad \dots \text{ (F-58)}$$

and the derivative of dimensionless time is defined as

$$\partial t_{aLfD} = \frac{k \partial t_a}{\phi(\mu c_t)_i L_f^2} \quad \dots \text{ (F-59)}$$

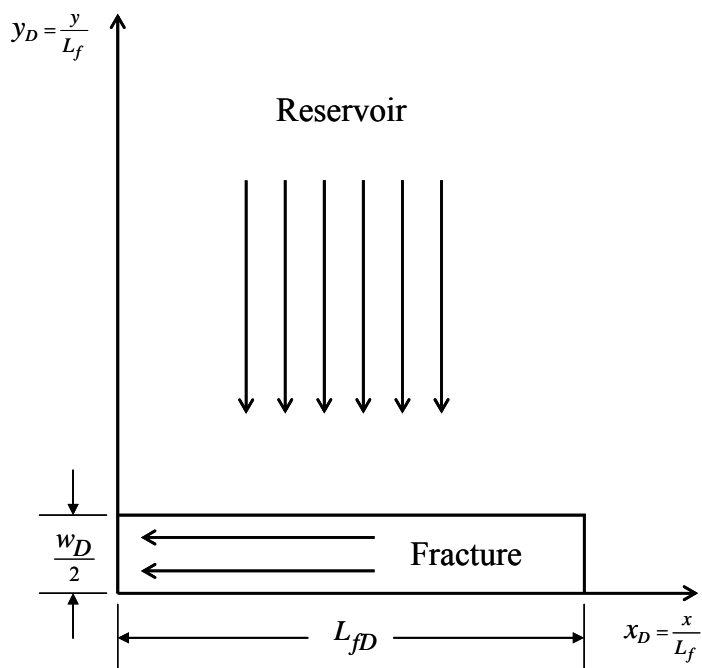


Fig. F-1—Flow directions in the reservoir and a finite-conductivity fracture.

Assuming two-dimensional flow in the fracture, the governing partial differential equation is written as

$$\frac{\partial^2 p_{afD}}{\partial x_D^2} + \frac{\partial^2 p_{afD}}{\partial y_D^2} = \frac{1}{\eta_{fD}} \frac{\partial p_{afD}}{\partial t_{aLfD}}, \dots\dots\dots (F-60)$$

where the dimensionless diffusivity is defined as

$$\eta_{fD} = \frac{k_f}{\phi_f(\mu c_t)_i} \frac{\phi_f(\mu c_t)_i}{k_f} \dots\dots\dots (F-61)$$

The boundary conditions are written for the fracture as

$$\left. \frac{\partial p_{afD}}{\partial x_D} \right|_{x_D=1} = \left. \frac{\partial p_{afD}}{\partial y_D} \right|_{y_D=0} = 0, \dots\dots\dots (F-62)$$

and the interface condition is written as

$$k \left. \frac{\partial p_{aD}}{\partial y_D} \right|_{y_D=w_D/2} = k_f \left. \frac{\partial p_{afD}}{\partial y_D} \right|_{y_D=w_D/2} \dots\dots\dots (F-63)$$

Following the pseudofunction approach and derivation of Bennett *et al.*,¹¹⁶ assume that

$$\frac{\partial p_{afD}}{\partial x_D}, \frac{\partial p_{afD}}{\partial t_{aLfD}} \neq f(y_D), \dots\dots\dots (F-64)$$

and integrate the fracture equation from $y_D = 0$ to $y_D = w_D/2$, which is written as

$$\int_0^{w_D/2} \frac{\partial^2 p_{afD}}{\partial x_D^2} dy_D + \int_a^b d \left(\frac{\partial p_{afD}}{\partial y_D} \right) = \frac{1}{\eta_{fD}} \int_0^{w_D/2} \frac{\partial p_{afD}}{\partial t_{aLfD}}, \quad \text{..... (F-65)}$$

where at $y_D = 0$,

$$a = \frac{\partial p_{afD}}{\partial y_D} \Big|_{y_D=0} = 0, \quad \text{..... (F-66)}$$

and at $y_D = w_D/2$, the interface condition applies and is written as

$$b = \frac{\partial p_{afD}}{\partial y_D} \Big|_{y_D=w_D/2} = \frac{k}{k_f} \frac{\partial p_{aD}}{\partial y_D} \Big|_{y_D=w_D/2} \quad \text{..... (F-67)}$$

Evaluation of the integrals results in

$$\frac{\partial^2 p_{afD}}{\partial x_D^2} + \frac{2}{w_D} \frac{k}{k_f} \frac{\partial p_{aD}}{\partial y_D} \Big|_{y_D=w_D/2} = \frac{1}{\eta_{fD}} \frac{\partial p_{afD}}{\partial t_{aLfD}}, \quad \text{..... (F-68)}$$

which can be written as

$$\frac{\partial^2 p_{afD}}{\partial x_D^2} + \frac{2}{C_{fD}} \frac{\partial p_{aD}}{\partial y_D} \Big|_{y_D=w_D/2} = \frac{1}{\eta_{fD}} \frac{\partial p_{afD}}{\partial t_{aLfD}}, \quad \text{..... (F-69)}$$

where dimensionless conductivity is defined as

$$C_{fD} = \frac{w_f k_f}{k L_f} \quad \text{..... (F-70)}$$

The flow rate is defined as

$$q_w B = 2L_f \tilde{q}(x, t), \quad \text{..... (F-71)}$$

where the flux must account for both fracture wings, which is written as

$$\tilde{q}(x, t) = \frac{(-2)A_x u_x}{L_x}, \quad \text{..... (F-72)}$$

or written as

$$\tilde{q}(x, t) = \frac{(-1) 2\pi kh}{\pi \mu} \frac{\partial p}{\partial y} \quad \text{..... (F-73)}$$

In terms of adjusted pseudopressure, the flux is written as

$$\tilde{q}(x, t) = \frac{(-1)B}{\pi} \frac{2\pi kh}{B_i \mu_i} \frac{\partial p_a}{\partial y}, \quad \text{..... (F-74)}$$

where the reference condition is the initial reservoir pressure, p_i .

Dimensionless adjusted flux is defined as

$$\tilde{q}_{aD} = \frac{2L_f \tilde{q}}{q_w B} = \frac{(-2)L_f}{\pi} \frac{2\pi k h}{B_i \mu_i} \frac{\partial p_a}{\partial y} = \frac{(-2)}{\pi} \frac{\partial p_{aD}}{\partial y_D} \Big|_{y_D=w_D/2}, \dots\dots\dots (F-75)$$

and can also be expressed as

$$-\pi \tilde{q}_{aD} = 2 \frac{\partial p_{aD}}{\partial y_D} \Big|_{y_D=w_D/2} \dots\dots\dots (F-76)$$

The governing partial differential equation can be written in terms of adjusted pseudovariabls as

$$\frac{\partial^2 p_{afD}}{\partial x_D^2} - \frac{\pi \tilde{q}_{aD}}{C_{fD}} = \frac{1}{\eta_{fD}} \frac{\partial p_{afD}}{\partial t_{aLFD}} \dots\dots\dots (F-77)$$

When steady flow is assumed in the fracture, the equation reduces to

$$\frac{\partial^2 p_{afD}}{\partial x_D^2} - \frac{\pi \tilde{q}_{aD}}{C_{fD}} = 0, \dots\dots\dots (F-78)$$

which can be written in the Laplace domain as

$$\frac{\partial^2 \bar{p}_{afD}}{\partial x_D^2} - \frac{\pi \bar{q}_{aD}}{C_{fD}} = 0, \dots\dots\dots (F-79)$$

The fracture-flow “wellbore” boundary condition for a constant rate is written in the Laplace domain as

$$\frac{\partial \bar{p}_{afD}}{\partial x_D} \Big|_{x_D=0} = -\frac{\pi}{s C_{fD}}, \dots\dots\dots (F-80)$$

and the boundary condition for no flow through the fracture tip is written in the Laplace domain as

$$\frac{\partial \bar{p}_{afD}}{\partial x_D} \Big|_{x_D=\pm 1} = 0 \dots\dots\dots (F-81)$$

Eq. F-76 is integrated twice with respect to x_D , and the general Laplace domain pressure distribution in a finite-conductivity fracture is written as

$$\bar{p}_{afD}(s) - \bar{p}_{aD}(x_D, s) = \frac{\pi x_D}{s C_{fD}} - \frac{\pi}{C_{fD}} \int_0^{x_D} \int_0^{x'} \bar{q}_{aD}(x'', s) dx'' dx' \dots\dots\dots (F-82)$$

where $p_{aD}(x_D, t_{aLFD})$ is the reservoir solution for production through a vertical fracture written in terms of adjusted pseudovariabls.

From Appendix E, the finite-conductivity fracture solution is written in the Laplace domain for a reservoir containing a slightly-compressible liquid as

$$\bar{p}_{fD}(s) - \bar{p}_D(x_D, s) = \frac{\pi x_D}{s C_{fD}} - \frac{\pi}{C_{fD}} \int_0^{x_D} \int_0^{x'} \bar{q}_{LFD}(x'', s) dx'' dx' \dots\dots\dots (F-83)$$

Note that the two solutions have the same form. Provided the solution for a reservoir containing a real gas and formulated in terms of adjusted pseudovariabls, $p_{aD}(x_D, t_{aLFD})$, and the reservoir solution for a

reservoir containing a slightly-compressible fluid, $p_D(x_D, t_{aLFD})$, are equivalent, then the finite-conductivity fracture pressure-transient solution written in terms of adjusted pseudovariabes, $p_{aFD}(t_{aLFD})$, is equivalent to the solution for a slightly-compressible fluid, $p_{FD}(t_{aLFD})$.

Reservoir Solution for a Well Producing a Real-Gas Through a Uniform-Flux Fracture

Appendix D contains the derivation of the the fully-penetrating vertical uniform-flux fracture solution for a reservoir containing a slightly compressible fluid where the solution is derived in the Laplace domain from the point-source solution as shown by Ozkan and Rhagavan.⁹⁵ The Laplace domain point-source solution is derived from the spherical-flow diffusivity equation,⁹⁵ which for real-gas flow and in terms of adjusted pseudovariabes is written as (Eq. F-54)

$$\frac{1}{r^2} \frac{\partial}{\partial r} \left(r^2 \frac{\partial p_a}{\partial r} \right) = \frac{\phi(\mu c_t)_i}{k} \left(\frac{\partial p_a}{\partial t_a} \right), \dots\dots\dots (F-84)$$

or in terms of dimensionless variables as

$$\frac{1}{r_D^2} \frac{\partial}{\partial r_D} \left(r_D^2 \frac{\partial p_a}{\partial r_D} \right) = \left(\frac{\partial p_a}{\partial t_{aD}} \right), \dots\dots\dots (F-85)$$

were $r_D = r/L_c$, L_c is a characteristic length, and a general dimensionless adjusted pseudotime is defined as

$$\partial t_{aD} = \frac{k \partial t_a}{\phi(\mu c_t)_i L_c^2} \dots\dots\dots (F-86)$$

The initial condition for solution of the governing differential equation requires that

$$p_a(r_D > \varepsilon \rightarrow 0^+, t_{aD} = 0) = 0, \dots\dots\dots (F-87)$$

and the boundary conditions are written as

$$p_a(r_D \rightarrow \infty, t_{aD} \geq 0) = 0, \dots\dots\dots (F-88)$$

and

$$\lim_{\varepsilon \rightarrow 0^+} \frac{4\pi k}{q(B\mu)_i} L_c \left(r_D^2 \frac{\partial p_a}{\partial r_D} \right) = -q_{aD} \delta(t) \dots\dots\dots (F-89)$$

The governing differential equation and boundary conditions for a reservoir containing a real gas are linear and identical in form to the governing differential equation and boundary conditions for a reservoir containing a slightly compressible liquid.⁹⁵ Consequently, the point-source solutions, and reservoir solutions developed from the point-source solutions, are the same. In the present context, the conclusion means that the reservoir solution formulated in terms of dimensionless adjusted pseudopressure for a well producing a real-gas through a vertical fracture is the same as the dimensionless pressure solution for a well producing a slightly-compressible liquid, which can be written as

$$p_{aD}(t_{aD}) = p_D(t_{aD}) \dots\dots\dots (F-90)$$

When the reservoir solutions are the same, the finite- and infinite-conductivity fracture solutions are also the same, which is written as

$$p_{afD}(t_{aD}) = p_{fD}(t_{aD}), \dots\dots\dots (F-91)$$

and when the finite- and infinite-conductivity solutions are the same, the fracture-injection/falloff solution for a dilating fracture formulated in terms of adjusted pseudopressure and adjusted pseudotime with the wellbore, fracture, and reservoir containing a real gas can be written as

$$p_{awsD}(t_{aLfD}) = \left[\begin{array}{l} q_{awsD} \left[p_{acD}(t_{aLfD}) - p_{acD}(t_{aLfD} - (t_e)_{aLfD}) \right] \\ + p_{awsD}(0) C_{acD} p'_{acD}(t_{aLfD}) \\ - (C_{abcD} - C_{aacD}) \int_0^{(t_c)_{aLfD}} p'_{acD}(t_{aLfD} - \tau_D) p'_{awsD}(\tau_D) d\tau_D \end{array} \right] \dots\dots\dots (F-92)$$

All fracture-injection/falloff solutions presented in Chapters III and IV can be cast in terms of adjusted pseudopressure and adjusted pseudotime, and in each fracture-injection/falloff solution, the reservoir and fracture solution derived in terms of adjusted pseudovariabes can be replaced by a slightly-compressible liquid solution evaluated in terms of adjusted pseudotime.

VITA

Name: David Paul Craig

Born: May 14, 1961
Fort Worth, Texas

Permanent Address: 14459 Williams Street
Thornton, CO 80602-7000

Phone: 720-929-0515

E-mail Address: doctorbubba@earthlink.net

Education: Texas A&M University, College Station, Texas, USA
Doctor of Philosophy in Petroleum Engineering
May 2006

Texas A&M University, College Station, Texas, USA
Master of Science in Petroleum Engineering
December 1991

Texas Tech University, Lubbock, Texas, USA
Bachelor of Science in Petroleum Engineering
December 1989